WOODHEAD PUBLISHING SERIES IN COMPOSITES SCIENCE AND ENGINEERING

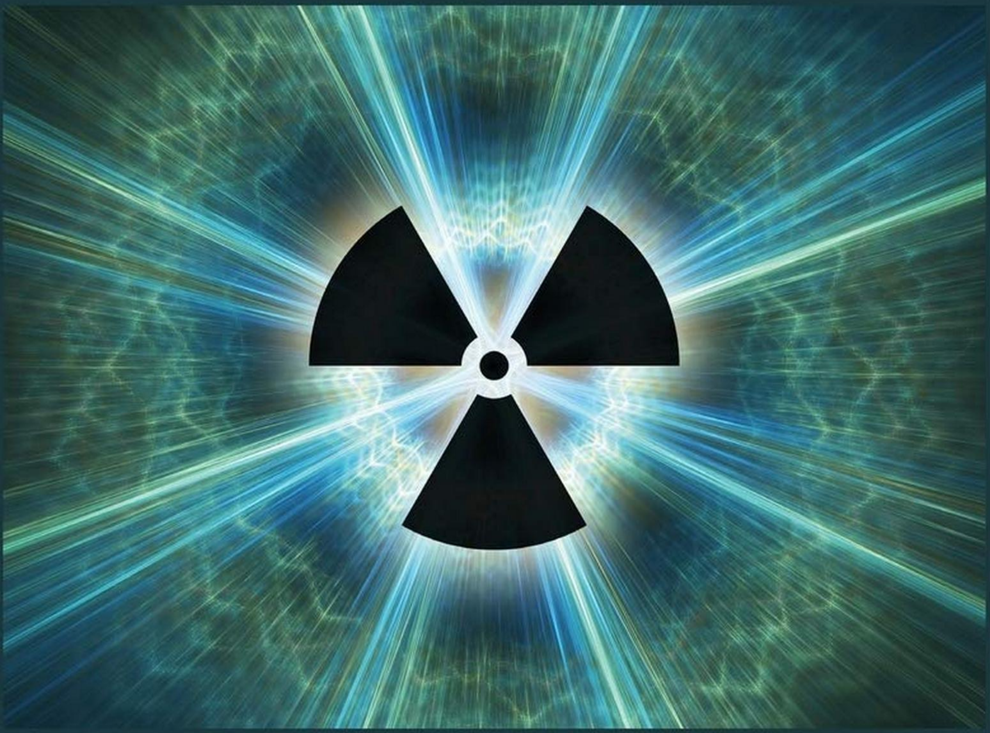

MICRO AND NANOSTRUCTURED COMPOSITE MATERIALS FOR NEUTRON SHIELDING APPLICATIONS

Edited by

SAJITH THOTTATHIL ABDULRAHMAN,
SABU THOMAS AND ZAKIAH AHMAD

ELSEVIER

MICRO AND NANOSTRUCTURED COMPOSITE MATERIALS FOR NEUTRON SHIELDING APPLICATIONS

Woodhead Publishing
Series in Composites
Science and Engineering

MICRO AND NANOSTRUCTURED COMPOSITE MATERIALS FOR NEUTRON SHIELDING APPLICATIONS

Edited by

SAJITH THOTTATHIL ABDULRAHMAN
Faculty of Civil Engineering, Universiti Teknologi Mara,
Shah Alam, Selangor, Malaysia

SABU THOMAS
Mahatma Gandhi University, Kottayam, Kerala, India

ZAKIAH AHMAD
Faculty of Civil Engineering, Universiti Teknologi Mara,
Shah Alam, Selangor, Malaysia

ELSEVIER
WP
WOODHEAD
PUBLISHING
An imprint of Elsevier

Woodhead Publishing is an imprint of Elsevier
The Officers' Mess Business Centre, Royston Road, Duxford, CB22 4QH, United Kingdom
50 Hampshire Street, 5th Floor, Cambridge, MA 02139, United States
The Boulevard, Langford Lane, Kidlington, OX5 1GB, United Kingdom

© 2020 Elsevier Ltd. All rights reserved.

No part of this publication may be reproduced or transmitted in any form or by any means, electronic or mechanical, including photocopying, recording, or any information storage and retrieval system, without permission in writing from the publisher. Details on how to seek permission, further information about the Publisher's permissions policies and our arrangements with organizations such as the Copyright Clearance Center and the Copyright Licensing Agency, can be found at our website: www.elsevier.com/permissions.

This book and the individual contributions contained in it are protected under copyright by the Publisher (other than as may be noted herein).

Notices
Knowledge and best practice in this field are constantly changing. As new research and experience broaden our understanding, changes in research methods, professional practices, or medical treatment may become necessary.

Practitioners and researchers must always rely on their own experience and knowledge in evaluating and using any information, methods, compounds, or experiments described herein. In using such information or methods they should be mindful of their own safety and the safety of others, including parties for whom they have a professional responsibility.

To the fullest extent of the law, neither the Publisher nor the authors, contributors, or editors, assume any liability for any injury and/or damage to persons or property as a matter of products liability, negligence or otherwise, or from any use or operation of any methods, products, instructions, or ideas contained in the material herein.

Library of Congress Cataloging-in-Publication Data
A catalog record for this book is available from the Library of Congress

British Library Cataloguing-in-Publication Data
A catalogue record for this book is available from the British Library

ISBN: 978-0-12-819459-1 (print)

ISBN: 978-0-12-819462-1 (online)

For information on all Woodhead publications
visit our website at https://www.elsevier.com/books-and-journals

Publisher: Matthew Deans
Acquisitions Editor: Gwen Jones
Editorial Project Manager: Emily Thomson
Production Project Manager:
Surya Narayanan Jayachandran
Cover Designer: Greg Harris

Typeset by SPi Global, India

ELSEVIER
Book Aid International
Working together
to grow libraries in
developing countries
www.elsevier.com • www.bookaid.org

Contributors

Sajith Thottathil Abdulrahman
Faculty of Civil Engineering, Universiti Teknologi Mara, Shah Alam, Selangor, Malaysia

Zakiah Ahmad
Faculty of Civil Engineering, Universiti Teknologi Mara, Shah Alam, Selangor, Malaysia

İskender Akkurt
Suleyman Demirel University, Isparta, Turkey

J. Alonso
Construction Engineering, Research and Project Development (INGECID S.L.), University of Cantabria. E.T.S. de Ingenieros de Caminos, Canales y Puertos, Santander, Spain

James Baciak
University of Florida, Nuclear Engineering Program, Gainesville, FL, United States

Lynsey Baxter
Oklahoma State University, Materials Science and Engineering Department, Tulsa, OK, United States

Eric Benton
Oklahoma State University, Physics Department, Stillwater, OK, United States

J.J. Bevelacqua
Bevelacqua Resources, Washington, WA, United States

Franco Cataldo
Actinium Chemical Research Institute, Rome, Italy

A. Cimentada
LADICIM (Laboratory of Materials Science and Engineering), University of Cantabria. E.T.S. de Ingenieros de Caminos, Canales y Puertos, Santander, Spain

C. Danani
Institute for Plasma Research, Gandhinagar, India

Andreas Enqvist
University of Florida, Nuclear Engineering Program, Gainesville, FL, United States

Yuan Gao
University of Florida, Nuclear Engineering Program, Gainesville, FL, United States

Korey Herrman
Oklahoma State University, Materials Science and Engineering Department, Tulsa, OK, United States

Antony Joseph
University of Calicut, Kerala, India

Kunal Mishra
Oklahoma State University, Mechanical Engineering Department, Stillwater, OK, United States

S.M.J. Mortazavi
Diagnostic Imaging Department, Fox Chase Cancer Center, Philadelphia, PA, United States; Medical Physics Department, School of Medicine, Shiraz University of Medical Sciences, Shiraz, Iran

S.V. Naydenov
Institute for Single Crystals of the NAS of Ukraine, Kharkov, Ukraine

G.M. Onyshchenko
Institute for Scintillation Materials of the NAS of Ukraine, Kharkov, Ukraine

Tonguç Özdemir
Mersin University Chemical Engineering Department, Mersin, Turkey

Rajesh Panthi
Oklahoma State University, Physics Department, Stillwater, OK, United States

Tomasz Piotrowski
Faculty of Civil Engineering, Warsaw University of Technology, Warsaw, Poland

J.A. Polanco
LADICIM (Laboratory of Materials Science and Engineering), University of Cantabria. E.T.S. de Ingenieros de Caminos, Canales y Puertos, Santander, Spain

Michele Prata
Laboratorio Energia Nucleare Applicata—Università degli Studi di Pavia, Pavia, Italy

Azerai Ali Rahman
Faculty of Civil Engineering, Universiti Teknologi Mara, Shah Alam, Selangor, Malaysia

Noureddine Ramdani
Polymer Materials Research Center, College of Materials Science and Chemical Engineering, Harbin Engineering University, Harbin, China; Department of Advanced Materials, RDI-IDT, Blida, Algeria

J. Rico
Construction Engineering, Research and Project Development (INGECID S.L.), University of Cantabria. E.T.S. de Ingenieros de Caminos, Canales y Puertos, Santander, Spain

V.D. Ryzhikov
Institute for Scintillation Materials of the NAS of Ukraine, Kharkov, Ukraine

J. Setién
LADICIM (Laboratory of Materials Science and Engineering), University of Cantabria. E.T.S. de Ingenieros de Caminos, Canales y Puertos, Santander, Spain

Raman Singh
Oklahoma State University, Mechanical Engineering Department, Stillwater, OK, United States

C.F. Smith
Naval Postgraduate School, Monterey, CA, United States

R. Srinivasan
Institute for Plasma Research, Gandhinagar, India

H.L. Swami
Institute for Plasma Research, Gandhinagar, India

P. Tamayo
LADICIM (Laboratory of Materials Science and Engineering), University of Cantabria. E.T.S. de Ingenieros de Caminos, Canales y Puertos, Santander, Spain

Sheila Thibeault
NASA Langley Research Center, Advanced Materials and Processing Branch, Hampton, VA, United States

C. Thomas
LADICIM (Laboratory of Materials Science and Engineering), University of Cantabria. E.T.S. de Ingenieros de Caminos, Canales y Puertos, Santander, Spain

Sabu Thomas
International and Inter University Centre for Nanoscience and Nanotechnology, Mahatma Gandhi University, Kottayam, Kerala, India

Ranji Vaidyanathan
Oklahoma State University, Materials Science and Engineering Department, Tulsa, OK, United States

ER Zuhal
Istanbul Technical University, Istanbul, Turkey

Editors biography

Sajith Thottathil Abdulrahman is a senior researcher at Universiti Teknologi Mara, Shah Alam, Malaysia. He was formerly an assistant professor at the School of Engineering at the Cochin University of Science and Technology, India. His doctoral thesis focused on the development of flexible materials for neutron radiation protection. He holds an MTech in nanotechnology and a BTech in mechanical engineering. His areas of research include nanotechnology, mechanical engineering, materials engineering, and polymer composites. He has published several books and journals in international journals and conferences.

Prof. Sabu Thomas is currently the *vice chancellor of Mahatma Gandhi University* and the founder director and professor of the International and Interuniversity Centre for Nanoscience and Nanotechnology. He is also a full professor of polymer science and engineering at the School of Chemical Sciences at Mahatma Gandhi University, Kottayam, Kerala, India. Professor Thomas is an outstanding leader with sustained international acclaims for his work in nanoscience, polymer science and engineering, polymer nanocomposites, elastomers, polymer blends, interpenetrating polymer networks, polymer membranes, green composites and nanocomposites, nanomedicine and green nanotechnology. Dr. Thomas's groundbreaking inventions in polymer nanocomposites, polymer blends, green bionanotechnological and nano-biomedical sciences have made transformative differences in the development of new materials for automotive, space, housing and biomedical fields. In collaboration with India's premier tyre company, Apollo Tyres, Professor Thomas's group invented new high-performance barrier rubber nanocomposite membranes for inner tubes and inner liners for tyres. Professor Thomas has received a number of national and international awards which include:

Fellowship of the Royal Society of Chemistry, London FRSC, Distinguished Professorship from Josef Stefan Institute, Slovenia, MRSI medal, Nano Tech Medal, CRSI medal, Distinguished Faculty Award, Dr. APJ Abdul Kalam Award for Scientific Excellence—2016, Mahatma Gandhi University—Award for Outstanding Contribution—Nov. 2016, Lifetime Achievement Award of the Malaysian Polymer Group, Indian Nano Biologists award 2017, and *Sukumar Maithy Award* for the best polymer researcher in the country. He is in the list of *most productive researchers in India* and holds a position of No. 5. Because of the outstanding contributions to the field of nanoscience and polymer science and engineering, Professor Thomas has been conferred *Honoris Causa (DSc) Doctorate by the University of South Brittany,* Lorient, France and *University of Lorraine, Nancy, France*. Very recently, Professor Thomas has been awarded *Senior Fulbright Fellowship* to visit 20 universities in the United States and most productive faculty award in the domain materials sciences. Very recently, he was also awarded with *National Education Leadership Award—2017* for Excellence in Education. Professor Thomas also won *6th contest of "mega-grants"* in the grant competition of the Government of the Russian Federation *(Ministry of Education and Science of the Russian Federation)* designed to support research projects implemented under the supervision of the world's leading scientists. He has been honoured with *Faculty Research Award* of India's brightest minds in the field of academic research in May 2018. Professor Thomas was awarded with *Trila—Academician* of The Year in June 2018 acknowledging his contribution to tyre industry. This year, Professor Thomas was also awarded with *H.G. Puthenkavu Mar Philoxenos Memorial Best Scientist Award.* In 2019 Professor Thomas received prestigious *CNR Rao Prize Lecture Award*. Professor Thomas has published over 900 peer-reviewed research papers, reviews, and book chapters. He has coedited 130 books published by Royal Society, Wiley, Woodhead, Elsevier, CRC Press, Springer, Nova, etc. He has five patents to his credit. The *H index* of Professor Thomas is *100* and has more than *48,266 citations*. Professor Thomas has delivered over 300 plenary/inaugural and invited lectures in national/international meetings over 30 countries.

Prof. Dr. Zakiah Ahmad is the dean of faculty of civil engineering, Universiti Teknologi Mara. Zakiah specialises in timber engineered composite and nanopolymer composites. She has secured and leads more than 50 research grants worth more than 5 million Euro. Dr. Ahmad has published more than 300 papers in journals and proceedings and 8 books. She has received several gold and silver awards for her research projects at national and international research competitions. She is the recipient of the following awards: Top Research Scientist Malaysia, Standard Malaysia Award, Best Researcher Award, Gold Consultant Award, and Best Academic. Dr. Ahmad is also active in giving keynote papers at numerous seminars and conferences at national and international level. Zakiah has served as consultant, committee member, and advisor to numerous public agencies and institutions. She also has been appointed as visiting scientist at BRE Research Institute, University of Bath, United Kingdom and tje Centre for Nanoscience and Nanotechnology, School of Chemical Sciences, Mahatma Gandhi University India.

CHAPTER 1

Introduction to neutron-shielding materials

Sajith Thottathil Abdulrahman[a], Zakiah Ahmad[a],
Sabu Thomas[b], Azerai Ali Rahman[a]
[a]Faculty of Civil Engineering, Universiti Teknologi Mara, Shah Alam, Selangor, Malaysia
[b]International and Inter University Centre for Nanoscience and Nanotechnology, Mahatma Gandhi University, Kottayam, Kerala, India

1.1 Introduction

Developments in neutron science and technology have led to the emission of unwanted neutron particle, which often occur in nuclear power plants, medical sector, and aerospace industry [1, 2]. A wide range of applications that emit neutron radiation show the need for protection in accordance with appropriate safety standards. Advances in the use of neutron sources such as neutron activation analysis (NAA), neutron radiography, active neutron interrogation technique, and neutron capture therapy over the past two decades show its importance. During operating conditions in such applications, unwanted neutron particle radiation escapes and interacts with the atoms of the surrounding materials which make the environment radioactive. Consequently, shielding materials with structural and functional integrity are important for the safer use of these applications. Table 1.1 lists the application of neutron-shielding materials in various sectors according to the incident energy of the undesired neutron radiations.

Nuclear power plants are an alternate source of energy to traditional fossil fuels with negligible carbon emissions, thus being relatively clean and efficient. Neutron emitted in reactors during the nuclear fission process must be shielded with suitable shielding materials. Specifically, high-energy neutrons exceeding 2 MeV energy during operation must be shielded to protect workers and the environment [3, 4]. Concrete has been generally used to attenuate the very fast neutrons with sufficient additives, including hydrogen-rich neutron moderators (water and polymer) and slow neutron absorbers. Additional shielding materials (flexible polymer-based) were applied to the curved and irregular plumbing surface ducts, etc., to prevent

Micro and Nanostructured Composite Materials for Neutron Shielding Applications
https://doi.org/10.1016/B978-0-12-819459-1.00001-5
© 2020 Elsevier Ltd.
All rights reserved.

Table 1.1 Neutron-shielding material application in various sectors.

Sl. no.	Categories	Energy of neutrons	Shielding material	Reference
1.	Nuclear power plants	>2 MeV	Concrete wall Water (moderator) Polymer composites Metal cask (spent fuel)	[3–5]
2.	Medical hospitals	10–25 MeV	Concrete wall Metal composites Polymer composites	[6–9]
3.	Aerospace	>1 MeV	Polymer composites	[10–12]
4.	Neutron radiography Neutron activation analysis Active neutron interrogations	~4 MeV	Polymer composites	[13–17]

the neutrons from escaping through them [18]. Furthermore, radiations from the radioactive waste material (spent fuel) from reactors also require proper disposal. The storage casks, based on metal materials with long-term durability, are usually used to dispose of spent nuclear fuel, which is another environmental issue that needs to be addressed.

Understanding the radiobiological effectiveness of by-product neutron doses occurring during radiation therapy treatment has been very important due to public health consequences [6]. Photo neutrons of 25–10 MeV generated during the acceleration of the electron in radiation therapy will result in in-room contamination, which is a threat to the patient [7,8]. Most neutrons are generated on collimation systems, applicators, and scattering foils in the accelerator. Metal-based and polymer-based shielding materials are provided to protect the patient from exposure to these neutron radiations and, in particular, flexible materials are needed to protect ventilation ducts, air conditioning, etc. [9]. In addition, boron neutron capture therapy is an emerging cancer therapy in circumstances where traditional radiation therapies become ineffective.

Galactic cosmic rays and solar energetic particles in outer space contains neutrons and protons of high energy (>1 MeV to 1 GeV) [11, 12]. Proper shielding has always been needed to protect electronics and humans from these radiation exposures. High secondary radiation is produced during interaction between radiation and heavy atoms in metals and concrete, so polymer-based composites were commonly preferred, which also helps to reduce the weight of the spacecraft, making it cost effective.

Neutron radiography has been used as a nondestructive test of objects in security applications, engineering studies, geology, biological medicine, and industry to determine structural defects. The unique chargeless characteristics of neutrons make them suitable for nondestructive testing of bulk compounds. They can provide excellent contrast for light atoms even in the presence of heavy atoms and can also easily distinguish between isotopes of the same element due to the significant variation in scattering and absorption cross sections during neutron interaction [13]. NAA technique is widely used in elemental composition studies related to environmental and industrial applications. It helps to analyze trace elements in vegetables [14] and to understand the spatial distribution of elements and isotopes in samples [15]. Prompt gamma NAA technique has emerged as an effective technique for monitoring heavy metals in groundwater contamination, which is a matter of serious concern to agriculture and modern industry [16]. Active neutron interrogation techniques are also used to detect bombs, land mine, and reliably identify elements in prehistoric utensils [17]. The neutron source used for the above techniques is Am/Be, Pu/Be, etc., which emits 4–5 MeV neutrons requiring adequate protection. Polymer composites such as polyethylene, paraffin, etc., are used to cover this neutron source in order to generate an isostatic neutron beam for the application. In turn, the portable neutron source should be lightweight and easy to transport from place to place.

In all of the above applications, proper protective measures should be taken considering unwanted neutron radiation generated during operating conditions. Neutron radiation is a type of ionizing radiation consisting of uncharged particles that pass-through electron clouds and interact directly with the nucleus of the atom. Apart from neutron sources and reactors, many high-energy radiations like X-rays, proton rays, γ-rays, etc., used in different applications often emit unwanted neutrons [6]. Compared with other radiations, these neutrons may cause severe damage to the nucleus of human tissues resulting in diseases such as cancer, cardiovascular disease, hemopoietic syndrome, etc. [19,20]. All nuclear-related activities are implemented with radiation safety concept “ALARA” or “as low as reasonably achievable” in order to ensure the safety of workers and the general public [21–25].

The demand for reliable neutron-shielding materials has risen over the last decade as unwanted radiation is harmful to man and the environment. The physical entity that is placed between the ionizing radiation source and protected objects is generally called a shield. The main function of this shield is to reduce the level of radiation at the position of the object. The object can be anything that is sensitive to ionizing radiations such as human beings, electronic items, etc.

1.2 Mechanism of neutron shielding

The shielding mechanism of neutron radiation is quite complex due to chargeless nature compared to other radiations. Neutrons interact directly with the nucleus because they are not affected by electrical fields. The interaction of cross sections of neutrons with the nucleus of the isotope depends on the energy of the incoming neutrons. Inelastic scattering, elastic scattering, and neutron absorption are three types of phenomena in which neutrons interact with matter. Fast neutrons with energy exceeding 10 MeV are subject to inelastic scattering with the nucleus. Neutrons with energy between 1 and 10 MeV shall lose their energy by means of elastic scattering in which energy is conserved. Slow neutrons (thermal neutrons) are assimilated into the nucleus in the absorption process without the emission of any particles. Absorption of neutrons lead to the excitation of the nucleus, followed by the liberation of γ-rays and α-rays [26].

The traditional way of shielding includes deceleration of fast neutrons through several elastic collisions to reduce the energy. According to the conservation of energy, isotopes with an equal mass of neutrons like hydrogen can cause maximum energy loss during elastic scattering. Further, the slow neutrons were absorbed using neutron-absorbing elements with relatively large neutron absorption cross sections. Therefore, for effective shielding of neutrons, the material should have a large number of hydrogen atoms together with neutron-absorbing elements with a large cross-section absorption of neutrons [27]. The schematic representation of the thermal neutron-shielding mechanism is shown in Fig. 1.1.

1.3 Neutron-shielding materials

Since 1950, the researchers have focused on nuclear reactors for power generation and associated radiation shielding materials due to biological damage directly caused by neutrons. Due to the advancement in nuclear technology, the neutron-shielding materials have gained significant attention in the last two decades. Trends in neutron-shielding material research publications over the past two decades are shown in Fig. 1.2. In the current scenario, the increase in the number of publications per year reveals their importance.

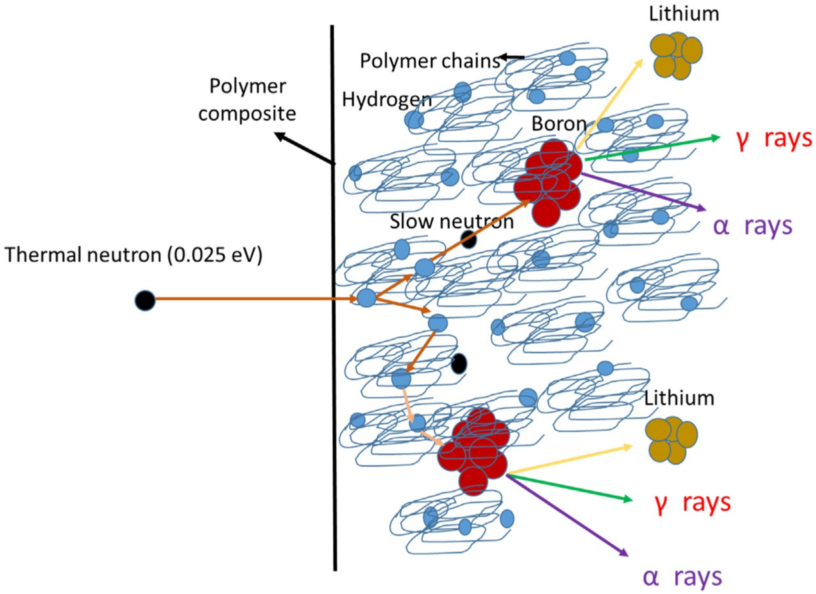
Lithium
Polymer chains
Polymer composite
Hydrogen
Boron
γ rays
α rays
Slow neutron
Thermal neutron (0.025 eV)
Lithium
γ rays
α rays

Fig. 1.1 Schematic representation of the thermal neutron-shielding process.

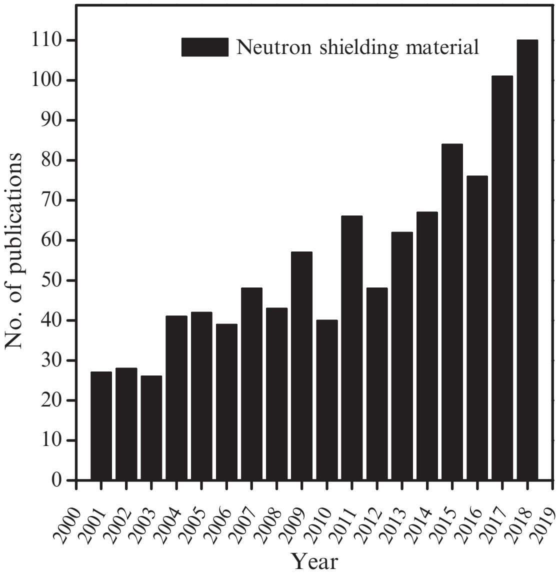

Fig. 1.2 Trends in neutron-shielding materials from year 2000 (SCI-Expanded, SSCI, A&HCI).

The choice of neutron-shielding material solely relies on the mechanism of shielding. Hydrogenous materials such as water, polymers, are therefore used as a matrix to decelerate the energy of fast neutron radiation through elastic scattering. In nuclear reactors, concrete containing neutron-absorbing fillers are traditionally used to block neutrons [5]. Concrete castings have also been used for the safe storage of radioactive waste removed from these reactors [28]. Metal [29,30] and ceramic [31,32] composites have been widely used as structural shielding materials due to their high mechanical properties, chemical resistance, and thermal stability. Borated steel has exceptional mechanical and thermal properties as a structural material, but the maximum boron content that can be incorporated is <2.23 wt% that makes it unsuitable for the absorption of thermal neutrons. However, in specific applications including aerospace, these materials have limitations due to heavy weight and size requirements.

Polymer composites filled with neutron absorbers are the most versatile neutron-shielding materials because of their properties like lightweight, low cost, compatibility, easiness of handling, etc. The tailorable nature of the polymer that can accommodate fillers like neutron absorbers makes it a suitable candidate for necessity wide range of applications. However, borated polymer composites usually have durability issues and their combustible nature makes them hazardous during application.

Several fillers are incorporated into the polymer matrix for enhancing their properties like neutron shielding, mechanical, thermal, etc. Boron, lithium, and cadmium are neutron-absorbing fillers with high thermal neutron absorption cross sections. The absorption cross section of boron compounds is 760 barns (1 barn $= 10^{-24}$ cm^2) and cadmium is 2520 barns. Lithium-6 (Li^6) isotope has thermal neutron absorption cross section of 940 b, but is less abundant. Some of the rare-earth elements like promethium, samarium, europium, gadolinium, and dysprosium also show high absorbing cross sections. However, boron compounds are used as neutron-absorbing fillers due to abundance and cost effectiveness [33,34].

The classification of the neutron-shielding materials based on the matrix type is presented in Fig. 1.3. Concrete, metal, and polymer materials filled with various additives are widely used to meet the application requirements. Here we will discuss each classification of neutron-shielding materials in detail.

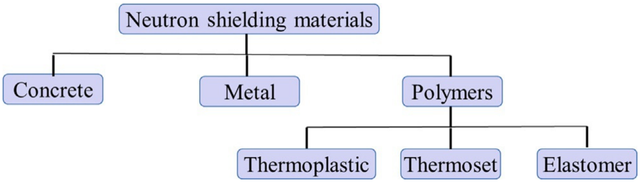

Fig. 1.3 Classification of neutron-shielding materials.

1.3.1 Concrete neutron-shielding materials

The most common material used for the attenuation of biological radiation is concrete because of its low cost and convenience of construction [35]. Fig. 1.4 illustrates an increase in the number of publications for concrete-based shielding materials over the past few years. The material properties such as radiation shielding safety, mechanical and thermal stability over a long lifetime of nuclear reactors are of primary concern in reactor shielding. The key factors affecting neutron and gamma shielding are hydrogen content, elemental composition, and concrete density. On the basis of that, special concretes have been designed with a combination of materials considering the known intensity of the spectrum of radiation. The heavy

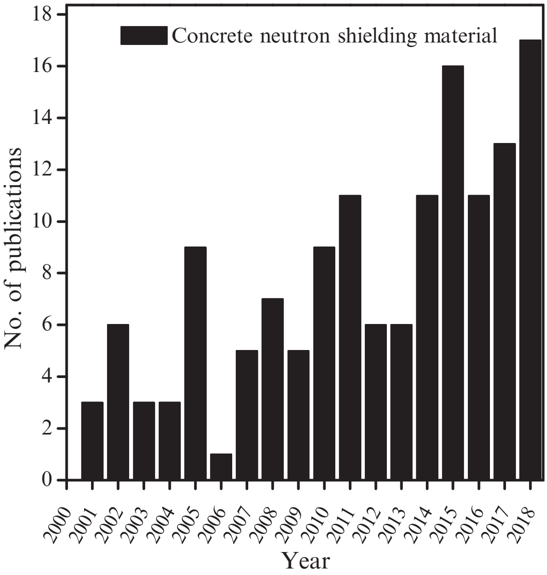

Fig. 1.4 Trends in concrete neutron-shielding materials from 2000 (SCI-Expanded, SSCI, A&HCI).

concrete, borated concrete, and high-temperature concrete are different types of concrete based on various compositions used for shielding purposes [36,37].

Elements such as barium, iron, hydrogen, and carbon are well known to moderate the rapid neutrons due to their large inelastic and elastic cross sections. As a result, carbon aggregates, iron ores (hematite), barium, lead, etc., are widely used to enhance the fast neutron moderation properties of concrete. These aggregates, however, increase the density of concrete from 2 to 5.5 g/cc. The addition of carbon powder to the hematite cement enhances the compressive strength of the concrete without compromising the shielding properties [38]. Silica fume, fly ash, and furnace blast display only marginal differences in the neutron attenuation property of concrete while the reduction in greenhouse gas emissions make it environmentally friendly [39]. In another experiment, the hematite proportion in the concrete increased the concrete strength without changing the shielding property. The hematite fillers also have greater cement adhesion and can be used at high temperatures [40]. A study on the transport of neutrons through cement mortar, PCC mortar, normal weight, and magnetite heavyweight concrete indicates that a 1% rise in humidity will boost the shielding by 10% due to an increase in atomic hydrogen density. In addition, only a slight increase in fast neutron attenuation was observed with concrete density suggesting that heavyweight concrete is not an appropriate candidate for fast neutron shielding. Nevertheless, due to increased iron content over silicon and oxygen, it has high thermal neutron absorption potential [41]. Another issue identified was the formation of heavier isotope impurities during neutron interactions, which may act as sources of secondary gamma radiation.

In order to suppress secondary gamma radiation, neutron-absorbing fillers, such as boron compounds, are introduced into concrete [42]. Thermal neutrons can be absorbed easily through borated concrete, thereby reducing the heat generated during the liberation of secondary gamma radiations. Boron fillers may be introduced into concrete using three different methods: (a) aggregates, (b) boron-containing cement, and (c) boron-dissolved water [26]. Boron compounds such as boric acid and borax are cheap aggregates mostly used for thermal neutron absorption in concrete, although these compounds cause a delay in setting time which eventually lowers the final properties of the composites. Borax-filled concrete shows improved neutron attenuation if the thickness of the shield is higher [43]. Boron carbide is an alternate aggregate material used in concrete composites, but its distribution is poor due to its high density. Comparative investigation of Fe-B and B_4C aggregates added to concrete indicates that Fe-B concrete has better neutron attenuation efficiency than B_4C [44].

In the meantime, taking into account the use of material at extreme temperatures, high-temperature concrete was developed by incorporating minerals such as serpentine and limonite. They provide temperature stability of up to 500°C and the loss of hydrogen due to heating, thereby reducing concrete density [36]. The analysis of the fast neutron removal cross sections of various mineral aggregates shows the combined effect of higher energy gains and lower energy losses of neutron beam attenuation [45]. The hydrogen content of limonite and serpentine improves neutron attenuation when used in combination with illuminate, magnetite, and hematite ores in concrete [46].

The potential use of colemanite ($2CaO:3B_2O_3:5H_2O$) enhances the efficiency of baryte and concrete neutron protection owing to the boron and hydrogen elements in it [47]. Colemanite shows better neutron-shielding performance among the ores of colemanite, ulexite, and tincal. The study also found the dependence of macroscopic cross section and boron atomic density [48]. An investigation into the setting time and hydration heat of cement of boron aggregates (colemanite, ulexite, borax, and boron carbide) and nanosilica revealed that colemanite aggregate significantly increases the boron content without altering the hydration process compared to other aggregates [49].

The use of polymer to improve the shielding and other properties of the concrete has gained great interest owing to its hydrogen enrichment and compatibility. Polypropylene fibers are introduced to retain structural integrity lost by colemanite, which indicates that 50% of the aggregate can be replaced by colemanite with this combination [50]. Concrete filled with polyethylene and B_4C enhances the shielding of thermal energy neutrons by a factor of 40 particularly in comparison to ordinary concrete. But the addition of PE and B_4C reduced the concrete density and strength [51]. Investigation of nonisocyanate polyurethane-filled concrete shows the gamma and neutron radiation effect on the destruction of hydrocarbon bonds. The radiation-resistant indices have been degraded to a maximum of 25% of the original value, but the structural changes enhance the composite's strength [52]. After exposure to high temperatures concrete containing limestone aggregates, PVA fiber, and boron carbide exhibited a decrease in mechanical properties and an increase in temperature porosity. The compressive strength enhanced up to 500°C and the strength reduced drastically above 500°C [53].

The influence of the size of the aggregates on the neutron-shielding concrete was also extensively studied. Borosilicate glass of 13 μm slightly improves the concrete's compressive strength and thermal neutron attenuation parameters and the pozzolanic behavior of borosilicate glass is also demonstrated [54]. Boron-infused basalt fiber-reinforced concrete samples show negligible changes in fast neutron attenuation but decreased the thickness of the thermal spectrum reactor radiation shield [55]. The influence of PbO_2, Fe_2O_3, WO_3, and H_4B (boronium) on particle size suggests that nanosized fillers have a 7% higher cross section of neutron removal than microparticles [56]. It is noted that B_4C can replace 40% of the quartz sand in the cement without altering the setting kinetics. In addition, the delay caused by boron can be overcome by adding 1%–2% nanosilica [49]. The cement paste incorporated with nano TiO_2 strengthened the low-energy neutron-shielding properties with the addition of filler. For nano cement paste, compressive strength and bulk density are higher than the normal Portland cement [57].

In summary, the concrete should contain a sufficient mixture of heavy atomic materials, neutron moderators, and absorbers for efficient shielding of neutron radiation. The addition of neutron absorbers reduces the secondary gamma radiation emitted during the shielding process. With the proper addition of mineral aggregates, the thermal stability of the concrete can be improved. The use of natural ores with neutron absorbers would increase the concrete's attenuation property but reduces structural properties. The addition of a polymer will maintain the structural properties lost when minerals are added and increase the atomic density of hydrogen. It is also observed that the nanosized fillers and cement fillers themselves will increase the concrete's neutron shielding and overall properties.

1.3.2 Metal neutron-shielding composites

In areas where extreme temperatures and chemical conditions are generated, heavy metal with neutron absorber was mostly used as a neutron-shielding material [58]. Fig. 1.5 illustrates an increase in the number of metal shielding material publications throughout the past decade. Metal storage container is the most suitable candidate as a convenient storage mode for the handling of the spent nuclear fuel, as it is a serious environmental problem. Since the casks are designed for long-term storage, they should have sufficient mechanical properties, resistance to corrosion, high-temperature stability, and low impact resistance [59].

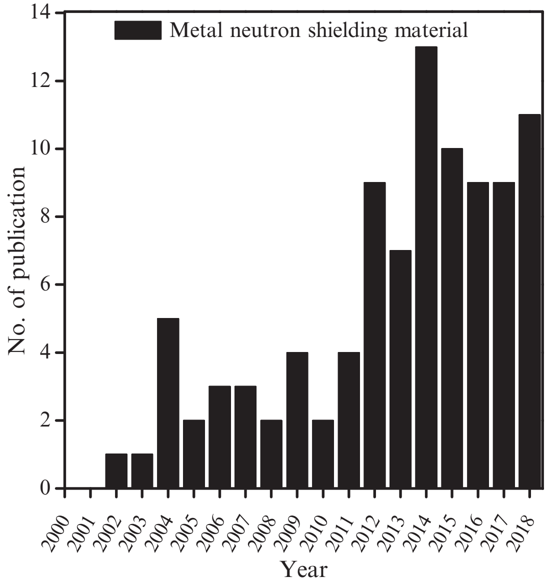

Fig. 1.5 Trends in metal neutron-shielding materials from 2000 (SCI-Expanded, SSCI, A&HCI).

A comparative study on neutron-shielding properties of aluminum boron carbide, tungsten boron carbide, bismuth borosilicate glass, and metathene shows tungsten B_4C as effective neutron attenuating material. The findings also show that the ability of neutron shielding mainly depends on materials having low atomic number [60]. The synthesis of lead borate compounds using a solvothermal process using pyridine and ammonium hydroxide results in the growth of lead borate fibers and nanostructured crystals. Among other structures, the developed lead borate crystal has better neutron and gamma shielding properties [61].

Boral is a widely used neutron-shielding composite made of hot-rolled composite plate material consisting of a core of mixed aluminum and boron carbide particles. The B_4C density (2.53 g/cm^3) is similar to aluminum (2.7 g/cm^3) making it an effective aluminum reinforcement. Different manufacturing methods for particulate aluminum reinforced metal composites includes stir casting, powder metallurgy, squeeze casting, hot pressing, hot isostatic pressing, and spark plasma sintering. Aluminum composites with B_4C prepared by sintering were highly porous and the presence of Al_3BC and AlB_2 intermetallic compounds was observed. While composites developed using hot isostatic pressing technique indicate that the distribution of B_4C has increased with negligible porosity [29]. The temperature of the hot press and extrusion process is held below 580°C to prevent the development of high-temperature phases and replaces the hot rolling process with hot extrusion. The composites show greater strength while the fracture ductility decreased slightly. A relationship has been found between the [10]Boron atomic density (BAD) and the neutron transmission ratio, which indicates that composites will shield 99% when BAD exceeds 0.034 g/cm^2 [62]. Neutron-absorbing composites of aluminum and B_4C developed using spark plasma sintering shows homogeneous distribution of B_4C in aluminum together with good interfacial bonding. The neutron transmission decreased with B_4C content and the strength enhanced due to the grain refinement and dislocation strengthening. Indeed, the generation of high heat produces intermetallic compounds such as AlB_{12}, Ti_2B_5, and B [59]. In order to enhance the ductility of Al/B_4C composites, a small amount of Gd was incorporated as a neutron-absorbing material. These composites exhibit enhanced mechanical properties with ductility. The developed $Al/B_4C/Gd$ composites displayed an equivalent boron areal density of 0.1105 g/cm^2 with 99% attenuation of neutrons [63]. However, the porosity and the formation of intermetallic phases significantly weaken the properties of the shielding material.

In order to overcome the issues caused by the incorporation of neutron absorbers, the authors tried to embed it over metal surfaces as coatings and laminates. Cost-effective B_4C coatings in aluminum alloy using cold spray additive manufacturing technique show crack-free and homogeneous deposition. The heat treatment of the coating at 500°C results in enhanced ductility and mechanical properties of the composites. The neutron attenuation properties of the composites increased with the thickness of the B_4C coating and 50% shielding was achieved with 5-mm-thick coating [64]. Neutron-shielding fiber metal laminates (NSFML) fabricated using the hot molding process show enhanced mechanical properties and B_4C distribution. With the increase in laminate layers, the neutron-shielding ability of laminates improved. Carbon fiber is also used in combination with aluminum as a neutron moderator, but the elongation of laminates declined due to its rupture [65]. In another study, the NSFML shows good thermal stability up to 300°C but dramatically degraded above 400°C due to pyridine pyrolysis. In addition, B_4C particles serve as pins between laminates that resist the relative motion of the plate between neutron-shielding layers [66].

Fe-based amorphous ribbons containing 25 at% boron and 10 at% gadolinium were developed using melt-spinning technique. The intermediate metal compounds were absent in the formed composites, thus retaining the mechanical properties and resistance to corrosion [67]. Investigations into the neutron-shielding properties of electroslag remelting steel demonstrate a greater macroscopic cross section compared to stainless steel and ordinary concrete [68]. The microstructural and physical properties of Mo-based gray control rods have been investigated. Mo-based Tb_2O_3-Dy_2O_3 composites produced by ball milling and sintering indicate the uniform distribution of Tb_2O_3-Dy_2O_3 in Mo matrix. The sintering temperature and chemical content of lanthanide oxides enhanced the compressive strength and microhardness of the composite. The coefficient of thermal expansion decreased with the chemical content of lanthanide oxides and increased with sintering temperature [69].

In summary, metal-based neutron-shielding materials are important for applications where high strength, temperature, and durability are required. The atomic density of the metal is an important parameter for attenuating fast neutrons. Due to the compact nature of most of the metals, the quantity of neutron-absorbing fillers added is very less, which affects the shielding property. Among the metals, aluminum is the most suitable metal-based neutron attenuating material.

1.3.3 Polymer neutron-shielding composites

Low weight and secondary gamma emissions are key requirements for neutron-shielding materials for specific applications such as space missions, portable devices, etc. The use of concrete or metal shields is very costly, spacious, and will cause rise in cancer incidence. Choosing polymers as a neutron-shielding matrix has several advantages such as hydrogen richness, lightweight, ease of production, compatibility, etc. These are giant molecules consisting of atoms of hydrogen and carbon with a range of repeating units called monomers. They are primarily classified into three categories: thermoplastic, thermoset, and elastomers. Fig. 1.6 reflects the recent increase in the number of polymer-based neutron-shielding materials research outcomes.

1.3.3.1 Thermoplastic neutron-shielding composites

The mechanical and morphological properties of HDPE/boron nitride (BN) composites for spacecraft radiation shielding have been reported. The surface modification of the BN improves the adhesion to the HDPE matrix and thus increases the mechanical properties. In addition, the radiation-shielding efficiency of the HDPE/BN composites, which are only one-third the weight aluminium, was similar to that of aluminum [11]. The morphology

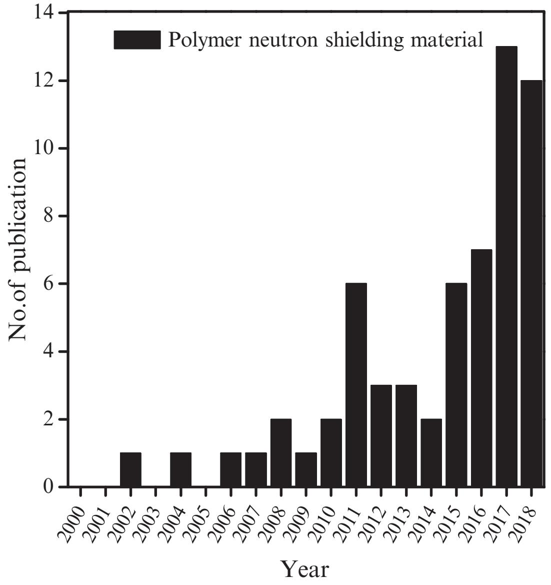

Fig. 1.6 Trends in polymer neutron-shielding materials from 2000 (SCI-Expanded, SSCI, A&HCI).

of UHMWPE/Sm_2O_3 shows the continuous distribution of Sm_2O_3 in UHMWPE but with lower tensile properties due to the agglomeration of the fillers [70]. Better distribution in HDPE composites for silane-modified BN than unmodified composites has been achieved and the tensile modulus of modified BN/HDPE composites surpassed unmodified composites by 23%. The neutron-shielding characteristics of modified BN/HDPE composites are also much higher than those of unmodified BN and B_4C/HDPE composites due to improved filler-matrix adhesion [71].

The effect of nanosize B_4C on the properties of the composites PVA and HDPE was examined [27]. The macroscopic cross section of PVA/B_4C increased from 1.49 to 1.72 cm^{-1} due to the nanosize of B_4C when compared to its micro counterparts. A similar type of macroscopic cross-section improvement was also observed in the case of composites HDPE/B_4C. In another study, the ball milling technique was used to reduce the size of B_4C. The size reduction of B_4C helps to achieve uniform distribution in the HDPE matrix and this intern enhances the mechanical and neutron-shielding characteristics of composites of HDPE with BN and B_4 [72]. Boron-doped MWCNT/HDPE composites enhanced the macroscopic cross section to 1.06 m^{-1} with high tensile characteristics [19].

In conclusion, the neutron-absorbing filler size and surface interaction play an important role in enhancing the properties of thermoplastic neutron-shielding materials. The lightweight, high hydrogen content together with boron-based absorber makes it an alternate shielding material. Nevertheless, these materials are rigid and are not suitable to be used on curved and irregular surfaces.

1.3.3.2 Thermoset neutron-shielding composites

Epoxy-based thermoset neutron-shielding composites are widely studied due to their excellent properties like dimensional stability, chemical resistance, heat resistance, easiness in fabrication, etc., over concrete and polyethylene. The aromatic backbone showed efficiency in shielding secondary gamma radiations. The neutron and gamma radiations were effectively shielded by LiF/B_4C metathene composites, which is suitable for biological applications like boron neutron capture therapy [33]. Investigations on epoxy/lithium borate that can be used as wall tiles to protect patients and workers in radiotherapy laboratories were performed. The homogeneous morphology of lithium borate in epoxy/lithium borate composites is attained through proper solidifying technique. Epoxy/lithium borate composites with a 20% filler addition show optimum mechanical properties with a half-value layer of 6.7 cm which is unaltered with gamma irradiation [34]. Epoxy-/boric-acid-based lightweight material with a mean free path of 7 cm and enhanced hardness shows better shielding efficiency than cement and concrete [73].

Adeli et al. [74] investigated the effect of B_4C size on low viscosity amine-based epoxy resins for neutron-shielding applications. A significant increase in neutron attenuation for 20-μm B_4C particle-filled epoxy composites was observed. B_4C/epoxy composites with 20 μm thickness show macroscopic cross section of 0.34 cm^{-1}. Moreover, the addition of WO_3 to shield secondary gamma radiation, and ATH to increase the flame retardancy enhanced the thermal neutron-shielding property of the composites.

In summary, thermoset polymers show better shielding with better dimensional stability and are easy to fabricate in curved and irregular surfaces, unlike thermoplastic. Its adhesion with reinforcements, lightweight, chemical resistance, mechanical and thermal properties makes it suitable for aerospace applications.

1.3.3.3 Elastomeric neutron-shielding composites

Elastomer-based neutron-shielding materials are used in applications where flexibility is a major requirement, especially for applications like wearable clothing, glovebox, curved and irregular surfaces, etc. The flexible elastomeric neutron-shielding materials reported were mostly based on natural rubber, EPDM rubber, silicon rubber, and styrene-butadiene rubber. Neutrons absorbers are distributed in the rubber matrix for absorbing the thermal neutron radiations. Elastomer composites were used rather than rigid thermoplastic materials for shielding the hazardous neutron radiations escaping through the curved and irregular surfaces.

Investigation on the neutron-shielding natural rubber with varying boric acid concentration shows 30 parts of H_3BO_3 improved the thermal neutron macroscopic cross section from 0.14 to 0.29 cm^{-1}. Besides, the thermal diffusivity of the composites increased at higher boric acid content but electrical characteristics decreased [75]. NR filled with H_3BO_3 and B_2O_3 indicates enhanced shielding efficiency with boron concentration. Moreover, the incorporation of wood particles gives additional dimensional stability to the composites without effecting the shielding property. The H_3BO_3 and B_2O_3 filler loading decreased the curing and mechanical properties of the composites [76]. Blocks of NR-borax and NR-boric acid composites illustrate that boron concentration enhanced the neutron-shielding properties. The distribution of the borax and boric acid also influence the shielding characteristics. Moreover, the loss occurring due to the bubble formation during the preparation of boric acid composites results in lower shielding for the same amount of borax-filled composites [77].

The incorporation of B_4C as an absorbing filler in the natural rubber matrix shows a neutron absorption cross section of 0.34 cm^{-1} for 20 phr B_4C-filled composites. In addition, the electrical and thermal conductivity of material increased with the addition of B_4C filler [78]. The flexible films of NR latex/B_4C composites indicate the uniform distribution of the B_4C that is prepared by latex mixing. The macroscopic cross section increased to 2 mm^{-1} with the addition of 55 wt% B_4C filler. However, the tensile properties decreased with B_4C loading and the molecular structure of the composites remains unchanged [79]. When comparing the neutron-shielding characteristics among the fillers, NR-B_4C composites were found to show higher attenuation due to the higher boron atomic density of B_4C than H_3BO_3. But, the cost of the NR filled with B_4C composites will be higher than the low-cost fillers H_3BO_3 and borax.

A flexible material based on methyl vinyl silicon rubber/B_4C material with improved mechanical, thermal, and flame retardancy was developed with the proper addition of B_4C, hollow beads, and zinc borate. The composites indicate a reduction of 53% in neutron transmission at higher

B_4C concentration. In addition, the surface modification of the B_4C fillers results in improved distribution in rubber matrix thereby enhancing the neutron-shielding characteristics, and mechanical and thermal properties of the material [21]. In another investigation, considering the secondary gamma attenuation, the fillers B_4C, PbO, and benzophenone were incorporated to develop a flexible neutron-shielding material based on methyl vinyl silicon rubber. The powder surface modification improved the dispersion of fillers in the matrix and thus enhanced the material properties. The composites show only 12% neutron transmission for 2-mm-thick 25 wt% B_4C-filled composites. Moreover, the irradiation of gamma radiation improved the cross-linking by benzophenone, which results in better properties of the material [80]. Silicone rubber composites with 17% H_3BO_3 reduced the neutron radiation by 70% and hence can be used as wearable clothing. Moreover, the contribution of newly generated thermal neutrons was negligible compared to the total neutron count [81].

The EPDM rubber composites show neutron absorption cross section of 1.46 cm^{-1} with a 20% H_3BO_3 filler addition. The H_3BO_3 fillers accelerate the vulcanization kinetics of the composites and consequently enhance the mechanical properties but marginally decrease thermal properties. [82]. In another study, boron trioxide (B_2O_3) shows the uniform distribution in the EPDM matrix which also accounts for increase in mechanical and thermal properties of the composites due to better interaction between filler and matrix. Further, 20% of B_2Os_3 filled composites show 2.57 cm^{-1} neutron macroscopic absorption cross section [83]. So, it can be concluded that the higher boron atomic density of B_2O_3 than H_3BO_3 results in enhanced neutron-shielding characteristics. Also, the better mechanical and thermal properties are due to good interaction of B_2O_3 with EPDM rubber.

In summary, the B_2O_3 and H_3BO_3 composites improve the cross-linking of silicone and EPDM rubber, but decrease the cross-linking in natural rubber composites. In the meantime, the hard filler B_4C enhances the neutron attenuation characteristics of all the rubbers with comparatively less amount than other fillers.

The blends of EPDM/LDPE (50/50) with 57% B_4C shows a macroscopic cross section of 0.215 cm^{-1} for slow neutrons. An enhancement in thermal and electrical properties with B_4C filler addition was also noticed [84]. Investigation on the NR/HDPE/liquid natural rubber with various B_4C fillers prepared in Haake internal mixer indicates the importance of the filler concentration in improving neutron absorption and mechanical properties [85]. NR/SBR with 60 phr B_2O_3 composites with

10-mm thickness attenuates the neutron radiations by 57%. Also, the 100-mm-thick composites with four alternating layers of NR/SBR/B_2O_3 and NR/SBR/Fe_2O_3 material decrease the neutron radiations by 72% [86]. The neutron-shielding characteristics of TPNR with varying B_4C composites prepared through melt mixing represent a macroscopic cross section of 14.8 cm^{-1} [87].

1.4 Conclusion

In this chapter, the growing demand for the use of neutron radiation shielding materials as structural materials in various sectors was discussed. Developments in the application of neutron radiations in the last decade such as neutron radiography and neutron capture therapy show the necessity of advanced neutron-shielding materials. Neutron attenuating material selection depends on the incoming neutron energy. The neutron-shielding materials are mainly categorized into concrete, metal, and polymer-based composites. In concrete, heavy atomic fillers like hematite, iron ore, etc., show enhanced attenuation toward very fast neutrons. The hydrogen content in the concrete is a significant factor for shielding fast neutrons through elastic collision and slow neutron attenuation was found to be dependent on the neutron absorber content in concrete which is mainly achieved through the incorporation of boron compounds. Metal-based neutron-shielding materials are applied in the regions were high strength, temperature, and durability are required. Difficulty in the incorporation of neutron absorbers in metals due to their compact structure is one of the major challenges. Polymer-based neutron-shielding composites have several advantages such as lightweight, ease of manufacturing, better distribution of neutron absorbers, excellent chemical resistance, etc. Portable neutron sources used in advanced technologies are covered with thermoplastic or thermoset composites. At the same time, elastomer and flexible resin-based composites are used for shielding curved and irregular surfaces.

References

[1] A.V. Mozhayev, R.K. Piper, B.A. Rathbone, J.C. McDonald, Moderator design studies for a new neutron reference source based on the D-T fusion reaction, Radiat. Phys. Chem. 123 (2016) 87–96, https://doi.org/10.1016/j.radphyschem.2016.02.004.

[2] S. Chandra, T. Ahmad, R.F. Barth, G.W. Kabalka, Quantitative evaluation of boron neutron capture therapy (BNCT) drugs for boron delivery and retention at subcellular-scale resolution in human glioblastoma cells with imaging secondary ion mass spectrometry (SIMS), J. Microsc. 254 (3) (2014) 146–156.

[3] S.J. Zinkle, G.S. Was, Materials challenges in nuclear energy, Acta Mater. 61 (3) (2013) 735–758.

[4] S.J. Zinkle, J.T. Busby, Structural materials for fission & fusion energy, Mater. Today 12 (11) (2009) 12–19, https://doi.org/10.1016/S1369-7021(09)70294-9.

[5] A.M. Sukegawa, Y. Anayama, S. Ohnishi, S. Sakurai, A. Kaminaga, K. Okuno, Development of flexible neutron-shielding resin as an additional shielding material, J. Nucl. Sci. Technol. 48 (March 2014) (2011) 585–590.

[6] L. Walsh, Neutron relative biological effectiveness for solid cancer incidence in the Japanese A-bomb survivors: an analysis considering the degree of independent effects from γ-ray and neutron absorbed doses with hierarchical partitioning, Radiat. Environ. Biophys. 52 (1) (2013) 29–36.

[7] A. Konefał, A. Orlef, M. Bieniasiewicz, Measurements of neutron radiation and induced radioactivity for the new medical linear accelerator, the Varian TrueBeam, Radiat. Meas. 86 (2016) 8–15.

[8] W.S. Liu, S.P. Changlai, L.K. Pan, H.C. Tseng, C.Y. Chen, Thermal neutron fluence in a treatment room with a Varian linear accelerator at a medical university hospital, Radiat. Phys. Chem. 80 (9) (2011) 917–922, https://doi.org/10.1016/j.radphyschem.2011.03.022.

[9] L. Deng, N. Zhou, Y.S. Chen, Y. Tu, Photoneutron radiation field of ducts in barrier of 15 MV medical electron accelerators, Radiat. Phys. Chem. 140 (199) (2017) 340–344.

[10] C. Harrison, E. Burgett, N. Hertel, E. Gmlke, Polyethylene/Boron Composites for Radiation Shielding Applications, AIP Conf. Proc. (2008) 484–492.

[11] C. Harrison, S. Weaver, C. Bertelsen, E. Burgett, N. Hertel, E. Grulke, Polyethylene/boron nitride composites for space radiation shielding, J. Appl. Polym. Sci. 109 (4) (2008) 2529–2538. Available from: http://doi.wiley.com/10.1002/app.27949.

[12] S. Nambiar, J.T.W. Yeow, Polymer-composite materials for radiation protection, ACS Appl. Mater. Interfaces 4 (11) (2012) 5717–5726.

[13] T. Minniti, W. Kockelmann, G. Burca, J.F. Kelleher, S. Kabra, S.Y. Zhang, et al., Materials analysis opportunities on the new neutron imaging facility IMAT@ISIS, J. Instrum. 11 (3) (2016).

[14] A. Ittipongse, Fungklin R, Neutron activation for analyzing elements in material. 675–676 (i) (2016) 700–703.

[15] M.H. Choopan Dastjerdi, H. Khalafi, Y. Kasesaz, S.M. Mirvakili, J. Emami, H. Ghods, et al., Design, construction and characterization of a new neutron beam for neutron radiography at the Tehran Research Reactor, Nucl. Instrum. Methods Phys. Res. Sect. A Accel. Spectrom. Detect. Assoc. Equip. 818 (2016) 1–8, https://doi.org/10.1016/j.nima.2016.02.040.

[16] L. Yongsheng, J. Wenbao, H. Daqian, S. Qing, C. Can, Z. Haojia, et al., A new Am-Be PGNAA setup for element determination in aqueous solution, Appl. Radiat. Isot. 95 (2015) 233–238, https://doi.org/10.1016/j.apradiso.2014.11.005.

[17] Z.D. Whetstone, K.J. Kearfott, A review of conventional explosives detection using active neutron interrogation, J. Radioanal. Nucl. Chem. 301 (3) (2014) 629–639.

[18] A.M. Sukegawa, Y. Anayama, S. Ohnishi, A. Kaminaga, K. Okuno, Development of flexible neutron-shielding resin as an additional shielding material, J. Nucl. Sci. Technol. 3131 (May) (2017).

[19] Wei-Hung C, Huang S-J. (19) United States (12). 2008;1(19).

[20] R. Madan, R. Benson, D.N. Sharma, P.K. Julka, G.K. Rath, Radiation induced heart disease: pathogenesis, management and review literature, J. Egypt Natl. Cancer Inst. 27 (4) (2015) 187–193, https://doi.org/10.1016/j.jnci.2015.07.005.

[21] H. Chai, X. Tang, M. Ni, F. Chen, Y. Zhang, D. Chen, et al., Preparation and properties of flexible flame-retardant neutron shielding material based on methyl vinyl silicone rubber, J. Nucl. Mater. 464 (2015) 210–215, https://doi.org/10.1016/j.jnucmat.2015.04.048.

[22] H.-B. Chen, Y.-Y. Ao, D. Liu, H.-T. Song, P. Shen, Novel neutron shielding alginate based aerogel with extremely low flammability, Ind. Eng. Chem. Res. 56 (30) (2017) 8563–8567. Available from: http://pubs.acs.org/doi/abs/10.1021/acs.iecr.7b01999.

[23] T.J. McGiff, R.A. Danforth, E.E. Herschaft, Maintaining radiation exposures as low as reasonably achievable (ALARA) for dental personnel operating portable hand-held X-ray equipment, Health Phys. 103 (2 Suppl. 2) (2012).

[24] S. Orak, D.Y. Baysoy, Neutron shielding properties of concrete with boron and boron containing mineral, Acad. Platf. J. Eng. Sci. 1 (1) (2013) 15–19.

[25] T. Tanimoto, N. Uchida, Y. Kodama, T. Teshima, S. Taniguchi, Safety of workers at the Fukushima Daiichi nuclear power plant, Lancet 377 (9776) (2011) 1489–1490, https://doi.org/10.1016/S0140-6736(11)60519-9.

[26] R.G. Jaeger, E.P. Blizard, A.B. Chilton, M. Grotenhuis, A. Honig, T.A. Jaegar, H. H. Eisenlohr, Engineering Compendium on Radiation Shielding. Vol. 21. Nuclear Engineering and Design, 1–531 pp. Available from: http://linkinghub.elsevier.com/retrieve/pii/0029549372900969%5Cnhttp://link.springer.com/10.1007/978-3-662-25858-3, 1968.

[27] Kim J, Uhm YR, Lee BC, Jung J, Rhee CK, Lee HM-K, et al. Magn. US 2010/0102279 A1, 2010.

[28] R.E. Hayner, Techniques and Compositions for Shielding Radioactive Energy, Vol. 2, (2008).

[29] J.J. Park, S.M. Hong, M.K. Lee, C.K. Rhee, W.H. Rhee, Enhancement in the microstructure and neutron shielding efficiency of sandwich type of 6061Al-B 4 C composite material via hot isostatic pressing, Nucl. Eng. Des. 282 (2015) 1–7, https://doi.org/10.1016/j.nucengdes.2014.10.020.

[30] H.S. Chen, W.X. Wang, Y.L. Li, J. Zhou, H.H. Nie, Q.C. Wu, The design, microstructure and mechanical properties of B4C/6061Al neutron absorber composites fabricated by SPS, Mater. Des. 94 (2016) 360–367.

[31] M. Celli, F. Grazzi, M. Zoppi, A new ceramic material for shielding pulsed neutron scattering instruments, Nucl. Instrum. Methods Phys. Res. Sect. A Accel. Spectrom. Detect. Assoc. Equip. 565 (2) (2006) 861–863.

[32] I. Tadadjeu Sokeng, B.D. Ngom, M. Msimanga, Z.Y. Nuru, L. Kotsedi, M. Maaza, et al., Coatings synthesised by the pulsed laser ablation of a B4C/W2B5 ceramic composite, Thin Solid Films 593 (2015) 5–9, https://doi.org/10.1016/j.tsf.2015.09.030.

[33] Y. Sakurai, A. Sasaki, T. Kobayashi, Development of neutron shielding material using metathesis-polymer matrix, Nucl. Instrum. Methods Phys. Res. Sect. A Accel. Spectrom. Detect. Assoc. Equip. 522 (3) (2004) 455–461.

[34] G. Eid, M.M. El-Toony, A.I. Kany, I.I. Bashter, S.A. Eman, F.A. Gaber, Neutron shielding using lithium tetraborate/epoxy composite, Researchers 3 (12) (2011).

[35] K.J. Singh, N. Singh, R.S. Kaundal, K. Singh, Gamma-ray shielding and structural properties of PbO-SiO_2 glasses, Nucl. Instrum. Methods Phys. Res. Sect. B Beam Interact. Mater. Atoms. 266 (6) (2008) 944–948.

[36] U. Ursu, Physics and technology of nuclear materials, [cited 2019 Aug 27]. Available from: https://inis.iaea.org/search/search.aspx?orig_q=RN:20075276, 1988.

[37] I. Akkurt, C. Basyigit, S. Kilincarslan, B. Mavi, The shielding of γ-rays by concretes produced with barite, Prog. Nucl. Energy 46 (1) (2005) 1–11.

[38] M.H. Kharita, S. Yousef, M. AlNassar, The effect of carbon powder addition on the properties of hematite radiation shielding concrete, Prog. Nucl. Energy 51 (2) (2009) 388–392, https://doi.org/10.1016/j.pnucene.2008.10.002.

[39] E. Yılmaz, H. Baltas, E. Kırıs, İ. Ustabas, U. Cevik, A.M. El-Khayatt, Gamma ray and neutron shielding properties of some concrete materials, Ann. Nucl. Energy 38 (10) (2011 Oct) 2204–2212. Available from: https://linkinghub.elsevier.com/retrieve/pii/S0306454911002222.

[40] O. Gencel, A. Bozkurt, E. Kam, T. Korkut, Determination and calculation of gamma and neutron shielding characteristics of concretes containing different hematite proportions, Ann. Nucl. Energy 38 (12) (2011) 2719–2723, https://doi.org/10.1016/j.anucene.2011.08.010.

[41] T. Piotrowski, M. Mazgaj, A. Zak, J. Skubalski, Importance of atomic composition and moisture content of cement based composites in neutron radiation shielding, Procedia Eng. 108 (2015) 616–623.

[42] M.F. Kaplan, Concrete radiation shielding : nuclear physics, concrete properties, design and construction, Longman Sci. Tech. (1989). [cited 2019 Aug 26], 457 p. Available from: https://inis.iaea.org/search/search.aspx?orig_q=RN:22004467.

[43] M.H. Kharita, S. Yousef, M. Alnassar, Review on the addition of boron compounds to radiation shielding concrete, Prog. Nucl. Energy 53 (2) (2011) 207–211, https://doi.org/10.1016/j.pnucene.2010.09.012.

[44] D. Sarıyer, R. Küçer, N. Küçer, Neutron shielding properties of concretes containing boron carbide and ferro-boron, Procedia Soc. Behav. Sci. 195 (2) (2015) 1752–1756. Available from: http://linkinghub.elsevier.com/retrieve/pii/S1877042815037994.

[45] I.I. Bashter, Calculation of radiation attenuation coefficients for shielding concretes, Ann. Nucl. Energy 24 (17) (1997) 1389–1401.

[46] A.A. El-Sayed, Calculation of the cross-sections for fast neutrons and gamma-rays in concrete shields, Ann. Nucl. Energy 29 (16) (2002) 1977–1988.

[47] T. Korkut, A. Ün, F. Demir, A. Karabulut, G. Budak, R. Şahin, et al., Neutron dose transmission measurements for several new concrete samples including colemanite, Ann. Nucl. Energy 37 (7) (2010) 996–998.

[48] T. Korkut, A. Karabulut, G. Budak, B. Aygün, O. Gencel, A. Hançerlioĝullari, Investigation of neutron shielding properties depending on number of boron atoms for colemanite, ulexite and tincal ores by experiments and FLUKA Monte Carlo simulations, Appl. Radiat. Isot. 70 (1) (2012) 341–345.

[49] M.A. Glinicki, A. Antolik, M. Gawlicki, Evaluation of compatibility of neutron-shielding boron aggregates with Portland cement in mortar, Constr. Build. Mater. 164 (2018) 731–738, https://doi.org/10.1016/j.conbuildmat.2017.12.228.

[50] A. Yadollahi, E. Nazemi, A. Zolfaghari, A.M. Ajorloo, Optimization of thermal neutron shield concrete mixture using artificial neural network, Nucl. Eng. Des. 305 (2016) 146–155, https://doi.org/10.1016/j.nucengdes.2016.05.012.

[51] D.D. DiJulio, C.P. Cooper-Jensen, H. Perrey, K. Fissum, E. Rofors, J. Scherzinger, et al., A polyethylene-B4C based concrete for enhanced neutron shielding at neutron research facilities, Nucl. Instrum. Methods Phys. Res. Sect. A Accel. Spectrom. Detect. Assoc. Equip. 859 (February) (2017) 41–46, https://doi.org/10.1016/j.nima.2017.03.064.

[52] D.E. Barabash, A.D. Barabash, Y.B. Potapov, D.V. Panfilov, O.E. Perekalskiy, Radiation-resistant composite for biological shield of personnel, IOP Conf. Ser. Earth Environ. Sci. 90 (1) (2017).

[53] C. Thomas, J. Rico, P. Tamayo, J. Setién, F. Ballester, J.A. Polanco, Neutron shielding concrete incorporating B4C and PVA fibers exposed to high temperatures, J. Build. Eng. 26 (June) (2019) 100859, https://doi.org/10.1016/j.jobe.2019.100859.

[54] B.K. Jang, J.C. Lee, J.H. Kim, C.W. Chung, Enhancement of thermal neutron shielding of cement mortar by using borosilicate glass powder, Appl. Radiat. Isot. 123 (February) (2017) 1–5, https://doi.org/10.1016/j.apradiso.2017.01.047.

[55] E. Zorla, C. Ipbüker, A. Biland, M. Kiisk, S. Kovaljov, A.H. Tkaczyk, et al., Radiation shielding properties of high performance concrete reinforced with basalt fibers infused with natural and enriched boron, Nucl. Eng. Des. 313 (2017) 306–318.

[56] A. Mesbahi, H. Ghiasi, Shielding properties of the ordinary concrete loaded with micro- and nano-particles against neutron and gamma radiations, Appl. Radiat. Isot. 136 (February) (2018) 27–31, https://doi.org/10.1016/j.apradiso.2018.02.004.

[57] J. Park, H. Suh, S.M. Woo, K. Jeong, S. Seok, S. Bae, Assessment of neutron shielding performance of nano-TiO_2-incorporated cement paste by Monte Carlo simulation, Prog. Nucl. Energy 117 (April) (2019) 103043, https://doi.org/10.1016/j.pnucene.2019.103043.

[58] C. Beidler, W. Hauth, A. Goel, Development of a B4C/Al cermet for use as an improved structural neutron absorber. Wolfenden A, editor, J. Test. Eval. 20 (1) (1992) 67–70. Available from: https://www.astm.org/DIGITAL_LIBRARY/JOURNALS/TESTEVAL/PAGES/JTE11899J.htm.

[59] H.S. Chen, W.X. Wang, Y.L. Li, J. Zhou, H.H. Nie, Q.C. Wu, The design, microstructure and mechanical properties of B4C/6061Al neutron absorber composites fabricated by SPS, Mater. Des. 94 (2016) 360–367.

[60] B.R. Evans, J. Lian, W. Ji, Evaluation of shielding performance for newly developed composite materials, Ann. Nucl. Energy 116 (2018) 1–9, https://doi.org/10.1016/j.anucene.2018.01.022.

[61] Y. Wu, Q.P. Zhang, D. Zhou, Y.L. Zhou, J. Zheng, Controlled synthesis of anisotropic lead borate crystals and its co-shielding of neutron and gamma radiations, J. Alloys Compd. 727 (2017) 1027–1035, https://doi.org/10.1016/j.jallcom. 2017.08.219.

[62] Y. Li, W. Wang, J. Zhou, H. Chen, P. Zhang, 10B areal density: a novel approach for design and fabrication of B4C/6061Al neutron absorbing materials, J. Nucl. Mater. 487 (2017) 238–246, https://doi.org/10.1016/j.jnucmat.2017.02.020.

[63] L.T. Jiang, Z.G. Xu, Y.K. Fei, Q. Zhang, J. Qiao, G.H. Wu, The design of novel neutron shielding (Gd+B4C)/6061Al composites and its properties after hot rolling, Compos. Part B Eng. 168 (March 2018) (2019) 183–194.

[64] N.H. Tariq, L. Gyansah, J.Q. Wang, X. Qiu, B. Feng, M.T. Siddique, et al., Cold spray additive manufacturing: a viable strategy to fabricate thick B 4 C/Al composite coatings for neutron shielding applications, Surf. Coat. Technol. 339 (February) (2018) 224–236, https://doi.org/10.1016/j.surfcoat.2018.02.007.

[65] X. Fu, X. Tang, Y. Hu, H. Li, J. Tao, Effect of different lay-ups on the microstructure, mechanical properties and neutron transmission of neutron shielding fibre metal laminates, J. Nucl. Mater. 475 (2016) 227–236, https://doi.org/10.1016/j.jnucmat.2016.04.021.

[66] X.L. Fu, Y.B. Hu, H.G. Li, J. Tao, Study on the thermal and mechanical properties of novel neutron shielding composite laminates at elevated temperature, Mater. Sci. Eng. A 697 (November 2016) (2017) 101–110, https://doi.org/10.1016/j.msea.2017.04.100.

[67] J.S. Park, J. Kim, S.H. Yi, Effects of Gadolinium in Fe based amorphous ribbons with high boron contents on the neutron shielding efficiency, Ann. Nucl. Energy 109 (2017) 365–369, https://doi.org/10.1016/j.anucene.2017.05.046.

[68] A.M. Reda, H. Halfa, Evaluation of neutron shielding properties of steel slag waste, J. Environ. Chem. Eng. 6 (4) (2018) 5544–5551, https://doi.org/10.1016/j.jece.2018.08.043.

[69] D. Lv, J. Lu, G. Ran, W. Zhou, M. Wang, Q. Feng, et al., Ball milling and sintering of neutron absorber Mo-based Tb_2O_3-Dy_2O_3 composite and its characterization, Powder Technol. 331 (2018) 226–235, https://doi.org/10.1016/j.powtec.2018.03.004.

[70] X. Cao, X. Xue, T. Jiang, Z. Li, Y. Ding, Y. Li, et al., Mechanical properties of UHMWPE/Sm_2O_3 composite shielding material, J. Rare Earths 28 (SUPPL. 1) (2010) 482–484, https://doi.org/10.1016/S1002-0721(10)60269-4.

[71] J.W. Shin, J.W. Lee, S. Yu, B.K. Baek, J.P. Hong, Y. Seo, et al., Polyethylene/boron-containing composites for radiation shielding, Thermochim. Acta 585 (2014) 5–9, https://doi.org/10.1016/j.tca.2014.03.039.

[72] J. Kim, B.C. Lee, Y.R. Uhm, W.H. Miller, Enhancement of thermal neutron attenuation of nano-B4C, -BN dispersed neutron shielding polymer nanocomposites, J. Nucl. Mater. 453 (1–3) (2014) 48–53, https://doi.org/10.1016/j.jnucmat.2014.06.026.

[73] E.I. Khalil, H.A. Elez, D. Anwar, Modern trends in epoxy based materials used for shielding Am-Be neutron source, Int. J. Sci. Eng. Res. 4 (11) (2016) 94–98.

[74] R. Adeli, S.P. Shirmardi, S.J. Ahmadi, Neutron irradiation tests on B4C/epoxy composite for neutron shielding application and the parameters assay, Radiat. Phys. Chem. 127 (2016) 140–146, https://doi.org/10.1016/j.radphyschem.2016.06.026.

[75] S. Gwaily, H. Hassan, M. Badawy, M. Madani, Natural rubber composites as thermal neutron radiation shields-II—H3BO3/NR composites, Polym. Test. 21 (5) (2002) 513–517. Available from: http://www.sciencedirect.com/science/article/pii/S014294 1801001179.

[76] K. Ninyong, E. Wimolmala, N. Sombatsompop, K. Saenboonruang, Potential use of NR and wood/NR composites as thermal neutron shielding materials, Polym. Test. 59 (2017) 336–343, https://doi.org/10.1016/j.polymertesting.2017.02.020.

[77] O. Onjun, N. Laothong, R. Picha, W. Ratanathongchai, T. Onjun, Natural rubber blocks as thermal neutron shields, Prog. Nucl. Sci. Technol. 4 (2014) 631–634. Available from: http://www.aesj.or.jp/publication/pnst004/data/631_634.pdf.

[78] S.E. Gwaily, M.M. Badawy, H.H. Hassan, M. Madani, Influence of thermal aging on crosslinking density of boron carbide/natural rubber composites, Polym. Test. 22 (1) (2003) 3–7.

[79] Y.C. Liao, D.G. Xu, P.C. Zhang, B4C/NRL flexible films for thermal neutron shielding, Nucl. Sci. Tech. 29 (2) (2018) 1–9, https://doi.org/10.1007/s41365-018-0358-4.

[80] P. Gong, M. Ni, H. Chai, F. Chen, X. Tang, Preparation and characteristics of a flexible neutron and γ-ray shielding and radiation-resistant material reinforced by benzophenone, Nucl. Eng. Technol. 50 (3) (2018) 470–477, https://doi.org/10.1016/j.net.2018.01.005.

[81] S.U. El-Kameesy, W.A. Kansouh, E. Salama, M.K. El-Mansy, S.A. El-Khateeb, R.M. Megahid, A developed material as a nuclear radiation shield for personal wearing, J. Appl. Math. Phys. 05 (03) (2017) 596–605. Available from: http://www.scirp.org/journal/doi.aspx?DOI=10.4236/jamp.2017.53051.

[82] T. Özdemir, I.K. Akbay, H. Uzun, I.A. Reyhancan, Neutron shielding of EPDM rubber with boric acid: mechanical, thermal properties and neutron absorption tests, Prog. Nucl. Energy 89 (May) (2016) 102–109.

[83] T. Ozdemir, A. Gungor, A. Reyhancan, Flexible neutron shielding composite material of EPDM rubber with boron trioxide: mechanical, thermal investigations and neutron shielding tests, Radiat. Phys. Chem. 131 (2017) 7–12, https://doi.org/10.1016/j.radphyschem.2016.10.012.

[84] M.M. Abdel-Aziz, S.E. Gwaily, A.S. Makarious, A.A. El-Sayed, Ethylene-propylene diene rubber/low density polyethylene/boron carbide composites as neutron shields, Polym. Degrad. Stab. 50 (2) (1995) 235–240.

[85] A. Mohamed, H. Yazid, S. Ahmad, Experimental optimization in polymer BLEND composite preparation based on mix level of taguchi robust design, J. Nucl. Relat. Technol. 9 (1) (2012) 23–32. Available from: http://www.nuklearmalaysia.org/nuklearmalaysia_org/media/JNRT2012-9-1-04.pdf.

[86] C. Jumpee, D. Wongsawaeng, Innovative neutron shielding materials composed of natural rubber-styrene butadiene rubber blends, boron oxide and iron(III) oxide, J. Phys. Conf. Ser. 611 (1) (2015) 012019. Available from: http://iopscience.iop.org/1742-6596/611/1/012019.

[87] N.M. Zali, H. Yazid, M.H.A.R. Megat Ahmad, Neutron shielding behavior of thermoplastic natural rubber/boron carbide composites, IOP Conf. Ser. Mater. Sci. Eng. (2018).

CHAPTER 2

Review on neutron-absorbing fillers

P. Tamayo[a], **C. Thomas**[a], **J. Rico**[b], **A. Cimentada**[a], **J. Setién**[a], **J.A. Polanco**[a]
[a]LADICIM (Laboratory of Materials Science and Engineering), University of Cantabria. E.T.S. de Ingenieros de Caminos, Canales y Puertos, Santander, Spain
[b]Construction Engineering, Research and Project Development (INGECID S.L.), University of Cantabria. E.T.S. de Ingenieros de Caminos, Canales y Puertos, Santander, Spain

2.1 Introduction

The term filler is used in many fields to refer to a material (usually particles) that improves some of the properties of another material that acts as a matrix. These properties can be of any type—physical, chemical, or mechanical but generally improving some properties entails the worsening of others. The size of these particles can range from nanometer (nanofillers) to micrometer orders (microfillers), the size along with filler quantity being the factors that most influence their effectiveness. Fillers for neutron shielding are based on the use of compounds that incorporate elements with a high thermal neutron capture cross section, which are typically added to polymeric, metal, alloy or concrete matrices, in order to obtain more effective shielding.

There are three modes of interaction between the atomic nuclei of the fillers and the incident neutrons: elastic scattering, inelastic scattering, and radiative capture (Fig. 2.1). In the first case, the total kinetic energy before and after the collision between a neutron (red) and a nucleus (blue) remains the same. In the second, the total kinetic energy after the collision is less than that before the collision and hence, the nucleus is in an excited state. In the third, the nucleus absorbs the incident neutron, being excited and generally emitting γ-radiation, neutron-absorbing fillers must include nuclei that favor this type of interaction.

When lightweight polymer filler compounds are required (e.g., in the aerospace industry), the level of incorporation is an important issue, because fillers increase the density of the compound, also negatively affect its processability [1]. In concretes, the incorporation of fillers generally involves the substitution of cement, negatively affecting the mechanical properties. In metals or alloys, it is common to find bonding defects

https://doi.org/10.1016/B978-0-12-819459-1.00002-7
© 2020 Elsevier Ltd.
All rights reserved.

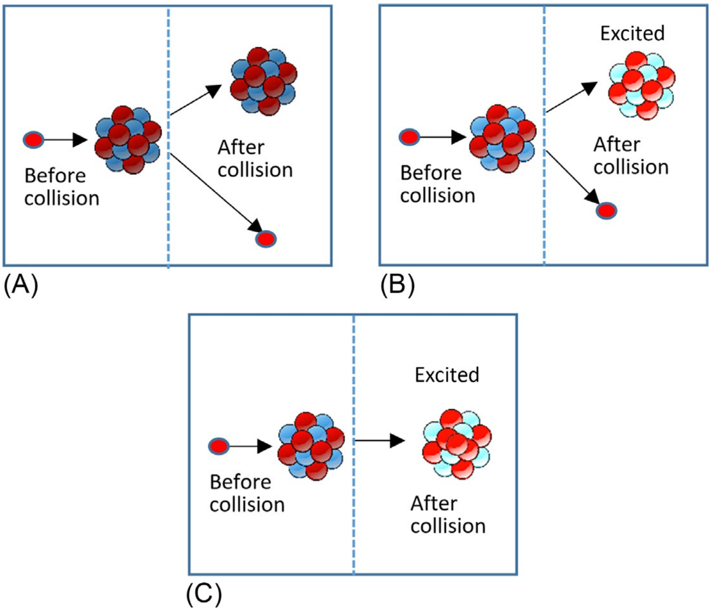

Fig. 2.1 Types of interaction between the nuclei of the filler's atoms and the incident neutrons: (A) elastic scattering, (B) inelastic scattering, and (C) radiative capture.

between matrix and fillers, and also problems of wettability. However, in many cases, the fillers provide an improvement not only in shielding properties but also in stiffness, toughness, thermal stability, and insulation characteristics, among others.

The size of the filler particles affects the radiation shielding properties of the material. The mean free path that a thermal neutron can penetrate in a material is reduced by incorporating nanofillers instead of microfillers, and by increasing the amount of filler. On the other hand, both physical and chemical properties are significantly affected when the characteristic dimension of the filler is modified when it is in the nanometer size [1]. Likewise, a better dispersion or distribution of the particles can be achieved in the shielding material with smaller particle dimensions, which can be more effectively homogenized in the medium. In the aerospace sector, for example, materials should be as light as possible, which can be done by adding small-sized fillers, as less material is required to obtain equally effective shielding. In all fields of the neutron shielding industry, this also leads to a reduction in costs because these fillers are generally more expensive than the material in which they are embedded. For these reasons, the use of fillers in the radiation shielding industry requires the use of more effective compounds, whose optimization and development are constantly evolving and from which significant cost savings are derived.

Currently, there are two families of fillers for neutron shielding applications worldwide: boron-based fillers and rare-earth fillers. This chapter discusses the main characteristics of each of them, as well as the main applications and the advantages or disadvantages of their use for neutron shielding. In addition, the main characteristics of the compounds commonly produced with each of these fillers are presented and the main characteristics of each one are listed in Table 2.1.

Lithium-based compounds (LiF, Li_2CO_3, or LiH) have been excluded from the review for several reasons. The first and main one is that its use in literature as neutron-absorbing material is very scarce. For neutron shielding, although ^{6}Li has a cross-section absorption of 940 b for thermal neutrons (almost one-third of that of ^{10}B), this element has an abundance of only 7.5% (^{10}B is 20%), so for use it has to be enriched (to ~96%) [2]. The advantage of Li-based compounds is that they do not generate gamma particles, but the much lower thermal neutron absorption, as well as the price make borated compounds much more functional [3]. Secondly, today the main use of LiF lies in the manufacture of neutron detection modules [4] or as a neutron scintillator due to its high refractive index [5]. For this application, LiF has higher thermal neutron detection efficiencies than devices with ^{10}B as converter [6]. Similarly, with LiH, although less used yet, there have been experiences in the past where it was considered a promising material in radiation shielding [7] mainly due to its lightness, but its high cost and the existence of other alternatives have not allowed the progress the last decades. Similarly, cadmium is a good material traditionally used as a neutron thermal absorber, but its use is deprecated. This disuse is derived from the restrictions on the use of cadmium in the European Union after the adoption of the European Union Directive 2002/95/EC (RoHS), which significantly limited the use of this element to combat environmental pollution.

2.2 Boron-based fillers

Boron as filler is par excellence in thermal neutron shielding. The macroscopic absorption cross section of ^{10}B is very high and ^{11}B is very low. The effect of the noncentral part of neutron-target interaction is that the neutron, being captured with given orbital angular momentum, may transfer some additional angular momentum to the target nucleus. This mechanism can explain the angular distribution of the protons and the different macroscopic absorption cross section [8]. In nature, there are two boron isotopes, ^{10}B has a natural abundance of 19.9% and a very high neutron capture cross section for thermal neutrons (0.025 eV) of around 3840 barns (10^{-24} cm^2), while ^{11}B has a natural abundance of 81.1% and a neutron capture cross section of 0.005 barns, so it practically does not capture thermal neutrons [9]. With these proportions, natural boron shows a thermal neutron absorption cross section of around 760 barns, a value between ^{6}Li (940 barns) and ^{235}U (549 barns), which makes it one of the best materials for neutron shielding. The capture reactions generate atoms of He and Li, as shown in the following equations [10]:

$$ {}^{10}_{5}B + {}^{1}_{0}n \rightarrow \left[{}^{11}_{5}B\right] \rightarrow 4{}^{4}_{2}He\,(1.47\,MeV) + 7{}^{7}_{3}Li\,(0.84\,MeV) + \gamma(0.48\,MeV) \tag{2.1} $$

$$ {}^{10}_{5}B + {}^{1}_{0}n \rightarrow 4{}^{4}_{2}He\,(1.79) + {}^{7}_{3}Li\,(1.01\,MeV) \tag{2.2} $$

Corresponding to Eq. (2.1) with 93.7% of reactions and Eq. (2.2) with 6.3% of reactions. Boron-based fillers provide thermal and mechanical stability to the matrix, and some of them are cheap compared to other neutron-absorbing materials such as Gd, Cd, Sm, and Li [4]. Boron-based materials are used as neutron absorbers because they are the safest and easiest materials for making fillers, in addition do not suffer a cut off in the absorption cross section at higher energies, as for example, Gd or Cd [11]. At higher energies, ^{10}B absorption cross section is reduced monotonically with increasing neutron energy and without resonance [12]. The main materials based on boron for neutron-absorbing applications are boron carbide (B_4C), boron nitride (BN), boron trioxide (B_2O_3), boric acid (H_3BO_3), and colemanite ($Ca_2B_6O_{11}$)·$5H_2O$. Theoretically, B_4C has the highest absorption cross section for both thermal and epithermal neutrons, boric acid and colemanite the lowest, while H_3BO_3 and B_2O_3 create the most secondary gamma rays, and additional dose radiation. On the other hand, both BN and B_4C (especially the latter) produce secondary photons with low energy [12]. An exhaustive analysis of each of them is provided next.

2.2.1 Boron carbide

Boron carbide is a ceramic material that has a rhombohedral structure and is composed of 12-atom icosahedral clusters joined by covalent bonds, through 3-atom intericosahedral chains [13]. Industrial preparation methods of B_4C include the direct combination of C and B and carbothermal routes, which are based on the reduction of compounds such as boric acid, boric oxide, or borax with carbon or magnesium in the presence of carbon in an electric furnace at temperatures close to the melting point [14]. An important process for the manufacture of components with B_4C is sintering, a process that seeks to improve the mechanical properties of the product as well as its densification. In the case of B_4C, due to the strong union of the covalent bonds of C and B (low self-diffusion coefficient), the high resistance to grain boundary sliding and absence of plasticity, stoichiometric boron carbide densification is not possible without the use of additives or the use of great pressures [15, 16]. Pressureless sintering is based on the use of inorganic additives such as C, TiB_2, or TiC or without additives, at very high temperatures close to the melting point. Hot pressing sintering uses fine pure powders, high temperatures, and high pressures, but is limited to simple shapes and requires diamond machining [13].

Chemically, B_4C is one of the most stable compounds. Its oxidation in oxygen and chlorine attack begins above 600°C; it is resistant to cold chemical reagents; it is oxidized by hot oxidizing acids such as HNO_3 or H_2SO_4 and reacts with many metals that form borides or carbides at 1000°C such as iron, titanium, or nickel [17]. Boron carbide is a lightweight material, with a bulk density of 2.52 g/cm^3 and a thermal expansion coefficient of $4–8 \times 10^{-6}\ K^{-1}$ [18], which is used with both the natural isotopic content of ^{10}B (19.9%) and enriched up to 90% of ^{10}B [13]. A high melting point of around 2763°C [19] gives thermal stability to compounds, such as polymer-based materials, that deteriorate at lower temperatures. Mechanically, it is a compound with a high elastic modulus, as well as a high wear resistance and hardness, being the third hardest material known after diamond and hexagonal boron carbide. Compared to other current alternatives such as Sm_2O_3 and Gd_2O_3, B_4C is more readily available and releases low-energy secondary gamma photons [19]. B_4C has also been included as a potential candidate for use in fusion reactors due to the low atomic number of C and B, which leads to low X-ray absorption. Moreover, neutron radiation exposure does not cause radioactive decay [20].

Although the use of B_4C filler significantly improves neutron shielding, the drawback of its use is the reduction in the elastic modulus, reduction in tensile strength and break elongation, properties that decrease as the level of incorporation of the filler in the matrix increases (polymeric, metallic, or concrete) [21]. With a large number of benefits, the main problem with B_4C is low fracture toughness (the lowest of all advanced ceramics), strength, and poor sinterability [20]. A low fracture toughness generally means a high fragility (low crack resistance) and this is a problem when working with this material under extreme conditions (e.g., in nuclear engineering). To improve this issue, doping B_4C with the dispersion of various nanopowders is proposed, which leads to the formation of microcracks due to thermal expansion mismatch between dispersed particles and the matrix [22]. Some nanopowders have been successfully developed for this purpose, such as TiB_2 [22] or TiC [23], improving strength and toughness.

This material is commonly used with particle sizes of several μm. Significant differences in shielding performance using various particle sizes have been obtained. Thus, B_4C particle size of 20 μm instead of 150 μm has shown improvements of around 50% [24], achieving better dispersion of the particles in the matrix. The use of B_4C filler with nano-sized particles and the improvement of the homogenization of its distribution in the matrix are two variables that affect the neutron shielding of the material, increasing the probability of collision with thermal neutrons [25], in addition to increasing protection against X-rays and gamma radiation [26]. Currently, there are several techniques to prepare nano-sized B_4C particles, such as chemical vapor condensation (CVC), reactive sputtering, and high-energy milling [27].

Furthermore, its viability in incorporating matrices of different nature has been shown. One of the main uses of B_4C is in B_4C/Al composites, a common material widely used in the nuclear, aerospace, and military weapons industries, mainly due to its lightness, ductility, chemical resistance, and very high hardness [28]. These compounds are manufactured using powder metallurgy (the most commonly used, typically ball-milled pressing, sintering, hot-extrusion, and hot-rolling processes [28]), casting (higher efficiency and less cost than metallurgy [29]), and pressureless infiltration (simple, low cost, high efficiency with high ceramic volume fraction [30]). The benefits offered by this product are similar to those provided by each material separately; good wear resistance, good behavior under high temperatures, high stiffness, and high strength characterize this compound [16]. The bond interfaces between matrix/filler and between layers of these compounds are strong, although the addition of large amounts of B_4C can cause bond defects between particle and matrix or may even affect wettability [31]. The wettability between B_4C and Al is inherently bad [27], so the dispersion of B_4C particles in the liquid phase is carried out at high temperatures (>1100°C) or by using reinforcing particles.

The use of polymers as a matrix in which B_4C particles are dispersed, supposed to be a source of H that acts as a neutron moderator, thermalizing (scattering) the incident fast neutrons and thus favoring the capture of the neutrons thermalized by the boron atoms. A novel compound involves the use of a polyimide matrix, a polymer that provides good thermal stability and oxidation resistance, high resistance to radiation and solvents, and good mechanical properties. On the other hand, these compounds have low solubility and high softening temperatures, which makes their production process difficult and/or expensive [32]. B_4C/polyimide compounds can be manufactured by polymerization in situ and as the content of B_4C is increased, good mechanical properties, enhanced neutron shielding properties, and great thermal stability are obtained [33]. This thermal stability is favored by better dispersion of B_4C particles.

Currently, there are compounds based on PE/B_4C. Polyethylene is used in space radiation shielding composites due, above all, to the advantages offered by its manufacture, in different forms as sheets, extruded or injection-molded profiles of various geometries can be easily manufactured [34]. With the incorporation of B_4C filler, density, crystallinity, stiffness, and thermal stability increase [35] in comparison with the compound without addition. The use of LDPE with embedded B_4C particles is an alternative to obtain a flexible and lightweight material, where a replacement of 1% by weight of B_4C can improve the neutron radiation shielding by almost 40% and can cause an ostensible improvement in tensile strength and impact resistance [36]. The concept of using HDPE as a matrix is basically the same, although obtaining a slightly stronger compound, with greater tensile strength, lower resilience, higher density and having similar economic benefits. Furthermore, the inclusion of B_4C filler in rubbers can form thermally conductive pathways with high thermal conductivity that can help reduce the accumulation of heat generated by cyclic deformation; heat that accelerates fatigue of the rubber and can cause temporary degradation of the material [37]. This also improves the shielding properties of the material. B_4C/epoxy compounds are used for neutron shielding of spent fuel located outside the nuclear reactor, preventing neutrons from escaping [38]. The dispersion of B_4C filler in epoxy resins does not seem to affect its degree of conversion during curing, but it does seem to affect (accelerating or retarding) the kinetic reactions depending on the particle size and the amount of B_4C used, to reduce the glass transition and to increase the abrasive wear of the material [39].

2.2.2 Hexagonal boron nitride

Hexagonal boron nitride (hBN) is a nonoxide ceramic material whose hexagonal structure is analogous to that of graphite, and is formed by strong covalent bonds between nitrogen and boron in each layer, and weak bonds between layers by van der Waals forces [40]. Another way in which boron nitride is found is amorphous (aBN) or cubic (cBN), with a structure analogous to that of diamond although less stable. The most common hBN powder preparation methods include hot pressing methods or via chemical vapor deposition (CVD). The weak links between layers make sintered BN materials susceptible to producing complex shapes using hot-pressing machines. To improve sintering by hot pressing, additives such as mullite [41] are mixed in a ball-milling process and then sintered at temperatures around 1900°C at pressures ranging from 10 to 30 MPa. CVD routes include the use of a precursor such as borazine ($B_3H_6N_3$) or ammonia-borane (H_3BNH_3) [42] in a thermally driven process where the precursor reacts to form a solid coating on the heated substrate.

hBN is a material with extraordinary insulating properties due to the covalent bonding between its layers, which localizes the free electrons [43], in addition to having a low dielectric constant, good optical properties, very high chemical resistance, an equally high corrosion resistance, great thermal stability (up to 2300°C [44]), a high melting point (about 3000°C [45]), and low density (2.34 g/cm^3). Its thermal properties include a high heat conductivity, high electrical resistivity from low to high temperatures, and a low thermal expansion coefficient [46]. In addition, it is not wetted by a lot of metallic and nonmetallic melts and has countless applications such as electrical insulation in high voltage applications, ceramics, high-temperature solid lubricant [47] (due to the sliding between layers), and of course, neutron shielding due to its high relative B content. The ease of its manufacture by hot-pressing methods, low density, thermal properties, and nontoxicity and environmental safety make it an increasingly demanded product. On the other hand, the weak bond between its layers makes it a relatively weak material mechanically and neutron interactions cause the formation of cBN (a material with poorer shielding properties) and a generalized amorphization of its structure [48].

As is known, boron has a high neutron absorption cross section, but ^{14}N has a much smaller cross section of 1.84 barns, about 2000 times lower than that of ^{10}B, and its capture reaction is as follows [44]:

$$^{14}_{7}\mathrm{N} + n \rightarrow {}^{14}_{6}\mathrm{C}\,(40\,\mathrm{keV}) + {}^{1}_{0}\mathrm{H}\,(580\,\mathrm{keV}) \tag{2.3}$$

Although the effective thermal neutron cross section of ^{14}N is about 500 times higher than that of ^{12}C (0.0034 barns), the greater stoichiometric proportion of ^{10}B atoms in B_4C makes it more effective as a neutron-absorbing material than hBN. In comparison with B_4C, hBN has a simpler crystalline structure that makes it a better candidate for manufacturing neutron detectors, because the epilayers possess higher crystalline quality and fewer defect-traps, providing better charge transport properties [49] and hence better intrinsic detection efficiency.

Another potential application of this material lies in the manufacture of hexagonal boron nitride nanotubes (BNNT). BNNTs show a structure similar to carbon nanotubes, with the difference that the former are insulators and more chemically and thermally stable. The use of carbon nanotubes is being developed and has potential applications in polymer composite reinforcement, thermal management packages, and neutron-shielding nanomaterials [50]. BNNT is a promising material in the aerospace industry for use against galactic cosmic radiation and secondary neutrons, due to the inherent high physical-mechanical performance of the material, excellent high-temperature stability, and high neutron absorption cross sections [51]. BNNT can be incorporated into a polymer matrix that thermalizes (attenuates) fast neutrons, with the advantage that these nanotubes have a molecular structure that favors hydrogenation (covalent bond between H and/or B and/or N) and hydrogen storage (large surface areas and high hydrogen binding energy) [52], two methods to introduce H into BNNT. Hydrogenated BNNT is a novel and very effective material both for slowing down the high-energy neutrons and for capturing thermal neutrons, being a perfect nanofiller for neutron-shielding applications. Hydrogenating BNNT entails a number of disadvantages, such as generalized losses of its mechanical properties (reduction in the elastic modulus by 10%) in comparison to nonhydrogenated BNNT, but the creation of covalent bonds between atoms of H and atoms of B and N (with the H attached externally to both, or the H attached externally to B and internally to N [53]) is a possible solution in the search for an optimal material for cosmic radiation shielding applications. There are already compounds that integrate BNNT and epoxy or polyurethane for the production of paper structures (buckypapers), compounds with a high BNNT content produced by resin infiltration, obtaining epoxy compounds with an improved modulus, ultimate tensile strength, and obtaining polyurethane compounds with greater resistance, elastic modulus and strain failure than the compounds that only integrate BNNT buckypapers [54]. Boron nitride microtubes (BNMTs) have also been synthesized, with the advantage of being less expensive to produce and that some properties such as electronic characteristics are independent of the geometry or morphology of the tube [55], although neutron-shielding properties depend largely on the size of the filler [1].

The addition of BN fillers are always of particular interest in polymer matrices (apart from its high H content to improve neutron scattering cross section) such as epoxies or rubbers, in order to reduce their thermal expansion or increase their thermal conductivity, as well as improve insulation properties, especially when it comes to sensitive electronic components [56]. In general, polymer materials are easy to manufacture, lightweight, flexible, inexpensive, and offer homogeneous shielding [57]. The dispersion of fillers in polymer matrices leads to an improvement in mechanical properties, impact strength, and viscosity. Similarly, the correct dispersion of nanomaterials in the polymer matrix is difficult because their high surface energy causes particles to agglomerate, increasing the viscosity of the compound and making it necessary to use coupling agents [58, 59].

There are examples in the production of HDPE/hBN compounds, which show that compounds generally manufactured by conventional methods (e.g., injection molding) exhibited better mechanical properties with respect to the neat polymer [60]. Melt fracture and sharkskin effect in PE can be suppressed by adding low BN contents due to the migration of hBN platelets to the die walls and due to the sorption of polyethylene chains on BN surfaces [34]. On the other hand, PE (and in general, polymers) has a poor adhesion with the inorganic filler due to the hydrophobicity of their surfaces, so polar compounds such as BN may not adhere properly and sometimes cause a worsening of the mechanical properties [34], so surface bonding powders are used to improve the adhesion between filler and polymer. In EPDM rubbers synthesized with hBN, the latter acts as a flame retardant (and even raises the glass transition temperature) [61], also increasing its modulus (lower elongation) and hardness. On the other hand, toughness and tensile strength are reduced, and at microscopic level the volume of voids has been observed to increase with replacement level, indicating a better thermal neutron absorption than with boric acid and boron oxide. hBN has also been added to silicon rubbers to obtain a composite with greater hardness, in which the glass transition temperature is reduced as the content of hBN increases due to the lubrication effect of hBN [62].

A new technique involves the use of 3D printing systems (fused deposition modeling or FDM) to obtain polymeric compounds with hBN, thermoplastic polymers, and additivation, obtained by extrusion and with which materials of very different geometry can be generated [63]. This technique could unseat traditional techniques such as injection molding although; at the moment, it is not so effective [64] (mechanically and thermally), so it still needs improvement. The material produced by this technique is specially aimed at the aerospace components sector, although its potential applications can also be found in radiation shielding.

2.2.3 Other boron compounds

Boric acid [H_3BO_3 or $B(OH)_3$] is a compound that is used in neutron radiation shielding because of its high B and H content. H_3BO_3 is presented as a powder, a weak acid, and with a melting point of 170.9°C, so its use is not prescribed for high doses of neutrons. Its layered intercrystalline structure makes it an excellent material as a solid lubricant and is considered an environmentally safe material. It is also soluble in water and is not toxic [65]. Its main applications are in fertilizers, glass industry, and as a fire retardant, which makes its use attractive in combination with polymers [66] favored by the generation of water and high melting point of B. In the nuclear industry, it is used in an aqueous solution in the emergency core cooling system. One of its main problems is corrosion and this is the main reason why it is not so widely used as other fillers. It can be obtained by the reaction of borax with an acidic mineral, or by hydrolysis. It has a density of 1.44 g/cm^3, limited mechanical properties (which make it unsuitable for structural elements), and high biological resistance.

The acidic nature of H_3BO_3 makes it unsuitable for use with metals or metallic alloys, and its use, although not very widespread, is focused on the production of polymer composites. There are examples of the production of EPDM/H_3BO_3 composites, producing an effective neutron moderating material which, at low temperatures, shows improved behavior due to the enhanced intermolecular bonds between the filler and the EPDM matrix [66]. However, the material degrades quickly at temperatures higher than the glass transition one, worsening the mechanical properties of the composite. Different amounts of H_3BO_3 have been used to make compounds based on natural rubbers, obtaining higher absorption of thermal neutrons for higher H_3BO_3 contents, as occurs analogously with thermal diffusivity [67]. The increase in H_3BO_3 content increases the thermal neutron shielding but reduces tensile strength, obtaining a flexible compound with potential applications in radiation shielding. One of the main uses of H_3BO_3 is in conjunction with borax ($Na_2[B_4O_5(OH)_4]\cdot 8H_2O$) for its flame-retarding properties; while borax tends to reduce flame-spread but can promote smoldering, boric acid suppresses smoldering but has little effect on flame spread [68]. Borax is a natural (mineral) compound rich in boron, which provides better mechanical properties than boric acid and whose use for neutron shielding is currently not widespread, its most common use being for the manufacture of boric acid.

Boric oxide (boron trioxide or B_2O_3) is an unhydrated version of boricacid (anhydrous form), characterized by a white glass-like solid, having a melting point of 450°C, and being a nontoxic environmentally safe material [69]. Due to its molecular structure, it is a good solid lubricant agent, it has a high hardness, good insulation properties, high refractive index, and low heat expansion coefficient [70], which gives it some interesting optical properties that make it ideal for the manufacture of glass systems. In addition to the manufacture of crystals, one of its main uses lies in the preparation of B_4C and in the ceramics industry. Boron oxide is used as a dopant in ceramics to improve conductivity and structural stability, although it has great disadvantages such as high hygroscopicity.

The use of this material in glass systems for radiation-shielding applications is very common, since it allows the passage of light (high visibility through it) at the same time effective in attenuating both gamma and neutron radiation. These glass systems are mostly generated by glass formers such as boron, silicon, and phosphorous oxides (B_2O_3, SiO_2, and P_2O_5, respectively) [71] mainly due to their high transmittance, thermal stability, and ability to form crystal structures. Compounds generated with B_2O_3 are commonly generated by heavy oxides, generally Pb (also Bi since it is also less toxic than Pb), some examples include glass systems formed by $PbO-B_2O_3-P_2O_5$ [72] or $PbO-SiO_2-B_2O_3-Na_2O$ [73] among many others.

There are also (although few) applications in which their incorporation is direct, as a powder, in shielding material compounds. Taking advantage of their relatively high boron content and reduced cost, they have been used for the manufacture of both natural rubbers/B_2O_3 [74] and EDPM/B_2O_3 compounds, where their addition as a filler provides advantages such as improving tensile and tear strength and also disadvantages such as the reduction in the elastic modulus as well as the increase in creep as the boron oxide content increases [69]. Many of the disadvantages that this filler induces are propitiated by its lubricating effect and, although slightly, its incorporation also improves the thermal stability of the compound. There are also examples of the use of B_2O_3 in paraffin composites [75], in which an addition of boron oxide leads to a systematic improvement of the neutron-shielding properties although mechanical properties such as tensile strength are slightly reduced.

Boron oxide is also used in a nonpure way, since many minerals (more than 200) naturally contain B_2O_3. Some of these minerals are inyonite

($CaB_3O_3(OH)_54{\cdot}H_2O$), inderite ($MgB_3O_3(OH)_55{\cdot}H_2O$), borax ($Na_2[B_4O_5(OH)_4]{\cdot}8H_2O$), kurnakivite ($MgB_3O_3(OH)_55{\cdot}H_2O$), ulexite ($NaCaB_5O_9{\cdot}8H_2O$), and colemanite ($Ca_2B_6O_{11}{\cdot}5H_2O$), the latter being the most important and the one with the highest content in B_2O_3 (about 45% [76]). Colemanite is a borated mineral, which has a density of 2.52 g/cm^3 and a monoclinical structure, being one of the cheapest existing borated materials, even more so than borax and boric acid [77], which makes it one of the most advantageous materials for the construction of neutron-shielding structures. In addition to its neutron-capturing properties, as it is a hydrated material, it also has neutron-scattering capabilities. This material can be used as a filler in thermoplastics, improving their strength, thermal stability, and flame retardant capacity [78], also reducing the cost of the polymer and being more eco-friendly than the latter. Polymer composites produced with polypropylene (PP)/colemanite show excellent corrosion resistance and good bonding strength with the polymer matrix, reducing the thermal expansion coefficient but increasing the viscosity of the compound for large replacement proportions, which creates some difficulty in molding the material [78]. When colemanite powder is added to an epoxy matrix, the mechanical properties of the polymer are reduced, as is the heat resistance, negative effects are circumvented using material curing operations [79]. There are positive examples with this compound [80], using colemanite filler, using additivation and sonic procedures to avoid the appearance of bubbles. The appearance of bubbles is more evident with larger particle size of the filler and causes, among others, loss of shielding efficiency, mechanical strength, and adhesion in the material. The addition of B_2O_3 filler in the epoxy compound causes improvements in tensile strength, elastic modulus, and offers good corrosion and cold resistance [80], providing the compound with better thermal properties than ulexite [80]. PMMA/colemanite compounds have been reported in radiation-shielding applications. The compound, prepared by in situ polymerization, is capable of improving the shielding capacity of both gamma photons and neutrons [57] while maintaining the excellent mechanical properties of the polymer compound.

Among all the compounds that can be found using colemanite filler, clearly the field in which its use is most promoted is mortars and concretes, because as it is an aggregate, its use is direct by replacing the traditional one either as an untreated aggregate or vitrified. The analysis of fillers for concrete is reviewed in Chapter 9.

2.3 Rare earths

The use of rare-earth oxides (Gd_2O_3 and Sm_2O_3) is expanding globally and are already playing an important role in glassmaking industries, metallurgy, or as a catalyst [81]. In the radiation-shielding industry, their use begins to extend due, above all, to their superior thermal neutron capture cross sections compared to boron, although their capture reactions are generally accompanied by the emission of very high-energy secondary gamma radiation compared to boron itself. Another thing that characterizes these materials is their high density (about 8 g/cm^3), which allows them to have lower half-value layers than boron, being much more effective attenuating photons. On the other hand, having a high density penalizes their use in the aerospace sector, where effective shielding materials are sought that are also light and resistant. In addition, while boron compounds when interacting with neutrons generate He bubbles that can affect the mechanical properties of the material, rare-earth elements maintain their structure virtually unchanged [82], remaining stable for longer periods of time. Finally, it should be noted that these compounds are often used together with boron compounds, enhancing the shielding properties of neutron shields.

2.3.1 Gadolinium

Gadolinium oxide (Gd_2O_3) is a ceramic compound that has two possible structures, a more stable cubic one, and a monoclinic structure that is achieved when the cubic structure reaches 1200°C. Gadolinium has seven isotopes (five stable and two quasi-stable), of which two, $^{155}_{64}\mathrm{Gd}$ Gd (abundance of 14.8%) and $^{157}_{64}\mathrm{Gd}$ (abundance of 15.65%), are natural isotopes with the largest thermal neutron absorption cross section, 60,900 barns (15 times higher than $^{10}\mathrm{B}$) and 254,000 barns (66 times higher than $^{10}\mathrm{B}$), respectively [83]. The other isotopes have negligible cross sections except in the case of $^{152}_{64}\mathrm{Gd}$, which has a cross section of 735 barns but an atomic fraction close to 0%. The cross section of the natural Gd, considering the atomic fraction of each isotope, is 48,800 barns, 64 times higher than that of the natural B for thermal neutrons. The main capture reactions are as follows [84]:

$$^{155}_{64}\mathrm{Gd} + {}^{1}_{0}n \rightarrow {}^{156}_{64}\mathrm{Gd}^{*} \rightarrow {}^{156}_{64}\mathrm{Gd} + \gamma(8.536\,\mathrm{MeV}) \tag{2.4}$$

$$^{157}_{64}\mathrm{Gd} + {}^{1}_{0}n \rightarrow {}^{158}_{64}\mathrm{Gd}^{*} \rightarrow {}^{158}_{64}\mathrm{Gd} + \gamma(7.937\,\mathrm{MeV}) \tag{2.5}$$

The isotopes $^{158}_{64}\mathrm{Gd}^{*}$ and $^{156}_{64}\mathrm{Gd}^{*}$ are excited nuclei that recover their fundamental energy, generating in both reactions gamma rays of very high

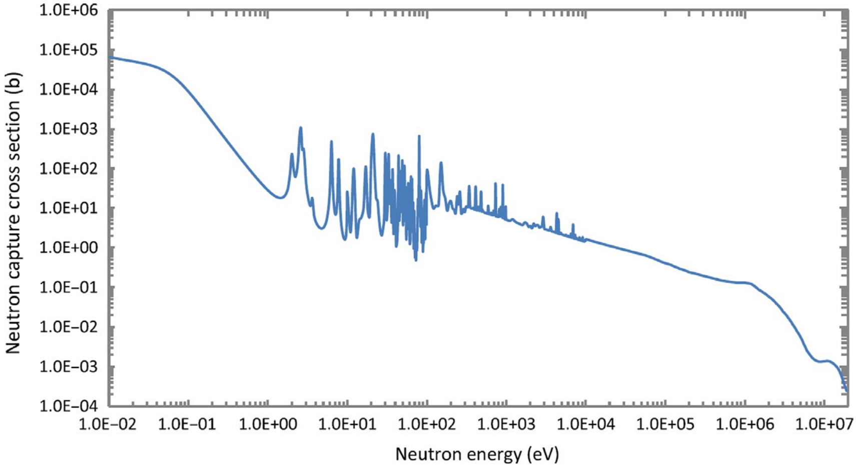

Fig. 2.2 Capture cross sections for natural Gd for different neutron energies. *(Reprinted with permission from J. Dumazert, R. Coulon, Q. Lecomte, G.H.V. Bertrand, M. Hamel, Gadolinium for neutron detection in current nuclear instrumentation research: a review, Nucl. Instruments Methods Phys. Res. Sect. A Accel. Spectrometers, Detect. Assoc. Equip. 882 (2018) 53–68. Copyright 2018 Nuclear Inst. and Methods in Physics Research, A).*

energy (about 8 MeV). This secondary gamma radiation generated in the capture reactions is the main disadvantage of Gd with respect to B, since it is approximately 15 times higher, which may require additional shielding in the radiation-proof component design. Another characteristic of Gd is its peculiar distribution of the neutron cross section for different energy ranges, being very effective in thermal energies, but not very effective in epithermal energies, in addition to having very variable cross sections (resonance) in a wide energy band from 1 to 100 eV approximately (Fig. 2.2).

Gd_2O_3 is produced on the surface of Gd metal by techniques that provoke the thermal decomposition of the hydroxide, carbonate, nitrate, or oxalates. The process of preparing the compound is complicated because Gd is a very reactive, combining easily with oxygen [85]. Nanoparticles of Gd_2O_3 can be obtained from colloidal and combustion methods [86]. Gd_2O_3 is a compound of high density (7.95 g/cm^3 [1]), which, on the one hand, makes it effective in attenuating gamma rays, and on the other hand, undesirable in polymer-based compounds aimed at the aerospace industry. It is an insoluble nanopowder with a melting point of 2420°C, high thermal stability, high mechanical strength due to its ceramic nature, excellent thermal conductivity, and very interesting optical properties such as a high refractive index (>1.9), large band gap (5.4 eV), and low phonon energy (phonon cutoff 600 cm^{-1}) [87].

Gd_2O_3 nanoparticles have potential applications as a nanomaterial in biomedicine, serving as a contrast agent for magnetic resonance imaging (MRI) due to their large magnetic moment [88], although they are components that can be toxic, so they needs to be treated to comply with safety conditions. Another potential application of Gd_2O_3, due to its high cross section, lies in the manufacture of neutron detectors. Due to the escalating cost of He^{-3} (the most widely used material) generated by the growing demand for detectors and the shortage of this material worldwide, Gd_2O_3 has become a potential candidate for this application [89], being cheaper and less critical than He^{-3}. Another application is the use of Gd_2O_3 for the manufacture of fuel pellets. Micro-sized particles of Gd_2O_3 are also incorporated in UO_2 nuclear fuel due to its high thermal neutron cross section, which acts as a burnable poison compensating the excess reactivity of the fuel during its useful life [90]. Likewise, the dispersion of Gd_2O_3 in UO_2 fuels achieves higher thermal conductivity and consequently greater burn-up [91].

In addition to the previous applications, Gd_2O_3 is beginning to have a great presence in neutron-shielding applications. Investigations into HDPE/Gd_2O_3 compounds verify that the lowest neutron transmission ratios correspond to this compound, in comparison with other common compounds such as B_2O_3, Sm_2O_3, or CdO (a toxic compound) when using the same quantity and size of filler [92]. On the contrary, lower neutral attenuation values have been obtained with Gd_2O_3 than with B_4C when an epoxy matrix is used, possibly due to the relatively lower dispersion ability of the former [93]. More advanced neutron shields are obtained by adding Gd_2O_3 to already used and very efficient substances based on the use of polymer/boron compounds. These new compounds are based on the combination of materials seeking synergies and taking advantage of each material in each energy range, obtaining more optimized shielding. Thus, it has been proven that the addition of hybrid nanoparticles (Gd_2O_3 + hBN) enables to obtain lower neutron transmissions than with each nanoparticle separately in a polymer matrix [94] (and of course, lower than the neat matrix) proving the effectiveness of multifunctional shielding and it is to bear in mind that the use of Gd_2O_3 in large quantities is limited due to the high emission of secondary gamma radiation. Even considering this limitation on the Gd_2O_3 content in a compound and considering that the cost of Gd_2O_3 is similar to that of B_4C, Gd_2O_3 has cost advantages [85].

Due to density concerns, the use of Gd_2O_3 is perhaps more widespread in metallic compounds. Compounds based on Gd_2O_3/6061Al have been successfully designed using spark plasma sintering and hot rolling; use of this filler instead of others, such as B_4C, with the aim of reducing the content of ceramic particles of the compound and thus improving its plasticity [85] demonstrate that the use of 10% of Gd_2O_3 is as effective as 30% of B_4C absorbing thermal neutrons (0.2 eV). In addition, the addition of Gd_2O_3 nanoparticles improves the mechanical properties of the metal compound due to the double reinforcement effect from the grain internal enhancement of nanoparticles and the grain boundary enhancement of micrometer particles, boundary enhanced by the formation of $Gd_3Al_5O_{12}$ particles during the preparation of the composite. On the other hand, when Al/Gd alloys are produced, the main problem that arises is the high brittleness of the material, making its use in structural materials difficult [95].

As with polymer compounds, Gd is also incorporated into B_4C/metal compounds with the aim of, once again, improving the plasticity (ductility) of the material while maintaining the shielding properties. B_4C/Al composites containing neat Gd can be prepared by vacuum hot-pressing methods, enabling the use of half the amount of B_4C (from 30% to 15%) by adding only 1% of Gd to obtain similar neutron-shielding properties [96]. In addition, this new compound enables to obtain better elongations by reducing the content of B_4C and reducing the cost of the composite, however, the emission of secondary gamma radiation is increased. On the other hand, the addition of Gd leads to a slight increase in tensile strength due to the enhancement effect produced by the improvement in the bonding interface with the Al matrix produced by hot extrusion [97].

A material with excellent corrosion resistance and good mechanical properties is required for spent fuel storage and transportation. The use of steels for neutron absorption applications offers better mechanical properties, thermal stability, and corrosion resistance than aluminum but has problems of solubility with boron, while Gd offers advantages, such as generation of He during neutron absorption and ease of alloy formation [98]. The addition of submicrometer particles of Gd in duplex stainless steel (via melting-casting hot-rolling) increases the neutron absorption coefficient three times and slightly increases the yield strength mainly due to precipitation hardening mechanisms [98]. Gd has also been added to Fe-based ribbons together with B where, due to the amorphous phase formation within ribbons, large amounts of Gd (around 10%) can be used without altering the mechanical properties or the corrosion resistance of the compound [99].

2.3.2 Samarium

Sm_2O_3 is a ceramic compound with a cubic crystalline structure (similar to that of Gd_2O_3), which has seven isotopes. Three are found in nature, ^{147}Sm (15%), ^{148}Sm (11%), and ^{149}Sm (14%), which have half-lives of several thousand trillion years, making them indistinguishable from stable isotopes [100]. ^{149}Sm is the isotope that has the greatest cross section for thermal neutron capture, with 40,650 barns, a value that when weighted with the natural occurrence of the isotope contributes to 99% of 5620 barns of cross section of the natural Sm [101]. Natural Sm is thus almost seven times more effective in capturing thermal neutrons than B. The capture reaction of the ^{149}Sm isotope is extremely exothermic and happens as shown in the following equation:

$$^{149}_{62}\mathrm{Sm} + ^{1}_{0}n \longrightarrow ^{150}_{62}\mathrm{Sm}^{*} \longrightarrow ^{150}_{62}\mathrm{Sm} + \mathrm{RP}\,(7.89\,\mathrm{MeV}) \tag{2.6}$$

where RP represents the reaction products (photons and electrons). The energy released in the emission of the reaction products is very similar to that released in the capture reaction of ^{157}Gd, however, in the latter case, 99% of the energy released corresponds to the emission of gamma rays, unlike with ^{149}Sm, where gamma emission is much lower. In addition, much of the decay and capture products of ^{149}Sm are other Sm isotopes, also good at absorbing neutrons, so Sm offers greater neutron capture properties than other elements such as B [101].

Sm_2O_3 is mainly produced from the thermal decomposition of samarium hydroxide, carbonate, or nitrate [102] and has a density of 8.35 g/cm^3, which together with its low secondary gamma-ray emission and its high neutron capture cross section make it an ideal candidate for both gamma and neutron shielding. The capture cross sections of Sm for different energies are shown in Fig. 2.3, where better shielding capabilities than B for almost any energy can be observed, although there is a large resonance zone between 1 and 2000 eV.

Sm_2O_3 has a melting point of 2335°C, which gives thermal stability to the composites it forms, especially to polymers [19]. Its use is less common than that of Gd_2O_3 and it is relatively abundant (the 40th most abundant element on earth), stable, and relatively low cost, approximately five times less than that of Gd_2O_3 [103]. In addition to use as shielding material, Sm_2O_3 has applications such as a refractory ceramic, dielectric resonators, resistance-based gas sensors, and capacitors, due to its high permittivity [104] and as optical and infrared absorbing glass to absorb infrared radiation [105].

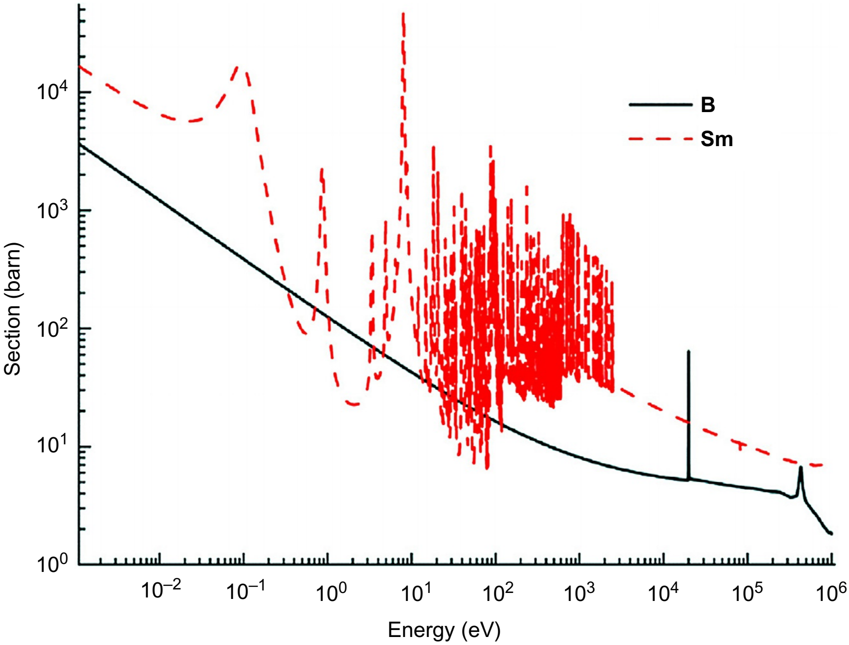

Fig. 2.3 Capture cross sections for natural Sm for different neutron energies. *(Reprinted with permission from P. Wang, X. Tang, H. Chai, D. Chen, Y. Qiu, Design, fabrication, and properties of a continuous carbon-fiber reinforced Sm_2O_3/polyimide gamma ray/neutron shielding material, Fusion Eng. Des. 101 (2015) 218–225. Copyright 2015. Fusion Engineering and Design).*

In its use as a sensor, as it is a material with great specific surface area and uniform nanoporosity (which increases the adsorption of gases), it has proven to be a very effective material in the detection of gases such as CO and CO_2, showing gas sensing properties similar to those of Sm_2O_3 or Nd_2O_3 [106]. The use of glasses containing Sm_2O_3 has interesting applications in nonlinear optical materials, communications by fiber optic, and medical applications, among others; in addition Sm ions are used to dope different glass hosts, facilitating crystallization and improving thermal stability of the glass [107]. As a neutron-shielding material, its use has been more intensively developed in recent years. Another application is its use in nanoparticles to improve the hardness, wear resistance, and corrosion resistance of nickel-based alloy coatings [108].

The use of Sm_2O_3 compounds is an alternative to the use of boron compounds when it is necessary to obtain radiation shielding that is effective against both gamma rays and neutrons. Ceramic materials, such as Sm_2O_3, provide physical cross-linking centers for polymers, reducing the tendency for polymer reorganization [109]. A problem in the use of Sm_2O_3 powders in polymeric materials is the great difference in density, causing the powder to sink when producing the compound and thus preventing homogeneous distribution [110], for which submicron sizes are recommended. Compounds based on polymeric materials are produced with the addition of Sm_2O_3. In the search for a material resistant to high pressures and temperatures and also resistant to corrosion, continuous carbon-fiber-reinforced Sm_2O_3/polyimide composites have been designed by hot-pressing methods [110]. This composite shows a good performance against neutrons and low-energy gamma photon production, showing a tensile strength 10 times higher than other compounds such as PE/Pb/B composites or HDPE-based composites, being able to operate at 300°C, which enables its use under almost any conditions in nuclear-shielding facilities. UHMWPE/Sm_2O_3 composites produced via hot pressing have potential as thermal neutron-shielding materials, composites that acquire greater hardness and tensile modulus; higher content of Sm_2O_3 negatively influences tensile strength as well as dielectric strength, making it necessary to optimize the amount of filler to be used [111]. Sm_2O_3 has also been successfully incorporated into PE oxide/lithium salt matrices, improving the mechanical properties and ion conductivity of the compound, due to the cross-link between the filler and the electrolyte, causing a synergetic effect among the three components [109] (Table 2.1).

2.4 Feature comparison chart

See Table 2.1.

2.5 Conclusions and future trends

The addition of fillers with high thermal neutron capture cross sections causes an improvement in shielding properties of radiation-proof compounds and therefore of their cost. This improvement is greater the smaller the size of the fillers, mainly due to a better dispersion of the particles in the matrix.

The use of fillers can also result in the improvement or loss of the physical-mechanical properties, so it is necessary to reach a compromise in the amounts of these materials added. Currently, two types of filler are commonly used worldwide: boron compounds and rare earths.

Table 2.1 Comparison of some characteristics of the main neutron absorbing fillers.

Compound	Neutron absorption	Behavior under high temperatures	Mechanical strength	Chemical resistance	Disadvantages	Price	Other applications	Observations
B_4C	High	Excellent	Very good	Excellent	Low fracture toughness and poor wettability	Very expensive	Abrasive grit or powder, wear resistance components, lightweight armor plates	The most widely used filler
hBN	Medium-high	Excellent	Good	Excellent	It degrades in c-BN losing neutron shielding	Very expensive	High-voltage applications, lubricant	Promising material in the aerospace industry
B_2O_3	Medium-high	Poor	Medium	Medium	High hygroscopicity	Cheap	Lubricant, insulate, glass	Commonly used to prepare B_4C
H_3BO_3	Medium	Very poor	Poor	Good	Corrosion	Cheap	Flame retardant, fertilizer	High H content, moderating material
$Ca_2B_6O_{11}$	Low	Medium	Medium	Medium	Low boron content	Very cheap	Glass, hi-tech ceramics	The most commonly used boron ore
Gd_2o_3	Very high	Very good	Good	Very good	High emission of secondary gamma radiation	Expensive	Biomedicine, neutron detectors, fuel dopant	Element with the largest cross section
Sm_2o_3	High	Very good	Good	Very good	High density	Medium	Optical, gas detectors, biomedicine	Low secondary gamma-ray emission

On the one hand, the addition of boron compounds, which are traditionally used, involves the use of a safe and easy-to-make material that does not suffer from cut off in the absorption cross section at higher energies. The cross section of these materials reduces monotically with the increase in energy and also does not suffer resonances. Boron compounds are lighter materials, which enables their use in the aerospace industry and also do not produce high-energy secondary photons.

On the other hand, the use of rare earths as fillers implies the use of stable materials with the greatest known thermal neutron capture cross sections (although not epithermal), so better shielding characteristics can be obtained with these compounds. However, the drawbacks are the capture reactions of these elements, which can generate high secondary gamma radiation, and their high density. This high density helps improve the attenuation of photons of the compound, but makes them less suitable for the manufacture of light-shielding materials.

The selection of one compound or another will always depend on the scope of the shielding component. The choice of the best material does not depend solely on its shielding properties. Often the selection criteria are imposed by economic, mechanical, and durability aspects. Nevertheless, other times the choice depends on the industrial experience in its use or by the accessibility of the material. In any case, future trends seem to be aimed at the greater use of rare-earth compounds, and strategies that include the selection of several filler compounds. These strategies are based on optimization processes for the use of specialized materials in each energy range and the cost of production.

References

[1] L. Schrempp-Koops, Size effects on the efficiency of neutron shielding in nanocomposites—a full-range analysis, Int. J. Nanosci. 12 (2013) 1350015.

[2] Y. Sakurai, A. Sasaki, T. Kobayashi, Development of neutron shielding material using metathesis-polymer matrix, Nucl. Instrum. Methods Phys. Res. Sect. A Accel. Spectrom. Detect. Assoc. Equip. 522 (2004) 455–461.

[3] X.P. Hou, S.F. Li, Y. Chen, D. Xu, W. Tang, Preparation of an ultra-thin, highly filled, neutron-shielding material, in: Mater. Sci. Forum, 2015, pp. 616–621.

[4] D.S. McGregor, S.L. Bellinger, D. Bruno, W.L. Dunn, W.J. McNeil, E. Patterson, B.B. Rice, J.K. Shultis, T. Unruh, Perforated diode neutron detector modules fabricated from high-purity silicon, Radiat. Phys. Chem. 78 (2009) 874–881.

[5] J. Jakubek, S. Pospíšil, J. Uher, J. Vacík, D. Vavrík, Properties of the single neutron pixel detector based on the Medipix-1 device, Nucl. Instruments Methods Phys. Res. Sect. A Accel. Spectrometers, Detect. Assoc. Equip. 531 (2004) 276–284.

[6] D.S. McGregor, S. Bellinger, D. Bruno, W.J. McNeil, E. Patterson, B.B. Rice, Perforated semiconductor neutron detector modules, in: Proc. 32nd Annu. GOMACTech Conf, 2007.

[7] F.H. Welch, Lithium hydride: a space age shielding material, Nucl. Eng. Des. 26 (1974) 444–460.

[8] N. Menyhárd, J. Zimányi, On the mechanism of the B10 (d, p) B11 ∗ stripping reaction, Nucl. Phys. 29 (1962) 687–689.

[9] Y.J. Zhang, S.L. Tan, R. Bin Wei, S.H. Ai, H. Bin Sun, Preparation of ^{10}B enriched B_4C Ceramics by Pressureless Sintering, in: Key Eng. Mater., 2014, pp. 540–543.

[10] J.E. Martin, Physics for Radiation Protection: A Handbook, John Wiley & Sons, 2006.

[11] C.L. Cramer, A.M. Elliott, J.O. Kiggans, B. Haberl, D.C. Anderson, Processing of complex-shaped collimators made via binder jet additive manufacturing of B_4C and pressureless melt infiltration of Al, Mater. Des. 107956 (2019).

[12] R. Adeli, S.P. Shirmardi, R. Bagheri, Theory and simulation investigation of low-energy neutron shielding for different boron compounds, J. Test. Eval. 45 (2016) 1570–1576.

[13] F. Thevenot, Boron carbide—a comprehensive review, J. Eur. Ceram. Soc. 6 (1990) 205–225.

[14] A. Sinha, T. Mahata, B.P. Sharma, Carbothermal route for preparation of boron carbide powder from boric acid-citric acid gel precursor, J. Nucl. Mater. 301 (2002) 165–169.

[15] T. Kumazawa, T. Honda, Y. Zhou, H. Miyazaki, H. Hyuga, Y. Yoshizawa, Pressureless sintering of boron carbide ceramics, J. Ceram. Soc. Jpn. 116 (2008) 1319–1321.

[16] R. Bin Wei, Y.J. Zhang, H.Y. Gong, X.J. Liu, Y.Z. Jiang, Y.J. Zhao, Pressureless sintering of B_4C neutron absorbing material with nano-sized rare-earth compounds addition, in: Adv. Mater. Res., 2013, pp. 503–507.

[17] K.A. Schwetz, Boron Carbide, Boron Nitride, and Metal Borides, Ullmann's Encycl. Ind, Chem, 1985.

[18] G.W. Hollenberg, Thermally induced stresses and fractures in boron carbide pellets, Am. Ceram. Soc. Bull. 59 (1980) 538.

[19] D. Castley, C. Goodwin, J. Liu, Computational and experimental comparison of boron carbide, gadolinium oxide, samarium oxide, and graphene platelets as additives for a neutron shield, Radiat. Phys. Chem. 165 (2019) 108435.

[20] M. Rafiei, M. Salehi, M. Shamanian, Formation mechanism of B_4C-TiB_2-TiC ceramic composite produced by mechanical alloying of Ti-B_4C powders, Adv. Powder Technol. 25 (2014) 1754–1760.

[21] T. Yasin, M.N. Khan, High density polyethylene/boron carbide composites for neutron shielding, E-Polymers 8 (2008).

[22] S. Tuffe, J. Dubois, G. Fantozzi, G. Barbier, Densification, microstructure and mechanical properties of TiB_2-B_4C based composites, Int. J. Refract. Met. Hard Mater. 14 (1996) 305–310.

[23] H. Wang, S. Sun, D. Wang, G. Tu, Characterization of the structure of TiB_2/TiC composites prepared via mechanical alloying and subsequent pressureless sintering, Powder Technol. 217 (2012) 340–346.

[24] R. Adeli, S.P. Shirmardi, S.J. Ahmadi, Neutron irradiation tests on B_4C/epoxy composite for neutron shielding application and the parameters assay, Radiat. Phys. Chem. 127 (2016) 140–146.

[25] Z. Soltani, A. Beigzadeh, F. Ziaie, E. Asadi, Effect of particle size and percentages of Boron carbide on the thermal neutron radiation shielding properties of HDPE/B_4C composite: experimental and simulation studies, Radiat. Phys. Chem. 127 (2016) 182–187.

[26] M.I. Alymov, S.I. Averin, S.A. Tikhomirov, V.A. Zelenskii, Effect of the annealing temperature on the minimum size of metallic nanoparticles, Russ. Metall. Met. C/C Izv. Nauk SSSR Met. 5 (2005) 427.
[27] M. Khakbiz, F. Akhlaghi, Synthesis and structural characterization of Al-B_4C nano-composite powders by mechanical alloying, J. Alloys Compd. 479 (2009) 334–341.
[28] L. Zhang, J. Shi, C. Shen, X. Zhou, S. Peng, X. Long, B_4C-Al composites fabricated by the powder metallurgy process, Appl. Sci. 7 (2017), https://doi.org/10.3390/app7101009.
[29] Y. Zhang, Y. Yu, G. Xu, Y. Fu, T. Li, T. Wang, Q. Guo, Microstructure and performance of a three-layered Al/7075-B_4C/Al composite prepared by semi continuous casting and hot rolling, Metals (Basel) 8 (2018) 600.
[30] Y.T. Yao, L.Q. Chen, B_4C/Al composites processed by metal-assisted pressureless infiltration technique and its characterization, Mater. Manuf. Process. 31 (2016) 1286–1291.
[31] H. Chen, H. Nie, W. Wang, J. Zhou, R. Liu, A novel neutron shielding AA6061/B_4C laminar composite fabricated by powder metallurgy: "SPS-HER", J. Alloys Compd. 806 (2019) 1445–1452.
[32] D.-J. Liaw, K.-L. Wang, Y.-C. Huang, K.-R. Lee, J.-Y. Lai, C.-S. Ha, Advanced polyimide materials: syntheses, physical properties and applications, Prog. Polym. Sci. 37 (2012) 907–974.
[33] X. Li, J. Wu, C. Tang, Z. He, P. Yuan, Y. Sun, W. Lau, K. Zhang, J. Mei, Y. Huang, High temperature resistant polyimide/boron carbide composites for neutron radiation shielding, Compos. B Eng. 159 (2019) 355–361.
[34] C. Harrison, S. Weaver, C. Bertelsen, E. Burgett, N. Hertel, E. Grulke, Polyethylene/boron nitride composites for space radiation shielding, J. Appl. Polym. Sci. 109 (2008) 2529–2538.
[35] Z. Uddin, T. Yasin, M. Shafiq, A. Raza, A. Zahur, On the physical, chemical, and neutron shielding properties of polyethylene/boron carbide composites, Radiat. Phys. Chem. 166 (2020) 108450.
[36] S. Avcioglu, M. Buldu, F. Kaya, C.B. Üstündag, E. Kam, Y.Z. Menceloglu, H.Y. Kaptan, C. Kaya, Processing and properties of boron carbide (B_4C) reinforced LDPE composites for radiation shielding, Ceram. Int. (2019).
[37] G. Weng, G. Huang, L. Qu, P. Zhang, Y. Nie, J. Wu, Natural rubber with low heat generation achieved by the inclusion of boron carbide, J. Appl. Polym. Sci. 118 (2010) 2050–2055.
[38] R.E. Sund, R.B. Walton, Gamma rays from short-lived fission-fragment isomers, Phys. Rev. 146 (1966) 824.
[39] J. Abenojar, M.A. Martínez, F. Velasco, V. Pascual-Sánchez, J.M. Martín-Martínez, Effect of boron carbide filler on the curing and mechanical properties of an epoxy resin, J. Adhes. 85 (2009) 216–238.
[40] R.T. Paine, C.K. Narula, Synthetic routes to boron nitride, Chem. Rev. 90 (1990) 73–91.
[41] X. Duan, D. Jia, Z. Wu, Z. Tian, Z. Yang, S. Wang, Y. Zhou, Effect of sintering pressure on the texture of hot-press sintered hexagonal boron nitride composite ceramics, Scr. Mater. 68 (2013) 104–107.
[42] B. Sompalle, J. Borme, F. Cerqueira, T. Sun, R. Campos, P. Alpuim, Chemical vapour deposition of hexagonal boron nitride for two dimensional electronics, U. Porto J. Eng. 3 (2017) 27–34.
[43] J. Eichler, C. Lesniak, Boron nitride (BN) and BN composites for high-temperature applications, J. Eur. Ceram. Soc. 28 (2008) 1105–1109.
[44] F. Cataldo, S. Iglesias-Groth, Neutron damage of hexagonal boron nitride: h-BN, J. Radioanal. Nucl. Chem. 313 (2017) 261–271.

[45] Y. Kubota, K. Watanabe, O. Tsuda, T. Taniguchi, Deep ultraviolet light-emitting hexagonal boron nitride synthesized at atmospheric pressure, Science (80-) 317 (2007) 932–934.

[46] Y. Gong, W. Zhou, Y. Kou, L. Xu, H. Wu, W. Zhao, Heat conductive h-BN/CTPB/epoxy with enhanced dielectric properties for potential high-voltage applications, High Volt. 2 (2017) 172–178.

[47] R. Haubner, M. Wilhelm, R. Weissenbacher, B. Lux, Boron nitrides—properties, synthesis and applications, in: High Perform. Non-Oxide Ceram. II, Springer, 2002, pp. 1–45.

[48] K. Arslan, H.K. Seval, Ö.F. Murathan, K. Soysal, Multiwalled boron nitride microtubes (BNMTs) shielding in thermal neutron absorbing, Radiat. Eff. Defects Solids 173 (2018) 555–566.

[49] A. Maity, S.J. Grenadier, J. Li, J.Y. Lin, H.X. Jiang, High-efficiency and high-sensitivity thermal neutron detectors based on hexagonal BN epilayers, in: Hard X-Ray, Gamma-Ray, Neutron Detect. Phys. XIX, 2017, p. 103920L.

[50] J.H. Kim, T.V. Pham, J.H. Hwang, C.S. Kim, M.J. Kim, Boron nitride nanotubes: synthesis and applications, Nano Converg. 5 (2018) 1–13.

[51] J.H. Kang, G. Sauti, C. Park, V.I. Yamakov, K.E. Wise, S.E. Lowther, C.C. Fay, S.A. Thibeault, R.G. Bryant, Multifunctional electroactive nanocomposites based on piezoelectric boron nitride nanotubes, ACS Nano. 9 (2015) 11942–11950.

[52] S.A. Thibeault, C.C. Fay, S.E. Lowther, K.D. Earle, G. Sauti, J.H. Kang, C. Park, A.M. McMullen, Radiation Shielding Materials Containing Hydrogen, Boron, and Nitrogen: Systematic Computational and Experimental Study. Phase I, 2012.

[53] J.E. Estevez, M. Ghazizadeh, J.G. Ryan, A.D. Kelkar, Simulation of hydrogenated boron nitride nanotube's mechanical properties for radiation shielding applications, Int. J. Chem. Sci. Eng. 8 (2014) 63–67.

[54] K.S. Kim, M.B. Jakubinek, Y. Martinez-Rubi, B. Ashrafi, J. Guan, K. O'neill, M. Plunkett, A. Hrdina, S. Lin, S. Dénommée, et al., Polymer nanocomposites from free-standing, macroscopic boron nitride nanotube assemblies, RSC Adv. 5 (2015) 41186–41192.

[55] P. Ahmad, M.U. Khandaker, Y.M. Amin, N. Muhammad, Synthesis and characterization of boron nitride microtubes, Mater. Express. 5 (2015) 249–254.

[56] R. Haubner, M. Herrmann, B. Lux, G. Petzow, R. Weissenbacher, M. Wilhelm, High Performance Non-Oxide Ceramics II, Springer, 2003.

[57] T. Bel, C. Arslan, N. Baydogan, Radiation shielding properties of poly (methyl methacrylate)/colemanite composite for the use in mixed irradiation fields of neutrons and gamma rays, Mater. Chem. Phys. 221 (2019) 58–67.

[58] J.W. Krumpfer, T. Schuster, M. Klapper, K. Müllen, Make it nano-keep it nano, Nano Today 8 (2013) 417–438.

[59] J. Fu, L. Shi, D. Zhang, Q. Zhong, Y. Chen, Effect of nanoparticles on the performance of thermally conductive epoxy adhesives, Polym. Eng. Sci. 50 (2010) 1809–1819.

[60] J.W. Shin, J.-W. Lee, S. Yu, B.K. Baek, J.P. Hong, Y. Seo, W.N. Kim, S.M. Hong, C.M. Koo, Polyethylene/boron-containing composites for radiation shielding, Thermochim. Acta 585 (2014) 5–9.

[61] A. Güngör, I.K. Akbay, T. Özdemir, EPDM Rubber with hexagonal boron nitride: a thermal neutron shielding composite, Radiat. Phys. Chem. 165 (2019) 108391.

[62] T. Özdemir, S.N. Yılmaz, Hexagonal boron nitride and polydimethylsiloxane: a ceramic rubber composite material for neutron shielding, Radiat. Phys. Chem. 152 (2018) 93–99, https://doi.org/10.1016/J.RADPHYSCHEM.2018.08.008.

[63] S. Woosley, N.A. Galehdari, A. Kelkar, S. Aravamudhan, Fused deposition modeling 3D printing of boron nitride composites for neutron radiation shielding, J. Mater. Res. 33 (2018) 3657–3664.

[64] T.J. Quill, M.K. Smith, T. Zhou, M.G.S. Baioumy, J.P. Berenguer, B.A. Cola, K. Kalaitzidou, T.L. Bougher, Thermal and mechanical properties of 3D printed boron nitride-ABS composites, Appl. Compos. Mater. 25 (2018) 1205–1217.

[65] P. Deshmukh, M. Lovell, W.G. Sawyer, A. Mobley, On the friction and wear performance of boric acid lubricant combinations in extended duration operations, Wear 260 (2006) 1295–1304.

[66] T. Özdemir, İ.K. Akbay, H. Uzun, İ.A. Reyhancan, Neutron shielding of EPDM rubber with boric acid: mechanical, thermal properties and neutron absorption tests, Prog. Nucl. Energy 89 (2016) 102–109, https://doi.org/10.1016/J.PNUCENE.2016.02.007.

[67] S. Gwaily, H. Hassan, M. Badawy, M. Madani, Natural rubber composites as thermal neutron radiation shields: II—H_3BO_3/NR composites, Polym. Test. 21 (2002) 513–517, https://doi.org/10.1016/S0142-9418(01)00117-9.

[68] S.L. LeVan, J.E. Winandy, Effects of fire retardant treatments on wood strength: a review, Wood Fiber Sci. 22 (2007) 113–131.

[69] T. Özdemir, A. Güngör, I.A. Reyhancan, Flexible neutron shielding composite material of EPDM rubber with boron trioxide: mechanical, thermal investigations and neutron shielding tests, Radiat. Phys. Chem. 131 (2017) 7–12.

[70] O.M. Moon, B.-C. Kang, S.-B. Lee, J.-H. Boo, Temperature effect on structural properties of boron oxide thin films deposited by MOCVD method, Thin Solid Films 464 (2004) 164–169.

[71] M.S. Al-Buriahi, A.S. Abouhaswa, H.O. Tekin, C. Sriwunkum, F.I. El-Agawany, T. Nutaro, E. Kavaz, Y.S. Rammah, Structure, optical, gamma-ray and neutron shielding properties of NiO doped B_2O_3-$BaCO_3$–Li_2O_3 glass systems, Ceram. Int. (2019).

[72] A.M.A. Mostafa, S.A.M. Issa, M.I. Sayyed, Gamma ray shielding properties of PbO-B_2O_3-P_2O_5 doped with WO_3, J. Alloys Compd. 708 (2017) 294–300.

[73] S.A. Issa, Y.B. Saddeek, H.O. Tekin, M.I. Sayyed, K. Shaaban, Investigations of radiation shielding and elastic properties of PbO-SiO_2-B_2O_3-Na_2O glasses using Monte Carlo method, Curr. Appl. Phys. (2018).

[74] C. Jumpee, D. Wongsawaeng, Innovative neutron shielding materials composed of natural rubber-styrene butadiene rubber blends, boron oxide and iron (III) oxide, in: J. Phys. Conf. Ser, 2015, p. 12019.

[75] D. Toyen, K. Saenboonruang, Development of paraffin and paraffin/bitumen composites with additions of B_2O_3 for thermal neutron shielding applications, J. Nucl. Sci. Technol. 54 (2017) 871–877.

[76] E. Derun, A. Kipcak, Characterization of some boron minerals against neutron shielding and 12 year performance of neutron permeability, J. Radioanal. Nucl. Chem. 292 (2011) 871–878.

[77] A. Bayulken, C. Aksut, Utilization of Colemanite as a Radiation Protection Material, 1986.

[78] A. Güldacs, A. Güllü, A. Çankaya, Determination of the rheological properties of polypropylene filled with colemanite, Polym. Adv. Technol. 28 (2017) 1179–1184.

[79] K. Okuno, Neutron shielding material based on colemanite and epoxy resin, Radiat. Prot. Dosimetry 115 (2005) 258–261.

[80] G. Guzel, O. Sivrikaya, H. Deveci, The use of colemanite and ulexite as novel fillers in epoxy composites: influences on thermal and physico-mechanical properties, Compos. B Eng. 100 (2016) 1–9.

[81] G. Charalampides, K.I. Vatalis, B. Apostoplos, B. Ploutarch-Nikolas, Rare earth elements: industrial applications and economic dependency of Europe, Procedia Econ. Financ. 24 (2015) 126–135.

[82] L. Li, S. Zhaohui, W. Youping, Radiation shielding and magnetic properties of rare earth/polymer composites, China Synth. Rubber Ind. 3 (2001).
[83] J. Dumazert, R. Coulon, Q. Lecomte, G.H.V. Bertrand, M. Hamel, Gadolinium for neutron detection in current nuclear instrumentation research: a review, Nucl. Instruments Methods Phys. Res. Sect. A Accel. Spectrometers, Detect. Assoc. Equip. 882 (2018) 53–68.
[84] R.B. Firestone, H.D. Choi, R.M. Lindstrom, G.L. Molnar, S.F. Mughabghab, R. Paviotti-Corcuera, Z. Revay, A. Trkov, C.M. Zhou, V. Zerkin, Database of Prompt Gamma Rays From Slow Neutron Capture for Elemental Analysis, 2004.
[85] P. Zhang, J. Li, W. Wang, X. Tan, L. Xie, F. Guo, The design, microstructure and mechanical properties of a novel Gd_2O_3/6061Al neutron shielding composite, Vacuum 162 (2019) 92–100.
[86] F. Söderlind, H. Pedersen, R.M. Petoral Jr., P.-O. Käll, K. Uvdal, Synthesis and characterisation of Gd_2O_3 nanocrystals functionalised by organic acids, J. Colloid Interface Sci. 288 (2005) 140–148.
[87] H. Guo, X. Yang, T. Xiao, W. Zhang, L. Lou, J. Mugnier, Structure and optical properties of sol-gel derived Gd_2O_3 waveguide films, Appl. Surf. Sci. 230 (2004) 215–221.
[88] N. Sakai, L. Zhu, A. Kurokawa, H. Takeuchi, S. Yano, T. Yanoh, N. Wada, S. Taira, Y. Hosokai, A. Usui, et al., Synthesis of Gd2O3 nanoparticles for MRI contrast agents, in: J. Phys. Conf. Ser., 2012, p. 12008.
[89] Managing Critical Isotopes, Weaknesses in DOE's Management of Helium-3 Delayed the Federal Response to a Critical Supply Shortage, GAO-11-472, U.S. Government Accountability Office, Washington, DC, 2011.
[90] D. Tobia, E.L. Winkler, J. Milano, A. Butera, R. Kempf, L. Bianchi, F. Kaufmann, Determination of Gd concentration profile in UO_2-Gd_2O_3 fuel pellets, J. Nucl. Mater. 451 (2014) 207–210.
[91] K. Iwasaki, T. Matsui, K. Yanai, R. Yuda, Y. Arita, T. Nagasaki, N. Yokoyama, I. Tokura, K. Une, K. Harada, Effect of Gd_2O_3 dispersion on the thermal conductivity of UO_2, J. Nucl. Sci. Technol. 46 (2009) 673–676.
[92] W. Poltabtim, D. Toyen, K. Saenboonruang, Comparative neutron-shielding properties of metal oxide/HDPE composites using a Monte Carlo Code of PHITS, in: IOP Conf. Ser. Mater. Sci. Eng, 2019, p. 12013.
[93] N.A. Galehdari, A.D. Kelkar, Effect of neutron radiation on the mechanical and thermophysical properties of nanoengineered polymer composites, J. Mater. Res. 32 (2017) 426–434.
[94] Ş.G. İrim, A.A. Wis, M.A. Keskin, O. Baykara, G. Ozkoc, A. Avcı, M. Doğru, M. Karakoç, Physical, mechanical and neutron shielding properties of h-BN/Gd_2O_3/HDPE ternary nanocomposites, Radiat. Phys. Chem. 144 (2018) 434–443, https://doi.org/10.1016/J.RADPHYSCHEM.2017.10.007.
[95] Y. Choi, B.M. Moon, D.-S. Sohn, Fabrication of Gd containing duplex stainless steel sheet for neutron absorbing structural materials, Nucl. Eng. Technol. 45 (2013) 689–694, https://doi.org/10.5516/NET.07.2013.015.
[96] Z.G. Xu, L.T. Jiang, Q. Zhang, J. Qiao, D. Gong, G.H. Wu, The design of a novel neutron shielding B_4C/Al composite containing Gd, Mater. Des. 111 (2016) 375–381.
[97] Z.G. Xu, L.T. Jiang, Q. Zhang, J. Qiao, G.H. Wu, The microstructure and influence of hot extrusion on tensile properties of (Gd + B_4C)/Al composite, J. Alloys Compd. 729 (2017) 1234–1243.
[98] Y. Baik, Y. Choi, B.M. Moon, D.S. Sohn, S.G. Bogdanov, A.N. Pirogov, Effect of gadolinium addition on the corrosion, wear, and neutron absorbing behaviors of duplex stainless steel sheet, Phys. Met. Metallogr. 116 (2015) 1135–1142.

[99] J.-S. Park, J. Kim, S.-H. Yi, Effects of gadolinium in Fe based amorphous ribbons with high boron contents on the neutron shielding efficiency, Ann. Nucl. Energy 109 (2017) 365–369.

[100] M.S. Uddin, M.H. Chowdhury, S.M. Hossain, S.A. Latif, M.A. Islam, M.A. Hafiz, S.H. Mubin, A.K.M. Zakaria, S.M. Yunus, S.M.A. Islam, Thermal neutron capture cross sections for the 152Sm (n, \$γ\$) 153Sm and 154Sm (n, \$γ\$) 155Sm reactions at 0.0536 eV energy, Nucl. Instruments Methods Phys. Res. Sect. B Beam Interact. with Mater. Atoms. 266 (2008) 4855–4861.

[101] R. Florez, H.A. Colorado, C.H.C. Giraldo, A. Alajo, Preparation and characterization of Portland cement pastes with Sm_2O_3 microparticle additions for neutron shielding applications, Constr. Build. Mater. 191 (2018) 498–506.

[102] R. Mohammadinasab, M. Tabatabaee, H. Aghaie, M.A. Seyed Sadjadi, A simple method for synthesis of nanocrystalline Sm_2O_3 powder by thermal decomposition of samarium nitrate, Synth. React. Inorganic, Met. Nano-Metal Chem. 45 (2015) 451–454.

[103] P. Wang, X. Tang, F. Chen, D. Chen, The design, fabrication and safety evaluation of a novel spent fuel storage basket material, Nucl. Eng. Des. 284 (2015) 91–96.

[104] B.T. Sone, E. Manikandan, A. Gurib-Fakim, M. Maaza, Sm_2O_3 nanoparticles green synthesis via Callistemon viminalis' extract, J. Alloys Compd. 650 (2015) 357–362.

[105] R.S. Niranjan, B. Rudraswamy, N. Dhananjaya, Effective atomic number, electron density and kerma of gamma radiation for oxides of lanthanides, Pramana 78 (2012) 451–458.

[106] C.R. Michel, A.H. Martínez-Preciado, R. Parra, C.M. Aldao, M.A. Ponce, Novel CO_2 and CO gas sensor based on nanostructured Sm_2O_3 hollow microspheres, Sens. Actuators B Chem. 202 (2014) 1220–1228.

[107] Y. Zhang, C. Lu, L. Sun, Z. Xu, Y. Ni, Influence of Sm_2O_3 on the crystallization and luminescence properties of boroaluminosilicate glasses, Mater. Res. Bull. 44 (2009) 179–183.

[108] S.H. Zhang, M.X. Li, J.H. Yoon, T.Y. Cho, Characterization on the coatings of Ni-base alloy with nano-and micron-size Sm_2O_3 addition prepared by laser deposition, Mater. Chem. Phys. 112 (2008) 668–674.

[109] P.P. Chu, M.J. Reddy, Sm_2O_3 composite PEO solid polymer electrolyte, J. Power Sources 115 (2003) 288–294.

[110] P. Wang, X. Tang, H. Chai, D. Chen, Y. Qiu, Design, fabrication, and properties of a continuous carbon-fiber reinforced Sm_2O_3/polyimide gamma ray/neutron shielding material, Fusion Eng. Des. 101 (2015) 218–225.

[111] D. Toyen, E. Wimolmala, N. Sombatsompop, T. Markpin, K. Saenboonruang, Sm_2O_3/UHMWPE composites for radiation shielding applications: mechanical and dielectric properties under gamma irradiation and thermal neutron shielding, Radiat. Phys. Chem. 108366 (2019).

CHAPTER 3

Thermoplastic micro- and nanocomposites for neutron shielding

Lynsey Baxter[a], Korey Herrman[a], Rajesh Panthi[b], Kunal Mishra[c], Raman Singh[c], Sheila Thibeault[d], Eric Benton[b], Ranji Vaidyanathan[a]
[a]Oklahoma State University, Materials Science and Engineering Department, Tulsa, OK, United States
[b]Oklahoma State University, Physics Department, Stillwater, OK, United States
[c]Oklahoma State University, Mechanical Engineering Department, Stillwater, OK, United States
[d]NASA Langley Research Center, Advanced Materials and Processing Branch, Hampton, VA, United States

3.1 Introduction and background

This chapter discusses recent research regarding the use of thermoplastic materials combined with micro- and nano-additives to form multifunctional composites for the use of neutron radiation shielding, particularly in reference to space applications.

3.1.1 Historical approaches to radiation shielding

In the past, neutron shielding was not considered to be a significant risk in terms of space-related radiation shielding. The lack of data regarding the biological risks of neutron radiation exposure as well as the belief that astronauts would likely only partake in a single space mission led scientists to be less concerned with developing radiation shielding materials to combat neutron radiation [1]. As such, traditionally, the majority of spacecraft were composed of aluminum alloys as aluminum is lightweight and met the other needs and necessary material requirements for space flight. However, as data from space expeditions were analyzed, neutron radiation was established to be a significant biological threat, and shielding against it was necessary in order to protect astronauts from the risks associated with this very prevalent form of radiation [2–4].

3.1.1.1 Neutron Shielding

In order to properly design materials for the shielding of neutron-based radiation, it is essential to understand the environments and phenomenon in which this radiation can be found and how neutron radiation propagates

Micro and Nanostructured Composite Materials for Neutron Shielding Applications
https://doi.org/10.1016/B978-0-12-819459-1.00003-9

© 2020 Elsevier Ltd.
All rights reserved.

and moves within these environments due to interactions with other materials. Neutron radiation is frequently produced as a secondary radiation source in a variety of space radiation phenomena such as galactic cosmic radiation (GCR) and solar particle events (SPE) [3–8]. The types of neutron radiation are diverse, ranging between high-energy or low-energy particles, albedo neutrons, and back-scattered neutrons, all of which require different considerations [4, 6] for protection. High-energy neutrons, also known as fast neutrons, are more effectively slowed by selecting materials which have cross sections that promote interactions resulting in neutron energy decreasing due to scattering [9–11]. Low-energy neutrons, often termed as slow neutrons or thermal neutrons, require materials that possess specific capture cross sections in order to prevent further radiation penetration through the shielding material [10–12]. Both high-energy and low-energy neutrons are commonly found in high-altitude environments [6].

It is also believed that neutron radiation will become more of a problem in future space travel expeditions. One significant example is the goal to reach the surface of Mars. Due to the interactions of "solar particle events" or SPE and the Martian atmosphere, secondary neutrons can easily become trapped within the areas of low orbit as well as close to the planetary surface [4, 5, 8]. This places particular importance in developing radiation shielding materials which are sufficient in shielding against high levels of neutron radiation as future missions to Mars are discussed and prioritized by space exploration organizations in the future.

3.1.1.2 Prevalence of aluminum

Traditionally, aluminum has been favored for use in the major structural components of spacecraft despite knowledge that materials containing high amounts of hydrogen provide superior radiation shielding [3, 6, 8, 13]. This is partially due to aluminum being easy to obtain as the most abundant metal on Earth and also partially due to aluminum being a highly versatile metal due to its ability to form alloys with different material properties. With future goals of landing once more on the moon as well as traveling to Mars, aluminum is no longer going to be sufficient to provide long-term protection to astronauts from the dangerous radiation of deep space. The current solution to this is the investigation of multifunctional structural composites with high hydrogen content. In particular, many studies have been conducted regarding micro- and nanocomposites made primarily from polyethylene-based materials combined with structural additives, or polyimide resins with additives to supplement the radiation shielding capacity (Table 3.1).

Table 3.1 Mechanical properties of various aluminum alloys used in spacecraft.

Material	Density (g/cm^3)	Melting point (°C)	Tensile yield strength (MPa)	Ref.
Al 2219	2.84	510	352	[8, 9, 14, 15]
Al 6061	2.70	588	276	[9, 16, 17]
Al 2024	2.78	510	324	[6, 18, 19]

3.1.2 Necessary and desired shielding applications

Radiation exposure poses various risks to astronauts as well as electronics and equipment that are placed into the harsh environment of space. Not only do these materials need to possess the ability to withstand extreme temperatures and stress, but they also need to be used in various applications such as habitats, vehicles, and rocket components. The materials used need to provide sufficient shielding against radiation as well as create lesser degrees of secondary radiation as by-products of the material's interactions with various radiation sources.

3.2 Thermoplastics of interest

The thermoplastics discussed in this chapter is mostly high-density polyethylene (HDPE) and polyimide resins. These materials are high in hydrogen content and have been well documented in various studies over the years. Polyethylene also has been a focal point of radiation shielding materials by professional organizations such as the National Aeronautics and Space Administration (NASA) [3, 5, 6, 9, 20]. Hydrogen- and carbon-based materials are capable of attenuating low-energy neutrons more efficiently than traditional metals such as aluminum [4, 6, 7, 9, 20]; this is due to the mass similarity of the hydrogen nucleus to that of the neutron radiation [3, 6, 21, 22]. Hydrogen also provides the added benefit of the absence of secondary neutron radiation due to the lack of neutrons in the hydrogen nucleus [23].

3.2.1 Polyethylene $(C_2H_4)_n$

Polyethylene (PE) is a thermoplastic composed solely of hydrogen and carbon atoms and possesses a variety of classifications based on density and structure such as HDPE that exhibits higher tensile strength [24] or low-density polyethylene (LDPE) which possesses a lower coefficient of thermal expansion [25]. These variations provide a wide range of mechanical

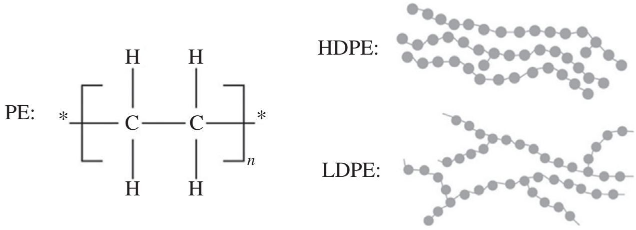

Fig. 3.1 The basic chemical structure of polyethylene and cross-linking behaviors of high-density polyethylene and low-density polyethylene. This modified image was originally created by Thorsten Graunke et al. and is licensed under CC BY 3.0. *(This modified image was originally created by Thorsten Graunke, Katrin Schmitt, J. Wöllenstein, Organic membranes for selectivity enhancement of metal oxide gas sensors, J. Sens. (2016) 1–22, https://doi.org/10.1155/2016/2435945 and is licensed under CC BY 3.0.)*

properties and provide the ability to fine-tune the desired final material characteristics (Fig. 3.1).

Polyethylene is considered lightweight with a density ranging from about 0.9 to 1 g/cm^3 depending on which form of polyethylene is used [24, 25]. Comparing the density of polyethylene (1 g/cm^3) to that of aluminum (2.7 g/cm^3), polyethylene provides equivalent shielding with less material and in result could be a cost-effective alternative [5, 8, 9, 26]. Because of its highly effective shielding capabilities and low density, polyethylene is considered to be an ideal base material for radiation shielding applications.

The current desired radiation shielding material is considered to be a multifunctional composite that exhibits high strength and could therefore be used as load-bearing structural materials. However, despite its superior radiation shielding properties, pure polyethylene lacks the necessary structural strength and stable thermal properties to be used as a shielding material alone [3, 5, 7, 8, 27]. As such, many research groups have sought to create multifunctional composites that use polyethylene as a base matrix. Many studies have been conducted to analyze the effects of the addition of micro- and nano-additives as well as the use of polyethylene in sandwich composites with carbon fiber and other structurally strong materials (Tables 3.2 and 3.3).

3.2.2 Polyimide, $C_{35}H_{28}N_2O_7$

Polyimides (PI) are high-performance thermoplastic polymers. Similar to polyethylene, polyimides have a high hydrogen content and have shown promise for future use in neutron shielding applications. Polyimides can

Table 3.2 Comparative properties of HDPE and LDPE.

Material	Density (g/cm^3)	Melting point (°C)	Tensile yield strength (MPa)	Ref.
HDPE	0.96	130	26.3	[24]
LDPE	0.91	114	11.5	[25]

Table 3.3 Thermal properties of HDPE and LDPE.

Material	T_g (°C)	Coefficient of thermal expansion (10^{-5}/°C)	Ref.
HDPE	−110	15.3	[24, 28]
LDPE	−110	2.0	[25, 28]

be made into films and matrix resins, which allow for ease of manufacturing, as well as providing higher mechanical and thermal properties when compared with pure PE [27, 29–31]. Despite these benefits, it is still necessary to combine polyimides with other materials in order to produce a multifunctional material that could meet the strength requirements for structurally important applications. There is, however, a substantial downside to the use of polyimides for radiation shielding applications.

Kapton, a polyimide film produced by DuPont in the 1960s, was initially used as insulation for electric wires (Fig. 3.2). The use of polyimide films was widespread in the aerospace industry and was often used in spacecraft [32]. However, it was later discovered that mechanical wear of the film resulted in rapid material failure [33]. As such, use of polyimides is often limited to particular formulations and applications are carefully considered [34] (Tables 3.4 and 3.5).

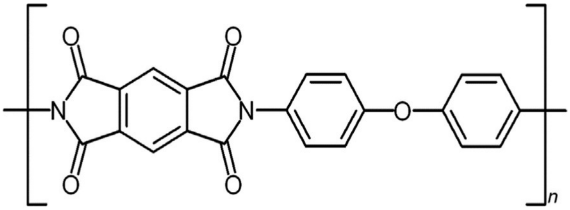

Fig. 3.2 Chemical structure of poly-oxydiphenylene-pyromellitimide, also known as Kapton HN. This image is licensed under CC BY-SA 3.0. *(Chemical structure of poly-oxydiphenylene-pyromellitimide, also known as Kapton HN. This image is licensed under CC BY-SA 3.0.)*

Table 3.4 Mechanical properties of common polyimides.

Material	Density (g/cm^3)	Melting point (°C)	Tensile yield strength (MPa)	Ref.
AURUM PL450C PI Resin	1.33	388	92	[35, 36]
Kapton 100 HN Film	1.42	–	69	[37]

Some data used was obtained from research published by Shota Kazano, Toshiko Osada, Satoshi Jobayashi, Ken Goto, Experimental and analytical investigation on resin impregnation behavior in continuous carbon fiber reinforced thermoplastic polyimide composites, Mech. Adv. Mater. Modern Process. (2016), https://doi.org/10.1186/s40759-018-0039-3 and is licensed under CC BY 4.0.

Table 3.5 Thermal properties of common polyimides.

Material	T_g (°C)	Coefficient of thermal expansion (10^{-5}/°C)	Ref.
AURUM PL450C PI Resin	250	5.5	[35]
Kapton 100 HN Film	360–410 (difficult to detect accurately due to concomitant degradation)	2.0	[37]

3.3 Additives of interest

Studies have shown that both boron- and nitrogen-containing materials exhibit excellent neutron radiation shielding capabilities as well as possess desirable mechanical properties [13, 21, 38]. Carbon fiber provides superior mechanical and structural properties but does not provide as effective radiation shielding as boron- and nitrogen-containing materials [11]. These differences will be discussed and compared later in the chapter. For now, a brief synopsis of each additive of interest will be given as well as information regarding their general exhibited properties.

3.3.1 Boron nitride

Boron nitride (BN) has been used as an additive for radiation shielding materials due to favorably low Z nuclei of boron and nitrogen and scattering of few neutrons as a secondary radiation by-product of interaction of radiation with the shielding material [10–12]. Boron possesses a cross section suitable for the attenuation of low-energy neutrons [38], making it an ideal additive for high-energy neutron attenuating polyethylene and polyimide.

Table 3.6 Typical material properties of BNs.

Density (g/cm^2)	Melting point (°C)	Hardness (MPa)	Young's Modulus (GPa)	Ref.
2.3	3000	1830	60	[40]

Boron nitride can be produced as micro-powders, nano-powders, as well as in the form of nanotubes which will be discussed as well. The variety in available additives promotes balance between radiation shielding efficiency and total composite production costs for applications which require sufficient but cheap solutions.

Boron nitride is found in a few common atomic structures such as cubic boron nitride (cBN) and hexagonal boron nitride (hBN). In the case of hBN, material properties are anisotropic, and any resulting composite will also feature anisotropy. Therefore, alignment of the hBN may be necessary to obtain optimum mechanical properties.

Boron nitride when combined with polyethylene results in a composite material with increased structural integrity and mechanical properties with minor reductions to the radiation shielding capacity when compared to shielding results of pure polyethylene [39]. The specifics of these effects will be discussed in further detail in Section 5 (Table 3.6).

3.3.2 Boron carbide

Traditionally valued for its extremely high hardness, boron carbide (B_4C) is another boron-based additive which is frequently found in studies which focus on the creation of new neutron radiation shielding composite materials. Along with a valuable neutron capture cross section and low risk of secondary neutron radiation resulting from neutron-material interactions, boron carbide possesses remarkable mechanical properties [21].

When compared with boron nitride, boron carbide has the hardness and Young's Modulus values which are over 2000% and 650% higher, respectively [40, 41]. Such dramatic differences mean there is likely to be substantial differences in the degree of improvement to the mechanical properties of a resultant composite with the use of boron carbide compared to the use of boron nitride. The increased mechanical properties of boron carbide provide significant motivation to include its use in thermoplastic-based composites. However, it should also be noted that carbon is less effective at neutron radiation shielding than nitrogen in most energy ranges [5, 42].

Table 3.7 Typical material properties of B_4C.

Density, g/cm^2	Melting Point, °C	Hardness, MPa	Young's Modulus, GPa	Ref
2.4	2445	41100	460	[41]

Also, some studies have shown boron carbide to be more difficult to uniformly disperse within polyethylene composites [39, 42] (Table 3.7).

3.3.3 Boron nitride nanotubes

Boron nitride nanotubes (BNNTs) have recently caught the attention of radiation shielding researchers, particularly those at the NASA Langley Research Center. NASA has put forth many years of research into the production and testing of BNNTs for radiation shielding applications, particularly for the use in multifunctional composites for space-based applications in fabrics as well as primary structures [5].

First theorized and synthesized in the 1990s, BNNTs have been found to possess valuable thermal, mechanical, and radiation attenuating properties, making these nanotubes an ideal additive material for use in hydrogen-rich polymer composites [3, 5, 7]. One of the significant drawbacks of the implementation of the nanotubes, however, is the difficulty in their synthesis. High-quality thin-walled nanotubes with small diameters exhibit the best relative properties; however, this type of nanotube can only be produced in lengthy, multistep procedures at high temperatures and pressures. More simplistic and low-temperature procedures such as ball milling result in the production of wide, multiwalled nanotubes which often possess defects in their structure, lessening their valuable properties [7].

Scientists at the NASA Langley Research Center have been researching how to synthesize high-purity BNNTs using high-temperature and high-pressure procedures in order to gain an understanding of how to mass-produce this valuable material. According to NASA's 2014 report, production rates of BNNTs in their laboratory are approximately 20 mg of material per hour [7].

Similar to the other additives discussed, proper dispersion of BNNTs into PE has proven to be a challenging task due to the complex relationships of matrix-additive chemical compatibility and the processing techniques used in the dispersion process [7]. As such, properties of composites with the inclusion of BNNTs can differ dramatically depending on the dispersion solvents and specific dispersion methods used, if not paired properly. This can result in their mechanical advantages being reduced due to agglomerations if the BNNTs are not properly dispersed within the matrix material.

3.3.4 Carbon fiber

Unlike the boron-contained additives previously discussed, carbon fiber does not possess a high neutron capture cross section, making it less effective in terms of neutron radiation shielding capacity. However, while carbon fiber (CF) additives may not provide significant improvements to the radiation shielding capacity of polyethylene and polyimide thermoplastics, carbon fiber does provide excellent mechanical and structural properties which the thermoplastics of interest dramatically lack. Along with impressive mechanical properties, carbon fiber is also lightweight and an excellent electrical conductor [11], which is mass-produced and therefore relatively easy to obtain and process. Furthermore, the benefits of the creation of reinforced sandwich composites will be discussed later in this chapter. The inclusion of carbon fiber in such sandwich composites is of significant research interest, and therefore it is important to bring attention to the properties of value.

3.4 Other considerations

There are various other considerations that need to be accounted for when discussing micro- and nanocomposites. These are of particular interest in terms of radiation shielding in space applications. For instance, particle size can have dramatic effects on the overall efficiency of radiation shielding [21, 42], and as such, it is often more advisable to use nano-sized additives over micro-sized additives. Also, the concentration [21, 43] and thickness [26, 27] of the material in the composite can allow for thinner materials which can save on the volume of material needed to mitigate the encountered radiation [21] which can, in turn, reduce the overall costs and production times of the composite components. It is also essential to understand how these materials are degraded over time and how that damage can have serious consequences in long-term space exploration missions [12, 44–47].

3.4.1 Particles size effects

The particle size of additives can have dramatic effects on the resultant properties of composites. The common trend of particle size effects is also seen in differences in the radiation shielding capabilities of materials. In specific to the additives of interest discussed in this chapter, the effects of the use of micro-sized and nano-sized particles will be briefly examined to provide insight on preferred material selections for neutron shielding applications.

A study conducted by Zahra Soltani et al. found that the inclusion of nano-sized boron carbide particles resulted in an approximately 40% decrease in the neutron transmission fraction compared to the transmission fraction values from micro-sized particle materials. However, in smaller weight percentages the difference in transmission fraction was only around 8% and 9% [21]. The dramatic difference in results requires later discussion of the concentration effects of additives in composites.

From the same study, results showed that the resultant thermal neutron absorption cross section was affected depending on which sized particle was used, as well. Differences of the cross-section ranged from around 20% to 50% in samples with 1–5 wt% of boron particles [21]. The increase in neutron absorption cross sections can be explained by the reduction in particle size. As the particle size of the boron additives decreases, the incident radiation will experience an increase in the number of collisions with the boron additive within the composite. These collisions are responsible for the mitigation of thermal neutrons to an energy state which can be easily stopped within smaller penetration depths of the shielding material [21, 42].

Overall, similar radiation attenuation results were found in an earlier study by Jaewoo Kim et al. who studied both boron nitride and boron carbide particles of micro- and nanoscales. In terms of particle size effects on mechanical properties, the study conducted mechanical testing experiments that showed that nano-sized particles provided a substantial increase in both tensile and flexural strengths compared to the respective micro-sized particles at a 10 wt% inclusion, as presented in Table 3.8 [42]. When using particles in composites, there are many physical properties improve as additive surface area increases. Since nanoparticles possess higher surface-area-to-volume ratios, these results are to be expected. These benefits should also be considered in the material selection process to ensure the most effective balance in resultant material properties.

Table 3.8 Approximate increase in properties of micro/nano BN and B_4C (at 10 wt% in HDPE) [42].

Property examined	Micro BN	Nano BN	% increase	Micro B_4C	Nano B_4C	% increase
Flexural strength (MPa)	32.1	36.6	13.1	28.0	34.3	20.2
Tensile strength (MPa)	29.4	30.8	4.7	27.8	33.6	18.9

While nanoparticles will have greater benefits in terms of theoretical resultant properties, a significant detriment comes from the fact that nanoparticles suffer from high surface energies resulting in nonuniform distribution of particles within a polymer matrix material [21, 42]. Thus, it is necessary to include preparation steps that can ensure better homogeneity in the resultant composite materials. Examples of such processes include ultra-sonication or the use of solvents in the mixing stage of the composite fabrication.

3.4.2 Concentration effects

The effects of varying additive concentration have been briefly touched upon in previous sections of this chapter; however, as it is an important consideration to take into account, the concept deserves a more in-depth discussion. It is intuitive to consider that the further inclusion of more additives will result in the final composite expressing behaviors and properties which are more closely related to the additive.

While concentration effects are typically well understood in the materials field, research has shown that in terms of radiation shielding materials, these effects can sometimes behave counterintuitively. For example, earlier in this chapter the concept of pure polyethylene being the ideal radiation shielding material was discussed and supported; however, the shielding efficiency can actually be increased with the addition of additives such as BN above specific material thicknesses [43].

Additionally, if nanoparticles are used at low weight percentages, there is greater risk of poor dispersion of the additives [21]. Poor dispersion will result in agglomerations of the additive material, which can dramatically affect the resultant radiation shielding capacity of the composite material. This will be discussed in more detail later in this chapter. It is important to examine the relationship between the concentration of additives and the resultant properties in order to produce a composite material with the proper balance of desired characteristics.

3.4.3 Thickness effects

Thickness effects are another particularly important consideration in terms of neutron radiation shielding for space applications. Thickness and weight are two of the most important measures to limit when considering composites for space exploration. Shielding materials need to be thin in order to allow space to be more widely distributed among other essential

Table 3.9 Required thickness to achieve neutron permeability of 0.4 in PI/B_4C composite [27].

Weight percent of B_4C	Thickness (mm)
15	0.48
30	0.41
40	0.26
45	0.22

components. Weight is directly related to the cost required to send materials into space. Due to these thickness and weight limitations, research has focused on the creation of multifunctional composites for radiation shielding so as to ensure the use of materials that could provide a variety of valuable properties within a single composite piece.

The resultant material thickness can be increased or decreased in order to meet specific requirements for various applications. For example, compare a traditional aluminum shielding material to that of a pure polyethylene shield. To obtain the same degree of radiation shielding as 0.1-in.-thick aluminum, it was found that a 0.2-in.-thick shield of polyethylene would be required. However, as the density of polyethylene is much lower than aluminum, the relative mass of the polyethylene shield would be approximately 28% less than that of aluminum [26]. In applications where an additional 0.1 in. could be reasonably added, there would be an immediate weight saving while in locations where space is extremely limited, such an alternative shield would not be feasible. Shield thickness can be further reduced by the inclusion of micro- and nano-additives, as presented in Table 3.9.

From the data provided, the required thickness of the material to obtain the same degree of neutron shielding was reduced by one half when the concentration of B_4C was increased from 15 to 45 wt% [27]. However, careful consideration of other material properties is needed as high concentrations of additives may degrade valuable matrix material properties. Variability in the material thickness is essential for the discussion and study of potential sandwich composite configurations which may prove to be beneficial for multifunctional composites. This will be discussed briefly in the following section for reference.

3.4.4 Multilayer composites

Multilayer and sandwich composites have been described as one of the most effective types of radiation shield due to the ability to place specific materials in

Table 3.10 Layered composite material configuration [48].

Group name	Layer configuration[a]
A	Mixed Material (PE, B_4C, Pb)
B	PE, B_4C, Pb
C	Pb, PE, B_4C, Pb
D	Pb, B_4C, PE, Pb
E	Pb, Mixed Material (PE, B_4C), Pb
F	Three layers of mixed material (PE, B_4C, Pb)

[a] It should be noted that each configuration had differing layer thicknesses, totaling 20 cm for all groups, and as such the resulting weight percentages of each material differs in each group.

different portions of the overall composite to achieve ideal functional layering [48]. To test this, Guang Hu et al. [48] ran simulations and radiation beam testing using six distinct configurations of three base materials to examine the effects that different layers may have on the composite's overall radiation shielding capabilities. Their configurations are presented in Table 3.10.

Results of the study show that group A, a single layer of mixed material, performed better in terms of radiation shielding than groups B–D. Group E, a traditional sandwich composite configuration, performed approximately 5% better in terms of total radiation shielding [48]. This is due to the ability to tailor specific depths of the resultant composite to perform highly specialized tasks which can allow for positive compounding effects if layered in proper order.

In an example composite like group E, an initial lead layer provides an excellent shield for heavy-ion radiation as well as excellent wear resistance to the composite. As secondary forms of radiation are released from the interactions of lead and heavy ions, the sandwiched mixed-material layer is intended to specifically target these resultant forms of radiation. As Hu's results show, this methodology of composite fabrication can allow for the creation of highly specific material properties and capabilities [48].

Yiping Huang et al. tested neutron shielding sandwich composites and found that by spraying a 0.4-mm B_4C layer on a CF/epoxy composite, a dramatic decrease in the radiation counts was experienced by the composite during testing by 100%; this study also found that the same thickness layer also exhibited an almost 11% improvement in tensile strength [11]. Hu and Huang both found that simple, traditional sandwich composites exhibit superior radiation capabilities compared to simply mixed composite material [11, 48]; however, there was not adequate testing or discussion of how varying the number of layers may affect a resultant composite's properties.

Table 3.11 Effects of n layers on neutron transmittance in HDPE/HDPE+BN composite [22].

No. of layers	Approximate neutron transmittance (I/I_0)
2	0.68
4	0.65
8	0.63
16	0.67
32	0.50
64	0.47
128	0.45

Xianlong Zhang et al. provided an excellent study of how the number of layers in a structure affects shielding capabilities [22]. It was found that radiation shielding efficiency was significantly improved as the number of alternative layers increased. Results from Zhang's testing show a total neutron transmittance improvement of approximately 40% when comparing the results of a two-layered composite to a composite consisting of 128 layers [22]. However, the improvement between 32- and 64-layered composites may not be seen as worthwhile, as the extra effort required to fabricate these composites is comparable to the small benefit in terms of properties increased per layer. These results are believed to be due to the initial layering creating an adequate distribution of BN particles within the depth of the composite layers where additional layers do not provide a high probability of significantly increased interactions [22] (Table 3.11).

3.4.5 Material degradation resulting from radiation

The final consideration to be discussed in this chapter is how radiation degrades and damages polymer-based composites. As the polymer matrix is broken down one can expect to quickly begin losing radiation shielding capacity which could lead to catastrophic health risks in terms of applications in the environment of space. Polymers which are exposed to radiation often go through structurally altering reactions such as chain scission and cross-linking [12, 44–47]. It is important to understand these reactions in order to discuss prevention measures or alternative methods to ensure that neutron shielding composites can successfully withstand varying degrees of radiation exposure.

Chain scission frequently occurs as a result of the irradiation of branched polymers (such as LDPE) by gamma radiation [12, 44–47]. The breaking of the structural bonds in the polymer chain results in the formation of free radicals [46, 47]. These free radicals can then create new cross-links within the polymer chains, altering the known mechanical properties [33, 44, 45, 49], cross-link with micro- and nano-additives, or become trapped within the shielding material and over time cause autocatalytic oxidative degradation which can likely result in premature failure of the polymer matrix [46]. Because scission typically happens between C—C bonds, hydrogen atoms will be released as a result of the irradiation initiated cross-linking [12, 44, 45, 47].

In studies conducted by Calcagno et al. and Polvi it was found that polymers with a low degree of branching such as HDPE-based materials are only likely to form cross-links as a result of high-energy radiations such as heavy-ion and gamma radiation [44, 47]. It is important that, during the material selection process, these irradiation effects are taken into account. For example, a sandwich composite wrapped in a nonpolymer material may be able to prevent some damage to the radiation shielding material, prolonging the overall composite's service life.

3.5 Current research approaches

This section focuses on specific research regarding the use of the thermoplastics and additives of interest discussed earlier. Published radiation shielding model simulation results from codes such as FLUKA (FLUktuierende KAskade) and HZETRN (High charge (Z) and Energy TRaNsport) will be compared to gain a theoretical understanding of how these composite materials may interact in environments where radiation is a substantial concern. The mechanical and thermal stability testing will be reviewed, and the findings will be discussed regarding their feasible utilization as primary structural or secondary bulk shielding applications. Conclusive radiation testing results supported by relevant neutron and space radiation studies will also be covered.

3.5.1 Radiation shielding models

3.5.1.1 FLUKA simulations

In order to model radiation absorption through mediums consisting of polyethylene and boron nitride, FLUKA simulations were performed in the setup shown in Fig. 3.3 in a study by Scott and Vaidyanathan [23].

Absorbers in each simulation run consisted of the same material composition, pure PE, pure BN, or a PE/BN composite with BN concentrations ranging from 10% to 90%. The radiation source simulated was a Fe-56 beam

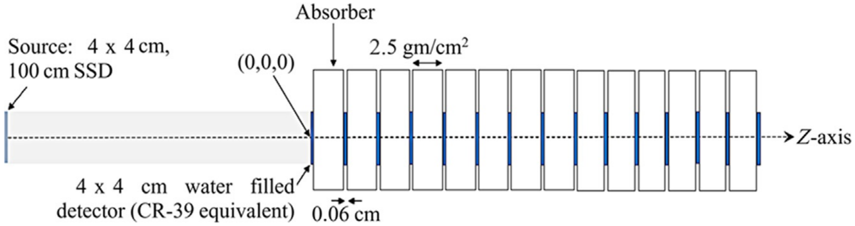
Absorber
Source: 4 x 4 cm,
100 cm SSD
(0,0,0)
2.5 gm/cm²
Z-axis
4 x 4 cm water filled
detector (CR-39 equivalent)
0.06 cm

Fig. 3.3 Schematic of the FLUKA simulation setup [23].

operating at 500 MeV/n. Water-filled CR-39 equivalent detectors were placed every 2.5 g/cm^2 along the *z*-axis in order to appropriately measure radiation transmission through the depth of the absorbers [23]. Varying weight percentages were used in order to analyze the concentrations at which BN may be added to PE without significantly effecting the depth-dose profile (Fig. 3.4).

These results show the depth required to absorb the radiation dose supplied by the source beam. As discussed in this chapter, pure polyethylene is considered to possess the ideal radiation shielding effectiveness for this range of simulations. The depth-dose profile resulting from the FLUKA

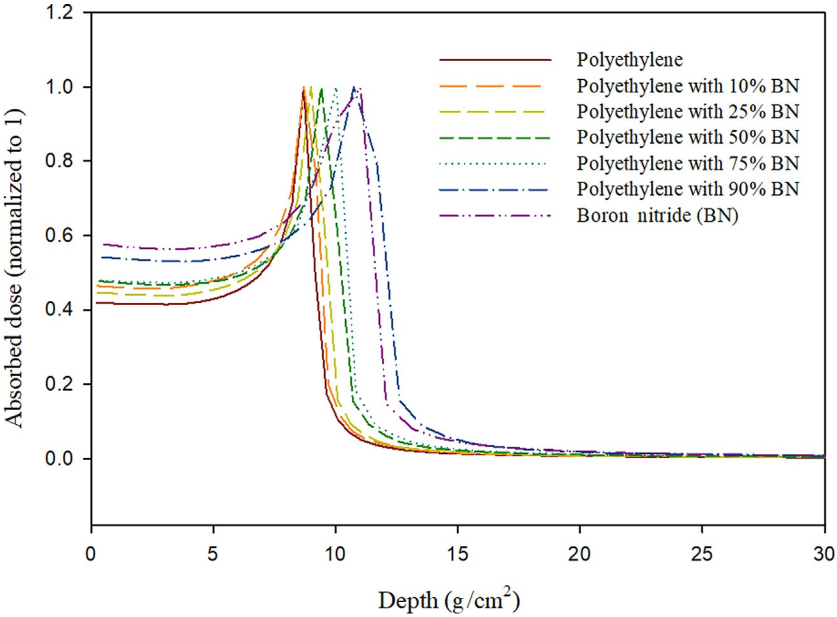

Fig. 3.4 Depth-dose profile acquired from FLUKA simulation testing using a Fe-56 source [23].

simulations shows the full dose absorption in pure polyethylene occurred at a depth of approximately 9 g/cm^2. For pure boron nitride, full absorption occurs at around 11 g/cm^2. From these results, one could reasonably expect similar absorption in radiation shields composed of pure polyethylene and composite shields of BN concentrations up to 50%. This provides polyethylene with sufficient levels of additives in order to improve the composite's mechanical properties.

3.5.1.2 HZETRN simulations

Thibeault et al. proposed that the use of BNNTs could allow the additives to carry more hydrogen atoms in the composite itself, increasing its radiation shielding capacity [3]. Results from some of Thibeault's early simulations show evidence of their claim. Fig. 3.5 shows that BNNTs loaded with a

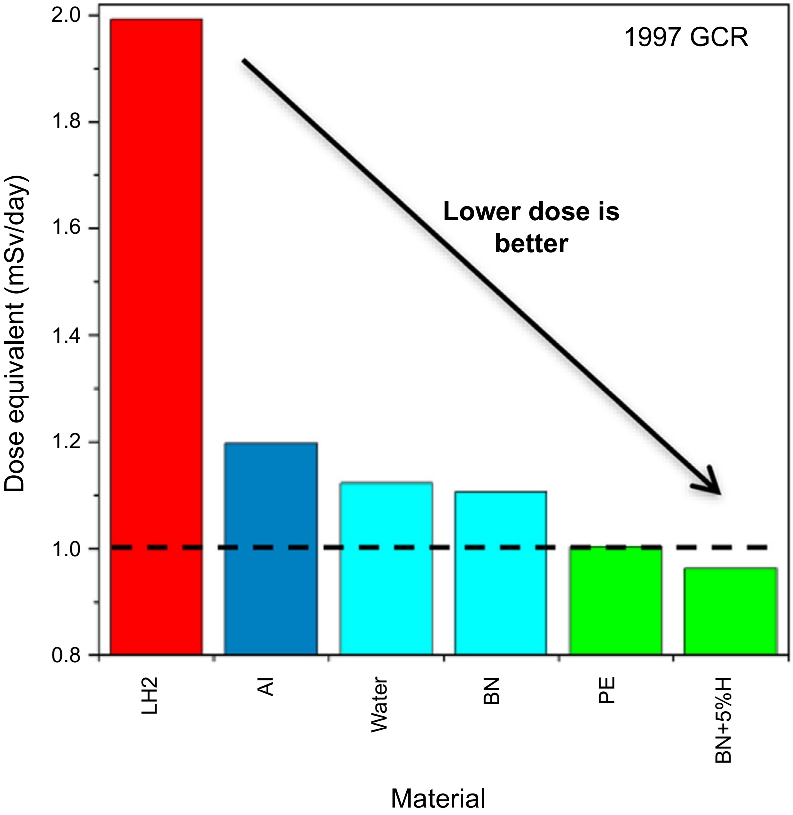

Fig. 3.5 Calculated exposure behind constant 30-cm thick shielding for various materials in a radiation environment similar to the GCR of 1997 [3].

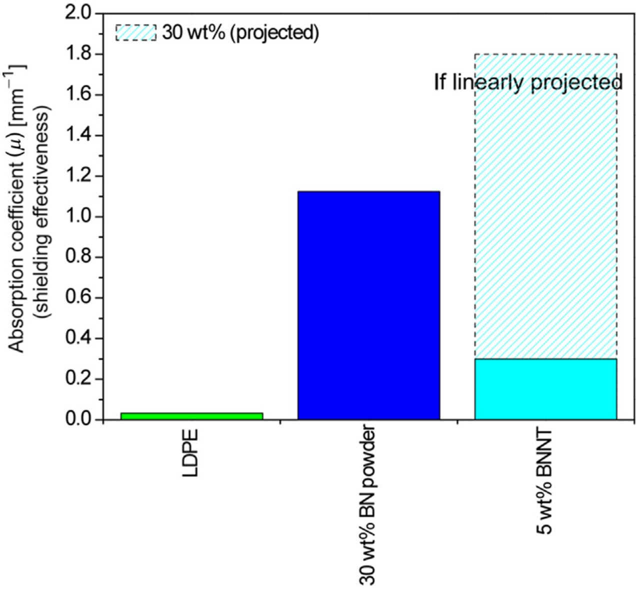

Fig. 3.6 Simulated and projected neutron shielding effectiveness comparing boron nitride powder and boron nitride nanotubes [5].

modest amount of hydrogen (labeled as BN + 5%H) provides better shielding than pure polyethylene and is far more effective at shielding against radiation than one could expect of a simple PE/BN composite.

These results are further supported by other simulations performed by Thibeault et al. as shown in Fig. 3.6 which illustrate the degree of which boron nanotubes may improve the overall shielding effectiveness if the composite's resultant properties can be linearly defined.

3.5.2 Mechanical testing

3.5.2.1 Atomic force microscopy

Atomic force microscopy (AFM) performed in contact mode can be used to generate phase maps which provide information regarding superficial level dispersion profiles. Proper dispersion of the additives will be shown as uniform or similar gradient colors. The greater the color difference, the more different the mechanical properties of those sections are from one another. Graham et al. performed such a test on PE/B_4C and PE/BN composites and their results are shown in Fig. 3.7 [50].

Large red (dark gray color in print version) portions in Fig. 3.7A show the presence of severe B_4C agglomeration. These dramatic differences between the

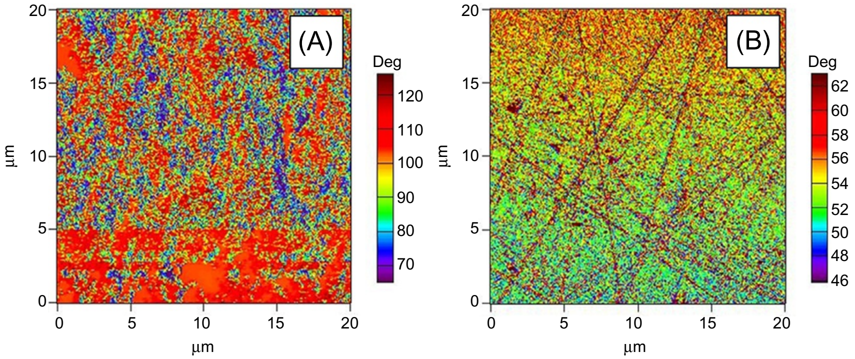

Fig. 3.7 Dispersion profiles of additives in PE: (A) 7 wt% B_4C and (B) 7 wt% BN [50].

red and blue/purple sections show that even at a 7 wt% addition of B_4C, there are issues with the mixing of the matrix and additives used. As previously discussed, agglomerations of such opposing properties can lead to severe problems such as poor radiation shielding as well as mechanical detriments as regions of agglomeration are likely to be more brittle. In contrast, Fig. 3.7B shows more uniform dispersion of BN within the polyethylene sample. One can expect to attain more uniform radiation and mechanical properties making these types of composites more reliable for their respective applications.

These results were used as a primary starting point for Baxter et al.'s research regarding the addition of various weight percentages of BN into HDPE for space radiation shielding composites [39]. Force maps produced using AFM shown in Fig. 3.8 were used to carefully examine the relationship of dispersion of BN with mechanical stiffness at concentrations ranging from pure PE to 15 wt% BN. Please take note of the different color scales when reviewing this data.

The average approximate elastic modulus values for the samples were found to be as follows: (A) 1.0 GPa, (B) 0.7 GPa, (C) 0.4 GPa, (D) 0.6 GPa, and (E) 1.0 GPa. Additive agglomeration became severe at loadings for 15 wt% BN, signaled by the rapid increase in material stiffness shown in red. Samples consisting of 1–10 wt% BN indicated more uniform material dispersion was achieved. Interestingly, low BN content samples displayed a dramatic decrease in material stiffness. This has been attributed to the lubricating effects of BN [39]. If testing with high additions of BN was continued, it can be expected that the resultant composite's stiffness would trend toward that of boron nitride, however, the problem of the occurrence of agglomerates would need to be solved.

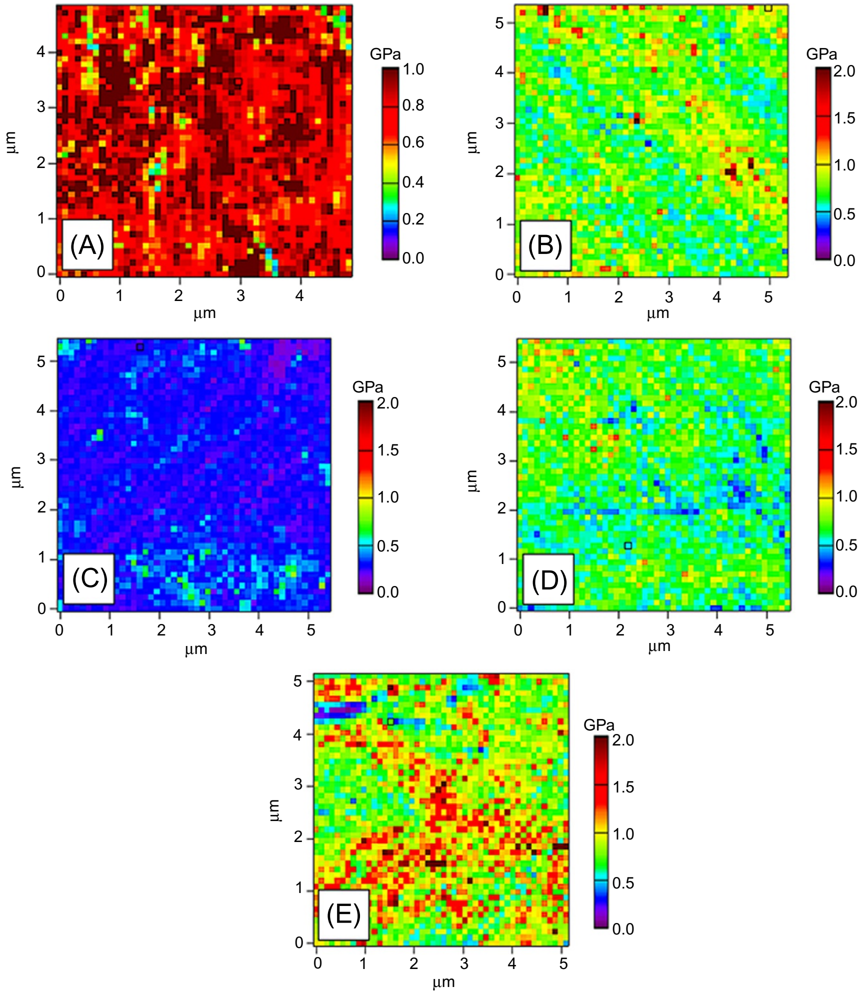

Fig. 3.8 Elastic modulus maps for (A) pure HDPE, (B) HDPE/1 wt% BN, (C) HDPE/5 wt% BN, (D) HDPE/10 wt% BN, and (E) HDPE/15 wt% BN [39].

3.5.2.2 Compression testing

Baxter et al. performed compression tests of HDPE/BN composite samples to further examine the stiffening effect of the BN additive. The results of these tests were compiled and are shown in Fig. 3.9. Overall, compression testing supported the AFM results previously discussed. Initial low weight percent additions of boron nitride resulted in a reduced compressive modulus in the samples, while higher loadings showed a dramatic increase in the compressive modulus from the stiff boron nitride filler [39].

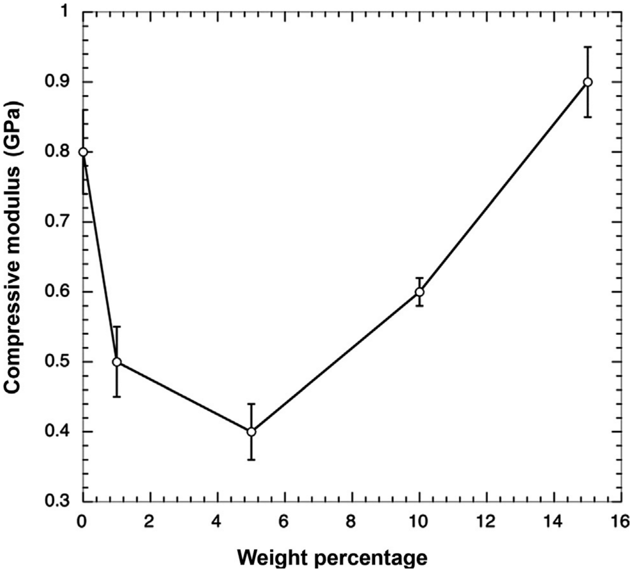

Fig. 3.9 Compressive properties of HDPE/BN composites of various weight percentages [39].

3.5.2.3 Flexural testing

Graham et al.'s results of their flexural testing provide more evidence of the potential risk posed by increasing additive concentrations to the point of agglomerate formation [50]. These results corroborate the claims from another mechanical testing. It was found that samples with inclusion of higher weight percentages of boron nitride and boron carbide suffered from a significant decrease in composite ductility which resulted in brittle failure at lower mechanical loads. This decrease in mechanical strength is attributed to poor dispersion, resulting in accelerated failure due to the extreme difference in mechanical properties between the matrix and additive materials (Fig. 3.10).

3.5.3 Thermal behavior

3.5.3.1 Differential scanning calorimetry

Differential scanning calorimetry (DSC) can be used to determine the glass transition temperature of a given sample. This is an important factor in determining the necessary processing temperature and the maximum curing temperature for composite specimens [50]. Graham et al. completed a study of the glass transition temperate of composites consisting of PE and varying weight percentages of B_4C and BN.

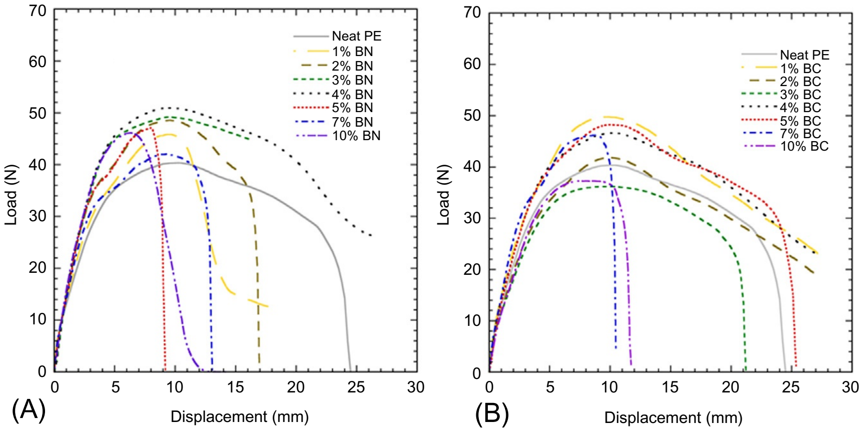

Fig. 3.10 Load-displacement results for composites composed of: (A) PE/BN and (B) PE/B_4C [50].

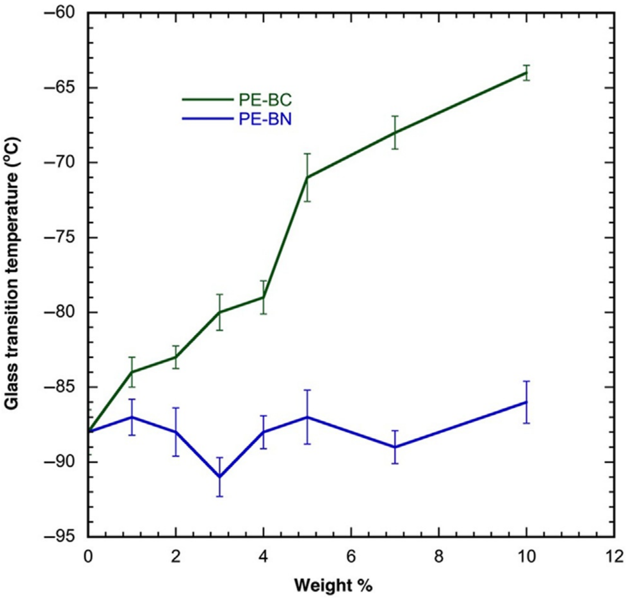

Fig. 3.11 DSC data were compiled to show the additive concentration effect on T_g [50].

Based on the results shown in Fig. 3.11, the glass transition temperature of neat PE is approximately −88°C. With the addition of boron carbide to the polyethylene matrix there is a dramatic increase in glass transition temperature. The addition of boron nitride shows no significant change in the glass transition temperature. These results could be explained with the

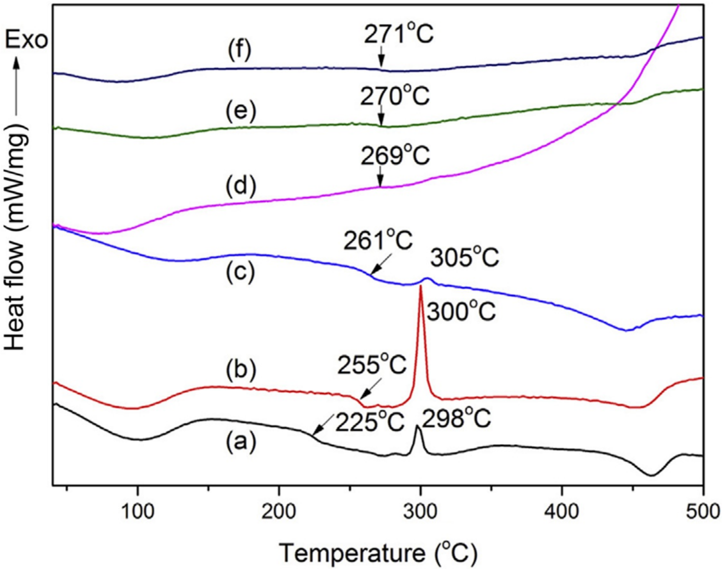

Fig. 3.12 DSC data displaying the effects of varying B_4C content on PI composite T_g. Figure is referenced from a study conducted by Li et al. (A) Pure PI, (B) 15 wt%, (C) 30 wt%, (D) 40 wt%, (E) 45 wt%, and (F) 50 wt% [27].

lubricating effect of boron nitride, whereas boron carbide has a restrictive effect on the molecular chains of polyethylene.

Li et al. also conducted a study on the glass transition temperature of B_4C with varying weight percent in polyimide resin. The results of this are shown in Fig. 3.12. Based on the data, it is shown that the pure resin has a glass transition temperature of approximately 225°C. Similar to the effects shown in Graham's study, the glass transition temperature increases with the addition of boron carbide. However, when the boron carbide content reaches above 30%, the increase in glass transition temperature levels off. This could be explained by the restrictive qualities of boron carbide, as mentioned in the previous study discussion.

3.5.3.2 Thermogravimetric analysis

Thermogravimetric analysis (TGA) was also performed on the materials. Fig. 3.13 shows the results of a TGA experiment conducted by Li et al. to determine if adding boron carbide to polyimide affects the composites at high temperatures. Based on the data, it appears that the polyimide has decomposed at the high temperatures, whereas the boron carbide does not, leaving the boron carbide behind.

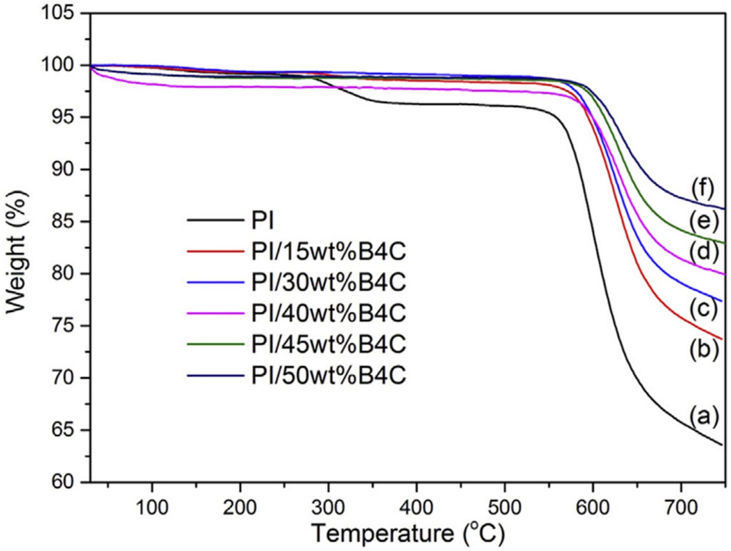

Fig. 3.13 TGA data displaying the effects of varying B_4C content on the composites. The figure is referenced from a study conducted by Li et al. (A) Pure PI, (B) 15 wt%, (C) 30 wt%, (D) 40 wt%, (E) 45 wt%, and (F) 50 wt% [27].

3.5.4 Radiation testing of composites

3.5.4.1 Neutron permeability results

In order to determine the neutron radiation shielding abilities of a material, the neutron permeability I/I_0 can be measured, where I_0 is the intensity of the incident neutron beam and I is the intensity of the neutron beam transmitted through the sample. Li et al. conducted a study on the neutron radiation characteristics of BPDA/ODA/B_4C polyimide composite films with varying B_4C content (0–50 wt%) using a CMRR neutron radiography device [27]. The results of this study are shown in Fig. 3.14. It can be seen that with an increase in B_4C the neutron permeability decreases. This suggests that the addition of B_4C improves the neutron radiation shielding abilities of the polyimide composite material.

In another study, modified boron nitride (mBN) fillers, functionalized with an organosilane, were studied; the neutron transmission (I/I_0) was compared for HDPE/BN, HDPE/mBN, and HDPE/B_4C composites with varying filler contents (0–200 phr) [51]. This experiment was conducted using a ^{252}Cf neutron source of 2.1 MeV, and was moderated by passing through an HDPE plate to allow for the focus on low-energy neutrons. The results are shown in Fig. 3.15.

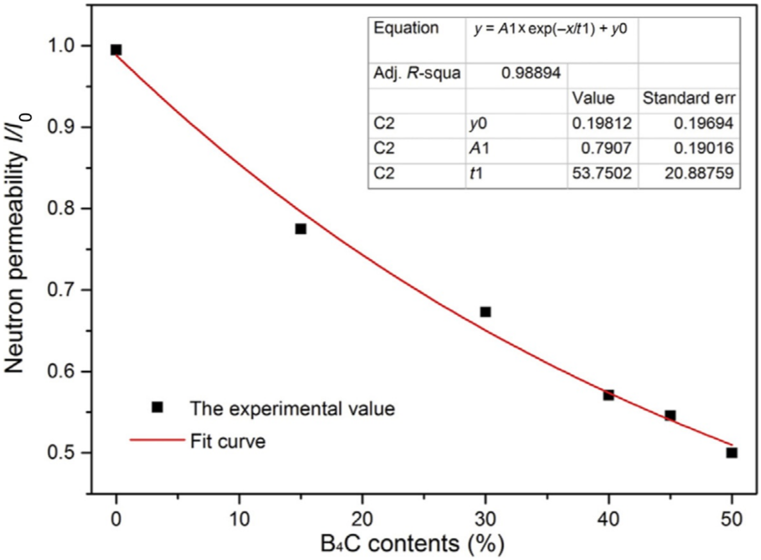

Fig. 3.14 The relationship of neutron permeability and B_4C filler content in PI composite films [27].

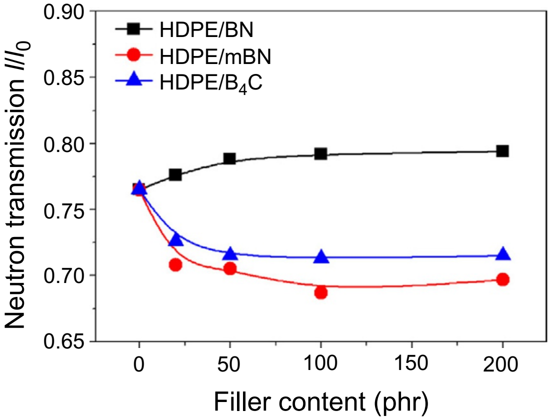

Fig. 3.15 Neutron transmission plotted against boron-based filler content [51].

The HDPE/B_4C data was consistent with the data presented in the previous study by Li. The addition of B_4C to HDPE and PI both resulted in the I/I_0 value decreasing and therefore shows an enhancement in the neutron shielding abilities of the composites. The HDPE/BN values showed an increase in the neutron transmission number, which was unexpected. This result could be due to a weak interfacial adhesion between the HDPE and BN [51]. The HDPE/mBN data gave the best results during this study with the lowest values for neutron transmission factor.

3.5.4.2 Neutron absorption results

Neutron exposure can also be measured by determining the mass absorption cross section for neutrons, or the shield effectiveness. Herrman et al. conducted a study to determine this value for HDPE/BN composite materials using 1%, 5%, and 30% BN content. The neutron exposure was performed at NASA Langley Research Center using a 1-Curie Americium-Beryllium (AM-BE) neutron source, which was moderated using a polyethylene block. Like the previously discussed study done by Shin et al., the polyethylene block is used to slow the fast neutrons to thermal neutrons. The mass absorption cross section was found by using the following equation:

$$\mu_m = \frac{-1}{d^* t} \ln\left(\frac{A}{A_0}\right)$$

where μ_m is the mass absorption cross section for thermal neutrons, t is the sample thickness, d is the sample density, A_0 is the average initial activity of the unshielded foil, and A is the average initial activity of the shielded foil [52].

The mass absorption, also discussed as shield effectiveness, for the HDPE/BN samples can be seen in Fig. 3.16. This data shows that the amount of boron nitride in the sample does affect the mass absorption of the composite. At higher amounts of boron nitride better shielding effectiveness is achieved.

3.6 Conclusions

This chapter focused on providing a basic understanding of thermoplastic micro- and nanocomposites and the considerations that must be given when designing these composites for applications that are sensitive to radiation environments, specifically those consisting of exposure to neutron radiation. As the potential materials for such applications are numerous, only a few were selected for discussion. Matrix and additive materials were chosen based on their recent increased interest in research conducted by universities and organizations with vested interests in shielding against neutron radiation such as space exploration organizations like NASA. As the future aims toward in-depth space exploration and final touchdown on the Martian

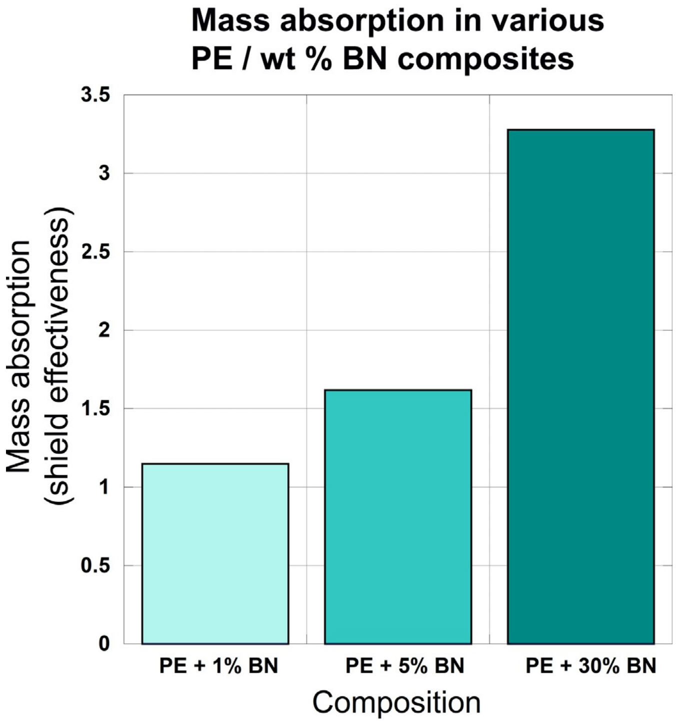

Fig. 3.16 Resultant data from neutron radiation exposure tests of PE/BN composites [52].

surface, there is extensive research which must be performed to further improve upon previous studies regarding composite materials with valuable radiation shielding properties.

References

[1] J.W. Wilson, M. Kim, W. Schimmerling, F.F. Badavi, S.A. Thibeault, F.A. Cucinotta, J.L. Shinn, R. Kiefer, Issues in space radiation protection: galactic cosmic rays, Health Phys. 68 (1995) 50–58.

[2] K. Hurlbert, B. Bagidigian, C. Carroll, A. Jeevarajan, M. Kliss, B. Singh, Human Health, Life Support and Habitation Systems, Technology Area 06, 2012, pp. 1–27.

[3] S.A. Thibeault, C.C. Fay, S.E. Lowther, K.D. Earle, G. Sauti, J.H. Kang, C. Park, A.M. McMullen, Radiation Shielding Materials Containing Hydrogen, Boron, and Nitrogen: Systematic Computational and Experimental Study—Phase I, NIAC Final Report, (2012) pp. 1–29.

[4] J.W. Norbury, T.C. Slaba, S. Aghara, F.F. Badavi, S.R. Blattnig, M.S. Clowdsley, L.H. Heilbronn, K. Lee, K.M. Maung, C.J. Mertens, J. Miller, R.B. Norman, C.A. Sandridge, R. Singleterry, N. Sobolevsky, J.L. Spangler, L.W. Townsend,

C.M. Werneth, K. Whitman, J.W. Wilson, S.X. Xu, C. Zeitlin, Advances in space radiation physics and transport at NASA, Life Sci. Space Res. (2019), https://doi.org/10.1016/j.lssr.2019.07.003.

[5] Sheila A. Thibeault, Catharine C. Fay, Kevin D. Earle, Godfrey Sauti, Jin Ho Kang, Cheol Park, Radiation Shield Materials Containing Hydrogen, Boron, and Nitrogen: Systematic Computational and Experimental Study, Presented at NIAC.

[6] R.C. Singleterry Jr., S.A. Thibeault, Materials for Low-Energy Neutron Radiation Shielding, NASA TP, 2000, pp. 1–14.

[7] A.L. Tiano, C. Park, J.W. Lee, H.H. Luong, L.J. Gibbons, S.-H. Chu, S. Applin, P. Gnoffo, S. Lowther, H.J. Kim, P.M. Danehy, J.A. Inman, S.B. Jones, J.H. Kang, G. Sauti, S.A. Thibeault, V. Yamakov, K.E. Wise, J. Su, C.C. Fay, Boron Nitride Nanotube: Synthesis and Applications, SPIE 9060 Nanosensors, Biosensors, and Info-Tech Sensors and Systems 2014 906006, 2014, pp. 1–19, https://doi.org/10.1117/12.2045396.

[8] R.K. Tripathi, J.W. Wilson, F.A. Cucinotta, J.E. Nealy, M.S. Clowdsley, M.H. Y. Kim, Deep Space Mission Radiation Shielding Optimization, 2001, https://doi.org/10.4271/2001-01-2326.

[9] J. Miller, C. Zeitlin, F.A. Cucinotta, L. Heilbronn, D. Stephens, J.W. Wilson, Benchmark studies of the effectiveness of structural and internal materials as radiation shielding for the international space station, Radiat. Res. 159 (3) (2003) 381–390, https://doi.org/10.1667/0033-7587(2003)159[0381:BSOTEO]2.0.CO;2.

[10] M.H. Kharita, S. Yousef, M. AlNassar, Review on the addition of boron compounds to radiation shielding concrete, Progr. Nucl. Energy 53 (2) (2011) 207–211, https://doi.org/10.1016/j.pnucene.2010.09.012.

[11] Y. Huang, W. Zhang, L. Lu, J. Xu, Z. Chen, A "Sandwich" type of neutron shielding composite filled with boron carbide reinforced by carbon fiber, Chem. Eng. J. 220 (2013) 143–150, https://doi.org/10.1016/j.cej.2013.01.059.

[12] A. Labouriau, T. Robison, C. Shonrock, S. Simmonds, B. Cox, A. Pacheco, C. Cady, Boron filled siloxane polymers for radiation shielding, Radiat. Phys. Chem. 144 (2018) 288–294, https://doi.org/10.1016/j.radphyschem.2017.08.027.

[13] J.W. Wilson, F.A. Cucinotta, J. Miller, J.L. Shinn, S.A. Thibeault, R.C. Singleterry, L.C. Simonsen, M.H. Kim, Materials for Shielding Astronauts From the Hazards of Space Radiations, (1997), https://doi.org/10.1557/PROC-551-3.

[14] https://www.azom.com/article.aspx?ArticleID=6616, Last Accessed: August 13, 2019.

[15] http://asm.matweb.com/search/SpecificMaterial.asp?bassnum=MA2219T851, Last Accessed: August 13, 2019.

[16] https://www.azom.com/article.aspx?ArticleID=6636, Last Accessed: August 13, 2019.

[17] http://asm.matweb.com/search/SpecificMaterial.asp?bassnum=MA6061T6, Last Accessed: August 13, 2019.

[18] https://www.azom.com/article.aspx?ArticleID=6615, Last Accessed: August 13, 2019.

[19] http://asm.matweb.com/search/SpecificMaterial.asp?bassnum=MA2024T4, Last Accessed: August 13, 2019.

[20] C. Lobascio, M. Briccarello, R. Destefanis, M. Faraud, G. Gialanella, G. Grossi, V. Guarnieri, L. Manti, M. Pugliese, A. Rusek, P. Scampoli, M. Durante, Accelerator-based tests of radiation shielding properties of materials used in human space infrastructures, Health Phys. 94 (2008) 242–247, https://doi.org/10.1097/01.HP.0000288560.21906.4e.

[21] Z. Soltani, A. Beigzadeh, F. Ziaie, E. Asadi, Effect of particle size and percentages of Boron carbide on the thermal neutron radiation shielding properties of HDPE/B4C composite: Experimental and simulation studies, Radiat. Phys. Chem. 127 (2016) 182–187, https://doi.org/10.1016/j.radphyschem.2016.06.027.

[22] X. Zhang, M. Yang, X. Zhang, H. Wu, S. Guo, Y. Wang, Enhancing the neutron shielding ability of polyethylene composites with an alternating multi-layered structure, Compos. Sci. Technol. 150 (2017) 16–23, https://doi.org/10.1016/j.compscitech.2017.06007.

[23] M. Scott, R. Vaidyanathan, Radiation Smart Structures With H-rich Nanostructured Multifunctional Materials Annual Performance Report YR3, NASA EPSCoR 2014-2017, (2017).

[24] https://polymerdatabase.com/Commercial%20Polymers/HDPE.html, Last Accessed: August 13, 2019.

[25] https://polymerdatabase.com/Commercial%20Polymers/LDPE.html, Last Accessed: August 13, 2019.

[26] P.D. McCormack, Radiation dose and shielding for the space station, Acta Astron. 17 (2) (1988) 231–241.

[27] X. Li, J. Wu, C. Tang, Z. He, P. Yuan, Y. Sun, W.-m. Lau, K. Zhang, J. Mei, Y. Huang, High temperature resistant polyimide/boron carbide composites for neutron radiation shielding, Compos. B: Eng. 159 (2019) 355–361, https://doi.org/10.1016/j.compositesb.2018.10.003.

[28] https://omnexus.specialchem.com/polymer-properties/properties/glass-transition-temperature, Last Accessed: August 13, 2019.

[29] F. Xuelong, X. Tang, Y. Hu, H. Li, J. Tao, Effect of different lay-ups on the microstructure, mechanical properties and neutron transmission of neutron shielding fibre metal laminates, J. Nucl. Mater. 475 (2016) 227–236, https://doi.org/10.1016/j.jnucmat.2016.04.021.

[30] Y. Mülazim, C. Kızılkaya, M.V. Kahraman, Thermal and neutron shielding properties of $^{10}B_2O_3$/polyimide hybrid materials, M.V. Polym. Bull. 67 (9) (2011) 1741–1750, https://doi.org/10.1007/s00289-011-0481-4.

[31] P. Wang, X. Tang, H. Chai, D. Chen, Y. Qiu, Design, fabrication, and properties of a continuous carbon-fiber reinforced Sm_2O_3/polyimide gamma ray/neutron shielding material, Fusion Eng. Des. 101 (2015) 218–225, https://doi.org/10.1016/j.fusengdes.2015.09.007.

[32] D.H. Berkebile, D.L. Stevenson, The Use of "Kapton" Polyimide Film in Aerospace Applications, in: SAE International, 1981, https://doi.org/10.4271/811091.

[33] ARES Corporation, National Aeronautics and Space Administration, Wire to Wire, System Failure Case Studies, vol. 4(2), (2010) pp. 1–4.

[34] J. Megusar, Low temperature fast-neutron and gamma irradiation of Kapton polyimide films, J. Nucl. Mater. 245 (2–3) (1997) 185–190, https://doi.org/10.1016/S0022-3115(97)00012-3.

[35] Mitsui Chemicals Inc., Technical Data Sheet: AURUM PL450C Thermoplastic Polyimide, https://www.dupont.com/content/dam/dupont/products-and-services/plastics-polymers-and-resins/parts-and-shapes/vespel/documents/pl450c.pdf, Last Accessed: August 13, 2019.

[36] S. Kazano, T. Osada, S. Jobayashi, K. Goto, Experimental and analytical investigation on resin impregnation behavior in continuous carbon fiber reinforced thermoplastic polyimide composites, Mech. Adv. Mater. Modern Process. (2016), https://doi.org/10.1186/s40759-018-0039-3.

[37] DuPont, DuPont KAPTON Summary of Properties, https://www.dupont.com/content/dam/dupont/products-and-services/membranes-and-films/polyimde-films/documents/DEC-Kapton-summary-of-properties.pdf, Last Accessed: August 13, 2019.

[38] M.H. Kharita, S. Yousef, M. AlNassar, Review on the addition of boron compounds to radiation shielding concrete, Progr. Nucl. Energy 53 (2) (2011) 207–211, https://doi.org/10.1016/j.pnucene.2010.09.012.

[39] L. Baxter, K. Herrman, N. Graham, K. Mishra, R. Panthi, E. Benton, R.P. Singh, R. Vaidyanathan, Fabrication, testing and characterization of polyethylene-based thermoplastic composite materials for radiation shielding, in: Annual Society for Advanced Manufacturing and Process Engineering (SAMPE) Meeting, Long Beach, CA, May 21–24, 2018.

[40] https://www.azom.com/article.aspx?ArticleID=78, Last Accessed: August 13, 2019.

[41] https://www.azom.com/properties.aspx?ArticleID=75, Last Accessed: August 13, 2019.

[42] J. Kim, B.-C. Lee, Y.R. Uhm, W.H. Miller, Enhancement of thermal neutron attenuation of nano-B4C, -BN dispersed neutron shielding polymer nanocomposites, J. Nucl. Mater. 453 (1–3) (2014) 48–53, https://doi.org/10.1016/j.jnucmat.2014.06.026.

[43] C. Harrison, S. Weaver, C. Bertelsen, E. Burgett, N. Hertel, E. Grulke, Polyethylene/boron nitride composites for space radiation shielding, J. Appl. Polym. Sci. 109 (2008) 2529–2538, https://doi.org/10.1002/app.27949.

[44] J. Polvi, K. Nordlund, Irradiation effects in high-density polyethylene, Nucl. Instrum. Methods Phys. Res. Sect. B: Beam Interact. Mater. Atoms 312 (2013) 54–59, https://doi.org/10.1016/j.nimb.2013.07.002.

[45] M.F. Zaki, Y.H. Elshaer, D.H. Taha, The alterations in high density polyethylene properties with gamma irradiation, Radiat. Phys. Chem. 139 (2017) 90–96, https://doi.org/10.1016/j.radphyschem.2017.02.058.

[46] M.J. Saif, M. Naveed, H.M. Asif, R. Akhtar, Irradiation applications for polymer nanocomposites: a state-of-the-art review, J. Ind. Eng. Chem. 60 (2018) 218–236, https://doi.org/10.1016/j.jiec.2017.11.009.

[47] L. Calcagno, G. Compagnini, G. Foti, Structural modification of polymer films by ion irradiation, Nucl. Instrum. Methods Phys. Res. B65 (1993) 413–422.

[48] G. Hu, H. Hu, Q. Yang, B. Yu, W. Sun, Study on the design and experimental verification of multilayer radiation shield against mixed neutrons and gamma rays, Nucl. Engi. Technol. (2019), https://doi.org/10.1016/j.net.2019.07.016.

[49] J. Cassidy, S. Nesaei, R. McTaggart, F. Delfanian, Mechanical response of high density polyethylene to gamma radiation from a Cobalt-60 irradiator, Polym. Test. 52 (2016) 111–116, https://doi.org/10.1016/j.polymertesting.2016.04.005.

[50] N. Graham, K. Mishra, J. Bejarano, R.P. Singh, R. Vaidyanathan, Evaluation of thermal and physical properties of boron compound reinforced high density polyethylene (HDPE), in: Annual Society for Advanced Manufacturing and Process Engineering (SAMPE) Meeting, Seattle, WA, May 22–25, 2017.

[51] J.W. Shin, J.-W. Lee, S. Yu, B.K. Baek, J.P. Hong, Y. Seo, W.N. Kim, S.M. Hong, C.M. Koo, Polyethylene/boron-containing composites for radiation shielding, Thermochim. Acta 585 (2014) 5–9, https://doi.org/10.1016/j.tca.2014.03.039.

[52] K. Herrman, L. Baxter, K. Mishra, E. Benton, R. Singh, R. Vaidyanathan, Mechanical characterization of polyethylene-based thermoplastic composite materials for radiation shielding, Compos. Commun. 13 (2019) 37–41, https://doi.org/10.1016/j.coco.2019.02.007.

CHAPTER 4

Thermosetting micro- and nanocomposites for neutron radiation shielding

Noureddine Ramdani[a,b]
[a]Polymer Materials Research Center, College of Materials Science and Chemical Engineering, Harbin Engineering University, Harbin, China
[b]Department of Advanced Materials, RDI-IDT, Blida, Algeria

4.1 Introduction

Energetic radiation particles including α/β particle, γ-ray, and neutron particle emissions are usually produced as a by-product in various industries including nuclear power plants, health-care industry, and aerospace. Unexpected exposures to such radiations can provoke carcinogenesis, cell mutations, and organ failure in workers. However, the implications of these exposures are related to several factors including the kind of radiation and its inherent energy, the amount of subjected dose that the body absorbed, time of exposure, etc.

Neutron radiation is the most harmful kind of radiation. Due to their strong penetration power, they could engender significant damage to both equipment and human beings [1]. Prolonged exposure to neutron radiation can provoke serious radiobiological effects such as carcinogenesis and DNA damage [2]. To mitigate the dangerous effects of neutron radiation, scientists should try to understand the mechanism of interaction between neutrons and target materials. Neutrons are not electrically charged particles which could easily pass through electron clouds, and collide with the target nuclei, thus fusing with the target nuclei and simultaneously emitting harmful radiation such as X-rays and gamma radiation present great challenges for the researchers in studying neutron-shielding materials. The most polymer composites used for shielding neutrons can only be effective for low-energy neutrons; they are unable to shield high-energy or high doses of neutrons. Moreover, after the scattering process of fast neutrons on the target, the slower or thermal neutrons could generally be absorbed by boron-containing fillers [3].

Micro and Nanostructured Composite Materials for Neutron Shielding Applications
https://doi.org/10.1016/B978-0-12-819459-1.00004-0
© 2020 Elsevier Ltd.
All rights reserved.

To mitigate the danger of nuclear radiation exposures, researchers have firstly utilized heavy metals or their reinforced concretes to attenuate such radiation. However, protective articles made of these materials are not only weighty but also generate more penetrative secondary radiations which require more expensive and heavy additional shielding. Thus, the tendency of research is directed to design economic, perfromant, lightweight, and flexible shields for protection against these radiations. In this aspect, thermosetting micro- and nanocomposites are considered suitable materials for designing an effective attenuate neutron radiation shields.

In this chapter, the state of the art of thermosetting polymer composites reinforced with micro/nanofillers, for their use as neutron radiation shields, is targeted. In addition, the properties and the shielding mechanisms involved during the protection against neutron radiation of these composites are reviewed along with some examples from the literature.

4.2 Polymer composites for neutron radiation shielding

To determine neutron attenuation, the effective removal cross section (Σ_R) of any material is considered as a macroscopic cross section. Since all interactions help in removing energy from the fast neutron beam and as a result Σ_R value is slightly lower than that of the total (scattering and capture) macroscopic cross section Σ_t of the material. Thus, Σ_R (cm^{-1}) can be determined experimentally for each shielding material by combining its removal coefficients. These effective removal cross sections are utilized by applying the exponential absorption equation to validate the results of the fast neutrons attenuation [4].

In Ref. [5], authors concluded from their finding that the composite 12.5, 37.5, 25, and 25 wt% (C_6) had the most efficient performance as a shielding material against Am-Be neutrons with energy 4.5 MeV and ^{60}Co gamma radiation as compared with the other composites. The half-value thickness for neutron was 6.9 cm and gamma was 5.5 cm. This new composite demonstrated outstanding performance when applied as a paste on various surfaces which makes it suitable for practical uses as compared with the present commercial shielding materials. The application of this shielding is promising for shielding and transporting the chemical isotopes due to its lower cost; in addition, it can play an important role as a shielding for experiments in experimental nuclear reactor.

To produce an efficient shielding for attenuating fast neutrons, light elements such as hydrogenous compounds mixed with boron material can be used to attenuate fast neutrons through elastic scattering process and that is recommended for increasing neutrons reaction $^{10}B_5$ (n, α) $^{7}Li_3$ cross section [6]. By absorbing neutrons, gamma rays with an energy of 2.2 MeV (secondary gamma) are generated, which demand more enhancement in the thickness of the shield [7]. Thus, an effective radiation shield consists of a combination of hydrogenous materials or other low-A materials to control neutron, thermal neutron absorbs, and high-Z materials for absorbing gamma rays.

Recently, numerous studies have been conducted to develop novel concrete by varying the properties of their various compositions and cement [8, 9]. Trials were made to decrease the thickness of concrete by adding borated polyethylene/borax and composite materials for enhancing their shielding efficiency and it was demonstrated that the research activities on the concrete significantly decreased with this replacement [10, 11]. Moreover, addition of borax ($Na_2B_4O_{75}H_2O$) has no significant affect on the mechanical strength of concrete, but it reduces the capture gamma rays up to 80% better than unborated concretes [12]. Besides, processing of the main components of concrete through mineral additives at different ratios can influence the attenuation parameters for neutron including linear attenuation coefficient (μ, cm^{-1}), mass attenuation coefficients (μ/ρ, cm^2 g^{-1}), and effective atomic numbers of the concrete [13]. For example, many previous studies have only evaluated the photon attenuation coefficients and treatment for neutron attenuation subjects is not reported [14, 15].

As the most efficient shielding material for mixed-radiation of neutron and gamma rays is usually prepared by blending borated hydrogenous materials with heavy metal elements so that it produces very thick barrier of large thickness, which need and has relatively expensive fabrication cost [16]. Therefore, many studies have been conducted to compromise between materials that can attenuate fast neutrons and γ-rays simultaneously. For instance, by using high-density polyethylene and borax mixed with cement and sand a composite paste (mold) can be prepared, which can be used in radiation attenuation shields suitable for various applications.

According to previous researches, scientists have focused investigation on the morphologies and types of functional fillers, which mainly control the shielding efficiency and mechanical performance of thermoplastic composites. For example, Kim et al. [17] have developed nano-boron carbide (B_4C) and boron nitride (BN) particle-reinforced polymer composites using a conventional melt mixing technique. Their results revealed that the homogeneous dispersion of boron-containing fillers improved the neutron-shielding efficiency and mechanical performance of their resulted composites. To enhance the interfacial adhesion between BN and the polymer matrix, BN was regularly modified using coupling agents [18].

In Ref. [19], a new kind of neutron-shielding polyamide sandwich composite coated with carbon fiber was studied in view of the urgent need for nuclear protective materials. Compared to the B_4C filler directly incorporated in the composite, it generated a marked performance enhancement in the mechanical properties as the content of B_4C reached 20 wt%, the neutron-shielding performance significantly upgraded in the presence of carbon fiber as illustrated in Fig. 4.1.

The attenuation capacities of some locally available wood and fiber-reinforced polyethylene polymer composite samples were investigated by Shamsuzzaman et al. [20] in terms of relative attenuation factor (RAF), linear

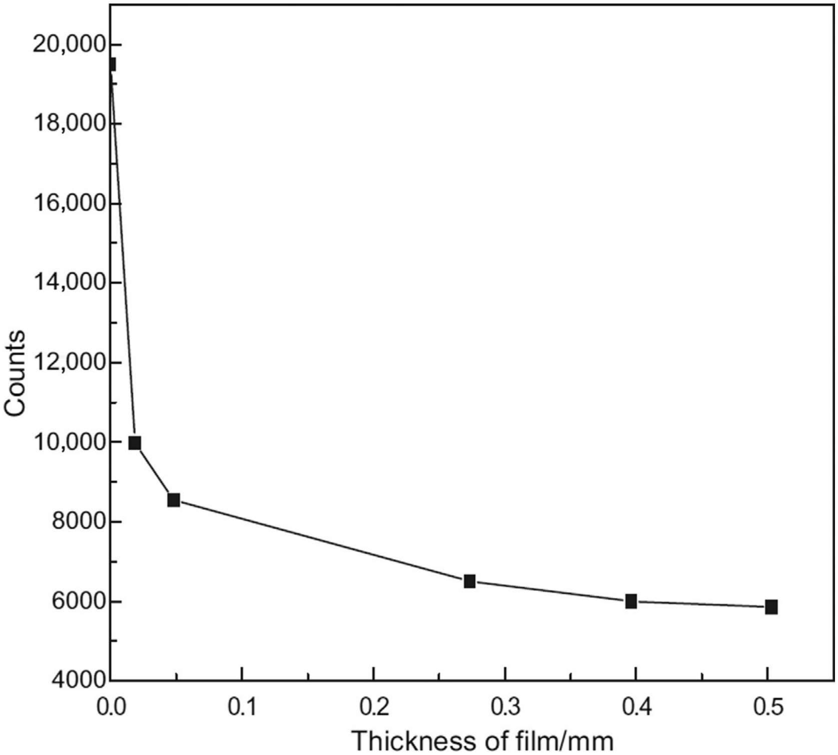

Fig. 4.1 Relationship between counts and the thickness of film. *(Reprinted from Y. Huang, W. Zhang, L. Liang, J. Xu, Z. Che, A "Sandwich" type of neutron shielding composite filled with boron carbide reinforced by carbon fiber, Chem. Eng. J. 220 (2013) 143–150. Copyright 2013, with permission from Elsevier.)*

attenuation (μ), and mass-attenuation coefficients (μ/ρ). A descending trend of RAF was observed for all the studied polyethylene composites for both gamma photon and neutron beams. For neutron beam, both glass fiber composite and jute composite specimens showed increased attenuation capacity compared to wood samples in terms of μ. Therefore, glass fiber and jute composites had an excellent shielding worth in the case of neutron beam. Thus, the explored materials have great chance for the potential shielding applications in scientific laboratory, medical, and industrial shielding purposes.

Evans et al. investigated the contributing factors behind the success of newly designed composite materials for neutron shielding [21]. Monte Carlo simulation methods were utilized to assess the shielding capabilities for neutron and the secondary radiation production characteristics in several composite materials: aluminum boron carbide, tungsten boron carbide, bismuth borosilicate glass, and metathene. The collected data relative to shielding performance and the generation of secondary radiation revealed that tungsten boron carbide had the highest ability to shielding composite. The obtained results show that increased thermal absorber loading caused improvement in neutron-shielding ability within both the thermal and epithermal neutron energy regions and that composites containing low-Z material showed better shielding efficiency within the faster neutron energy regions. Megusar [22] prepared S2-glass fiber/epoxy composites by deformation and fracture processes followed by 4.2 K fast-neutron and gamma irradiation technique. Irradiation to fast-neutron fluences of 0.9 and 1.8×10^{22} n/m^2 eased the glass/epoxy interface debonding by lowering its interface strength.

4.3 Concrete-based neutron-shielding materials

Tuna and Bayrak studied the neutron-shielding capabilities of colemanite-reinforced materials with concrete matrix. Composite having 20, 40, and 60 mm thicknesses and containing 70 wt% colemanite were prepared by hand mixing technique and their performance of neutron radiation shielding was experimentally analyzed with Am-Be neutron source measurement system [23]. It was found that the shielding capacity of the produced composite material increased with increase in its thickness.

Concretes that are designed for applications in neutron-generating facilities, including fission reactors become radioactive due to neutron irradiation. Low-activation and neutron-shielding materials are highly recommended at the dismantling stage with the increasing need for radioactive waste management. To improve these parameters, synthetic thermoset-based mortar was elaborated by Min et al. [24]. The mass of hydrogen in these concrete composites is similar to that of a neutron, and it effectively absorbs neutrons through increasing the probability of elastic scattering. It is well known that thermosetting polymers are composed of numerous hydrogen atoms. Resins containing mortar mixtures were studied to understand the effect of resin on the mechanical properties of mortar as well as on its neutron-shielding performance. The experimental data revealed that the neutron dose equivalent to a thermoset-based blend decreased by 63.86% compared to that of conventional mortar, although the mechanical properties need to be improved via a special modification. It indicated great potential to decrease not only the thickness of the neutron shields but also the amount of radioactive waste.

Neutrons shielding polymeric materials are widely applied in fields like aeronautic, medical, space, and nuclear sector and there is an increasing need for neutron-shielding materials exhibiting high-temperature resistance. This is difficult to achieve with the current approach of using borated or lithium-enriched polyethylene or polyamide composites because their hydrogen content limits temperature resistance to 200°C. Thus, the design and production of thermosetting-based composites can overcome these serious practical problems which are usually associated with thermoplastic-based neutron-shielding materials. Another way to address this challenge is using elastomer-based neutron-shielding material developed with a degradation temperature greater than 300°C and a macroscopic neutron cross section better than that of 5 wt% borated polyethylene. By compensating for the low number of hydrogen atoms in such composite, compared to some thermoplastic polymers, iron or other inorganic fillers with a high neutron absorption cross section can be included to reach the recommended attenuation performance [25].

4.4 Thermosetting matrices

Thermosetting matrices are predominant today than thermoplastic polymeric materials for manufacturing advanced composite materials. Thermosetting resins play a critical role in many industries owing to their high modulus, mechanical strength, durability against weather change, good thermal stability, and the high chemical resistance, which are promoted by high cross-linking density. These thermoset can be synthesized using different methods such as polycondensation reaction of two or more raw materials in the presence or absence of catalyst. For practical aspects, the cured thermosets can be effectively recycled if they were grounded into fine particles, before incorporating them into new laminates or other products as reinforcing fillers.

Thermosetting matrices have a restricted use as pure systems, thus they generally need the inclusion of other chemicals to facilitate their processability. For reinforced plastics, they usually constitute a modified resin system (with curing agents, hardeners, inhibitors, plasticizers) and one or more reinforcing phase. The resin matrix plays the role of a binder, to a large extent controlling the cost, dimensional stability, heat and chemical resistance, and flammability property. The reinforcing agents can be tailored (particularly heat and dimensional stability) but the main effect is on tensile strength and toughness. High-performance fibers, such as carbon, glass, and Kevlar, also have a fundamental effect on production cost of thermosetting composites.

Specific fillers or modifiers can significantly affect the mechanical properties of a thermosetting composite, especially for the dimensional stability, but they are essentially utilized to confer other specific properties, including flame retardancy, ultraviolet (UV) resistance, and electrical conductivity. Thermosetting matrices are generally used as viscous liquid which solidify and harden upon curing process. With some thermosets known as the B-stage resin, it is possible to partly cure them and then stored for completing their cure at a later time.

4.5 Thermosetting micro- and nanocomposites for neutron radiation shielding

From the past to the present day, neutron radiation shielding has been explored with various types of materials and different shielding products have been developed and tested. In a large part of recent works thermosetting composites are mostly preferred for this application. The main target in neutron-shielding studies based on both polymer and metal matrix composite materials is to thermalize the neutrons with light nucleus in these matrics, then absorbing the thermalized neutrons with high thermal neutron cross-sectioned reinforcement materials. Lightweight thermosetting shielding composites can be produced with polymer matrix materials to replace the heavy conventional metal matrixed shielding materials. In the following sections, various thermosetting composites designed for neutron-shielding applications are summarized.

4.5.1 Epoxy composites

Epoxy resin is a chemically adhesive thermoset showing a stable strength over time under aggressive weathering conditions. It is commonly used to fabricate fiber-reinforced polymer composites. It is extensively used in textile manufacturing, food industry, pharmaceutical industry, automobile services, petrochemical plants, printers, aerospace, plastics industry, coatings, and many other industries. Epoxy matrix was widely used to prepare composite materials exhibiting improved thermal, mechanical, and electrical properties.

Due to its good thermal and mechanical properties compared with other polymers, epoxy resin was widely used in the nuclear safety industry and has been investigated as radiation-shielding material in the past decade. Shielding/absorbing characteristics of carbon nanotube (CNT)-embedded epoxy composites were determined and electromagnetic interference (EMI)-shielding effectiveness and sheet resistance made of these composites were scrutinized with variation of thickness [26]. Insulating epoxy/barite and cross-linked unsaturated polyester/barite composites were developed and their radiation attenuation and shielding capabilities were evaluated. To design these new radiation shields MCNP4C Monte Carlo code was utilized [27]. A new epoxy thermoset reinforced with boron carbide (B_4C) was studied and demonstrated two main functions of adhesive and radiation shielding efficiency [28]. To protect against a high-frequency radiation attack, new epoxy composites were developed by adding graphite, lead, and boron nitride fillers [29]. High-performance electromagnetic radiation-shielding composites composed of short carbon fiber-filled epoxy were explored and irradiation, thermal, and mechanical properties were determined [30].

Hsu et al. developed a glass fiber/epoxy/silica nanoparticle/c-APTES hybrid composite as a shielding material against high-energy radiation [31]. Many types of functional particle-modified epoxy multilayer composites for gamma radiation-shielding purpose, which were composed of lead acrylate/erbium oxide/epoxy and tungsten oxide/erbium oxide/epoxy layer by layer, were successfully elaborated [32]. PbO/epoxy and Pb_3O_4/epoxy composites for X-ray radiation-shielding applications were produced, and mass attenuation characteristics were determined [33]. Usability of epoxy/ilmenite composite material as an attenuator for radiation and a restoration mortar for cracks was investigated, and fast neutron, thermal neutron, and gamma ray-shielding experiments and MCNP Monte Carlo simulations were studied [34].

Recently, epoxides reinforced with different inorganic fillers have been used as radiation-shielding materials against both gamma rays and neutron particles. Aygün et al. evaluated the neutron-shielding capacity of an epoxy filled by molybdenum powder additive, which was increased with the inclusion of the metallic fillers [35]. With the addition of molybdenum particles, the simulation and experimental results showed that the total neutron macroscopic cross section value increased from 0.1597 to 0.4522 cm^{-1} and equivalent dose rate attenuation was increased by almost 12%, respectively. This new composite material can be used for neutron-shielding purposes. Okuno incorporated colemanite mineral into the epoxy matrix, which found to exhibit high neutron-shielding capacity and are suitable for practical use [36].

In another study [37], a low-viscosity epoxy resin modified with amine-based curing agent was used as matrix reinforced with B_4C particle by applying low speed stirring via the application of ultrasonic waves. The purpose of adding B_4C particle size (20 and 150 μm) on neutron shielding was scrutinized. In addition, to produce high-performance composites, the influence of ATH (flame retardant) and WO_3 fillers (for shielding from gamma rays) on neutron-shielding characteristic was also taken into account. The neutron experiments were based on foil activation analysis in thermal column of Tehran research reactor (TRR). Results show that the required shield thickness (B_4C, 150 μm, 3 wt%) for 80% absorption of neutron fluence was almost 9.8 mm. Thus, the thermal neutron absorption is directly related the size of the B_4C filler and exhibit a significant enhancement in shielding performance for smaller particle size. On the other hand, the addition of WO_3 and ATH additive had a strong influence on the thermal neutron shielding where hybrid shield reveals an increase of more than 60%.

Fig. 4.2 illustrates the effect of B_4C loading on neutron-shielding performance of reinforced composites. All specimens have a fixed thickness of 2 mm and same filler size of 20 μm. Experimental data revealed that the neutron attenuation coefficient of reinforced composites increases with enhancing B_4C loading due to high absorbability of boron element of the filler. The results show that total neutron attenuation coefficient increased from 0.076 cm^{-1} for the neat matrix to 0.345 cm^{-1} for composite containing 5 wt% B_4C. The bubbles and porosity formation, agglomeration, and homogeneity of dispersed reinforcing agent in epoxy matrix influence the shielding performance.

Kiani et al. [38] reported that the elaborated new epoxy/clay/B_4C hybrid nanocomposite having improved mechanical and thermal stability

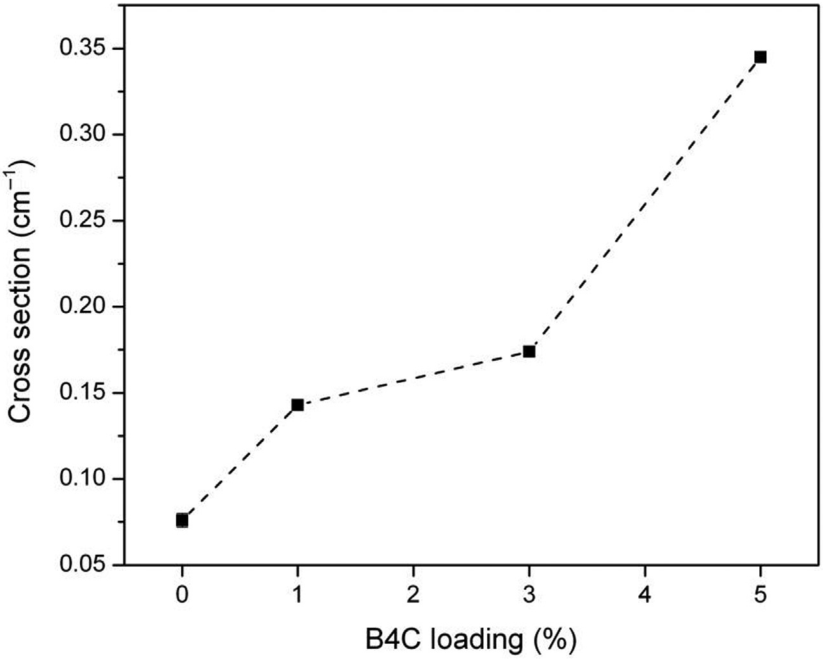

Fig. 4.2 Effect of B_4C (20 μm) loading on neutron shielding performance of reinforced composites. *(Reprinted from R. Adeli, S.P. Shirmardi, S.J. Ahmadi, Neutron irradiation tests on b4c/epoxy composite for neutron shielding application and the parameters assay, Radiat. Phys. Chem. 127 (2016) 140–146. Copyright 2016, with permission from Elsevier.)*

can be used as neuron shielding application. XRD patterns show that the exfoliation occurred for nanocomposites containing 3 wt% nanoclay while morphological analysis revealed uniform distribution of nanoclay and B_4C particles in the epoxy matrix. The neutron absorption test show that for thicknesses higher than 10 mm, the dependency of neutron shield efficiency on thickness is insignificant, regardless of B_4C loadings. Table 4.1 depicts that macroscopic absorption cross section increases with increasing B_4C concentration in a nonlinear trend, which could be related to the formation of the bubbles and porosity which is more probable at higher nanofiller contents.

El-Sarraf et al. [39] measured and calculated the shielding parameters of epoxy/ilmenite composite and found that the measured spectra of fast neutrons and total gamma rays, as well as, slow neutron fluxes lowered in intensity as the energy and thickness increased. The calculated attenuation parameters including effective removal cross section Σ_R, macroscopic cross

Table 4.1 Macroscopic absorption cross section of Epoxy/Clay/B_4C nanocomposite (ECBCN) at high concentration of boron carbide [38].

Nanocomposite	Macroscopic absorption cross section (cm^{-1})
Epoxy/3 wt% Clay/5 wt%B_4C	0.739
Epoxy/3 wt% Clay/10 wt%B_4C	0.818
Epoxy/3 wt% Clay/20 wt%B_4C	1.047

section R, and attenuation coefficient μ are very close to the experimentally determined parameters. Thus, the obtained results indicate that the produced composite is suitable for shielding applications and restoration/injection mortar for biological shields. Measured fluxes of fast neutrons (2–10 MeV) and total gamma rays (2–6 MeV) behind the studied composite having different thicknesses have been integrated and illustrated in Fig. 4.3. The plotted attenuation relations show that the flux intensity decreases exponentially with increasing thicknesses. Also, it appeared that the falloff of two radiations is nearly the same, but the composite is more effective for fast neutrons than the gamma rays, and this is due to high hydrogenous contents the epoxy.

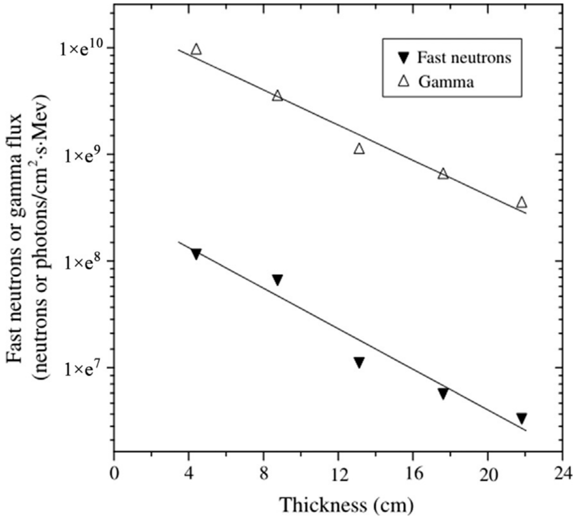

Fig. 4.3 Measured fast neutron and gamma integral fluxes behind epoxy/ilmenite composite. *(Reprinted from M.A. El-Sarraf, A. El-Sayed Abdo, M.A. Abdul-Waha, Usability of epoxy/ilmenite composite material as an attenuator for radiation and a restoration mortar for cracks, Ann. Nucl. Energy 60 (2013) 362–367. Copyright 2013, with permission from Elsevier.)*

El-Sayed et al. [40] studied a new epoxy/ilmenite composite material designed as an injecting mortar for cracks developed in some biological concrete shields. Thermal neutrons and γ-rays attenuation in the epoxy/ilmenite composites containing 75 and 80 wt% of ilmenite ratios were also investigated. According to the measured and calculated shielding data for epoxy/ilmenite composites at various ilmenite contents, they concluded that the mechanical strengths enhanced as the ilmenite filler particle size was reduced. In addition, 80 wt%/500-mm filler loading exhibited denser medium and improved attenuation capacity despite its inferior mechanical properties.

Hu and coworkers [41] optimized lightweight, compact, and high-temperature sustaining shielding epoxy/Fe/Pd/TiO_2 nanocomposites for both neutron and γ-ray radiation by means of genetic algorithms (GA) combined with the Monte Carlo N-Particle (MCNP) code. The results show that the designed samples have improved radiation shielding performance compared to the *Nuclear Power Institute of China* (PB202) and the *KRAFTON-XP3* developed by Sanoya Industry Co. Ltd. of Japan, especially for Cakes radiation shielding with multilayered structures of Fe-interlayer-Pb. The attenuation experiments on the specimens were carried out using tandem electrostatic accelerator neutron source, spontaneous fission neutron source of ^{252}Cf, and γ-ray source of ^{60}Co. The experimental results are in line with optimal design and craft. The prepared Cakes are quite useful for practical applications in nuclear science and technology.

Jun et al. [42] reported on the improvement in the mechanical properties of the B_4C/epoxy composites, which are developed by direct ultrasonic dispersion of the B_4C particles in the hardener using an immersed horn as neutron-shielding materials for spent nuclear fuel cask. The tensile strength of the B_4C/epoxy composites produced by direct ultrasonic dispersion was maintained (or increased) compared to that for the unfilled epoxy matrix, while those prepared without ultrasonic dispersion were significantly decreased. Thus, direct ultrasonic dispersion process achieved uniform dispersion as well as strong adhesion of the B_4C particles in/with the epoxy matrix enhancing the material properties without any chemical treatment.

High functional epoxy nanocomposites with three different filler materials, B_4C, PbO, and $Al(OH)_3$, were produced via an effective fabrication method consisting of an ultrasonic dispersion of nanoparticles in low-viscosity hardener and a subsequent mixing of a hardener-nanoparticle colloid with epoxy resins [43]. Results confirmed that this technique provide not only a homogenous dispersion but also an excellent wetting with improved interfacial adhesion of nano-particulate fillers within the matrix. By adding those three fillers, a synergistic effect was recorded in multiple properties such as mechanical strength properties, thermal degradation, flame retardancy, and radiation shielding performance.

Fig. 4.4A and B illustrates the change in thermal neutron flux attenuation properties of the micro- and nano-particulate B_4C composites as a function of the thickness of the specimen. For all specimens, the neutron flux attenuation (I/I_0) exponentially decreased with increasing thickness. Those exponential linear trends are well established in the insets of each figure. As the B_4C composition increased from 0 to 20 wt%, the effect of the neutron flux attenuation became more remarkable. However, the dependency of the shielding effect on the B_4C content gradually decreased as the thickness of sample increases. It was also noted that the attenuation performance for the composites with three fillers in Fig. 4.4C was almost comparable to that for the composites with the identical B_4C content (Fig. 4.4A and B), indicating that the addition of PbO and $Al(OH)_3$ had a small effect

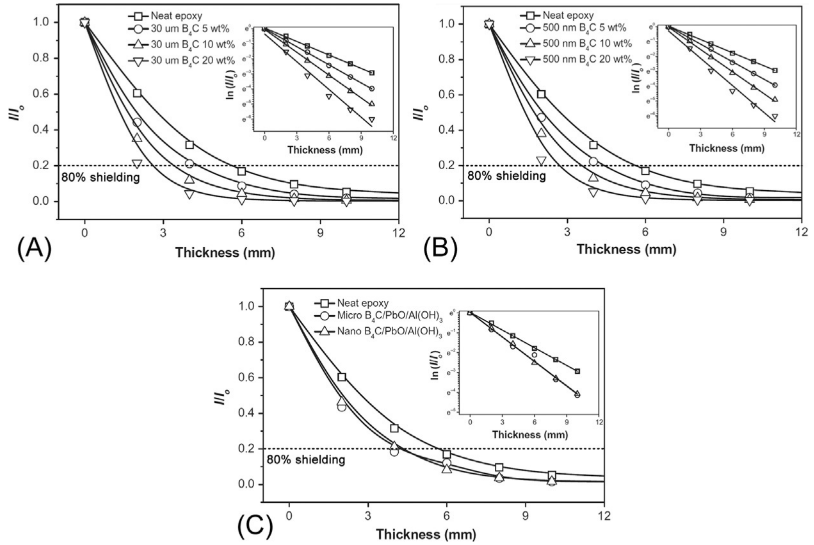

Fig. 4.4 Thermal neutron flux attenuations for (A) the microcomposites with B_4C, (B) the nanocomposites with B_4C, and (C) the microcomposite and nanocomposites with $B_4C/PbO/Al(OH)_3$. The insets show an exponential linear relationship between I/I_0 and the thickness. *(Reprinted from M.K. Lee, J.K. Lee, J.W. Kim, G.J. Lee, Properties of B4C-PbO-Al (OH)3-epoxy nanocomposite prepared by ultrasonic dispersion approach for high temperature neutron shields, J. Nucl. Mater. 445 (2014) 63–71. Copyright 2014, with permission from Elsevier.)*

on the thermal neutron attenuation property. From the exponential relationship between the neutron attenuation and the sample thickness, the linear attenuation coefficients μ was determined using the following equation:

$$I = I_o \exp(-\mu x) \tag{4.1}$$

where μ is the linear attenuation coefficient and x is the thickness of the specimen.

As a parameter of the neutron-shielding performance, the linear attenuation coefficients μ and the thicknesses required for 80% of thermal neutron shielding for various composites are listed in Table 4.2. The measured μ increased with an increase in B_4C loading owing to a high absorbability of boron with respect to thermal neutrons. The microcomposite and nanocomposite dispersed with three fillers provided μ values of nearly 0.41 cm^{-1}. As compared to the composites with only 5 wt% B_4C, the almost equivalent thicknesses obtained from the composites reinforced with three fillers show that the thermal neutron-shielding ability was significantly related to the presence of B_4C, irrespective of the addition of PbO and $Al(OH)_3$.

Three types of low-cost shielding composite materials composed of boron-containing natural green ores and epoxy matrix were produced by Li and coworkers [44]. The shielding performance of slow neutron and ^{60}Co γ-ray among the three shielding materials were studied. The results show that boron-rich slag as neutron absorber exhibited relatively improved

Table 4.2 The linear attenuation coefficients μ and the thicknesses required for 80% of thermal neutron shielding for various composites [43].

Material	Linear attenuation coefficient, μ (cm^{-1})	Thickness required for 80% shielding (mm)
Neat epoxy	0.2972 ± 0.0043	5.6
Microcomposite (5 wt% B_4C)	0.3992 ± 0.0040	4.2
Microcomposite (10 wt% B_4C)	0.5037 ± 0.0090	3.3
Microcomposite (20 wt% B_4C)	0.6123 ± 0.0488	2.1
Nanocomposite (5 wt% B_4C)	0.3964 ± 0.0052	4.3
Nanocomposite (10 wt% B_4C)	0.5001 ± 0.0107	3.4
Nanocomposite (20 wt% B_4C)	0.6123 ± 0.0397	2.3
Microcomposite with $B_4C/PbO/Al(OH)_3$[a]	0.4101 ± 0.0214	4.1
Microcomposite with $B_4C/PbO/Al(OH)_3$[a]	0.4121 ± 0.0061	4.2

[a] Filler composition: 5 wt% B_4C, 10 wt% PbO, and 10 wt% $Al(OH)_3$.

slow neutron-shielding ability, its macroscopic cross section (Σ) is 0.271 cm^{-1} which is about 1.72 times higher than lead-boron polyethylene B201 whose macroscopic cross section (Σ) is only 0.158 cm^{-1}.

Li et al. [45] developed four novel boron-containing ores/epoxy composites by using nature ludwigite green ore (NLGO), artificial ores including boron-containing iron ore concentrate (BCIOC), boron-rich slag (BRS), and boron mud (BM) as neutron absorbers, which were obtained by dressing from NLGO, blast furnace separation from BCIOC, and borax production, respectively. Shielding properties of the composites against thermal and Cf-252 fast neutron were measured. Energy deposition, absorbed dose, and half-value layers (HVLs) of the composites against neutron penetration were simulated by Monte Carlo method. Increasing the boron mole numbers per unit volume (nB) in these composites can obviously increase the macroscopic absorbing cross section (Σ thermal) and enhance the shielding properties for thermal neutron. Increase in the shielding efficiency against Cf-252 fast neutron can be obtained by developing composites containing low average atomic number.

Saiyad et al. [46] studied the effect of dispersion of various fillers in epoxy matrix to develop radiation-hardened plastic packaging which can be applied as a shielding against a high-frequency radiation attack. Three types of compositions are produced using epoxy/graphite, epoxy/lead, and epoxy/boron nitride nanopowder. Scanning electron microscope (SEM) images are used to investigate the dispersion state in the polymeric matrix. Results of linear absorption coefficient were obtained using Am-Be neutron source. The best dispersion, which is necessary to restrict radiation to be passed through, is recorded in the graphite-, boron-, and lead-based epoxy composites, respectively. They also found that a graphite/epoxy composite has the best linear absorption coefficient.

Canel et al. [47] designed a series of Ta, Fe, WC, and Bi powder filled epoxy composites for neutron and gamma irradiation and modeled effective neutron removal cross sections and gamma linear attenuation coefficients by GEANT4 and FLUKA codes to estimate with 10 wt% adding ratio. As against 4.5 MeV ^{241}Am-Be neutrons, Ta40 showed the best shield with 0.677 cm^{-1} value compared to the other tested specimens. The incorporation of metallic powders into prepared epoxy composites was an excellent path to develop new shielding materials for both neutron-gamma mixed fields. Fig. 4.5 illustrates effective neutron removal cross sections of WC/epoxy composite. This figure shows that Ta40 presets the best neutron

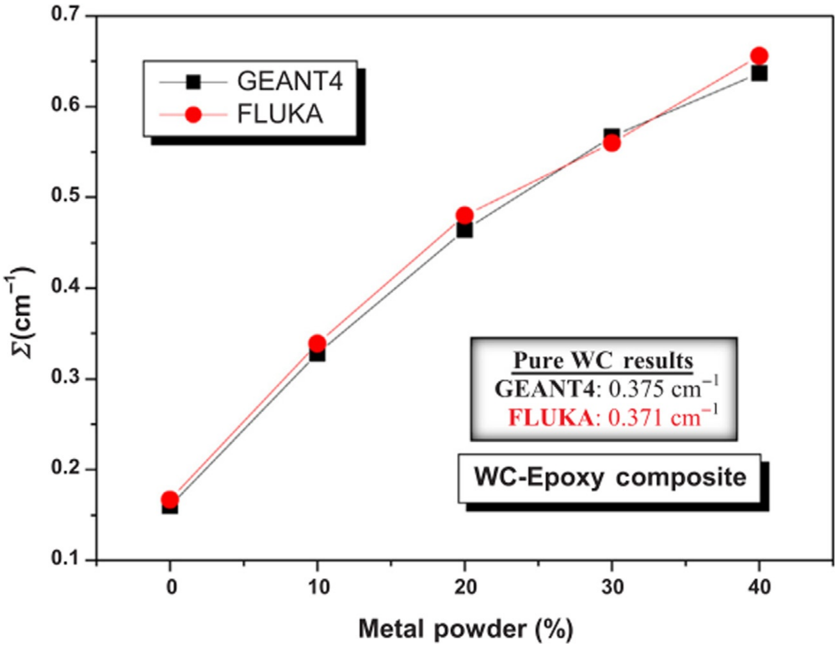

Fig. 4.5 Neutron effective removal cross sections of WC epoxy composite. *(Reprinted from A. Canel, H. Korkut, T. Korkut, Improving neutron and gamma flexible shielding by adding medium-heavy metal powder to epoxy based composite materials, Radiat. Phys. Chem. 158 (2019) 13–16. Copyright 2019, with permission from Elsevier.)*

shield with the value of $0.667\ \text{cm}^{-1}$. It was also noted that epoxy/WC composite materials are better than Fe- and Bi-filled epoxy composites in neutron-shielding performance.

Galehdari and Kelkar [48] in their study addressed the effects of neutron radiation on the mechanical properties of lightweight multifunctional epoxy composite with improved radiation shielding properties, produced by dispersing boron nanopowder, gadolinium, and boron carbide nanoparticles into an epoxy matrix, to form core sheets for final hybrid sandwich structure. The neutron radiation shielding parameters of the prepared nanocomposites and their mechanical and thermophysical properties were studied. The mechanical and thermophysical analysis results demonstrate that the developed core materials can retain their structural integrity after an exposure to the highly thermalized neutron radiation in steady-state mode with a flux of $3 \times 10^{13}\ \text{n/cm}^2/\text{s}$. In addition, their study revealed that the neutron-shielding efficiency increased significantly with the addition of nanoparticles.

The neutron attenuation is measured using one or two independent counting systems, each consisting of a BF3 neutron detector. As reactor flux is unstable, precision was enhanced by monitoring the incident neutron beam and normalizing the test counts and subtracting system background counts. The neutron attenuation data for four composites are shown in Fig. 4.6. As it can be seen from Fig. 4.6A, the neutron transmission declines remarkably in the specimens that were reinforced with nanoparticle, which reflected the increase in neutron-shielding efficiency (Fig. 4.6B) by introduction of 3 wt% nanofillers. The collected data also proved that boron nanopowders gave the best thermal neutron-absorbing efficiency. Although gadolinium particles showed the highest neutron absorption cross section among all the reinforcing agents used, their composites exhibited lower shielding efficiency compared to boron nanopowder, which is ascribed to their larger particle size and relatively lower dispersion state into the matrix. Generally, the improvement in radiation resistance upon the inclusion of fillers is due to the type of filler as well as, homogenous dispersion of the filler within the polymer matrix, in addition to the size effect of the filler [49].

In order to perform dry interim storage and transportation of the spent fuel assemblies of the Bushehr Nuclear Power Plant (NPP), dual purpose casks can be used. Rezaeian et al. [50] analyzed the effectiveness of different neutron shield materials, for the dual purpose cask, through a set of calculations achieved by the MCNP code. The dose rate for the dual purpose cask utilizing the fabricated materials of epoxy/clay/B_4C and epoxy/clay/B_4C/carbon fiber was lower than the allowable radiation level of 2 mSv/h at any point, and 0.1 mSv/h at 2 m from the external surface of the cask. By replacing ethylene glycol/water mixture with epoxy/clay/B_4C, the dose rates on the side surface of the cask caused by neutron sources and consequent secondary gamma rays decreased by almost 17.5% and 10%, respectively. In the case of the DPC with neutron shield material of epoxy/clay/B_4C/CF, the overall dose rate reached the highest value. However, the calculated dose rate in this case was also lower than the allowable radiation level of 2 mSv/h at any point on the external surface of the DPC.

In an original work, Gaber et al. [51] studied the use of boron oxide glass/epoxy ilmenite assembly (BOG/EI) as a two-layer shield. Experimental work regarding measurements of fast neutrons and gamma ray leaking behind homogenous and two-layer shield of (BOG) and (EI) composite have been carried out to investigate their radiation attenuation capabilities in terms of flux degradation. The MCNP-4C2 code was utilized to simulate

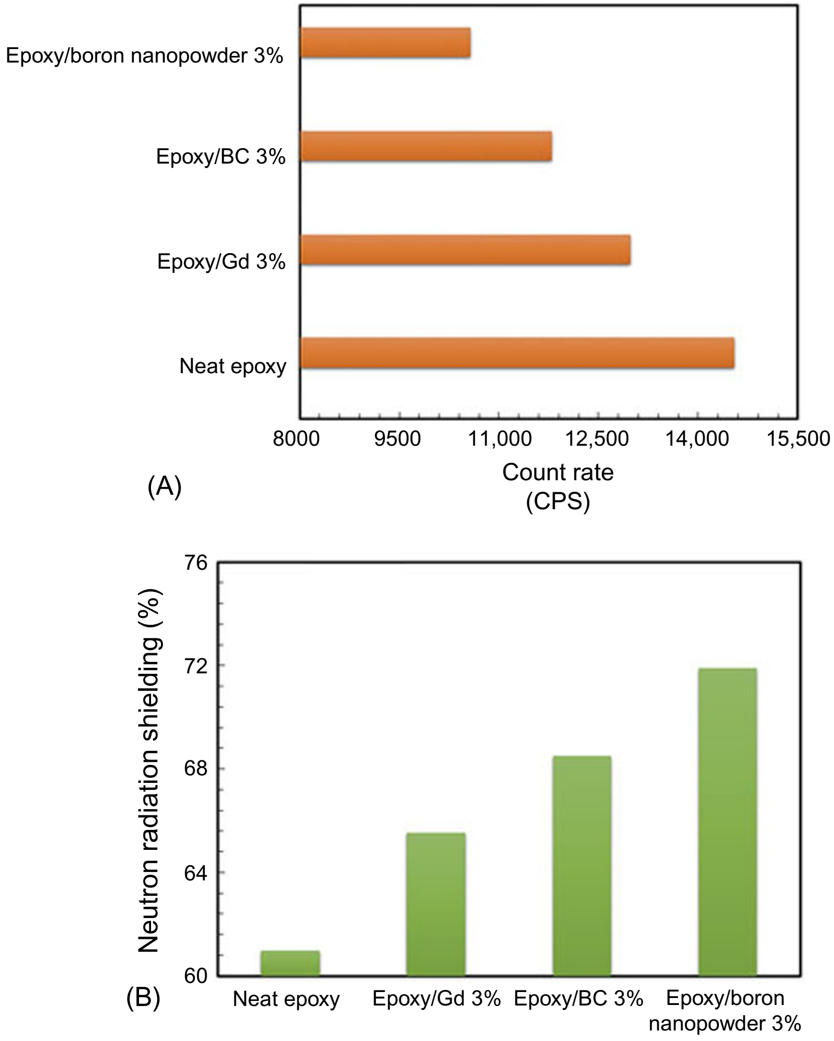

Fig. 4.6 Neutron attenuation results: (A) corrected count rate and (B) shielding efficiency. *(Reprinted from J. Kim, B.C. Lee, Y.R. Uhm, W.H. Miller, Enhancement of thermal neutron attenuation of nano-B4C, -BN dispersed neutron shielding polymer nanocomposites, J. Nucl. Mater. 453 (2014) 48–53. Copyright 2017, with permission from Cambridge University Press.)*

the experimental transmission of fast neutrons and gamma ray fluxes data for validation. The two-layer shield BOG/EI composite demonstrated the highest fast neutron attenuation capability for the highest high densely EI proportioned assembly and lowest capability for the highest low densely BOG proportioned assembly.

4.5.2 Poly(methyl methacrylate) composites

The role of CNTs in reducing the generation of secondary neutrons upon interaction with high-energy particle radiation has not been widely explored. In comparison with single-walled carbon nanotubes (SWCNTs), multi-walled carbon nanotubes (MWCNTs) have better resistance to radiation. Carbon atoms of MWCNTs have a higher atom displacement threshold than those of SWCNTs and the knocked-off carbon atoms can be quickly relocated to the neighboring wall, minimizing the structural damage [52]. The MWCNTs also need less energy than SWCNTs to break the van der Waals force within the CNT bundles, thus MWCNTs exhibit improved dispersion in the polymeric matrices, providing better reinforcement effect. The composition of PMMA contains low-Z elements (carbon, hydrogen, and oxygen) resulting in a lower possibility of secondary neutron generation. In a study conducted by Li et al. [53], the PMMA/MWCNT nanocomposite was produced with 3 wt% of MWCNTs and the proton transmission and secondary neutron generation properties were studied under proton radiation with energy up to ~80 MeV. The shielding performance of the nanocomposite was also compared with that of pure PMMA matrix and aluminum.

To enhance the radiation shielding efficiency of poly(methyl methacrylate) (PMMA), this thermoset was reinforced by colemanite $Ca_2B_6O11\cdot 5H_2O$ (CMT) by using in situ polymerization with atom transfer radical polymerization (ATRP) technique described in the study by Bel et al. [54]. To evaluate the radiation protective shielding performance of PMMA/CMT composite, in terms of the attenuation coefficient (μ) and the HVL, the reinforcement effect of CMT was investigated at four different filler ratios (5, 15, 30, and 40 wt%) as displayed in Fig. 4.7. Neutron transmission tests on the PMMA/CMT composite were carried out by using a neutron howitzer

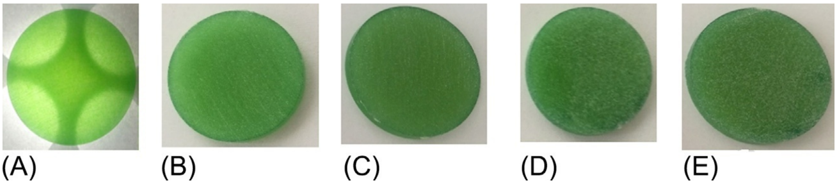

Fig. 4.7 Pictures of (A) PMMA and composite containing, (B) 5 wt%, (C) 15 wt%, (D) 30 wt%, and (E) 40 wt% CMT. *(Reprinted from T. Bel, C. Arslan, N. Baydogan, Radiation shielding properties of poly(methyl methacrylate)/colemanite composite for the use in mixed irradiation fields of neutrons and gamma rays, Mater. Chem. Phys. 221 (2019) 58–67. Copyright 2019, with permission from Elsevier.)*

(^{239}Pu-Be neutron source). Results show an increase of 11.1% in the radiation shielding capacity for gamma photons of Cs-137 radioisotope and 38.56% for neutrons emitted from Pu-Be neutron source.

4.5.3 Polyimide composites

Generally, thermosetting polyimides and their composites either possess inferior thermal oxidative stability or have nonfunctional properties. Wu et al. [55] designed a new type of polyimide composite exhibiting good neutron shielding and thermal performance. They fabricated a carbon fiber-reinforced carborane containing bis(o-carborane)-containing diamine 1,4-bis[2-(4-aminophenyl)-o-carboranyl]benzene-based polyimides by a hot press processing technique. The cured polyimide resins showed char yield at 800°C above 97.7% under air atmosphere. Moreover, carbon fiber-reinforced polyimide composites exhibited glass transition temperatures above 500°C without lowering their storage moduli. Neutron-shielding permeability of polyimide/carbon fiber composites having 2 mm-thickness was evaluated and results revealed excellent neutron-shielding capability. The reported results can encourage the production and design of polyimides composites with outstanding thermal- and neutron-shielding performance for nuclear-shielding applications.

Further, the macroscopic cross section (Σ) is a key factor to evaluate neutron-shielding property of the prepared composites. The macroscopic cross-section value is 0.192 cm^{-1} for carborane-containing polyimide-based composite shield with 5.44 wt% B (Table 4.3). More importantly, the chemical interaction between matrix and boron particles in these polymers could overcome the problems of nonhomogenous dispersion and boron particles shedding due to the traditional blending of boron particles in matrix polymers. Besides, it is reported that the thickness and boron content of the

Table 4.3 Neutron performance of carbon fiber reinforced composites [55].

Sample	B content (wt%)[a]	Thickness (mm)[b]	I/I_0[c]	$I/I_0 \times 100$ (%)[d]	Σ (cm^{-1})[e]
Carbon fiber/PI-PDA-1	0	2	1	100	/
Carbon fiber/PI-1	5.44	2	0.962	96.2	0.192

[a] Boron content in the tested composite.
[b] Thickness of the tested material.
[c] Neutron transmission factor.
[d] Neutron permeability.
[e] The macroscopic cross-section.

materials have an effect on neutron-shielding performance. The addition of carborane groups into polyimide matrix reduced the transmission factor I/I_0 of the carborane-containing polyimide-based composite till 0.962, which reflects its good neutron-shielding property. The neutron-shielding property of these composites was increased markedly due to their large thickness or high boron loading. Thus, carborane-containing polyimide composites have excellent practical application value to mitigate neutron radiation danger.

Recently, reinforced epoxy composites have been applied as radiation-shielding materials against gamma rays and neutron particles. In the study by Aygün et al. [56], the neutron-shielding capacity of epoxy was increased by adding molybdenum powder. Results of the Monte Carlo simulation demonstrated that the total neutron macroscopic cross section value increased from 0.1597 to 0.4522 cm^{-1}. Also an increase of approximately 12% for equivalent dose rate attenuation was reached as the experimental results revealed.

Neutron-shielding fiber metal laminates (NSFMLs) containing 10–50 wt% of boron

B_4C powder were produced using hot molding process as reported by Fu et al. [57]. The testing results indicated that good interfacial adhesion between different layers, uniform distribution of B_4C particles, and carbon fibers tightly surrounded by polyimide (PI) resin were crucial to improve the mechanical properties of composite laminates. In addition, the prepared composite laminates still retain the good interlaminar shear strength even at 300°C. NSFMLs with a 3/2 configuration, consisting of three AA6061 alloy plates coated with the newly developed neutron-shielding polyimide composite (NSC) and two carbon fiber-reinforced polyimide (CFRP) layers were also produced using hot molding process.

Fig. 4.8 illustrates the process of preparing NSFMLs. The NSFMLs with a 3/2 configuration, constituting stacking layer of AA6061 plates, neutron-shielding composite (NSC), and carbon fiber-reinforced polyimide (CFRP), were firstly stacked in the compression mold by hand lay-up, and then placed into the vulcanizing machine, and finally hot compressed under the pressure of 2–3 MPa when the mold temperature exceeded 280°C. The detailed curing process of all composite laminates is 80°C/1 h, 120°C/1 h, 160°C/1 h, 200°C/1 h, 280°C/1/2 h, and 320°C/2 h.

The design and fabrication of shielding materials with good heat resistance and mechanical properties can cause serious problem in the radiation shielding field. Wang et al. [58] prepared new composites for gamma ray and neutron shielding applications based on a continuous carbon-fiber reinforced Sm_2O_3/polyimide by hot-pressing technique. The mechanical

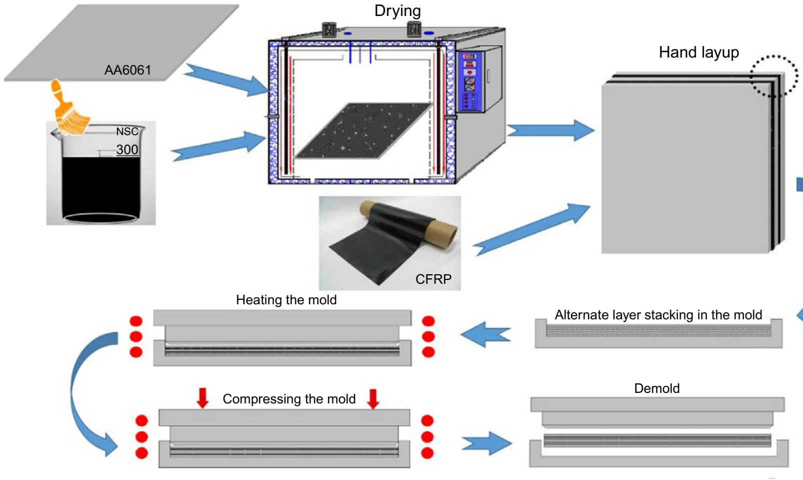

Fig. 4.8 Schematic illustration of preparing process of the NSFMLs. *(Reprinted from X.L. Fu, Y.B. Hu, H.G. Li, J. Tao, Study on the thermal and mechanical properties of novel neutron shielding composite laminates at elevated temperature, Mater. Sci. Eng. A 697 (2017) 101–110. Copyright 2017, with permission from Elsevier.)*

results show that the tensile strength of the novel shielding material exceeded 200 MPa, which makes it of similar strength to aluminum alloy. The prepared composites showed cross-linking and decomposition reactions at 300°C and can be used in such environments for long periods of time. The continuous carbon fiber-reinforced Sm_2O_3/polyimide material exhibited improved shielding performance with respect to gamma rays and neutrons. These materials can be used in fusion reactor system and nuclear waste disposal applications.

According to theory, neutron transmissivity decreases with increasing composite thickness as shown in Fig. 4.9. The evolution in neutron transmissivity with thickness is quantitatively well described by Eq. (4.2)

$$\eta = {}^{I_i}\!/_{I_0} = Be^{\sum d_i} + a \tag{4.2}$$

where η is the transmittance of gamma, I_i, I_0 are the count rate before and after shielding, B is cumulative factor, d_i is the thickness of the shielding material, a is the background count, and Σ is the macroscopic cross section (representing the neutron shielding ability for a specific energy range).

As depicted in Fig. 4.9B, the neutrons were categorized into four groups according to their energy. The transmissivity of all energies neutrons

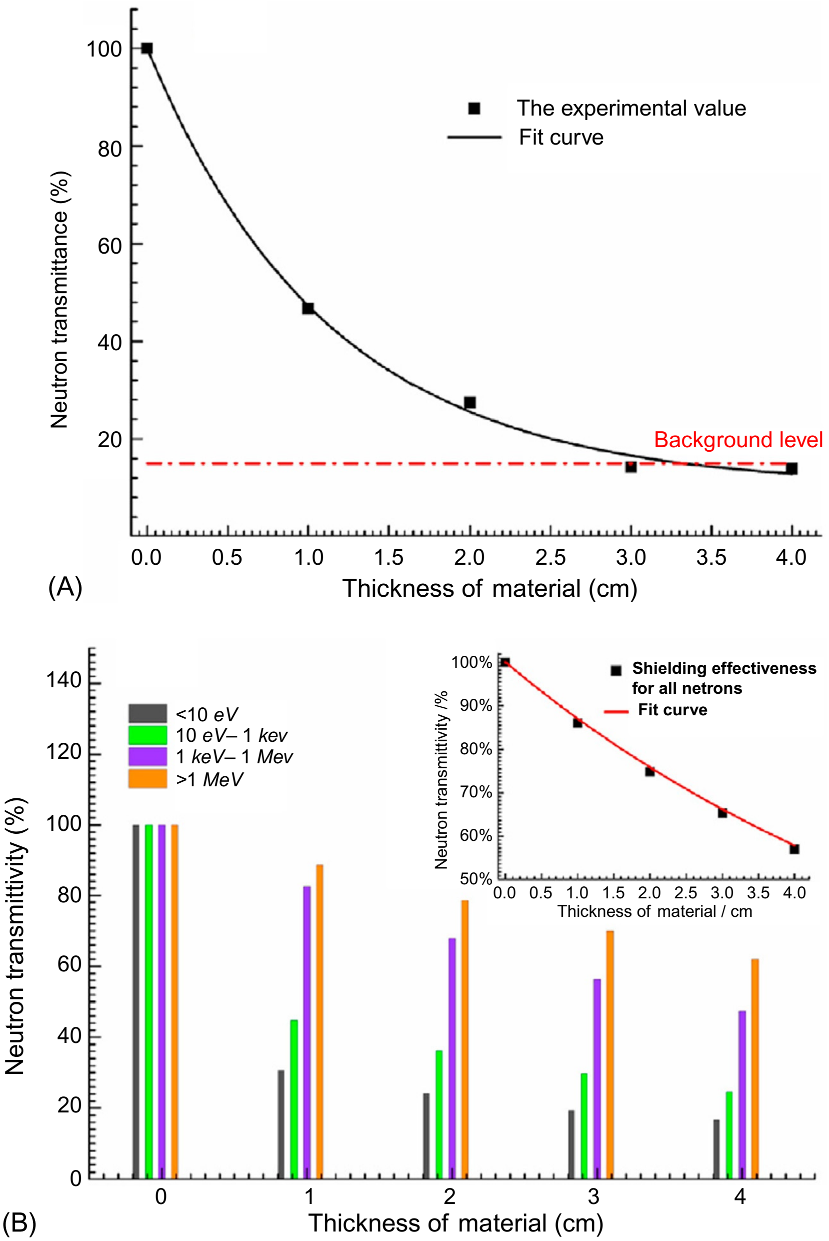

Fig. 4.9 Neutron shielding properties of continuous carbon-fiber reinforced Sm_2O_3/polyimide shielding material: (A) experimental values and (B) calculated values. *(Reprinted from P. Wang, X. Tang, H. Chai, D. Chen, Y. Qiu, Design, fabrication, and properties of a continuous carbon-fiber reinforced Sm2O3/polyimide gamma ray/neutron shielding material, Fusion Eng. Des. 101 (2015) 218–225. Copyright 2015, with permission from Elsevier.)*

decreased with increasing sample thickness but for the low-energy neutrons this trend was more remarkable due to fact that the neutron absorption cross section decreases with increasing neutron energy. As the average energy of the neutrons emitted by the Am-Be neutron source reached 4.5 MeV, no matter where the ^{3}He proportional counter was moved to in the laboratory, some neutrons were still able to penetrate the detector after being scattered. In the beginning, the number of background neutrons was detected using a ^{3}He proportional counter, before the shielding tests on composite samples was started. As shown in Fig. 4.9A, when 3 cm of shielding composite was used, the neutron irradiation level had reduced to the environmental level.

When comparing Fig. 4.9A and B, it appears that the experimentally determined values of neutron transmissivity are different than those calculated by Monte Carlo codes (MCNP/4C). However, the experimental data well-fitted the predicted ones for specimens whose energy was lower than 10 eV. This was attributed to large thermal neutron absorption cross sections of ^{3}He as the ^{3}He proportional counter only reflects the shielding performance for low-energy neutrons but high-energy neutrons are also included in the calculations. The macroscopic cross sections for the experimental and simulated curves reach 0.88 and 0.15 cm^{-1}, respectively. This reflects that the ^{3}He proportional counter is mainly useful for recording the low-energy neutrons. In conclusion, the continuous carbon-fiber reinforced Sm_2O_3/polyimide neutron-shielding composite material not only can exhibit good thermal neutron-shielding performance, but also is capable of absorbing some of the high-energy neutrons and even gamma rays.

Thakur et al. [59] studied the development of novel composite based on polymethyl methacrylate (PMMA) matrices reinforced with neodymium oxide and extensively evaluated their neutron-shielding ability. The neutron-shielding parameters were assessed from the fast neutron removal cross sections. The developed PMMA/neodymium oxide composite showed improved neutron-shielding properties than the commonly used neutron shields likes B_4C, polyethylene grains, and conventional concrete. The explored lightweight and flexible PMMA resin doped with neodymium oxide composites can serve as protective neutron shields for the personnel involved in radiation applications.

The polyimide composite provides a great potential for use in applications which require materials with high thermal stability and neutron radiation shielding ability, such as fusion reactor system and nuclear waste disposal. Li et al. [60] evaluated the neutron-shielding properties of new type the polyimide/B_4C composite films with different micro-sized B_4C contents prepared by in situ polymerization. Silane coupling agent KH550 was used to functionalize outer surface of B_4C particles for enhancing the dispersion rate of these particles within the polyimide matrix and also to promote the strength interfacial interaction. Results show that the micro-sized B_4C functional particles can be well dispersed in the polyimide matrix. Meanwhile, the polyimide/B_4C composite films exhibit an improved thermal neutron radiation shielding capacity. The neutron permeability I/I_0 changed exponentially with a change in B_4C content. At 30 wt% B_4C, the polyimide composite films exhibited optimum properties in combination with thermal decomposition temperature (Td_{10}) of 622°C, neutron permeability (I/I_0) of 0.24 (800 μm in thickness), and tensile strength of 406 MPa.

The neutron radiation shielding characteristics of polyimide/B_4C composite films at various B_4C ratios (0–50 wt%) and thicknesses (20–800 μm) were detected by CMRR neutron radiography device. As revealed from Fig. 4.10, the neutron permeability I/I_0 values of the BPDA/ODA/B_4C

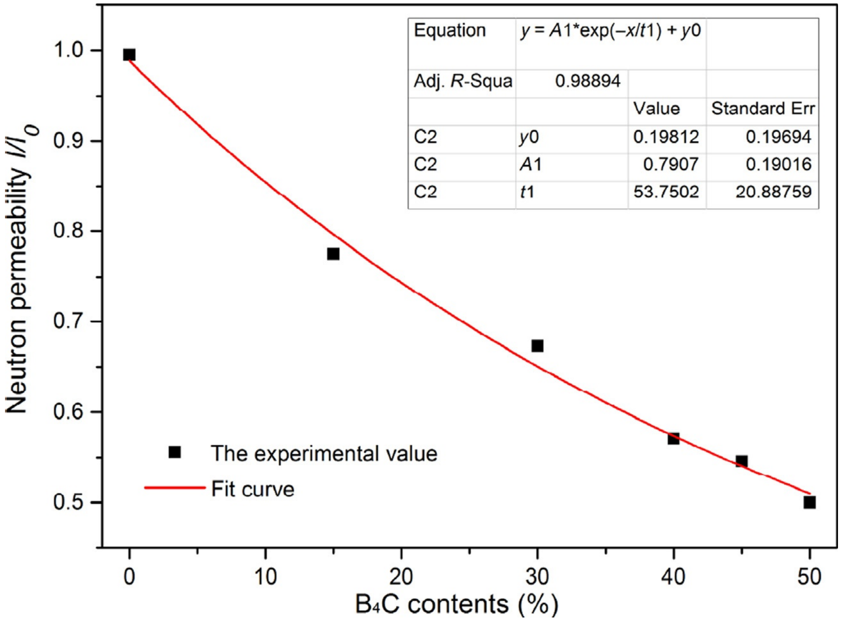

Fig. 4.10 Relationship between neutron permeability and B_4C content for polyimide/B_4C composite films. *(Reprinted from X. Li, J. Wu, C. Tang, Z. He, P. Yuan, Y. Sun, et al., High temperature resistant polyimide/boron carbide composites for neutron radiation shielding, Compos. Part B 159 (2019) 355–361. Copyright 2019, with permission from Elsevier.)*

polyimide composite films reduced significantly with increasing B_4C loading. The neat polyimide matrix demonstrated small ability to shield neutron radiation given the I/I_0 value is as high as 0.995. Moreover, the neutron permeability I/I_0 value lowered from 0.775 at 15 wt% B_4C to 0.5 at 50 wt% B_4C. It suggests that the addition of B_4C increased significantly the neutron radiation shielding performance of their newly developed polyimide composites films. As shown in Fig. 4.10, the fitted relationship between the neutron permeability I/I_0 and B_4C fractions follows exponential trend, as expressed by the following equation:

$$y = 0.7907 \times \exp(-x)75.53 + 0.1981 \tag{4.3}$$

where y is the neutron permeability I/I_0 and x is the B_4C content.

To investigate the effect of thickness on the neutron permeability I/I_0, the neutron radiation shielding properties of polyimide/B_4C composite films with various B_4C contents ranging from 15 to 45 wt% at different thicknesses (20–800 μm) were tested. The measurement results are shown in Fig. 4.11. For instance, the value of I/I_0 was reduced from 0.55 to 0.48, 0.35, and 0.30 when the B_4C content was increased from 15 wt% to 30 wt%, 40 wt%, and 45 wt% at the thickness of 300 μm.

4.5.4 Polyurethane composites

The thermal neutron radiation shielding efficiency of polyurethane (PUR) composites loaded with 20.9% by weight of B_4C or by 20.4% graphite micronized fillers was evaluated in the study by Cataldo and Prata [61]. The produced composite was more effective in thermal neutron radiation shielding compared with those of other PUR composites loaded with about 20% of amorphous boron or 20% boron nitride (BN). However, the PUR composite reinforced with graphite was not found to be suitable for shielding thermal neutrons.

By comparing with the unfilled PUR as reference, the value of μ and μ/ρ were indexed making 100 times the values recorded on the unfilled PUR. Thus, shield A with amorphous boron is 3.1 times more efficient as mass shield against thermal neutrons than reference. Shield B filled with B_4C is 2.44 times more efficient as thermal neutron shield than reference unfilled PUR. In its turn, shield C loaded with BN is 1.78 times more efficient than reference. Since the boron amount in BN is only 43.6% of the filler, the real boron load on shield C is only 9.1%. Consequently, the μ/ρ value of shield C is reduced roughly to about half the μ/ρ value of shield A with 20.4% amorphous boron. Finally shield D composed of PUR filled with graphite

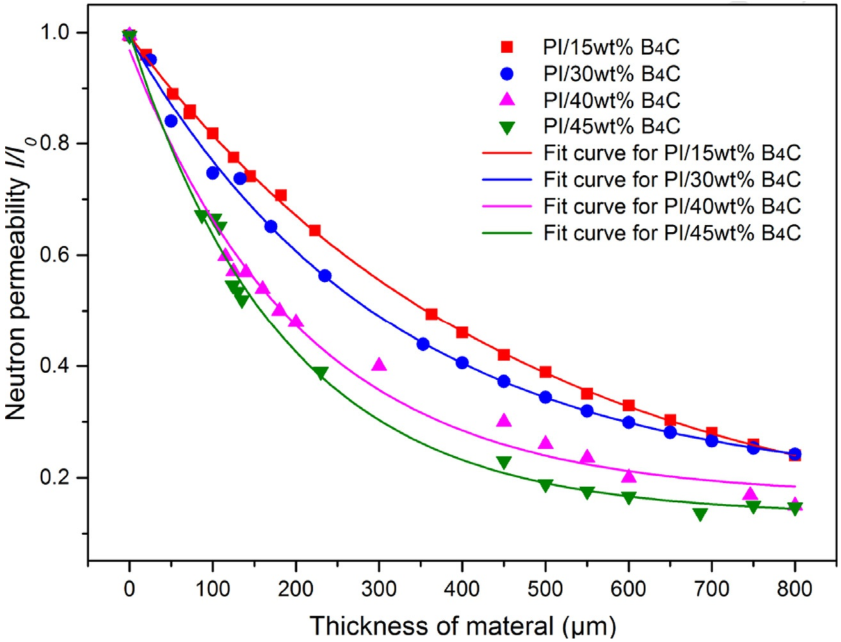

Fig. 4.11 Relationship of neutron permeability and thickness for BPDA-ODA polyimide/ B_4C composite films. *(Reprinted from X. Li, J. Wu, C. Tang, Z. He, P. Yuan, Y. Sun, et al., High temperature resistant polyimide/boron carbide composites for neutron radiation shielding, Compos. Part B 159 (2019) 355–361. Copyright 2019, with permission from Elsevier.)*

did not demonstrate shielding properties against thermal neutrons, since elemental carbon does not have a high neutron capture cross section compared to boron compounds.

The facile fabrication of the low-density boron-containing PUR material makes it very suitable in neutron-shielding applications. Chen et al. [62] produced a new highly efficient neutron-shielding aerogel materials by adding boron compounds into polyurethane matrix. Morphological analysis of the prepared composites revealed layered or network structure of both boron-containing aerogels and the control as depicted in Fig. 4.12. The developed aerogel composites exhibited high neutron-shielding efficiency, with neutron-shielding rate up to 99%. The neutron-shielding efficiency is mostly tailored by B content, which is also affected by the boron compounds. Combustion test showed that all the studied boron-containing neutron-shielding compounds exhibited a very low fire risk.

The neutron transmission factor I/I_0 of boron-containing aerogels and the control were studied with a typical reactor-based pinhole SANS, as listed

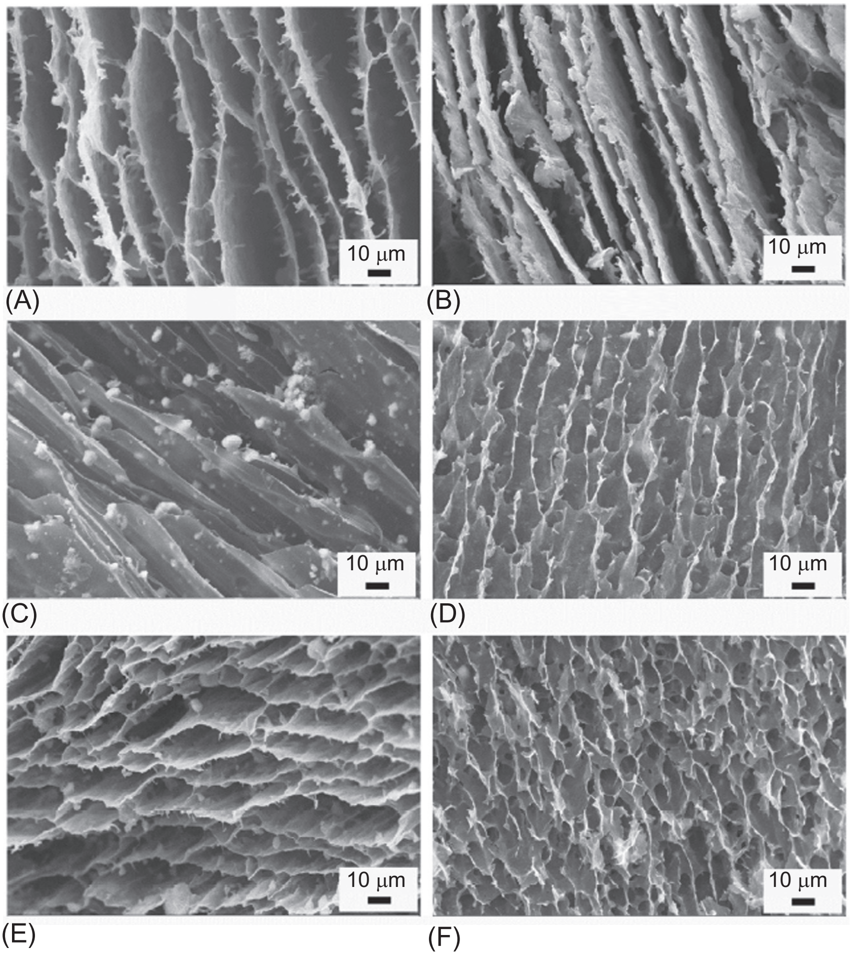

Fig. 4.12 SEM micrographs of neutron shielding aerogel materials and the control: (A) the control; (B) composite 1 (8 wt% boron); (C) composite 2 (8 wt% boron); (D) composite 3 (8 wt% boron); (E) composite 4 (8 wt% boron); and (F) composite 5 (15 wt% boron) [62]. *(Reprinted from H-B. Chen, Y.-Y. Ao, D. Liu, H-T. Song, P. Shen, Novel neutron shielding alginate based aerogel with extremely low flammability, Ind. Eng. Chem. Res. J. 56(30) (2017) 8563–8567. Copyright 2017, with permission from ACS publication.)*

in Table 4.4. I_0 and I are the intensities of the incident neutron beam and neutron beam transmitted through the thickness direction of the specimen composites, respectively. The control material has an I/I_0 value of 73.0% ± 2.1%. By adding 8 wt% B content, the transmission factor of composites 1, 2, and 3 all decreased: composite 1 with 8 wt% B (boron carbide) has a

Table 4.4 Neutron shielding parameters of neutron shielding aerogel materials [62].

Sample	Control	Composite 1	Composite 2	Composite 3	Composite 4	Composite 5
Thickness (mm)	26.0 ± 0.5	26.0 ± 0.5	26.0 ± 0.5	26.0 ± 0.5	26.0 ± 0.5	26.0 ± 0.5
Areal density ($g\ cm^{-2}$)	0.26	0.25	0.27	0.30	0.26	0.28
Porosity (%)	95.2	95.3	94.8	95.5	95.4	95.3
Transmittance (%)	73.0 ± 2.1	7.3 ± 1.0	5.7 ± 0	5.6 ± 1.0	5.7 ± 0.1	0.9 ± 0

transmission factor of 7.3% ± 1.0%; composite 2 with 8 wt% B (boron nitride) has transmission factor of 5.7% ± 0%; and composite 3 with 8 wt% B (zinc borate) has transmission factor of 5.6% ± 1.0%. These indicate that B_4C has the worst shielding efficiency in the three boron-containing compounds, although close to each other. Compared to the used fillers, B_4C has the highest boron (B) content, thus it has the least mass at a fixed B content. This was attributed to the lower dispersion degree and the poor distribution of B_4C in these composites which is responsible for increasing neutron transmittance. Composite 4 also has 8 wt% B (four parts of boron in boron carbide, three parts of boron in boron nitride, and three parts of boron in zinc borate), with transmission factor of 5.7% ± 0.1%. With the same proportion of boron compounds, composite 5 with 15 wt% B has transmission factor of 0.9% ± 0%, conforming high-performance neutron-shielding efficiency of the newly designed aerogel composites.

Cataldo and Prata used a castable polyurethane (PUR) with soft segment made by polytetrahydrofuran polyol (or polytretramethylene ether glycol = PTMEG) derived from renewable sources as polymer matrix to develop new types of neutron shields [63]. The PUR polymer matrix was reinforced with 20.4 wt% of amorphous boron or with 20.9 wt% by weight of hexagonal boron nitride (h-BN). The PUR composites were cast in foils of 2 mm thickness and tested as thermal neutron shields against reference pure PUR foils. Neutron-shielding tests in terms of the linear (μ) and mass attenuation coefficient (μ/ρ) for the two prepared PUR composites were determined. Making 100 as the linear attenuation coefficient μ of unfilled PUR, the μ value of 20.4 wt% amorphous boron filled composite was reached at 224 while that of 20.9 wt% filled BN was attained at 182. Making 100 as the mass attenuation coefficient μ/ρ of the unfilled PUR the amorphous boron PUR filled composite was found at 311 while the BN filled PUR composite stopped at 178.

4.5.5 Polyester composites

Novel polyester is reinforced with red mud, obtained from aluminum industry waste, based composites for neutron-shielding application. A method for making neutron-shielding materials utilizing processed red mud with boric acid with polyester matrix has been investigated by Guru et al. [64]. The fabricated neutron-shielding polyester composites have been explored for fast and thermal neutron shielding by using 12 Ci Am-Be radiation source. The total macroscopic cross section of red mud-polyester composites had been also calculated and compared in this study. The attenuation factor was measured as the ratio of count rates resulted without and with sample in between the source and detector. The Σ_t value was calculated using Eq. (4.4). However, thermal neutron absorption is determined mainly by the type of material and its atomic number density. The recorded results of the thermal neutron irradiation experiment for developed neutron-shielding composites show that red mud-reinforced polyester composites have better neutron absorption capabilities and exhibited better total macroscopic cross section (Σ_t) and mass removal cross section (Σ_t/ρ) than the composite reinforced with simulated red mud with pure chemical components that contained red mud from industrial waste.

$$I = I_0 \exp^{[-\Sigma_t x]} \tag{4.4}$$

where I_0 and I are the intensities of neutrons before and after absorption, respectively, and x (cm) represents the thickness of the material medium.

Wu et al. [65] prepared two series of carborane-containing copolyesters by copolymerization of newly designed 5-(1-methoxy-o-carborane) dimethyl isophthalate (BDMI) and conventional polyester monomers. Then carborane-containing copolyester fibers were fabricated through melt spinning and the spinning conditions were explored to produce the continuous fibers meters long. The neutron-shielding characteristics of the resulting carborane-containing polyester films were measured. The neutron absorption cross section (Σ) is an important factor to evaluate neutron-shielding performance of these materials. Fig. 4.13 shows the macroscopic cross section of copolyester films at a fixed shield thickness value. It was shown that the value of Σ enhanced with the increasing carborane content in the copolyester, suggesting that boron concentration could properly promote the neutron-shielding property of materials. The neutron absorption cross section of the neat matrix was 1.93 cm^{-1}. At a 10% loading level of BDMI, the carborane-containing copolyester polybutylene terephthalate (PBT)-B10 with 5.16% boron content showed Σ value at 8.70 cm^{-1}. However, at a 10 wt% loading level of BDMI, the Σ value of PBT-B10 was only 6.74 cm^{-1} due to its relatively low boron content (4.55%). Obviously, the highest value of Σ was recorded as 17.04 cm^{-1} for the copolyester PBT-B20. This value was about 50 times higher than that of the unmodified PBT, implying that the inclusion of carborane groups into polyester matrix had a positive effect on neutron-shielding efficiency. Interestingly, the resulting copolyesters possessed outstanding neutron-shielding properties.

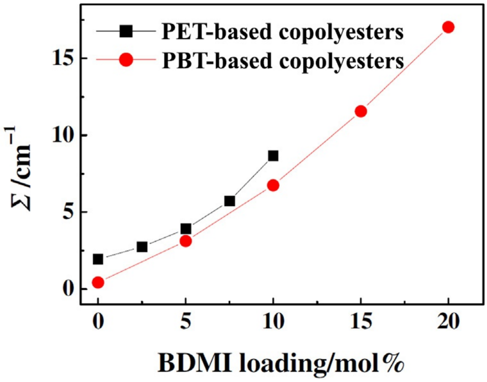

Fig. 4.13 Neutron absorption cross section (Σ) of the PET-based and PBT-based copolyesters versus the carborane-containing monomer BDMI loading in copolyester synthesis process. *(Reprinted from Y. Wu, J. Hu, C. Feng, G. Chen, J. Yan, Carborane-containing copolyester fibers with unique neutron shielding properties, Mater. Des. 172 (2019) 107772–107778. Copyright 2019, with permission from Elsevier.)*

Especially, at a 20% loading level of the carborane-containing monomer BDMI, the resulting polybutylene terephthalate-based copolyester showed the highest neutron absorption cross section of 17.04 cm^{-1}. On the other hand, the thickness of composite film was only about 0.02 mm. Thus, if these fibers are produced into nonwoven cloth with a certain thickness, the shielding performance will be markedly increased.

In their study, the carborane groups are joined through chemical interaction in copolyester chains. Thus, their cores, which are responsible for the neutron-shielding performance, are unremovable from the fibers, justifying the long-term use without significant performance degradations. In addition, compared to inorganic reinforcing fillers, there is no need to consider the problems of interfacial adhesion control and the compatibility between the matrix and the filler. Therefore, the prepared carborane-containing copolyester composite fibers can be fabricated as nonwoven cloth for the designing neutron-shielding protection clothing and high-performance radiation shielding textile materials.

The radiation shielding properties of isophthalic-bismuth polymer composites have been investigated by Tijani and Al-Hadeethi [66], at the energies of interest in diagnostic nuclear medicine. The mass attenuation coefficients, half-value layers, and the percentage of heaviness of isophthalic/Bi_2O_3 polymeric composites with the composition formula: $(100\text{-}x)C_8H_6O_4\text{-}xBi_2O_3$ (where $x = 40, 30, 20, 10, 5$, and 0 percentage fractions) were evaluated. It was found that the mass attenuation coefficients of these thermosetting composites exceeded that of conventional concrete. The authors found that these composites can replace concretes for constructing radiation barriers at nuclear medicine centers.

4.5.6 Other types of thermosetting composites for neutron shielding

In their study, Wang et al. [67] scrutinized the shielding properties of polyacrylonitrile reinforced with gadolinium nanofibers for thermal neutron protection were produced by electrospunning, followed by in situ self-polymerization. Morphological test was conducted by the SEM and images of the newly developed polyacrylonitrile nanofibers reflected a high purity of these materials. The leaching rate of Gd^{3+} was reduced from 79.97% to 10.74%, tested by low-field nuclear magnetic resonance (LF-NMR) technique after the self-polymerization of gadolinium methacrylate in the matrix when the nanofibers were immersed in water for 7 days. The thermal neutron-shielding data calculated by MCNP program showed that above 99% thermal neutrons are absorbed when traveling through the 2-mm-thick polyacrylonitrile containing gadolinium nanofibers.

Comparatively, the neat polyacrylonitrile nanofibers exhibited a slight thermal neutron-shielding ability. More than 90% thermal neutron penetrated the 2-mm-thick neat polyacrylonitrile nanofibers. The PAN containing Gd nanofibers demonstrated a significant thermal neutron-shielding capacity due to high Gd content (theoretical Gd content is 11.43 wt% and real Gd content is 12.11 wt%). More than 99% of thermal neutron was absorbed when traveling through the 2-mm-thick polyacrylonitrile reinforced with Gd nanofibers.

4.6 Application of thermosetting composites for neutron radiation shielding

Neutron shielding involves mainly three steps: slowing neutrons, absorption of neutrons, and impregnation of gamma rays. Neutrons decelerate with thermal energy by hydrogen, water, paraffin, and plastic. Hydrogenated materials are also very useful for the absorption of neutrons. Gamma rays are produced by neutron (radiation) retention on the neutron shield, inelastic scattering, and degradation of activation products. If a source emits gamma rays at various energies, high-energy gamma rays sometimes specify shielding requirements. Multifunctional materials for neutron shields, concrete, especially with barium mixed in, can decrease and absorb the neutrons, and shield the gamma rays. Plastic with boron is also a promising multipurpose shielding material.

As the radioactivity decreases with time because of decay, the highest shielding performance is thus recommended at the beginning of the storage period. However, a continuous shielding capability is needed for the whole storage, even in the case of a long-term period. Degradation in neutron-shielding material performance occurs over time and is caused by irradiation, temperature, or thermal cycling. Concrete is subjected to several degradation phenomena such as carbonation or other chemical degradation process, and also to freeze-thaw degradations. The most effective shielding material used for nuclear reactors is produced by mixed hydrogenous materials, heavy metal elements, and other neutron absorbers. Inelastic scattering by heavy elements and elastic scattering by hydrogen are relatively effective to decelerate fast and intermediate energy neutrons, and the absorbers can decrease secondary gamma rays as well as thermal neutrons. Thus, the hydrogenous epoxy resin with excellent radiation resistant ability and high thermal stability are generally chosen as the substrate for the composite material with some reinforced metallic filler such as Fe, Pb, W, and Gd powder. In addition, low ratios of nanopowder can be utilized to improve the thermal stability and toughness of the composite material [68–70].

Korkut et al. [71] developed epoxy-ferrochromium slag composites including commercial epoxy resin and ferrochromium (FeCr) slag were tested against neutron ionizing radiations. Attenuation coefficients and absorbed doses as shielding parameters were recorded experimentally and by FLUKA Monte Carlo simulations. The addition of FeCr slag in epoxy resin up to 50% improves X-ray-, gamma-, and neutron-shielding performance of epoxy matrix. Such composites can be used in radiation applications such as radiotherapy rooms, nuclear industry, and radioactive source containers.

A new type of epoxy/colemanite shielding material was fabricated for practical use. These composites show that the new material has mechanical strength about three times that of concrete and exhibited a heat resistance temperature of 133°C. A liquid neutron-shielding material may be made if the curing agent is not used. An activation experiment was also carried out at the JRR-4 nuclear reactor installed at JAERI (Japan Atomic Energy Research Institute) [72].

The incorporation of B_4C particles into thermosetting polymer to prepare high-performance neutron radiation shielding composites has been in demand for the safe operation of nuclear power in the defense industry and nuclear power plant. Polyester vinylester compounds (e.g., TN Vyal-B by

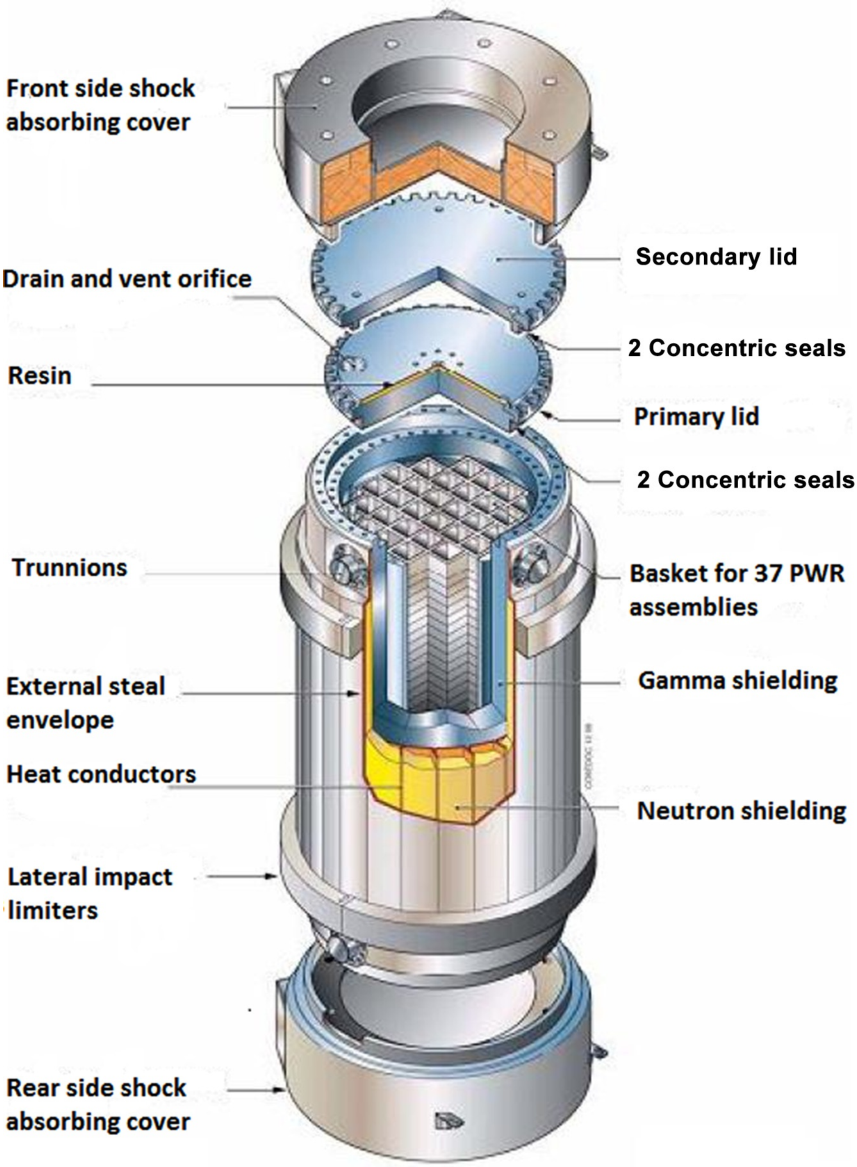
Front side shock absorbing cover
Secondary lid
Drain and vent orifice
2 Concentric seals
Resin
Primary lid
2 Concentric seals
Trunnions
Basket for 37 PWR assemblies
External steal envelope
Gamma shielding
Heat conductors
Neutron shielding
Lateral impact limiters
Rear side shock absorbing cover

Fig. 4.14 Shielding walls of dual purpose casks (AREVA). *(Reprinted from H. Issard, Radiation protection by shielding in packages for radioactive materials, in: K. Sorenson (Ed.), Safe and Secure Transport and Storage of Radioactive Materials, 1st ed., Elsevier, 2015, p. 123–140. Copyright 2015, with permission from Elsevier.)*

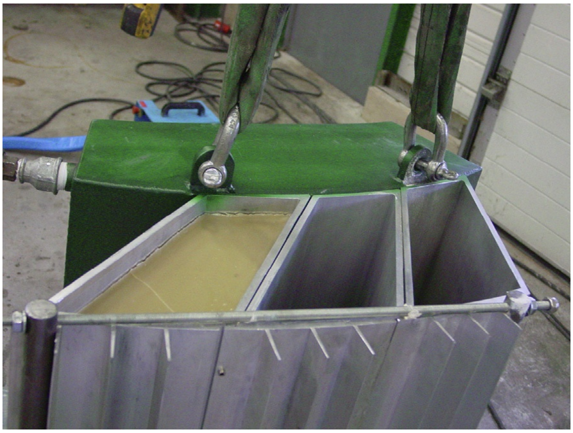

Fig. 4.15 Qualification of vinylester compound neutron shielding pouring process in an AREVA TN transport storage cask. *(Reprinted from H. Issard, Radiation protection by shielding in packages for radioactive materials, in: K. Sorenson (Ed.), Safe and Secure Transport and Storage of Radioactive Materials, 1st ed., Elsevier, 2015, p. 123–140. Copyright 2015, with permission from Elsevier.)*

AREVA TN) are made of polyester or vinylester with alumina fillers [73]. There is a chance to include boron-containing fillers. It meets a good compromise with high hydrogen content. This material shows very good fire resistance due to the addition of reinforcing agents while it self-extinguished after a fire test. The product can be mixed and prepared at ambient temperature and poured in situ (Fig. 4.14). Polyester compound neutron-shielding TN Vyal-B is used in transport storage casks for used nuclear fuel as a layer around the steel shell (Fig. 4.15).

Epoxy and epoxy phenolic compounds (e.g., NS4-FR) are prepared from epoxy filled with alumina fillers [74]. They are generally reinforced with boron-containing fillers. They exhibit a good compromise with a high hydrogen ratio. Under a fire test, the compound demonstrates self-extinguishing behavior. Due to the thermosetting nature of the epoxy matrix, the temperature resistance in long-term operation is good (150°C). The NS4-FR epoxy product is procured in the form of shielding blocks to be assembled to form a layer around the transport or storage equipment. In addition, the NS4-FR epoxy neutron-shielding is utilized in storage casks for used nuclear fuel as a layer around the main shell (e.g., in Japan, USA). Various other products exhibited relative efficiency in neutron shielding in several cases, such as polyamide, polycarbonate, different types of glass, methyl polymethacrylate, and polyurethane [75].

4.7 Conclusions

The high demand for lightweight radioprotective gear and structural materials in different industries has expanded researches in neutron-shielding materials based on polymeric composites. The shielding effectiveness of these materials is directly dependent on a various factors that include the type of radiation, its origin (cosmos, nuclear reactor, laboratories, natural radioactivity, etc.), the range of energies tested, exposure time, secondary radiations, and other external physical parameters. Additional factors involved in selecting an effective shielding material include conformability, cost-effectiveness, toxicity, durability, etc. In this aspect, polymer composites offer numerous outstanding performances over conventional materials such as concrete. Based on the studies covered in this chapter, polymer composites filled with micro- or nanoscale structures have great potential to be utilized as radiation shielding materials in various industries. Moreover, researchers are focusing on the development of novel, multifunctional polymer nanocomposites by exploiting the properties of nanofillers. However, the radiation-resistant properties of these nanomaterials under different types of radiation still remain to be further understood. In nuclear industry, low-Z materials alone failed in attenuating highly penetrative rays like γ-rays. One of the emerging solutions is the use of a graded shield material that are composed of heavy atoms impregnated within hydrogen-rich polymer matrix along with other micro- or nanofillers such as boron, ceramics, graphitic fibers, metallic fibers, etc. In nuclear reactors, composite shields consisting of a mixture of different atomic numbers incorporated within hydrogenous polymer-matrix along with some neutron absorbers are very suitable. The inelastic scattering by heavy atoms and elastic scattering by hydrogen are the most effective mechanism for attenuating fast and intermediate neutrons, and the neutron absorbers can decrease secondary gamma radiations and thermal neutrons.

References

[1] A.M. Osman, M.A. El-Sarraf, A.M. Abdel-Monem, A.E. Abdo, Studying the shielding properties of lead glass composites using neutrons and gamma rays, Ann. Nucl. Energy 78 (2015) 146–151.

[2] F.A. Cucinotta, M.-H.Y. Kim, L. Ren, Evaluating shielding effectiveness for reducing space radiation cancer risks, Radiat. Meas. 4 (2006) 1173–1185.

[3] X. Fu, X. Tang, Y. Hu, Effect of different lay-ups on the microstructure, mechanical properties and neutron transmission of neutron shielding fibre metal laminates, J. Nucl. Mater. 475 (2016) 227–236.

[4] J.E. Martin, Physics for Radiation Protection, sixth ed., APA, Wiley, New York, 2000, p. 593.

[5] N.R. Abd Elwahab, N. Helal, T. Mohamed, F. Shahin, F.M. Ali, New shielding composite paste for mixed fields of fast neutrons and gamma rays, Mater. Chem. Phys. 233 (2019) 249–253.

[6] J. Rochus Paul, Adding boron compounds to increase the neutron shielding properties of materials, McMaster J. Eng. Phys. 1 (1) (2017) 1395.

[7] J. Wood, Computational Methods in Reactor Shielding, Pregamon Press, New York, 1982.

[8] E. Yılmaz, H. Baltas, E. Kırıs, I. Ustabas, U. Cevik, A.M. El-Khayatt, Gamma ray and neutron shielding properties of some concrete materials, Ann. Nucl. Energy 38 (2011) 2204–2212.

[9] M.S. Hossain, S.M.A. Islam, M.A. Quasem, M.A. Zaman, Study of shielding behavior of some multilayer shields contain PB and BX, Indian Journal of Pure & Applied Physics 48 (2010) 860–868.

[10] K. Karimi-Shahri, L. Rafat-Motavalli, H. Miri-Hakimabad, Finding a suitable shield for mixed neutron and photon fields based on an Am-Be source, J. Radioanal. Nucl. Chem. 298 (1) (2013) 33–39.

[11] S.J. Park, J.G. Jang, H.K. Lee, Computational investigation of the neutron shielding and activation characteristics of borated concrete with polyethylene aggregate, J. Nucl. Mater. 452 (2014) 205–211.

[12] M.H. Kharita, S. Yousef, M. AlNassar, Review on the addition of boron compounds to radiation shielding concrete, Prog. Nucl. Energy 53 (2) (2011) 207–211.

[13] S.E. Liverhant, Elementary Introduction to Nuclear Reactor Physics, Wiley, New York, 1960.

[14] M. Kurudirek, M. Buyukyıldız, Y.O. Zdemir, Effective atomic number study of various alloys for total photon interaction in the energy region of 1 keV–100 GeV, Nucl. Instrum. Methods Phys. Res. 613 (2010) 251–256.

[15] I. Akkurt, H. Akyıldırım, B. Mavi, S. Kilincarslan, C. Basyigit, Photon attenuation coefficients of concrete includes barite in different rate, Ann. Nucl. Energy 37 (2010) 910–914.

[16] K.Y. Noh, C.J. Park, Y.D. Lee, J.Y. Hyeon, G.I. Park, Shielding analysis of high density polyethylene and borax for lead slowing down time spectrometer system, Trans. Korean Nucl. Soc. 24 (45) (2011) 26–27.

[17] J. Kim, B.C. Lee, Y.R. Uhm, W.H. Miller, Enhancement of thermal neutron attenuation of nano-B4C, -BN dispersed neutron shielding polymer nanocomposites, J. Nucl. Mater. 453 (1–3) (2014) 48–53.

[18] X. Zhang, X. Zhang, S. Guo, Simple approach to developing high-efficiency neutron shielding composites, Polym. Eng. Sci. 59 (2019) E348–E355.

[19] Y. Huang, W. Zhang, L. Liang, J. Xu, Z. Che, A "Sandwich" type of neutron shielding composite filled with boron carbide reinforced by carbon fiber, Chem. Eng. J. 220 (2013) 143–150.

[20] M. Shamsuzzaman, M.A.M. Khan, M.M.H. Bhuiyan, M.S. Rahman, M.J.H. Khan, D. Paul, et al., Attenuation property of wood and fiber reinforced polymer composite materials for neutron and gamma radiation shielding, Am. J. Mater. Sci. 9 (1) (2019) 8–14.

[21] B.R. Evans, J. Lian, W. Ji, Evaluation of shielding performance for newly developed composite material, Ann. Nucl. Energy 116 (2018) 1–9.

[22] J. Megusar, Low temperature fast-neutron and gamma irradiation of glass fiber/epoxy composite. Part 1. Deformation and fracture, J. Nucl. Mater. 228 (1996) 168–175.

[23] T. Tuna, K. Bayrak, Investigation of the shielding capability of concrete matrixed colemanite reinforced shielding material, J. Eng. Technol. Appl. Sci. 2 (2) (2017) 57–63.

[24] J. Min, B. Lee, J.S. Lee, Development of synthetic resin-based mortar for low activation and neutron shields, Constr. Build. Mater. 124 (2016) 992–998.

[25] D. Castley, C. Goodwin, J. Liu, Computational and experimental comparison of boron carbide, gadolinium oxide, samarium oxide, and graphene platelets as additives for a neutron shield, Radiat. Phys. Chem. 165 (2019) 108435–108443.

[26] I.W. Nam, H.K. Lee, J.H. Jang, Electromagnetic interference shielding/absorbing characteristics of CNT-embedded epoxy composites, Compos. A Appl. Sci. 42 (9) (2011) 1110–1118.

[27] M. El-Sarraf, A.E. Abdo, Insulating epoxy/barite and polyester/barite composites for radiation attenuation, Appl. Radiat. Isot. 79 (2013) 18–24.

[28] T. Korkut, O. Gencel, E. Kam, W. Brostow, X-ray, gamma, and neutron radiation tests on epoxy-ferrochromium slag composites by experiments and Monte Carlo simulations, Int. J. Polym. Anal. Charact. 18 (3) (2013) 224–231.

[29] Y.P. Huang, L. Liang, J. Xu, W.J. Zhang, The design study of a new nuclear protection material, Nucl. Eng. Des. 248 (2012) 22–27.

[30] M. Saiyad, N.M. Devashrayee, R.K. Mevada, Study the effect of dispersion of filler in polymer composite for radiation shielding, Polym. Compos. 35 (7) (2014) 1263–1266.

[31] P.Y. Hsu, S. Lin, C.F. Yang, J.J. Lin, Improvement of radiation-induced degradation in MOSFET by using glass fiber/epoxy/silica nanoparticles/c-APTES composite as shielding materials for high-energy radiation, in: Intelligent Technologies and Engineering Systems, Springer, New York, 2013. p. 901–906.

[32] H.X. Zhang, S. Chang, B. Kang, B. Sheng, Y.D. Dai, Preparation of functional particles modified epoxy multilayer composite and their radiation shielding properties, Adv. Mater. Res. 900 (2014) 150–153.

[33] N.Z.N. Azman, S.A. Siddiqui, R. Hart, I.M. Low, Microstructural design of lead oxide–epoxy composites for radiation shielding purposes, J. Appl. Polym. Sci. 128 (5) (2013) 3213–3219.

[34] M.A. El-Sarraf, A.E. Abdo, M.A. Abdul-Wahab, Usability of epoxy/ilmenite composite material as an attenuator for radiation and a restoration mortar for cracks, Ann. Nucl. Energy 60 (2013) 362–367.

[35] B. Aygün, T. Korkut, A. Karabulut, O. Gencel, A. Karabulut, Production and neutron irradiation tests on a new epoxy/molybdenum composite, Int. J. Polym. Anal. Charact. 20 (4) (2015) 323–329.

[36] K. Okuno, Neutron shielding material based on colemanite and epoxy resin, Radiat. Prot. Dosim. 115 (1–4) (2005) 258–261.

[37] R. Adeli, S.P. Shirmardi, S.J. Ahmadi, Neutron irradiation tests on B_4C/epoxy composite for neutron shielding application and the parameters assay, Radiat. Phys. Chem. 127 (2016) 140–146.

[38] M.A. Kiani, S.J. Ahmadi, M. Outokesh, R. Adeli, A. Mohammadi, Preparation and characteristics of Epoxy/Clay/B_4C nanocomposite at high concentration of boron carbide for neutron shielding application, Radiat. Phys. Chem. Radiat. Phys. Chem. 141 (2017) 223–228.

[39] M.A. El-Sarraf, A. El-Sayed Abdo, M.A. Abdul-Waha, Usability of epoxy/ilmenite composite material as an attenuator for radiation and a restoration mortar for cracks, Ann. Nucl. Energy 60 (2013) 362–367.

[40] A. El-Sayed Abdo, M.A. El-Sarraf, F.A. Gaber, Utilization of ilmenite/epoxy composite for neutrons and gamma rays attenuation, Ann. Nucl. Energy 30 (2003) 175–187.

[41] H. Hu, Q. Wang, J. Qin, Y. Wu, et al., Study on composite material for shielding mixed neutron and γ-rays, IEEE Trans. Nucl. Sci. 55 (4) (2008) 2376–2384.

[42] J. Jun, J. Kim, Y. Bae, Y.S. Seo, Enhancement of dispersion and adhesion of B_4C particles in epoxy resin using direct ultrasonic excitation, J. Nucl. Mater. 416 (2011) 293–297.

[43] M.K. Lee, J.K. Lee, J.W. Kim, G.J. Lee, Properties of B_4C-PbO-$Al(OH)_3$-epoxy nanocomposite prepared by ultrasonic dispersion approach for high temperature neutron shields, J. Nucl. Mater. 445 (2014) 63–71.
[44] Z. Li, X. Xue, T. Jiang, H. Yang, M. Zhou, Study on the properties of boron-containing ores/epoxy composites for slow neutron shielding, Adv. Mater. Res. 201-203 (2011) 2767–2771.
[45] Z. Li, X. Xue, P. Duan, A. Tian, S. Li, Z. Yin, Preparation and thermal/fast neutron shielding properties of novel boron containing ore composites, Mater. Sci. Forum 743-744 (2013) 613–622.
[46] M. Saiyad, N.M. Devashrayee, R.K. Mevada, Study the effect of dispersion of filler in polymer composite for radiation shielding, Polym. Compos. 35 (2014) 1263–1266.
[47] A. Canel, H. Korkut, T. Korkut, Improving neutron and gamma flexible shielding by adding medium-heavy metal powder to epoxy based composite materials, Radiat. Phys. Chem. 158 (2019) 13–16.
[48] N.A. Galehdari, A.D. Kelkar, Effect of neutron radiation on the mechanical and thermophysical properties of nanoengineered polymer composites, J. Mater. Res. 32 (2) (2017) 426–434.
[49] J. Kim, B.C. Lee, Y.R. Uhm, W.H. Miller, Enhancement of thermal neutron attenuation of nano-B_4C, -BN dispersed neutron shielding polymer nanocomposites, J. Nucl. Mater. 453 (2014) 48–53.
[50] M. Rezaeian, J. Kamali, S.J. Ahmadi, M.A. Kiani, Effectiveness of the neutron shield nanocomposites for a dual purpose cask of Bushehr's VVER 1000 NPP spent fuels, Nucl. Eng. Technol. 49 (7) (2017) 1563–1570.
[51] F.A. Gaber, M.A. El-Sarraf, W.A. Kansouh, Utilization of boron oxide glass and epoxy/ilmenite assembly as two layer shield, Annu. Nucl. Energy 57 (2013) 106–110.
[52] F. Banhart, Irradiation effects in carbon nanostructures, Rep. Prog. Phys. 62 (1999) 1181.
[53] Z. Li, S. Chen, S. Nambiar, PMMA/MWCNT nanocomposite for proton radiation shielding applications, Nanotechnology 27 (2016) 234001–234010.
[54] T. Bel, C. Arslan, N. Baydogan, Radiation shielding properties of poly(methyl methacrylate)/colemanite composite for the use in mixed irradiation fields of neutrons and gamma rays, Mater. Chem. Phys. 221 (2019) 58–67.
[55] Y. Wu, G. Chen, M. Zhan, J. Yan, High heat resistant carbon fiber/polyimide composites with neutron shielding performance, Prog. Org. Coat. 132 (2019) 184–190.
[56] B. Aygün, T. Korkut, A. Karabulut, O. Gencel, A. Karabulut, Production and neutron irradiation tests on a new epoxy/molybdenum composite, Int. J. Polym. Anal. Charact. 20 (4) (2015) 323–329.
[57] X.L. Fu, Y.B. Hu, H.G. Li, J. Tao, Study on the thermal and mechanical properties of novel neutron shielding composite laminates at elevated temperature, Mater. Sci. Eng. A 697 (2017) 101–110.
[58] P. Wang, X. Tang, H. Chai, D. Chen, Y. Qiu, Design, fabrication, and properties of a continuous carbon-fiber reinforced Sm_2O_3/polyimide gamma ray/neutron shielding material, Fusion Eng. Des. 101 (2015) 218–225.
[59] S. Thakur, P. Kaur, L. Singh, Investigation of polymethyl methacrylate incorporated neodymium oxide for gamma-ray and neutron shielding behaviour, AIP Conf. Proc. 2142 (2019) 120007–120011.
[60] X. Li, J. Wu, C. Tang, Z. He, P. Yuan, Y. Sun, et al., High temperature resistant polyimide/boron carbide composites for neutron radiation shielding, Compos. Part B 159 (2019) 355–361.
[61] F. Cataldo, M. Prata, Neutron radiation shielding with PUR composites loaded with B_4C or graphite, Fullerenes, Nanotubes Carbon Nanostruct. 27 (7) (2019) 1–7.

[62] H.-B. Chen, Y.-Y. Ao, D. Liu, H.-T. Song, P. Shen, Novel neutron shielding alginate based aerogel with extremely low flammability, Ind. Eng. Chem. Res. J. 56 (30) (2017) 8563–8567.

[63] F. Cataldo, M. Prata, New composites for neutron radiation shielding, J. Radioanal. Nucl. Chem. 320 (2019) 831–839.

[64] S. Guru, S.S. Amritphale, J. Mishra, S. Joshi, Multicomponent red mud-polyester composites for neutron shielding application, Mater. Chem. Phys. 224 (2019) 369–375.

[65] Y. Wu, J. Hu, C. Feng, G. Chen, J. Yan, Carborane-containing copolyester fibers with unique neutron shielding properties, Mater. Des. 172 (2019) 107772–107778.

[66] S.A. Tijani, Y. Al-Hadeethi, The use of isophthalic-bismuth polymer composites as radiation shielding barriers in nuclear medicine, Mater. Res. Express 6 (2019) 055323–055329.

[67] C.H. Wang, L.M. Hu, Z.F. Wang, M. Zhang, Electrospun and in situ self-polymerization of polyacrylonitrile containing gadolinium nanofibers for thermal neutron protection, Rare Metals 38 (2019) 252–258.

[68] J.M. Brown, D. Curliss, R.A. Vaia, Thermoset-layered silicate nanocomposites. Quaternary ammonium montmorillonite with primary diamine cured epoxies, Chem. Mater. 12 (11) (2000) 3376–3384.

[69] X. Kornmann, H. Lindberg, L.A. Berglund, Synthesis of epoxy-clay nanocomposites. Influence of the nature of the curing agent on structure, Polymer 42 (10) (2001) 4493–4499.

[70] E.P. Giannelis, Polymer-layered silicate nanocomposites: synthesis, properties and applications, Appl. Organomet. Chem. 12 (10–11) (1998) 675–680.

[71] T. Korkut, O. Gencel, E. Kam, W. Brostow, X-Ray, gamma, and neutron radiation tests on Epoxy-Ferrochromium slag composites by experiments and Monte Carlo simulations, Int. J. Polym. Anal. Charact. 18 (3) (2013) 224–231.

[72] K. Okuno, Neutron shielding material based on colemanite and epoxy resin, Radiat. Prot. Dosim. 115 (1–4) (2005) 258–261.

[73] H. Issard, T.N. International, France Development of neutron shielding materials for high burn up nuclear fuel storage facilities, in: A. Alami, H. Issard, S. Momon (Eds.), SMIRT 20 Conference Espoo, Finland (2009). TN International France. Development of Neutron Shielding Materials for Transport/Storage Casks and Installations, INMM Conference, 2011.

[74] N. Yamada, R. Horita, K. Kusunoki, A. O-iwa, R. Asano, Thermal behavior of neutron shielding material, NS-4-FR, under long term storage conditions, in: PATRAM, Berlin, Germany, September 20–24, 2004.

[75] H. Issard, Radiation protection by shielding in packages for radioactive materials, in: K. Sorenson (Ed.), Safe and Secure Transport and Storage of Radioactive Materials, first ed., Elsevier, 2015, pp. 123–140.

CHAPTER 5

Elastomeric micro- and nanocomposites for neutron shielding

Tonguç Özdemir
Mersin University Chemical Engineering Department, Mersin, Turkey.

5.1 Introduction

Neutron particles have been discovered by J. Chadwick [1] in 1932 and since then neutrons have been utilized in many different application areas including industry, research, and agriculture, among others. Materials are exposed to neutron radiation in different environments such as nuclear industry and outer space. Neutrons are conventionally shielded by paraffin that has high hydrogen content and it is also used for shielding in howitzer-type neutron sources. The limitation of the paraffin is with the flexibility and it burns easily [2]. However, elastomeric materials are materials with extreme flexible nature and could also have superior material properties.

Neutron sources are widely used in industry and research applications including nuclear gauges, nondestructive testing, material analysis, radioisotope production, etc. It is important to have a safe workplace environment to protect public and radiation workers. International Atomic Energy Agency (IAEA) establishes safety standards for protection against ionizing radiation from peaceful nuclear activities [3]. Neutrons have high radiation weighting factors that depend on neutron energy, high radiation weighting factors lead to high equivalent dose in anyone exposed.

Neutrons could be produced from nuclear reactors, accelerators, neutron generators, and alpha-neutron radiation sources [4]. Neutron shielding comprises two main steps: first one is the deceleration of fast neutrons to thermal energies and the second step is the absorption of thermalized neutrons [5]. Low atomic weight materials and hydrogen-rich materials, for example, water and paraffin, could be used for the deceleration of the fast neutrons. Consequently, the thermalized neutrons are absorbed by materials that have a high neutron absorption cross section, for example, boron and its compounds [5]. Although many different materials have been used for

Micro and Nanostructured Composite Materials for Neutron Shielding Applications
https://doi.org/10.1016/B978-0-12-819459-1.00005-2
© 2020 Elsevier Ltd.
All rights reserved.

neutron shielding, the elastomers provide flexibility for the shielding materials, and that is why the development flexible neutron shielding materials is increasing.

Radiation incidents and accidents, unfortunately, occur in spite of many safety-related precautions within the facilities and activities. Incidents and accidents are classified according to INES Scale [6] developed by international organizations. According to this classification system, accidents refer to more severe events compared to incidents. The elastomeric neutron shielding materials could be a useful tool for the intervention actions to the incidents. In addition, neutron shielding is necessary for the protection of workers who are occupationally exposed to the neutron radiation. People engaged in outer space activities are also exposed to neutron radiation.

A study reported that nanocomposites show more effective shielding performance compared to the microcomposites and it was stated that "the shielding effectiveness significantly decreases for filler radii in the micrometer range and above" [7]. It is theoretically correct that the small-sized materials with relatively high surface-area-to-volume ratio have higher shielding efficiency. The increased efficiency due to high surface-area-to-volume ratio of the functional additive would lead the relatively less use of the functional filler for neutron shielding. This might, as well, provide an opportunity to develop lightweight neutron-attenuating materials.

5.2 Elastomers

Elastomers are a class of polymeric materials with flexible nature. Elastomers have low intermolecular forces that allow them to have high degrees of elongation. The typical stress versus strain diagram for elastomers is illustrated in Fig. 5.1. Elastic modulus is low for elastomeric materials and they are in amorphous state. When elastomers are stretched, some crystalline regions occur within the elastomeric structure. The cross-links within the elastomers provide the ability to regain the original form after the applied stress, that is either dynamic or static, is removed. Glass transition temperature (T_g) of the elastomers is lower than the room temperature. In addition, elastomeric materials have very high toughness values; in other words, they are able to absorb very high energies under stress. Elastomers, in general, have other superior properties such as high abrasion resistance and impermeability. Elastomers have also good adhesion properties and are used in adhesive industry [8]. Good adhesion to different types of fillers and all other properties allow the elastomers to be used widely in daily applications.

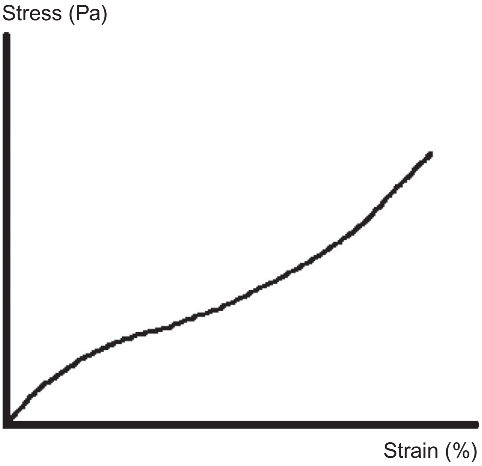

Fig. 5.1 A typical stress-strain diagram for the elastomers.

Elastomeric materials are also used in nuclear industry mostly for the sealing applications and electrical wire insulation.

5.3 Types of elastomers used in neutron shielding

The present literature shows that both synthetic and natural rubbers are good candidates for the development of neutron shielding composite materials. In this regard, natural rubber, EPDM rubber, silicone rubber, natural rubber, and styrene butadiene rubber elastomers have mainly been used for the incorporation of functional fillers for neutron particles' attenuation. The physical properties of elastomeric materials are given in Ref. [9]. Elastomers have been used to incorporate suitable fillers for X/gamma-ray shielding applications, as well. For this purpose, high atomic weight materials are employed due to the interaction mechanism of the photons with matter.

The polymeric structures that have high hydrogen content are advantageous for neutron shielding purpose. It is worth to state that the conventional polymeric material that has been used for the neutron shielding is polyethylene due to its high hydrogen content. There are many literature reports available (such as Refs. [10, 11]) about incorporation of functional fillers into polyethylene. High-density poly ethylene (HDPE) is mostly used due to relatively low branching of polymeric chains and high-density compared to that of low-density polyethylene (LDPE).

5.4 Typical additives used for elastomer-based neutron shielding composite material development

The typical additives used for neutron-shielding applications using elastomeric matrix are mainly hexagonal boron nitride (hBN), boron carbide, boron oxide, boric acid, and zinc borate. It is important to note that hexagonal boron nitrate is a ceramic material and has a structure similar to graphite that is used as a neutron moderation in nuclear reactors.

Boron compounds due to high neutron cross-section value are mostly used for embedding materials into an elastomer matrix. Size of the incorporated particles and homogeneity of the functional filler within the polymer matrix are two important parameters for ensuring the interaction of the incoming neutron particles with the functional fillers [7].

5.5 Neutron shielding with elastomeric micro- and nanocomposites developed

There are ongoing efforts to develop flexible neutron shielding materials. One of the motivation is to end up with a flexible neutron shielding composite contrary to inflexible nature of conventional materials used for neutron radiation shielding. Many different elastomeric composites have been developed for the purpose of neutron shielding and some studies were also carried out for attenuating neutron particles and gamma-ray photons. Another motivation for using elastomer in neutron shielding is the reduction in the weight of the shielding material. In particular for the space studies, development of lightweight shielding material is very vital. A summary of studies carried out on the development of micro- and nanostructured composites of elastomers for neutron shielding is presented in Table 5.1.

It is obvious from Table 5.1 that some of the composite materials were designed to shield mixed radiation of gamma, neutrons, and heavy ions [13, 14, 19, 26].

For the development of rubber composites, mainly two-roll mill equipment is used, many different chemical agents (activators, coactivator, accelerators, cross-linker, reinforcing filler, etc.) should also be added for the proper completion of vulcanization process. The functional fillers for neutron attenuation are added to the rubber compound, in general, at the two-roll mill for the purpose of ending up with a homogeneous rubber compound before the vulcanization step. The homogenized rubber compound is then vulcanized to have a stable material matrix including functional fillers for required neutron particle attenuation.

Table 5.1 A summary of studies carried out on developing micro and nanostructured composites of elastomers for neutron shielding.

Elastomer type	Functional additive(s)	Shielding purpose	Reference
Silicone rubber	Boron carbide, hollow beads, and zinc borate	Neutron	[12]
Chloroprene rubber/ natural rubber	Boron carbide (as the thermal neutron absorber) and tungsten (as the gamma-ray shielding material)	Neutron and gamma	[13]
Baypren 210 (KAU) (rare earth doped high-density rubber)	Rare earth doping	Neutron and heavy ions	[14]
Natural rubber	Boric acid	Neutron	[15]
Ethylene-propylene diene rubber (EPDM) and low-density polyethylene (LDPE)	Boron carbide powder	Neutron	[16]
EPDM	Boric acid	Neutron	[17]
EPDM	Boron oxide	Neutron	[18]
Silicone rubber	Hexagonal boron nitride, boron oxide, bismuth oxide	Neutron and gamma	[19]
Silicone rubber	Hexagonal boron nitride	Neutron	[20]
EPDM	Hexagonal boron nitride (hBN)	Neutron	[21]
Natural rubber/wood particles	Boron oxide and boric acid	Neutron	[22]
Poly-diphenyl-methylsiloxane	Boron-10	Neutron	[23]
Polyurethane (PUR)	Hexagonal boron nitride (hBN) and boron	Neutron	[24]
Silicone rubber	Boron carbide, gadolinium oxide, samarium oxide, and graphene	Neutron	[25]
Silicone rubber	Boron carbide, PbO, and benzophenone (BP)	Neutron	[26]
Natural rubber latex	Boron carbide	Neutron	[27]
Natural rubber (NR) and styrene butadiene rubber (SBR)	Boron oxide	Neutron	[28]
Natural rubber	Boron carbide	Neutron	[29]

Additives such as antirads could help to have a more radiation-resistant elastomer-based composite material. This could be effective especially in the environments where the materials are exposed to the mixed radiation types. When developing the elastomer-based composite material, compatibility of the fillers for radiation shielding with the polymeric matrix is necessary. Coupling agents could be used for the improvement of the compatibility of the fillers with the polymer matrix.

Chai et al. [12] reported a flexible flame-retardant microcomposite for neutron shielding. In that study, VMQ-type silicone rubber was used as the main elastomeric matrix. Boron carbide (about 50 μm), hollow bead material (about 80 μm), and zinc borate (about 2 μm) were incorporated into the elastomer matrix. The hollow bead material was reported to be used for heat insulation, whereas zinc borate was used not only for its flame retardancy function but also due to its boron content to increase the neutron attenuation performance [12]. The filler incorporation changed the tensile properties of microcomposite and Shore hardness increased with the increase in filler content. Am/Be neutron source was used for the neutron attenuation tests, I/I_0 value for a 2-cm sample was reported as 47.8%. Surface modification for filler materials was reported to improve the neutron shielding performance of the composite material developed.

Salimi [13] reported an elastomeric microcomposite material for the shielding of neutron and gamma radiation. Chloroprene and natural rubber blend were used as composite matrix. Tungsten (10 μm) was used in the composite as gamma shielding functional material and boron carbide (98%, <10 μm) was used for neutron absorption. Monte Carlo simulation results were reported, and they [13] concluded that the simulations confirmed that the incorporation of 5% by weight of boron carbide would end up with best thermal neutron attenuation capacity. Tungsten content for the composite was reported to be adjustable depending on the required degree of shielding from gamma radiation.

Shielding properties of rare earth-doped high-density rubber was studied for neutron particle and heavy ion shielding by Vana et al. [14]. The results of the shielding performance were compared with that of aluminum and polyethylene. Results reported that tested new materials might be more effective up to 10% regarding neutron attenuation in comparison with aluminum shielding. Vana et al. [14] have also reported that due to lower density of polymer and rubber samples compared to conventional shielding materials, a weight reduction in shielding materials could be achieved. This situation would also contribute to the reduction in space mission launch cost.

Gwaily et al. [15] developed an elastomer composite of natural rubber and boric acid and the effect of boric acid content on the attenuation of thermal neutron radiation was investigated. The maximum value of the macroscopic cross section for thermal neutrons was reported as 0.29 cm^{-1} for composite containing 30 part per hundred (phr) boric acid. Thermal neutron attenuation of 30-phr boric acid containing boric acid/natural rubber composite was about 107% higher than that for natural rubber without any boric acid content.

Abdel-Aziz et al. [16] studied the development of a composite including ethylene-propylene diene rubber, low-density polyethylene, and boron carbide. Contents of boron carbide powder in the composites developed were 47% and 57%, by weight. The composites were investigated for their gamma and thermal neutron radiation shielding properties. Pu/Be source was used as the radiation source for neutron attenuation tests. As one of the results reported, the thermal neutron attenuation of the composite with 57% by weight of boron carbide is about 45% higher than that of composite with 47% by weight of boron carbide.

Neutron shielding of EPDM rubber with boric acid and boron oxide were studied by Özdemir et al. [17, 18] and mechanical, thermal, and neutron shielding tests were carried out.

The reason for the selection of EPDM as candidate material for flexible neutron shielding materials was being the presence of high hydrogen content within EPDM's polymeric chain structure [17]. Experimental and theoretical calculations were carried out within the scope of that study. Microwave irradiation-assisted sol-gel analysis tests and in parallel Soxhlet extraction studies were conducted to find out the gel fraction of the developed polymer composite. The neutron attenuation tests were carried out for elastomeric composite containing 20% by weight of boric acid. The attenuation coefficient for EPDM rubber with boric acid was calculated to be 0.53 cm^{-1} [17] and experimental results for attenuation ratio was reported to be lower than the theoretical calculations. It was reported that EPDM rubber with boric acid functional filler forms an efficient neutron moderating flexible composite material. Özdemir et al. [18] have also reported that the incorporation of boron trioxide into EPDM matrix led to an increase in the tensile properties and tear strength of the composite material. The attenuation coefficient of EPDM containing 20% by weight of boron trioxide was reported to be 0.56 cm^{-1}. It was stated that the EPDM and boron trioxide composite material could be used as a flexible neutron shielding material like EPDM and boric acid composite.

In another study, Özdemir and Yilmaz [19] reported the development of a novel silicone-based three-layered composite material consisting of hexagonal boron nitrate, boron oxide and bismuth oxide containing silicone layers; this composite material was developed for both gamma and neutron shielding. Bismuth oxide was used as a gamma-ray shielding functional material. Silicone rubber used was a high-temperature vulcanization (HTV)-type silicone rubber due to flexibility, high transparency, and superior mechanical properties [19]. Hexagonal boron nitrite and bismuth oxide have a very good compatibility with the silicone matrix, and have been very homogeneously mixed with the silicone within the two-roll mill equipment. Mechanical, thermal, and neutron attenuation tests were performed by Özdemir and Yilmaz [19]. A composite having a lead (Pb) equivalent thickness of 0.35 mmPb was developed. In addition, I/I_0 value for neutron particles was 30.8% for elastomeric composite developed having hBN content of 30%, by weight. The authors [19] concluded that the composite material with layered structure could attenuate either neutrons or gamma-rays and concluded that the developed composite material can successfully be used during intervention actions to the incidents.

Özdemir research group used hexagonal boron nitrate ceramic filler within two different rubber matrices, silicone rubber and EPDM rubber, for neutron particle attenuation [20, 21]. Özdemir and Yilmaz [20] stated that "hexagonal boron nitride with its unique properties could be used for neutron attenuation as the ceramic filler for the rubber matrix." Silicone rubber VMQ-type polydimethylsiloxane incorporated with hexagonal boron nitride was cured, and mechanical, thermal, and neutron attenuation tests were carried out. The attenuation rate (I/I_0) was reported to be 60.7% for the developed composite material consisting of 30 wt% hBN with thickness 6.9 mm. Hexagonal boron nitride incorporation modified tensile properties of silicone rubber matrix and increasing the content of hBN in the composite material causes the rise in the hardness value of the developed composite material. The glass transition temperature of the hBN/silicone rubber composite decreased with the rise in the hBN content. Silicone rubber incorporated with hBN with flexible nature was reported as a composite material that can be used in the areas where the neutron shielding is desired [20].

In another study that included hexagonal boron nitride filler, Güngör et al. [21] have developed flexible hBN/EPDM composite. The authors [21] have carried out kinetic analysis for this rubber composite and concluded that the nonautocatalytic reaction was the main reaction type during the vulcanization process. They have also reported that the increase in hBN content has changed the nature and the flexibility of the rubber composite. Thermal stability of the composite was improved with the further addition of hBN. Thermal neutron attenuation tests showed that hBN/EPDM composite attenuated the neutron radiation up to 61.5%. They reported that the developed composite of hBN/EPDM is a good neutron shielding material having a flexible nature depending on the hBN filler content.

Bio-based materials were also used in the fabrication of composite materials for the neutron shielding [22]. In a study, thermal neutron attenuation, vulcanization parameters of natural rubber, and wood particles/natural rubber composites having either boron oxide or boric acid as functional fillers have been investigated [22]. It was concluded that increase in the boron oxide or boric acid content within the elastomer improve thermal neutron attenuation performance, and, on the other hand, the tensile properties improved with the incorporation of 20 phr wood particles in wood/natural rubber composites.

Labouriau et al. [23] studied boron-10 filled siloxane-based polymer that was exposed to nuclear reactor irradiation for neutron attenuation testing. Highly filled polysiloxanes were synthesized for shielding high neutron flux. The developed composite material consisted of cross-linked poly-diphenylmethylsiloxane as main elastomeric matrix whereas natural boron and carbon nanofibers were used as functional fillers. The aromatic groups present in the siloxane backbone provide resistance to ionizing radiation. Highly isotopically enriched boron-10 was used for neutron shielding and carbon nanofibers were used for mechanical strength improvement. They have reported that the composite developed was resistant to ionizing radiation due to the presence of high concentrations of aromatic groups in the polymer chain and the composite was effective in capturing thermal neutrons owing to the presence of isotopically enriched boron-10 within the polymeric matrix [23].

Cataldo and Prata [24] used castable polyether-polyurethane (PUR) composite for which amorphous boron and hexagonal boron nitride were used as functional fillers for neutron shielding. The developed composite was reported to be flexible after filler incorporation. Shielding properties of the developed composite improved with the incorporation of the functional fillers. PUR composite incorporated with amorphous boron showed better shielding performance compared to composite incorporated with boron nitrate.

Castley et al. [25] developed a nanocomposite that is high-temperature-resistant neutron shielding material using an elastomer-based material. Additives of boron carbide nanopowder (<50 nm), gadolinium oxide nanoparticles (<100 nm), and samarium oxide nanoparticles (~ 100 nm) were used for incorporation into silicone matrix to achieve neutron attenuation. Graphene platelets were used to assess the ability of graphene to mitigate secondary gamma photons coming from the neutron absorption by gadolinium and samarium. The sample containing 10% gadolinium oxide and 2% boron carbide attenuated neutron particles better than the borated polyethylene with a fast neutron cross section of 0.026 cm^{-1}. On the other hand, graphene platelets did not provide a noticeable improvement for neutron attenuation [25]. Samples with 3% by weight of gadolinium oxide and samples with 3% by weight of samarium oxide have shown better neutron attenuation than the borated polyethylene sample.

Gong et al. [26] used VMQ (methyl vinyl silicone rubber)-type silicone matrix for the development of flexible gamma and neutron shielding material. For that study, boron carbide, lead oxide, and benzophenone were incorporated into the silicone matrix. In order to end up with a proper dispersion in the rubber composite, the fillers were exposed to surface modification. The function of the aromatic benzophenone was to improve the radiation resistance of the composite matrix. The authors [26] have reported that the hardness and cross-link density of the polymeric matrix increased while the tensile properties diminished. The addition of benzophenone improved the mechanical properties; in this regard the incorporation of benzophenone had a positive effect on the composite matrix. Am/Be neutron source was used for neutron attenuation tests. The I/I_0 value for neutron particles with a sample thickness of 2 mm was reported to be 0.12. The authors [26] concluded that "developed neutron and γ-ray shielding material displayed excellent flexibility, radiation resistance, thermal stability, neutron and γ-ray shielding performance."

Liao et al. [27] developed a boron carbide and natural rubber composite with flexible nature for thermal neutron attenuation. Boron carbide content of the composite was varied within the range of 5%–55%, by weight. The authors [27] reported that boron carbide was homogeneously dispersed in the rubber latex. A three-dimensional "shielding efficiency" diagram was reported, from this diagram it is obvious that the thickness and boron carbide content are the parameters that determine the ability of the composite developed to attenuate thermal neutrons.

Natural rubber (NR) and styrene butadiene rubber (SBR) blend was developed by Jumpee et al. [28], boron oxide was used as functional filler for neutron shielding. Both experimental and Monte Carlo simulations were carried out within the scope of the study. The thickness of the samples used for experimental studies were 10 and 100 mm. A 10-mm shielding material of natural rubber (NR) and styrene butadiene rubber (SBR) blend with 60 phr boron oxide was reported to decrease the neutron intensity by about 53.9% using an Am-Be neutron source. In addition, the 100-mm rubber sample having four alternating layers consisting of 100 phr Fe_2O_3 and 20 phr B_2O_3 was reported to attenuate neutron particles by about 72.6%.

Nurazila et al. [29] studied the development of high-density polyethylene (HDPE) and natural rubber composite with varying weight content of boron carbide for neutron attenuation. Developed samples were tested using the thermal neutron flux from a research reactor. I/I_0 value for 0%, 10%, 20%, and 30% by weight of boron carbide composites were found to be 0.369, 0.106, 0.05, and 0.025 with test sample thickness of 0.3 cm.

5.6 Conclusions

The elastomers provide a stable matrix for the incorporation of functional materials for neutron-shielding applications. The flexible nature and relatively lower density (lightweight) of elastomers are important factors for their selection as the host matrix for shielding applications. The studies have shown that micro- and nanolevel elastomeric composite materials could be effectively used in the shielding of neutron particles. Many different types of elastomeric materials have been developed using different functional fillers. The hydrogen-rich elastomeric materials are also advantageous for the neutron particle deceleration. The increase in the use of neutrons for different applications would lead to further studies to benefit from elastomer materials for neutron shielding purpose.

References

[1] J. Chadwick, The existence of a neutron, Proc. R. Soc. Lond. A 136 (1932), https://doi.org/10.1098/rspa.1932.0112.

[2] B. Viswanathan, Petroleum, in: B. Viswanathan (Ed.), Energy Sources, Elsevier, 2017. ISBN 9780444563538, pp. 29–57, https://doi.org/10.1016/B978-0-444-56353-8.00002-2 (Chapter 2).

[3] Radiation Protection and Safety of Radiation Sources: International Basic Safety Standards, IAEA Safety Standards Series No. GSR Part 3, IAEA, ISBN 978-92-0-135310-8, Vienna, 2014.

[4] J.E. Martin, Physics for Radiation Protection: A Handbook, WILEY-VCH Verlag GmbH & Co. KGaA, Weinheim, 2006. ISBN 3-527-40611-5.

[5] C. Herman, E. Johnson Thomas, Introduction to Health Physics, fourth ed., McGraw Hill Companies, Inc, New York, NY, 2008.

[6] International Atomic Energy Agency, Ines, The International Nuclear and Radiological Event Scale User's Manual, IAEA, Vienna, 2013.

[7] Schrempp-Koops Lily, Size effects on the efficiency of neutron shielding in nanocomposites—a full-range analysis, Int. J. Nanosci. 12 (3) (2013) 1350015, https://doi.org/10.1142/S0219581X13500154.

[8] S. Ebnesajjad, A.H. Landrock, Classification of Adhesives and Compounds, in: S. Ebnesajjad, A.H. Landrock (Eds.), Adhesives Technology Handbook, third ed., William Andrew Publishing, 2015, pp. 67–83, https://doi.org/10.1016/B978-0-323-35595-7.00004-8 (Chapter 4).

[9] R.A. Shanks, I. Kong, General purpose elastomers: structure, chemistry, physics and performance, in: P. Visakh, S. Thomas, A. Chandra, A. Mathew (Eds.), Advances in Elastomers I. Advanced Structured Materials, vol. 11, Springer, Berlin, Heidelberg, 2013.

[10] Ş. Gözde Irim, A.A. Wis, M.A. Keskin, O. Baykara, G. Ozkoc, A. Avci, M. Doğru, M. Karakoç, Physical, mechanical and neutron shielding properties of h-BN/Gd_2O_3/HDPE ternary nanocomposites, Radiat. Phys. Chem. 144 (2018) 434–443.

[11] Z. Soltani, A. Beigzadeh, F. Ziaie, E. Asadi, Effect of particle size and percentages of boron carbide on the thermal neutron radiation shielding properties of HDPE/B4C composite: experimental and simulation studies, Radiat. Phys. Chem. 127 (2016) 182–187.

[12] H. Chai, X. Tang, M. Ni, F. Chen, Y. Zhang, D. Chen, Y. Qiu, Preparation and properties of flexible flame-retardant neutron shielding material based on methyl vinyl silicone rubber, J. Nucl. Mater. 464 (2015) 210–215.

[13] M. Salimi, N. Ghal-Eh, E.A. Amirabadi, Nucl. Sci. Tech. 29 (2018) 36, https://doi.org/10.1007/s41365-018-0371-7.

[14] N. Vana, M. Hajek, T. Berger, M. Fugger, P. Hofmann, Novel shielding materials for space and air travel, Radiat. Prot. Dosim. 120 (1–4) (September 2006) 405–409, https://doi.org/10.1093/rpd/nci670.

[15] S.E. Gwaily, H.H. Hassan, M.M. Badawy, M. Madani, Natural rubber composites as thermal neutron radiation shields: II—H_3BO_3/NR composites, Polym. Test. 21 (5) (2002) 513–517.

[16] M.M. Abdel-Aziz, S.E. Gwaily, A.S. Makarious, A. El-Sayed Abdo, Ethylene-propylene diene rubber/low density polyethylene/boron carbide composites as neutron shields, Polym. Degrad. Stab. 50 (2) (1995) 235–240.

[17] T. Özdemir, I.K. Akbay, H. Uzun, I.A. Reyhancan, Neutron shielding of EPDM rubber with boric acid: mechanical, thermal properties and neutron absorption tests, Prog. Nucl. Energy 89 (2016) 102–109.

[18] T. Özdemir, A. Güngör, I.A. Reyhancan, Flexible neutron shielding composite material of EPDM rubber with boron trioxide: mechanical, thermal investigations and neutron shielding tests, Radiat. Phys. Chem. 131 (2017) 7–12.

[19] T. Özdemir, S.N. Yilmaz, Mixed radiation shielding via 3-layered polydimethylsiloxane rubber composite containing hexagonal boron nitride, boron (III) oxide, bismuth (III) oxide for each layer, Radiat. Phys. Chem. 152 (2018) 17–22.

[20] T. Özdemir, S.N. Yilmaz, Hexagonal boron nitride and polydimethylsiloxane: a ceramic rubber composite material for neutron shielding, Radiat. Phys. Chem. 152 (2018) 93–99.

[21] A. Güngör, I.K. Akbay, T. Özdemir, EPDM rubber with hexagonal boron nitride: a thermal neutron shielding composite, Radiat. Phys. Chem. 165 (2019) 108391.

[22] K. Ninyong, E. Wimolmala, N. Sombatsompop, K. Saenboonruang, Potential use of NR and wood/NR composites as thermal neutron shielding materials, Polym. Test. 59 (2017) 336–343.

[23] A. Labouriau, T. Robison, C. Shonrock, S. Simmonds, B. Cox, A. Pacheco, C. Cady, Boron filled siloxane polymers for radiation shielding, Radiat. Phys. Chem. 144 (2018) 288–294.

[24] F. Cataldo, M. Prata, J. Radioanal. Nucl. Chem. 320 (2019) 831, https://doi.org/10.1007/s10967-019-06526-5.

[25] D. Castley, C. Goodwin, J. Liu, Computational and experimental comparison of boron carbide, gadolinium oxide, samarium oxide, and graphene platelets as additives for a neutron shield, Radiat. Phys. Chem. 165 (2019) 108435.

[26] P. Gong, M. Ni, H. Chai, F. Chen, X. Tang, Preparation and characteristics of a flexible neutron and γ-ray shielding and radiation-resistant material reinforced by benzophenone, Nucl. Eng. Technol. 50 (3) (2018) 470–477.

[27] Y.C. Liao, D.G. Xu, P.C. Zhang, Nucl. Sci. Tech. 29 (2018) 17, https://doi.org/10.1007/s41365-018-0358-4.

[28] C. Jumpee, D. Wongsawaeng, J. Phys.: Conf. Ser. 611 (2015) 012019.

[29] N.M. Zali, et al., IOP Conf. Ser.: Mater. Sci. Eng. 298 (2018) 012018.

CHAPTER 6

Metal and alloy composites for neutron shielding

İskender Akkurt[a], **ER Zuhal**[b]
[a]Suleyman Demirel University, Isparta, Turkey
[b]Istanbul Technical University, Istanbul, Turkey

6.1 Introduction

Next-generation shielding systems will be built on versatile intelligent systems. In versatile intelligent designs for the shielding systems, concepts need to be developed for the use of new materials, weight reduction, and control of excessive deformation. In many technical fields, for example, in aerospace engineering, the materials used are expected to meet high demands. Materials for shielding of neutrons must not only withstand high mechanical loads, but also withstand thermal stresses and meet nuclear requirements. Simple metals generally do not meet these requirements. Therefore, several metals are usually produced together to achieve completely new properties. In this respect, such mixtures of two or more metals, i.e., mixtures of metallic character substances, are called alloys. In general, alloys are produced by melting, mixing, and then solidifying.

An atom consists of three basic particles: electron, proton, and neutron. All particles have their own importance. Without neutrons, the only element would be hydrogen. Together with protons, the neutrons form the nucleus held together by a strong (nuclear) force. The ratio of neutrons to protons increases with increasing radioactivity. The nucleus is unstable. The neutron is a baryon and is thought to consist of two down quarks and one up quark. On the other hand, neutrons contain details of the results of their interaction with matter due to their special properties. For example, when neutrons interact with matter, they can not only see the atomic nucleus of the material under investigation, but can also interact dynamically with vibration and magnetism in the material. As such, neutron radiation makes it possible to examine both the structural property of the material and the dynamic effects such as vibrations in the atomic grid. Neutrons play a role in understanding the material world. They can show where the atoms are and what they do [1–103].

Micro and Nanostructured Composite Materials for Neutron Shielding Applications
https://doi.org/10.1016/B978-0-12-819459-1.00006-4

© 2020 Elsevier Ltd.
All rights reserved.

Radiation interacts with matter. It forms the basis of radiation protection principles. Furthermore, with this information, the effects of radiation on material interaction can be determined while the radiation makes changes in the material. The most important element of these influences is the change in radiation energy. The radiation that interacts with the material may lose some or all of its energy. This reduction in radiation energy can be expressed as the radiation shielding property of the material.

The radiation shielding property produces different results in different materials for different types of radiation. Therefore, the materials used in radiation shielding vary for different types of radiation. The activation mechanism depends on the type and energy of the particle, as well as on the number and density of protons of the atom of the medium it enters. Therefore, the interaction of charged and uncharged particles with matter needs to be considered separately [3, 5, 18, 30, 31, 59, 85, 89, 94, 96, 99, 100, 120–126].

As a part of this study, when we look at understanding the basics of interaction of neutrons with matter, it can be stated that neutron-matter interaction is an important step to work safely in areas where neutron radiation can be encountered.

There are applications using neutrons, gamma rays, and X-rays to look at the materials in depth. Neutrons are used in scientific studies and industrial applications. For example, it can be used to study the dynamics of chemical reactions at interfaces for chemical and biochemical engineering, food science, drug synthesis, welding controls in the aircraft, car, and ship industries, turbine blades, gas pipelines, and health services. Thus, the study of neutrons provides a deeper look at solid objects and provides a microscopic view of stresses that affect the service life of very important engineering components. In addition, nanoparticles, low-dimensional system and magnetism studies, new generation computer and IT technology, data storage, sensors, and neutrons are used for the development of superconducting materials [1–104, 127–132].

6.2 Neutrons and neutron shielding

The neutron is about 0.2% larger than a proton, which corresponds to an energy difference of 1.29 MeV. However, a neutron is stable when combined with the nucleus; a free neutron will decay with a half-life of about 10.3 min. To find the number of neutrons in an atom, one needs to find the mass number of each element. On the other hand, neutrons have unique advantages as atomic level probes [1–100, 104, 122–125].

Neutrons and protons are the particles that make up the atomic nucleus. A nuclear reaction in which a neutron collides with target nucleus and form a heavier nucleus (compound nucleus) is called a neutron capture reaction. Free neutron is a nucleus unconnected neutron and, unlike a limited neutron, is subject to radioactive beta degradation (Fig. 6.1). The measure of the intensity of neutron radiation, the neutron flux (neutron/cm^2), corresponds to the flow rate of neutrons [1–104, 131].

The aim of modern materials science is to understand the properties of matter on an atomic scale and to use this knowledge to optimize properties or to develop new materials (Fig. 6.2). Neutrons are neutral subatomic particles without electrical charge. Therefore, it is nondestructive and can penetrate into substances much deeper than charged particles such as electrons. In addition, since they have a property called spin, neutrons can be used to investigate magnetism on an atomic scale.

Neutrons need a low-mass material as they are weakened by a decrease in energy and subsequent absorption. The most well-known substance that naturally releases neutrons is 252Cf with a half-life of 2.65 years. In addition, neutron sources are generated by using some binary systems. Neutrons need a low-mass material that absorbs energy because of the fact that the elastic scattering will be provided by lighter materials.

In 2014, An and Xue [105] have asserted "Boron reserve of China ranks fourth in the world next to Turkey, USA, and Russia. In China, the main boron-containing ores are szaibelyite, ludwigite, and brine. However, ludwigite resource is relatively abundant and account for 58.4% of the total Chinese boron reserve."

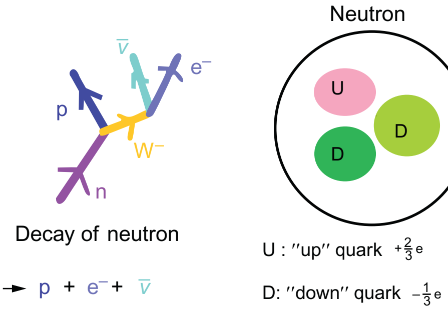
$\bar{\nu}$
e$^-$
p
W$^-$
n
Decay of neutron
$n \rightarrow p + e^- + \bar{\nu}$
Neutron
U
D
D
U : "up" quark $+\frac{2}{3}e$
D: "down" quark $-\frac{1}{3}e$

Fig. 6.1 Neutrons in atomic view.

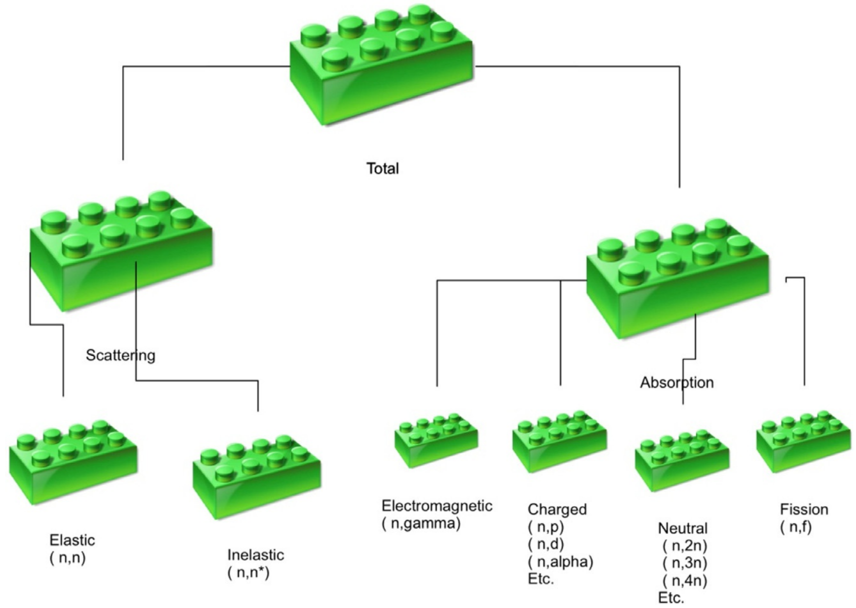
Total
Scattering
Absorption
Elastic
(n,n)
Inelastic
(n,n*)
Electromagnetic
(n,gamma)
Charged
(n,p)
(n,d)
(n,alpha)
Etc.
Neutral
(n,2n)
(n,3n)
(n,4n)
Etc.
Fission
(n,f)

Fig. 6.2 Various categories of neutron interactions.

Roughly the purpose of radiation shielding is twofold:

(i) To protect against damage caused by radiation and prevent direct contact between the source and its surroundings/environments.

(ii) Provide the physical configuration of collimation of radiation (neutron) source.

The main characteristics required for a shielding material are as follows:

(i) High cross section for neutron capture or absorption.

(ii) Low cross section for neutron scattering.

(iii) Low energy loss per collision event between neutron and shielding material.

(iv) The shielding material used in thermal reactors should have a low absorption cross section for neutrons.

(v) Temperature and the shielding material must not have a high melting point.

(vi) The shielding material must not be damaged by continuous neutron radiation (radiation stability).

(vii) The preferred material for shielding should be robust enough to ensure that impact resistance and shielding do not change over time.

The neutrons move in random directions and hence may not flow; however, neutrons will exhibit a net flow when there are spatial differences in their density. As neutrons are known to exhibit a net flow in the least density direction, it is a natural consequence that there is more collision density at more neutron density positions. A material with a low mass number and high cross section is suitable for the absorption of neutron radiation. They can be easily manufactured as desired. The material to be used as shielding material must have high corrosion resistance.

In recent years, as all in all technologies, a great deal of effort has been devoted to developing and improving a new generation of materials for radiation shielding applications. The driving forces behind this effort are preferably the small size of flexible materials, the reduction in costs, extension of the service life of material parts (structural and radiation protection), and decrease in radiation-induced damage, weight, and radiation penetration range.

This chapter examines the most important classes of composite alloy shielding materials for neutrons with the scope to provide an overview of recent advancements and to highlight current problems and perspectives related to shielding materials for neutrons. Comparisons with other scientific studies in terms of the criteria set in the literature reviews, which constitute the main structure of this section, have been made. This chapter's literature search is set on the composite alloy materials in neutron shielding. In addition to the limits of review and evaluation are also based on the criterias such as neutron absorber, multipurpose materials, English.

Absorber

- for slow neutron
- for fast neutron
- for slow and fast neutrons
- other (gamma rays)

Capturing

- microscopic cross section
- macroscopic cross section
- mass attenuation factor
- reaction rate density
- calculations—dose
- calculations—others
- simulation

Reflecting

- reflection coefficient
- shielding performance

- patented options
- comments

Shielding material

- composite
- alloy
- other types are used polymer

6.3 Composites and alloys in the material classification

Substances can be classified according to their structural composition. Pure substances contain only one type of particle. If the substance consists of several types of particles (atoms or molecules) that do not have a certain atomic ratio due to chemical bonds, these substances are called mixtures. Such mixtures can also be classified into heterogeneous mixtures and homogeneous mixtures. Homogeneous mixtures with alloys have a uniform distribution of different particles [39, 50, 99–103, 106, 107]. The material classifications representing the relationships between composites, metals, and alloys are illustrated in the Fig. 6.3.

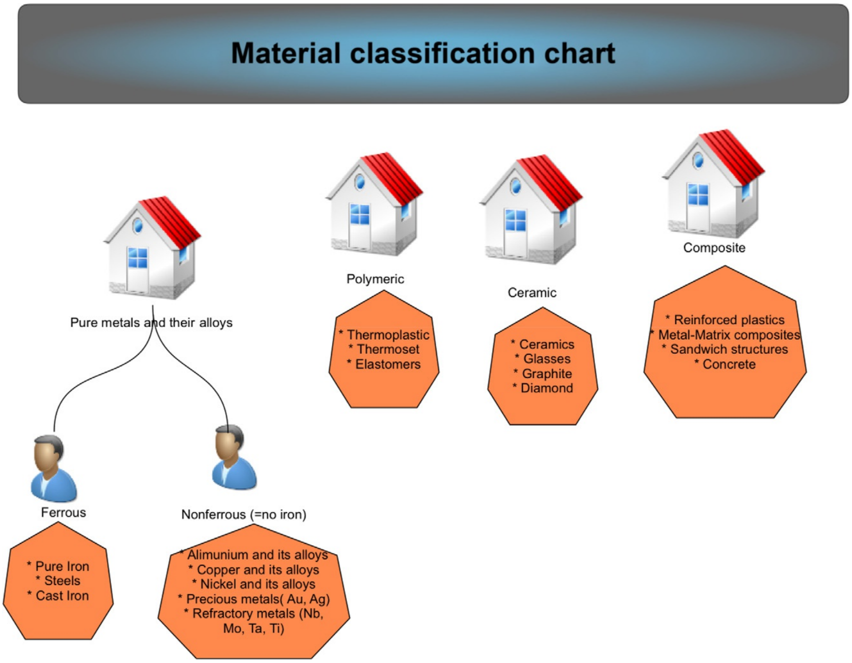
Material classification chart
Pure metals and their alloys
Polymeric
Ceramic
Composite
* Thermoplastic
* Thermoset
* Elastomers
* Ceramics
* Glasses
* Graphite
* Diamond
* Reinforced plastics
* Metal-Matrix composites
* Sandwich structures
* Concrete
Ferrous
Nonferrous (=no iron)
* Pure Iron
* Steels
* Cast Iron
* Alimunium and its alloys
* Copper and its alloys
* Nickel and its alloys
* Precious metals(Au, Ag)
* Refractory metals (Nb, Mo, Ta, Ti)

Fig. 6.3 The chart of material classification in general perspective.

Since the usage areas and needs for composite materials occupy a significant place in the digital age and include strategic importance as an additional factor for the increase in competitiveness, many studies are being carried out in order to contribute in the context of national technological upgrades and focal unity. Engineering metals are generally considered alloys [1–3, 5, 24, 25, 30, 38, 39, 48, 50, 61, 90, 99–103, 106, 107].

The metals can be characterized by high electrical and thermal conductivity as well as by malleability, ductility, and high reflectivity of light, and also good mechanical properties such as hardness, ability to withstand repeated stress (fatigue strength), ductility-malleability.

The composite (Fig. 6.5) is a combination of two or more different materials that results in a superior (often stronger) product. The composite material is a combination of two or more materials, as shown in the Fig. 6.4.

An alloy is a substance made by melting two or more elements together, one of which has to be metallic. In the other words, as mentioned previously, alloys are metallic materials formed by mixing two or more elements such as mild steel (Fe + C), stainless steel (Fe + C + Cr + Mn, …, etc.), and Cr, which improve the corrosion resistance, etc. [39, 50, 99–103, 106, 107, 132].

General Classification of Engineering Materials (Fig. 6.4) can be listed such as 1-Metals and Alloys 2-Ceramics, Glasses, and Glass-ceramics

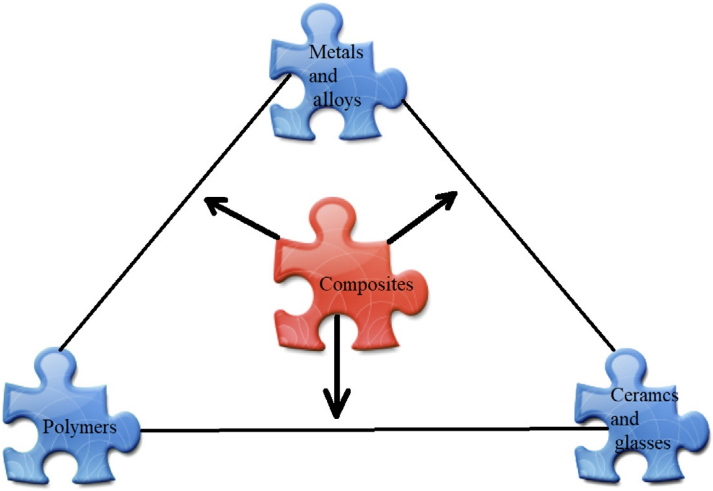

Fig. 6.4 Relationships between the composite materials and other materials.

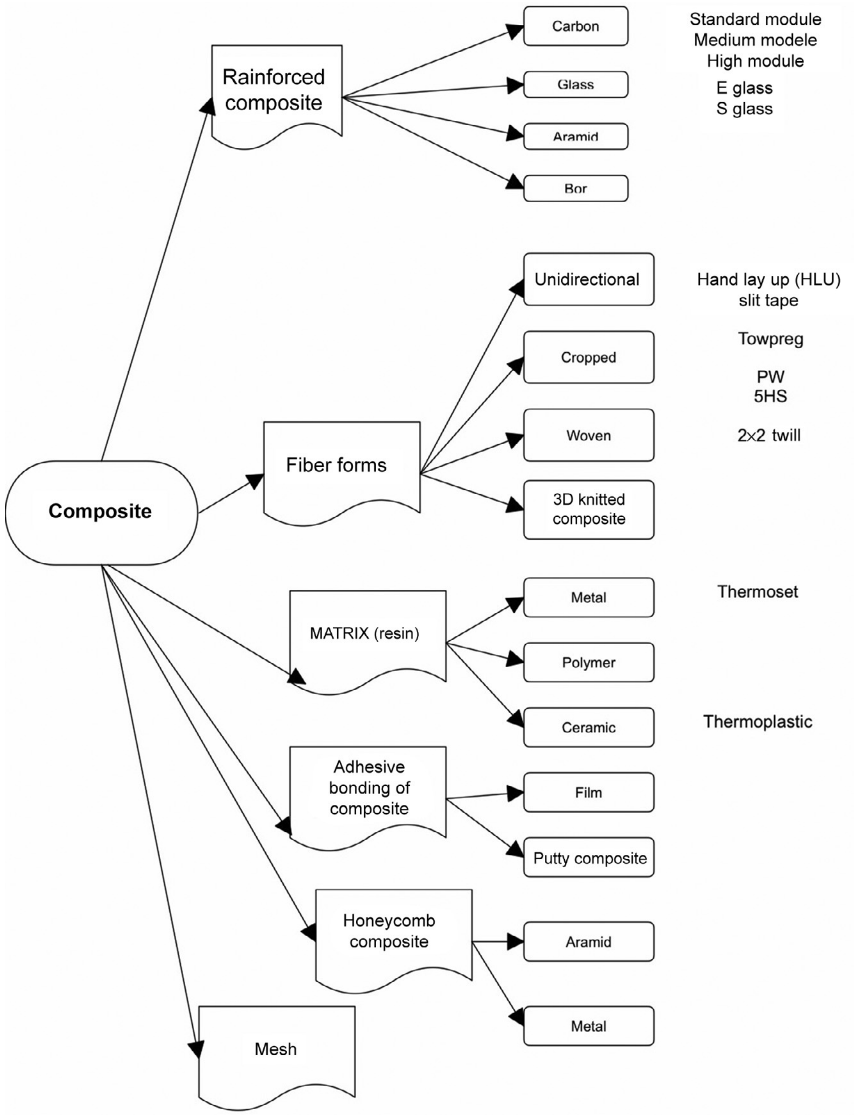
Composite
Rainforced composite
Carbon
Glass
Aramid
Bor
Standard module
Medium modele
High module
E glass
S glass
Fiber forms
Unidirectional
Cropped
Woven
3D knitted composite
Hand lay up (HLU)
slit tape
Towpreg
PW
5HS
2×2 twill
MATRIX (resin)
Metal
Polymer
Ceramic
Thermoset
Thermoplastic
Adhesive bonding of composite
Film
Putty composite
Honeycomb composite
Aramid
Metal
Mesh

Fig. 6.5 Classification of composite, and alloys.

3-Polymers (plastics), Thermoplastics and Thermosets, 4 Semiconductors, and 5-Composite Materials.

As shown in Fig. 6.3, metals and alloys are classified as ferrous (plain carbon steel, alloy steel, cast iron) and nonferrous [light alloys (Al, Mg, Ti, Zn), heavy alloys (Cu, Pb, Ni), refractory metals (Mo, Ta, W), precious metals (Au, Ag, Pt)]. On the other hand, the crystalline structure of an alloy is reinforced by the presence of foreign atoms. This is the reason why pure metals are not used in industrial applications. In other words, a particular alloy (e.g., steel) is stronger than the pure metal (Fe). In industry pure metals are not used due the low properties. The purpose of putting two (or more) ingredients together is to have a mixture; alloys offer better properties and/or significantly different qualities than the isolated components due the inclusion of foreign atoms in the crystalline structure [39, 50, 99–103, 106, 107].

Aluminum alloys
- Al-Cu alloys
- Al-Zn alloys
- Al-Li Alloys

Aluminum composites
- Metal matrix composites of light alloys (Al, Ti, Mg) with reinforced by ceramics (SiC, Al2O3, TiC, B4C)

Ceramic matrix composites
- Polymer matrix composites (polyethylene or paraffin)

Borated polyethylene, layers of B4C and aluminum, boron-aluminum alloys
- Ti alloys
- α-Ti
- β-Ti
- α-β–Ti

Ti composites reinforced with SiC fibers
- Mg alloys
- Steels
- Ni-based super alloys

Hafnium, aluminum, beryllium, lithium, magnesium, magnesium alloy, zirconium, zirconium alloy, Ni super alloys, Ti alloys, metal matrix composites (MMC), stainless steel, iron-cobalt-vanadium soft magnetic alloy, silver-indium-cadmium alloys, cadmium, gadolinium, boron, and boron carbide are the widely used materials for absorption of neutrons. Iron and concrete are good neutron absorbers [1–3, 5, 24, 25, 30, 38, 39, 48, 50, 62, 90, 99–103, 106, 107].

Compressions between the alloy and the composite are briefly explained in the following. An alloy is a mixture of metals or a mixture of a metal and another element; however, a composite is a tailor-made substance of any combination. For alloy, the element getting introduced (solute) dissolves into the metal getting alloyed (solvent) to form a solid solution. Alloy cannot be distinguished. For composite, the component forming the base of the composite (matrix) and the added element remain undissolved and could be identified.

Alloy is homogeneous mixture, even though composite can be homogeneous or heterogeneous. Whereas the constituent elements do not retain their original properties in alloy, the materials forming the composite retain their original properties in composites. Alloys have completely different enhanced properties than the reactant elements; by contrast the composites carry traces of elemental characteristics. Also alloys do not have strict proportions in elemental composition, but composites do have strict proportions in elemental composition [1–3, 5, 24, 25, 30, 38, 39, 48, 50, 61, 90, 99–103, 106, 107].

6.4 Methodology

The properties and uses of different alloys and metals are important in recent technological investments. Metal, alloy, and composite are discussed in this study with some brief schema, sketch, figure, which document the material elements of the examination and help to explain the results for neutron shielding evaluations.

Therefore, the obtained schemes, sketches, figures, and other reviews that document the material elements of the examination and help explain the results are also evaluated in the context of creating a neutron shielding technology roadmap.

In this section, the importance and test market predictions of the materials are made. Financial statements have not been presented in all subunits of the all materials.

In this respect, this study focuses on the following which is evaluated completely under the state of art of the technology and science in the neutron shielding subject.

1. Evaluation of prioritization criteria;
2. Activities, current situation trends, prioritization analysis, acquisition plan studies, and evaluations—evaluation of proposals;
3. Review of the neutron shielding studies.

6.4.1 Evaluation of prioritization criteria

In this section, the steps followed in the literature review of the composite technologies roadmap in the context of neutron shielding are schematically shown in Fig. 6.6. The methodology of the literature reviews is presented in Table 6.1 in to five method steps. Six key attributes for each assessment subject (criticality, situation in the world, limits for health, infrastructure, latest technology opportunities, scientific advances), totally 23 criteria {6-4-3-3-3

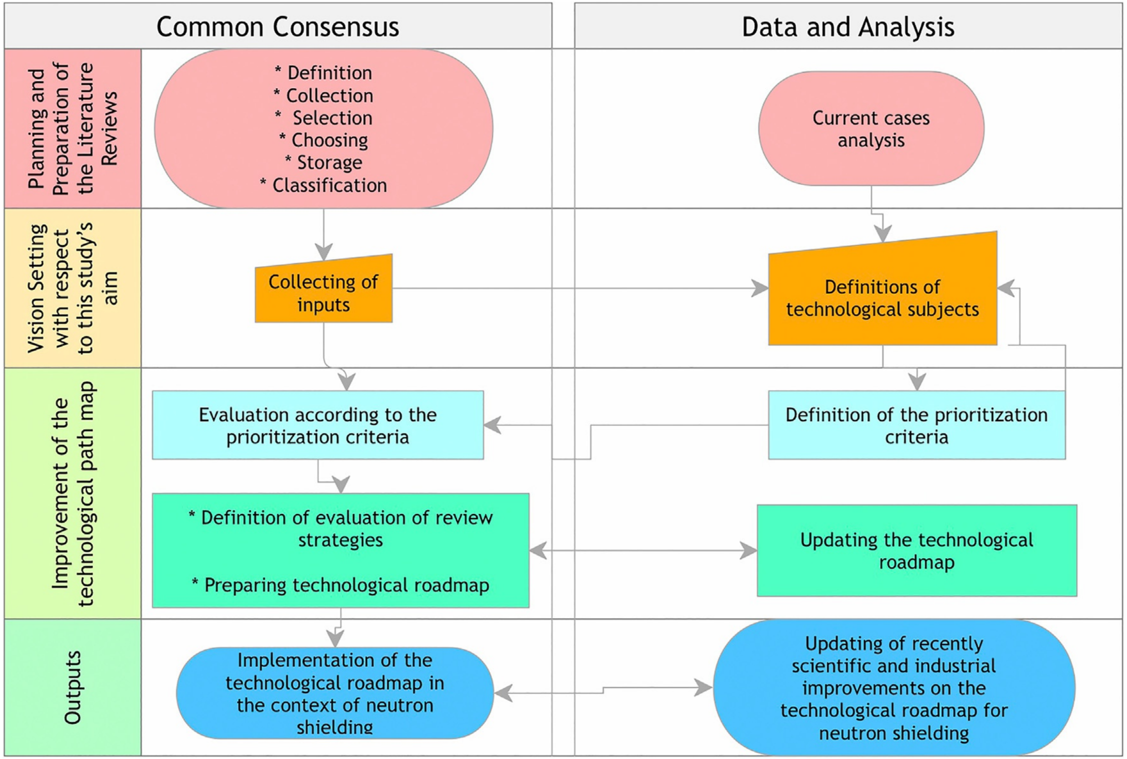

Common Consensus
Data and Analysis
Planning and Preparation of the Literature Reviews
Vision Setting with respect to this study's aim
Improvement of the technological path map
Outputs
* Definition
* Collection
* Selection
* Choosing
* Storage
* Classification
Current cases analysis
Collecting of inputs
Definitions of technological subjects
Evaluation according to the prioritization criteria
Definition of the prioritization criteria
* Definition of evaluation of review strategies
* Preparing technological roadmap
Updating the technological roadmap
Implementation of the technological roadmap in the context of neutron shielding
Updating of recently scientific and industrial improvements on the technological roadmap for neutron shielding

Fig. 6.6 Technological road map for alloys and composites.

Table 6.1 Short-term (1–5 years) first priority material technology issues to be acquired.

Subject	Technology
Composite technologies for ballistic protection	Ceramic matrix materials
Fiber design and production technology	High module carbon fiber Medium module carbon fiber
Trace reducer composite technologies	Absorber coatings (radar)
Thermoplastic material technologies	PEEK prepreg
Thermoset material technologies	Towpreg/Epoxy resin (120°C cure)/Epoxy resin prepreg (120°C cure)/Autoclave external production resin (180°C cure)

prioritization evaluations} were made. The classification of composites as a result of the classification studies after the technological road map scaling activities are shown in Fig. 6.6.

Selection of the appropriate shielding material (smart or not) for recent technological improvement in today's digital world requires consideration of many factors including less thickness and weight of the material, neutron moderation and capture properties, production of secondary radiation (n,g), potential neutron activation reactions which can induce radioactivity in the shielding material, and technological and radiological and also mechanical compatibility of the shielding material with the environment in which it will be used.

6.4.2 Literature studies, current situation trends, prioritization analyzes, acquisition plan studies, and evaluations: Evaluation of proposals

In this section, the focus is on material, design analysis, manufacturing, and nondestructive testing. In the short term (1–5 years), priority technology issues related to the material are presented in Table 6.1; design and analysis are presented in Table 6.2 ; manufacturing are presented in Table 6.3; and the test for nondestructive testing is presented in Table 6.4.

The volume of the composite industry in the world, according to 2018 global market analysis, is 11.4 million tons (Mt) and is worth 83 billion dollars. Asia has become the region with the largest volume in recent years. The United States and EMEA (Europe, the Middle East, Africa) maintained their position of having higher value-added practices when compared with other regions as shown in the Fig. 6.7.

Table 6.2 Short-term (1–5 years) first priority technology issues for the design and analysis to be acquired.

Subject	Technology
Design and analysis of the composite technologies for ballistic protection	Methods and tools for stiffness (deformation)/strength control
Design and analysis of composite structures	Methods and tools for stiffness (deformation)/strength control Methods and tools for environmental resistance control Maintenance and modification design methods and tools
Design and analysis of the trace reducer composite technologies	Methods and tools for stiffness (deformation)/strength control Methods and tools for environmental resistance control
Design and analysis of non-autoclave integrated composite structures	Methods and tools for stiffness (deformation)/strength control Methods and tools for damage tolerance control Methods and tools for environmental resistance control Maintenance and modification design methods and tools Methods and tools for operational and special case strength
Design and analysis for thermoplastics	Methods and tools for stiffness (deformation)/strength control Methods and tools for environmental resistance control
Design and analysis for thermo-sets	Methods and tools for stiffness (deformation)/strength control Methods and tools for environmental resistance control Maintenance and modification design methods and tools

Natural boron consists of two stable isotopes, ^{11}B (80.1%) and ^{10}B (19.9%). In the nuclear industry, boron is widely used as a neutron absorber due to the high neutron cross section of the isotope ^{10}B. The reaction cross section for thermal neutrons (n, alpha) is approximately 3840 barns (for 0.025 eV neutrons). Isotope ^{11}B has an absorption cross section of approximately 0.005 barns (for 0.025 eV neutrons) for thermal neutrons.

Table 6.3 Short-term (1–5 years) first priority technology issues for manufacturing to be acquired.

Subject	Technology
Composite manufacturing technologies for ballistic protection	Manufacturing Composite forming/processing
Trace reducer composite manufacturing technologies	Patterned composite manufacturing 3D (multilayer) composite manufacturing Granular/doped composite manufacturing
Mold-tool-fixture and auxiliary apparatus manufacturing technologies	Manufacturing with thermoplastic materials
Thermoplastic material manufacturing technologies	Thermoforming (press-forming)

Table 6.4 Short-term (1–5 years) first priority technology issues for non-destructive methods to be acquired.

Subject	Technology
Environmental tests	MIL STD 810 Tests/DO 160 G Firing Tests
Multiscale tests	Nano, micromeasuring abilities
High-speed deformation, impact and fatigue tests	Internal and external ballistic tests
Nondestructive test methods	Neutron radiography/tomography/spectrometry

Most of the reactions of thermal neutrons (n, alpha) are ^{10}B(n, alpha)^{7}Li reactions with 0.48 MeV gamma emission. Boron has another positive contribution as a neutron absorber. Reaction products after a neutron absorption, helium and lithium, are stable isotopes. But, there are minor problems with used absorbers. Cadmium is also a neutron absorber. Natural cadmium consists of eight isotopes: ^{106}Cd (1.3%), ^{108}Cd (0.9%), ^{110}Cd (12.5%), ^{111}Cd (12.8%), ^{112}Cd (24.3%), ^{113}Cd (12.2%), ^{114}Cd (28.7%), and ^{116}Cd (7.5%). As is known, ^{113}Cd (7.7 × 1015 y) and ^{116}Cd (2.9 × 1019 y) have very long half-life radioactive isotopes. In nuclear industry, ^{113}Cd is widely used as a thermal neutron absorber due to very high neutron absorption cross section.

^{113}Cd has a specific absorption cross section and the neutrons with kinetic energy below the cutoff energy (~0.5 eV) are strongly absorbed by ^{113}Cd. Therefore, cadmium is widely used to absorb thermal neutrons in thermal neutron filters [1–3, 5, 24, 25, 30, 38, 47, 49, 62, 90, 99, 101, 106].

Both alloys and composites are mixtures of at least two components mixtures. But, there are also several differences between them that make them suitable for different applications. Still, the present technologies often have requirements for the neutron shielding that cannot be met by conventional alloys. Many industries today need materials that are characterized with better mechanical properties such as low density, high strength, and resistance to abrasion and corrosion. This combination of properties can be realized with composite materials. In the shielding, there are strongly many factors in choosing aluminum versus composites [1–3, 6, 8, 16, 21, 25, 26, 37–39, 45–47, 57, 62, 64, 76, 79, 81, 82, 95, 104, 108–111].

6.5 Results and discussion

In this study; second-, third-, and fourth-order grams of composite and alloy shielding materials associated with neutron shielding are subtracted to feature vectors of different sizes. Therefore, the dimensions of these feature vectors were reduced by using correlation-based feature selectors and feature vectors of different sizes were obtained. These feature vectors based on the *n*-gram model were used to determine whether a shielding material document is a composite, alloy, and neutron shielding material with the help of selected (high classification success) classification methods. The data set used consists of 100 search engines (World Wide Science, Google Scholar, Online Journals Search Engine, Directory of Open Access Journals, Springer Link, CERN Document Server, Pub Med, Education Resources Information Center, Academic Index, etc.) for academic research, taken from 16 journals belonging to 16 papers written on different disciplines such as material, nuclear, chemistry, economy, health, and standards. Furthermore, 13,068,758 documents by title, author, DOI, and arxiv id were searched and the results were found: 289; 304; 764; 8 documents with respect to keywords "neutron shielding," "neutron composite," "neutron alloy," "neutron composite alloy," respectively. Any document with respect to the keywords "neutron composite alloy shielding" could not be found. This represents the originality of this chapter and it would not be wrong to underline that the novelty of this study is what the document classification process will show that if it is done using some methods, it will shorten the time spent for document classification. In order to determine whether the document is about composite, alloys, and neutron shielding material, the data set on hand is arranged in three different formats. In addition, cross validations were taken into account in all experiments to show that the classification success was not accidental.

n-Order gram model is a model in which n character slices belong to the string of character. The *n*-order gram-based classification method is a process based on the frequency of use of *n* grams of characters in the document. In this study, second grams, third grams, and fourth grams were used as few different lengths of *n*-order grams. We can explain the path followed in obtaining *n*-order grams with an example; in the example, the underscore character "_" is used to represent the space character.

If our sentence is "Composite Neutron Shielding," *n*-order grams of this sentence; 2-grams: "Co," "mp," "os," "it," "e_," "Ne," "ut," "ro," "n_," "Sh," "ie," "Ld," "in,", "g_" 3-grams: "Com," "pos," "ite," "_ Ne," "utr," "on_," "Shi," "eld," " ing" 4-grams: It will be " Comp," "osit," "e_Ne," "utro," "n_Sh," "ield," "ing_." Since the classification is based on the frequency of use of the characters in the article, we can easily classify with the frequency of the *n*-order grams we obtain the relevant forms of a word ("radiation," "to radiation," "with radiation" or "attenuation," "by attenuation," "via attenuation") in a nuclear article.

In a boutique science branch, some words are used more than other sciences. This is the right approach for words that are specific to a particular subject. Therefore, a threshold value is used to distinguish *n*-grams with significant frequency values from others. When the documents from the same category are compared, we see that the documents have similar *n*-gram frequencies. In this study, 2-gram, 3-gram, and 4-gram of each document in the data sets were obtained. Considering that *n*-grams, which are used most frequently in composite, alloy, and neutron hielding determination studies, have a significant effect on classifying documents, whose frequency value (usage frequency) is greater than 100. Three feature vector tables named General *n*-gram Table, Main *n*-gram Table, and Result *n*-gram Table were used to extract the properties that are specific to the document. General *n*-gram Tables are obtained from the 2-grams, 3-grams, and 4-grams of the documents in each data set. Briefly, since three different *n*-gram models are used, $n \times 3$ General *n*-gram Tables were created for n documents. For each data set, a common scrutiny table was created, expressing all the documents in the data set. This common scrutiny table is called the Composite Alloy Neutron Shielding Material *n*-order gram evaluations' table and is provided in Table 6.5. Considering

Table 6.5 Evaluations of *n*-order grams for the composite alloy neutron shielding material.

Journal name	Article #	WoSID	Year	Absorbing	Capturing	Microscopic cross-section	Macroscopic cross-section	Mass attenuation factor	Reaction rate density	Calculation dose	Calculation others (photon energy Penetration depth)	Reflecting	Shielding performance	Alloy	Composite	Buildup factor	Effective atomic number	Standards and Patented options
NUKLEONIKA	1	Doi: 10.2478/nuka-2019-0012	2019	x				x			x	x	x	x	x			
Results in Physics, Elsevier	2	Doi: 10.1016/j.rinp.2019.01.060	2019	x	X	x	x	x					x					
American Journal of Materials Science	3	Doi: 10.5923/j.materials.20190901.02	2019	x		x	x						x					
International Journal of Emerging Trends in Engineering and Development	4	Doi: 10.26808/rs.ed.i8v4.02	2018	x	X	x	x						x					
Radiation Physics and Chemistry	5	Doi: 10.1016/j.radphyschem.2016.10.012	2017	x	X	x	x						x					
International Journal of Radiation Research	6	Doi: 10.18869/acadpub.ijrr.14.4.379	2016	x		x	x						x					
	7		2015	x	X	x	x						x					

Continued

Table 6.5 Evaluations of *n*-order grams for the composite alloy neutron shielding material—cont'd

Journal name	Article #	WoSID	Year	Absorbing	Capturing	Microscopic cross-section	Macroscopic cross-section	Mass attenuation factor	Reaction rate density	Calculation dose	Calculation others (photon energy Penetration depth)	Reflecting	Shielding performance	Alloy	Composite	Buildup factor	Effective atomic number	Standards and Patented options
Acta Physica Polonica A		Doi: 10.12693/APhysPolA.128.B-14																
Nuclear Engineering and Design	8	Doi: 10.1016/j.nucengdes.2014.10.020	2015											x	x			
Thermochimica Acta	9	Doi: 10.1016/j.tca.2014.03.039	2014	x	X	x												
Annals of Nuclear Energy [1]	10	DOI: 10.1016/j.anucene.2012.08.002	2013							x	x					x		
Fusion Engineering and Design	11	Doi: 10.1016/j.fusengdes.2013.05.042	2013								x				x			
Nuclear Instruments and Methods in Physics Research Section B: Beam Interactions with Materials and Atoms	12	Doi: 10.1016/j.nimb.2013.01.032	2013								x				x			

Central European Journal of Engineering	13	Doi: 10.2478/s13531-011-0063-0	2012	x	X					x								
Nuclear Instruments and Methods in Physics Research A	14	Doi: 10.1016/j.nima .2010.12.239	2011	x	X	x	x						x					
Nuclear Instruments and Methods in Physics Research Section B	15	Doi: 10.1016/j.nimb .2007.04.222	2007	x	X	x	x						X					
Materials Science and Engineering: A	16	Doi: 10.1016/j.msea. 2006.04.063	2006	x	x	x	x	x	x		x	x	x	x	x			
Journal of Nuclear Science and Technology	17	Doi: 10.1080/ 18811248. 1992.9731634	1992	x	x	x	x						x					

the abovementioned issues, in this chapter, for comparisons of the studies available from the literature, we look at the distribution of publications in the criteria presented in Table 6.5 and Fig. 6.8.

It plays an important role in many areas such as document classification, information retrieval, information extraction, document indexing, document filtering, obtaining metadata automatically, and hierarchically editing web pages. In the past, categories were created by people, and in order to be able to assign to the correct category, it was necessary to read documents irrelevant to the subject; however, papers accessed by search engines offer the ease of finding a related article faster. In order to find and review related studies, we randomly selected and examined 10–100 different subsets from both the data set and the attribute set. The most frequently encountered studies in search results were selected with our *n*-order model reviews. According to the keywords determined for the subject, the details of the graphical evaluations of the scrutiny results are presented in Figs. 6.9 and 6.12.

The journals are shown in Fig. 6.10 and a total of 41 papers are distributed with several journals. The journal of Fusion Engineering and Design has high number of papers with 7 (Figs. 6.11–6.13).

The main *n*-gram table (Table 6.4) was created by subtracting common second-order grams, third-order grams, and fourth-order grams for each data set. In the formation of this table, the work of each journal in the data set was taken. If we take the journal determination process, the data set (5 × 3 from neutron and composite and alloy data sets +1 from neutron, composite, alloy) from 16 studies were examined.

These results are illustrated in Table 6.5.

The results obtained give a clear idea about the behavior of the neutron shielding materials under variation in main parameters like neutron energies, cross-sectional areas, vulnerabilities, and temperature and also depending on factors, including the nuclear properties of the target core. The Table 6.5 presents the review of literature studies about neutron shielding and materials of composites and/or alloys (Tables 6.6–6.10). A list of the journal with respect to the selected keywords using *n*th group model for the relevant papers in this study are presented in Tables 6.6 and 6.11. Therefore, the results of the tables represent literature studies that focused on several parameters, the specific studies which have directly focused on neutron shielding by composite and alloy materials have recently been published.

The motivation of the study comes from the fact that, besides the increase in space studies, the ozone layer is thinning, there are cases of

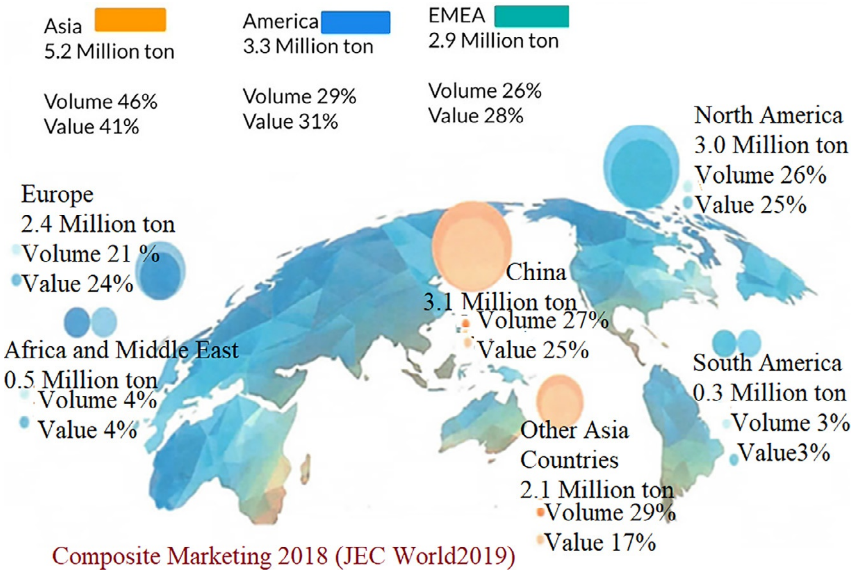
Asia
5.2 Million ton
Volume 46%
Value 41%
America
3.3 Million ton
Volume 29%
Value 31%
EMEA
2.9 Million ton
Volume 26%
Value 28%
North America
3.0 Million ton
Volume 26%
Value 25%
Europe
2.4 Million ton
Volume 21 %
Value 24%
China
3.1 Million ton
Volume 27%
Value 25%
Africa and Middle East
0.5 Million ton
Volume 4%
Value 4%
South America
0.3 Million ton
Volume 3%
Value3%
Other Asia Countries
2.1 Million ton
Volume 29%
Value 17%
Composite Marketing 2018 (JEC World2019)

Fig. 6.7 Composite industry and market in the world.

exposure to atmospheric radiation, and material options have improved with new technological investments.

Numerous materials are produced every day to make our lives easier. Thanks to the information provided, the efficiency, quality, and price of cars, planes, trains, turbines, cosmetics, laundry detergents, drugs, neutron experiments, have improved. Moreover, development of advanced materials that support new technologies depends on scientists' ability to manipulate their properties at the atomic level, and neutron science is key to these efforts. On the other hand, the use of some mobile radiation devices is becoming widespread. In addition, the investigation of the properties of new energy storage materials is largely based on neutron scattering.

Detailed analyses are made using neutrons for the analysis of suitable storage materials. Neutron scattering can help improve lithium batteries. The development of superconductors for energy transport is based on information from neutron scattering. In photovoltaic and solar energy research, neutrons are used to study the performance of solar cells.

Another environmental factor is the geomagnetic field, which strongly affects plasma/particle movements and locations. A geomagnetic storm is the result of injection of solar storm particles into the Earth's magnetic field. Geomagnetic storms are directly related to the incidence of spacecraft

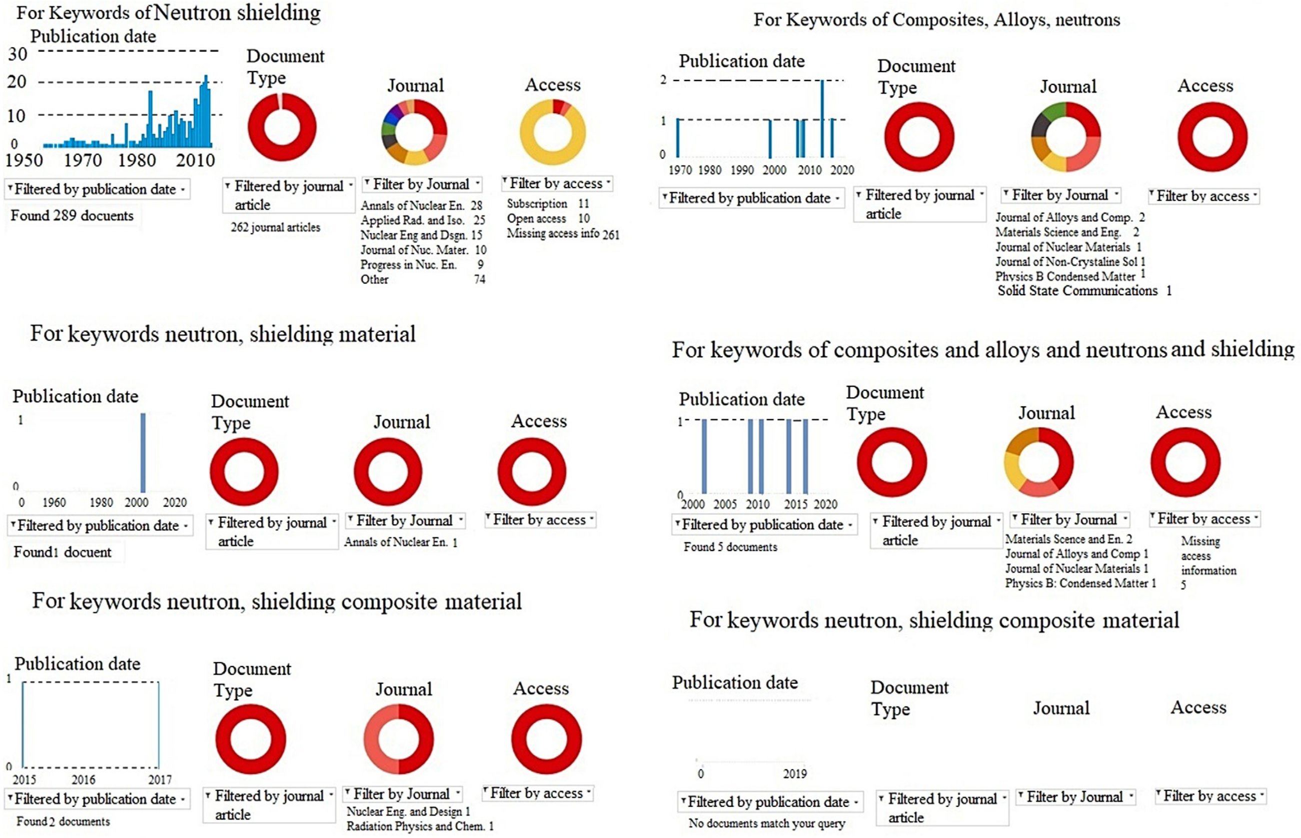

Fig. 6.8 The interaction with more than 1 million academic papers in multidisciplinary studies for neutron composite-alloy shielding materials.

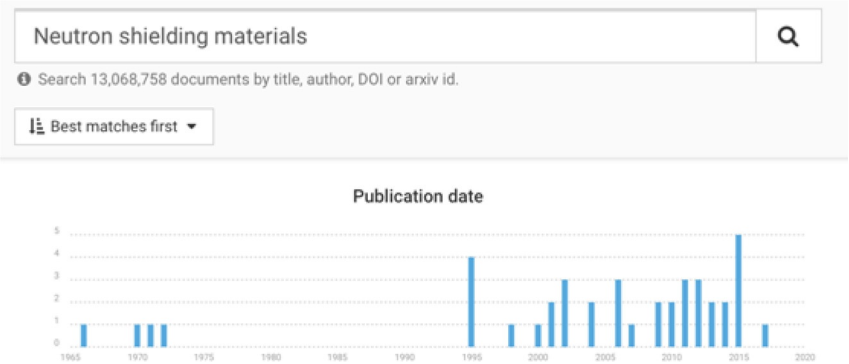

Neutron shielding materials

Search 13,068,758 documents by title, author, DOI or arxiv id.

Best matches first
Publication date
5
4
3
2
1
0
1965
1970
1975
1980
1985
1990
1995
2000
2005
2010
2015
2020

Fig. 6.9 Academic study distribution with respect to the keyword of "neutron shielding materials" for 13,068,758 documents.

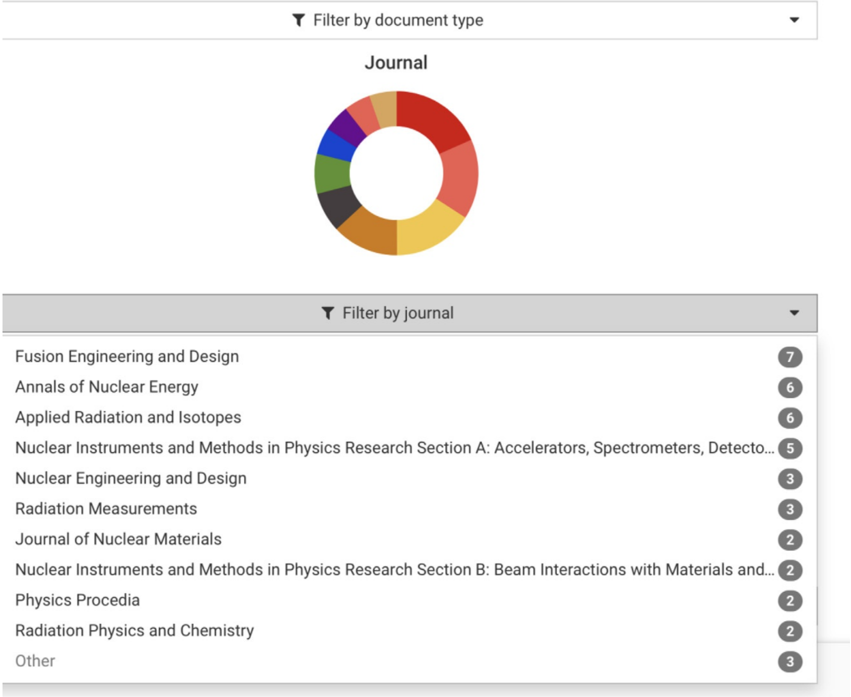

Filter by document type
Journal
Filter by journal

Fusion Engineering and Design	7
Annals of Nuclear Energy	6
Applied Radiation and Isotopes	6
Nuclear Instruments and Methods in Physics Research Section A: Accelerators, Spectrometers, Detecto...	5
Nuclear Engineering and Design	3
Radiation Measurements	3
Journal of Nuclear Materials	2
Nuclear Instruments and Methods in Physics Research Section B: Beam Interactions with Materials and...	2
Physics Procedia	2
Radiation Physics and Chemistry	2
Other	3

Fig. 6.10 Academic studies' journal distribution with respect to the keyword "neutron shielding materials" for 13,068,758 documents.

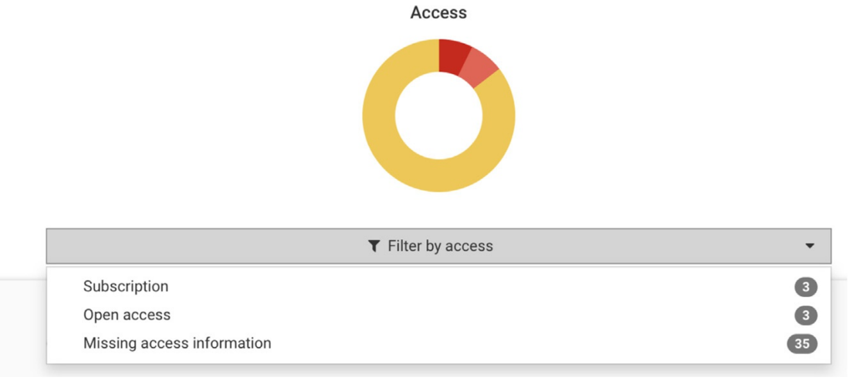

Subscription 3
Open access 3
Missing access information 35

Fig. 6.11 Academic studies' access distribution with respect to the keyword "neutron shielding materials" for 13,068,758 documents.

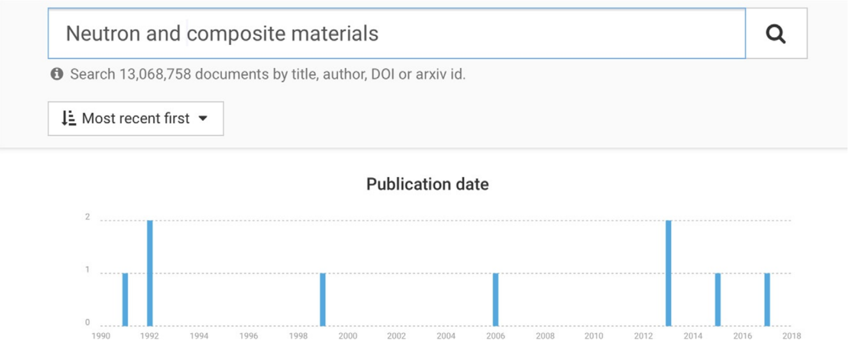
Neutron and composite materials

Search 13,068,758 documents by title, author, DOI or arxiv id.

Most recent first

Fig. 6.12 Academic studies' publication date distribution with respect to the keyword "neutron shielding materials" for 13,068,758 documents.

charge [95]. Geomagnetic data are also important in science, being among the most widely used spacecraft data. The knowhow of the literature studies can also be used to validate large-scale shielding material environment models of the neutron radiation; recently artificial intelligence (AI) has created opportunities for the implementation of such a model in the near future. Industrial innovation and competitiveness are based on the basic knowledge provided by neutrons on the behavior of molecules or the determination of internal stresses to develop components with higher performance.

As the neutron shielding material thickness becomes minimum requirement neutron attenuation of the material becomes acceptable and safe. The effect of temperature variation on the neutron shielding is very important

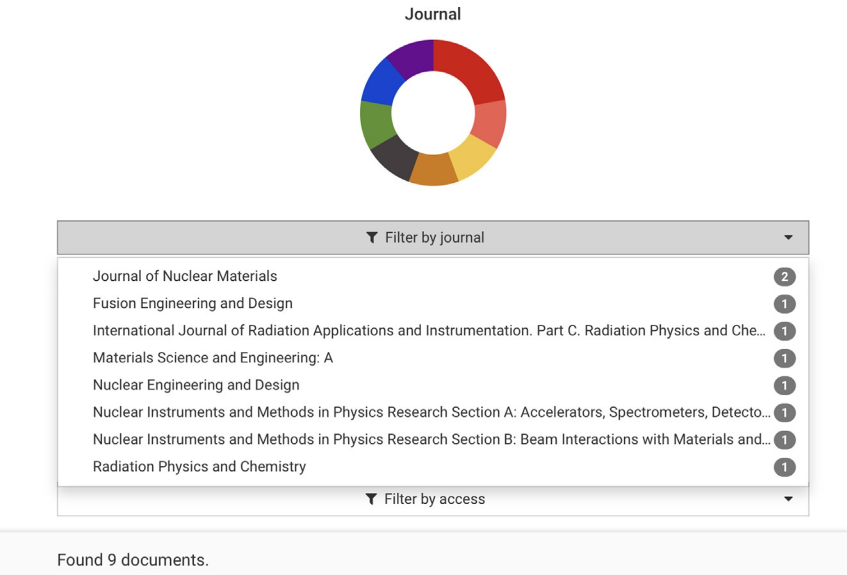

Journal of Nuclear Materials	2
Fusion Engineering and Design	1
International Journal of Radiation Applications and Instrumentation. Part C. Radiation Physics and Che...	1
Materials Science and Engineering: A	1
Nuclear Engineering and Design	1
Nuclear Instruments and Methods in Physics Research Section A: Accelerators, Spectrometers, Detecto...	1
Nuclear Instruments and Methods in Physics Research Section B: Beam Interactions with Materials and...	1
Radiation Physics and Chemistry	1

Found 9 documents.

Fig. 6.13 Academic studies' journal distribution with respect to the keyword "neutron, composite, and alloy materials" for 13,068,758 documents.

Table 6.6 Journals for absorbing in our selected and relevant papers via *n*th-order group mode model.

Acta Physica Polonica A [112]
American Journal of Materials Science [103]
Central European Journal of Engineering [113]
International Journal of Emerging Trends in Engineering and Development [105]
International Journal of Radiation Research [114]
Journal of Nuclear Science and Technology [115]
Materials Science and Engineering: A [96]
Nuclear Instruments and Methods in Physics Research A [80]
Nuclear Instruments and Methods in Physics Research Section B [116, 117]
NUKLEONIKA [101]
Radiation Physics and Chemistry [1]
Results in Physics, Elsevier [102]
Thermochimica Acta [118]

and cannot be neglected, while the effect of temperature variation on the interaction of neutron and material combined with the effect of material temperature of shielding target can be clearly noticed in the literature reviews where the higher temperature has a negative effect on the amount of the vulnerability of the material.

Table 6.7 Journals for capturing in our selected and relevant papers via *n*th-order group mode model.

Acta Physica Polonica A [112]
Central European Journal of Engineering [113]
International Journal of Emerging Trends in Engineering and Development [105]
Journal of Nuclear Science and Technology [115]
Materials Science and Engineering: A [96]
Nuclear Instruments and Methods in Physics Research A [80]
Nuclear Instruments and Methods in Physics Research Section B [117]
Radiation Physics and Chemistry [1]
Results in Physics, Elsevier [102]
Thermochimica Acta [118]

Table 6.8 Journals for the Shielding performance in our selected and relevant papers via *n*th-order group mode model.

Acta Physica Polonica A [112]
American Journal of Materials Science [103]
International Journal of Emerging Trends in Engineering and Development [99]
International Journal of Radiation Research [114]
Journal of Nuclear Science and Technology [115]
Materials Science and Engineering: A [96]
Nuclear Instruments and Methods in Physics Research A [80]
Nuclear Instruments and Methods in Physics Research Section B [117]
NUKLEONIKA [101]
Radiation Physics and Chemistry [1]
Results in Physics, Elsevier [102]
Thermochimica Acta [118]

Table 6.9 Journals for the Shielding performance and alloy our selected and relevant papers via *n*th-order group mode model.

Acta Physica Polonica A [112]
American Journal of Materials Science [103]
International Journal of Emerging Trends in Engineering and Development [105]
International Journal of Radiation Research [114]
Journal of Nuclear Science and Technology [115]
Materials Science and Engineering: A [96]
Nuclear Engineering and Design [23]
Nuclear Instruments and Methods in Physics Research A [80]
NUKLEONIKA [101]
Radiation Physics and Chemistry [1]
Results in Physics, Elsevier [102]

Table 6.10 Journals for the Shielding performance and composite in our selected and relevant papers via *n*th-order group mode model.

Acta Physica Polonica A [112]
American Journal of Materials Science [103]
Fusion Engineering and Design [119]
International Journal of Emerging Trends in Engineering and Development [105]
International Journal of Radiation Research [114]
Journal of Nuclear Science and Technology [115]
Materials Science and Engineering: A [96]
Nuclear Engineering and Design [23]
Nuclear Instruments and Methods in Physics Research A [80]
Nuclear Instruments and Methods in Physics Research Section B [117]
Nuclear Instruments and Methods in Physics Research Section B: Beam Interactions with Materials and Atoms [116]
NUKLEONIKA [101]
Radiation Physics and Chemistry [1]
Results in Physics, Elsevier [102]

Table 6.11 Journals for the Shielding performance and composite and also alloy in our selected and relevant papers via *n*th-order group mode model.

Acta Physica Polonica A [112]
American Journal of Materials Science [103]
Fusion Engineering and Design [119]
International Journal of Emerging Trends in Engineering and Development [105]
International Journal of Radiation Research [114]
Journal of Nuclear Science and Technology [115]
Materials Science and Engineering: A [96]
Nuclear Engineering and Design [23]
Nuclear Instruments and Methods in Physics Research A [80]
Nuclear Instruments and Methods in Physics Research Section B: Beam Interactions with Materials and Atoms [116]
NUKLEONIKA [101]
Radiation Physics and Chemistry [1]
Results in Physics, Elsevier [102]

Especially polyethylene (PE) and polymethylmethacrylate (PMMA), which were proposed as polymeric matrices with neutron adsorbing materials such as graphite and boron carbide for radiation shielding, can accept a really limited loading of filler before losing both mechanical properties and flexibility.

6.6 Conclusions

The main reason for the negative effect on the amount of elimination of neutron radiation was the higher neutron energies on the neutron shielding material which depends on attenuation factors and absorption parameters. Therefore, as a result of analysis of the neutron shielding materials according to Alloy and Composite material choosing records, it is observed that neutron shielding affects using composite or/and alloy yield is nonlinear with neutron energies and temperature. It is recommended to focus on use the methodology in literature review which is about designing and performance assessment of composite and alloy materials for neutron shielding. As new studies are added to scientific studies anytime, anywhere: there will always be inputs and continuous outputs for the model to examine publications on composite-alloy materials in neutron shielding. Therefore, this study's literature review evaluation has feature life. This study can be improved by combining the smart (IoT) neutron shielding alloy and composite material evaluations.

References

[1] T. Özdemir, A. Güngör, I.A. Reyhancan, Flexible neutron shielding composite material of EPDM rubber with boron trioxide: mechanical, thermal investigations and neutron shielding tests, Radiat. Phys. Chem. 131 (2017) 7–12, https://doi.org/10.1016/j.radphyschem.2016.10.012.

[2] Z.G. Xu, L.T. Jiang, Q. Zhang, J. Qiao, D. Gong, G.H. Wu, The design of a novel neutron shielding B4C/Al composite containing Gd, J. Eng. Technol. Appl. Sci. 2 (2) (2017) 57–63, https://doi.org/10.30931/jetas.336562.

[3] R. Adeli, S.P. Shirmardi, S.J. Ahmadi, Neutron irradiation tests on B4C/epoxy composite for neutron shielding application and the parameters assay, Radiat. Phys. Chem. 127 (2016) 140–146, https://doi.org/10.1016/j.radphyschem.2016.06.026.

[4] J. Min, B. Lee, J.S. Lee, Development of synthetic resin-based mortar for low-activation and neutron shieldsublic, Constr. Build. Mater. 124 (2016) 992–998, https://doi.org/10.1016/j.conbuildmat.2016.08.100.

[5] Z. Soltani, A. Beigzadeh, F. Ziaie, E. Asadi, Effect of particle size and percentages of Boron carbide on the thermal neutron radiation shielding properties of HDPE/B4C composite: experimental and simulation studies, Radiat. Phys. Chem. 127 (2016) https://doi.org/10.1016/j.radphyschem.2016.06.027.

[6] B. Oto, A. Gür, E. Kavaz, T. Çakır, N. Yaltay, Determination of gamma and fast neutron shielding parameters of magnetite concretes, J. Progr. Nucl. Energy 92 (2016) 71–80, https://doi.org/10.1016/j.pnucene.2016.06.011.

[7] S. Sen, S. Bagchi, R.R. Prasad, D. Venkatasubramanian, P. Mohanakrishnan, R.S. Keshavamurty, A. Haridas, A.J. Arul, P. Puthiyavinayagam, Determination of neutron energy spectrum at KAMINI shielding experiment location, Appl. Radiat. Isot. 115 (2016) 165–171, https://doi.org/10.1016/j.apradiso.2016.06.025.

[8] K.S. Bang, S.H. Yu, J.C. Lee, K.S. Seo, W.S. Choi, Experimental assessment on the thermal effects of the neutron shielding and heat-transfer fin of dual purpose casks on

open pool fire, Nucl. Eng. Des. 304 (2016) 63–69, https://doi.org/10.1016/j.nucengdes.2016.04.040.

[9] Z.D. Whetstone, K.J. Kearfott, Layered shielding design for an active neutron interrogation system, Radiat. Phys. Chem. 125 (2016) 69–74, https://doi.org/10.1016/j.radphyschem.2016.03.018.

[10] M. Košťál, F. Cvachovec, F. Jánský, V. Rypar, V. Juříček, D. Harutyunyan, M. Schulc, J. Milčák, E. Novák, S. Zaritsky, Neutron deep penetration through reactor pressure vessel and biological concrete shield of VVER-1000 Mock-Up in LR-0 reactor, Ann. Nucl. Energy 94 (2016) 672–683, https://doi.org/10.1016/j.anucene.2016.04.014.

[11] P. Wang, X. Tang, H. Chai, D. Chen, Y. Qiu, Design, fabrication, and properties of a continuous carbon-fiber reinforced Sm2O3/polyimide gamma ray/neutron shielding material, Fusion Eng. Design 101 (2015) 218–225, https://doi.org/10.1016/j.fusengdes.2015.09.007.

[12] L.H. Heilbronn, T.B. Borak, L.W. Townsend, P.E. Tsai, C.A. Burnham, R.F. McBeth, Neutron yields and effective doses produced by Galactic Cosmic Ray interactions in shielded environments in space, Life Sci. Space Res. 7 (2015) 90–99, https://doi.org/10.1016/j.lssr.2015.10.005.

[13] J. Stenander, D.D. DiJulio, Application of automated weight windows to spallation neutron source shielding calculations using Geant4, Nucl. Instrum. Meth. Phys. Res. Sect. A 798 (2015) 167–171, https://doi.org/10.1016/j.nima.2015.07.037.

[14] K. Kondo, F. Arbeiter, U. Fischer, L. Lu, Y. Qiu, K. Tian, Shielding performances analysis for the IFMIF test facility based on high-fidelity Monte Carlo neutronic calculations, Fusion Eng. Design 98–99 (2015) 1998–2002, https://doi.org/10.1016/j.fusengdes.2015.01.019.

[15] H. Chai, X. Tang, M. Ni, F. Chen, Y. Zhang, D. Chen, Y. Qiu, Preparation and properties of flexible flame-retardant neutron shielding material based on methyl vinyl silicone rubber, J. Nucl. Mater. 464 (2015) 210–215, https://doi.org/10.1016/j.jnucmat.2015.04.048.

[16] S. Ali, M. Laherty, J.W. Laprade, P.M. Cala, F.P. Lipschultz, B. Neuhauser, A portable shield for a neutron howitzer used for instructional and research purposes, Appl. Radiat. Isot. 103 (2015) 37–42, https://doi.org/10.1016/j.apradiso.2015.05.011.

[17] S.M. Malkapur, H. Satdive, M.C. Narasimhan, N.B. Karkera, P. Goverdhan, V. Sathian, Effect of mix parameters and hydrogen loading on neutron radiation shielding characteristics of latex modified concrete mixes, Prog. Nucl. Energy 83 (2015) 8–12.

[18] M.K. Sharma, A.B. Alajo, X. Liu, Adjoint acceleration of Monte Carlo simulations using SCALE: a radiation shielding evaluation of the neutron generator room at Missouri S&T, Nucl. Instrum. Meth. Phys. Res. A 792 (2015) 47–55, https://doi.org/10.1016/j.nima.2015.04.035.

[19] D. Sarıyer, R. Küçer, N. Küçer, Neutron shielding properties of concretes containing boron carbide and Ferro-boron, Procedia Soc. Behav. Sci. 195 (2015) 1752–1756, https://doi.org/10.1016/j.sbspro.2015.06.320.

[20] A. Roberts, A.N. Villano, A.M. Howard, J.J. Kolata, A simple cosmic-ray veto shield for low-rate neutron measurements, Nucl. Instrum. Meth. Phys. Res. Sect. A 783 (2015) 28–34, https://doi.org/10.1016/j.nima.2015.02.013.

[21] M. Pouryavi, S.F. Masoudi, F. Rahmani, Radiation shielding design of BNCT treatment room for D-T neutron source, Appl. Radiat. Isot. 99 (2015) 90–96, https://doi.org/10.1016/j.apradiso.2015.02.016.

[22] A.M. Osman, M.A. El-Sarraf, A.M. Abdel-Monem, A.E.S. Abdo, Studying the shielding properties of lead glass composites using neutrons and gamma rays, Erzincan Univ. J. Sci. Technol. 12 (2) (2015) 1141–1148, https://doi.org/10.18185/erzifbed.587514.

[23] J.J. Park, S.M. Hong, M.K. Lee, C.K. Rhee, W.H. Rhee, Enhancement in the microstructure and neutron shielding efficiency of sandwich type of 6061Al–B4C composite material via hot isostatic pressing, Nucl. Eng. Des. 282 (2015) 1–7, https://doi.org/10.1016/j.nucengdes.2014.10.020.

[24] M.J. Radebe, S. Korochinsky, W.J. Strydom, F.C. De Beer, au foil activation measurement and simulation of the concrete neutron shielding ability for the proposed new SANRAD facility, Phys. Procedia 69 (2015) 392–398, https://doi.org/10.1016/j.phpro.2015.07.055.

[25] S.V. Singh, V.M. Badiger, H.R. Vega-Carrillo, Neutron kerma coefficients of compounds for shielding and dosimetry, in: Conference: ISSSD 2014, Cusco. Peru, Vol. 1, 2014, pp. 1340–1355.

[26] R.W. Babai, I.S. Napadensky, D. Bar, I. Mor, N. Tamim, V. Dangendorf, K. Tittelmeier, B. Bromberger, M. Weierganz, Fast neutron tomography of low-Z object in high-Z material shielding, Phys. Procedia 69 (2015) 275–283, https://doi.org/10.1016/j.phpro.2015.07.039.

[27] F.C. De Beer, M.J. Radebe, B. Schillinger, R. Nshimirimana, M.A. Ramushu, T. Modise, Upgrading the neutron radiography facility in South Africa (SANRAD): concrete shielding design characteristics, Phys. Procedia (2015) 115–123, https://doi.org/10.1016/j.phpro.2015.07.017.

[28] T. Piotrowski, M. Mazgaj, A. Żak, J. Skubalski, Importance of atomic composition and moisture content of cement based composites in neutron radiation shielding, Procedia Eng. 108 (2015) 616–623, https://doi.org/10.1016/j.proeng.2015.06.188.

[29] S. Srinivasan, S. Priya, T. Patel, R.K. Gopalakrishnan, D.N. Sharma, Assessment of radiation shield integrity of DD/DT fusion neutron generator facilities by Monte Carlo and experimental methods, Nucl. Instrum. Methods Phys. Res., Sect. B 342 (2015) 125–132, https://doi.org/10.1016/j.nimb.2014.09.027.

[30] P.N. Martin, C.D. Clemett, C. Hill, J. O'Malley, B. Campbell, Active detection of shielded special nuclear material in the presence of variable high backgrounds using a mixed photon-neutron source, Phys. Procedia 66 (2015) 216–225, https://doi.org/10.1016/j.phpro.2015.05.028.

[31] G. Konrad, F.A. Guardia, S. Baeler, M. Borg, F. Glück, W. Heil, S. Hiebel, R. M. Horta, Y. Sobolev, The magnetic shielding for the neutron decay spectrometer aSPECT, Nucl. Instrum. Meth. Phys. Res. Sect. A 767 (2014) 475–486, https://doi.org/10.1016/j.nima.2014.09.014.

[32] R. Delunel, D.L. Bourlès, P.A. Van der Beek, F. Schlunegger, I. Leya, J. Masarik, E. Paquet, Snow shielding factors for cosmogenic nuclide dating inferred from long-term neutron detector monitoring, Quat. Geochronol. 24 (2014) 16–26, https://doi.org/10.1016/j.quageo.2014.07.003.

[33] M.K. Sharma, A.B. Alajo, X. Liu, MCNP modeling of a neutron generator and its shielding at Missouri University of Science and Technology, Nucl. Instrum. Meth. Phys. Res. Sect. A 767 (2014) 126–134, https://doi.org/10.1016/j.nima.2014.08.011.

[34] S. Henry, M. Pipe, A. Cottle, C. Clarke, U. Divakar, A. Lynch, Characterisation of superconducting capillaries for magnetic shielding of twisted-wire pairs in a neutron electric dipole moment experiment, Nucl. Instrum. Meth. Phys. Res. A 763 (2014) 155–162, https://doi.org/10.1016/j.nima.2014.06.021.

[35] D. Taylor, S. Lilley, A. Turner, A. Davis, Neutron shielding and activation of the MASTU device and surrounds, Fusion Eng. Design 89 (9–10) (2014) 2076–2082, https://doi.org/10.1016/j.fusengdes.2014.02.035.

[36] J. Kim, B.C. Lee, Y.R. Uhm, W.H. Miller, Enhancement of thermal neutron attenuation of nano-B4C, -BN dispersed neutron shielding polymer nanocomposites, J. Nucl. Mater. 453 (1-3) (2014) 48–53, https://doi.org/10.1016/j.jnucmat.2014.06.026.

[37] S.J. Park, J.G. Jang, H.K. Lee, Computational investigation of the neutron shielding and activation characteristics of borated concrete with polyethylene aggregate, J. Nucl. Mater. 452 (1-3) (2014) 205–211, https://doi.org/10.1016/j.jnucmat.2014.05.010.

[38] R. Pöllänen, T. Siiskonen, Detection of fast neutrons from shielded nuclear materials using a semiconductor alpha detector, Appl. Radiat. Isot. 90 (2014) 187–191, https://doi.org/10.1016/j.apradiso.2014.03.031.

[39] P. Holm, K. Peräjärvi, S. Ristkari, T. Siiskonen, H. Toivonen, A capture-gated neutron spectrometer for characterization of neutron sources and their shields, Nucl. Instrum. Meth. Phys. Res. Sect. A 751 (2014) 48–54, https://doi.org/10.1016/j.nima.2014.03.021.

[40] G. Chiba, A. Tsuji, T. Narabayashi, Resonance self-shielding effect in uncertainty quantification of fission reactor neutronics parameters, Nucl. Eng. Technol. 46 (3) (2014) 281–290, https://doi.org/10.5516/NET.01.2014.707.

[41] A. Razetti, R.O. Farías, S.I. Thorp, V.A. Trivillin, E.C.C. Pozzi, P. Curotto, A. E. Schwint, S.J. González, Design, construction and application of a neutron shield for the treatment of diffuse lung metastases in rats using BNCT, Appl. Radiat. Isot. 88 (2013) 50–54, https://doi.org/10.1016/j.apradiso.2013.12.021.

[42] V.P. Singh, N.M. Badiger, N. Chanthima, J. Kaewkhao, Evaluation of gamma-ray exposure buildup factors and neutron shielding for bismuth borosilicate glasses, Radiat. Phys. Chem. 98 (2014) 14–21, https://doi.org/10.1016/j.radphyschem.2013.12.029.

[43] V.P. Singh, N.M. Badiger, Gamma ray and neutron shielding properties of some alloy materials, Ann. Nucl. Energy 64 (2014) 301–310, https://doi.org/10.1016/j.anucene.2013.10.003.

[44] B. Merk, J. Konheiser, Neutron shielding studies on an advanced molten salt fast reactor design, Ann. Nucl. Energy 64 (2014) 441–448, https://doi.org/10.1016/j.anucene.2013.07.014.

[45] M.K. Lee, J.K. Lee, J.W. Kim, G.J. Lee, Properties of B4C–PbO–Al(OH)3-epoxy nanocomposite prepared by ultrasonic dispersion approach for high temperature neutron shields, J. Nucl. Mater. 445 (1-3) (2014) 63–71, https://doi.org/10.1016/j.jnucmat.2013.10.051.

[46] J.L. Thalhofer, H.S. Roque, W.F. Rebello, S.A. Correa, A.X. Silva, E.M. Souza, D.V.S. Batita, E.S. Sandrini, Effect of external shielding for neutrons during radiotherapy for prostate cancer, considering the 2300 CD linear accelerator and voxel phantom, Radiat. Phys. Chem. 95 (2014) 267–270, https://doi.org/10.1016/j.radphyschem.2013.02.013.

[47] U. Dahlborg, M. Besser, M.J. Kramer, J.R. Morris, M. Calvo-Dahlborg, Atomic dynamics in molten AlCu alloys of different compositions and at different temperatures by cold neutron scattering, Phys. B Condens. Matter 412 (2013) 50–60, https://doi.org/10.1016/j.physb.2012.12.019.

[48] A. Best, M. Couder, M. Famiano, A. Lemut, M. Wiescher, Study of the beam-induced neutron flux and required shielding for DIANA, Nucl. Instrum. Meth. Phys. Res. Sect. A 727 (2013) 104–108, https://doi.org/10.1016/j.nima.2013.06.032.

[49] J.B. Lin, H.C. Tseng, W.S. Liu, D.B. Lin, T.S. Hsieh, C.Y. Chen, Evaluating secondary neutron doses of a refined shielded design for a medical cyclotron using the TLD approach, Radiat. Phys. Chem. 92 (2013) 43–47, https://doi.org/10.1016/j.radphyschem.2013.06.019.

[50] S. Liu, J. Li, S. Zheng, N. Mitchell, Neutronics analysis of inboard shielding capability for a DEMO fusion reactor CFETR, Fusion Eng. Design 88 (9-10) (2013) 2404–2407, https://doi.org/10.1016/j.fusengdes.2013.04.031.

[51] C. Zweck, M. Zreda, D. Desilets, Snow shielding factors for cosmogenic nuclide dating inferred from Monte Carlo neutron transport simulations, Earth Planet. Sci. Lett. 379 (2013) 64–71, https://doi.org/10.1016/j.epsl.2013.07.023.

[52] A. Alizadeh, A.S. Shirani, S. Kashi, Neutron and gamma-ray deep penetration calculation through biological concrete shield of VVER-1000 reactor by a new technique based on variance reduction, Ann. Nucl. Energy 60 (2013) 86–92, https://doi.org/10.1016/j.anucene.2013.04.033.

[53] M.N. Nasrabadi, G. Baghban, Neutron shielding design for 241Am–Be neutron source considering different sites to achieve maximum thermal and fast neutron flux using MCNPX code, Ann. Nucl. Energy 59 (2013) 47–52, https://doi.org/10.1016/j.anucene.2013.03.030.

[54] H.R. Vega-Carrillo, L.E. Villagrana-Muñoz, E. Rivera-Perez, H.A. De Leon-Martinez, T.G. Soto-Bernal, V.M. Hernández-Davila, Concrete enclosure for shielding a neutron source, Appl. Radiat. Isot. 79 (2013) 37–41, https://doi.org/10.1016/j.apradiso.2013.04.030.

[55] A.S. Kipcak, P. Gurses, E.M. Derun, N. Tugrul, S. Piskin, Characterization of boron carbide particles and its shielding behavior against neutron radiation, Energy Convers. Manag. 72 (2013) 39–44, https://doi.org/10.1016/j.enconman.2012.08.026.

[56] M. Fragopoulou, M. Zamani, Phenomenological calculations of shielding spallation neutron sources, Nucl. Instrum. Meth. Phys. Res. Sect. A 714 (2013) 24–30, https://doi.org/10.15761/NMBI.1000138.

[57] M. Košťál, F. Cvachovec, J. Milčák, F. Mravec, The effect of biological shielding on fast neutron and photon transport in the VVER-1000 mock-up model placed in the LR-0 reactor, Appl. Radiat. Isot. 75 (2013) 37–43, https://doi.org/10.1016/j.apradiso.2013.01.034.

[58] Y. Huang, W. Zhang, L. Liang, J. Xu, Z. Chen, A "Sandwich" type of neutron shielding composite filled with boron carbide reinforced by carbon fiber, Chem. Eng. J. 220 (2013) 143–150, https://doi.org/10.1016/j.cej.2013.01.059.

[59] M. Kurudirek, D. Sardari, N. Khaledi, C. Çakır, K.S. Mann, Investigation of X- and gamma ray photons buildup in some neutron shielding materials using GP fitting approximation, Ann. Nucl. Energy 53 (2013) 485–491, https://doi.org/10.1016/j.anucene.2012.08.002.

[60] M. Nyarku, R.S. Keshavamurthy, V.D. Subramanian, A. Haridas, E.T. Glover, Experimental neutron attenuation measurements in possible fast reactor shield materials, Ann. Nucl. Energy 53 (2013) 135–139, https://doi.org/10.1016/j.anucene.2012.10.019.

[61] M. Mocko, G. Muhrer, Fourth-generation spallation neutron target-moderator-reflector-shield assembly at the Manuel Lujan Jr. neutron scattering center, Nucl. Instrum. Meth. Phys. Res. Sect. A 704 (2013) 27–35, https://doi.org/10.1016/j.nima.2012.11.103.

[62] M. Košťál, J. Milčák, V. Rypar, V. Juříček, E. Novák, A. Kolros, The effect of biological shielding on neutron transport in the VVER-1000 mock-up on the LR-0 research reactor, Appl. Radiat. Isot. 78 (2013) 38–45, https://doi.org/10.1016/j.apradiso.2013.03.094.

[63] I. Akkurt, A.M. El-Khayatt, The effect of barite proportion on neutron and gamma-ray shielding, Ann. Nucl. Energy 51 (2013) 5–9, https://doi.org/10.1016/j.anucene.2012.08.026.

[64] H. Kira, Y. Sakaguchi, J. Suzuki, T. Oku, M.N. Nakamura, M. Arai, K. Kakurai, Y. Endo, Y. Arimoto, T. Ino, H.M. Shimizu, T. Kamiyama, K. Ohoyama, H. Hiraka, K. Tsutsumi, K. Yamada, L.J. Chang, Magnetic shield design of in-situ SEOP polarized 3He neutron spin filter system, Phys. Procedia 42 (2013) 200–205, https://doi.org/10.1016/j.phpro.2013.03.195.

[65] A. Lafuente, J.F. Latkowski, K.J. Kramer, A.M. Dunne, Neutronic studies for the optimization of shield wall penetrations for laser IFE systems, Fusion Eng. Design 88 (1) (2013) 57–64, https://doi.org/10.1016/j.fusengdes.2012.11.007.

[66] A.M. Guimarães, M.A.S. Lacerda, J.A.L. Santos, P.G.M. Maletta, S.L.M. Rodrigues, R.S. Andrade, E.C. Vilela, T.A. Da Silva, Use of a TLD-based multisphere spectrometry system to measure the neutron spectra around a not-self-shielded PET cyclotron: preliminary results, Appl. Radiat. Isot. 71 (2012) 92–95, https://doi.org/10.1016/j.apradiso.2012.05.014.

[67] L.B. Rees, J.B. Czirr, Optimizing moderation of He-3 neutron detectors for shielded fission sources, Nucl. Instrum. Meth. Phys. Res. Sect. A 691 (2012) 72–80, https://doi.org/10.1016/j.nima.2012.07.004.

[68] M. Albarhoum, A.H. Soufan, H. Mustafa, Experimental determination of the shielding characteristics of the dwelling houses' building materials against neutrons in the Central Region of Syria, Ann. Nucl. Energy 47 (2012) 134–139, https://doi.org/10.1016/j.anucene.2012.04.019.

[69] M. Mera, L. Pereira, E. Meilan, A.T. Garcia, F. Gomez, V. Fuentes, J.M. Caruncho, D. Medal, F. Salvador, A. Lopez, EP-1488 new concrete designed specifically for neutron shielding, Radiother. Oncol. 103 (Suppl 1) (2012) S568, https://doi.org/10.1016/S0167-8140(12)71821-2.

[70] A. Trkov, G. Žerovnik, C. Destouches, S. Bourganel, G. Grégoire, J.M. Girard, Self-shielding factor calculations of heterogeneous samples in activation measurements for neutron spectrum unfolding, Nucl. Eng. Des. 246 (2012) 69–74, https://doi.org/10.1016/j.nucengdes.2011.06.039.

[71] A. Donzella, G. Bonomi, E. Giroletti, A. Zenoni, Biological shielding assessment and dose rate calculation for a neutron inspection portal, Radiat. Phys. Chem. 81 (4) (2012) 414–420, https://doi.org/10.1016/j.radphyschem.2011.12.038.

[72] M. Krmar, N. Jovančević, D. Nikolić, Measurement of 56Fe activity produced in inelastic scattering of neutrons created by cosmic muons in an iron shield, Appl. Radiat. Isot. 70 (1) (2012) 269–273, https://doi.org/10.1016/j.apradiso.2011.08.003.

[73] A. Proctor, T.A. Gabriel, A.W. Hunt, J. Manges, T. Handler, Detecting fissionable materials in a variety of shielding matrices via delayed gamma and neutron photofission signatures-Part 2: experimental results, Nucl. Instrum. Meth. Phys. Res. Sect. A 662 (1) (2012) 71–80, https://doi.org/10.1016/j.nima.2011.09.016.

[74] O. Gencel, A. Bozkurt, E. Kam, T. Korkut, Determination and calculation of gamma and neutron shielding characteristics of concretes containing different hematite proportions, Ann. Nucl. Energy 38 (12) (2011) 2719–2723, https://doi.org/10.1016/j.anucene.2011.08.010.

[75] S. Merz, M. Djuricic, M. Villa, H. Böck, G. Steinhauser, Neutron flux measurements at the TRIGA reactor in Vienna for the prediction of the activation of the biological shield, Appl. Radiat. Isot. 69 (11) (2011) 1621–1624, https://doi.org/10.1016/j.apradiso.2011.05.019.

[76] A.M. Sukegawa, Y. Anayama, K. Okuno, S. Sakurai, A. Kaminaga, Flexible heat resistant neutron shielding resin, J. Nucl. Sci. Technol. 48 (4) (2011) 585–590, https://doi.org/10.1080/18811248.2011.9711737.

[77] E. Yılmaz, H. Baltas, E. Kırıs, I. Ustabas, U. Cevik, A.M. El-Khayatt, Gamma ray and neutron shielding properties of some concrete materials, Ann. Nucl. Energy 38 (10) (2011) 2204–2212, https://doi.org/10.1016/j.anucene.2011.06.011.

[78] A.M. Reda, Monte Carlo simulations of a D-T neutron generator shielding for landmine detection, Radiat. Meas. 46 (10) (2011) 1187–1193, https://doi.org/10.1016/j.radmeas.2011.07.013.

[79] J. Ghassoun, N. Senhou, A. Jehouani, Neutron and photon doses in high energy radiotherapy facilities and evaluation of shielding performance by Monte Carlo method, Ann. Nucl. Energy 38 (10) (2011) 2163–2167, https://doi.org/10.1016/j.anucene.2011.06.020.

[80] E. Calzada, F. Grünauer, B. Schillinger, H. Türck, Reusable shielding material for neutron- and gamma-radiation, Nucl. Instrum. Meth. Phys. Res. Sect. A 651 (1) (2011) 77–80, https://doi.org/10.1016/j.nima.2010.12.239.

[81] L. Lakosi, C.T. Nguyen, E. Serf, Neutron interrogation of shielded/unshielded uranium by a 4MeV linac, Appl. Radiat. Isot. 69 (9) (2011) 1251–1254, https://doi.org/10.1016/j.apradiso.2011.04.003.

[82] S.-E. Huang, K. Wang, Y. Dong, An advanced approach to calculation of neutron resonance self-shielding, Nucl. Eng. Des. 241 (8) (2011) 3051–3057, https://doi.org/10.1016/j.nucengdes.2011.05.014.

[83] H. Soltner, U. Pabst, M. Butzek, M. Ohl, T. Kozielewski, M. Monkenbusch, D. Sokol, L. Maltin, E. Lindgren, S. Koch, D. Fugate, Design, construction, and performance of a magnetically shielded room for a neutron spin echo spectrometer, Nucl. Instrum. Meth. Phys. Res. Sect. A 644 (1) (2011) 40–47, https://doi.org/10.1016/j.nima.2011.01.094.

[84] M.E. Medhat, M. Fayez-Hassan, Elemental analysis of cement used for radiation shielding by instrumental neutron activation analysis, Nucl. Eng. Des. 241 (6) (2011) 2138–2142, https://doi.org/10.1016/j.nucengdes.2011.03.025.

[85] I. Yosuke, R.M. Ronningen, Attenuation of ambient dose equivalent from neutrons by thick concrete, cast iron and composite shields for high energy proton, 3He, 48Ca and 238U ions on Cu targets for shielding design, Nucl. Instrum. Methods Phys. Res., Sect. B 269 (3) (2011) 353–363, https://doi.org/10.1016/j.nimb.2010.11.046.

[86] Z. Zhong, Y. Gohar, Shielding design and analyses of KIPT neutron source facility, Nucl. Eng. Technol. 50 (6) (2011) 989–995, https://doi.org/10.1016/j.net.2018.03.016.

[87] M. Albarhoum, Graphite reflecting characteristics and shielding factors for Miniature Neutron Source Reactors, Ann. Nucl. Energy 38 (1) (2011) 14–20, https://doi.org/10.1016/j.anucene.2010.08.021.

[88] R.S. Keshavamurthy, D.V. Subramanian, R.R. Prasad, A. Haridas, P. Mohanakrishnan, S. Chetal, Experimental measurements of neutron attenuation in the advanced shield material Ferro Boron in KAMINI reactor, Energy Procedia 7 (2011) 273–278, https://doi.org/10.1016/j.egypro.2011.06.035.

[89] G. Fehrenbacher, T. Radon, Generation of shielding data for neutron radiation produced by heavy ions, Radiat. Meas. 45 (10) (2010) 529–1531, https://doi.org/10.1016/j.radmeas.2010.05.027.

[90] H. Liu, M.A. Abdou, R.J. Reed, A. Ying, M.Z. Youssef, Neutronics assessment of the shielding and breeding requirements for FNSF (standard aspect ratio), Fusion Eng. Design 85 (7-9) (2010) 1296–1300, https://doi.org/10.1016/j.fusengdes.2010.03.023.

[91] Y. Romanets, J. Bermudez, J.C. David, D. Ene, I.F. Goncalves, Y. Kadi, C. Kharoua, R. Luis, F. Negoita, R. Rocca, L. Tecchio, P. Vaz, EURISOL-DS multi-MW target unit: neutronics performance and shielding assessment, dose rate and material activation calculations for the MAFF configuration, Radiat. Meas. 45 (10) (2010) 1350–1354, https://doi.org/10.1016/j.radmeas.2010.08.001.

[92] A.C. Fernandes, M. Felizardo, A. Kling, J.G. Marques, T. Morlat, Studies on the efficiency of the neutron shielding for the SIMPLE dark matter search, Nucl. Instrum. Meth. Phys. Res. Sect. A 623 (3) (2010) 960–967, https://doi.org/10.1016/j.nima.2010.07.044.

[93] C. Chilian, R. Chambon, G. Kennedy, Neutron self-shielding with k0-NAA irradiations, Nucl. Instrum. Meth. Phys. Res. Sect. A 622 (2) (2010) 429–432, https://doi.org/10.1016/j.nima.2010.01.042.

[94] H.T. Phuong, M.V. Nhon, V.T.T. Trang, E. Ishitsuka, Application of Pade approximation for calculation of epithermal neutron self-shielding factors of some materials

dealing with Doppler broadening effects, Appl. Radiat. Isot. 68 (6) (2010) 1177–1179, https://doi.org/10.1016/j.apradiso.2009.12.041.

[95] U. Dahlborg, M. Besser, M.C. Dahlborg, S. Janssen, F. Juranyi, M.J. Kramer, J.R. Morris, D.J. Sordelet, Public diffusion of Cu in AlCu alloys of different composition by quasielastic neutron scattering, J. Non-Cryst. Solids 353 (32–40) (2007) 3295–3299, https://doi.org/10.1016/j.jnoncrysol.2007.05.074.

[96] Y. Akiniwa, S. Machiya, H. Kimura, K. Tanaka, N. Minakawa, Y. Morii, T. Kamiyama, Evaluation of material properties of SiC particle reinforced aluminum alloy composite using neutron and X-ray diffraction, Mater. Sci. Eng. A 437 (1) (2006) 93–99, https://doi.org/10.1016/j.msea.2006.04.063.

[97] M. Eldrup, B.N. Singh, Influence of composition, heat treatment and neutron irradiation on the electrical conductivity of copper alloys, Information Service Department, Riso, 1998. ISBN 87-550-2350-9. ISSN 0106-2840.

[98] Y. Nakai, N. Kunitomi, Y. Endoh, Y. Ishikawa, Diffuse scattering of neutrons near the critical composition in Au-Cr alloy, J. Phys. Soc. Jpn. 34 (5) (1973) 1197–1202, https://doi.org/10.1143/JPSJ.34.1197.

[99] J. An, X. Xue, Life cycle environmental impact assessment of borax and boric acid production in China, J. Clean. Prod. 66 (2014) 121–127, https://doi.org/10.1016/j.jclepro.2013.10.020.

[100] Z. Er, I. Akkurt, A brief review on atmospheric radiation dose estimations, in: Proceedings of ICCESEN-2019. 6th International Conference on Computational and Experimental Science and Engineering, 23–27 October, Antalya, Turkey, 2019, pp. 248–251.

[101] E. Kam, I.A. Reyhancan, R. Biyik, A portable fast neutron radiography system for non-destructive analysis of composite materials, Nukleonika 64 (3) (2019) 97–101, https://doi.org/10.2478/nuka-2019-0012.

[102] H.O. Tekin, E.E. Altunsoy, E. Kavaz, M.I. Sayyed, O. Agar, M. Kamislioglu, Photon and neutron shielding performance of boron phosphate glasses for diagnostic radiology facilities, Results Phys. 12 (2019) 1457–1464, https://doi.org/10.1016/j.rinp.2019.01.060.

[103] M. Shamsuzzama, M.A.M. Khan, M.M.H. Bhuiyan, M.S. Rahman, M.J.H. Khan, D. Paul, D.R. Sarkar, Attenuation property of wood and fiber reinforced polymer composite materials for neutron and gamma radiation shielding, Am. J. Mater. Sci. 9 (1) (2019) 8–14, https://doi.org/10.5923/j.materials.20190901.02.

[104] T. Korkut, A. Karabulut, G. Budak, B. Aygün, O. Gencel, A. Hançerlioğulları, Investigation of neutron shielding properties depending on number of boron atoms for colemanite, ulexite and tincal ores by experiments and FLUKA Monte Carlo simulations, Appl. Radiat. Isot. 70 (1) (2012) 341–345, https://doi.org/10.1016/j.apradiso.2011.09.006.

[105] A.M. Madbouly, A.A. ElSawy, Calculation of gamma and neutron parameters for some concrete materials as radiation shields for nuclear facilities, Int. J. Emerg. Trends Eng. Devel. 3 (8) (2018). https://doi.org/10.26808/rs.ed.i8v4.02.

[106] P. Litwa, K. Perkowski, D. Zasada, I. Kobus, G. Konopka, T. Czujko, R.A. Varin, A novel Fe–Cr–Nb matrix composite containing the TiB2 neutron absorber synthesized by mechanical alloying and final hot isostatic pressing (HIP) in the Ti-tubing, J. Alloys Compd. 674 (2016) 425–434, https://doi.org/10.1016/j.jallcom.2016.03.079.

[107] M. Calvo-Dahlborg, P.S. Popel, M.J. Kramer, M. Besser, J.R. Morris, U. Dahlborg, Superheat-dependent microstructure of molten Al–Si alloys of different compositions studied by small angle neutron scattering, J. Alloys Compd. 550 (2013) 9–22, https://doi.org/10.1016/j.jallcom.2012.09.086.

[108] Z. Zhong, Y. Gohar, Electron accelerator shielding design of KIPT neutron source facility, Nucl. Eng. Technol. 48 (3) (2016) 785–794, https://doi.org/10.1016/j.net.2016.01.004.

[109] K. Hadad, M. Nematollahi, H. Sadeghpour, R. Faghihi, Moderation and shielding optimization for a 252Cf based prompt gamma neutron activation analyzer system, Int. J. Hydrog. Energy 41 (17) (2016) 7221–7226, https://doi.org/10.1016/j.ijhydene.2015.12.208.

[110] B. Oto, N. Yıldız, T. Korkut, E. Kavaz, Neutron shielding qualities and gamma ray buildup factors of concretes containing limonite ore, Nucl. Eng. Des. 293 (2015) 166–175, https://doi.org/10.1016/j.nucengdes.2015.07.060.

[111] T. Vasilopoulou, I.E. Stamatelatos, P. Batistoni, S. Conroy, B. Obryk, S. Popovichev, D.B. Syme, Neutron streaming along ducts and labyrinths at the JET biological shielding: effect of concrete composition, Radiat. Phys. Chem. 116 (2015) 359–364, https://doi.org/10.1016/j.radphyschem.2015.04.015.

[112] A. Akkasa, A.B. Tugrul, B. Buyuk, A.O. Addemir, M. Marsoglu, B. Agacan, Shielding Effect of boron carbide aluminium metal matrix composite against gamma and neutron radiation, Acta Phys. Pol. A 128 (2B) (2015). https://doi.org/10.12693/APhysPolA.128.B-14.

[113] T. Piotrowski, D.B. Tefelski, A. Polański, J. Skubalski, Monte Carlo simulations for optimization of neutron shielding concrete, Central Eur. J. Eng. 2 (2) (2012) 296–303, https://doi.org/10.2478/s13531-011-0063-0.

[114] S.M.J. Mortazavi, M. Kardan, S. Sina, H. Baharvand, N. Sharafi, Design and fabrication of high density borated polyethylene nanocomposites as a neutron shield, Int. J. Radiat. Res. 14 (4) (2016)https://doi.org/10.18869/acadpub.ijrr.14.4.379.

[115] H. Kobayashi, H. Wakao, Y. Ikeda, K. Ohokubo, A. Tsuruno, Macroscopic cross section measurements and defect detection in materials using neutron radiography technique, J. Nucl. Sci. Technol. 29 (11) (2012) 1045–1053, https://doi.org/10.1080/18811248.1992.9731634.

[116] R. Uhlář, P. Alexa, J. Pištora, A system of materials composition and geometry arrangement for fast neutron beam thermalization: an MCNP study, Nucl. Instrum. Methods Phys. Res., Sect. B 298 (2013) 81–85, https://doi.org/10.1016/j.nimb.2013.01.032.

[117] D.L. Chichester, B.W. Blackburn, Radiation fields from neutron generators shielded with different materials, Nucl. Instrum. Methods Phys. Res. Sect. B 261 (1-2) (2007) 845–849, https://doi.org/10.1016/j.nimb.2007.04.222.

[118] J.W. Shin, J.W. Lee, S. Yu, B.K. Baek, J.P. Hong, Y. Seo, W.N. Kim, S.M. Hong, C. M. Koo, Polyethylene/boron-containing composites for radiation shielding, Thermochim. Acta 585 (2014) 5–9, https://doi.org/10.1016/j.tca.2014.03.039.

[119] A. Aures, L.W. Packer, S. Zheng, Tritium self-sufficiency of HCPB blanket modules for DEMO considering time-varying neutron flux spectra and material compositions, Fusion Eng. Design 88 (9–10) (2013) 2436–2439, https://doi.org/10.1016/j.fusengdes.2013.05.042.

[120] D.D. DiJulio, H. Björgvinsdóttir, C. Zendler, P.M. Bentley, Population-based metaheuristic optimization in neutron optics and shielding design, J. Nucl. Instrum. Meth. Phys. Res. Sect. A 835 (2016) 157–162, https://doi.org/10.1016/j.nima.2016.08.035.

[121] Y.K. Leei, Analysis of the ITER computational shielding benchmark with the Monte Carlo TRIPOLI-4 neutron gamma coupled calculations, Fusion Eng. Design 109-111 (B) (2016) 1163–1168, https://doi.org/10.1016/j.fusengdes.2015.12.062.

[122] R. Pampin, A. Suarez, A. Arnould, N. Casal, R. Juarez, A. Martin, F. Moro, F. Mota, E. Polunovskiy, F. Sabourin, Study of shielding options for lower ports for mitigation

of neutron environment and shutdown dose inside the ITER cryostat, J. Fusion Eng. Design 109-111 (2016) 1408–1411, https://doi.org/10.1016/j.fusengdes.2015.12.010.

[123] A. Yadollahi, E. Nazemi, A. Zolfaghari, A.M. Ajorloo, Optimization of thermal neutron shield concrete mixture using artificial neural network, J. Nucl. Eng. Design 305 (2016) 146–155, https://doi.org/10.1016/j.nucengdes.2016.05.012.

[124] M.S. McArthur, L.B. Rees, J.B. Czirr, Reliability of Monte Carlo simulations in modeling neutron yields from a shielded fission source, Nucl. Instrum. Meth. Phys. Res. Sect. A 827 (2016) 46–51, https://doi.org/10.1016/j.nima.2016.04.062.

[125] X. Fu, X. Tang, Y. Hu, H. Li, J. Tao, Effect of different lay-ups on the microstructure, mechanical properties and neutron transmission of neutron shielding fibre metal laminates, J. Nucl. Mater. 475 (2016). https://doi.org/10.1016/j.jnucmat.2016.04.021.

[126] T. Ozdemir, I.K. Akbay, H. Uzun, I.A. Reyhancan, Neutron shielding of EPDM rubber with boric acid: mechanical, thermal properties and neutron absorption tests, Prog. Nucl. Energy 89 (2016) 102–109, https://doi.org/10.1016/j.pnucene.2016.02.007.

[127] T. Dang, D. Ying, Q. Yang, M. Loughlin, A. Davis, First neutronics analysis for ITER bio-shield equatorial port plug, Fusion Eng. Design 87 (7–8) (2012) 1447–1452, https://doi.org/10.1016/j.fusengdes.2012.03.036.

[128] M. Angelone, P. Batistoni, F. Moro, M. Pillon, R. Villari, M. Laubenstein, M. Loughlin, Neutronics analysis and nuclear heating measurement up to the TFC in a mock-up of the ITER inboard shield, Fusion Eng. Design 87 (5–6) (2012) 910–915, https://doi.org/10.1016/j.fusengdes.2012.02.045.

[129] J. Ghassoun, N. Senhou, The evaluation of neutron and gamma ray dose equivalent distributions in patients and the effectiveness of shield materials for high energy photons radiotherapy facilities, Appl. Radiat. Isot. 70 (4) (2012) 620–624, https://doi.org/10.1016/j.apradiso.2011.12.041.

[130] R. Remetti, G. Andreoli, S. Keshishian, Monte Carlo calculation of the neutron effective dose rate at the outer surface of the biological shield of HTR-10 reactor, Nucl. Eng. Des. 243 (2012) 148–152, https://doi.org/10.1016/j.nucengdes.2011.12.003.

[131] A. Trkov, G. Žerovnik, L. Snoj, M. Ravnik, On the self-shielding factors in neutron activation analysis, Nucl. Instrum. Meth. Phys. Res. Sect. A 610 (2) (2009) 553–565, https://doi.org/10.1016/j.nima.2009.08.079.

[132] R.F. Castrillo, G. Bruno, G.G. Doncel, Neutron and synchrotron radiation diffraction study of the matrix residual stress evolution with plastic deformation in aluminum alloys and composites, Mater. Sci. Eng. A 487 (1–2) (2008) 6–32, https://doi.org/10.1016/j.msea.2007.09.067.

CHAPTER 7

Shielding concrete with neutron attenuating and absorbing components

Tomasz Piotrowski
Faculty of Civil Engineering, Warsaw University of Technology, Warsaw, Poland

7.1 Introduction

Concrete has been used as a radiation shielding material since the beginning of use of nuclear reaction in energy production, medicine, and research. The main function of concrete in civil structures is always to bear load but due to its composite character it can be modified to achieve other desired properties. One of such actions is to improve the shielding efficiency against ionizing radiation, both gamma and neutron. The problem is that while in case of gamma radiation the shielding efficiency strongly depends on the density of the material (especially in the medium energy range when Compton scattering is dominant), the protection against neutrons is a much more complex phenomenon.

Neutrons are uncharged particles and they can only interact with the nuclei of atoms. The type of this interaction strongly depends on the neutron energy (speed). In general, when neutrons of high energy, so-called fast neutrons, hit a nucleus, they will bounce off and lose some of their energy as a result elastic scattering. It is known from the laws of mechanics that if a neutron collides with a large nucleus it will lose a small part of its energy, and if its mass is close to the mass of a nucleus it is colliding with, the energy loss will be large. For this reason, the best neutron attenuation is obtained on hydrogen and other elements of low atomic number. The second stage of neutron radiation shielding is the absorption of attenuated, slow neutrons, also called the thermal neutrons. Their energy is less than 0.025 eV. As a result of such radiation stop, a new isotope of the element is formed, and the excess energy is emitted in the form of a gamma quantum. The so-called secondary gamma radiation is then observed. Its intensity depends on the target nuclei.

Micro and Nanostructured Composite Materials for Neutron Shielding Applications
https://doi.org/10.1016/B978-0-12-819459-1.00007-6
© 2020 Elsevier Ltd.
All rights reserved.

Sometimes, fast neutrons are also captured and proton or α particle and gamma quantum are emitted from the nucleus. The other reaction that can occur is inelastic scattering. It is possible when the neutron energy is above so-called threshold energy, i.e., >1 MeV, which is greater than the typical energy of the lowest excited state of the nuclei. In an inelastic scattering, some energy of the incident neutron is absorbed by the recoiling nucleus and the nucleus remains in the excited state. The neutron is absorbed by the target nucleus and the interaction take place via compound nucleus formation. The compound nucleus then emits a neutron of lower kinetic energy which leaves the original nucleus in an excited state. An excited intermediate nucleus emits its excess energy through a nuclear transformation, which is accompanied by gamma emission or nuclear fission. However, these phenomena are relatively rare in relation to the fast neutron attenuation and thermal neutron absorption already described.

Taking the above simplified approach into consideration it is clear that neutron radiation shielding concrete should contain both neutron attenuation and absorbing components. Moreover, due to secondary gamma radiation high-density concrete would be advantageous.

The aim of the chapter is to present the achievements, both historical and the newest, relating to improvement of neutron radiation shielding concrete as a result of material modification, explicit by addition neutron attenuating and absorbing components. Since the neutron shielding is one of the hardest and very rarely treated in publications this review could be useful for scientists, professionals, faculty, and students in areas such as civil engineering, nuclear engineering, nuclear power, and radiation shielding.

7.2 Neutron shielding by particular atoms of concrete

Effectiveness in neutron shielding by individual atoms of a matter is described by the so-called microscopic cross-sections σ. Intuitively, the cross section is the surface of the atom in which a neutron can hit and be attenuated or absorbed—it should not, however, be identified with the size of the nuclei or atoms of individual elements. In the case of neutrons, for each element a cross section is distinguished for a given type of reaction, i.e., scattering cross section σ_s, including coherent σ_{cs} and incoherent σ_{is} and absorption cross section σ_a. By analyzing the cross-section values (Tables 7.1 and 7.2) it can be concluded that the atoms that are common in concrete are not the best absorbers, however, some of them are quite efficient in neutron attenuation. The most effective in attenuation by inelastic

Table 7.1 Cross-section values for common nuclei in ordinary concrete (in the order of increasing atomic number *Z* and atomic mass *A* [1].

Z	Symbol	Name	*A* [u]	σ_{cs} [barn]	σ_{is} [barn]	σ_s [barn]	σ_a [barn]
1	H	Hydrogen	1.0	1.757	80.267	82.03	0.3327
8	O	Oxide	16.0	4.233	0.001	4.23	0.0002
11	Na	Sodium	23.0	1.662	1.623	3.28	0.5305
12	Mg	Magnesium	24.3	3.631	0.087	3.71	0.0633
13	Al	Aluminum	27.0	1.495	0.008	1.50	0.2313
14	Si	Silicon	28.1	2.163	0.005	2.17	0.1713
15	P	Phosphorous	31.0	3.307	0.005	3.31	0.1727
16	S	Sulfur	32.1	1.109	0.007	1.03	0.5311
17	Cl	Chlorine	35.5	11.526	5.355	16.80	33.5333
19	K	Potassium	39.1	1.692	0.271	1.96	2.1111
20	Ca	Calcium	40.1	2.782	0.053	2.83	0.4322
26	Fe	Iron	55.8	11.225	0.401	11.62	2.5633

σ_a—absorption cross section for 2200 m/s neutrons ($E = 25.3$ meV).

Table 7.2 Cross-sections values of the best neutron absorbers (in the order of increasing absorption cross-section value) [1].

Z	Symbol	Name	A [u]	σ_{cs} [barn]	σ_{is} [barn]	σ_s [barn]	σ_a [barn]
64	Gd	Gadolinium	157.3	29.388	151.222	180.22	49.700
62	Sm	Samarium	150.4	0.422	39.333	39.33	5.922
63	Eu	Europium	152.0	6.754	2.544	9.24	4.530
48	Cd	Cadmium	112.4	3.046	3.461	6.50	2.520
66	Dy	Dysprosium	162.5	35.988	54.412	90.39	994
5	B	Boron	10.80	3.545	1.701	5.24	767
77	Ir	Iridium	192.2	14.189	0.333	14.33	452
80	Hg	Mercury	200.6	20.245	6.611	26.81	372.3
79	Au	Gold	197.0	7.321	0.435	7.75	98.65
47	Ag	Silver	107.9	4.407	0.583	4.99	63.30
27	Co	Cobalt	58.9	0.779	4.833	5.63	37.18
17	Cl	Chlorine	35.5	11.526	5.355	16.85	33.13

σ_a—absorption cross section for 2200 m/s neutrons ($E = 25.3$ meV).

scattering are elements with high atomic mass (although this is not the rule), but since the contribution of this reaction in the total attenuation of neutron radiation is negligible, the influence of heavy elements on neutron attenuation will also be hardly visible. The best solution is therefore a high content of hydrogen that acts by elastic scattering. Since no significant effect for the changes in simple water to cement (w/c) ratio of concrete on its shielding properties has been reported [2], it can be present additionally by water in capillarity and chemically bound water by cement, hydrated aggregate (limonite, serpentine) and as a component of various types of admixtures and additives, especially polymer ones. Chloride (Cl) and iron (Fe) appear to be the best neutron absorbers in ordinary concrete. Unfortunately, chloride is not recommended as a component of reinforced concrete due to possible corrosion of reinforcing steel, and absorption of slow neutrons on iron emits high-energy secondary gamma radiation and as a result causes a significant activation of concrete. For this reason, it seems beneficial to use other elements than those found in ordinary concrete like gadolinium (Gd), cadmium (Cd), boron (B), or cobalt (Co), whose absorption cross sections are rather high.

7.3 Quantities for the description of neutron attenuation and absorption

The most common parameter used for the evaluation of radiation shielding is linear attenuation coefficient μ [cm^{-1}]. Following ICRU Report [3] its definition is

$$\mu = \frac{1}{dl} \cdot \frac{dN}{N} \tag{7.1}$$

where

dN/N, mean fraction of the particles that experience interactions in traversing a distance dl in the material of density ρ.

In other words $\mu \cdot dl$ is the probability that at normal incidence an uncharged particle undergoes an interaction in a material layer of thickness dl. Another definition of linear attenuation coefficient results from Beer-Lambert law:

$$N = N_0 e^{-\mu l} \tag{7.2}$$

where

N, number of neutrons behind the shield, N_0, number of neutrons in front of the shield, and l, material thickness.

Transformation of Eq. (7.2) leads to.

$$\mu = \frac{1}{l} \ln \frac{N_0}{N} \left[\mathrm{cm}^{-1}\right] \tag{7.3}$$

Some researchers, especially for the evaluation of experimental results, apply this equation using instead of number of neutrons other values, e.g., dose transmission [4, 5].

The next physical quantity used for the evaluation of neutron shielding is the fast neutron effective removal cross sections (Σ_R) or fast neutron mass removal cross section (Σ_R/ρ). In this case, the term "removal" means removal from the group of fast neutrons, which in most cases is the result of elastic scattering. As mentioned earlier, the other types of fast neutron-material interaction such as inelastic scattering and fast neutron capture are also possible. Therefore, the so-called fast neutron effective removal cross section (Σ_R) is smaller than the total fast neutron removal cross section (Σ_t). In the range of 6–8 MeV, their ratio is about two-thirds, except for materials with high hydrogen in their structure, for which these values are practically the same. It is also assumed that in the range of 2–12 MeV, both values of removal cross sections are constant.

It is calculated by analogy to the mass attenuation coefficient (μ/ρ) equation for any chemical compounds or homogeneous mixture of *i*-elements [6–8]. It is a sum of the individual microscopic removal cross sections of its constituents:

$$\mathrm{\mu}/\mathrm{\rho} = \sum_i w_i \cdot (\mu/\rho)_i \tag{7.4}$$

where

w_i, weight fraction of the *i*th element and $(\mu/\rho)_i$, mass attenuation coefficient of the *i*th element.

The mass removal cross section may be calculated as the value of (Σ_R/ρ) for various elements in the compounds or mixtures as in Eq. (7.4) but the mass removal cross section (Σ_R) is replaced by mass attenuation (μ).

$$\Sigma_R/\rho = \sum_i w_i \cdot (\Sigma_R/\rho)_i \tag{7.5}$$

Weight fraction (w_i) is proportional to partial density (W_i) by its density according to formula:

$$\mathrm{W}_i = w_i \cdot \rho_s \tag{7.6}$$

Then fast neutron effective removal cross section (Σ_R) can be calculated as

$$\Sigma_R = \sum_i W_i \cdot (\Sigma_R/\rho)_i \tag{7.7}$$

where

W_i, partial density of ith constituent and $(\Sigma_R/\rho)_i$, fast neutron mass removal cross section of the ith element.

The value of fast neutron mass removal cross section of constituents depends only on microscopic nuclear properties and varies smoothly with the atomic weight. They can be calculated using empirical equations related to the atomic mass A and the atomic number Z of the element proposed by Wood [8]:

$$\Sigma_R/\rho = 0.21 \cdot A^{-0.56}; A \le 12 \tag{7.8}$$

$$\Sigma_R/\rho = 0.00662 \cdot A^{-\frac{1}{3}} + 0.33 \cdot A^{-\frac{2}{3}} - 0.211 \cdot A^{-1}; A > 12 \tag{7.9}$$

$$\Sigma_R/\rho = 0.190 \cdot Z^{-0.743}; Z \le 8 \tag{7.10}$$

$$\Sigma_R/\rho = 0.125 \cdot Z^{-0.565}; Z > 8 \tag{7.11}$$

or by Chilton et al. [9] in 1984:

$$\Sigma_R/\rho = 0.0206 \cdot A^{\frac{1}{3}} \cdot Z^{-0.294} \tag{7.12}$$

Experimental and theoretical values of the mass removal cross sections for most elements and some compounds have been presented in tables [6, 9–11]. Using the above additivity, values for any compound or material not listed can be obtained.

In 2009 El-Khayatt and El-Sayed Abdo [12] presented a program for calculating the macroscopic effective cross section of fast neutrons based on the programming language FORTRAN 90—MERCSF-N (macroscopic effective removal cross section of fast neutrons). It allows to determine this value for homogeneous mixtures, composites, and concretes. In 2011 El Khayatt [13] proposed to upgrade this software in the form of NXcom, which gives the ability to simultaneously calculate the total mass attenuation coefficient for gamma radiation (μ/ρ) and the macroscopic effective cross section for fast neutrons (Σ_R). In 2015, Mann [14] proposed the WinNC-toolkit tool written in C++, in which the database of mass values was supplemented with a fast neutron weakening factor for nine elements (Tc, Pm, Po, At, Rn, Fr, Ra, Ac, and Pa), while Elmahroug et al. [15]

presented the ParShield program, in which the novelty is the ability to calculate for gamma radiation using two additional characteristics, the effective atomic mass (Z_{eff}), i.e., the ratio of the effective total atomic cross section to the total effective electrical active cross section and the effective electron density (N_{eff}) defined as the number of electrons per mass unit [16–18].

The last quantity used for shielding evaluation is half-value layer (HVL) and less often tenth value layer (TVL) that describe the thickness of the shield needed to reduce the radiation intensity by half or by one-tenth of the intensity value in front of the shield. These values can be obtained from the basic law of attenuation of radiation:

$$\frac{n}{n_0} = \frac{1}{2} = e^{-\mu \cdot \mathrm{HVL}}; \mathrm{HVL} = \frac{\ln 2}{\mu} = \frac{0.693}{\mu}\mathrm{cm} \tag{7.13}$$

$$\frac{n}{n_0} = \frac{1}{10} = e^{-\mu \cdot \mathrm{TVL}}; \mathrm{TVL} = \frac{\ln 10}{\mu} = \frac{2.31}{\mu}\mathrm{cm} \tag{7.14}$$

They can also be determined graphically based on figures presenting the results of radiation intensity measurements (expressed in, e.g., gamma radiation intensity, neutron count, dose, etc.) as a function of shield thickness.

7.4 Neutron shielding evaluation methods

The quantities for the evaluation of neutron shielding efficiency of concrete can be obtained by three procedures:

- calculation
- computer simulation (Monte Carlo method)
- experimental measurements

First two methods are based on elemental (atomic) composition of concrete. It can be obtained again by calculating concrete mix composition or by measurements, especially using energy dispersive X-ray fluorescence (EDXRF) technique. Calculation of atomic composition of concrete could be performed using chemical composition of its constituents. For example, Portland cement is a hydraulic mineral binder whose composition can be obtained by standard XRF measurement and is presented in the oxide form of chemical compounds. To calculate the atomic composition of cement, it is necessary to know the atomic mass of each element and to calculate the molecular weight of a molecule. One calculates the percentage of each element by dividing the atomic mass of an element (multiplied by the quantity in the molecule) by the atomic mass of the whole molecule and multiplying by the percentage of particles in the cement. To calculate the total amount of a given element in the cement one should sum up the amount of all the molecules in which it appeared. Then proceeding similarly the amount of the atoms from other constituents (aggregate, additives, admixtures, and water) can be calculated by multiplying the percentage of the component of the concrete in which the element is located. An example of such calculation was presented in detail by Piotrowski et al. [19]. An important factor in such calculation is especially the bound water content in the hardened composite, as it can be different depending on the cement type and class [20]. Normally it is assumed to be 20%–25% of the cement mass but this rage seems to be really wide. As a consequence, since the variations in hydrogen content for concretes with different types of cement are noted, differences in theoretical Σ_R values should be observed as well.

Alongside calculations the computer simulation methods are used for shielding evaluation. Most of them are based on Monte Carlo (MC) method. It is a statistical method based on the pseudo-random number generator, the cross sections for reactions in material already known, and the assumed model of particle motion. A complete set of simulation must also include the geometry of the shielding material, atomic composition of the material, parameters of radioactive source, and a type and placement of radiation detectors. The most advanced MC computational package is Monte Carlo N-Particle Transport Code System (MCNPX) from Los Alamos National Laboratory—the Monte Carlo N-Particle Transport Code System including MCNP6.1, MCNP5-1.60, MCNPX-2.7.0, and Data Libraries was released in 2013 and additionally version 6.2 of MCNP was released in 2018. The other well-known codes are Fluka [21, 22], Geant4 [23–25], Serpent [26], and Tripoli [27]. Also minor software like OpenMC [28] and SPOT [29] have been developed as well.

Both calculation and simulation results are often compared to experimental results. In these experiments both neutron flux beam from reactor core and neutron reference fields from radionuclides sources are used. The reference radionuclide sources are Am-Be, Pu-Be, and Cf-252. Am-Be and Pu-Be sources produce approximately the same count rate as that of about 4.5 MeV gamma-ray per unit of alpha emitter activity [30]. Cf-252 source characteristic is different. It has an average neutron energy of about 2.0 MeV and emits spectrum more similar to that obtained from fission reactors [31]. An important parameter is also yield describing how many neutrons are emitted per second as differences in intensity could be important [32].

The general idea of tests is to place the investigated sample of concrete between neutron source and detector—in most cases BF_3 or helium counter for flux measurement and Roentgen Equivalent Man (REM) counter for dose measurement. In order to direct the beam, part of the system are the collimators, e.g., made from HDPE. Sometimes, additional cadmium (Cd) and/or boron carbide (B_4C) filters are used to eliminate the thermal component of a neutron spectrum as well. To attenuate fast neutrons in the beam, the most common moderators used are rich-in-hydrogen water and paraffin moderators.

Recently, simple laboratory setups (Fig. 7.1) were used by Oto et al. [4] and Malkapur et al., who additionally added collimators [5, 33].

The problem is that while Am-Be source emits a wide spectrum of neutrons, both fast and thermal ones, only the second are detected in this arrangement. It has to be remembered that some of the neutrons, especially thermal after attenuation by the sample, are absorbed in the volume as well. This is not taken into account. An interesting idea was presented in 2015 by Piotrowski et al. [19, 34], who proposed two measuring systems: one for neutron absorption evaluation and the other one for fast neutron attenuation (Fig. 7.2). In the first one, all the emitted fast neutrons were attenuated to thermal ones before the sample by elastic scattering and inelastic collisions with hydrogen atoms which were in the paraffin moderator surrounding the source in a special paraffin block. An a consequence, only thermal neutrons reach the sample and can be absorbed and no increase in such neutrons due to fast neutron attenuation is possible. In the second one, only fast neutrons penetrate the sample, as all thermal ones are absorbed by a cadmium filter channel between the source and the sample. The increase in the number of thermal neutrons counted by a helium detector is a result of almost

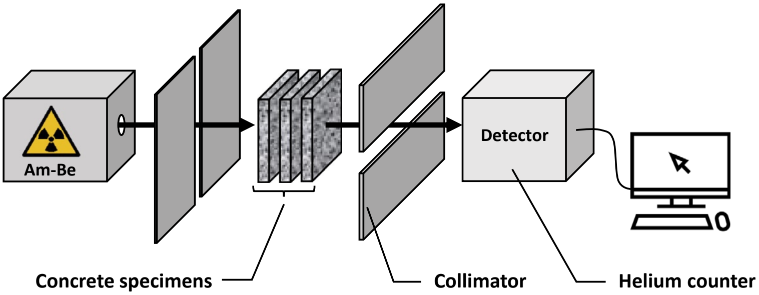

Fig. 7.1 Experimental setup with reference radionuclide source for neutron shielding evaluation of concrete following Oto et al. [4] and Malkapur et al. (additional collimators) [5, 33].

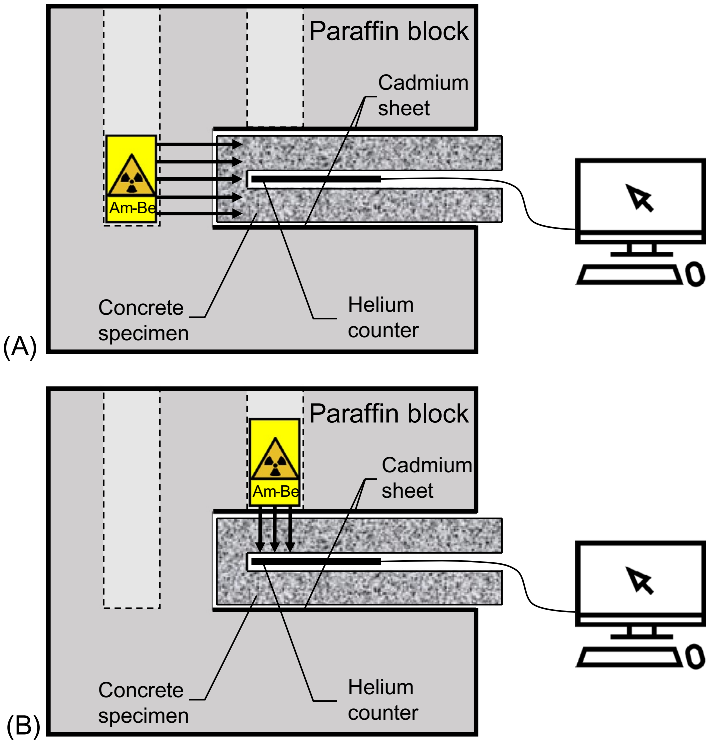
Paraffin block
Cadmium sheet
Am-Be
Concrete specimen
Helium counter
(A)
Paraffin block
Cadmium sheet
Am-Be
Concrete specimen
Helium counter
(B)

Fig. 7.2 Experimental setups with reference Am-Be neutron source for separate evaluation of thermal neutron absorption (A) and fast neutron attenuation (B) proposed by Piotrowski [19, 34].

pure fast neutron attenuation, as only limited number of fast neutrons could be attenuated and absorbed within a volume of sample.

Mixed neutron gamma experimental arrangement in front of a collimated beam emitted from the horizontal channel No 2 of the ET-RR-1 reactor (Egypt) was presented by Bashter et al. [35] and Abdo and Megahid [36, 37]. The fast neutron and gamma-ray spectra were measured using a neutron-gamma spectrometer with a stilbene crystal and results for flux were presented as energy spectra in neutrons/cm^2 s and photons/cm^2 s for gamma. Fast neutron total macroscopic cross sections and total gamma-ray attenuation coefficients were calculated as well (Fig. 7.3).

It has to be mentioned that both neutron and gamma shielding efficiency and their intensity depends not only on the atomic composition but also on the structure of the barrier (e.g., heterogeneities) [38] and local defects (e.g., cracks) [39]. These factors are not taken into account in calculations and simulations or in experiments.

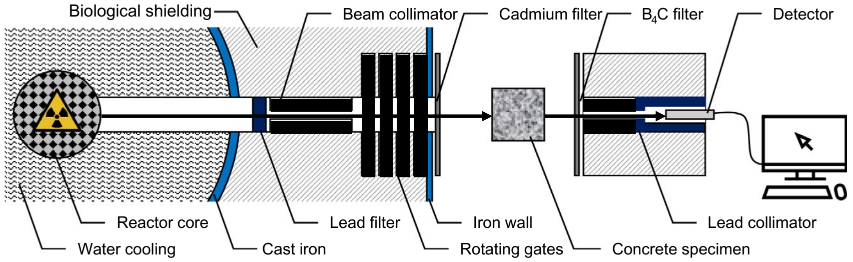

Fig. 7.3 Experimental setup with reactor neutron flux for neutron shielding evaluation of concrete [35].

7.5 Neutron attenuation and absorption by concrete with different aggregates

The biggest part of concrete volume takes an aggregate so the most important changes of neutron shielding can bring aggregate change. Moreover, aggregate is the most important factor which influences the concrete performance and density significantly in both the fresh and the hardened state. A number of investigation results have been already presented in this field (Table 7.3).

At first, it has to be stated that when a mixed (neutron and gamma) radiation is needed to be shielded heavyweight aggregate has to be used. Iron-based aggregates (hematite, magnetite, ilmenite, limonite) and lead-based aggregates (galena) rather than barite ones are recommended for this purpose due to their high density and good mechanical properties. For neutron radiation shielding, the influence of aggregate density is minor. An improvement in fast neutron attenuation could be a result of the use of rich-in-hydrogen aggregate. An example is a serpentine that was used separately or in different mixes with ilmenite and hematite. The concrete composition that contains only serpentine [46] (which contains considerable amount of hydrogen) come off second best after hematite that alongside iron contain iron hydroxides. The best solution in this case seems to be a mixed aggregate, e.g., hematite-serpentine [42, 44] or ilmenite-serpentine [40]. If additionally thermal neutron absorption is the goal, then the colemanite aggregate containing both hydrogen and boron is a good candidate. Due to its poor mechanical properties it is recommended to use it just as a part of aggregate. Research shows that the neutron dose transmission is linearly dependent on colemanite quantity but at the level of 15% allows for 2% increase only [47].

Table 7.3 References of neutron shielding evaluation of concrete with different aggregates (chronologically).

Year	Author(s)	Ref	Aggregate	Calculations/ simulation/ experiment	Conclusions
1994	Kany et al.	[40]	Ordinary (OC) Ilmenite + serpentine (ISC)	Exp	ISC proved to be a better thermal, epithermal, and thermalized neutron attenuator than OC shields preheated at different temperatures up to 873 K. The thermal neutron macroscopic cross-section decreases slightly as the temperature increases up to 673 K for the ISC. The epithermal and thermalized neutron macroscopic cross sections decrease exponentially as the temperature increases for both ISC and OC shields
1996	Makarious et al.	[41]	Ilmenite (± iron punchings)	Exp/calc	The relaxation length of fast neutrons for the ilmenite concrete in the present work ($\rho = 3.5$ g/cm^3) is less than the other previously investigated ilmenite concrete ($\rho = 4.6$ g/cm^3), so its shielding efficiency for fast neutrons is higher. The addition of iron punchings to the previously investigated ilmenite concrete is the main source for the production of the most penetrating hard capture secondary gamma-rays (7.7 MeV)

Continued

Table 7.3 References of neutron shielding evaluation of concrete with different aggregates (chronologically)—cont'd

Year	Author(s)	Ref	Aggregate	Calculations/ simulation/ experiment	Conclusions
1996	Bashter et al.	[42]	Hematite-serpentine, ilmenite-limonite	Exp	The fast neutron flux measured behind hematite-serpentine concrete is higher than that measured behind ilmenite-limonite concrete. This can be attributed to the fact that ilmenite-limonite concrete has higher density than hematite-serpentine concrete. Also the percentage weight of iron oxide in ilmenite-limonite concrete is higher than in hematite-serpentine concrete so that the probability of inelastic scattering of fast neutrons in ilmenite-limonite concrete increases. The flux intensity decreases more rapidly in the case of ilmenite-limonite concrete than in the case of hematite-serpentine for neutrons of all energies
1996	Bashteret al.	[35]	Gravel (ordinary) Ilmenite Ilmenite-limonite	Exp	Ilmenite concrete is better for slow and thermal neutron attenuation than both ordinary and ilmenite-limonite concretes. Thermal neutrons emitted directly from the reactor core are highly absorbed within the first few centimeters of each type of concrete

1997	Bashter	[43]	Gravel Steel scrap	Exp/calc	Steel scrap concrete is better than ordinary, hematite-serpentine, ilmenite-limonite and ilmenite concretes investigated in Ref. [35] from the radiation shielding point of view. The calculated neutron effective removal cross section (Σ_R) for steel scrap concrete and other types of concretes using the modified equation due to Schmidt are in good agreement with the corresponding measured values
1997	Bashter	[44]	Ordinary (gravel), hematite-serpentine, ilmenite-limonite, basalt-magnetite, ilmenite, steel-scrap, steel-magnetite	Calc	For photon shielding, the ilmenite, steel-scrap, and steel-magnetite concretes have better properties than ordinary, hematite-serpentine, ilmenite-limonite, and basalt-magnetite concretes. With regard to neutron shielding, the ilmenite may be used in combination with limonite as aggregate for concrete shielding. The object is to obtain a concrete of maximum density for the attenuation of photons, whilst retaining an adequate amount of hydrogen, derived from the water of

Continued

Table 7.3 References of neutron shielding evaluation of concrete with different aggregates (chronologically)—cont'd

Year	Author(s)	Ref	Aggregate	Calculations/ simulation/ experiment	Conclusions
					crystallization of limonite, for the attenuation of neutrons. Serpentine aggregate is used in concrete because this hydrous aggregate retains most of its water of crystallization at temperatures up to ~500°C. Therefore, hematite-serpentine concrete has a practical use for neutron shielding. The steel-magnetite concrete under investigation is a much better radiation attenuator than the other concretes from the shielding point of view
1998	El-Sayed Abdo et al.	[36, 37]	Magnetite-limonite (Mag-Lim) Ilmenite-ilmenite (Ilm-Ilm) Magnetite-magnetite (Mag-Mag)	Exp	The spectra of fast neutrons measured behind homogeneous barriers having the same thickness show that Mag-Lim is the best neutron attenuator while Mag-Mag with 10% content of silica is the poorest attenuator for fast neutrons of all energies. The displayed spectra of total gamma-rays indicate also that Mag-Lim is the best for gamma-ray attenuation while Mag-Mag is the poorest gamma-ray attenuator

2002	El-Sayed Abdo	[45]	Dolomite-sand, barite-barite, magnetite-limonite, ilmenite-ilmenite	Calc	With regarded to neutron shielding, magnetite, hematite, and ilmenite ores may be used with combination of limonite or serpentine ores to obtain a maximum density for gamma-ray shielding and retaining an adequate amount of hydrogen, derived from water of crystallization of limonite or serpentine for neutron shielding. It is concluded that, the elemental composition, hydrogen content and the concrete density contribute an important rule for neutrons and gamma rays attenuation. Therefore when concrete is used for both neutrons and gamma-rays shielding, the concrete density, as well as, the water content as crystallization water in mixing ores must be taken in consideration
2008	Kharita et al	[46]	River clay and silts Dolomite Hematite Serpentine	Exp	For shielding of neutron radiation, it is clear that samples (2 and 3—hematite) are the best for shielding of neutrons. This behavior may be the result of the high content of iron is

Continued

Table 7.3 References of neutron shielding evaluation of concrete with different aggregates (chronologically)—cont'd

Year	Author(s)	Ref	Aggregate	Calculations/ simulation/ experiment	Conclusions
					there samples and the presence of iron hydroxides (as limonite). The concrete composition that contains serpentine (which contains considerable amount of hydrogen) comes as second best. This composition was expected to show good results for the attenuation of neutrons. It can be noticed that sample 4 (dolomite) gives good results too, which could be attributed to the high content of carbon
2010	Korkut et al.	[47]	Normal/barite + colemanite	Exp	The neutron dose transmission values decrease when the colemanite percentages increase in both barite and ordinary concrete samples. Colemanite ($2CaO{:}3\text{-}B_2O_3{:}5H_2O$) includes both boron and hydrate. Thereof, colemanite can shield fast and thermal neutrons. We have successfully enhanced the neutron shielding property of barite and ordinary concrete by adding different proportions of colemanite

2011	Gencel et al.	[48]	Limestone Hematite	Calc/exp	Although concretes containing hematite have desired gamma-ray shielding capability, there has been no effect for hematite addition on neutron shielding properties of the investigated concretes
2012	Piotrowski et al.	[29]	Granite Barite	Sim	The investigation showed that increasing density of material has a marginal influence on neutron shielding efficiency
2013	Tefelski et al.	[49]	Ordinary Barite	Sim	The worst concrete for this purpose (when not only thermal neutrons should be attenuated) seems to be the barite heavy concrete commonly used against gamma and other radiation. It is full of high mass elements with very small cross sections for neutron capture
2013	Akkurt and El-Khayat	[50]	Barite	Calc	It was found that increasing barite proportion in the concrete increased the gamma attenuation coefficient while it decreased the neutron removal cross section. The selection of a material for neutron and gamma-rays shield requires that there be heavy atoms and light atoms mixed in the proper ratio. It was found that while barite improved concrete

Continued

Table 7.3 References of neutron shielding evaluation of concrete with different aggregates (chronologically)—cont'd

Year	Author(s)	Ref	Aggregate	Calculations/ simulation/ experiment	Conclusions
					shielding properties against gamma-rays, it is not an ideal material to improve shielding properties against neutron radiation. If a high barite proportion is required for concrete used against both neutron and gamma-ray it is recommended to back up it by hydrogen absorber
2015	Piotrowski et al.	[19]	Granite Magnetite	Sim/exp	Increasing density of material has a marginal influence on fast neutron shielding efficiency, so performance-based design of such concrete should take into account other conditions like atomic composition and moisture (hydrogen) content. It is proved that heavyweight concrete is not proper solution for shielding against fast neutrons but its efficiency is visible in the case of thermal neutrons absorption, probably due to increase of Fe content at the expense of Si and O in the atomic composition

2015	Oto et al.	[4]	Gravel Limonite	Calc/exp	The highest value of Σ_R for FCL concrete (limonite) have observed due to higher partial density value (0.06053) of hydrogen in this sample despite all of concrete samples having the same amount of water/cement ratio. In this manner, the attenuation of neutrons depends largely on hydrogen content derived from the water of crystallization of limonite ore. As well as, removal macroscopic cross sections of concrete samples is to a large extent dependent on their density, … Limonite concrete is effective neutron shielding material in compared to the normal concrete sample
2016	Oto et al.	[51]	Gravel Magnetite	Calc	Since the hydrogen content for all studied concretes is almost same, small variations between theoretical Σ_R values have been observed. These variations are due to the density of concrete samples and Σ_R values is highest for the M100 sample. This result leads to the conclusion that magnetite aggregate is more effective

Continued

Table 7.3 References of neutron shielding evaluation of concrete with different aggregates (chronologically)—cont'd

Year	Author(s)	Ref	Aggregate	Calculations/ simulation/ experiment	Conclusions
					material for neutron shielding than the ordinary aggregate and the concrete density plays an important role for neutron attenuation
2018	Aygun et al.	[52]	Barite Galena (PbS)	Sim/exp	Use of appropriate galena concentration and barite can improve cross section value of hybrid fiber heavyweight aggregate concrete and enhance properties of neutron shielding

7.6 Influence of cement type on neutron attenuation and absorption

The important concrete component next to aggregate is cement. The main constituent of cement is Portland cement clinker made by sintering a precisely specified mixture of raw materials containing elements, usually expressed as oxides: CaO, SiO_2, Al_2O_3,Fe_2O_3, and small quantities of other materials. Portland cement clinker is a hydraulic material that consists of at least two-thirds by mass calcium silicates ($3CaO \cdot SiO_2$ and $2CaO \cdot SiO_2$), the remainder consisting of aluminum and iron containing clinker phases and other compounds. The mass ratio of (CaO)/(SiO_2) should be not less than 2.0. The content of magnesium oxide (MgO) should not exceed 5.0% by mass. Alongside Portland cement clinker the other main constituents in the family of common cements according to EN 197-1 are granulated blast furnace slag (GGBS), pozzolanic materials, fly ash, burnt shale, limestone, and silica fume. Based on composition the family of common cement are grouped into five cement types:

- CEM I—Portland cement
- CEM II—Portland-composite cement
- CEM III—Blast furnace cement
- CEM IV—Pozzolanic cement
- CEM V—Composite cement

In the United States, separate classification for Portland (ASTM C150) and blended hydraulic cements (ASTM C595) is used. Blended cements are divided into the following types:

- Type IL—Portland-Limestone cement
- Type IS—Portland-Slag cement
- Type IP—Portland-Pozzonlan cement
- Type IT—Ternary Blended cement

Portland cement classification is based more on characteristics description:

- Type I—Normal
- Type II—Moderate sulfate resistance
- Type II (MH)—Moderate heat of hydration (and moderate sulfate resistance)
- Type III—High early strength
- Type IV—Low heat hydration
- Type V—High sulfate resistance

Also with an interest in the industry for performance-based specifications, ASTM C1157 describes cements by their special performance attributes:

- Type GU—General use
- Type HE—High early strength
- Type MS—Moderate sulfate resistance
- Type HS—High sulfate resistance
- Type MH—Moderate heat of hydration
- Type LH—Low heat of hydration

It is clear that variety of cement is quite wide but for radiation shielding structures due to its massive characteristic moderate and low heat hydration Portland cements are used especially. Hydration heat could also be reduced by the use of slag and pozzolans as well (e.g., CEM III and CEM V). The influence of cement type (CEM I and CEM II) alongside aggregate change (granite to barite) on neutron radiation shielding was evaluated by Piotrowski et al. [29] and some but not important changes have been found. It is probably due to assumption concerning water demand in 25% of mass of cement used for hydration. In fact bound water content can vary a lot. Prochoń and Piotrowski [20] found by experiment that surprisingly the w/c ratio change has a linear influence on the bound water content in a cement matrix—it is contrary to stoichiometric analysis. Nevertheless, it is strongly dependent on cement type—the lowest bound water content have been examined for CEM III (8%–12%) and the highest for CEM II/A-LL containing up to 20% of limestone (17%–21%). As the fast neutron attenuation is mainly due to collisions with hydrogen atoms such big difference need to have an effect on total neutron radiation shielding. Piotrowski et al. [34] have measured standard cement mortar with Portland cement—CEM I is almost twice greater in fast neutron flux attenuation than in the mortar of other cements: CEM III/A 42.5 N-LH/HSR/NA and CEM IV/B(V)32.5-LH/HSR, which is in line with the results of the bound water measurement mentioned before.

7.7 Efficiency of neutron attenuation and absorption by special components of concrete

The special components used to improve neutron attenuation can be decided into two groups: neutron attenuating components and neutron absorbing components. A number of investigation results have been already presented on this field as well (Table 7.4). In the first group, there are rich-in-hydrogen materials, generally polymers: epoxy [34, 62, 64, 65, 70],

Table 7.4 References in neutron shielding evaluation of concrete with special neutron attenuating and absorbing components (chronologically)

Year	Author(s)	Ref	Components	Calculations/ simulation/ experiment	Conclusions
2010 2014	Abdullach et al.	[53, 54]	Boron carbide (B_4C)	Exp	The results show that the density of concrete was reduced by the addition of boron carbide in concretes. Attenuation coefficient of concrete/boron carbide increases as boron carbide content in concretes increased. This study shows that the addition of boron carbide particles to concretes able to increase the capability of neutron absorption compared to regular concrete. However, concrete strength was reduced by the increasing of boron carbide in concretes
2010	Mortazavi et al.	[55]	Datolite $CaBSiO_4(OH)$ + galena (DaGa)	Sim/exp	DaGa concrete samples (densities of 3000 and 7500 kg/m^3) had a 20% more neutron absorption compared to reference concrete (density 2600 kg/m^3)
2011	Kharita et al.	[56]	Boric acid (H_3BO_3) Boric frit Borax ($Na_2B_4O_7$)	Sim/exp	Boric acid and its frit have deleterious effect on the setting of ordinary cement in ratios 0.5%–1% of the total weight of the concrete. The changes in attenuation efficiency for neutrons are within errors range. This is in good agreement with the measurements. The benefit gained by addition of borax was the decrease of the dose due to gamma capture rays

Continued

Table 7.4 References in neutron shielding evaluation of concrete with special neutron attenuating and absorbing components (chronologically—cont'd

Year	Author(s)	Ref	Components	Calculations/ simulation/ experiment	Conclusions
2011	Ylmaz et al.	[57]	Silica fume (SF) Fly ash (FA) Blast furnace slag (GGBS)	Calc	For neutron attenuation, due to constant ratios of water to cementitious materials and water to aggregate for the all samples a small variation was observed for the calculated removal cross-section values
2012	Mohd Reusmaazran et al.	[58]	Boron carbide (B_4C)	Exp	The result show that the attenuation coefficient of the sample with 20 wt% B_4C is 0.299 cm^{-1} and the sample without B_4C is 0.238 cm^{-1} and hence, concrete/B_4C is suitable as a shielded for thermal neutron radiation
2013	Tefelski et al.	[49]	Borated concrete	Sim	The results of neutron attenuation for borated concrete in comparison to heavy concrete is of one or two orders of magnitude
2013	Aghamiri et al.	[59]	Galena Ulexite	Sim/exp	Neutron attenuation in thin ulexite-galena slabs does not offer better shielding properties compared with those of ordinary concrete. However, in case of thick slabs, the shielding properties of ulexite-galena slabs against neutrons do significantly increase. The variation in the behavior of ulexite-galena

					slabs originates from the fact that neutrons in the current experiment were originally fast and thin slabs were unable to moderate these neutrons to thermal neutrons that can be captured by boron nuclei. In this light, it can be concluded that the efficiency of ulexite-galena slabs in neutron shielding is thickness-dependent and also depends on incident neutron energy
2014	Aghamiri et al.	[60]	Galena Tourmaline (Alumina borosilicate with fluorine)	Sim/exp	Neutron attenuation measurements showed that thin ToGa concrete samples had 16% greater neutron absorption in comparison with the reference concrete (density of 2.35 g/cm^3). Although there is a negligible discrepancy (5%), the MC simulation matches the experimental measurements reasonably well. Furthermore, MC-calculated results showed that thick ToGa concrete shields had up to 10 times greater neutron attenuation compared to ordinary concrete
2015	Piotrowski et al.	[34]	Epoxy	Exp	A significant benefit on neutron shielding properties by polymer addition was obtained. PCC repair mortars exhibit superior properties in terms of both thermal neutron absorption and fast neutrons attenuation. This is probably due to bigger number of the hydrogen atoms resulting from the content of the hydrocarbon chains of the polymers

Continued

Table 7.4 References in neutron shielding evaluation of concrete with special neutron attenuating and absorbing components (chronologically—cont'd

Year	Author(s)	Ref	Components	Calculations/ simulation/ experiment	Conclusions
2015	Piotrowski et al.	[61]	Epoxy (E) Gadolinium oxide (Gd_2O_3)	Sim/exp	Concerning the epoxy resin: it improves shielding properties of mortars and concrete against neutron radiation, addition of such polymer into heavyweight concrete (used against gamma radiation) can improve its usability properties and neutron shielding efficiency as well. Concerning the gadolinium: it is an efficient additive for low energy neutron attenuation but it is useless from the fast neutron-shielding point of view—no decrease of flux was observed for all thickness. Increasing gadolinium content from 1% to 5% in relation to cement does not make an important progress in neutron shielding efficiency
2015	Mazgaj et al.	[62]	Epoxy (E) Gadolinium oxide (Gd_2O_3)	Exp	The experimental test showed that the path of adding epoxy and other rare earth elements like gadolinium could be a good way in design the new generation shielding concrete. The influence of the epoxy resin in ordinary concrete (Z) was obtain but the

					difference in attenuation coefficient between the magnetite and magnetite (M) epoxy is not observed. Next test were performed on fast neutron attenuation. Both in ordinary concrete and magnetite heavyweight concrete there is noted a significant influence of epoxy. Less thermal neutrons on the counter in case of MG5 and MEG5 than corresponding MG2 and MEG2 confirms that gadolinium is very effective in thermal neutron absorption. Moreover an increase of content from 2% to 5% plays an important role
2015	Sariyer et al.	[63]	Boron carbide (B_4C) Ferro-boron (Fe-B)	Sim	High-density concretes are more suitable if the neutron sources possess high energy. This study shows that the high density Fe-B added to concrete is better neutron shielding material than B_4C added to concretes. It is known that boron is good thermal neutron absorber material and iron is important shielding materials to slow down fast neutrons below 1 MeV. Therefore, we should be recommended that Fe-B added to concrete as a promising shield material for the fast neutron application

Continued

Table 7.4 References in neutron shielding evaluation of concrete with special neutron attenuating and absorbing components (chronologically—cont'd

Year	Author(s)	Ref	Components	Calculations/ simulation/ experiment	Conclusions
2016	Piotrowski et al.	[64, 65]	Epoxy (PCC1) Acrylic dispersion (PCC2) Gadolinium oxide (Gd_2O_3) Polypropylene fibers Sodium borohydride ($NaBH_4$)	Exp	As a result of interpolation with the 3rd degree polynomial function, HVL and QVL values were determined for the Pu-Be source. It can be seen that ordinary concrete gains slightly worse protective properties than heavy concrete (by approx. 10%–12% for HVL). The material modification of heavy concrete gives very good results with gadolinium, polymer fibers, and polymer additive (HVL decrease by another 10% compared to unmodified heavy concrete M). The most advantageous turned out to be the use of the polymer together with gadolinium oxide (decrease by 20%)—it can therefore be concluded that in this case the synergistic effect of modification appeared
2017	Malkapur et al.	[33]	Natural river sand HDPE powder Crushed granite	Exp	By using polymeric material as a partial replacement to sand, it was possible to attain better neutron shielding characteristics compared to the conventional concrete. The flux transmission values reduced in a range of 5%–8.5% and the dose transmission values reduced in a range of 9.8%–16.1%. The half value layer (HVL) thicknesses reduced in a range of 3.2%–5.4%

2017	Malkapur et al.	[5]	Natural river sand Virgin HDPE powder/waste HDPE powder Crushed granite	Exp	The reduction in flux transmission is only up to 8.5% (max.) vis-à-vis control concrete mix. As hydrogen is a good moderator, it can reduce the kinetic energy of the neutrons to a great extent but cannot absorb all the neutrons. Hence the reductions in dose transmission factor values are more predominant than the flux transmission factor values
2018	Satish et al	[66]	Boron carbide (B_4C) Silica fumes (SF) Metakaolin (MET)	Calc	The increase in the macroscopic removal cross-section values from specimen B to D (increase in B_4C from 15% to 25%) shows that boron carbide has neutron attenuating property and the neutron attenuation nature of a sample increases with increase in boron carbide content. The decrease in the removal cross section values on addition of pozzolans in specimen E and H (5% replacement of cement by pozzolans: SF, MET) when compared with specimen B (15% B_4C) shows that the microscopic removal cross section of the components of the pozzolanic material like microsilica and metakaolin is actually lesser than the microscopic cross-section values of the components present in the Portland pozzolana cement which is being replaced

Continued

Table 7.4 References in neutron shielding evaluation of concrete with special neutron attenuating and absorbing components (chronologically—cont'd

Year	Author(s)	Ref	Components	Calculations/ simulation/ experiment	Conclusions
2018	Aygun et al.	[52]	Steel fiber Mono- and Multi-filament polypropylene fiber	Sim/exp	Cross section is increasing with the using of monofilament polypropylene fiber in the samples and decreasing absorbed dose by detector of hybrid fiber heavyweight aggregate concretes. It is seen successfully that the neutron cross section are strongly dependent on the using of monofilament polypropylene fiber in the concretes. The using of monofilament polypropylene fiber effect on neutron shielding capability of matter. It is more effective shielding material because it has high cross section, high neutron capture values, and low absorbed dose rate
2018	Sarkawi et al.	[67]	Ferro-boron (Fe-B)	Sim	Concrete containing ferro-boron capable to block almost all the gamma radiation and thermal neutrons at thickness of 40 and 30 cm, respectively, while standard concrete needs shielding thickness around 60 cm for shielding gamma and thermal neutron radiation. Concrete containing ferro-boron has better shielding properties for thermal

					neutron as compared to gamma radiation. This is due to ferro-boron that contain boron compound which has high neutron absorption cross section. Hence, it shows that ferro-boron is capable of enhancing shielding properties of concrete
2018	Mesbahi et al.	[68]	Lead oxide (PbO_2) Iron oxide (Fe_2O_3) Tungsten oxide (WO_3) Boronium (H_4B)	Sim	Adding all four particles increased the neutron and photon attenuation of ordinary concrete. The nanosized particles showed higher neutron removal cross section (7%) and photon attenuation coefficient (8%) relative to microparticles
2019	Roslan et al.	[69]	Ferro-boron (Fe-B)	Exp	Aimed to reduce neutron and gamma radiation, this study examined the shielding capability of high density concretes mixed with Ferro boron in different proportions (25%, 50%, and 75%) replacing granite aggregate, denoted as 25FB, 50FB, and 75FB, respectively, with control specimen designated as CC. Ferro boron concrete showed better radiation shielding, where 25FB, 50FB, and 75FB shielded transmission of neutron and gamma 2, 2.57, and 3.27 times as well as 1.35, 1.72, and 2.92 times, respectively, better than CC

Continued

Table 7.4 References in neutron shielding evaluation of concrete with special neutron attenuating and absorbing components (chronologically—cont'd

Year	Author(s)	Ref	Components	Calculations/ simulation/ experiment	Conclusions
2019	Zalegowski et al.	[70]	Epoxy (PCC1) Acrylic dispersion (PCC2) Gadolinium oxide (Gd_2O_3) Polypropylene fibers Sodium borohydride ($NaBH_4$)	Calc/exp	Regarding the effectiveness of an ordinary concrete modification in order to improve its shielding properties against neutron radiation (half value layer *HVL* and effective macroscopic cross section Σ_R) it can be stated that the addition of gadolinium oxide has no influence of on calculated Σ_R for fast neutrons but it influenced on measured *HVL* due to the fact that attenuated neutrons are absorbed and dose in decreased. The modification of shielding concrete by combination of acrylic resin and gadolinium oxide was considered as the most effective in neutron shielding.

HDPE [5, 33], latex [71], and polypropylene fibers [52, 64, 65, 70]. The second group are the neutron absorbers containing boron compounds mainly boron carbide [53, 54, 58, 63, 66], datolite [55], boric acid, boric frit, and borax [56], ulexite [59], tourmaline [60], and ferro-boron [63, 67, 69]. Recently, hydro-borated components like boronium H_4B [68] and sodium borohydride $NaBH_4$ [64, 65, 70] were tried as well. Finally, some simulation and experiment have been made with gadolinium oxide [62, 64, 65, 70].

The possibility of improving neutron shielding properties of concrete by polymer additives has been already presented in the 1970s by Belyakov et al. [72, 73]. Modification introduces up to 300 kg/m^3 of polyethylene filler into concrete, which is quite effective from physicomechanical and technicoeconomic aspects. It was proved that such polymer cement composite can have a comparatively easily adjustable hydrogen content (up to 60 kg/m^3) and the empirical exponential relation between relaxation length of fluxes of fast neutron with energies 1.5–10.0 MeV and hydrogen content of the concrete has been found [72]. Also a nomogram for the calculation of comparative thickness of technological shielding against radiations from reactor spectra depending on hydrogen content in concrete of density 2000–2400 kg/m^3 has been drawn [73]. Analysis of the nomograms shows that the use of polymer-cement concrete allows for 30%–40% reduction in the thickness of the shielding compared with reference cement concrete with a hydrogen content of 6 kg/m^3. Moreover, it was concluded that as the thickness of the shielding concrete increases, the use of concretes with increased hydrogen content becomes less effective. The most pronounced decrease in the shielding size can be achieved at a thickness of 75–150 cm and it is inadvisable to increase the hydrogen content in the composition above 50 kg/m^3. New approach in this field was presented by Malkapur et al. [71] in a study on the effect of mix parameters and hydrogen loading on the neutron radiation shielding characteristics of latex modified concrete mixes. In general, an increasing trend of total neutron cross section and decreasing trend of dose transmission values with increased hydrogen loading were observed compared with control concrete with a few exceptions, which need to be explored taking into account the effect of other parameters (contribution of carbon and other lighter elements) and combined effect of parameters on the shielding performance. Evaluation of epoxy performed by Piotrowski [34, 64, 65] Zalegowski et al. [70], and Mazgaj and Piotrowski [62] show that this modifier can improve neutron attenuation significantly. PCC mortars showed slowing up to be twice more effective than cement mortars [34].

Materials with high capture cross sections for thermal neutrons such as gadolinium, cadmium, or boron have high potential in thermal neutrons capture. Boron addition into concrete also advantageous for reduction in the secondary gamma radiation produced after the thermal neutron capture. As a result emission of soft capture gamma rays (less penetrating) are easily absorbed by the shielding material. There are a number of studies on the addition of different boron compounds in concrete such as boric acid (H_3BO_3) and borax ($Na_2B_4O_7$) [56] or the use of specific aggregates such as colemanite ($CaB_3O_4(OH)\ H_2O$) [47]. The addition of boron carbide (B_4C) seems to be the most effective due to its high boron weight fraction. Moreover, the smaller the size of the B_4C particle the higher the shielding effectiveness. The problem in particle minimization is that it generates cost increase [68]. Nevertheless, the use of nanoparticle size additives has recently been reported to aid in achieving better neutron removal cross sections [68]. It is assumed that optimal proportion of B_4C is around 5% wt. of concrete. It is a compromise solution between an increase in the attenuation effect and a compressive strength reduction [53, 56, 74].

Investigations on the use of borohydrides are at the early stage—they seems to be effective but the increase in air content and decrease in density can be a problem. The addition of gadolinium in the form of gadolinium oxide (Gd_2O_3) is very promising. Chemically it is similar to titanium oxide (TiO_2) that is widely used in concrete. It does not influence negatively the cement hydration as it is in the case of ulexite [75] and the shielding efficiency improvement was observed both in computer simulations and experiments [61, 64, 65, 70].

7.8 Conclusions

This study suggests that many aspects of neutron shielding should be taken into account when designing an efficient barrier. The first step is to define neutron radiation characteristic including neutron energy and intensity.

Next, it has to be checked if gamma radiation emission is present as well. From such intro data the concrete design can be proceeded. When a mixed (neutron and gamma) radiation is needed to be shielded heavyweight aggregate has to be used. Iron-based aggregates (hematite, magnetite, ilmenite, limonite) and lead-based aggregates (galena) rather than barite ones are recommended for this purpose due to their higher density and better mechanical properties. Some improvement in thermal neutron attenuation can be a result of the use of rich-in-hydrogen aggregate like serpentine. If additionally thermal neutron absorption is the goal then the colemanite containing both hydrogen and boron is a candidate.

Cement type due to small differences in its chemical composition has no big influence of neutron radiation shielding but it is important for bound water content after cement hydration. This parameter is really important when fast neutron attenuation is considered.

The last possibility for neutron radiation shielding efficiency improvement is the use of special components. Their action is both neutron attenuation and absorption. In the first group (attenuation) there are generally polymers in the form of polymer additives (epoxy) and polymer fibers (polypropylene). In the second group (absorption), mostly boron compound are added but in this case the influence on mechanical properties of concrete should be checked—influence of boron-carbide (B_4C) is minimal in this group. Recent investigation shows that gadolinium oxide has high thermal neutron attenuation potential—even in very small amounts (less than 1% in relation to cement mass). Moreover, it has a positive influence on cement hydration. To increase mixed radiation shielding, ferro-boron (Fe-B) appears to be the best solution alongside iron- and lead-based material additives like steel fibers.

References

[1] V.F. Sears, Neutron scattering lengths and cross sections, Neutron News 3 (3) (1992) 29–37.

[2] M.H. Kharita, S. Yousef, M. AlNassar, The effect of the initial water to cement ratio on shielding properties of ordinary concrete, Prog. Nucl. Energ. 52 (5) (2010) 491–493, https://doi.org/10.1016/j.pnucene.2009.11.005.

[3] ICRU, Fundamental quantities and units for ionizing radiation (ICRU Report 85a-Revised), J. ICRU 11 (1) (2011). Report 85, Oxford University Press.

[4] B. Oto, N. Yıldız, T. Korkut, E. Kavaz, Neutron shielding qualities and gamma ray buildup factors of concretes containing limonite ore, Nucl. Eng. Des. 293 (2015) 166–175, https://doi.org/10.1016/j.nucengdes.2015.07.060.

[5] S.M. Malkapur, L. Divakar, M.C. Narasimhan, N.B. Karkera, P. Goverdhan, V. Sathian, N.K. Prasad, Neutron radiation shielding properties of polymer incorporated self compacting concrete mixes, Appl. Radiat. Isot. 125 (2017) 86–93, https://doi.org/10.1016/j.apradiso.2017.03.029.

[6] M.F. Kaplan, Concrete Radiation Shielding, John Wiley & Sons, New York, 1989.

[7] M.S. Seltzer, Calculation of photon mass energy-transfer and mass energy absorption coefficients, Radiat. Res. 136 (2) (1993) 147–170, https://doi.org/10.2307/3578607.

[8] J. Wood, Computational Methods in Reactor Shielding, Pergamon Press, Inc, New York, 1982.

[9] A.B. Chilton, J.K. Shultis, R.E. Faw, Principles of Radiation Shielding, Prentice-Hall, Englewood Cliffs, NJ, 1984.

[10] A.M. El-Khayatt, Calculation of fast neutron removal cross-sections for some compounds and materials, Ann. Nucl. Energy 37 (2) (2010) 218–222, https://doi.org/10.1016/j.anucene.2009.10.022.
[11] A.E. Profio, Radiation Shielding and Dosimetry, John Wiley & Sons, New York, 1979.
[12] A.M. El-Khayatt, A. El-Sayed Abdo, MERCSF-N: a program for the calculation of fast neutron removal cross sections in composite shields, Ann. Nucl. Energy 36 (6) (2009) 832–836, https://doi.org/10.1016/j.anucene.2009.01.013.
[13] A.M. El-Khayatt, NXcom—a program for calculating attenuation coefficients of fast neutrons and gamma-rays, Ann. Nucl. Energy 38 (1) (2011) 128–132, https://doi.org/10.1016/j.anucene.2010.08.003.
[14] K.S. Mann, Toolkit for fast neutron removal cross-section, in: Presentation for International Conference on Advanced Engineering and Technology (ICAET), 2015. Available at https://www.researchgate.net/profile/Kulwinder_Mann/publication/328927463_Use_WinNC-Toolkit/data/5bebc64b4585150b2bb4f236/WinNC-Toolkit.pdf.
[15] Y. Elmahroug, B. Tellili, C. Souga, K. Manai, ParShield: a computer program for calculating attenuation parameters of the gamma rays and the fast neutrons, Ann. Nucl. Energy 76 (2) (2015) 94–99, https://doi.org/10.1016/j.anucene.2014.09.044.
[16] S. Gowda, S. Krishnaveni, R. Gowda, Studies on effective atomic numbers and electron densities in amino acids and sugars in the energy range 30–1333 keV, Nucl. Instrum. Methods, B 239 (2005) 361–369, https://doi.org/10.1016/j.nimb.2005.05.048.
[17] O. Içelli, Z. Yalçin, M. Okutan, R. Boncukçuoğlu, A. Şen, The determination of the total mass attenuation coefficients and the effective atomic numbers for concentrated colemanite and Emet colemanite clay, Ann. Nucl. Energy 38 (9) (2011) 2079–2085, https://doi.org/10.1016/j.anucene.2011.06.003.
[18] S.R. Manohara, S.M. Hanagodimath, K.S. Thind, L. Gerward, On the effective atomic number and electron density: a comprehensive set of formulas for all types of materials and energies above 1 keV, Nucl. Instrum. Methods, B 266 (18) (2008) 3906–3912, https://doi.org/10.1016/j.nimb.2008.06.034.
[19] T. Piotrowski, M. Mazgaj, A. Żak, J. Skubalski, Importance of atomic composition and moisture content of cement based composites in neutron radiation shielding, Procedia Eng. 108 (2015) 616–623, https://doi.org/10.1016/j.proeng.2015.06.188.
[20] P. Prochoń, T. Piotrowski, Bound water content measurement in cement pastes by stoichiometric and gravimetric analyses, J. Build. Chem. 1 (1) (2016) 18–25. https://dx.doi.org/10.17461/j.buildchem.2016.103.
[21] T.T. Böhlen, F. Cerutti, M.P.W. Chin, A. Fassò, A. Ferrari, P.G. Ortega, A. Mairani, P.R. Sala, G. Smirnov, V. Vlachoudis, The FLUKA code: developments and challenges for high energy and medical applications, Nucl. Data Sheets 120 (2014) 211–214, https://doi.org/10.1016/j.nds.2014.07.049.
[22] A. Ferrari, P.R. Sala, A. Fassò, J. Ranft, FLUKA: A Multi-Particle Transport Co de, CERN-2005-10, (2005)INFN/TC_05/11, SLAC-R-773.
[23] S. Agostinelli, et al., Geant4—a simulation toolkit, Nucl. Instrum. Methods Phys. Res A 506 (2003) 250–303, https://doi.org/10.1016/S0168-9002(03)01368-8.
[24] J. Allison, et al., Geant4 developments and applications, IEEE T. Nucl. Sci. 53 (1) (2006) 270–278, https://doi.org/10.1109/TNS.2006.869826.
[25] J. Allison, et al., Recent developments in Geant4, Nucl. Instrum. Methods Phys. Res A 835 (2016) 186–225, https://doi.org/10.1016/j.nima.2016.06.125.
[26] J. Leppänen, M. Pusa, T. Viitanen, V. Valtavirta, T. Kaltiaisenaho, The Serpent Monte Carlo code: status, development and applications in 2013, Ann. Nucl. Energy 82 (2015) 142–150, https://doi.org/10.1016/j.anucene.2014.08.024.
[27] OECD-NEA, TRIPOLI-4 Version 8.1, 3D General Purpose Continuous Energy Monte Carlo Transport Code, Available at https://www.oecd-nea.org/tools/abstract/detail/nea-1716, 2013.

[28] P.K. Romano, N.E. Horelik, B.R. Herman, A.G. Nelson, B. Forget, K. Smith, OpenMC: a state-of-the-art monte carlo code for research and development, Ann. Nucl. Energy 82 (2015) 90–97, https://doi.org/10.1016/j.anucene.2014.07.048.

[29] T. Piotrowski, D.B. Tefelski, A. Polański, J. Skubalski, Monte Carlo simulations for optimization of neutron shielding concrete, Cent. Eur. J. Eng. 2 (2) (2012) 296–303, https://doi.org/10.2478/s13531-011-0063-0.

[30] H.R. Vega-Carrillo, E. Manzanares-Acuña, A.M. Becerra-Ferreiro, A. Carrillo-Nuñez, Neutron and gamma-ray spectra of 239PuBe and 241AmBe, Appl. Radiat. Isot. 57 (2) (2002) 167–170, https://doi.org/10.1016/S0969-8043(02)00083-0.

[31] S.-T. Park, Neutron energy spectra of ^{252}Cf, Am—Be source and of the D(d,n)^{3}He reaction, J. Radioanal. Nucl. Chem. 256 (1) (2003) 163–166, https://doi.org/10.1023/A:1023333016692.

[32] J. Schezinger, R. Al, J.R.M.A. Jebali, K.G. Fissum, R. Hall-Wilton, S. Koufigar, N. Mauritzson, F. Messi, H. Perrey, E. Rofors, Comparison of untagged gamma-ray and tagged-neutron yields from ^{241}AmBe and ^{238}PuBe sources, Appl. Radiat. Isot. 127 (2017) 98–102, https://doi.org/10.1016/j.apradiso.2017.05.014.

[33] S.M. Malkapur, L. Divakar, M.C. Narasimhan, N.B. Karkera, P. Goverdhan, V. Sathian, N.K. Prasad, Fresh and hardened properties of polymer incorporated self compacting concrete mixes for neutron radiation shielding, Constr. Build. Mater. 157 (2017) 917–929, https://doi.org/10.1016/j.conbuildmat.2017.09.127.

[34] T. Piotrowski, D. Tefelski, J. Skubalski, A. Żak, Experiments on neutron transport through concrete member and the potential for the use in material investigation, Acta Phys. Pol. A 128 (2B) (2015) B14–B18. https://doi.org/10.12693/APhysPolA.128.B-14.

[35] I.I. Bashter, A. El-Sayed Abdo, A.S. Makarious, A comparative study of the attenuation of reactor thermal neutrons in different types of concrete, Ann. Nucl. Energy 23 (14) (1996) 1189–1195, https://doi.org/10.1016/0306-4549(95)00122-0.

[36] A. El-Sayed Abdo, R.M. Megahid, Attenuation of Neutrons and Gamma-Rays in Homogeneous and Multilayered Shields, AREAEA/Rep.344(1988).

[37] A. El-Sayed Abdo, R.M. Megahid, Homogeneous and multilayered shields for neutrons and gamma-rays, Jpn. J. Appl. Phys. 40 (2001) 2460–2464, https://doi.org/10.1143/JJAP.40.2460.

[38] I. Murata, S. Yoshida, A. Takahashi, Effect of heterogeneities in heavy concrete on shielding of fusion neutrons, Fusion Sci. Technol. 36 (2) (1999) 181–193. https://doi.org/10.13182/FST99-A101.

[39] C.-M. Lee, Y.H. Lee, K.J. Lee, Cracking effect on gamma-ray shielding performance in concrete structure, Prog. Nucl. Energ. 49 (4) (2007) 303–312, https://doi.org/10.1016/j.pnucene.2007.01.006.

[40] A.M.I. Kany, M.I. El-Gohary, S.M. Kamal, Thermal, epithermal and thermalized neutron attenuation properties of ilmenite-serpentine heat resistant concrete shield, Radiat. Phys. Chem. 44 (l/2) (1994) 157–160, https://doi.org/10.1016/0969-806X(94)90122-8.

[41] A.S. Makarious, I.I. Bashter, A. El-Sayed Abdo, M.S.A. Azim, W.A. Kansouh, On the utilization of heavy concrete for radiation shielding, Ann. Nucl. Energy 23 (3) (1996) 195–206, https://doi.org/10.1016/0306-4549(95)00021-1.

[42] I.I. Bashter, A. El-Sayed Abdo, A.S. Makarious, Investigation of hematite-serpentine and ilmenite-limonite concretes for reactor radiation shielding, Ann. Nucl. Energy 23 (1) (1996) 65–71, https://doi.org/10.1016/0306-4549(95)00011-G.

[43] I.I. Bashter, Radiation attenuation and nuclear properties of high density concrete made with steel aggregates, Radiat. Eff. Defects S. 140 (3–4) (1997) 351–364, https://doi.org/10.1080/10420159708216859 Incorporating Plasma Science and Plasma Technology.

[44] I.I. Bashter, Calculation of radiation attenuation coefficients for shielding concretes, Ann. Nucl. Energy 24 (17) (1997) 1389–1401, https://doi.org/10.1016/S0306-4549(97)00003-0.

[45] A. El-Sayed Abdo, Calculation of the cross-sections for fast neutrons and gamma-rays in concrete shields, Ann. Nucl. Energy 29 (16) (2002) 1977–1988, https://doi.org/10.1016/S0306-4549(02)00019-1.

[46] M.H. Kharita, M. Takeyeddin, M. Alnassar, S. Yousef, Development of special radiation shielding concretes using natural local materials and evaluation of their shielding characteristics, Prog. Nucl. Energy 50 (1) (2008) 33–36, https://doi.org/10.1016/j.pnucene.2007.10.004.

[47] T. Korkut, A. Ün, F. Demir, A. Karabulut, G. Budak, R. Şahin, M. Oltulu, Neutron dose transmission measurements for several new concrete samples including colemanite, Ann. Nucl. Energy 37 (2010) 996–998, https://doi.org/10.1016/j.anucene.2010.04.005.

[48] O. Gencel, A. Bozkurt, E. Kam, T. Korkut, Determination and calculation of gamma and neutron shielding characteristics of concretes containing different hematite proportions, Ann. Nucl. Energy 38 (12) (2011) 2719–2723, https://doi.org/10.1016/j.anucene.2011.08.010.

[49] D.B. Tefelski, T. Piotrowski, V. Blideanu, A. Polanski, J. Skubalski, Monte-Carlo aided design of neutron shielding concretes, Bull. Pol. Acad. Sci.-Tech. 61 (1) (2013) 161–171, https://doi.org/10.2478/bpasts-2013-0015.

[50] I. Akkurt, A.M. El-Khayatt, The effect of barite proportion on neutron and gamma-ray shielding, Ann. Nucl. Energy 51 (2013) 5–9, https://doi.org/10.1016/j.anucene.2012.08.026.

[51] B. Oto, A. Gür, E. Kavaz, T. Çakır, N. Yaltay, Determination of gamma and fast neutron shielding parameters of magnetite concretes, Prog. Nucl. Energy 92 (2016) 71–80, https://doi.org/10.1016/j.pnucene.2016.06.011.

[52] B. Aygun, R. Mehrnejad, E. Şakar, S. Unvar, T. Korkut, A. Karabulut, R. Durak, Improving heavy concrete shielding materials against fast neutron radiation leaks with experimental and Monte Carlo simulation (Geant4) code, Int. J. Sci. Eng. Res. 9 (5) (2018) 107–111.

[53] Y. Abdullah, M.R. Yusof, A. Muhamad, Z. Samsu, N.E. Abdullah, Cement-boron carbide concrete as radiation shielding material, J. Nucl. Relat. Technol. 7 (2) (2010) 74–79.

[54] Y. Abdullah, F.N.T. Ariffin, R. Hamid, M.R. Yusof, N.M. Zali, M.H.A.R. M. Ahmad, H. Yazid, S. Ahmad, A.A. Mohamed, Preliminary study of neutron absorption by concrete with boron carbide addition, AIP Conf. Proc. 1584 (2014) 101–104, https://doi.org/10.1063/1.4866112.

[55] D.S.M.J. Mortazavi, M.A. Mosleh-Shirazi, M.R. Maheri, H. Yousefnia, S. Zolghadri, A. Haji-Pour, Production of an economic high-density concrete for shielding megavoltage radiotherapy rooms and nuclear reactors, Iran. J. Radiat. Res. 8 (1) (2010) 11–15. http://ijrr.com/article-1-328-en.html.

[56] M.H. Kharita, S. Yousef, M. Alnassar, Review on the addition of boron compounds to radiation shielding concrete, Prog. Nucl. Energ. 53 (2) (2011) 207–211, https://doi.org/10.1016/j.pnucene.2010.09.012.

[57] E. Yılmaz, H. Baltas, E. Kırıs, İ. Ustabas, U. Cevik, A.M. El-Khayatt, Gamma ray and neutron shielding properties of some concrete materials, Ann. Nucl. Energy 38 (2011) 2204–2212, https://doi.org/10.1016/j.anucene.2011.06.011.

[58] M.R. Yusof, Y. Abdullah, Z. Samsu, Study of the effect of boron carbide content in concrete as radiation shielding application, Adv. Mat. Res. 535–537 (2012) 1877–1880, https://doi.org/10.4028/www.scientific.net/AMR.535-537.1877.

[59] S.M.R. Aghamiri, S.M.J. Mortazavi, Z. Razi, M.A. Mosleh-Shirazi, M. Baradaran-Ghahfarokhi, F. Rahmani, F. Faeghi, Ulexite-galena intermediate-weight concrete

as a novel design for overcoming space and weight limitations in the construction of efficient shields against neutrons and photons, Radiat. Prot. Dosim 154 (3) (2013) 375–380, https://doi.org/10.1093/rpd/ncs249.

[60] S.M.R. Aghamiri, S.M.J. Mortazavi, M.A. Mosleh Shirazi, M. Baradaran-Ghahfarokhi, F. Rahmani, A. Amiri, S. Jarideh, Production of a novel high strength heavy concrete using tourmaline and galena for neutron and photon radiation shielding, Int. J. Radiat. Res. 12 (3) (2014) 277–282. http://ijrr.com/article-1-1287-en.html.

[61] T. Piotrowski, D.B. Tefelski, J.J. Sokołowska, B. Jaworska, NGS-concrete—new generation shielding concrete against ionizing radiation—the potential evaluation and preliminary investigation, Acta Phys. Pol. A 128 (2B) (2015) B9–13. https://doi.org/10.12693/APhysPolA.128.B-9.

[62] M. Mazgaj, T. Piotrowski, Improvement of neutron shielding properties of concrete by innovative material modification, in: A.M. Brandt, J. Olek, M.A. Glinicki, C.K. Y. Leung, J. Lis (Eds.), Proc. Int. Symp. "Brittle Matrix Composites 11", Warsaw, Sept. 28–30, Institute of Fundamental Technological Research, 2015, p. 2015.

[63] D. Sarıyer, R. Küçer, N. Küçer, Neutron shielding properties of concretes containing boron carbide and ferro-boron, Procedia Soc. Behav. Sci. 195 (2015) 1752–1756, https://doi.org/10.1016/j.sbspro.2015.06.320.

[64] T. Piotrowski, M.A. Gryziński, Effectiveness evaluation of new generation shielding concrete against ionizing radiation based on measurements in standard radiation fields, J. Civ. Eng. Environ. Archit. 33 (63/1/1) (2016) 141–148. (in Polish). https://doi.org/10.7862/rb.2016.16.

[65] T. Piotrowski, A. Garbacz, Efektywność modyfikacji materiałowej w celu poprawy właściwości osłonowych betonu przed promieniowaniem jonizującym, in: IX Konferencja Dni betonu. Tradycja i nowoczesność. Monografie technologii betonu (1–2), 2016, pp. 649–667 Stowarzyszenie Producentów Cementu (in Polish).

[66] A.J. Satish, P.N. Aravind, P.V. Hakesh, V. Vignesh, D.K.M. Mini, Influence of boron carbide addition on performance and neutron shielding ability of cement mortar mix, Int. J. Eng. Technol. 7 (4.5) (2018) 48–55, https://doi.org/10.14419/ijet.v7i4.5.20008.

[67] M.S. Sarkawi, M.R.M. Zain, M.H. Rabir, F.M. Idris, J. Zainal, Radiation shielding properties of ferro-boron concrete, IOP Conf. Ser. Mater. Sci. Eng. 298 (2018) 12,037, https://doi.org/10.1088/1757-899X/298/1/012037.

[68] A. Mesbahi, H. Ghiasi, Shielding properties of the ordinary concrete loaded with micro- and nano-particles against neutron and gamma radiations, Appl. Radiat. Isot. 136 (2018) 27–31, https://doi.org/10.1016/j.apradiso.2018.02.004.

[69] M.K.A. Roslan, M. Ismail, A.B.H. Kueh, M.R.M. Zin, High-density concrete: exploring ferro boron effects in neutron and gamma radiation shielding, Constr. Build. Mater. 215 (2019) 718–725, https://doi.org/10.1016/j.conbuildmat.2019.04.105.

[70] K. Zalegowski, T. Piotrowski, A. Garbacz, G. Adamczewski, Relation between microstructure, technical properties and neutron radiation shielding efficiency of concrete, Constr. Build. Mater. 235 (2020) 117389, https://doi.org/10.1016/j.conbuildmat.2019.117389.

[71] S.M. Malakpur, H. Satdive, M.C. Narasimhan, B.N. Karkera, P. Goverdhan, V. Sathian, Effect of mix parameters and hydrogen loading on neutron radiation shielding characteristics of latex modified concrete mixes, Prog. Nucl. Energ. 83 (2015) 8–12, https://doi.org/10.1016/j.pnucene.2015.02.010.

[72] V.V. Belyakov, V.A. Grigorev, V.V. Kozlov, P.A. Lavdanskii, V. Nazarov, Shielding characteristics of polymer based concretes in neutron radiation fields, Sov. Atom. Energ. 43 (4) (1977) 913, https://doi.org/10.1007/BF01117999.

[73] V.V. Belyakov, V.A. Grigoriev, P.A. Lavdanskii, O.A. Remeiko, V.F. Khokhlov, Calculation of shielding made of concrete with an increased hydrogen content, Sov. Atom. Energ. 44 (5) (1978) 526–528, https://doi.org/10.1007/BF01119280.

[74] F.N.T. Ariffin, R. Hamid, Y. Abdullah, S.H. Ahmad, Y.H. Muhammad, Effect of boron carbide addition on the strength and physical properties of concrete, Adv. Mater. Res. 895 (2014) 385–389, https://doi.org/10.4028/www.scientific.net/AMR.895.385.

[75] T. Piotrowski, J. Glinicka, M.A. Glinicki, P. Prochoń, Influence of gadolinium oxide and ulexite on cement hydration and technical properties of mortars for neutron radiation shielding purposes, Constr. Build. Mater. 195 (2019) 583–589, https://doi.org/10.1016/j.conbuildmat.2018.11.076.

CHAPTER 8

Neutron shielding concrete in medical applications

J.J. Bevelacqua[a], **S.M.J. Mortazavi**[b,c]
[a]Bevelacqua Resources, Washington, WA, United States
[b]Diagnostic Imaging Department, Fox Chase Cancer Center, Philadelphia, PA, United States
[c]Medical Physics Department, School of Medicine, Shiraz University of Medical Sciences, Shiraz, Iran

8.1 Introduction

Neutrons are an important consideration in treating various medical conditions. Medical applications utilize a variety of facilities, physical processes, medical protocols, and require knowledge of neutron physics and the associated shielding techniques [1–4].

Neutron radiation facilitates the delivery of high radiation doses to treat various cancer types. Neutrons are generated using a number of radiation-generating devices including fission reactors, cyclotrons, linear accelerators, and specific nuclear reactions. These devices are used in a variety of therapy applications including fast neutron therapy and neutron capture therapy.

The neutron-generating devices produce radiation levels that require a shielded structure to reduce exposures to facility staff, patients, and the public to levels that meet regulatory requirements [5]. Neutron shielding is complex. The neutron is uncharged and numerous interactions [e.g., (n, γ), (n, p), and (n, α)] are induced by its passage through matter [6]. These reactions are determined by the available neutron energy. Current medical applications involve relatively low-energy neutrons (<100 MeV), which greatly simplify the shielding problem [4, 7]. With this energy consideration, concrete becomes a cost-effective shielding material that has a number of desirable characteristics for use in medical facilities.

This chapter focuses on the use of concrete in medical shielding applications. Section 8.2 outlines the various medical facilities that utilize neutron radiation. Neutron physics is addressed in Section 8.3. Section 8.4 outlines neutron shielding considerations and methodology including the use of micro- and nanomaterials. The use of concrete for neutron shielding and the advantages and disadvantages of heavy concrete for neutron and photon shielding are addressed in Sections 8.5 and 8.6, respectively.

Micro and Nanostructured Composite Materials for Neutron Shielding Applications
https://doi.org/10.1016/B978-0-12-819459-1.00008-8

© 2020 Elsevier Ltd.
All rights reserved.

8.2 Medical facilities utilizing neutron radiation

A variety of medical facilities have used or currently utilize neutron radiation in medical research and treatment protocols Ashraf and Khan [8], Svensson, and Landberg [9], Zyga [10], IAEA [11], Kroc and Welsh [12], NTCW [13]. Table 8.1 summarizes a selection of these facilities by their country, type of facility, and methodology utilized to produce the neutron source. As noted in Table 8.1, neutron facilities are located throughout the world, and use a number of techniques to produce neutrons [1, 2, 4, 7].

The dominant modes of neutron production are based on cyclotrons and fission reactors. Linear accelerators and deuterium-tritium (D-T) sources are also used, but to a lesser extent.

Cyclotrons produce a neutron source using a variety of nuclear reactions. The machines accelerate protons or deuterons, and strike a target to produce the neutron source. Most facilities produce neutrons using a beryllium target and utilize the reactions $^{9}Be(p,n)^{9}B$ and $^{9}Be(d,n)^{10}B$. Other reactions could also be used including $^{3}H(p,n)^{3}He$ and $^{3}H(d,n)^{4}He$. The neutron energy is

Table 8.1 Partial list of historical world neutron therapy centers.[a]

Country	Facility type	Methodology
Argentina	Reactor	Fission neutrons
Belgium	Cyclotron	$^{9}Be(p,n)^{9}B$
China	Proton linear accelerator	$^{9}Be(p,n)^{9}B$
Finland	Reactor	Fission neutrons
France	Cyclotron	$^{9}Be(p,n)^{9}B$
Germany	Reactor	Fission neutrons
Germany	D-T generator	$^{3}H(^{2}H,n)^{4}He$
Japan	Cyclotron	$^{9}Be(d,n)^{10}B$
Japan	Reactor	Fission neutrons
Netherlands	Reactor	Fission neutrons
Russia	Reactor	Fission neutrons
Saudi Arabia	Cyclotron	$^{9}Be(p,n)^{9}B$
South Africa	Cyclotron	$^{9}Be(p,n)^{9}B$
Taiwan	Reactor	Fission neutrons
United Kingdom	Cyclotron	$^{9}Be(p,n)^{9}B$
United Kingdom	Cyclotron	$^{9}Be(d,n)^{10}B$
United States	Cyclotron	$^{9}Be(p,n)^{9}B$
United States	Cyclotron	$^{9}Be(d,n)^{10}B$
United States	Proton linear accelerator	$^{9}Be(p,n)^{9}B$
United States	Reactor	Fission neutrons

[a] Derived from IAEA [11] and NTCW [13].

governed by the reaction Q value and energy of the incident proton or deuteron. However, the neutrons utilized in medical applications are relatively low energy (<100 MeV), which greatly simplifies the shielding considerations. This is addressed in more detail in Sections 8.3 and 8.4.

Reactor-generated neutrons rely on the thermal fission of ^{235}U. Following the thermal fission of ^{235}U, 2–3 neutrons are emitted. Fission neutrons have an energy distribution, and most neutrons have energy below 7 MeV. The neutron distribution has a most probable energy of about 0.7 MeV and a mean energy of about 2.0 MeV [7].

8.3 Review of neutron physics

The neutron is uncharged, has a mass of 939.6 MeV/c^2, and interacts with a material medium by a variety of energy-dependent processes [6]. In broad terms, these processes can be classified as elastic and inelastic scattering [7].

The neutron energy is reduced by elastic scattering from target nuclei in the scattering medium. If the neutron mass is m, an initial energy (E), and the target nucleus mass is M, the maximum energy transferred in a single collision ($E_{\max}$) is obtained from the conservation of energy and momentum [7]:

$$E_{\max} = E\left[1 - \left(\frac{M-m}{M+m}\right)\right]^2 \tag{8.1}$$

The average energy transferred in a single collision ($\overline{E}$) is

$$\overline{E} = E\frac{2Mm}{(M+m)^2} \tag{8.2}$$

The maximum energy transferred in a collision is achieved if $M = m$ which occurs in the target contains nuclei with a mass similar to that of the neutron. This occurs for materials with a high hydrogen concentration (e.g., concrete, polyethylene, and water) [14–16]. The elastic scattering reaction of most significance is ^{1}H(n,n)^{1}H. This reaction is discussed in additional detail in Section 8.4.

Inelastic scattering results in the excitation of the target nucleus. The excitation depends on the target nucleus and incident neutron energy. Section 8.4 addresses several inelastic interactions of interest in neutron shielding including ^{1}H(n,γ)^{2}H, Fe(n,n′)Fe, and Pb(n,n′)Pb [14–17].

Cyclotrons and other proton accelerators present unique challenges. Before limiting the discussion to the lower energy machines summarized in Table 8.1, it is illustrative to consider the general case of neutrons produced by a proton accelerator such as a cyclotron or linear accelerator [18]. Although interesting phenomena occur above 1 GeV, the discussion is limited to that energy. This is reasonable since the medical facilities are typically limited to proton beam energies below 100 MeV.

Under most operating conditions, neutrons are the dominant prompt radiation hazard at proton accelerators above 10 MeV. The interaction mechanisms that are associated with electromagnetic and hadronic cascades [1, 2, 4, 7, 18, 19] preferentially remove photons and charged particles. Accordingly, photons and charged particles normally contribute a small contribution to the total effective dose outside the shield. Neutrons normally dominate the effective dose.

An increased number of nuclear reactions occur for proton beam energies between 200 MeV and 1 GeV (ICRU [20] and NCRP [18]). Within this energy range highly excited compound nuclear states are formed. These excited states decay by neutron emission that leads to the development of hadronic cascades (see Table 8.2). Other radiation types (e.g., charged particles and light nuclei) are also emitted, but are absorbed in accelerator shielding. Protons and neutrons are produced in roughly equal numbers. As their energy increases (well beyond those encountered in neutron therapy), protons have a greater range in the shielding and are of increasing importance from a radiation protection standpoint. However, the issues associated with proton radiation are not usually an issue during neutron therapy.

8.4 Neutron shielding including micro- and nanomaterial structures

The approach to neutron shielding is significantly different than gamma-ray shielding. Gamma-ray shielding is a mass attenuation process that is governed by three basic interaction processes (i.e., photoelectric effect, Compton scattering, and pair production). Neutron shielding is a bulk attenuation process. Gamma-ray shielding depends on the density of the attenuating medium, but neutron shielding depends on the material thickness. Neutron shielding must also consider the reaction products of neutron-induced reactions including the activation of structures and components [11, 15, 17, 21].

In general, neutron shielding is a complex process that involves a number of interactions characterized by hadronic cascade interactions. The hadronic cascade is summarized in Table 8.2.

Table 8.2 Processes of the hadronic cascade.[a]

Process	Initial particles produced as a result of the incident hadron collision	Time scale (s)	Typical energy per particle (MeV)	Percent of energy deposition
Muon production	$\pi^+ \rightarrow \mu^+ + \nu_\mu$ $\pi^- \rightarrow \mu^- + \overline{\nu}_\mu$ $K^+ \rightarrow \mu^+ + \nu_\mu$ $K^- \rightarrow \mu^- + \overline{\nu}_\mu$	10^{-8}	Any	10
Electromagnetic cascade	$\pi^0 \rightarrow \gamma + \gamma$ $\gamma \rightarrow e^+ + e^-$ $\gamma \rightarrow \mu^+ + \mu^-$ (γ, n) reactions	10^{-16}	Any	20
Intranuclear cascade	Spallation products dominated by protons, neutrons, pions, and kaons	10^{-22}	<200	30
Extranuclear Cascade	Nuclear collisions produce a variety of radiation types including protons, neutrons, pions, and kaons	10^{-23}	>200	30
Evaporation of nucleons and nuclear fragments	Evaporation products are dominated by protons, neutrons, deuterons, and alpha particles	10^{-19}	<30	10
Induced activity	Activation reactions lead to the emission of radiation types dominated by photons, beta particles, and alpha particles	Seconds to years	<10	<1

[a] Derived from NCRP 144 [18] and ICRU [20].

As noted in Eqs. (8.1), (8.2), the reduction in initial neutron energy is facilitated by collisions with hydrogenous materials. Water, polyethylene, and concrete are typically used to shield neutrons. Most medical facilities incorporate concrete shields as part of the facility design. The effectiveness of these shields is based on the scattering cross section for the $^{1}H(n,n)^{1}H$ reaction. As low neutron energies (e.g., <5–10 MeV) the $^{1}H(n,\gamma)^{2}H$ reaction efficiently removes neutrons and produces photons [7, 14–17, 21]. These photons are effectively absorbed by additional concrete shielding. In general, the $^{1}H(n,n)^{1}H$ reaction has reduced cross sections as the proton energy increases. However, this physical consideration is minimized by designing a thicker concrete shield. For most facilities, space is not a limiting consideration, and concrete makes an effective neutron shield.

If space becomes a consideration then the shield thickness can be reduced by using a combined shield of concrete and lead or iron. For neutron energies above 5–10 MeV, the shield incorporates iron or lead closer to the source to reduce the neutron energy through inelastic scattering reactions (e.g., $Fe(n,n')Fe$, and $Pb(n,n')Pb$) [7, 14–17, 21]. These reactions reduce the neutron energy to the 5–10 MeV range where the elastic scattering reaction $^{1}H(n,n)^{1}H$ becomes effective again, and the neutrons are captured through the $^{1}H(n,\gamma)^{2}H$ reaction. A final layer of lead or iron attenuates the photons. Since space is not normally a limiting factor, concrete is effectively used without the necessity to incorporate iron or lead into the shield design.

Detailed shielding design is often accomplished using neutron transport codes including FLUKA [22], GEANT4 [23], MCNPX [23], and MCNP [24]. These codes are Monte Carlo simulation code packages that are frequently utilized in medical and shielding applications. The codes can be utilized to determine shield thickness values and dose rates for an input neutron source and a complex geometric configuration. An overview of these codes and their underlying principles are provided by Shultis and Faw [25] and NCRP [18].

Computer codes are extremely useful in shielding design applications, but users must exercise caution in their use. Knowledge of their internal operation, defining algorithms, data files, and limiting assumptions are essential to ensure credible results. Before utilizing the computer code, it is often advantageous to perform a deterministic calculation using methodology similar to that proposed by Rockwell [14], Shure et al. [15], Schaeffer [16], or Bevelacqua [2, 7]. In particular, an initial half-value layer calculation or more detailed point kernel calculation is performed.

The half-value layer calculation is used to provide an initial estimate of the shield thickness. A more accurate result can be obtained using a point kernel calculation [7, 15, 21]. These deterministic calculations are used to assess the validity of the more sophisticated computer model. The deterministic calculations provide confidence in the computational results. However, these deterministic calculations only provide an initial assessment and are not sufficiently accurate for final design calculations. The final calculations must account for equipment configuration, entry doors, penetrations, structural obstructions, and maze structures.

The half-value layer calculation is based on a relationship involving either desired fluence rate (ϕ) or dose rate ($\dot{H}$):

$$\phi(x) = \phi(0)2^{-N} \tag{8.3}$$

$$\dot{H}(x) = \dot{H}(0)2^{-N} \tag{8.4}$$

where $\phi(x)$ is the attenuated (shielded) fluence rate, x is the shield thickness, $\phi(0)$ is the unattenuated (unshielded) fluence rate, N is the number of neutron half-value layer (HVL) thicknesses for the source with energy E, $\dot{H}(x)$ is the attenuated dose rate, and $\dot{H}(0)$ is the unattenuated dose rate. Eqs. (8.3), (8.4) are written for a simple shield composed of only a single material. These equations can be generalized to more complex shields, but the results are not as accurate as those provided by the Monte Carlo models.

Example half-value thickness values are summarized in Table 8.3 for selected neutron energies. Similar relationships are written for 10th-value layers (TVL). The shield thickness (x) is written in terms of N and the half-value thickness t_{HVL}

$$x = Nt_{\mathrm{HVL}} \tag{8.5}$$

The Shure et al. methodology utilizes a point kernel relationship [14, 15]

Table 8.3 Neutron HVL and TVL values in concrete[a].

Neutron energy (MeV)	HVL (cm)	TVL (cm)
1	7	23
5	11	38
10	14	47
15	16	53

[a] Derived from Bevelacqua [7].

$$\dot{H}\left(\vec{r}\right)=\frac{S\left(\vec{r}\,'\right)}{4\pi\left|\vec{r}-\vec{r}\,'\right|}\sum_{i=1}^{N}A_i e^{-\Sigma_i t} \tag{8.6}$$

where the constants A_i are empirical values determined from a fit of exponential terms to (1) the measured fast neutron dose rate distribution and (2) the experimental thermal neutron dose rate distribution to theoretical transport calculations. In Eq. (8.6), $\dot{H}\left(\vec{r}\right)$ is the neutron dose rate at distance $\vec{r}$, $S\left(\vec{r}\,'\right)$ is the neutron source strength at distance $\vec{r}\,'$, $\sum_i$ are macroscopic neutron removal coefficients, t is the shield thickness, and N is the number of terms in the exponential fit.

For the fast neutron dose rate kernel, the A_i values contain dose conversion factors. The fast neutron dose rate kernel contains three terms in the exponential ($N=3$) and the thermal neutron dose rate kernel contains two terms ($N=2$). The use of Shure et al. [15] methodology is valid only if the shield is uniform and at least 15 cm of concrete must lie between the last nonhydrogenous material and the dose point.

The dose rate can also be obtained from the fluence using an appropriate fluence to dose conversion factor (k) [26]:

$$H(x)=k\phi(x) \tag{8.7}$$

ICRP 116 [26] provides fluence to dose conversion factors for neutron energies in the range 0.001 eV–10 GeV.

Eqs. (8.3)–(8.7) provide a basic estimate of the neutron fluence and associated equivalent dose. As noted previously, these results would be used as part of the evaluation of transport code results for a concrete shield supporting a neutron therapy facility.

Improved shield performance can be obtained by adding materials to the basic concrete structures. For example, this results in a denser concrete that improves the shielding of photons or borated concrete that improves the attenuation of neutrons. Neutron attenuation is facilitated by the materials having a large thermal neutron absorption cross section. A commonly used additive is boron that absorbs thermal neutron through the $^{10}B(n,\alpha)^{7}Li$ reaction.

The simple deterministic calculations summarized in Eqs. (8.3)–(8.7) assume uniform shields and do not accurately accommodate penetrations, ducts, and other structures that perturb the shield uniformity assumption. In order to accurately model structures penetrating the shield and detailed concrete content, transport codes must be utilized.

Transport codes are also useful in assessing a more recent improvement in neutron shielding. A recent development in neutron shielding further advances the concept of adding material to concrete to improve its neutron attenuation properties. This improvement incorporates the use of micro- and nanomaterials within the concrete shield. This development is a nature extension of the use of borated concrete to enhance the shield's neutron attenuation properties. Other added materials have also been used to enhance the photon-attenuating properties of concrete. These materials are discussed in Section 8.6.

As an illustration of the use of micro- and nanoparticles, Kim et al. [27] noted that the size dependence of imbedded particles is an important consideration in neutron shield development. Relative to microparticles, nanoparticles increase the total particle surface area. The area decrease of the individual particles results in an interparticle spacing reduction, and decreases the mean free path. The net effect of homogeneous nanoparticle dispersion in a shield matrix is an increase in neutron absorption efficiency.

In a 2008 study, Kim et al. [27] investigated B_2O_3 neutron absorption efficiency as a function of particle size. A point thermal neutron source (0.025 eV) was used to irradiate a high-density polyethylene shield of 0–3 cm thickness. Improved thermal neutron absorption was observed with decreasing particle radius. B_2O_3 particles of selected radii (i.e., 300 μm, 1 μm, and ~0.1 nm) were utilized and analyzed using MCNP [24]. The calculations suggest an enhancement of thermal neutron absorption efficiency ~25% for 1 cm shields, ~50% for 2 cm shields, and ~72% for 3 cm shields.

Mesbahi and Ghiasi [28] investigated the shielding characteristics of ordinary concrete supplemented with micro- and nanomaterials. MCNPX [23] was used to simulate narrow beams of neutrons (0.1–3.0 MeV) and photons (0.142–1.25 MeV) impinging upon ordinary concrete with added PbO_2, Fe_2O_3, WO_3, and H_4B. In comparison to microparticles, nanoparticles had a calculated neutron removal cross section 7% larger and photon attenuation coefficient that was 8% larger. The addition of nanoparticles to concrete shielding has the potential to reduce both neutron and photon radiation exposures, and reduce the shield thickness.

Park et al. [29] also suggest that the addition of micromaterials improves neutron shield performance. Nano-TiO_2 improved the shielding effectiveness of cement paste for thermal, slow, and intermediate neutrons. The neutron shielding performance also improved as nano-TiO_2 loading increased. Kim et al. [30] reported the use of B_4C and BN nanocomposites. In this work, the attenuation of thermal neutrons using high-density polyethylene nanomaterials was enhanced when compared to their micromaterial analogues. Mortazavi et al. [31] also observed improved neutron shield effectiveness using boron nanoparticles in polyethylene.

The importance of particle size in optimizing shield design is also suggested by Song et al. [32]. Small-angle neutron scattering results reinforce calculations that indicate that particle sizes influence the properties of materials doped with micro- and nanomaterials.

An alternative to imbedding materials within a concrete matrix is offered by Chkhartishvili [33]. Chkhartishvili suggests using thin coatings of ^{10}B-enriched material to create coatings that can be applied to existing structures to attenuate neutrons. These coatings have the potential to be applied to concrete structures and possibly to protective clothing (e.g., coveralls, gloves, shoe covers, and hoods) to reduce neutron radiation doses.

Micro- and nanomaterials have the potential to reduce both neutron and photon doses. However, the materials need to be validated experimentally, investigated at a range of neutron energies, and tested for longevity to verify sustained performance over extended periods in a medical facility environment. Concrete performance under various temperature, humidity, and environmental conditions should also be performed. The economics of the use of nanomaterials must be clearly demonstrated for this technology to be widely utilized in shielding applications.

8.5 Using concrete for neutron shielding

Recently, the utilization of nuclear technology in different fields of industry, medicine, and research has experienced rapid advancement. Radiation protection has become a public and worker safety concern due to the growing use of ionizing radiation in industry and medicine. Among the types of the ionizing radiations, X- and gamma-ray photons and neutrons merit attention, because their range is greater than the penetrating capability of charged particles. Insufficient or inappropriate shielding against such radiation types could potentially cause serious biological damages to human and other biological systems. Therefore, the design and construction of radiation shields are important nuclear engineering and radiation protection considerations. From the theoretical point of view, as long as the thickness is sufficient to attenuate the radiation to meet regulatory requirements, any material can be used as a radiation shield. However, the attenuation characteristics of lead and concrete validate their use in practical shielding applications for photons and neutrons, respectively.

The desired radiation attenuation depends on basic factors including the thickness and weight of the shield. While the properties such as high atomic number, density, stability, and ease of fabrication have made lead an excellent photon-shielding material, it is not self-supporting, highly toxic, and relatively transparent to neutrons. In contrast, concrete is a nontoxic, inexpensive, and self-supporting shielding material.

The lack of electrical charge in neutrons increases their penetration through different materials, because they primarily interact with the nuclei of atoms. Moreover, shielding high-energy neutrons is more difficult because their absorption cross section tends to decrease with energy. Moderating these higher energy neutrons through elastic or inelastic scattering interactions and then absorbing them in appropriate shielding materials are the key aspects of shielding energetic neutrons [34].

Concrete is the conventional material for shielding high-energy photons and neutrons in energy generation, medicine, and research applications. Given this consideration, concrete has been used for many years on Earth, and has recently been investigated for its utilization and production in space. A recent paper in the Frontiers in Materials [2] investigated key questions regarding the use of concrete in space (e.g., how it will harden in microgravity and what is the resulting microstructure?). The authors noted that lack of basic terrestrial physical properties in space (e.g., buoyancy, sedimentation, and fluid convection) led to the production of samples with a uniform phase distribution and distinct morphologies [35].

Concrete has been widely used in the construction of radiotherapy rooms and containers for spent nuclear fuel, nuclear power plant foundations, and many other industrial and research structures [36]. Concrete is an effective shielding material used for protection against gamma radiation. Moreover, an increase in concrete density (e.g., the utilization of high-density aggregates) significantly increases its photon attenuation properties. In addition to its cost effectiveness, concrete has an additional advantage over other shielding materials for high-energy radiotherapy machines (>10 MV). As long as the barrier thickness is adequate to shield against X-rays, it would also be adequate for shielding neutrons (NCRP 151). However, considering the major differences in the interactions of neutrons with the matter, increasing the density of concrete for protection against neutrons is more complex and high-density concrete may show a lower efficacy in neutron shielding compared to ordinary concrete [37]. An additional shielding consideration involves the appropriate treatment of shield penetrations. For high-energy radiotherapy machines, doors and large ducts require careful attention and specialized methods of neutron shielding to properly attenuate neutron streaming through shield penetrations (NCRP report #151, 2005).

High-density concrete materials are frequently employed in the construction of radiotherapy bunkers. Photoneutrons are produced via high-energy photon interactions with concrete walls. In the study by Mesbahi et al. [38], the influence of concrete composition on photoneutron doses at the isocenter and maze entrance door of a radiation therapy room was investigated. It was found that application of high-density concretes may result in higher neutron doses in the maze entrance door of radiation therapy bunkers [39]. In the other study by the same research group, a novel barite-colemanite concrete was designed to lower photoneutron production in radiation therapy bunkers. The findings show that the addition of colemanite to the barite concrete will lower the photoneutron fluence rate at the maze entrance door [38].

Neutron scattering properties as well as the photoneutron production probability of high-density concretes including steel-magnetite, ilmenite-ilmenite, barite, and Datolite-Galena were studied [8]. The results show that the scattered neutron fluence strongly depends on the scattering angle and shield composition [40]. Moreover, it was found that photoneutron production in these concrete materials markedly depends on their composition. It was also reported that the application of fillers made of Fe and Pb, increases photoneutron production in high-density concretes walls [41]. In a recent study, the doping effect of different nanoparticles on neutron removal cross section of the ordinary concrete was studied. Neutron energies of 100–3000 keV and several nano- and micro-fillers including PbO_2, Fe_2O_3, WO_3, and H_4B were evaluated using the MCNPX Monte Carlo code. The results indicated that up to 7% higher neutron attenuation by nano-fillers compared to micro-fillers [42].

Some light nanocomposites such as carbon nanotubes and either nano-sized or micro-sized boron carbide (B_4C) incorporated into low-density polyethylene (LDPE) demonstrated enhanced mechanical properties, and an enhanced shielding efficiency for neutrons [43]. Given this result, researchers added hydrogen-rich polyethylene and B_4C to concrete to investigate its neutron capture properties. The resulting concrete samples showed a 15% lower mass density, and a compressible strength of 50% relative to a standard concrete. However, the samples showed a significant increase in neutron shielding for MeV and lower energy neutrons [44]. In a recent study, concretes mixed with 25%, 50%, and 75% ferroboron (as a partial granite aggregate replacement) were studied. This experiment showed that while compressive strength increased with ferroboron (only up to 50% replacement), neutron and gamma transmission decreased with the ferroboron increment [45]. Moreover, some high-temperature-resistant heavy concretes (e.g., chromite and wolframite) provided better neutron absorption capacity than paraffin and conventional concrete [46].

8.6 Advantages and disadvantages of heavy concrete shielding for photon and neutron shielding

The neutron shielding properties of a material depend on the interactions of neutron with the shield. These interactions are determined by the neutron energy and the neutron attenuation properties of the shielding material. Improving the shielding properties of concrete is possible by changing its composition and density [47]. Due to low cost and versatility of concrete compared to steel or lead, concrete can be introduced as an effective shielding material against ionizing radiation. However, when it is used in radiotherapy rooms or nuclear power plant foundations, a large thicknesses of concrete is needed [36]. Iron, lead, barium, and other high atomic number elements have been added to concrete to increase its attenuation properties and hence, decrease the thickness of shield walls. Embedding steel in cement can also be used for reinforcing concrete. Given this consideration, high-density (heavy) concrete, which is composed of heavy weight aggregates, cement, water, and coarse and fine aggregates, is extensively used for the prevention of radiation leakage from radioactive sources as well as construction of radiotherapy bunkers and nuclear reactors.

High atomic number materials such as lead and iron can be used for protection against gamma and X-ray photons. However, by considering all the parameters involved in the selection of an appropriate radiation shield, concrete would be among the best choices. Concrete has appropriate structural properties such as load bearing and strength, and a specific concrete shield with desirable mechanical and radiation properties can be constructed by changing the type of aggregates [48, 49]. This versatility is due to the use of various materials with different densities and neutron attenuating properties. Furthermore, low construction cost, high strength, and ultra-durability are other reasons making the concretes most-used protection materials for nuclear reactors and radiotherapy bunkers.

In the energy ranges of X- and gamma-rays used in modern teletherapy rooms, the Compton Effect is dominant. Therefore, concretes are suitable shields in radiotherapy departments. The radiation attenuation ability of concrete improves by increasing the concrete density due to the increase in the probability of the photon interactions. However, shielding the newly established radiotherapy departments needs a considerable thickness of the ordinary concrete with the density of about 2350 kg/m^3. The shortage of space has always been an important issue, therefore the tendency to use the high-density concretes with densities more than 2350 kg/cm^3 [50] is increasing, to reduce the shield wall thickness [51]. Furthermore, replacing old and inefficient ^{60}Co units with modern accelerators in radiotherapy departments requires an increase in the concrete shield thickness. In such cases, heavyweight concrete can reduce the required shielding space [52]. Over the past decades, several effective high-Z material-based heavy concrete specimens have been produced for radiation protection purposes [51, 53–56]. The engineering and gamma-ray shielding properties of different heavy concrete samples compared to those of ordinary concrete are summarized in Table 8.4.

Table 8.4 Engineering and gamma-ray shielding properties of some heavy concrete samples compared to those of ordinary concrete.

	Physical properties		
Concrete type	**Density (kg/m^3)**	**HVL for ^{60}Co gamma-rays (cm)**	**Compression Strength (kg/cm^2)**
Ordinary concrete	2300–2500	5.25–6.2	300
Barite concrete [57]	3180–3550	3.6–4.0	140–394
Barite concrete [58]	3490	3.8	NI
Barite concrete [59]	NI	4.4	NI
Super heavy concrete [60]	3800–4200	NI	NI
Galena concrete [51]	4200–4600	2.56	500
Datolite-galena (DaGa) concrete [53, 54]	4420–4650	2.56	448–522
Colemanite-galena (CoGa) concrete [53, 54, 61]	4100–4650	2.49	398–464
Ulexite-galena (UlGa) concrete [55]	3640–3900	2.84[a] 2.87[b]	144–377
Tourmalin-galena (ToGa) concrete [56]	4000–4200	2.72[a] 2.77[b]	326–560

[a] Measured HVL.
[b] Calculated by MCNP simulation.
NI, not indicated by the authors.

Neutrons and photons interact with matter through unique and different mechanisms. Although the standard concrete density is 2.35 g/cm^3, density is quite variable in shielding applications. While increasing the density of concrete increases its photon shielding properties, shielding neutrons is more complex. High-density concrete does not demonstrate a better efficacy in neutron shielding compared to ordinary concrete [3]. Density is only changed by adding high atomic number components to concrete, but these materials are not effective in shielding high-energy neutrons. It was previously mentioned that concrete has an additional advantage over other materials for high-energy radiotherapy machines (>10 MV). Therefore, as long as the concrete barrier thickness is adequate to shield against photons, it would be adequate for shielding neutrons. However, with heavy concrete, this may not be universally applicable, and should be verified using detailed neutron shielding methods (e.g., GEANT4, FLUKA, MCNP, and MCNPX).

8.7 Conclusions

Concrete is the most common shielding material in medical facilities utilizing neutron sources. Neutron shielding in these facilities is a complex process that requires detailed knowledge of the physical properties of shield materials, and the fluence rate and energy distribution of the source. Neutron-induced reactions must also be evaluated in the shielding analysis. While concrete is the traditional choice for neutron shielding, appropriate additives with large neutron capture cross sections can improve its shielding performance.

Since the neutron absorption cross section tends to decrease with energy, shielding high-energy neutrons is a complex process. The two key aspects of shielding energetic neutrons are moderating these higher energy neutrons through elastic or inelastic scattering interactions, and then absorbing the reaction products in appropriate shielding materials. Improving the neutron shielding characteristics can be achieved by introducing various micro- and nanomaterials into the proposed shielding matrix. However, their cost, effectiveness, and long-term reliability require further studies. According to the NCRP, for high-energy radiotherapy machines (>10 MV), concrete has an advantage over other shielding materials. Given this consideration, as long as the barrier thickness is adequate to shield against photons, it would also be adequate for shielding neutrons. However, increasing the density of concrete for better protection against photons may show a lower efficacy in neutron shielding compared to ordinary concrete. Therefore, neutron shielding properties of heavy concrete should be verified using detailed neutron shielding methods including the use of the GEANT4, FLUKA, MCNP, and MCNPX transport codes.

References

[1] J.J. Bevelacqua, Health Physics in the 21st Century, John Wiley & Sons, 2008.

[2] J.J. Bevelacqua, Contemporary Health Physics: Problems and Solutions, John Wiley & Sons, 2009.

[3] J.J. Bevelacqua, Basic Health Physics: Problems and Solutions, Wiley Online Library, 1999.

[4] J.J. Bevelacqua, Health Physics: Radiation-Generating Devices, Characteristics, and Hazards, John Wiley & Sons, 2016.

[5] 10CFR20, Standards for Protection Against Radiation, National Archives and Records Administration, US Government printing Office, Washington, DC, 2018.

[6] K. Hagiwara, K. Hikasa, K. Nakamura, M. Tanabashi, M. Aguilar-Benitez, C. Amsler, et al., Review of particle physics: particle data group, Phys. Rev. D: Part., Fields, Gravitation, Cosmol. 66 (1 I) (2002) 100011–10001958.

[7] J.J. Bevelacqua, Basic Health Physics: Problems and Solutions, second ed., Wiley-VCH, Weinheim, 2010.

[8] M.M. Ashraf, A.R. Khan, Shielding Calculations for the Design of Neutron Radiography Facility Around PARR, Pakistan Institute of Nuclear Science and Technology, 1989.

[9] H. Svensson, T. Landberg, Neutron therapy—the historical background, Acta Oncol. 33 (3) (1994) 227–231.

[10] L. Zyga, Neutrons for Cancer Treatment, [cited 15 October 2019]; Available from: https://www.symmetrymagazine.org/article/april-2005/neutrons-for-cancer-treatment, 1976.

[11] IAEA. Report of the IAEA Technical Meeting (F1-TM-44771)- Research Reactor Users' Networks (RRUNs), Advances in Neutron Therapy, International Atomic Energy Agency, Vienna, Austria, 2014.

[12] T.K. Kroc, J.S. Welsh, Neutron Therapy in the 21st Century, arXiv preprint arXiv:14091928, 2014.

[13] NTWC, Neutron therapy centres worldwide, [cited 25 September 2019]; Available from:http://www.neutrontherapy.com/Worldwidecentres.asp, 2019.

[14] T. Rockwell III, Reactor Shielding Design Manual, United States Atomic Energy Commision, Washington, DC, 1956.

[15] K. Shure, J. O'Brien, D. Rothberg, Neutron dose rate attenuation by iron and lead, Nucl. Sci. Eng. 35 (3) (1969) 371–375.

[16] N.M. Schaeffer, Reactor Shielding for Nuclear Engineers, Radiation Research Associates, Inc, Fort Worth, TX, 1973.

[17] R. Jaeger, E. Blizard, A. Chilton, M. Grotenhuis, A. Hoenig, T.A. Jaeger, et al., Engineering Compendium on Radiation Shielding Volume I: Shielding Fundamentals and Methods, 1968.

[18] A. Upton, National Council on radiation protection and measurements scientific committee 1–6. The state of the art in the 1990s: NCRP report no. 136 on the scientific bases for linearity in the dose-response relationship for ionizing radiation, Health Phys. 85 (1) (2003) 15–22.

[19] Particle Data Group, Review of particle physics, Phys. Rev. D1 Part A 98 (3) (2018) 1–880.

[20] Units ICoR, Measurements. An International Neutron Dosimetry Intercomparison: Basic Aspects of High Energy Particle Interactions and Radiation Dosimetry; Dose Specification for Reporting External Beam Therapy with Photons and Electrons; Quantitative Concepts and Dosimetry in Radiobiology; Average Energy Required to Produce an Ion Pair; Methods of Assessment of Absorbed Dose in Clinical Use of Radionuclides, International commission on radiation units and measurements, 1978.

[21] O. Wallace, Analytic Flux Formulas and Tables of Shielding Functions, Bettis Atomic Power Lab, West Mifflin, PA, 1981.

[22] FLUKA, The Official FLUKA Site, http://www.fluka.org/fluka.php, 2019. (Accessed 25 September 2019).

[23] MCNPX, MCNPX, https://rsicc.ornl.gov/codes/ccc/ccc8/ccc-810.html, 2019. (Accessed 26 September 2019).

[24] MCNP, MCNP, https://rsicc.ornl.gov/codes/ccc/ccc8/ccc-810.html, 2019. (Accessed 26 September 2019).

[25] J.K. Shultis, R.E. Faw, Radiation Shielding, Prentice Hall, Upper Saddle River, NJ, 1996, ISBM 0-13-125691-2.

[26] ICRP, Publication116, Conversion Coefficients for Radiological Protection Quantities for External Radiation Exposures, Elsevier, Amsterdam, 2010.

[27] J. Kim, Y.R. Uhm, B.C. Lee, M. Lee, C.K. Rhee, Investigation of particle size-dependent neutron shielding efficiency, Korea 2008 (9) (2008) 16.

[28] A. Mesbahi, H. Ghiasi, Shielding properties of the ordinary concrete loaded with micro-and nano-particles against neutron and gamma radiations, Appl. Radiat. Isot. 136 (2018) 27–31.

[29] J. Park, H. Suh, S.M. Woo, K. Jeong, S. Seok, S. Bae, Assessment of neutron shielding performance of nano-TiO_2-incorporated cement paste by Monte Carlo simulation, Prog. Nucl. Energy 117 (2019) 103043.

[30] J. Kim, B.-C. Lee, Y.R. Uhm, W.H. Miller, Enhancement of thermal neutron attenuation of nano-B4C,-BN dispersed neutron shielding polymer nanocomposites, J. Nucl. Mater. 453 (1–3) (2014) 48–53.

[31] S.M.J. Mortazavi, M. Kardan, N. Sharafi, H. Baharvand, S. Sina, Design and fabrication of high density borated polyethylene nanocomposites as an efficient radiation shield for protecting astronauts, Int. J. Radiat. Res. 14 (4) (2016) 380–383.

[32] P. Song, X. Tu, L. Bai, G. Sun, Q. Tian, J. Gong, et al., Contrast variation small angle neutron scattering investigation of micro-and nano-sized TATB, Materials 12 (16) (2019) 2606.

[33] L. Chkhartishvili, Boron-Containing Nanostructured Materials for Neutron-Shields. Nanostructured Materials for the Detection of CBRN, Springer, 2018, pp. 133–154.

[34] D. Sarıyer, R. Küçer, N. Küçer, Neutron shielding properties of concrete and ferro-boron, Acta Phys. Pol. A 128 (2B) (2015).

[35] N. Jooyan, B. Goliaei, B. Bigdeli, R. Faraji-Dana, A. Zamani, M. Entezami, et al., Direct and indirect effects of exposure to 900MHz GSM radiofrequency electromagnetic fields on CHO cell line: evidence of bystander effect by non-ionizing radiation, Environ. Res. 174 (2019) 176–187.

[36] C. Thomas, J. Rico, P. Tamayo, J. Setién, F. Ballester, J.A. Polanco, Neutron shielding concrete incorporating B4C and PVA fibers exposed to high temperatures, J. Build. Eng. 26 (2019) 100859. 2019/11/01.

[37] T. Piotrowski, D.B. Tefelski, M. Mazgaj, J. Skubalski, A. Żak, J.J. Sokołowska (Eds.), Polymers in Concrete–The Shielding Against Neutron Radiation, Trans Tech Publ, 2015. Advanced Materials Research.

[38] A. Mesbahi, G. Alizadeh, G. Seyed-Oskoee, A.-A. Azarpeyvand, A new barite–colemanite concrete with lower neutron production in radiation therapy bunkers, Ann. Nucl. Energy 51 (2013) 107–111.

[39] A. Mesbahi, A.A. Azarpeyvand, H.R. Khosravi, Does concrete composition affect photoneutron production inside radiation therapy bunkers? Jpn. J. Radiol. 30 (2) (2012) 162–166.

[40] A. Mesbahi, R. Khaldari, Neutron and photon scattering properties of high density concretes used in radiation therapy facilities: a Monte Carlo study, Pol. J. Med. Phy. Eng. 23 (3) (2017) 61–65.

[41] A. Mesbahi, A.A. Azarpeyvand, A. Shirazi, Photoneutron production and backscattering in high density concretes used for radiation therapy shielding, Ann. Nucl. Energy 38 (12) (2011) 2752–2756.

[42] A. Mesbahi, H. Ghiasi, Shielding properties of the ordinary concrete loaded with micro- and nano-particles against neutron and gamma radiations, Appl. Radiat. Isot. 136 (2018) 27–31.

[43] F. Jamali, S. Mortazavi, M. Kardan, M. Mosleh-Shirazi, S. Sina, J. Rahpeyma, Developing light nano-composites with improved mechanical properties for neutron shielding, Kerntechnik 82 (6) (2017) 648–652.

[44] D. DiJulio, C.P. Cooper-Jensen, H. Perrey, K. Fissum, E. Rofors, J. Scherzinger, et al., A polyethylene-B4C based concrete for enhanced neutron shielding at neutron research facilities, Nucl. Instrum. Methods Phys. Res., Sect. A 859 (2017) 41–46.

[45] M.K.A. Roslan, M. Ismail, A.B.H. Kueh, M.R.M. Zin, High-density concrete: exploring Ferro boron effects in neutron and gamma radiation shielding, Constr. Build. Mater. 215 (2019) 718–725. 2019/08/10.

[46] B. Aygün, Neutron and gamma radiation shielding properties of high-temperature-resistant heavy concretes including chromite and wolframite, J. Radiat. Res. Appl. Sci. (2019) 1–8.

[47] D. Sariyer, R. Küçer, Development of neutron shielding concrete containing iron content materials, AIP Conf. Proc. 1935 (1) (2018) 100003.

[48] A.B. Chilton, J.K. Shultis, R.E. Faw, Principles of Radiation Shielding, Prentice-Hall, 1984.

[49] X. Wang, R. Faw, Transmission of neutrons and secondary gamma rays through concrete slabs, Radiat. Prot. Dosim. 60 (3) (1995) 213–222.

[50] J.F. Ahearne, Rapporteur's summary of presentations at the 2005 NCRP annual meeting, Health Phys. 91 (5) (2006) 531–536, https://doi.org/10.1097/01.HP.0000232851.45120.06.

[51] S. Mortazavi, M. Mosleh-Shirazi, M. Maheri, H. Yousefnia, S. Zolghadri, A. Hajipour, Production of an economic high-density concrete for shielding megavoltage radiotherapy rooms and nuclear reactors, Iran. J. Radiat. Res. 5 (3) (2007) 143–146.

[52] A. Facure, A.X. Silva, The use of high-density concretes in radiotherapy treatment room design, Appl. Radiat. Isot. 65 (9) (2007) 1023–1028.

[53] S. Mortazavi, M. Mosleh-Shirazi, M. Baradaran-Ghahfarokhi, Z. Siavashpour, A. Farshadi, M. Ghafoori, et al., Production of a datolite-based heavy concrete for shielding nuclear reactors and megavoltage radiotherapy rooms, Iran. J. Radiat. Res. 8 (1) (2010) 11–15.

[54] S. Mortazavi, M. Mosleh-Shirazi, P. Roshan-Shomal, N. Raadpey, M. Baradaran-Ghahfarokhi, High-performance heavy concrete as a multi-purpose shield, Radiat. Prot. Dosim. (2010) ncq265.

[55] S. Aghamiri, S. Mortazavi, Z. Razi, M. Mosleh-Shirazi, M. Baradaran-Ghahfarokhi, F. Rahmani, et al., Ulexite–galena intermediate-weight concrete as a novel design for overcoming space and weight limitations in the construction of efficient shields against neutrons and photons, Radiat. Prot. Dosim. 154 (3) (2013) 375–380.

[56] S. Aghamiri, S. Mortazavi, M. Shirazi, M. Baradaran-Ghahfarokhi, F. Rahmani, A. Amiri, et al., Production of a novel high strength heavy concrete using tourmaline and galena for neutron and photon radiation shielding, Int. J. Radiat. Res. 12 (3) (2014) 277–282.

[57] F. Bouzarjomehri, T. Bayat, R. Dashti, J. Ghisari, N. Abdoli, 60Co γ-ray attenuation coefficient of barite concrete, Iran. J. Radiat. Res. 4 (2) (2006) 71–75.
[58] A. Abdo, W. Kansouh, R. Megahid, Investigation of radiation attenuation properties for baryte concrete, Jpn. J. Appl. Phys. 41 (2002) 7512.
[59] I. Akkurt, C. Basyigit, S. Kilincarslan, B. Mavi, A. Akkurt, Radiation shielding of concretes containing different aggregates, Cem. Concr. Compos. 28 (2) (2006) 153–157.
[60] A. Proshin, V. Demyanova, D. Kalashnikov, Superheavy high-strength concrete on the base of secondary stuff, Asian J. Civil Eng. 6 (2005) 67–73.
[61] S. Mortazavi, M. Mosleh-Shirazi, P. Roshan-Shomal, N. Raadpey, M. Baradaran-Ghahfarokhi, High-performance heavy concrete as a multi-purpose shield, Radiat. Prot. Dosim. 142 (2–4) (2010) 120–124.

CHAPTER 9

Advancements in shielding materials for spent fuel storage

P. Tamayo[a], **C. Thomas**[a], **J. Rico**[b], **J. Setién**[a], **A. Cimentada**[a], **J.A. Polanco**[a], **J. Alonso**[b]

[a]LADICIM (Laboratory of Materials Science and Engineering), University of Cantabria. E.T.S. de Ingenieros de Caminos, Canales y Puertos, Santander, Spain

[b]Construction Engineering, Research and Project Development (INGECID S.L.), University of Cantabria. E.T.S. de Ingenieros de Caminos, Canales y Puertos, Santander, Spain

9.1 Introduction

The growing development of the nuclear technology in all its aspects (energy generation, industrial applications, medicine, or in the military industry) generates the need for the treatment of the generated waste. Nuclear waste, some of which has a half-life of thousands of years, poses a risk to human health and therefore both transport and storage must be carried out under adequate safety conditions. These safety conditions involve the use of materials that isolate spent fuel from the environment. The nature of these materials is very diverse, and their use prevents the interaction of the incident radiation with the environment. The materials used in the manufacture of spent fuel containers must satisfy the need to obtain a durable product, whose biggest issue is corrosion, the aggressive conditions of the environment and the physical-mechanical effects induced by the spent fuel. That is why the selection of materials involves an optimization process in which numerous variables are considered. Nuclear waste is classified according to its activity in three general levels according to the International Atomic Energy Agency (IAEA) [1]: low-level waste (LLW), intermediate-level waste (ILW), and high-level waste (HLW). LLW has a high concentration of short-lived radionuclides and a limited concentration of long-lived radionuclides that can generate the need for hundreds of years of containment. Contact dose rates below 2 mSv/h characterize these wastes. ILW has a long-lived radionuclide content (alpha emitting), which requires a higher level of containment and may require heat dissipation systems. This waste may need to be stored at great depths of the order of 100 m. HLW has high activity concentrations and many long-lived radionuclides,

https://doi.org/10.1016/B978-0-12-819459-1.00009-X
© 2020 Elsevier Ltd.
All rights reserved.

which emit a large amount of heat and make disposal and transport containment with high insulating capacity necessary. This chapter describes the materials that are currently used in containment media for the isolation of spent fuel, which are used in nuclear reactors and are considered HLW, whose activity concentration is typically 10^4–10^6 TBq/m^3 [1]. These containment elements are manufactured with design criteria aimed at heat dissipation and the attenuation of radioactive decay products, the characteristics of the shielding material playing an important role in addition to the energy spectrum of the source term. Elements of spent fuel containers such as baskets, canisters, or casks require materials of different natures that are capable of attenuating all types of ionizing radiation. Metal alloys are used as a structural base, due to their behavior against corrosion mechanisms and their ability to attenuate gamma radiation. Polymers such as paraffin, rubbers, or epoxy compounds are used as a fast neutron-scattering material, while composites based on the use of boron, cadmium, or rare-earth elements are used because of their high neutron absorption cross section. However, not only the appearance of new compounds, but also the emergence of new design strategies contribute to the latest advances in radiation shielding. The use of various specialized materials in the shielding of a specific energy spectrum requires researchers to carry out an optimization process that is supported by simulation software.

9.2 Factors that influence the material choice for spent fuel storage

The materials used in the manufacture of spent fuel containers must perform well in the presence of external agents, mechanical loads, and under the effects produced by the spent fuel during the intended target operation lifetimes. The structural behavior of cask- or canister-based containers is evaluated by impact and drop tests (of different types) to ensure their structural integrity both in transport and during their service in storage or disposal circumstances, for which both the design and the selection of materials must be adapted. Dry cask storage is based on containers that are placed on land and temporarily store spent fuel coming from the pools. The numbers of this type of container increased in the United States from 690 to 1300 between 2005 and 2010 [2] and will continue to do so as the reactor pools continue to fill. While expensive, the cost of dry cask storage is a fraction of the cost to build an additional used fuel pool or develop additional fuel reprocessing infrastructure [3]. In this case the exposure environment is the atmosphere and the soil, so the most aggressive agents to be confronted are air humidity, high temperatures, or salts in the air. In the case of reinforced concrete, an especially aggressive environment (e.g., the presence of carbonates in the groundwater or chlorides in the air) can reduce the pH of the concrete below 5.5, depassivating the reinforcement and reducing protection against corrosion. In the repositories the concentration of chlorine ions is determined by the composition of the rock formations. Soils with high chloride ion contents can corrode the reinforcing bars after penetrating the concrete and can react with the tricalcium aluminate of the cement to form Friedel salts [4]. Exposure to sulfate-rich soils can cause a reduction in durability. Typical reactions occur between calcium hydroxide present in cement and sulfate ions to form gypsum and the reaction between calcium aluminate and sulfate ions to form ettringite. Another reaction is the formation of thaumasite, a deterioration product formed from sulfate and carbonate ions (from limestone and atmospheric carbonation) at low temperature (5°C) [5]. To minimize these effects, the use of sulfate-resistant cements is recommended, as they have a low content of tricalcium aluminate (C3A). In repositories, the content of sulfides in the groundwater can corrode materials such as steel, copper, or nickel alloys [6] and sulfates can lead to sulfide formation. Another phenomenon to take into account, in environments with high relative humidity, where temperatures can reach negative values, is the effect produced by freezing-thawing cycles. The stress and strain caused by these cycles due to the pressure produced by the water in the pores can compromise the integrity of the material, especially near the surface of the concrete [7], which obliges the design of concrete with reduced porosity.

In dry cask storage, metal confinement elements are in contact with air through ventilation pipes. This air can be loaded with moisture or salts, which is deposited on stainless steel (or another metal) and is not washed away by rain because the structure is covered by an overpack [8]. This deposited salt can induce stress corrosion cracking (SCC) in the presence of humidity and high temperatures. Air humidity can cause corrosion, pitting corrosion (depends on the size of the cathodic area and creates cavities), or cracking corrosion (formed between the surface of a metal and another surface). Corrosion depends on the materials as well as on the environment. There are materials that allow corrosion under oxidizing conditions, such as carbon steel, cast irons, or low-alloy steels. In this case, the behavior against corrosion is predictable (uniform). In the case of carbon steel, its corrosion can have a negative or positive impact on other materials, generating H_2 and suppressing the alteration of spent fuel [9].

Corrosion-resistant materials such as stainless steels, nickel, or titanium alloys are characterized by having a layer that protects against oxidation. These materials are susceptible to punctual or localized corrosion (e.g., crevice corrosion), which are difficult to predict [10]. In repositories, microbially influenced corrosion (MIC) may develop in the long term. This is generally associated with corrosion under a biofilm (microorganisms adhered to a surface) by the action of bacteria that produce corrosive elements. Materials such as copper or carbon steel are susceptible to MIC, while stainless steel, Ti alloys, and alloy 22 (Ni-Cr-Mo-W) are more resistant to this type of corrosion [11].

In disposal containers, the water table is a key variable in the corrosion of materials. Most repositories are located below the level of the water table [9], which makes them cooler and can better dissipate the heat produced by the spent fuel in the canister. The temperature rise caused by the decay of radionuclides in materials containing spent fuel (canister temperature can reach 200°C) may limit the use of certain materials such as some polymers whose melting temperature is somewhat higher than 100°C. High temperatures reduce H due to the evaporation of water from concrete and other hydrogenous neutron-shielding materials [8]. Temperature can also affect the concrete used as a coating. Several studies show a loss of the mechanical properties of concrete above 300°C for conventional limestone concretes [12], and the improvement of this response with the use of iron-based aggregates such as magnetite [13].

One of the determining factors in the selection of materials is the behavior under ionizing radiation. Metals and metal alloys have the ability to reduce the intensity of electromagnetic radiation by half (half-value layer) with little thickness due to their high density. On the other hand, H-rich compounds are required to moderate fast neutrons and compounds with a high absorption cross section to capture thermalized neutrons. For the former, polymeric compounds are generally used for dry storage containers, or water for wet storage systems. In recent years, new H-rich compounds have been developed, such as epoxy compounds, or new polymers such as ultrahigh-molecular-weight polyethylene (UHMWP). Materials based on the use of boron, cadmium, or rare earth in concrete, in alloys, or in other compounds are used as dopants in the form of fillers or powders. In containers for spent fuel, the IAEA [1] defines safety distances during transport. The material selected should reduce the dose rate below 2 mSv/h to the accessible surface and below 0.1 mSv/h at a distance of 2 m from the conveyance, while in a storage place these limits vary depending on the country.

The container must be able to reduce the doses to very low values using these materials and appropriate thicknesses.

9.3 Types of containers for spent fuel storage

Depending on the purpose of the containers, they can be classified as single/dual or multipurpose systems. Single-purpose systems are only licensed to store or transport spent fuel, while dual-purpose systems allow transport and storage functions. Multipurpose systems can perform transport, storage, and disposal functions, although their use is not expected to be licensed in the near future [14]. Dual-purpose systems have the advantage of reducing the number of fuel handling operations compared to single-purpose systems (no fuel transfer between transport and storage operations) [15] in addition to facilitating transport to the reprocessing plant for spent fuel. The main disadvantages of these dual-purpose systems are the higher cost (the need to incorporate neutron-absorbing materials and additional hardware), the complexity of the designs, and the longer license time since they require separate licenses for storage and transport operations [16].

Depending on the typology, there are dry and wet storage systems. There is an increase in the global demand for dry cask storage facilities due to the global increase in nuclear waste production and due to a lack of progress in the implementation of facilities for the disposal of such waste. Another reason is the filling of the pools (wet storage) in nuclear facilities. Dry storage containers (casks) can be vertical or horizontal, although the former are usually more common. The vertical ones are stand-alone structures that have their own shielding, while the horizontal ones are not so heavily shielded and should be placed in steel-lined concrete bunkers in order to be safe [2].

According to the technology of the container used, spent fuel containers may be cask-based systems or canister-based systems. Both must meet the requirements of heat removal, radiation shielding, high integrity, and criticality control (using neutron absorber materials). Cask-based systems are based on the use of a single container (a metal cask generally), which fulfills the safety conditions required for transport and storage operations. These systems have the disadvantage that multipurpose cask-based containers are designed to meet the requirements of a particular environment for disposal (the disposal place must be known before design), while canister-based systems are more flexible, due to the possibility of coupling different overpacks according to need. Some current examples that incorporate this system are those developed by the GNS group (CASTOR, CONSTOR systems).

CASTOR casks are designed as transport and storage systems. The cask is cast iron and can incorporate polyethylene to improve neutron attenuation. Inside, the casks are made of nickel-plated compounds and coated with polyester resin. The basket is manufactured with borated stainless steel. The covers are made of stainless steel coated with carbon steel. During transport the covers are protected by a steel plate that protects the system from shocks. The CONSTOR system consists of a cask designed for transport and storage of the spent fuel. Its inner layer is made of stainless steel while its outer layer of steel and iron-based high-density concrete (CONSTORIT). The baskets are made of stainless steel and borated aluminum, while there is a hollow layer with helium sealed with stainless steel. The Transnucléaire company has also developed cask-based systems. One of the most in-demand cask-based systems is the TN24, which has dual purpose systems. It is constructed of forged steel and covered with borated resin, both layers integrate the radiation shielding structure. Copper plates are embedded in the resin and this is enclosed within an external steel envelope. The cask is protected during transport in both covers by stainless steel impact absorbers. During transport and storage, two concentric seals cover the cask. In storage, these seals are metallic and are filled with helium.

In canister-based systems the fuel is placed in a sealed cylinder filled with an inert gas (canister), covered with different overpacks (with different safety levels), which can be metal or concrete and serve as radiation shielding and as mechanical protection. These overpacks are different for each of the operations: transport, storage, and disposal. Some current examples of these systems are those produced by Holtec International (HI-STORM, HI-STAR systems). These systems incorporate Al/B_4C compounds such as neutron-absorbing materials attached to the fuel basket. HI-STORM overpacks use concrete and steel as shielding material and its arrangement is vertical, to improve natural convection. HI-STAR cask is composed of a multilayer compound that uses carbon steel together with Holtite-A (which is a polymeric neutron material attenuator) and B_4C as a neutron absorber. NAC International Universal employs dual-purpose transportable-storage canisters (TSC) using stainless steel and fuel basket canisters that incorporate Al/B_4C (Boral) compounds as neutron absorber material. This system is placed vertically for storage and uses a steel-concrete structure as overpack. A multilayer steel/lead/steel overpack (VCC) is used for transport, which incorporates a NS-4-FR composite (a borated epoxy resin) as the neutron shield. The Energy Solutions systems use cylindrical stainless steel canisters (W21M) with top and bottom covers made of carbon steel, stainless steel, and depleted uranium. The canister uses Boral compounds as neutron-shielding material. Storage is done with a vertical reinforced concrete overpack while the transport overpack consists of a multilayer steel/lead/steel composite.

9.4 Types of materials for spent fuel containers

Different types of materials are necessary for each of the parts that make up a spent fuel container. Parts such as storage cask, cask lid, canister, and fuel baskets are usually metallic as they are designed as effective barriers to corrosion and impacts. Other parts such as cask overpacks are usually made of concrete, while polymeric compounds and materials with high neutron absorption cross sections are usually included in neutron-shielding layers.

9.4.1 Metal alloys

9.4.1.1 Carbon steels

Carbon steel is one of the materials that "allow corrosion" so that its corrosion rate can be predicted. It is not very resistant to corrosion but its effects tend to cause less severe damage than stainless steel. The material has high weldability, ductility, manufacturing experience, high resistance to hydrogen-induced cracking (HIC), and good mechanical performance [9]. These steels are commonly used in the storage of ILW and, if their use is intended, for HLW. They are intended for saturated repositories without presence or with a low presence of O_2. The main corrosion mechanism is usually general corrosion and use is often combined with concrete due to the protection of this material, which is also responsible for reducing microbial activity and thus the MIC. One reason to select carbon steels is to avoid the risk of cracking due to adsorbed hydrogen generated by anaerobic corrosion [17]. One of the main advantages of this material is that it is not expensive and a great disadvantage is its impact on other barrier materials (e.g., bentonite) due to the production of Fe (II) and H_2 under certain anaerobic conditions.

9.4.1.2 Stainless steels

Stainless steels have good mechanical properties and are resistant to corrosion in general, but the corrosion produced by SCC and intergranular corrosion can cause severe damage [18] so their use is not specified for the manufacture of canisters for HLW (unless the concentrations of Cl^- are extremely low). The presence in disposal environments with Cl^- combined with the high temperatures generated by the spent fuel mean this material is too susceptible to SCC. Its use in ILW is contemplated in type 304 L or 306 L alloys commonly. The corrosion in ILW of this material depends on the alkalinity of the environment, usually cementitious material or concrete [9], since its response to localized corrosion or to SCC will depend on this cementitious backfill.

9.4.1.3 Copper

Copper is a material with very good durability, which can be used for the manufacture of the canister, can be found naturally in repositories [18], and can provide very long disposal times (>100,000 years) in very well-sealed deep repositories remaining below the water table [9]. Its use as an alloy is also possible, some of the most common are 70–30 Cu-Ni, UNS 71500, and an Al bronze, UNS 61300. Among its disadvantages is its thermodynamic instability in repositories under aerobic conditions, but it is stable in environments without O_2. This means that as the O_2 of the repository is consumed, the corrosion of copper ceases. The behavior under general corrosion is excellent and its use is justified in saline environments, where Cl ions promote the active dissolution of Cu, which prevents localized corrosion and SCC [19]. Its use is not recommended in repositories with a high presence of HS^- in the groundwater. Radiation induces enhanced corrosion of copper compared to nonirradiated samples, forming cuprite and the effects of radiolysis on corrosion appear to be smaller compared to other corrosion processes [20].

9.4.1.4 Titanium alloys

Titanium alloys provide very good mechanical joints, good corrosion resistance, and can be used as a containment material for very long periods of time. Their use in containers is frequent in the form of α Ti alloys or near-α Ti alloys (e.g., Ti Grade 7) [9] although they have also been used pure. Pure titanium is susceptible to crevice corrosion in Cl^- solutions. The corrosion of titanium alloys seems to be independent of the temperature and composition of the saline solution, and under repository conditions, the performance is excellent in preventing SCC and crevice corrosion. Moreover, gamma radiation does not seem to influence the corrosion processes of the material as is the case with water radiolysis [21]. Likewise, titanium alloys are immune to MIC due to the stability of the TiO_2 passive film [22]. However, the absorption of hydrogen (e.g., produced in general corrosion or when used with active metals) can cause the fragility of the material [18].

9.4.1.5 Nickel alloys

Nickel alloys have excellent resistance to corrosion that can be compared to that of titanium alloys, with the advantage of being more easy to weld and the disadvantage that they can be more expensive [18]. These alloys may allow material containment for very long periods. Some alloys used in containers include alloy 625, C-4, or C-22. C-22 is one of the most crevice corrosion-resistant alloys of all those used to manufacture canisters [9]. Nickel alloys have a wide range of elements (almost always using Cr and Mo) and can also offer a wide range of mechanical characteristics and corrosion resistance, so their use can be adapted to the needs of each repository. Their corrosion resistance is generally good in both aerobic and anaerobic environments. Compared to stainless steels, nickel alloys are less susceptible to SCC in environments with Cl^- [23] and also cause minimal impact on other containment materials [9]. Regarding the radiation condition, these alloys are affected by high doses of gamma radiation [6].

9.4.1.6 Ceramics

Ceramic materials have the advantage of not generating H_2 during the corrosion process. Some of these materials, such as silicon carbide or graphite, have high resistance to corrosion while being abundant [18]. Some of the disadvantages of this material consist in having a greater tendency to fracture and being unable to withstand the loads to which the canister is subjected in repository conditions [24]. The idea of using this material began in the 1980s and although there have been studies on its feasibility in the manufacture of canisters, there are still problems associated with its structural behavior.

9.4.1.7 Concretes

Concrete is a very cheap, easy-to-place, and durable material, used in container casks or in overpacks. Concrete has been manufactured incorporating natural high-density aggregates such as magnetite, goethite, hematite, barite, ilmenite, or limonite [25–28] given that density must be maximized to obtain lower half-value layers (HVLs) to attenuate gamma radiation. Sometimes various iron-nature materials such as iron punchings [29] or metal fibers are added to the mixture to increase density. Very-high-density concrete has also been obtained using depleted uranium dioxide (UO_2) as an aggregate [30], producing concrete which is twice as dense as the traditional one and with a large percentage of O_2 incorporated, increasing the neutron absorption cross section. The cost of manufacturing containers with high-density concrete is less than those using metals such as steel or lead, although it has the disadvantage of needing a larger volume of material to be equally effective.

To improve the scattering cross section of the concrete, polymeric fibers can be included or the effective water-cement ratio can be increased. The addition of the most common fibers such as polyethylene ($(C_2H_4)_n$), polypropylene ($(C_3H_6)_n$), or polyvinyl alcohol ($(C_2H_4O)_n$) provides more H. $(C_2H_4O)_n$ has the highest density and melting point (200°C), so its use is more appropriate when high temperatures are generated by spent fuel. Likewise, temperatures close to 200°C coincide with the temperatures of spalling in the concrete, so the cavities generated by the fusion of the fibers mean that they allow a better evacuation of the steam generated by heat, reducing the risk of cracking [31]. The use of natural aggregates rich in boron and hydrogen, such as colemanite ($CaB_3O_4(OH)_3 \cdot H_2O$), borocalcite, or ferroboron improves the moderating and thermalizing capacity of concrete.

The other factor that has a significant impact on the neutron radiation shielding of concrete is the combined water. The main source of H in concrete is water. Free or interstitial (unbound) water evaporates at temperatures close to 100°C while at temperatures between 180°C and 300°C the combined water in the calcium-silicate-hydrate gel (CSH) is lost [32] and thus most of the H stored in concrete. The amount of concrete hydration water depends on the amount and type of the cement. For Portland cements, the majority of hydration products obtained are as follows [33]:

$3CaO \cdot 2SiO_2 \cdot 3H_2O$: Hydrated calcium silicate (50%–60%).

$Ca(OH)_2$: Calcium hydroxide (20%–25%).

$3CaO \cdot Al2O_3 \cdot CaSO_4 \cdot 12H_2O$: Calcium sulfoaluminate (15%–20%).

Considering the molecular weight of each of the abovementioned compounds, the percentage weight of the elements that are part of the cement hydration is obtained. From this relationship, the amount of water combined with the cement can be extracted, after applying two correction factors: one that considers the amount of gypsum present in the cement to improve the setting of the mixture ($f_1 = 0.97$) and another factor that considers the minimum clinker content of a Portland CEM I ($f_2 = 0.95$) according to the standard EN 197-1: 2011 [34]. The average value of the water-cement ratio obtained is close to 20%.

The behavior of concrete under radiation by neutrons is good, although there are mechanisms that can alter the material. These cause mechanical losses due to the swelling derived from the neutron radiation-induced volumetric expansion (RIVE) [35] and thermal or gamma radiation-induced damage [36]. In any case, doses below 10^{19} n/cm^2 do not seem to affect the integrity of the concrete [37], a priori limits unattainable in spent fuel containers.

9.4.2 Polymer composites for neutron attenuation

H is the material that best thermalizes fast neutrons. Having only one proton in the nucleus, it has the same mass as the neutron, so the successive inelastic collisions between them result in the successive loss of neutron energy. Polymers are lightweight materials with a high H content, whose production cost is low and also provide some structural integrity. In neutron radiation shielding, the use of polymers usually consists of a matrix, in which various nano- or micromaterials that have a high effective cross section (are effective absorbing thermal neutrons) are dispersed. Polymers offer a number of advantages, such as geometric conformability and lightness [38]. As a main disadvantage, polymers usually have a higher thermal expansion coefficient and lower melting temperatures than metals and concretes, so exposure to high levels of radiation can degrade their structures.

9.4.2.1 High-density polyethylene

High-density polyethylene (HDPE) is one of the most used polymers in radiation shielding as a fast neutron thermalizer due to its high H content, good mechanical performance, and good corrosion resistance. Its most common use is as a matrix for neutron absorption powders. In many cases its use is accompanied by the presence of boron nitride (BN) additions, although it can accept a limited amount of filler before losing its mechanical properties. Under high-energy neutrons, HDPE shows the same shielding properties as Al and HDPE-BN compounds [39].

The latest trends with this material are aimed at obtaining multilayer compounds in order to optimize the shielding ability of the material. Compounds have been proposed that incorporate successive layers of HDPE/(HDPE/BN) and (HDPE/BN)/(HDPE/$BaSO_4$), obtained by coextrusion, verifying that the neutron transmittance is reduced with the increase in layers ostensibly up to 32 layers [40]. Increasing the number of layers also decreases the cross-link effect in HDPE due to secondary radiation [41].

9.4.2.2 Ultrahigh-molecular-weight polyethylene

Recently, the use of ultrahigh-molecular-weight polyethylene (UHMWPE) with characteristics similar to HDPE has been proposed, adding some advantages: it is extremely tough, has a higher impact strength, and is more resistant to concentrated acids and alkalis. Its capacity as a neutron thermalizer has been proven in various studies as a matrix of thermal neutron absorbers, generally generated by extrusion or by press molding methods [42, 43].

9.4.2.3 Rubbers (EPDM and silicon)

The most common materials based on polymer and epoxy composites cannot be used when, for example, the instruments or detectors of a measuring device have an abnormal shape or arrangement that requires curved surfaces or narrow spaces. Rubbers have the ability to adapt to irregular surfaces while retaining the neutron-shielding properties of other more rigid materials [44].

The EDPM is the most commonly used and economical rubber on the market. It is the designated term for a polymer chain that incorporates ethylene, propylene, and diene [45]. Due to its high H content, it is an excellent candidate for neutron-shielding applications although it is also used for radioactive waste embedding and shows high gamma radiation stability [46]. In addition, this material is compatible with boric acid, obtaining stable compounds offering good neutron-shielding properties [47]. This material undergoes pyrolysis in the range of 250–500°C so it can withstand relatively high working temperatures. One of the things that characterizes EPDM and rubbers in general is that the incorporation of neutron-absorbing additions reduces the elongation of the specimen due to the discontinuity of the composite [48]. The great drawback of these compounds is their behavior against fire, since they do not have flame-retardant properties, although there are already rubbers based on methyl vinyl silicone compounds that improve this issue [44]. Silicon rubbers have good electrical, heat, and chemical agent resistance making them excellent materials for neutron shielding.

9.4.2.4 Epoxy compounds

Epoxy resins are a type of thermosetting polymer, which are easier to manufacture than thermoplastic polymers such as polyethylene, have good dimensional stability and excellent adhesion to other materials, high heat resistance, resistance to chemical agents, and good mechanical performance [49]. Epoxies are electrically insulating materials providing good adhesion to any surface even in humid conditions. They are good thermal insulators and their properties can be modified according to the needs through the use of fillers, reducing the thermal stresses that are caused by the differences in thermal expansion coefficients [50]. The use of these resins is generally intended to encapsulate electrical components that are located near radiation sources

[51] and are more effective at attenuating rapid neutrons than polyesters, due to their higher H content. Their durability for gamma radiation and neutrons is excellent compared to polyethylene or concrete [52].

9.4.2.5 Polyamide

Polyamide, unlike other thermoplastic polymers (e.g., polyethylene), has high stability at high temperatures, in addition to good mechanical properties and good resistance to radiation [53], which makes it a good candidate for spent fuel storage materials. Continuous carbon fiber-reinforced polyimide composites have been developed in recent decades, offering resistant materials with high elastic moduli that behave excellently under high temperature conditions and also resist corrosion [54].

9.4.3 Composites for neutron absorption

There is a clear trend toward the use of powders (fillers) both with alloys, as in polymer matrix and in concrete for the improvement in the absorption cross sections of the materials used in spent fuel containers. Each material is capable of absorbing thermal neutrons of a given energy range, so the source's energy spectrum must be known before selecting an optimal absorber material. ^{10}B, which has an absorption cross section of 755 barns, is the main (almost unique) element used for this purpose, in any of its most common forms (B_4C, B_2O_3, and BN), providing thermal stability and good mechanical properties. Some of the current commercial compounds based on boron carbide use an Al matrix (e.g., Metamic, BORTEC, BORAL, BorAluminum), others employ a stainless steel matrix (e.g., NeutroSorb, Neutronit). Regarding the use of polymer matrices, there are also some examples in the container industry (e.g., BISCO NS-1, Boro-Silicon, Bocarsil) or phenolic resin-based compounds (BISCO NS-4-FR, Holtite-A). Borated concrete is also found in the market (e.g., BISCO NS-3). Another potential material as a neutron absorber is ^{113}Cd, with an absorption cross section of 2450 barns, whose use is not widespread because it is a toxic element. The use of rare earth elements implies the use of the best known neutron absorbers. Thus, there are successful studies on the use of Gd (200,000 barns) or Sm (46,000 barns) in the form of oxides incorporated into container elements. The detailed analysis of all these fillers is reported in Chapter 2.

9.5 Multilayer strategies

Currently, the selection of materials plays an equally important role as the design of a container. The containers currently arranged in the storage facilities are constituted by a set of elements that guarantee the safe storage of spent fuel and whose composition and structure is designed to attenuate both gamma and neutron radiation. Some examples of this strategy have been discussed in the previous section, namely a polymer-based matrix (HDPE, rubbers, epoxy, or polyamide) doped with fillers with a high absorption cross section (B_4C, BN, hBN, B_2O_3, or others) in alternating layers with different alloys or compounds. Since a large number of spent fuel containers are based on the use of concrete shields for this purpose, this section deals with a multilayer strategy applied to concrete overpacks, in whose optimization the selection of materials, the energy spectrum of the source terms, and the geometries come into play.

Since the necessary properties for the shielding of both types of radiation (gamma and neutron) are antagonistic, if a single layer of concrete is to be used for the manufacture of the container, it will be necessary to dose the concrete so that a balance is obtained between its properties as a neutron radiation shield and as a gamma radiation shield, so that the dose outside the container is reduced as much as possible. There are different container models proposing different numbers of layers with different materials but the general approach of what is intended to be achieved is explained in the following.

For the design of a multilayer barrier, it is a question of incorporating successive layers, composed of concrete specialized in protecting against each type of radiation, in Fig. 9.1 a new system that includes several layers of concrete is shown.

The inner concrete shielding is made of high-density concrete based on the use of iron aggregates, to which various iron pieces can be added, such as iron punchings or metal fibers in order to increase the specific gravity of the compound. This first layer is responsible for attenuating gamma radiation and can also incorporate bodies of a polymeric nature (e.g., polypropylene fibers) to thermalize fast neutrons. The amount of cement to be used should not be less than $350\ \text{kg/m}^3$, it being advisable to use amounts close to $400\ \text{kg/m}^3$ to maximize the amount of H combined. A second layer of ordinary concrete or concrete that incorporates boron (or another thermal neutron absorbing materials, which usually has a deleterious effect on compressive strength) in the aggregate or in the form of a filler acts as a

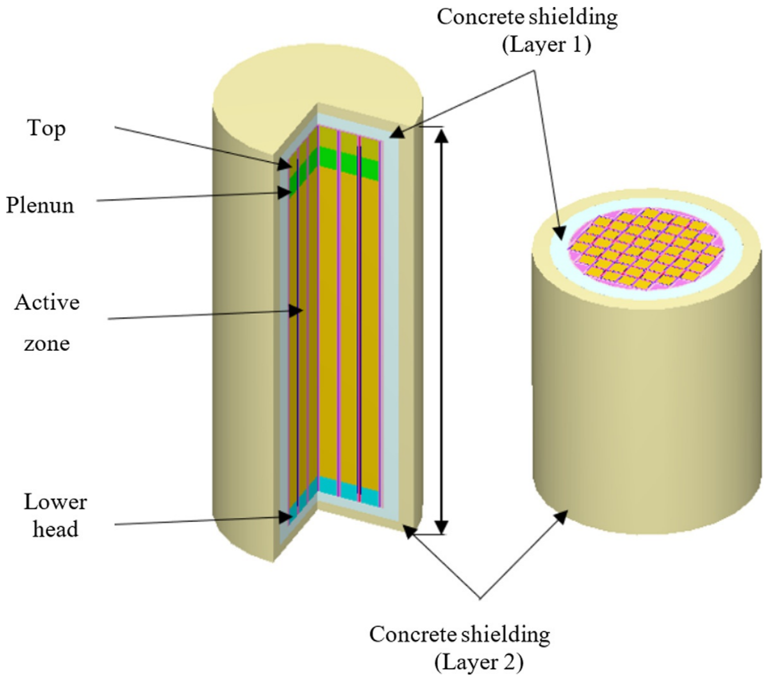

Fig. 9.1 Model of spent fuel container with multilayer configuration. *(Courtesy of INGECID S.L.)*

barrier against neutrons. With this method, it is possible not to use boron filler in the whole thickness of the concrete layer, with the consequent economic saving and with the improvement in the shielding properties. Intermediate layers of attenuating material (e.g., paraffin) may be added to this model or additional layers may be included, for example, to attenuate the secondary gamma radiation produced by the interactions of the neutrons with the core of the shielding material.

There are multilayer models optimized for each particular case. An example is the multilayer concrete designed for shielding in neutron-generating facilities in Japan consisting of three layers [55]: low-activation concrete, low-activation concrete doped with boron, and ordinary concrete. In the first layer, the neutrons are moderated to be efficiently captured by the boron of the second layer, and the first two layers reduce the radioactivity induced by the third. With this, the concentration of long-lived radionuclides in the concrete is diminished, thus reducing the cooling time of the material after operation. With the use of low-activation concrete, the concentration of short-lived nuclides in the third layer is also reduced.

Another example of this strategy is the one proposed in Korea, based on the use of double-layered concrete structures using polyethylene and boron, respectively. The first layer is composed of concrete with part of the aggregate replaced by polyethylene aggregate materials and the second layer by concrete doped with B_4C, managing to reduce the thicknesses by 25%–50% relative to using a monolithic borated concrete, producing as in the previous case notable economic savings derived from the savings in B_4C [56]. There are more examples, although scarce, in the literature [57] and in all of them it is concluded that the multilayer strategy is an advance in neutron radiation shielding, so that the use of several layers provides more effective shielding than each separately or even superior to the behavior of a monolithic layer that incorporates several compounds.

9.6 Numerical simulations

Today, numerical tools are required to optimize the selection of materials for spent nuclear fuel containers. Concrete is a heterogeneous material, which is not totally isotropic and whose chemical composition is variable, since it is composed of 80% aggregate, which in turn depends mostly on its origin. The characterization of concrete under neutron radiation requires laboratory tests to validate the simulation results and vice versa.

When it comes to studying the attenuation that occurs in a neutron flux that crosses a certain thickness x of material that contains a mixture of elements, the neutron flux $\Phi(x)$ does not decrease exponentially, as it does in the case of photons, not even in the case when considering a monoenergetic beam of neutrons. This is due to the influence of the neutrons dispersed mainly in the shield and, to a lesser extent, in the air until affecting the detector. This effect is usually represented by an "accumulation factor" or "build-up" Δ. Thus, the neutron flux can be expressed as follows [58]:

$$\Phi(x) = \Phi_0\left(1 + \Delta(\Sigma x)^2\right)e^{-\Sigma x} \tag{9.1}$$

where Φ_0 is the neutron flux that affects the material (n/cm^{2}s) and Σ is the neutron cross section (the sum of scattering and absorption cross sections, expressed in cm^{-1}) that characterizes the average attenuation in the medium. The equation refers to the neutron flux of a certain energy, monoenergetic, so that both Δ and Σ depend on the corresponding energy, in addition to the corresponding material. Δ and Σ are obtained for each material corresponding to an incident flux that has the energy spectrum produced by a neutron source, the most common being Am-Be [59]. This simplified equation is only used to fit the experimental measurements and to fit the calculated values in the simulations of the laboratory geometry and cannot be used for complex systems such as dry cask shielding analysis.

The typical structure of these test systems consists of a ^{241}Am source that, in contact with ^{9}Be, generates a neutron flux whose energy spectrum typically reaches 10 MeV. The source is usually placed in a paraffin container inside a steel tube. A hollow air cylinder allows access to the source and makes possible the introduction of a cadmium tube that acts as a neutron collimator, ensuring that the neutrons diffused by the paraffin do not reach the detector, as shown in Fig. 9.2.

The different concretes (or different shielding materials) are exposed to the emission of the source, making direct measurements of the neutron flux that penetrates the different thicknesses of the samples, using a neutron detector. The neutron detector, with a characteristic efficiency for each energy spectrum, consists of an LiF fluoride sheet enriched in ^{6}Li (to favor the nuclear reaction ^{6}Li(n,α)^{3}H), deposited on a glass support, which in turn is deposited on a silicon photodiode. In each reaction with a neutron, an alpha particle and a tritium nucleus are generated. These particles leave with opposite directions and with characteristic E(α) and E(3H) kinetic energies, so that only one of the particles is detected. From the total particle rate, a direct measurement of the neutron flux that affects the sheet can be made and the cross section of the material can be obtained.

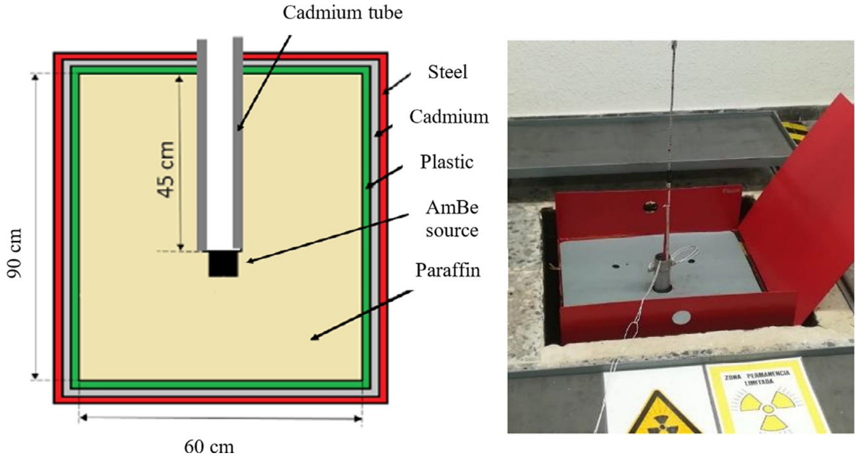

Fig. 9.2 Container scheme: location of the Am-Be source term and protection barriers. *(Courtesy of INGECID S.L.)*

The simulation enables the results obtained in laboratory tests to be contrasted. The characteristics of the material (chemical composition and specific gravity mainly) are required to provide the model's shielding properties. The characteristics of the laboratory equipment can be replicated through specific computing sequences such as MCNP (developed by Oak Ridge National Lab) or MAVRIC, which is part of the SCALE software packages (also developed by Oak Ridge National Lab), for simulating nuclear processes (i.e., neutron transport calculations). MAVRIC can perform radiation deep penetration problems with automatic variance reduction using adjoint-biased source and importance map to improve the Monte Carlo computational speed [60]. MCNP is most common for carrying out neutron flux calculations simulating particle interactions and microscopic cross sections, although among them there are differences in computational efficiencies or accuracy derived from different versions of cross-section libraries, continuous versus multigroup cross sections used, and differences in the calculation functions [61].

The simulations provide information not only about the flow (n/s) that reaches the detector, but also the flow by neutron energy groups. To establish a correlation between the measurements calculated by means of the laboratory model and the experimental ones, it is necessary to take into account the value of the effective absorption section of ^{6}Li for each neutron energy group. Thus, the calculated neutron flux for each energy interval is multiplied by a factor proportional to the average cross section for each range.

To obtain the values of parameters Δ and Σ, it must be ensured that all the neutron flux that reaches the sensing surface has traversed the entire thickness of concrete and does not come from successive collisions in the paraffin, for which a simulation is performed with a vacuum instead of paraffin. Making the adjustment to Eq. (9.1), taking Φ_0 as an incident flow in the concrete, the flow calculated by means of the simulation without placing concrete (or other shielding material) between the detector and the source, the values of Δ and Σ are obtained. Neutron attenuation is obtained by simulating the model with different thicknesses, obtaining the final neutron flux for each energy spectrum.

Subsequently, when the simulations have validated the results of the laboratory tests and vice versa, the modeling of the spent fuel container is performed. This model is used to evaluate the effectiveness of the multilayer strategy as well as the effectiveness of the preselected materials for its performance. For the calculation of the dose rate outside the containers, an evaluation of the neutron and gamma source terms is performed.

When considering spent fuel containers, there are two main sources of neutron radiation to consider: neutrons generated by spontaneous and subcritical fission and neutrons emitted by (α,n) reactions of fissile material. The spent fuel source term can be calculated using three factors: initial enrichment (IE), burn up, and cooling time (CT), and also the type of nuclear fuel. For this calculation, specialized computation sequences as ORIGEN (developed by Oak Ridge National Lab) using the subsequence called ORIGEN-ARP are used. With this modeling, the neutron dose can be determined both in the container wall and at various distances by previously defining cylindrical meshes, for each of the multilayer configurations and materials used.

Finally, once the container with the final disposition and materials has been modeled and simulated, the interaction with other containers has to be studied (Fig. 9.3), for which an individual temporary warehouse (in the case of dry cask storage) with a certain number of containers is simulated. Numerous examples are found in the literature with different numbers of containers and dispositions [62, 63]. In this case, both the relative position between containers and the spatial configuration are optimized, using the same assumptions as were adopted for the single container model.

It is also important to mention the effect of gamma radiation interactions, also needing to consider the evolution of fuel gamma-ray, structure gamma-ray, and secondary gamma-ray contributions to the total dose rate [64].

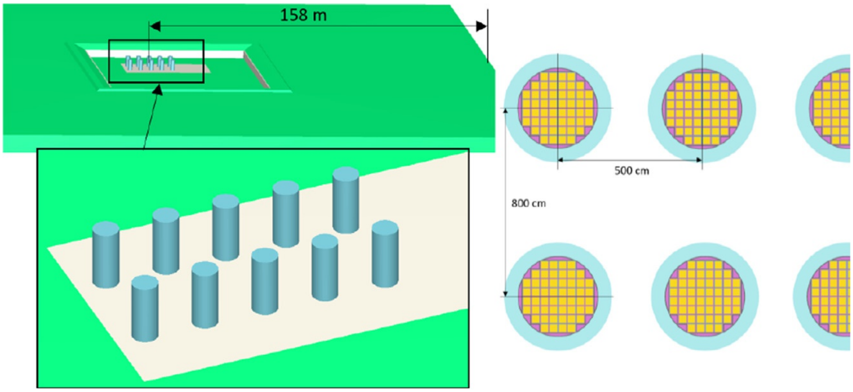

Fig. 9.3 Model of an individual temporary warehouse with 10 spent fuel containers using MAVRIC. *(Courtesy of INGECID S.L.)*

9.7 Conclusions and future trends

Since most of the pools where spent fuel is stored are being filled/have been filled, dry casks are the main storage systems today. The current trend is to use dual-purpose casks, although some of the current models are multipurpose, even though the license process of the latter is not yet regulated in most cases. This dry cask storage usually uses steels (carbon, stainless), aluminum, and lead for construction, although polymers (epoxy, rubbers, or PE) are used and powders such as B_4C (or other boron compounds) are incorporated to improve the neutron-scattering and absorption cross sections, respectively. The optimization in the design of these casks comprises a simultaneous selection of materials and geometries and depends fundamentally on the energy spectrum of the source and its geometry. To develop these designs, numerical simulation tools that use neutron transport models through different materials are used. Today, the use of multilayer strategies, which employ specialized layers for each type of radiation interaction, comprises one of the great advances in neutron-shielding strategies, especially in the design of concrete overpacks.

The future of the development of spent fuel containers will be based on the development of new more effective material shielding and the optimization of design. The most current research is aimed at the use of copper in the disposal container canisters due to its excellent performance against corrosion, as a coating, as is the case with the Swedish program [9], where its thickness is gradually being reduced due to the traditional tendency to use extremely conservative safety factors, a situation also exists with C-steel canisters. This idea of using a copper coating has also been developed by the Canadian program [65], further favored by economic factors. As for other materials, the use of passive materials such as Ni or Ti alloys will be incorporated in the design of the canister, corrosion-resistant materials classically discarded due to the difficulty in predicting their corrosion behavior, since they are materials that tend to suffer localized attacks.

Advances will also continue in aspects related to the behavior of certain alloys against corrosion in the interaction with the disposal medium. Dry cask storage systems are the preferred option to store spent fuel for now. The advance in the study of these designs will mean that the acquired industrial experience can be applied to disposal systems. Storage in casks under inert conditions offers advantages such as being a modular storage system and having a passive-convective cooling system that reduces operating costs. The development of new dry cask storage will focus more on the production of multipurpose canisters and there will be a greater commercial offer, due to the growing needs for storage systems. The tendency will be to increase the size of the casks to reduce the cost-volume ratio and also reducing maintenance operations, the size of the container being limited by restrictions on the transport load or lifting equipment.

References

[1] I.A.E. Agency, Classification of Radioactive Waste, https://www-pub.iaea.org/MTCD/Publications/PDF/Pub1419_web.pdf, 2009.

[2] J.D.B. Lambert, K.K. Kadyrzhanov, Safety Related Issues of Spent Nuclear Fuel Storage, Springer Science & Business Media, 2007.

[3] C. Greulich, C. Hughes, Y. Gao, A. Enqvist, J. Baciak, High energy neutron transmission analysis of dry cask storage, Nucl. Instrum. Methods Phys. Res. A 874 (2017) 5–11.

[4] A.K. Suryavanshi, R. Narayan Swamy, Stability of Friedel's salt in carbonated concrete structural elements, Cem. Concr. Res. 26 (1996) 729–741, https://doi.org/10.1016/S0008-8846(96)85010-1.

[5] M.E. Gaze, N.J. Crammond, The formation of thaumasite in a cement:lime:sand mortar exposed to cold magnesium and potassium sulfate solutions, Cem. Concr. Compos. 22 (2000) 209–222, https://doi.org/10.1016/S0958-9465(00)00002-0.

[6] B. Kursten, E. Smailos, I. Azkarate, L. Werme, N.R. Smart, G. Santarini, State-of-the-Art Document on the COrrosion BEhaviour of COntainer MAterials, 5th EURATOM Framew. Program, 1998, 2002.

[7] V. Penttala, F. Al-Neshawy, Stress and strain state of concrete during freezing and thawing cycles, Cem. Concr. Res. 32 (2002) 1407–1420.

[8] O.K. Chopra, D.R. Diercks, R.R. Fabian, Z.H. Han, Y.Y. Liu, Managing Aging Effects on Dry Cask Storage Systems for Extended Long-Term Storage and Transportation of Used Fuel (REV. 2), 2014.

[9] F. King, Nuclear waste canister materials: corrosion behavior and long-term performance in geological repository systems, in: Geological Repository Systems for Safe Disposal of Spent Nuclear Fuels and Radioactive Waste, Elsevier, 2017, pp. 365–408.

[10] D.G. Bennett, R. Gens, Overview of European concepts for high-level waste and spent fuel disposal with special reference waste container corrosion, J. Nucl. Mater. 379 (2008) 1–8.

[11] F. King, Microbiologically influenced corrosion of nuclear waste containers, Corrosion 65 (2009) 233–251.

[12] C. Thomas, J. Rico, P. Tamayo, J. Setién, F. Ballester, J.A. Polanco, J. Setién, J. A. Polanco, Neutron shielding concrete incorporating B4C and PVA fibers exposed to high temperatures, J. Build. Eng. 26 (2019) 100859.

[13] C. Thomas, J. Rico, P. Tamayo, F. Ballester, J. Setién, J.A. Polanco, Effect of elevated temperature on the mechanical properties and microstructure of heavy-weight magnetite concrete with steel fibers, Cem. Concr. Compos. 103 (2019) 80–88. https://doi.org/10.1016/j.cemconcomp.2019.04.029.

[14] National Research Council, Others, Safety and Security of Commercial Spent Nuclear Fuel Storage: Public Report, National Academies Press, 2006.

[15] A.T. Silva, M.M. Neto, R.P. Mourao, L.L. Silva, C.C. Lopes, M.C.C. Silva, Options for the interim storage of IEA-R1 research reactor spent fuels, Prog. Nucl. Energy 50 (2008) 836–844.

[16] W. Bak, V. Roland, Dual Purpose or Not? The Significant Factors, 1999.

[17] A. Turnbull, A Review of the Possible Effects of Hydrogen on Lifetime of Carbon Steel Nuclear Waste Canisters, 2009.

[18] M.-S. Yim, K.L. Murty, Materials issues in nuclear-waste management, JOM 52 (2000) 26–29.

[19] F. King, Container materials for the storage and disposal of nuclear waste, Corrosion 69 (2013) 986–1011.

[20] Å. Björkbacka, S. Hosseinpour, M. Johnson, C. Leygraf, M. Jonsson, Radiation induced corrosion of copper for spent nuclear fuel storage, Radiat. Phys. Chem. 92 (2013) 80–86.

[21] F. Hua, K. Mon, P. Pasupathi, G. Gordon, D. Shoesmith, A review of corrosion of titanium grade 7 and other titanium alloys in nuclear waste repository environments, Corrosion 61 (2005) 987–1003.

[22] C.S. Brossia, L. Browning, D.S. Dunn, O.C. Moghissi, O. Pensado, L. Yang, Effect of Environment on the Corrosion of Waste Package and Drip Shield Materials, Publ. Cent. Nucl. Waste Regul. Anal., 2001 (CNWRA 2001–03).

[23] A.J. Sedriks, Corrosion of Stainless Steel, seconnd ed., U.S. Department of Energy, Office of Scientific and Technical Information, United States, 1996.

[24] N. Diomidis, L.H. Johnson, Materials options and corrosion-related considerations in the design of spent fuel and high-level waste disposal canisters for a deep geological repository in opalinus clay, JOM 66 (2014) 461–470.

[25] I.I. Bashter, A.S. Makarious, A. El-Sayed Abdo, Investigation of hematite-serpentine and ilmenite-limonite concretes for reactor radiation shielding, Ann. Nucl. Energy 23 (1996) 65–71, https://doi.org/10.1016/0306-4549(95)00011-G.

[26] I.I. Bashter, Calculation of radiation attenuation coefficients for shielding concretes, Ann. Nucl. Energy 24 (1997) 1389–1401, https://doi.org/10.1016/S0306-4549(97)00003-0.

[27] C. Basyigit, The physical and mechanical properties of heavyweight concretes used in radiation shielding, J. Appl. Sci. 6 (2006) 762–766.

[28] A.S. Ouda, Development of high-performance heavy density concrete using different aggregates for gamma-ray shielding, Prog. Nucl. Energy 79 (2015) 48–55, https://doi.org/10.1016/j.pnucene.2014.11.009.

[29] J. Kazjonovs, D. Bajare, A. Korjakins, Designing of high density concrete by using steel treatment waste, in: 10th International Conference Modern Building Materials, Structures and Techniques, 2010, pp. 138–142.

[30] S.G. Ermichev, V.I. Shapovalov, N.V. Sviridov, V.K. Orlov, V.M. Sergeev, A. G. Semyenov, A.M. Visik, A.A. Maslov, A.V. Demin, D.D. Petrov, et al., High-density concrete with ceramic aggregate based on depleted uranium dioxide, in: IHLRWM, Las Vegas, NV, 30 2006, pp. 880–884.

[31] G. Sanjayan, L.J. Stocks, Spalling of high-strength silica fume concrete in fire, Mater. J. 90 (1993) 170–173.

[32] M. Lion, F. Skoczylas, Z. Lafhaj, M. Sersar, Experimental study on a mortar. Temperature effects on porosity and permeability. Residual properties or direct measurements under temperature, Cem. Concr. Res. 35 (2005) 1937–1942, https://doi.org/10.1016/j.cemconres.2005.02.006.

[33] P.K. Mehta, P.J.M. Monteiro, CONCRETE Microstructure, Properties and Materials, 2017.

[34] 197-1:2011 UNE-EN, Cemento. Parte 1: Composición, especificaciones y criterios de conformidad de los cementos comunes., (n.d.).

[35] I. Maruyama, O. Kontani, A. Ishizawa, M. Takizawa, O. Sato, Development of system for evaluating concrete strength deterioration due to radiation and resultant heat, in: Proceedings 3rd International Conference NPP Life Management Long Term Operations IAEA-CN-194-096, Salt Lake City, May, 2012, pp. 12–14.

[36] K.G. Field, I. Remec, Y. Le Pape, Radiation effects in concrete for nuclear power plants—Part I: Quantification of radiation exposure and radiation effects, Nucl. Eng. Des. 282 (2015) 126–143, https://doi.org/10.1016/j.nucengdes.2014.10.003.

[37] M.R. Elleuch, F. Dubois, J. Rappenau, Behavior of special shielding concretes and of their constituents under neutron irradiation, in: Fourth United Nations International Conference on the Peaceful Uses Atomic Energy, 1971.

[38] S. Nambiar, J.T.W. Yeow, Polymer-composite materials for radiation protection, ACS Appl. Mater. Interfaces 4 (2012) 5717–5726.

[39] C. Harrison, S. Weaver, C. Bertelsen, E. Burgett, N. Hertel, E. Grulke, Polyethylene/boron nitride composites for space radiation shielding, J. Appl. Polym. Sci. 109 (2008) 2529–2538.

[40] X. Zhang, M. Yang, X. Zhang, H. Wu, S. Guo, Y. Wang, Enhancing the neutron shielding ability of polyethylene composites with an alternating multi-layered structure, Compos. Sci. Technol. 150 (2017) 16–23.

[41] X. Zhang, X. Zhang, S. Guo, Simple approach to developing high-efficiency neutron shielding composites, Polym. Eng. Sci. 59 (2019) E348–E355.

[42] D. Toyen, E. Wimolmala, N. Sombatsompop, T. Markpin, K. Saenboonruang, Sm_2O_3/UHMWPE composites for radiation shielding applications: mechanical and dielectric properties under gamma irradiation and thermal neutron shielding, Radiat. Phys. Chem. 164 (2019) 108366.

[43] C.A.O. Xiaozhou, X. Xiangxin, T. Jiang, L.I. Zhefu, D. Yuefeng, L.I. Yong, Y. He, Mechanical properties of UHMWPE/Sm_2O_3 composite shielding material, J. Rare Earths 28 (2010) 482–484.

[44] H. Chai, X. Tang, M. Ni, F. Chen, Y. Zhang, D. Chen, Y. Qiu, Preparation and properties of flexible flame-retardant neutron shielding material based on methyl vinyl silicone rubber, J. Nucl. Mater. 464 (2015) 210–215.

[45] P.S. Ravishankar, Treatise on EPDM, Rubber Chem. Technol. 85 (2012) 327–349.

[46] T. Özdemir, Monte Carlo simulations of radioactive waste embedded into EPDM and effect of lead filler, Radiat. Phys. Chem. 98 (2014) 150–154.

[47] T. Özdemir, I.K. Akbay, H. Uzun, I.A. Reyhancan, Neutron shielding of EPDM rubber with boric acid: mechanical, thermal properties and neutron absorption tests, Prog. Nucl. Energy 89 (2016) 102–109.

[48] T. Özdemir, S.N. Yilmaz, Hexagonal boron nitride and polydimethylsiloxane: a ceramic rubber composite material for neutron shielding, Radiat. Phys. Chem. 152 (2018) 93–99.

[49] M.A. El-Sarraf, A.E.-S. Abdo, Insulating epoxy/barite and polyester/barite composites for radiation attenuation, Appl. Radiat. Isot. 79 (2013) 18–24.

[50] E.M. Petrie, Handbook of Adhesives and Sealants, McGraw-Hill, New York, 2000.

[51] M. Rezaeian, J. Kamali, S.J. Ahmadi, M.A. Kiani, Effectiveness of the neutron-shield nanocomposites for a dual-purpose cask of Bushehr's water–water energetic reactor (VVER) 1000 nuclear-power-plant spent fuels, Nucl. Eng. Technol. 49 (2017) 1563–1570.

[52] A.B. Chilton, J.K. Shultis, R.E. Faw, Principles of Radiation Shielding, Prentice Hall Inc., Old Tappan, NJ, 1984

[53] X. Li, J. Wu, C. Tang, Z. He, P. Yuan, Y. Sun, W. Lau, K. Zhang, J. Mei, Y. Huang, High temperature resistant polyimide/boron carbide composites for neutron radiation shielding, Compos. Part B Eng. 159 (2019) 355–361.

[54] P. Wang, X. Tang, H. Chai, D. Chen, Y. Qiu, Design, fabrication, and properties of a continuous carbon-fiber reinforced Sm_2O_3/polyimide gamma ray/neutron shielding material, Fusion Eng. Des. 101 (2015) 218–225.

[55] S. Sato, T. Maegawa, K. Yoshimatsu, K. Sato, A. Nonaka, K. Takakura, K. Ochiai, C. Konno, Development of a low activation concrete shielding wall by multi-layered structure for a fusion reactor, J. Nucl. Mater. 417 (2011) 1131–1134.

[56] S.J. Park, J.G. Jang, H.-K. Lee, Computational investigation of the neutron shielding and activation characteristics of borated concrete with polyethylene aggregate, J. Nucl. Mater. 452 (2014) 205–211.

[57] S.M.A. Islam, M.M. Akramuzzaman, M.A. Awal, M.N. Islam, A study of neutron shielding properties of some multilayers containing polyethylene, Appl. Radiat. Isot. 44 (1993) 1161–1164.

[58] B.T. Price, C.C. Horton, K.T. Spinney, Radiation Shielding, The International Series of Monographs on Nuclear Energy, 1957.

[59] A. Lorente Fillol, E.F. Gallego D'iaz, H.R. Vega-Carrillo, R. Méndez, Neutron shielding properties of a new high-density concrete, in: IRPA 12: 12. International Congress of the International Radiation Protection Association (IRPA): Strengthening Radiation Protection Worldwide, Buenos Aires (Argentina), 19–24 Oct 2008; Country of input: International Atomic Energy Agency (IAEA), SAR, Buenos Aires (Argentina), 2008, 10 p

[60] Y. Gao, C.R. Hughes, C.R. Greulich, J.E. Tulenko, A. Enqvist, J.E. Baciak, Radiation dose rate distributions of spent fuel dry casks estimated with MAVRIC based on detailed geometry and continuous-energy models, Ann. Nucl. Energy 117 (2018) 84–97.

[61] A.Y. Chen, Y.F. Chen, J.N. Wang, R.J. Sheu, Y.-W. Liu, S.H. Jiang, A comparison of dose rate calculations for a spent fuel storage cask by using MCNP and SAS4, Ann. Nucl. Energy 35 (2008) 2296–2305.

[62] S.E. Smith, X. Sun, C.A. Ford, A.W. Fentiman, MCNP simulation of neutron energy spectra for a TN-32 dry shielded container, Ann. Nucl. Energy 35 (2008) 1296–1300.

[63] I. Harkness, T. Zhu, Y. Liang, E. Rauch, A. Enqvist, K.A. Jordan, Development of neutron energy spectral signatures for passive monitoring of spent nuclear fuels in dry cask storage, in: EPJ Web Conference, 2018, p. 7004.

[64] Y. Gao, N.J. McFerran, A. Enqvist, J.E. Tulenko, J.E. Baciak, Dry cask radiation shielding validation and estimation of cask surface dose rate with MAVRIC during long-term storage, Ann. Nucl. Energy 140 (2019) 107145.

[65] P.G. Keech, P. Vo, S. Ramamurthy, J. Chen, R. Jacklin, D.W. Shoesmith, Design and development of copper coatings for long term storage of used nuclear fuel, Corros. Eng. Sci. Technol. 49 (2014) 425–430, https://doi.org/10.1179/1743278214Y.0000000206.

CHAPTER 10

Neutron radiation shielding composites for deep space exploration: An introduction

Franco Cataldo[a], **Michele Prata**[b]
[a]Actinium Chemical Research Institute, Rome, Italy
[b]Laboratorio Energia Nucleare Applicata—Università degli Studi di Pavia, Pavia, Italy

10.1 Introduction: The problem of high-energy radiation in deep space

Reliable radiation shielding materials are requested for traditional as well as for emerging and challenging applications. Radiation shielding in nuclear reactors and nuclear waste removal, processing, and storage as well as X-ray shielding in medical and industry, shielding in nuclear medicine, e.g., for cancer treatments, γ-ray facilities for sterilization and research, shielding of cyclotrons, represent some examples of traditional application [1–3]. However, for emerging and challenging applications, it is sufficient to talk about the problem of effective shielding of neutron streaming from Tokamak fusion reactors [4] and about space radiation shielding, which is especially demanding for deep space manned missions [5–8]. In these new demanding applications, the radiation shielding composites will certainly play a key role for a number of obvious positive reasons, including lightness, low density, possible flexibility, use (at least in part) of renewable sources for their production and, moreover, wide degrees of formulation margins to engineer their applications.

Regarding space exploration, it is necessary to distinguish low Earth orbit missions from deep space exploration. In low Earth orbit manned missions, as it is the case of the International Space Station (ISS), the space radiation does not pose major problems because the ISS is orbiting at about 410 km from the Earth surface, thus, well inside the protection exerted by the Earth's magnetic field. On the other hand, any space missions conducted outside the protection of the Earth's magnetic field are considered deep space missions [9–11]. Thus, even a trip to the Moon or to a near-Earth object is a deep

Micro and Nanostructured Composite Materials for Neutron Shielding Applications
https://doi.org/10.1016/B978-0-12-819459-1.00010-6
© 2020 Elsevier Ltd.
All rights reserved.

space mission, as it is obviously a mission toward Mars and beyond. It is worth to remind here that neither Mars nor the Moon possess a strong natural magnetic field as the Earth.

The key problem of a deep space mission is that the crew is exposed directly to both the solar wind and the galactic cosmic radiation (GCR) [5–8, 11, 12]. An additional source of risks for the manned mission in deep space is presented by solar flares or solar particle events (SPEs) occurring especially during solar maxima [9, 11, 13, 14]. While normal solar wind protons have in general an energy in the keV order of magnitude, SPE protons can reach from 100 MeV to 25 GeV and occur together with proton flux >100 particles/cm^2/s/ster [15, 16]. Thus, SPE protons and α-particles appear in their energy spectrum somewhat similar to that of cosmic rays but at a much higher flux. In case of SPE event there is a high risk of acute radiation exposure for the crew of a manned mission [9, 10, 12].

On the other hand, cosmic radiation is composed of a flux of protons (92.9%), α particles, i.e., ^{4}He nuclei (6.3%) and a smaller fraction of light and average nuclei (0.53%) by heavier nuclei (0.23%) of all elements with a minor electron component [17]. Cosmic rays are responsible for the chronic exposure to radiation in a manned mission in deep space [8]. A particularly dangerous component of the cosmic radiation are the heavier nuclei with energies of the order of GeV/nucleon or higher. Such particles are known as HZE particles and are heavy nuclei ($Z > 3$) heavily charged and accelerated to relativistic velocities [18, 19]. When these relativistic particles impinge on the outer surface of the spacecraft, an avalanche of secondary particles is generated through spallation nuclear reactions [7]. The secondary particles are mainly neutrons and protons. These secondary particles enter into the spacecraft and represent an important fraction of the radiation dose absorbed by the crew inside spacecraft. Indeed, according to NASA documents [20, 21], the action of cosmic rays and/or SPE particles on the metallic shell of a common spacecraft produces cascade neutrons which are directed toward the interior part of the spacecraft and contribute significantly to the radiation dose absorbed by the crew in a deep space mission. The traditional spacecraft building material is based on aluminum. For example, in the Apollo mission the external spacecraft building consisted of an Al skin followed by an internal layer of steel honeycomb and by another layer of internal Al surface. The irradiation of Al and Fe with cosmic rays and solar wind particles (especially those from SPE) produces a series of secondary protons and neutrons directed toward the inner part of the spacecraft. The secondary protons can undergo capture by nuclei without the necessary emission of a new nuclear fragment but only with the emission of γ quanta [22, 23]. Only when protons have very high energy, >50 MeV, then nuclear reactions occur with the production of secondary neutrons [22–24]. Relativistic protons can give rise to spallation reactions [22–24]. For example, protons with energy between 1 and 3 GeV have a devastating effect on ^{27}Al target nuclei:

$$^{27}\mathrm{Al} + \mathrm{p} \rightarrow 10\mathrm{p} + 11\mathrm{n} + {}^{7}\mathrm{Be} \tag{10.1}$$

In fact, the impact of a relativistic proton with ^{27}Al nucleus leads to its disintegration into an avalanche of protons and neutrons leaving a residual ^{7}Be nucleus as the main secondary product of this nuclear reaction. Indeed, reaction (10.1) represents just one of the numerous reactions occurring during ^{27}Al spallation with relativistic protons. In fact, with 0.8 GeV protons ^{27}Al spallation produces 12 different nuclides [25], while with 28 GeV protons ^{27}Al spallation produces at least 9 different nuclides with ^{7}Be as the most abundant [26]. The mentioned spallation reactions are applicable to a spacecraft in deep space mission.

Similarly, for ^{56}Fe nuclei, even protons of only 340 MeV can cause a spallation reaction on ^{56}Fe [22, 23]. However, protons of 0.8 GeV cause ^{56}Fe nuclei spallation with the production of 36 different nuclides [25]. It is important to note here that ^{27}Al and ^{56}Fe are also normal components in Lunar or Martian regolith together with ^{28}Si [20]. The latter undergoes spallation reaction with protons of 0.5 GeV threshold [27]:

$$^{28}\mathrm{Si} + \mathrm{p}\,(0.5\ \mathrm{GeV}) \rightarrow 3\mathrm{p} + 4\mathrm{n} + {}^{3}\mathrm{He} + {}^{18}\mathrm{F} \tag{10.2}$$

Thus, a silicon nucleus impacted by a relativistic proton produces three protons, four neutrons, and one ^{3}He and one ^{18}F nuclei.

Regolith is preconized as local building material for the future Lunar and Martian bases; however, it presents the same problems as the traditional spacecraft building materials in terms of spallation reaction sensitivity and products. The main difference between spacecraft and regolith toward cosmic ray spallation reactions is the fact that the spacecraft walls represent a thin target while the regolith in Lunar or Martian base represent thick target. Based on these considerations, the NASA documents [20, 21] strongly suggests that there is the need to study passive radiation shielding toward neutrons to protect the crew in deep space mission.

10.2 About spallation nuclear reactions in connection with deep space missions

Regarding the spallation nuclear reactions, the textbooks by Choppin [22], Friedlander et al. [24], and Krása [28] can be considered as useful introductory works. Following Shen and Merker [27], spallation reactions derive from inelastic nuclear collisions where the resulting complex nucleus is characterized by an available energy which exceeds the interaction energy of the nucleons in the given nucleus. In general, a spallation reaction involves an excess of 50–100 MeV/nucleon energy in the nucleon-nucleus, pion-nucleus, or nucleus-nucleus reaction. The most accepted spallation model involves a high-energy (say >0.5 GeV) incident particle which enters into the target nucleus, interacting with the other nucleons and leading to an intranuclear cascade. In this fast step a few nucleons are ejected out from the target nucleus. This stage is also called knock-on stage or cascade stage. The term "cascade" refers to the succession of self-multiplying collisions occurring inside the target nucleus. If the incident particle energy is high enough (i.e., >0.3 GeV) pions are also created and emitted from the nucleus. At this stage the target nucleus has less nucleons than that before the collision but is still at an excited stage. The de-excitation occurs by a delayed emission of a number of single nucleons and small clusters of nucleons leaving a final lighter nucleus as shown in reactions (10.1), (10.2). This second step of de-excitation process also is known as evaporation process and is somewhat analogous to that occurring in lower energy nuclear reactions and is a slow process.

In the context of deep space mission, the distinction between thin and thick targets is important. The case of thin targets, which applies to the external walls of a spacecraft, there are no secondary interactions, which means that the nucleons and nuclides produced by the interaction of the incident particle with the target nucleus do not encounter other nuclei in the target and are ejected directly into spacecraft. Secondary interactions hence start inside the spacecraft, with the artificial atmosphere or with the astronaut's bodies, for instance.

On the other hand, the case of thick targets can be represented by the regolith-based walls of the Lunar or Martian bases. The nuclides ejected as a result of primary interactions produce secondary particles and then further the secondaries directly inside the thick target. In these conditions, the speed of neutrons can be found equal to or even double the velocity of the impinging cosmic ray nuclei [20, 21]. The nuclear reactions induced by

1.6 GeV neutrons have been reviewed by Leya and Michel [29]. At this point the problem of radiation shielding of a crew in a spacecraft or in a Lunar or Martian base is defined in terms of slowdown of high-energy protons, proton capture, and slowdown of neutrons derived from the spallation reactions followed by capture.

10.3 Radiation dose to astronauts in deep space mission

The permanence of the astronauts on the surface of Mars and Moon represents a radiation hazard because of the lack of the natural magnetic field in both bodies of the Solar System, the absence of any atmosphere on the Moon, and the very thin atmosphere present on Mars. For example, the average radiation dose rate taken by humans on the Earth is in the range of 2–3 mSv/year with peaks at 6–7 mSv/year in certain regions with higher radiation background [30]. The radiation dose rate in deep space is estimated at 360 mSv/year but a SPE could deliver 10 mSv in a single day [6, 31, 32]. A round trip from Earth to Mars and back to Earth may take more than 2 years. Thus, with a dose rate of 360 mSv/year in deep space, with a single round trip to Mars the carrier limit of a male astronaut is reached in full, since the total radiation dose (as carrier limit) for a 35-year-old male is 720 and that for a female is 500 mSv [33]. Furthermore, on Mars surface the dose rate is similar to that estimated for deep space, i.e., 200–300 mSv/year [31, 32]. In this context, the study by Straume et al. [34] is absolutely interesting, which shows that the lightest elements (H and He) in GCR have by far the highest flux and therefore traversal rates in biological targets, but heavy nuclides contribute substantially to the mean dose and dose equivalent behind thin shielding producing large energy deposition in small biological targets such as cell nuclei. Behind a shield equivalent to 50 g/cm^2 of water, the main flux of secondaries derived from GCR is neutrons [20]. Although GCR contain <1% of HZE particles, about 16% of the neutron flux behind the shield is generated by the impact of HZE particles. On the other hand, alpha particles in GCR are less than 10% but are responsible for 15% of the secondary neutron flux behind the shield [20]. Protons represent more than 90% of the GCR constituents but generate only 69% of the secondary neutrons flux behind the shield [20].

For shielding high-energy high-Z particles it was shown that hydrogen-rich materials are the most effective materials and the preferred one is polyethylene in all its versions, i.e., UHMWPE, PE-foam, and so forth. [13, 35]. It is interesting to quote here a conclusion taken from the study by DeWitt et al. [35]: "*Relatively high-Z materials such as aluminum and copper do not fragment incident heavy ions as thoroughly as polyethylene. This is due to the hydrogen-rich content of the polymer, which translates into a high fragmentation cross-section per unit constituent of the material. The competing effects of nuclear fragmentation and the slowing of primaries by electromagnetic interactions varies depending on the charge of the projectile. A slowed primary acquiring a higher LET (thus making a higher dose contribution) is offset by the heavy ion fragmenting ability of the absorber. So while polyethylene slows the primary ions more relative to the higher Z of aluminum or copper, the increase in dose from this effect is counterbalanced by the amount of fragmentation undergone by the remaining primaries.*"

10.4 Composites for radiation shielding in deep space missions and elsewhere

It should be noted that simple composite shielding materials based on hydrogen-rich polymer matrices were proposed since long time [36]. Especially polyethylene (PE) and polymethylmethacrylate (PMMA) were proposed as polymeric matrices for radiation shielding as internal layers inside a spacecraft [36]. In addition, loading of these polymeric matrices with neutron adsorbing materials such as graphite and boron carbide were already proposed and tested [36]. It is however well known that PE can accept a really limited loading of filler before losing both mechanical properties and flexibility. Furthermore, PE is not suitable at all as polymeric matrix to be composed with reinforcing and shielding textile fabrics. On the other hand, PMMA shows poor radiation resistance and is plagued by chains scission phenomena under high-energy radiation hindering its potential application [37]. A similar drawback, although less dramatically, applies also to PE [37]. Currently, the main focus on composites for radiation shielding relies on PE which remains a very popular polymer matrix [38], conjugated under various grades such as HDPE [39–44], LLDPE [45], and UHMWPE [46] as well as UHMWPE fibers in epoxy composite [47]. Other polymer matrices studied much less frequently are EPDM [48–51], nitrile rubber [52], natural rubber [53–55], styrene-butadiene rubber [56], and silicon rubber [57]. Furthermore, apart from the known rigid epoxy-based composites [58], quite unusual flexible epoxy composites were studied as well [59].

Regarding the fillers used in the composite, graphite and graphite-based fabrics were used [60] mainly to slowdown fast neutrons, while for neutron capture the most preferred compounds are boron compounds and in particular boric acid (H_3BO_3) which is the most economic, followed by boron carbide B_4C and boron nitride BN. Gadolinium is sometimes used as filler as well [61]. It is useful to remind here that certain rare earth metals are characterized by very high thermal neutron capture cross section and the most useful is indeed Gd, which, however, is not widely available and cheap as boron [24, 40].

Natural elemental boron is composed of a mixture of about 20% ^{10}B isotope and about 80% ^{11}B isotope, and it is characterized by a thermal neutron absorption cross section of 760 barn, which reaches 3890 barn in the case of pure ^{10}B isotope [22, 24]. The thermal neutron capture reaction of ^{10}B can be summarized as follows [22, 24]:

$$^{10}\mathrm{B} + \mathrm{n} \rightarrow \left[^{11}\mathrm{B}\right]^{*} \rightarrow {}^{4}\mathrm{He}\,(1.47\,\mathrm{MeV}) + {}^{7}\mathrm{Li}\,(0.84\,\mathrm{MeV}) + \gamma\,(0.48\,\mathrm{MeV}) \tag{10.3}$$

$$^{10}\mathrm{B} + \mathrm{n} \rightarrow {}^{4}\mathrm{He}\,(1.79\,\mathrm{MeV}) + {}^{7}\mathrm{Li}\,(1.01\,\mathrm{MeV}) \tag{10.4}$$

with Eq. (10.3) weighing 93.7% and Eq. (10.4) only for 6.3% ^{4}He nuclei.

In conclusion, the key "ingredients" of an effective radiation shield for deep space mission could be just a hydrogen-rich polymer matrix to slow-down neutrons but which is also effective in HZE particle fragmentation [13, 35] and a boron-based filler to capture the thermalized neutrons derived from the spallation reactions.

10.5 Hydrogen-rich polymer matrix

As mentioned at the end of the previous paragraph, a number of different polymer matrices were used in the preparation of neutron radiation shields. Surprisingly, there are no reports on the use of polyurethanes as polymer matrix for radiation shielding. However, polyurethanes (PUR) can be prepared by using polyol prepolymers derived from renewable sources rather than from fossil raw materials. Thus, only the cross-linking must be achieved using bifunctional isocyanates. For example, in our recent studies [62, 63] 56% of polytetrahydrofuran polyol, 21% of boron-based filler, and 23% of 1,1-diphenylmethane diisocyanate polyol prepolymer were used as key ingredients for the preparation of the composite. It is worth to remind here that polytetrahydrofuran polyol is an hydrogen-rich polymer which is prepared by ring opening polymerization of tetrahydrofuran [64]. The latter derives from furfural, a molecule obtained by simple chemical processed from different biomasses and hence from fully renewable sources [65]. Thus, about 56% of our PUR-based composite was derived from renewable sources. It is worth mentioning here that another step ahead in future PUR-based composites for radiation shielding must involve polyurethanes prepared without using diisocyanates which is an emerging technology and will certainly phase out the use of the dangerous and reactive isocyanates [66].

Polyurethanes present numerous advantages as polymer matrix for radiation shielding composites with respect to other hydrogen-rich polymer matrices. First of all the molecular architecture can be changed with a certain degree of freedom which is lacking in the case of many other polymer matrices. Thus, flexible and rigid PUR matrices can be obtained by design. Furthermore, the mechanical properties of PUR also exceed those of many other more common polymer matrices. However, one of the main feature of PUR in radiation shielding is the excellent radiation resistance, a property which is known since long time [67]. In fact, it was reported that polyurethanes can resist a single γ-ray dose of 100 MGy [68], although different polyurethane grades may show different behavior toward high-energy radiation [69], which is also affected by soft and hard segment ratio [70–72]. PUR radiation resistance was also assessed on foams at low temperatures [73, 74], a condition which is met also in space environment. Based on these premises about the excellent radiation resistance of polyurethanes, certainly much better than PE and PP [69], it is not surprising to observe almost no changes in the FT-IR spectra of neutron treated (1.5×10^{13} n/cm^2) unfilled PUR either front foil of the shield facing the neutron beam or the rear foil behind the shield in comparison to pristine, unfilled PUR [62, 63]. Furthermore, the DSC analysis of the PUR used as radiation shield, after exposure to neutron fluence of 1.5×10^{13} n/cm^2, show no significant changes in the glass transition temperature [62, 63].

10.6 Boron fillers

Before preparation of PUR composites, a series of selected boron fillers were irradiated with thermal neutrons (fluence $\sim 1.5 \times 10^{13}$ n/cm^2) and studied with infrared, Raman spectroscopies, and thermal analysis [75–78] using an experimental setup and approach similar to that presented in previous studies on neutron treatment of carbon materials [79–82]. Hexagonal boron nitride (h-BN) having average particle size around 1 μm was used in our study [75]. Unfortunately, ^{14}N has low neutron cross section of only 1.84 barn and hence, the really effective neutron shielding activity is displayed only by 43.57% boron content in h-BN. This filler once treated with a thermal ($E \leq 0.5$ eV) and epithermal $0.5 \leq E \leq 500$ keV neutron field is sensitive to neutron damage as detected by both FT-IR and ESR (electron spin resonance) spectroscopies. Furthermore, neutron damaged h-BN shows new Raman line due to cubic boron nitride (c-BN) and due to cross-linking between the h-BN layers [75]. Thermal annealing of neutron damaged h-BN causes the release of Wigner energy due to recombination of defective structures. Boron carbide is commonly represented with the minimal formula B_4C. However, Cataldo et al. [76] have discussed that it is better to represent boron carbide with the minimal formula $B_{12}C_3$. In fact, the icosahedral structure of elemental boron is retained in boron carbide under the form of a β-rhombohedral boron unit cell and a BCC, CBC, or CCC interstitial chain in discrete B_{12} icosahedra. The most astonishing character of $B_{12}C_3$ is its self-healing properties under corpuscular radiation damage. In fact, even when heavily damaged by neutron treatment, it still shows a crystalline X-ray diffraction band pattern. However, both DSC analysis of neutron-damaged $B_{12}C_3$ and ESR spectroscopy show a dependence of the stored Wigner energy as well as the paramagnetic signal intensity on the neutron dose [76].

Amorphous boron powder having particle size ≤ 1 μm was neutron treated as in the case of h-BN and $B_{12}C_3$. However, being amorphous, it was quite impossible to get evidences of the neutron damage.

Boric acid is a quite popular and easily accessible filler in certain composites designed as neutron shields, mainly based on PE. However, boric acid is reactive with isocyanates and when incorporated into polytetrahydrofuran polyol and cross-linked with 1,1-diphenylmethane diisocyanate polyol prepolymer and tolylene diisocyanate, it gives a foamy composite, which tends on time to set into a hard sponge [83]. Thus, the side reaction of H_3BO_3 with isocyanates hinder the adoption of boric acid in PUR nanocomposites for radiation shielding. We then focused our attention toward a lithium salt of boric and oxalic acid known as LiBOB, i.e., lithium bis(oxalate)borate, which is used as electrolyte in certain energy storage devices. LiBOB is mixable with polyol prepolymer and does not interfere with the cross-linking of isocyanate groups, thus it is ideal to circumvent all the drawbacks presented by H_3BO_3. However, the neutron bombardment of pure LiBOB [77] has shown that this salt is heavily and easily damaged by corpuscular radiation as easily evidenced by infrared, Raman, and ESR spectroscopies. In addition, the LiBOB decomposition involves the release of CO_2 as a consequence of oxalate decomposition and formation of free H_3BO_3. Thus, LiBOB does not appear to be a suitable filler for neutron shield composites.

There are other two important aspects of boron fillers (and fillers in general) employed for neutron shielding. These fillers must be free from impurities which may be activated by the neutron field so that in front of an effective neutron shielding there is an unexpected induced radioactivity. The second aspect is with regard to particle size and particle size distribution, tendency of the filler particles to clump together, and incompatibility with the polymer matrix. All these parameters must be accurately evaluated as well as the uniformity of the filler dispersion in the polymer matrix to avoid the unwanted phenomena of "radiation channeling." In fact, particle clumping, incompatibility with the polymer matrix, and poor filler dispersion in the matrix may create undesired inhomogeneities in filler distribution so that once the shield in "cutting" a neutron field, thin neutron beams can filter through the shield giving rise to the radiation channeling phenomenon.

10.7 Evaluation of the boron-filled PUR composites as neutron radiation shields

This section is an illustration and a summary of the measurements we have made with our PUR shields loaded with 20% by weight of amorphous boron, $B_{12}C_3$, h-BN, or milled graphite (as reference).

The polyether-polyurethane (PUR) composites were prepared by loading the filler into the polytetrahydrofuran polyol, mixing thoroughly with a large spatula until complete filler incorporation and then pouring the second component, i.e., the 1,1-diphenylmethane diisocyanate polyol prepolymer into the mixture with the filler. Once completed the mixing and homogenization of the three components, the mixture was poured into a 12 × 12 cm square silicon template (in general it works also with an Al template and enameled steel). The compound was left to cure at room temperature for a couple of days before removal from the template as free-standing foil of 2 mm thickness.

For each compound, the typical composition by weight was as follows: 56% of polytetrahydrofuran polyol, 20%–21% of filler, and 23% of 1,1-diphenylmethane diisocyanate polyol prepolymer. The following samples were prepared:

Shield A consisting of PUR loaded with 20.4% by weight of amorphous boron.

Shield B consisting of PUR loaded with 21.9% by weight of boron carbide.

Table 10.1 Shield B; PUR loaded with 21.9% by weight of boron carbide.

Copper wire id	"Sandwich" thickness (cm)	Specific activity at saturation (Bq/g)	Attenuation factor $[I_x]/[I_0]$
CB1 (rif.)	0.000	11.1 ± 0.6	–
CB2	0.317 ± 0.005	0.59 ± 0.03	0.053 ± 0.005
CB3	0.585 ± 0.005	0.10 ± 0.01	0.009 ± 0.001
CB4	0.875 ± 0.005	0.05 ± 0.01	0.005 ± 0.001
CB5	1.161 ± 0.005	<0.01	–

Shield C consisting of PUR loaded with 20.9% by weight of boron nitride.

Shield D consisting of PUR loaded with 20.4% by weight of graphite.

Reference shield consisting of pure PUR foil without any filler

The irradiation was performed in the thermal column of the research reactor TRIGA Mark II at LENA of University of Pavia [84]. The position inside the thermal column employed for the irradiation (next to the BORAL shielding window) presents an integral neutron flux $1.2 \times 10^9\ \mathrm{cm}^{-2}\ \mathrm{s}^{-1}$ with the energy spectrum reported in Table 10.1 [85].

As reference, a copper wire of certified purity 99.99% was first neutron irradiated in the thermal column. The copper neutron treatment makes the copper wire radioactive due to the formation of ^{64}Cu radionuclide. Without any shielding at the selected neutron fluence the copper wire reaches a reference activity in 3 h 30 min irradiation. Afterwards, a series of similar copper wires 99.99% pure were sandwiched between the composite material (see Fig. 10.1) and irradiated in the thermal column with the same neutron spectra and neutron fluence always given at the nominal thermal power of 250 kW in 3 h 30 min. Because of the different thickness and shielding effectiveness of the shielding material, the activity level of the activated copper wires due to the radionuclide ^{64}Cu was found reduced by a certain factor with respect to the activity level achieved by the reference naked copper wire. Through these activity attenuation data were measured on the copper wires, following a procedure reported by Alloni et al. [86].

For high-energy radiation fields of indirectly ionizing radiation, such as gamma and neutron radiation, the linear attenuation coefficient μ of a material is defined as the radiation interaction probability of per path unit:

$$[I_x] \cdot [I_0]^{-1} = \exp\left(-\mu/\rho\right) \tag{10.5}$$

where

$I_{0,}$ intensity of the radiation field outside the shield,

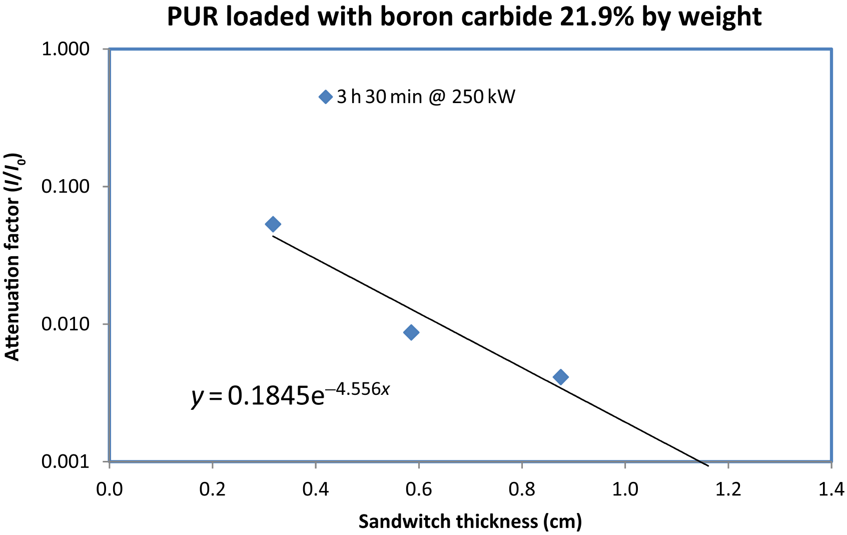

Fig. 10.1 The linear attenuation coefficient of PUR filled with 21.9% by weight of boron carbide was determined from the above graph and found $\mu \sim 4.56\ \text{cm}^{-1}$. Since the density of the PUR composite with boron was measured to be $0.99 \pm 0.07\ \text{g/cm}^3$, the mass attenuation coefficient was determined as $\mu/\rho \sim 4.61\ \text{cm}^2/\text{g}$.

$I_{x,}$ intensity of the radiation field after a shield of thickness x (cm),
μ, linear attenuation coefficient (cm^{-1}).

In order to compare the linear attenuation coefficients of different materials, we have introduced [62, 63] the mass attenuation coefficient μ/ρ (expressed in cm^2/g) with ρ being the density of the PUR composites.

As a first step the neutron attenuation provided by the reference PUR foil without any filler was determined. The results of such blank measurements were already reported in the previous work [62, 63]. For the determination of μ in the unfilled PUR, foils of increasing thickness were exposed to the neutron field [62, 63]. The increase in thickness of the radiation shield was achieved simply by overlapping PUR foils and irradiating the copper wire in the shield, measuring the activation by gamma spectrometry, and calculating the specific activity at saturation [62, 63].

From the experimental data regarding the activity of the copper wire and knowing that the total neutron fluence delivered to the samples in 3.5 h was $1.51 \times 10^{13}\ \text{n/cm}^2$, the attenuation factor $[I_x] \cdot [I_0]^{-1}$ specific for reference unfilled PUR was determined [62, 63]. The attenuation factor of the unfilled PUR shield was then plotted against the thickness of the shield. The data were fitted with an exponential law and the linear attenuation

Table 10.2 Shield D; PUR loaded with 20.4% by weight of graphite.

Copper wire id	"Sandwich" thickness (cm)	Specific activity at saturation (Bq/g)	Attenuation factor $[I_x]/[I_0]$
G1 (rif.)	0.000	21.2 ± 1.0	–
G2	0.270 ± 0.005	19.2 ± 1.0	0.91 ± 0.05
G3	0.552 ± 0.005	14.7 ± 0.7	0.70 ± 0.03
G4	0.987 ± 0.005	9.7 ± 0.5	0.46 ± 0.02
G5	1.045 ± 0.005	5.7 ± 0.3	0.27 ± 0.01

coefficient of unfilled PUR $\mu = 1.89\ \text{cm}^{-1}$ was determined. Since the density of the unfilled PUR composite was found at $1.00 \pm 0.04\ \text{g/cm}^3$, the mass attenuation coefficient of unfilled and reference PUR was found to be $\mu/\rho = 1.89\ \text{cm}^2/\text{g}$ [62, 63].

To illustrate the procedure for the determination of the linear attenuation coefficient of the PUR composite, the following part of this section is dedicated to the determination of μ and μ/ρ for the PUR composites filled with 21.9% by weight of boron carbide (see Table 10.1 for the experimental data regarding the activation of the copper wire till saturation and the resulting attenuation factor) and with 20.4% by weight of graphite (see Table 10.2 for the relative experimental data).

In Fig. 10.1 the data from Table 10.1, i.e., attenuation factors measured on PUR filled with 21.9% of boron carbide were graphed as a function of the shield thickness. The data were fitted according to the exponential law, yielding a linear attenuation coefficient of $\mu = 4.56\ \text{cm}^{-1}$. Since the density of the PUR composite with 21.9% content of boron carbide was found at $0.99 \pm 0.07\ \text{g/cm}^3$, the mass attenuation coefficient of boron carbide filled PUR was found to be $\mu/\rho = 4.61\ \text{cm}^2/\text{g}$.

Similarly, in Fig. 10.2 the experimental data from Table 10.2, i.e., attenuation factors measured on PUR filled with 20.4% of graphite were graphed as a function of the shield thickness. The data were fitted according to the exponential law, yielding a linear attenuation coefficient of $\mu = 1.52\ \text{cm}^{-1}$. Since the density of the PUR composite with 20.4% content of graphite was found at $1.03 \pm 0.03\ \text{g/cm}^3$, the mass attenuation coefficient of graphite filled PUR was found to be $\mu/\rho = 1.47\ \text{cm}^2/\text{g}$.

In Table 10.3 a complete summary of all the linear and mass attenuation coefficients determined both in the previous and in the present study is reported. For an easier comparison with the reference value of unfilled PUR, μ and μ/ρ were indexed making 100 the values found on the unfilled PUR. Thus, shield A with amorphous boron is 3.1 times more efficient as

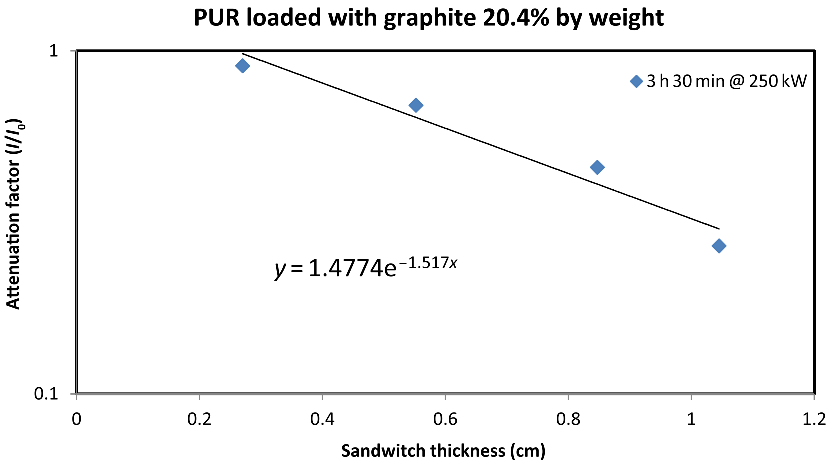

Fig. 10.2 The linear attenuation coefficient of PUR filled with 20.4% by weight of graphite was determined from the above graph and found $\mu \sim 1.52\ \mathrm{cm}^{-1}$. Since the density of the PUR composite with boron was measured to be $1.03 \pm 0.03\ \mathrm{g/cm}^3$, the mass attenuation coefficient was determined as $\mu/\rho \sim 1.48\ \mathrm{cm}^2/\mathrm{g}$.

mass shield against thermal neutrons than reference, shield B filled with B_4C is 2.44 times more efficient thermal neutron shield than reference unfilled PUR. In its turn, shield C loaded with BN is 1.78 times more efficient than reference. Since the boron amount in BN is only 43.6% of the filler, the real boron load on shield C is only 9.1%. Consequently, the μ/ρ value of shield C is reduced roughly to about half the μ/ρ value of shield A with 20.4% amorphous boron. Finally shield D composed of PUR filled with graphite does not show any shielding properties against thermal neutrons as expected, since elemental carbon does not have a high neutron capture cross section as in the case of elemental boron.

Another approach to visualize the effectiveness of the various composites in cutting the thermal neutron field is reported in Table 10.4. The experimental mass attenuation coefficient determined for each composite, i.e., the μ/ρ values are introduced into Eq. (10.1) and the resulting exponential is multiplied by I_0, intensity of the radiation field outside the shield, a value of $1.5 \times 10^{13}\ \mathrm{n/cm}^2$.

With this calculation the neutron fluence I_x for the unitary shield thickness of each composite is determined and presented in Table 10.4. Then the neutron attenuation index (NAI) is determined simply by the ratio:

$$\mathrm{NAI} = [I_0] \cdot [I_x]^{-1} \tag{10.6}$$

Table 10.3 Summary linear and mass attenuation coefficient of PUR composites.

		ρ (g/cm^3)	μ (cm^{-1})	μ/ρ (cm^3/g)	μ (index)	μ/ρ (index)	Reference
Ref PUR	Unfilled PUR	1.00	1.89	1.89	100	100	[62]
Shield A	PUR with 20.4% amorph. boron	0.72	4.23	5.88	224	311	[62]
Shield B	PUR with 21.9% B_4C	0.99	4.56	4.61	241	244	[63]
Shield C	PUR with 20.9% BN	1.02	3.44	3.37	182	178	[75]
Shield D	PUR with 20.4% graphite	1.03	1.52	1.48	80	78	[63]

Table 10.4 Effectiveness of the composites in shielding the neutron flux.

Composite material	μ/ρ (cm^2/g)	Neutron fluence 3.5 h (n/cm^2) behind the shield	Neutron attenuation (index)	Composite nucl. cross section in barn (10^{-28} m^2)
Neutron fluence in 3,5 h [I_0]	N.a.	1.51×10^{13}	1	0.0
unfilled PUR	1.89	2.28×10^{12}	7	0.1
PUR 20.4% amorph. B	5.87	4.27×10^{10}	354	155
PUR 21.9% B_4C	4.61	1.50×10^{11}	100	130
PUR 20.9% BN	3.37	5.20×10^{11}	29	69
PUR 20.4% Graphite	1.48	3.44×10^{12}	4	0.08

The resulting NAI values are reported in Table 10.4 and can be read as follows. A NAI = 7 as in the case of unfilled PUR, which means that the unfilled PUR is able to cut the thermal neutron radiation field by one-seventh of its original value. Consequently, Table 10.4 reports that the PUR composite filled with amorphous boron reduces to 1/354 of the neutron radiation field, while the composite filled with B_4C is effective in reducing the thermal neutrons field to 1/100. As already commented, the PUR composite filled with BN is much less effective than other composites which are benefitting from a larger boron content. In the latter case the neutron field is reduced by 1/29.

Using the nuclear cross section value σ for thermal neutron capture of natural mixture of isotopes of all elements composing the PUR composites under study [62,63], it is possible to estimate the cross section of each composite in barn. The results of such estimations are reported in Table 10.4. As expected the highest cross section for neutron capture is attributed to the amorphous boron-filled composite, which is the most effective thermal neutron shield, followed by B_4C and then by the BN. The graphite-filled PUR composite is characterized by a cross section for thermal neutrons capture which is even lower than that of pure unfilled PUR (which is richer in hydrogen than the former). In fact, nuclear cross section of natural hydrogen is 0.3326 versus 0.0035 barn of graphite. Thus, 20% graphite causes a reduced neutron cross section as presented in Table 10.4.

Consequently, the PUR composite loaded with graphite was found more "transparent" to a thermal neutrons field (attenuation 1/4) than the case of unfilled and reference PUR (attenuation 1/7). Fig. 10.3 shows a

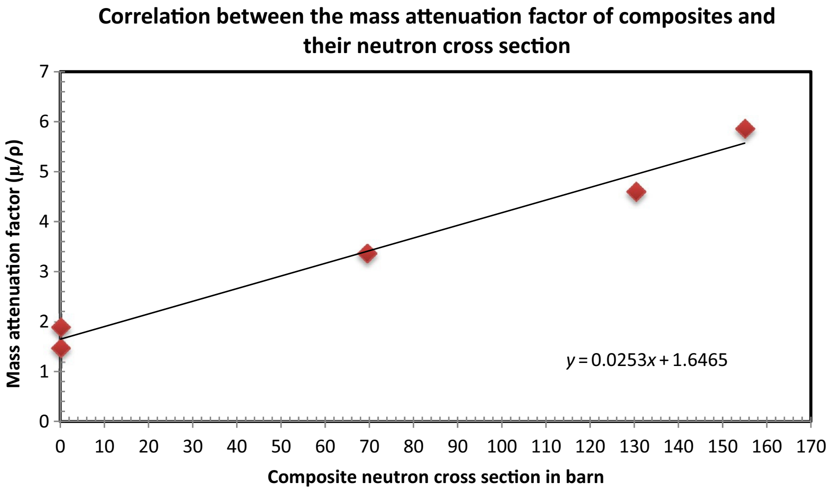

Fig. 10.3 Linear correlation between the mass attenuation coefficient μ/ρ and the calculated thermal neutrons cross section of the composites *(Data from Table 10.4.)*

linear correlation between the experimental mass attenuation coefficient μ/ρ and the neutron cross section of our composites so that.

$$\mu/\rho = 0.0253\,\sigma + 1.6454 \tag{10.7}$$

10.8 Summary and conclusions

The forthcoming manned space exploration missions toward the Moon, Mars, and asteroids are all deep space missions because these are conducted outside the protective shield of the Earth's magnetic field. In this chapter, the problems connected with the radiation hazard to the crews involved in such missions have been addressed. Essentially, it is possible to distinguish between acute and chronic radiation hazard. The former may occur during SPE phenomena (Solar Particle Events), for example, when the sun is at its maximum in the 11-year solar cycles. On the other hand, the chronic radiation exposure is either due to the normal solar wind or due to galactic cosmic ray (GCR) exposure. Particular emphasis is placed on the hazard due to relativistic particles and especially due to HZE particles, i.e., high atomic number and high-energy nuclei essentially representing a minor component of the GCR but also represent a major hazard for the crew. In fact, when relativistic protons or HZE particles impinge on thin targets as could be the walls of a spacecraft or a thick target as could be a regolith composite of a Lunar base, a spallation reactions occur in the target with the formation of secondary particles directed toward the inside of the spacecraft or the lunar or mars base facility. In these conditions the secondary particles are all relativistic particles and consist of atomic nuclei having Z lower than the target nuclei, accompanied by an avalanche of protons and neutrons. Especially in thick target the secondary nuclei are stopped and protons can experience both simple capture and capture with the emission of γ quanta. However, above a certain energy threshold also protons produce secondary neutrons by interaction with the target matter. Thus, a problem for the crew in the spacecraft or inside the base is due to the neutron flux which contribute significantly to the crew radiation dose.

It is therefore necessary to think about neutron radiation shields to be used inside the spacecraft and inside the Lunar or Martian bases. Recent studies have shown that it is advisable that these shields must be based on hydrogen-rich polymer matrix to maximize the neutron thermalization effect but also to slowdown effectively the other secondary particles, i.e., protons and low-Z nuclear fragments. Consequently, it has been found that a certain number of different polymers could be used as matrices for these shields. Furthermore, the thermalized neutrons should be removed by a neutron capture process by using as fillers in the composites, nuclei with high thermal neutrons absorption cross section. The best compromise in terms of neutron absorption cross section and cost can be found on boron and boron compounds.

Instead of focusing on classic hydrogen-rich polymer matrix like PE, our recent work was directed toward the preparation of neutron radiation shield based on polyurethane (PUR) composites. The advantage of PUR over PE and other more common polymer matrix was discussed in the chapter. In summary, it has been found that PUR, if adequately formulated, can have an excellent radiation resistance. For instance, our preference was toward polyether-polyurethane type composite, which can yield flexible and elastic composites, with excellent mechanical properties which can exceed by far those of a PE composite. Furthermore, our polyether-polyurethane matrix was based on a polyol known as polytetrahydrofuran, derived from completely renewable sources and this is in remarkable contrast to any other polymer composite for neutron radiation shielding which was prepared using polymer matrix derived from fossil fuels. Another feature of our PUR composite was the excellent compatibility with the amorphous boron filler as well as the other boron compounds tested, i.e., boron carbide ($B_{12}C_3$) and hexagonal boron nitride (h-BN). Excellent compatibility was also found with graphite filler, used as reference.

The last part of our chapter deals with the experimental results on the PUR shields prepared with the mentioned boron fillers, using thermal neutrons. In terms of thermal neutron radiation shielding of the PUR composites the results are summarized in Tables 10.3 and 10.4. At equal filler loading (about 20% by weight) the best results were achieved with PUR composite loaded with amorphous boron, followed by the composite filled with boron carbide and then with boron nitride. Micronized graphite filler was used as reference shield together with unfilled PUR composite. **ORCID:** Franco Cataldo http://orcid.org/0000-0003-2607-4414.

References

[1] F.H. Attix, Introduction to Radiological Physics and Radiation Dosimetry, John Wiley & Sons, New York, 2008.

[2] J.E. Martin, Physics for Radiation Protection: A Handbook, John Wiley & Sons, New York, 2006.

[3] M.G. Stabin, Radiation Protection and Dosimetry: An Introduction to Health Physics, Springer Science & Business Media, Berlin, 2007.

[4] Y. Song, W. Wu, S. Du, Tokamak Engineering Mechanics, Springer, Berlin-Heidelberg, 2014.

[5] L. Campajola, F. Di Capua, Applications of accelerators and radiation sources in the field of space research and industry, Top. Curr. Chem. 374 (2017) 84 (29 pages).

[6] J.R. Letaw, R. Silberberg, C.H. Tsao, Radiation hazards on space missions outside the magnetosphere, Adv. Space Res. 9 (1989) 285–291.

[7] L. Miroshnichenko, Radiation Hazard in Space, Springer Science & Business Media, New York, 2003.

[8] R.C. Singleterry, Radiation engineering analysis of shielding materials to assess their ability to protect astronauts in deep space from energetic particle radiation, Acta Astronaut. 91 (2013) 49–54.

[9] J. Preston, Board (Eds.), Technical Evaluation of the NASA Model for Cancer Risk to Astronauts due to Space Radiation, The National Academies Press, Washington, DC, 2012. https://doi.org/10.17226/13343.

[10] C.E.H. Scott-Conner, D.R. Masys, C.T. Liverman, National Academies of Sciences, Engineering, and Medicine (Eds.), Review of NASA's Evidence Reports on Human Health Risks: 2016 Letter Report, The National Academies Press, Washington, DC, 2017. https://doi.org/10.17226/23678.

[11] R. Setlow, Board (Eds.), Radiation Hazards to Crews of Interplanetary Missions: Biological Issues and Research Strategies, The National Academies Press, Washington, DC, 1997. https://doi.org/10.17226/5540.

[12] T. Straume, Space radiation effects on crew during and after deep space missions, Curr. Pathobiol. Rep. 6 (2018) 167–175.

[13] F.F. Badavi, D.O. Adams, J.W. Wilson, On the validity of the aluminum equivalent approximation in space radiation shielding applications, Adv. Space Res. 46 (2010) 719–727.

[14] M. Gargaud (Ed.), Encyclopedia of Astrobiology, Springer-Verlag, Berlin, 2011.

[15] S. Aminalragia-Giamini, I. Sandberg, C. Papadimitriou, I.A. Daglis, P. Jiggens, The virtual enhancements—solar proton event radiation (VESPER) model, J. Space Weather Space Clim. 8 (2018) A06 (10 pages).

[16] P. Jiggens, D. Heynderickx, I. Sandberg, P. Truscott, O. Raukunen, R. Vainio, Updated model of the solar energetic proton environment in space, J. Space Weather Space Clim. 8 (2018) A31 (23 pp).

[17] T. Stanev, High Energy Cosmic Rays, Springer-Verlag, Berlin, 2010.

[18] E. Catao, M. Hada, P.B. Saganti, K.A. George, F.A. Cucinotta, Relative biological effectiveness of HZE particles for chromosomal exchanges and other surrogate cancer risk endpoints, PLoS One 11 (2016) e0153998 (17 pages).

[19] M. Hada, L.J. Chappell, M. Wang, K.A. George, F.A. Cucinotta, Induction of chromosomal aberrations at fluences of less than one HZE particle per cell nucleus, Radiat. Res. 182 (2014) 368–379.

[20] J.W. Wilson, J. Miller, A. Konradi, F.A. Cucinotta, Shielding strategies for human space exploration, in: NASA Conference Publication N°3360; Proceedings of a workshop sponsored by the National Aeronautics and Space Administration and held at Lyndon B. Johnson Space Center, Houston, Texas, December 6–8,1995, 1997.

[21] J.W. Wilson, M.S. Clowdsley, J.L. Shinn, R.C. Singleterry, R.K. Tripathi, F.A. Cucinotta, J.H. Heinbockel, F.F. Badavi, W. Atwell, Neutrons in Space: Shield Models and Design Issues (No. 2000-01-2414, 2000), 2000. SAE Technical Paper.

[22] G.R. Choppin, J. Rydberg, Nuclear Chemistry. Theory and Applications, Pergamon Press, Oxford, 1980.

[23] D. Filges, F. Goldenbaum, Handbook of Spallation Research: Theory, Experiments and Applications, Wiley, New York, 2009.

[24] G. Friedlander, J.W. Kennedy, E.S. Macias, J.M. Miller, Nuclear and Radiochemistry, John Wiley & Sons, New York, 1981.

[25] H. Vonach, A. Pavlik, A. Wallner, M. Drosg, R.C. Haight, D.M. Drake, S. Chiba, Spallation reactions in ^{27}Al and ^{56}Fe induced by 800 MeV protons, Phys. Rev. C 55 (1997) 2458–2467.

[26] J.B. Cumming, G. Friedlander, J. Hudis, A.M. Poskanzer, Spallation of aluminum by 28- GeV protons, Phys. Rev. 127 (1962) 950–954.

[27] B.S.P. Shen, M. Merker (Eds.), Spallation Nuclear Reactions and their Applications, D. Riedel Publishing Co, Dordrecht, 1976.

[28] A. Krása, Spallation reaction physics, in: Manuscript for the Lecture "Neutron Sources for ADS" for Students of the Faculty of Nuclear Sciences and Physical Engineering at Czech Technical University, Prague, 2010, pp. 1–61. https://pdfs.semanticscholar.org/ba08/30dcab221b45ca5bcc3cfa8ae82558d624e7.pdf.

[29] I. Leya, R. Michel, Cross sections for neutron-induced reactions up to 1.6 GeV for target elements relevant for cosmochemical, geochemical, and technological applications, Nucl. Instrum. Methods Phys. Res., Sect. B 269 (2011) 2487–2503.

[30] T. Henriksen, H.D. Maillie, Radiation and Health, Taylor & Francis, London, 2003.

[31] C. Zeitlin, T. Cleghorn, F. Cucinotta, P. Saganti, V. Andersen, K. Lee, G. Badhwar, Overview of the Martian radiation environment experiment, Adv. Space Res. 33 (2004) 2204–2210.

[32] C. Zeitlin, D.M. Hassler, F.A. Cucinotta, B. Ehresmann, R.F. Wimmer-Schweingruber, D.E. Brinza, S. Burmeister, Measurements of energetic particle radiation in transit to Mars on the Mars Science Laboratory, Science 340 (2013) 1080–1084.

[33] S. McKenna-Lawlor, P. Gonçalves, A. Keating, G. Reitz, D. Matthiä, Overview of energetic particle hazards during prospective manned missions to Mars, Planet. Space Sci. 63 (2012) 123–132.

[34] T. Straume, T.C. Slaba, S. Bhattacharya, L.A. Braby, Cosmic-ray interaction data for designing biological experiments in space, Life Sci. Space Res. 13 (2017) 51–59.

[35] J.M. DeWitt, E.R. Benton, Y. Uchihori, N. Yasuda, E.V. Benton, A.L. Frank, Assessment of radiation shielding materials for protection of space crews using CR-39 plastic nuclear track detector, Radiat. Meas. 44 (2009) 905–908.

[36] J. Haffner, Radiation and Shielding in Space, Academic Press, New York, 1967.

[37] M. Dole (Ed.), The Radiation Chemistry of Macromolecules, Elsevier, Amsterdam, 2013.

[38] S. Guetersloh, C. Zeitlin, L. Heilbronn, J. Miller, T. Komiyama, A. Fukumura, Y. Iwata, T. Murakami, M. Bhattacharya, Polyethylene as a radiation shielding standard in simulated cosmic-ray environments, Nucl. Instrum. Methods Phys. Res. B 252 (2006) 319–332.

[39] C. Harrison, S. Weaver, C. Bertelsen, E. Burgett, N. Hertel, E. Grulke, Polyethylene/boron nitride composites for space radiation shielding, J. Appl. Polym. Sci. 109 (2008) 2529–2538.

[40] Ş.G. İrim, A.A. Wis, M.A. Keskin, O. Baykara, G. Ozkoc, A. Avcı, M. Dogru, M. Karakoç, Physical, mechanical and neutron shielding properties of h-BN/Gd_2O_3/HDPE ternary nanocomposites, Radiat. Phys. Chem. 144 (2018) 434–443.

[41] J. Jung, J. Kim, Y.R. Uhm, J.K. Jeon, S. Lee, H.M. Lee, C.K. Rhee, Preparations and thermal properties of micro-and nano-BN dispersed HDPE composites, Thermochim. Acta 499 (2010) 8–14.

[42] J. Kim, B.C. Lee, Y.R. Uhm, W.H. Miller, Enhancement of thermal neutron attenuation of nano-B_4C,-BN dispersed neutron shielding polymer nanocomposites, J. Nucl. Mater. 453 (2014) 48–53.

[43] S.M.J. Mortazavi, M. Kardan, S. Sina, H. Baharvand, N. Sharafi, Design and fabrication of high density borated polyethylene nanocomposites as a neutron shield, Int. J. Radiat. Res. 14 (2016) 379–383.

[44] J.W. Shin, J.W. Lee, S. Yu, B.K. Baek, J.P. Hong, Y. Seo, C.M. Koo, Polyethylene/boron-containing composites for radiation shielding, Thermochim. Acta 585 (2014) 5–9.

[45] E.E. Belgin, G.A. Aycik, Preparation and radiation attenuation performances of metal oxide filled polyethylene based composites for ionizing electromagnetic radiation shielding applications, J. Radioanal. Nucl. Chem. 306 (2015) 107–117.

[46] C.S. Cummings, E.M. Lucas, J.A. Marro, T.M. Kieu, J.D. DesJardins, The effects of proton radiation on UHMWPE material properties for space flight and medical applications, Adv. Space Res. 48 (2011) 1572–1577.

[47] W.H. Zhong, G. Sui, S. Jana, J. Miller, Cosmic radiation shielding tests for UHMWPE fiber/nano-epoxy composites, Compos. Sci. Technol. 69 (2009) 2093–2097.

[48] M.M. Abdel-Aziz, S.E. Gwaily, A.S. Makarious, A.E.S. Abdo, Ethylene-propylene diene rubber/low density polyethylene/boron carbide composites as neutron shields, Polym. Degrad. Stab. 50 (1995) 235–240.

[49] W. Huang, W. Yang, Q. Ma, J. Wu, J. Fan, K. Zhang, Preparation and characterization of γ-ray radiation shielding $PbWO_4$/EPDM composite, J. Radioanal. Nucl. Chem. 309 (2016) 1097–1103.

[50] T. Özdemir, I.K. Akbay, H. Uzun, I.A. Reyhancan, Neutron shielding of EPDM rubber with boric acid: mechanical, thermal properties and neutron absorption tests, Prog. Nucl. Energy 89 (2016) 102–109.

[51] T. Özdemir, A. Güngör, İ.A. Reyhancan, Flexible neutron shielding composite material of EPDM rubber with boron trioxide: mechanical, thermal investigations and neutron shielding tests, Radiat. Phys. Chem. 131 (2017) 7–12.

[52] A.K. Mheemeed, H.I. Hasan, F.M. Al-Jomaily, Gamma-ray absorption using nitrile rubber—lead mixtures as radiation protection shields, J. Radioanal. Nucl. Chem. 291 (2012) 653–659.

[53] S.E. Gwaily, M.M. Badawy, H.H. Hassan, M. Madani, Natural rubber composites as thermal neutron radiation shields: I. B_4C/NR composites, Polym. Test. 21 (2002) 129–133.

[54] S.E. Gwaily, M.M. Badawy, H.H. Hassan, M. Madani, Natural rubber composites as thermal neutron radiation shields: II H_3BO_3/NR composites, Polym. Test. 21 (2002) 513–517.

[55] S.E. Gwaily, M.M. Badawy, H.H. Hassan, M. Madani, Influence of thermal aging on crosslinking density of boron carbide/natural rubber composites, Polym. Test. 22 (2003) 3–7.

[56] N.A. Shaltout, Effect of electron beam irradiation and degree of boric acid loading on the properties of styrene-butadiene rubber, React. Funct. Polym. 69 (2009) 229–233.

[57] H. Chai, X. Tang, M. Ni, F. Chen, Y. Zhang, D. Chen, Y. Qiu, Preparation and properties of flexible flame-retardant neutron shielding material based on methyl vinyl silicone rubber, J. Nucl. Mater. 464 (2015) 210–215.

[58] A.E.S. Abdo, M.A. El-Sarraf, F.A. Gaber, Utilization of ilmenite/epoxy composite for neutrons and gamma ray attenuation, Ann. Nucl. Energy 30 (2003) 175–187.

[59] A.M. Sukegawa, Y. Anayama, K. Okuno, S. Sakurai, A. Kaminaga, Flexible heat resistant neutron shielding resin, J. Nucl. Mater. 417 (2011) 850–853.

[60] A. Emmanuel, J. Raghavan, Influence of structure on radiation shielding effectiveness of graphite fiber reinforced polyethylene composite, Adv. Space Res. 56 (2015) 1288–1296.

[61] N.A. Galehdari, A.D. Kelkar, Effect of neutron radiation on the mechanical and thermophysical properties of nanoengineered polymer composites, J. Mater. Res. 32 (2017) 426–434.

[62] F. Cataldo, M. Prata, New composites for neutron radiation shielding, J. Radioanal. Nucl. Chem. 320 (2019) 831–839.

[63] F. Cataldo, M. Prata, Neutron radiation shielding with PUR composites loaded with B_4C or graphite, Fuller. Nanotub. Carbon Nanostruct. 27 (2019) 531–537.

[64] M. Szycher (Ed.), Szycher's Handbook of Polyurethanes, CRC press, Boca Raton, FL, 2012.

[65] K.J. Zeitsch, The Chemistry and Technology of Furfural and its Many by-Products, Elsevier, Amsterdam, 2000.

[66] M. Wloch, J. Datta, Nonisocyanate polyurethane, in: S. Thomas, J. Datta, J.T. Haponiuk, A. Reghunadhan (Eds.), Polyurethane Polymers: Blends and Interpenetrating Networks, Elsevier, Amsterdam, 2017 (Chapter 7).

[67] A.K. Bhowmick, H. Stephens (Eds.), Handbook of Elastomers, Boca Raton, FL, CRC Press, 2001, p. 405.

[68] K. Gorna, S. Gogolewski, The effect of gamma radiation on molecular stability and mechanical properties of biodegradable polyurethanes for medical applications, Polym. Degrad. Stab. 79 (2003) 465–474.

[69] Q. Tian, E. Takács, I. Krakovský, Z. Horváth, L. Rosta, L. Almásy, Study on the microstructure of polyester polyurethane irradiated in air and water, Polymers 7 (2015) 1755–1766.

[70] A. Dannoux, S. Esnouf, J. Begue, B. Amekraz, C. Moulin, Degradation kinetics of poly (ether-urethane) Estane® induced by electron irradiation, Nucl. Instrum. Methods Phys. Res. B 236 (2005) 488–494.

[71] M. Walo, G. Przybytniak, K. Łyczko, M. Piątek-Hnat, The effect of hard/soft segment composition on radiation stability of poly(ester-urethane)s, Radiat. Phys. Chem. 94 (2014) 18–21.

[72] H. Wei, J. Xiong, X. Chen, X. Gao, Y. Xu, Y. Fu, Study on the radiation degradation of polyether-polyurethane induced by electron beam, J. Radioanal. Nucl. Chem. 274 (2007) 525–530.

[73] T.W. Kim, S.K. Kim, S. Park, K.H. Park, J.M. Lee, Effect of irradiation on the cryogenic mechanical characteristics of polyurethane foam, J. Radioanal. Nucl. Chem. 317 (2018) 145–159.

[74] H. Sui, X. Liu, F. Zhong, X. Li, B. Wang, X. Ju, Relationship between free volume and mechanical properties of polyurethane irradiated by gamma rays, J. Radioanal. Nucl. Chem. 300 (2014) 701–706.

[75] F. Cataldo, S. Iglesias-Groth, Neutron damage of hexagonal boron nitride: H-BN, J. Radioanal. Nucl. Chem. 313 (2017) 261–271.

[76] F. Cataldo, S. Iglesias-Groth, Y. Hafez, Neutron bombardment of boron carbide $B_{12}C_3$: A FT-IR, calorimetric (DSC) and ESR study, Fuller. Nanotub. Carbon Nanostruct. 25 (2017) 371–378.

[77] F. Cataldo, S. Iglesias-Groth, M. Prata, Neutron bombardment of lithium bis (oxalato) borate: LiBOB, Fuller. Nanotub. Carbon Nanostruct. 313 (2017) 239–247.

[78] S. Pascale, E. Scatena, F. Fabbri, F. Cataldo, Morphological and structural properties of neutron-irradiated $B_{12}C_3$ boron carbide microcrystals, Fuller. Nanotub. Carbon Nanostruct. 25 (2017) 585–588.

[79] F. Cataldo, O. Ursini, G. Nasillo, E. Caponnetti, M. Carbone, F. Valentini, G. Palleschi, T. Braun, Thermal properties, Raman spectroscopy and TEM images of neutron-bombarded graphite, Fuller. Nanotub. Carbon Nanostruct. 21 (2013) 634–643.

[80] F. Cataldo, G. Angelini, Z. Revay, E. Osawa, T. Braun, Wigner energy of nanodiamond bombarded with neutrons or irradiated with γ radiation, Fuller. Nanotub. Carbon Nanostruct. 22 (2014) 861–865.

[81] F. Cataldo, S. Iglesias-Groth, Y. Hafez, G. Angelini, Neutron bombardment of single wall carbon nanohorn (SWCNH): DSC determination of the stored Wigner-Szilard energy, J. Radioanal. Nucl. Chem. 299 (2014) 1955–1963.

[82] S. Iglesias-Groth, F. Cataldo, Y. Hafez, Neutron bombardment of C_{60} and C_{70} fullerenes: a spectroscopic and calorimetric study, Fuller. Nanotub. Carbon Nanostruct. 24 (2016) 547–554.

[83] N. Leventis, C. Sotiriou-Leventis, A.M. Saeed, S. Donthula, H. Majedi Far, P. M. Rewatkar, G. Churu, Nanoporous polyurea from a triisocyanate and boric acid: a paradigm of a general reaction pathway for isocyanates and mineral acids, Chem. Mater. 28 (2015) 67–78.

[84] M. Prata, D. Alloni, P. De Felice, M. Palomba, A. Pietropaolo, M. Pillon, L. Quintieri, A. Santagata, P. Valente, Italian neutron sources, Eur. Phys. J. Plus 129 (2014) 255 (15 pages).

[85] N. Protti, S. Bortolussi, M. Prata, P. Bruschi, S. Altieri, D. Nigg, Neutron spectrometry for the University of Pavia TRIGA™ thermal neutron source facility, Trans. Am. Nucl. Soc. 107 (2012) 1269–1272.

[86] D. Alloni, A.B. di Tigliole, J. Bruni, M. Cagnazzo, R. Cremonesi, G. Magrotti, F. Oddone, A. Panza, M. Prata, A. Salvini, Neutron flux characterization of the SM1 sub-critical multiplying complex of the Pavia University, Prog. Nucl. Energy 67 (2013) 98–103.

CHAPTER 11

Functional characterization of neutron-shielding materials

H.L. Swami, C. Danani, R. Srinivasan
Institute for Plasma Research, Gandhinagar, India

11.1 Introduction

Various shielding materials are playing a vital role in the development and operation of nuclear reactors and facilities [1–6]. The flexible shield materials are also used widely for space application where radiation environment is dominated. The applicability of shield materials in radiation facilities is very vast, such as medical radiation facilities, laboratory-based neutron generators, compact neutron generators, etc. [5–10]. The shield materials which are good for compact shield design, are used in radiation therapy facilities. The radiation shield phenomena can be better understood by the nature of particles and the nature of materials.

There are three kinds of basic nuclear particles or radiation, i.e., gamma rays, neutrons and charged particles [1–3, 11]. The radiations have specific nature of interaction with materials like gamma rays attenuate and transfer their energy through photoelectric and compton scattering whereas neutrons have various kinds of nuclear interactions such as elastic scattering, inelastic scattering, and transmutation process. Neutrons change the nuclide through transmutation process. And, charge particles interact through an electronic process. They lose their energy through radiation.

The behavior of neutron during interaction varies with nuclide, and it depends on the neutron interaction probability. The interaction probability is defined as a nuclide cross section available for a particular reaction. It is expressed in units of area (cm^2). The cross section depends on the nuclei internal structure and incident neutron energy. It plays an important role in nuclear shielding material design and development. Therefore, the elements or nuclides having the affinity of the capturing, absorbing, and attenuating neutrons in large capacity are considered in the composition of neutron-shielding materials [11]. As mentioned that neutron cross section depends on the energy of incident neutron, neutron-shielding

Micro and Nanostructured Composite Materials for Neutron Shielding Applications
https://doi.org/10.1016/B978-0-12-819459-1.00011-8
© 2020 Elsevier Ltd.
All rights reserved.

materials also have their specific objective to be fulfilled. Few materials are developed for thermal neutrons whereas few are made for fast neutron attenuation [1–5, 11].

The developed materials should be tested and evaluated for their application before their commercial application. The neutron shield capability testing of the materials is part of their development procedure. The neutron-shielding characterization of materials assures their objective of development. The capability of shielding is predicated by using the simulation and numerical methods at the time of design and development. Once the material is developed, the physical verification of the shielding efficiency is performed using active neutron source through experiments. However, the experiments are very expansive and cannot be processed iteratively. The simulation process helps enormously in the development of shielding materials. The iterative process of simulation can be done to get the best optimized shielding composition.

The realistic functional characterization experiment is necessary for material testing and has to be conducted in the facility as per the application of the developed material. The experimental designs for the evaluation of the shielding function are challenging. The design becomes more complicated where the available neutron source does not directly belong to functional zone of materials. In such a case, the neutron energy spectrum of the source has to be optimized to get the expected energy range. There are several diagnostics available to measure the neutrons as per their energy ranges. Some diagnostics work only for thermal energy range like ^{3}He, BF3 gas detectors whereas some measures fast neutrons such as proton recoil scintillators [12].

The chapter describes the detailed evaluation of the shielding capability of materials developed for various neutron-shielding applications. Shielding characterization techniques are described in Section 11.2. The section comprises the importance of elemental compositions, numerical method, and experimental procedure of neutron-shielding characterization. The complexities of the experiment as well as the easiness of numerical technique for the evaluation of shielding capability are explained in detail.

The shielding characterization depends on the neutron sources because the application of the developed materials is varied. The details of the various neutron sources which are required for the material evaluation are given in Section 11.3.

The measurement of shielding efficiency has to be done by neutron detectors. It is also necessary as a neutron source. The details of various neuron detectors are given in Section 11.4. The conclusive remarks on the shielding characterization of the materials are provided in Section 11.5.

11.2 Neutron-shielding characterization

The shielding efficiency of materials is characterized through the attenuation and absorbing capability estimations. The experiments are the well-established method for shielding estimation using the active neutron source and by measuring the outgoing neutrons against the incoming neutrons. The ratio of outgoing and incoming neutrons gives the attenuation efficiency of the material for a particular thickness. However, the experiments provide only details of macroscopic phenomena in terms of attenuation through a bulk material. In order to understand the microscopic physics, the numerical simulation of the attenuation process plays a significant part. It includes the microscopic cross section of each element for various types of interaction which contributes to neutron absorption and attenuation. The estimation of neutron shielding using numerical techniques can be understood through the simple schematic representation of neutron interaction shown in Fig. 11.1. The specific energy neutron falls on the material and the reaction with medium occurs as per the probability of interaction.

Neutron may lose its energy through elastic scattering and come out of the material with low energy. Elastic scattering of a neutron is similar to classic collision of two mass balls where one ball transfers its energy to other. If the masses of both are equal then it transfers half of its energy to other.

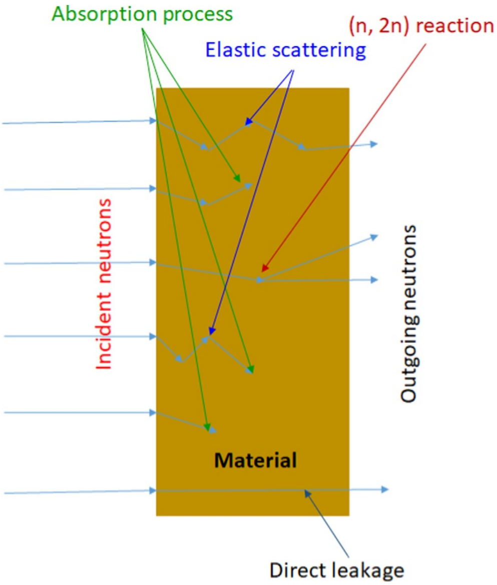

Fig. 11.1 Neutron interaction processes.

Thus, the elastic scattering cross sections of low-atomic weight elements are more because the atomic weight of neutron is almost equal to hydrogen atom. There is also a probability of direct absorption in the material. It eliminates the incident neutron and the atom of the material is transmuted in some other nuclei through the emission of charged particles or photons. The absorption process mainly happens with low-energy neutrons and high mass number elements. However, few isotopes like boron and cadmium have a high cross section of thermal neutron absorption. There is also a probability of increase in low-energy neutrons via (n, xn) reaction. In this process, the interacting atomic nuclide captures the incident neutron and emits two or more neutrons. The interacting nuclide is transmuted in some other nuclei through the process. Neutron multiplication kind of reaction happens mainly with high mass number elements except few such as beryllium. It is also possible that some neutrons come out without interacting with the material which is a direct leakage of the incident neutron as shown in Fig. 11.1. It happens because the probability of interaction is limited and there is always a chance that few neutrons skip out the medium without interaction. This phenomenon is more visible for high-energy neutrons [1–3, 11].

The neutron shielding cannot be predicated only through the absorption of the neutrons. The elastic scattering is also equally important to reduce the energy of neutrons and make it prominent for materials to absorb it. The account of the intermediately produced neutrons through multiplication reactions is also needed to get the actual shielding capability of material. Sometimes multiplication reaction is also useful to make the initial reduction in fast neutrons energy because emitting neutrons have less energy than the incident. Direct leakage is not good in the case of neutron shielding and should be reduced by enhancing more elastic and inelastic scatterings in the materials.

In order to estimate the overall attenuation, it is required to include all interactions and terms of elimination or removal. The diffusion of neutrons in the material also needs to account to get the actual built-up of neutrons in the material. The neutron interaction process phenomena are illustrated in Fig. 11.1. It is included to understand the numerical estimation of attenuation and shielding capability of the materials. Each process shown in Fig. 11.1 is represented by their microscopic cross section. The cumulative effect of microscopic phenomena is included in the macroscopic cross section which can easily represent the attenuation of neutrons. The microscopic cross sections, macroscopic cross sections and their role in estimating the shielding capability are explained in the following sections. The experimental technique of measuring the shielding capability is also described in following sections.

11.2.1 Importance of elemental composition of materials

The elemental composition of materials plays a vital role in the shielding capability of the particular materials because neutron interaction probability of atoms varies. Elastic and absorption processes play an equally important role to shield the neutrons. The shielding materials are made of various kinds of elements as per their objective of development. Materials for fast neutron shielding must have elements for the moderation of neutrons and also for absorption. In order to understand neutron attenuation and evaluation of neutron shielding, the microscopic cross section of each element with the function of energy should be analyzed. It is also essential to define the shielding characterization techniques in a better way. The cross sections of some elements with specific interaction probability are shown in the below figures.

All cross-section data have been taken from ENDF data library [13–17] and plotted using the online ENDF portal of nuclear data service [17]. The unit for measuring cross-section is the barn where 1 barn is equal to 10^{-24} cm^2.

The neutron cross sections of hydrogen are shown in Fig. 11.2. The plot shows the probability of elastic and nonelastic scatterings along with total cross section. The elastic scattering mainly dominates the neutron interaction with hydrogen. There is also a small possibility of inelastic scattering. The inelastic scattering data is taken from the JENDL library [18, 19]. Hydrogen has a large cross section for elastic scattering which plays a major role in slowing down the neutron energy. Therefore, hydrogen remains as an inherent part of all kinds of neutron shielding.

The cross sections of both lithium isotopes are shown in Fig. 11.3. Total cross section of lithium-6 is dominated by inelastic scattering, unlike the hydrogen. However, lithium-7 has elastic scattering cross section higher than inelastic. The cross section of lithium-6 for energy range below 0.1 MeV is quite higher than lithium-7 due to inelastic scattering mainly (n, α) reaction. For fast neutrons, the elastic scattering has a bit higher cross sections than inelastic. Lithium is not usually a choice of shielding ingredient because it produces tritium through (n, α) reaction which is a radioactive isotope. However, it is included here to represent its affinity for neutron interaction in comparison to hydrogen and other low-atomic weight nuclides. Moreover, when lithium cross section is compared with that of

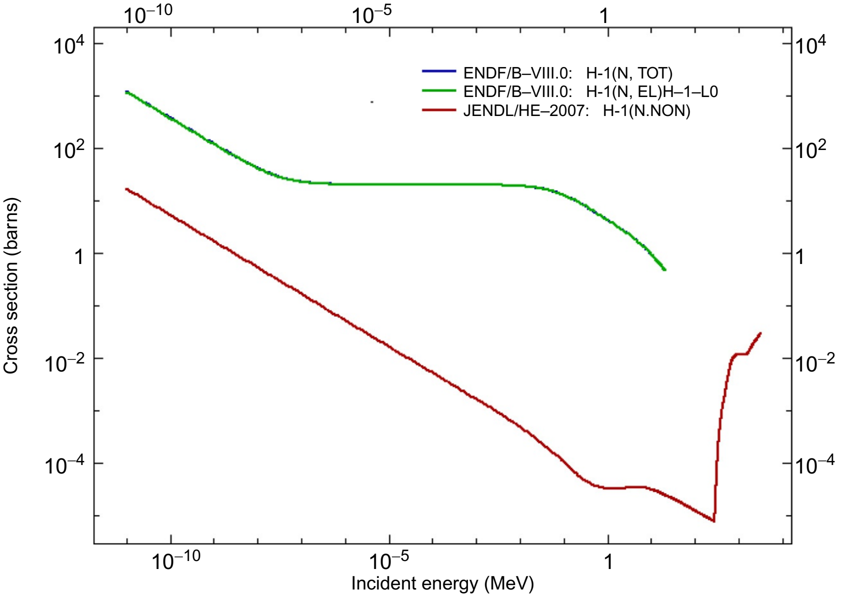

Fig. 11.2 Neutron interaction cross sections of hydrogen.

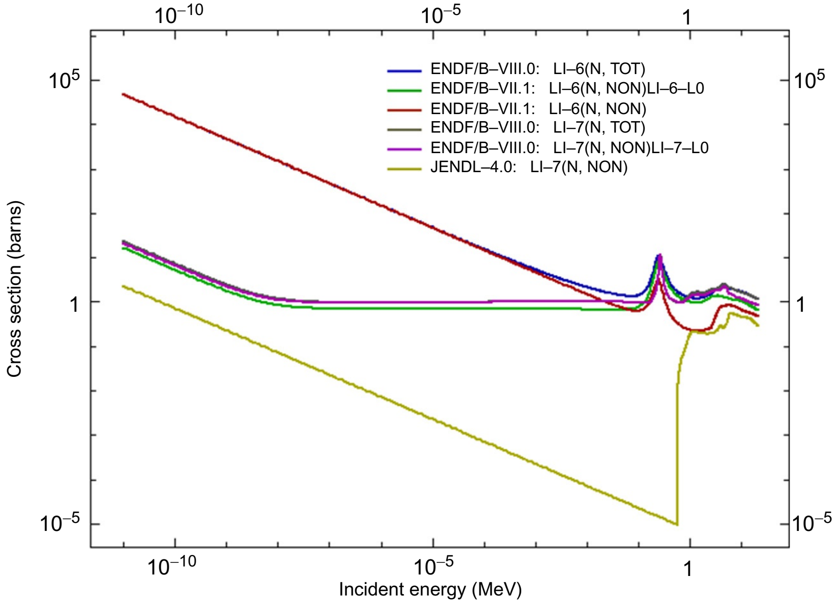

Fig. 11.3 Neutron interaction cross sections of lithium.

hydrogen for a particular energy 1 eV, it was found around 150 barns for lithium and only 20 barns for hydrogen.

The neutron cross section of beryllium is also plotted in sequence in Fig. 11.4 to analyze all lower atomic weight isotopes It is interesting to observe that beryllium does not follow the trend of lithium. The pattern of the total cross section is more similar to hydrogen except for (n, 2n) reaction cross section. It's cross section is also lower than hydrogen and lithium for the thermal energy range. For high energy, it is quite close to both lithium and hydrogen. Like lithium, beryllium is also not directly chosen for shielding design because of its toxicity and neutron multiplication feature. It is useful where neutron multiplication is demanded. The lithium and beryllium isotopes are more desired in fusion reactor fuel breeding applications [19–22].

The neutron interaction cross sections of boron isotopes are plotted in Fig. 11.5. It is clearly visible that B-10 is more prone to neutron interaction than B-11. It has huge cross section for inelastic scattering which is basically the (n, α) reaction. The reaction makes it a good absorber for thermal to slow energy range neutrons. It has a higher total cross section than hydrogen and lithium for 1 eV neutrons. The total cross section for boron-10 is around 610 barns for 1 eV neutrons. It has around 3870 barns cross section for thermal

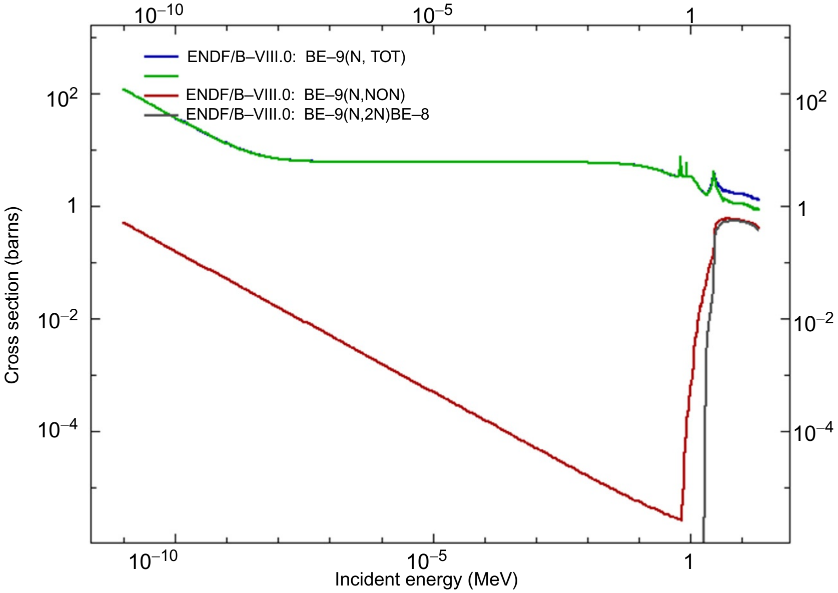

Fig. 11.4 Neutron interaction cross sections of beryllium.

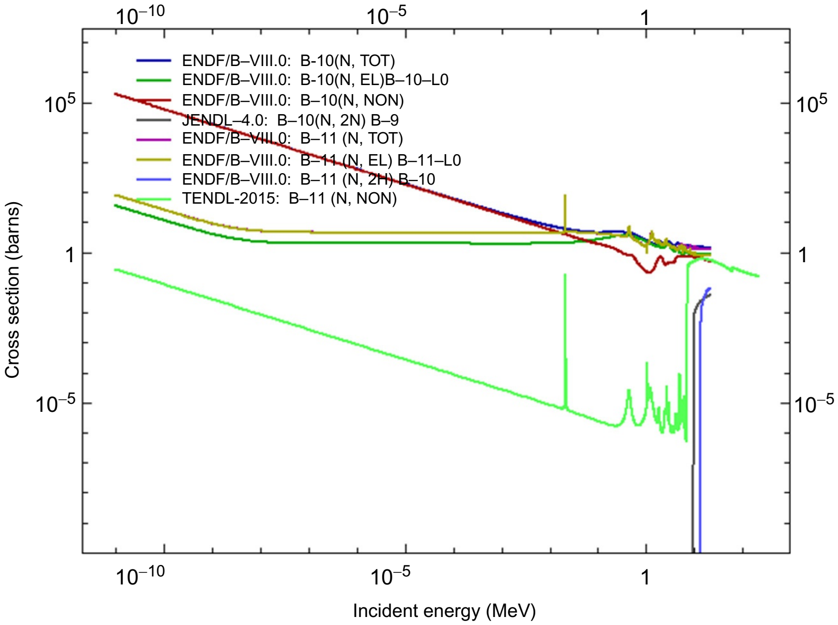

Fig. 11.5 Neutron interaction cross sections of boron.

neutrons (0.025 eV). Boron plays a significant role in neutron removal. Thus, boron is the most desirable material for neutron shielding like hydrogen. A lot of materials are made using boron for neutron-shielding application [23–26]. The combination of boron with hydrogen makes neutron-shielding effectual because hydrogen slows down the neutrons and makes them suitable for boron absorption.

The carbon cross section of neutron is also included and presented in Fig. 11.6 because carbon is most likely presented in various shielding materials [23, 24, 26]. As it is seen in cross-section plot in Fig. 11.6 carbon does not attract neutron as much as other lower atomic weight elements. The total cross section is dominated by elastic scattering only. Inelastic scattering has some visible contribution in total interaction probability for fast neutron range. The cross-section plot suggests that presence of carbon in materials may not have any significant impact on shielding of neutrons. However, it is also not a troublemaking element for neutron shielding. Moreover, carbon presence in structural materials is required for the enhancement of physical strength and intermediate chemical processes [27].

In sequence to lower atomic weight elements, nitrogen also has its presence in various structural materials as well as shielding materials. Nitrogen is

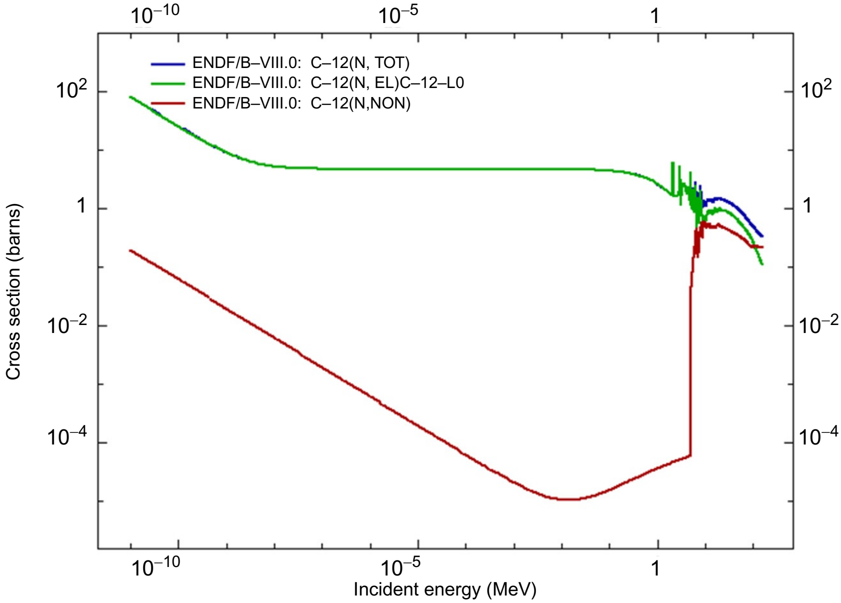

Fig. 11.6 Neutron interaction cross sections of carbon.

an inherent part of some materials like boron nitrides and high-nitrogen austenitic steels [28], which makes it necessary to analyze nitrogen as a part of shielding materials. The neutron cross section of nitrogen is shown in Fig. 11.7. The cross section of nitrogen is more similar to carbon with a bit higher probability of interaction. The elastic scattering is dominant in total cross section. Like carbon, nitrogen is also not a proactive element for neutron shielding but the presence of nitrogen cannot be eliminated for shielding materials. It is an essential part of steels and provides stability, corrosion residence, and good mechanical properties [28].

Oxygen is a part of various shielding materials, whether it is ceramic-based or polymer-based. It is also associated with the most classic shielding substance water (H_2O). It is also present in steels and plays an impactful role in their toughness [29]. The neutron cross section of oxygen, given in Fig. 11.8, does not differ much from nitrogen, it follows the same trend. The high-energy neutrons interact with oxygen and produce N-16 and N-17 radioactive isotopes which gets decay in few second and emit high-energy secondary gamma rays and neutrons. The production of N-16 and N-17 is quite huge in high-energy neutrons environment such as fusion reactor [30]. The generation of N-16 and N-17 in water reduces the chance

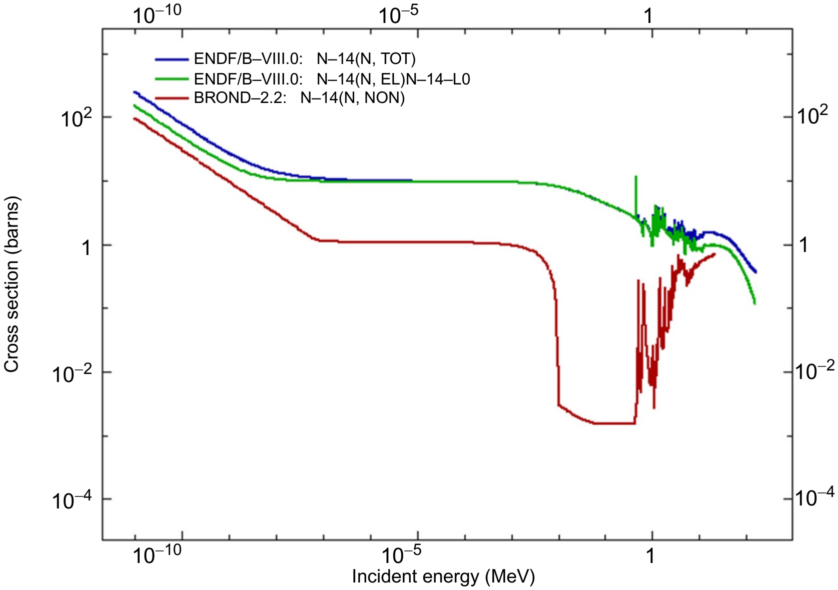

Fig. 11.7 Neutron interaction cross sections of nitrogen.

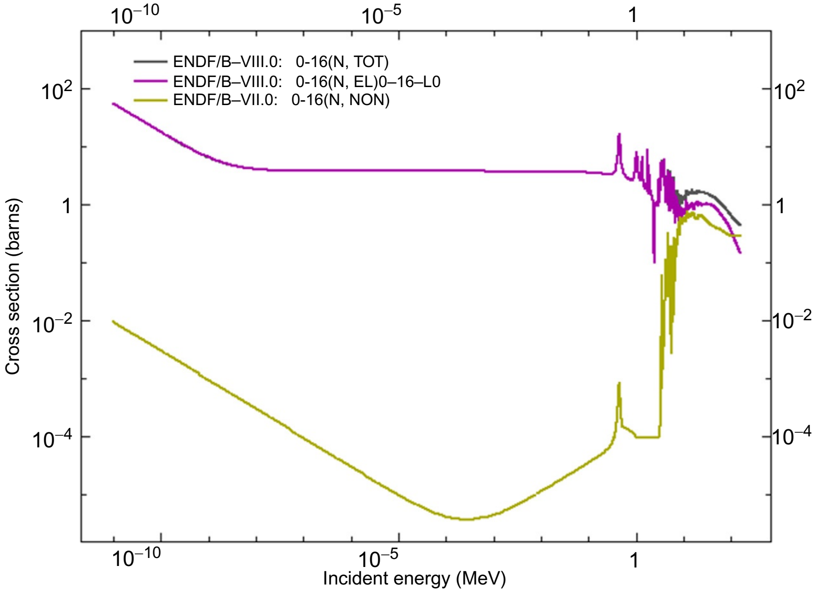

Fig. 11.8 Neutron interaction cross sections of oxygen.

of it as a shielding material in fusion reactor and opens the way for alternate materials as a solution of shielding as well as cooling [26].

Sulfur is used in the preparation of elastomer shielding materials as well as ceramic materials [31, 32]. The cross section of sulfur is presented in Fig. 11.9. The inelastic scattering cross section is higher for thermal energy range and drastically decreases after thermal energy range. Elastic scattering dominates after thermal energy range. There is a resonance region between 10 keV and 1 MeV. The resonance region has fluctuations in cross section and varies from low to high in a minor energy difference. Sulfur does not have any shielding features but it is presented in flexible shielding materials.

Neutron scatterings are more prominent with low-atomic weight elements but the structural materials of nuclear reactors and facilities (such as steels) have iron and its neighboring elements [33–35]. Structural materials are also utilized in neutron-shielding purposes like support for shielding, water-steel mixtures. Cross sections of few elements those are presented in the structural materials, i.e., chromium, iron, nickel, and zinc, are analyzed to observe the performance of such elements in neutron environment. The neutron cross section of chromium is shown in Fig. 11.10. It has a cross section of around 50 barns for thermal neutrons and 6 barns for 1 eV to 10 keV energy range. It also has a resonance region between 100 keV and 5 MeV.

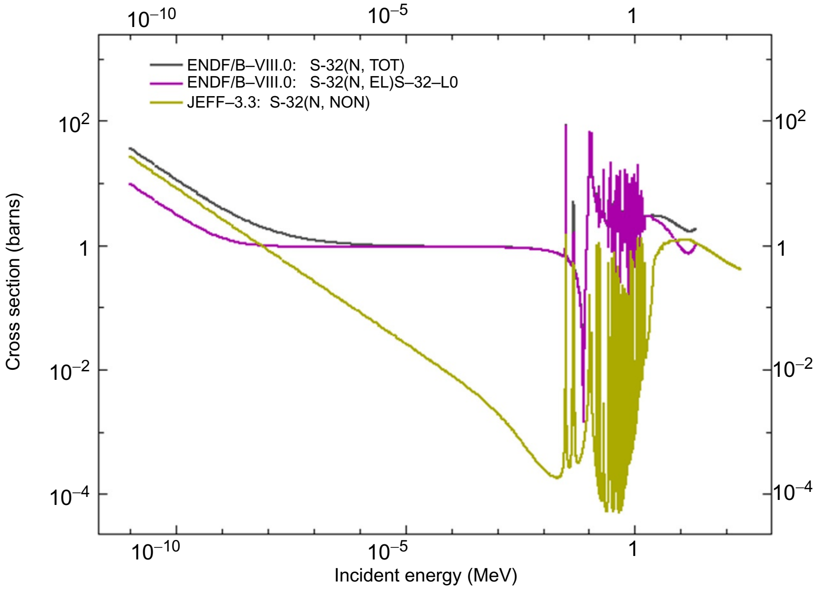

Fig. 11.9 Neutron interaction cross sections of sulfur.

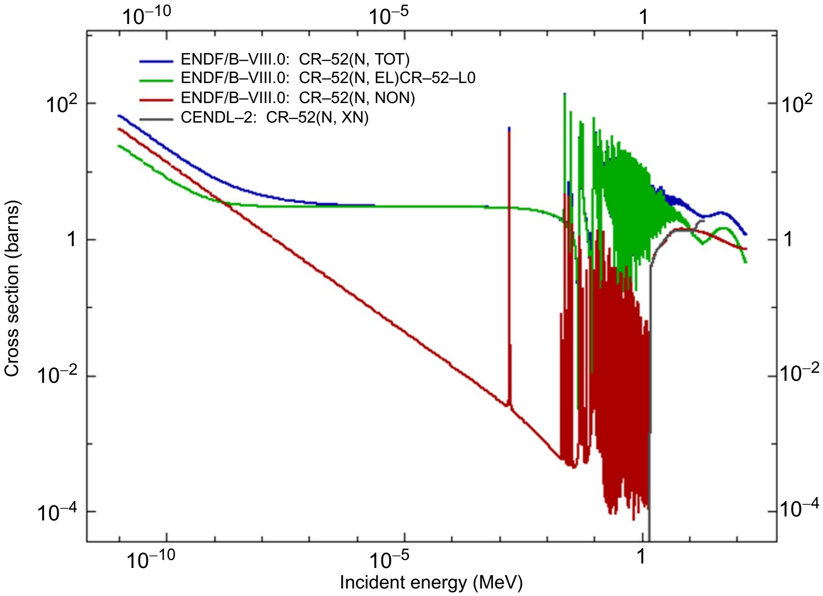

Fig. 11.10 Neutron interaction cross sections of chromium.

Iron is an inherent part of steel and is available as a base element in all kinds of steel. The cross-section profile of iron-56 is presented in Fig. 11.11. It has a pattern similar to chromium apart from the amplitude of cross section which is a bit higher than chromium. Iron is always considered a good absorber for thermal neutrons but it is not better than boron. For low-energy neutron, the (n, γ) reaction occurs whereas for high energy the (n, p) and (n, α) reactions dominate as the part of inelastic scattering.

However, it plays a considerable role where the mechanical strength is required in shielding. In fission and fusion reactor design, steel is used with water or hydrogenous materials as shielding options. The borated steels are also used as a favorable option for the shielding of nuclear reactors and facilities [34].

Nickel nuclide behaves similar to iron when it faces the neutrons. The interaction probability of nickel in terms of the cross section is shown in Fig. 11.12. The inelastic scattering cross-section equally contributes in total interaction for thermal neutrons and it decreases as temperature of neutrons increases up to 10 keV. It also has a resonance in cross-section between 10 keV and 1 MeV. Inelastic scattering again becomes equally important in the total probability of interaction for high energy. As a part of steel, nickel is equally good as iron for neutron shielding.

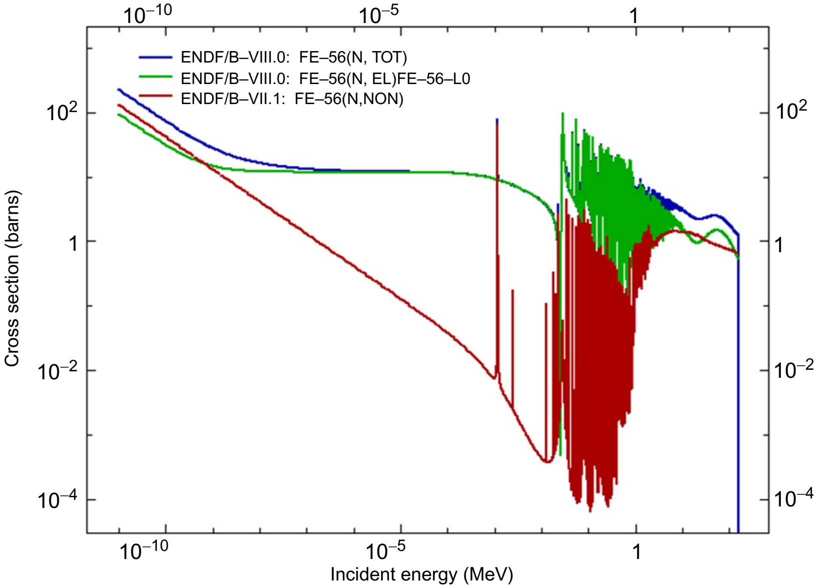

Fig. 11.11 Neutron interaction cross sections of iron.

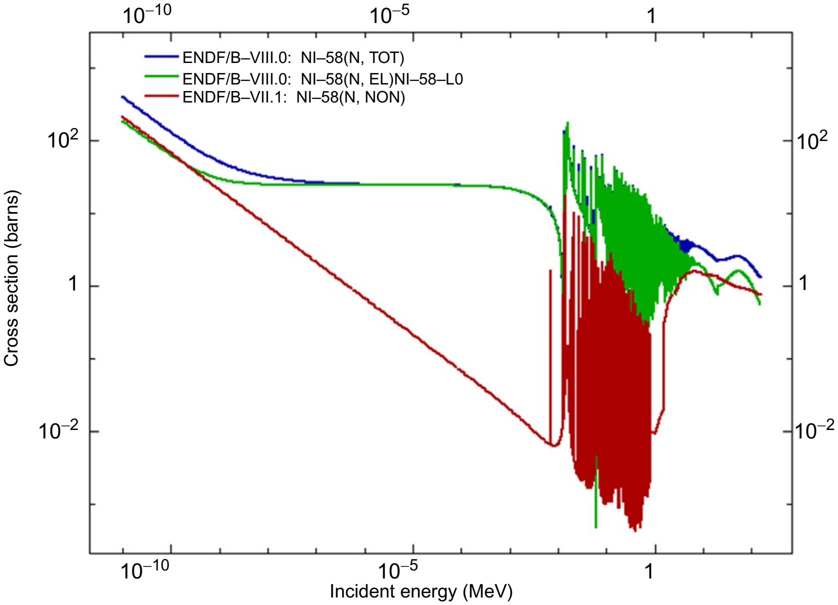

Fig. 11.12 Neutron interaction cross sections of nickel.

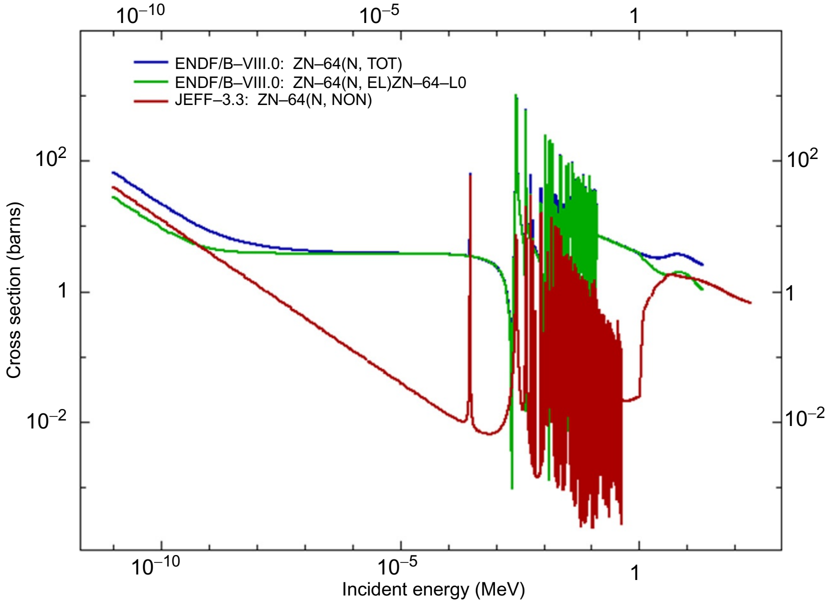

Fig. 11.13 Neutron interaction cross sections of zinc.

Zinc is also considered here to present a better understanding of intermediate-atomic weight elements. The zinc cross section with energy is shown in Fig. 11.13. Like other elements of intermediate-atomic weight, zinc cross section also varies between 10^2 and 10^{-3} barns. The interaction probability of elastic and inelastic scattering also follows a similar trend like iron and nickel. The shielding behavior of zinc is also as good as iron and nickel. Therefore, the presence of zinc in steel and other structural materials makes a positive contribution to shielding.

Cadmium is considered a special element for neutron absorption and was widely used earlier in the fission reactor as an absorber rod to control the fission chain rate. The cross-section profile of cadmium is shown in Fig. 11.14. It has a huge cross section of inelastic scattering up to 1 eV neutrons. The capture reaction (n, γ) is a reaction that plays a major role in the elimination of the neutrons. Cadmium also generates radioactive isotopes such as Cd113m, Cd113, and Cd109 when it interacts with high-energy neutrons.

In order to have a complete understanding of the neutron cross sections, it is also necessary to analyze the cross section of high-atomic weight elements like tungsten and lead. The cross section of tungsten is shown in Fig. 11.15. The profile does not show the substantial interaction probability

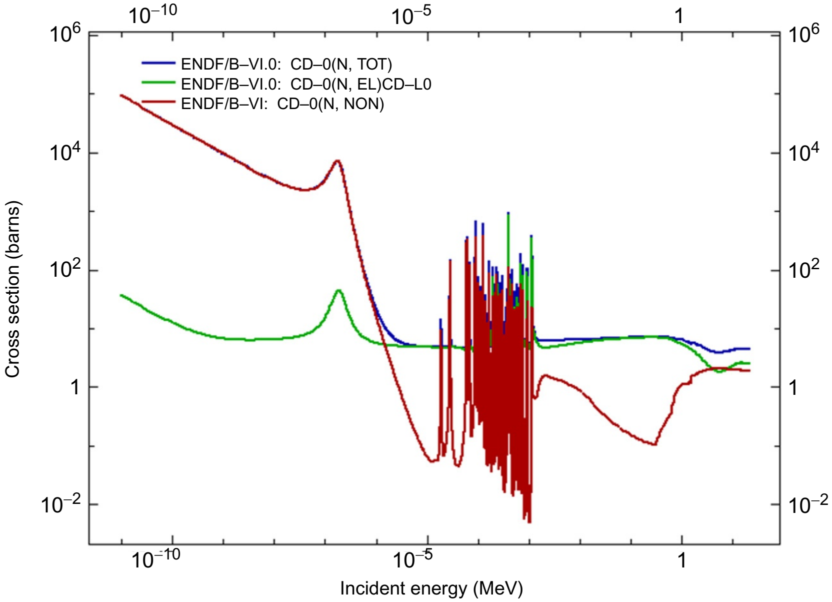

Fig. 11.14 Neutron interaction cross sections of cadmium.

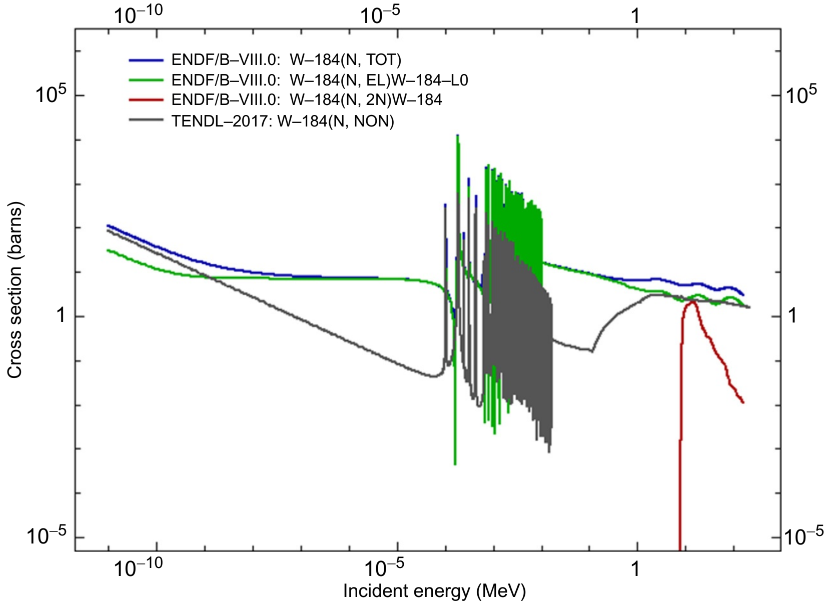

Fig. 11.15 Neutron interaction cross sections of tungsten.

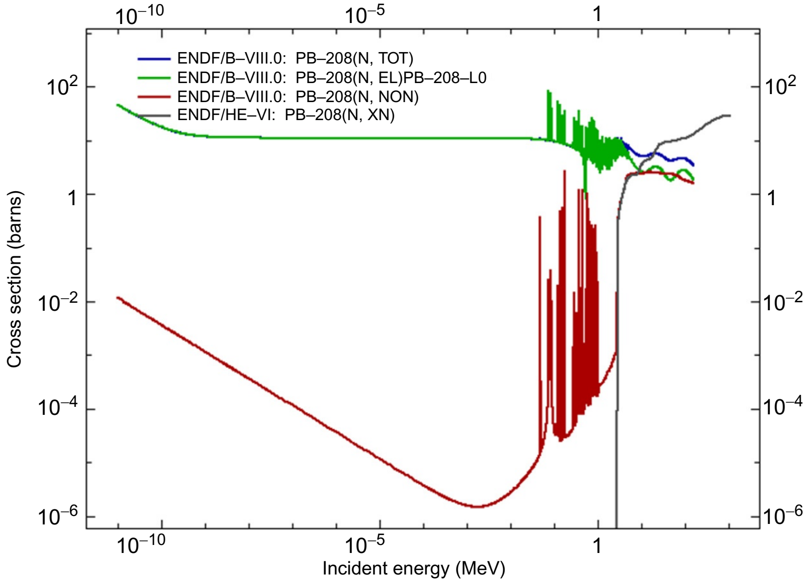

Fig. 11.16 Neutron interaction cross sections of lead.

of neutrons. Both elastic and inelastic scattering contribute equally to the total cross section. The high-atomic weight nuclides such as tungsten and lead do neutron multiplication reaction for high-energy neutrons.

The cross section of lead is also shown in Fig. 11.16. It is considered as a potential neutron multiplier for fusion reactor tritium breeding blankets. The cross section of inelastic scattering is low in comparison to elastic for low-energy neutron. The cross section of inelastic scattering considerably increases for high-energy neutrons. The threshold of (n, 2n) reaction of lead is around 7.5 MeV.

Lead is a very useful and most desirable candidate for the gamma-ray shielding because of its gamma absorption behavior. Tungsten is also good for gamma-ray shielding. They are not considered as a neutron-shielding material [3, 4].

11.2.2 Numerical estimation of macroscopic cross section and shielding efficiency of materials

The macroscopic cross section represents the interaction probability of neutron for a particular material. It is a summation over cross sections of all elements presented in a unit volume of the material. The unit of macroscopic

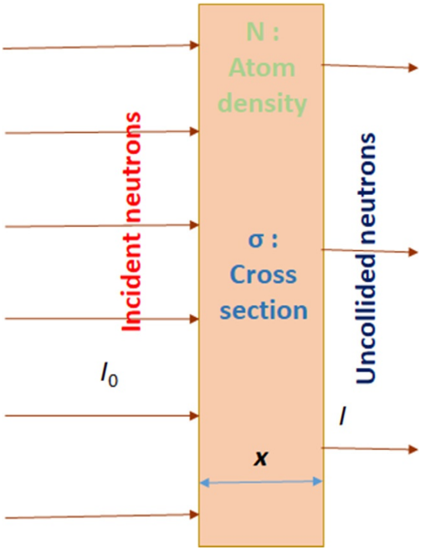

Fig. 11.17 Representation of uncollided flux.

cross section is cm^{-1} which comes from the multiplication of the atom density (N) and cross sections (σ).

The macroscopic cross section can be better understood by an example of uncollided flux estimation as shown in Fig. 11.17. For example, I_0 neutron flux fall on the material which has thickness x and atom density N. The total neutron cross section of the material is σ. The uncollided flux is simply estimated by the exponential law as [36–39].

$$I = I_0 e^{-N\sigma x} \tag{11.1}$$

where $N\sigma$ represent a macroscopic cross section $\sum$. The macroscopic cross section symbolizes the total probability of any interaction occurrence in a unit volume of the material. If the formulation of charge particle attenuation ($I = I_0 e^{-x/\lambda}$) is observed then λ represents the length of the collision occurrence, it is also called mean free path. For neutrons, the mean free path is inversely proportional to macroscopic cross section. It indicates that larger the macroscopic cross section shorter the mean-free path becomes. The better representation of macroscopic cross section and mean free path is made through an example of specific energy neutrons fall on a unit volume of materials. The results are presented in Table 11.1.

Hydrogen gas has a good microscopic cross section but has a very high mean free path. It is due to the density of the hydrogen, which is very low at

Table 11.1 Macroscopic cross section and mean free path of neutrons for specific materials.

Sr. no.	Material	Microscopic cross section (barns) at 0.025 eV	Atom density (atoms/cc)	Macroscopic cross-section (1/cm)	Mean free path (cm)
1	H	30.51	4.93E+19	1.51E-03	6.64E+02
2	B	778.23	1.16E+23	9.02E+01	1.11E−02
3	Fe	14.81	8.48E+22	1.26E+00	7.96E−01
4	H2O	64.93	3.35E+22	2.17E+00	4.60E−01
5	B4C	3117.87	2.70E+22	8.43E+01	1.19E−02

room temperature 8.20×10^{-5} g/cc [40]. It results in a transparent medium for neutrons. Hydrogen plays an important role as a constituent of water. The mean free path for water is quite low at around 4.6 mm for thermal neutrons. Boron is known for neutron absorbing quality, it shows the lowest mean free path among others (Table 11.1).

By incorporating macroscopic cross section, Eq. (11.1) can be rewritten as.

$$I = I_0 e^{-\sum x} \tag{11.2}$$

$$x = \frac{1}{\sum}(\ln I_0/I) \tag{11.3}$$

The thickness (x) to reduce the neutron by any factor is calculated by Eq. (11.3). A thickness equal to $0.693/\sum$ is required for the reduction of flux by a factor of 2. As per Eq. (11.3), 23.2 cm shield of water can reduce 14 MeV neutrons by a factor of 10.

The shielding efficiency of various elements for 1 eV neutrons are estimated using Eq. (11.3) and plotted in Fig. 11.18. The cross section of boron is quite high for low-energy neutrons which reflect in attenuation profile of boron. The uncollided flux of 1 eV is drastically reduced by a factor of 10^8 within a 2-cm thick boron. A very less attenuation is seen in hydrogen shield mainly due to the low density of hydrogen. Iron and cadmium attenuated the flux by a factor of 10^6 within 13- and 14-cm thick shields, respectively. Tungsten has lower attenuation in comparison to iron.

The attenuation of neutrons through water has been estimated for specific energies and plotted in Fig. 11.19. It represents a good example of

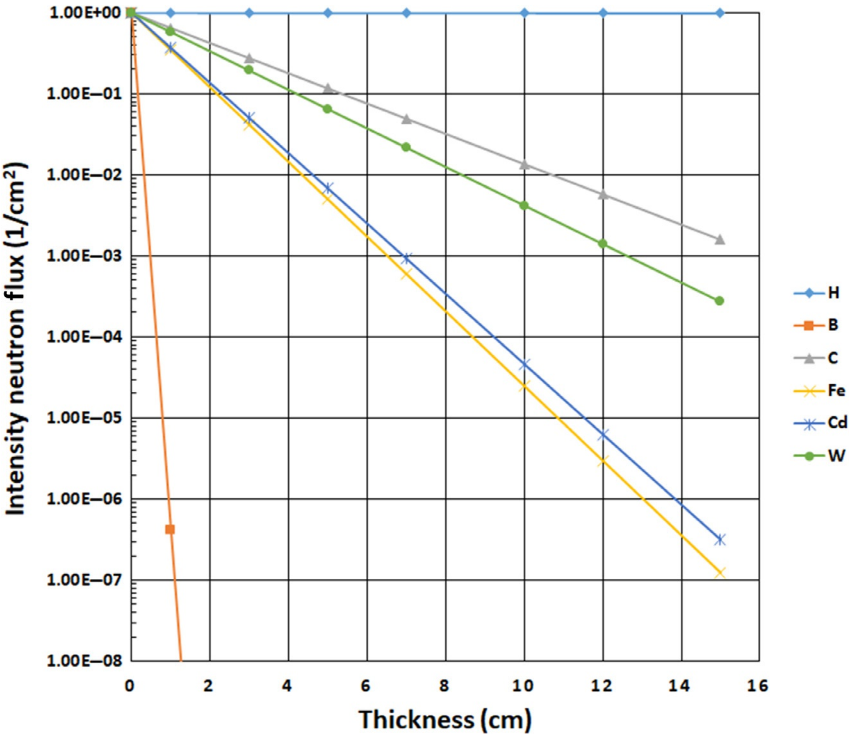

Fig. 11.18 Attenuation profile of 1 eV neutrons in the shield of specific elements.

attenuation with energy. High-energy neutrons penetrate deeper than low-energy neutrons. However, the attenuation of 1 keV and 1 eV neutrons is almost the same. It shows that there is no major change in cross section between 1 eV and 1 keV.

The formulation given for the estimation of the uncollided part of neutron fluence is only purposed to make the primary shielding estimation of developed or being developed material. If the elemental compositions of the materials are known, the uncollided fluence evaluation can be easily performed for any kind of material. The elemental composition of the materials can be obtained through various material testing approaches such as XRD, SEM, etc. [41]. For realistic estimation of shielding, secondary particles and their effects on the materials should be included. To conduct the detailed analyses, a lot of advanced computational tools are available for the simulation of neutron transport. Such tools are made considering advanced physics models [42–45].

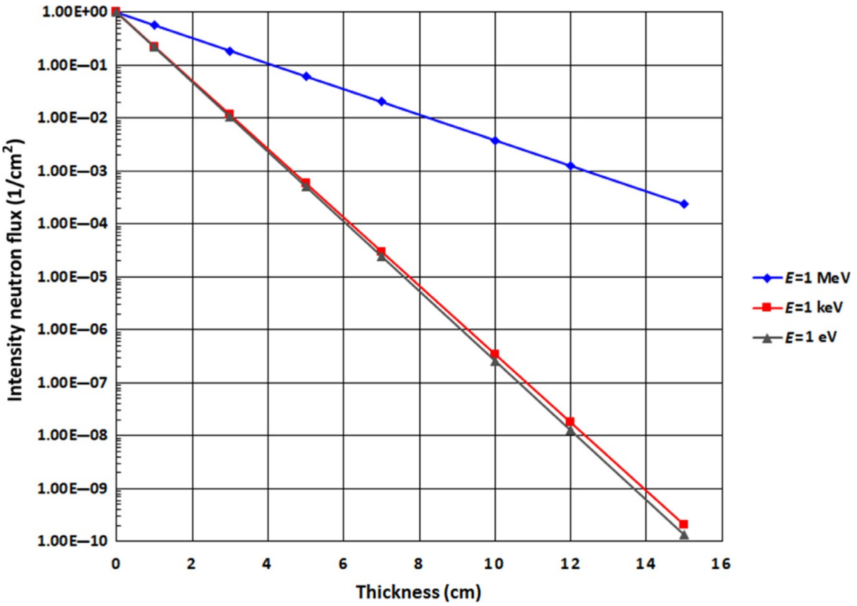

Fig. 11.19 Attenuation of specific energy neutrons through water shield.

11.2.3 Small-scale shielding experiments using various neutron source at laboratory

The shielding capability of a material can be characterized by small-scale shielding experiments at the laboratory [46–56]. A schematic representation of an experiment for the shielding efficiency evaluation is illustrated in Fig. 11.20. The neutron source is covered by a shield to reduce the occupational radiation doses during the experiment. There is a location for direct exposure of neutron where the placement of material for shield efficiency testing has to be made. The measurement of neutron flux is conducted by a neutron detector. The shielding efficiency testing experiments are generally conducted in two steps. In the first, the direct neutron fluence is measured before placing the material. In the second step, the material is placed in front of the source and neutron fluence is measured.

The shielding experiment can be directly performed using the source neutrons without any spectrum optimizer if the material is developed for the similar neutron energy range. However, the material developed for lower energy range can also be tested with high-energy source by placing a spectrum optimizer in front of the source. The spectrum optimizer is a material that can soft the energy spectrum of the source and make it desirable for the developed material.

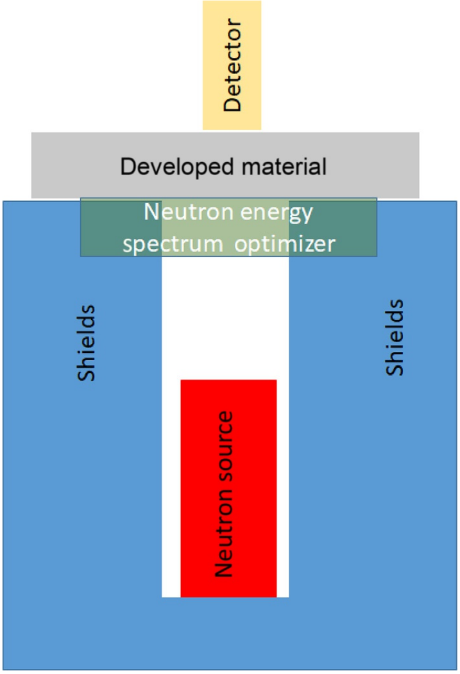

Fig. 11.20 Schematic representation of experimental setup for the evaluation of the shielding material.

A shielding experiment for the fusion reactor shielding design support has been conducted at the Institute for Plasma Research [56]. The experiment was conducted using the available 14 MeV D-T-based neutron source. A simulation model of the experiment is shown in Fig. 11.21. A neutron spectrum optimizer was used in the experiment to get the desired neutron spectrum for shield testing. The neutron flux was monitored using Helium-3 detector. In order to avoid the environmental effects or sky-sign effects, the entire experiment was covered with HDPE sheets. Fig. 11.22 shows an experimental arrangement of optimizer and shield mock-up at the laboratory. The complete description and results of the experiment can be found in the published article [56].

11.3 Neutron source for shielding efficiency measurement

The neutron source is an essential part of the neutron-shielding experiment. There are various neutron sources available worldwide [1, 2, 57, 58]. A fission reactor is a well-known neutron source; it is a very intense kind

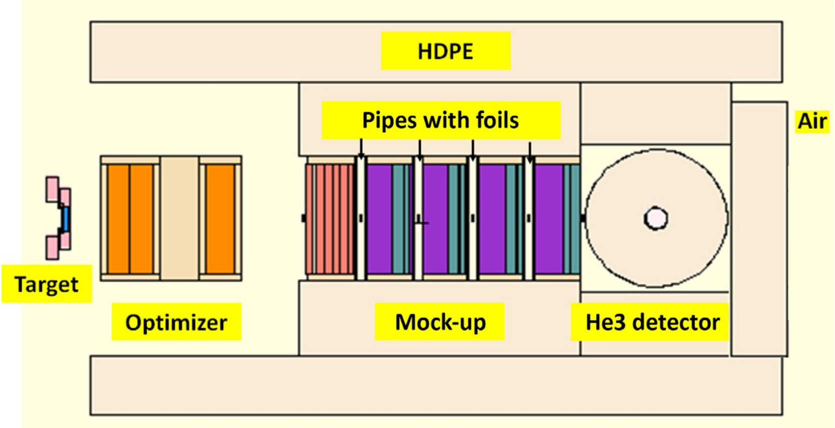
HDPE
Pipes with foils
Air
Target
Optimizer
Mock-up
He3 detector

Fig. 11.21 Simulation model of a shielding experiment [56].

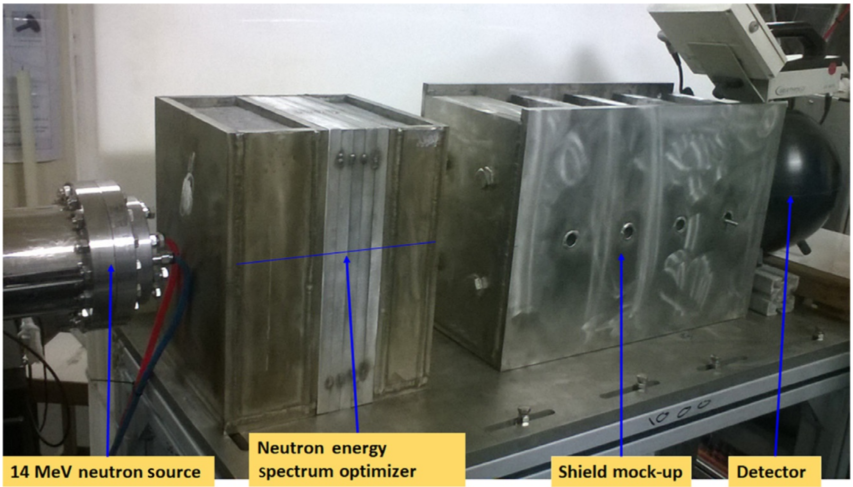
14 MeV neutron source
Neutron energy spectrum optimizer
Shield mock-up
Detector

Fig. 11.22 Shielding experiment conducted at IPR using 14 MeV Source.

of neutron source with a fluence of 10^{12}–10^{15} n/cm^2.s. The neutrons produced in the fission reactor are due to U-235 fission reaction and the average energy of neutrons is around 2 MeV. The fluence level varies with the location in the reactor. The reactors are primarily made for the power generation purpose but it has some dedicated port especially for the material sample testing and radiation damage studies.

There are also other fission neutron sources those are based on spontaneous fission process. Some high-mass radionuclides such as Pu-238, Cf-252, and Cm-244 undergo spontaneous fission and emit neutrons similar to fission reactors. Energy spectrum of emitting neutrons is also same as the fission reactor neutrons. Cf-252 is an important radionuclide for the spontaneous fission-based neutron source due to its high neutron yield per unit mass. It has $\sim 2 \times 10^{12}$ n/s/g yield and the effective half-life is around 2.6 years. Small capsule-based sources are created using Cf-252 for laboratory-scale experiments and dosimetry.

There are few nuclear reactions which can produce neutrons, i.e. alpha-beryllium reaction and gamma-beryllium reaction. The alpha emitter-based neutron sources are commonly used in laboratory scale.

$$Be^9 + \alpha \rightarrow C^{12} + Neutron + \gamma$$

Alpha emitters such as Am-241, Pu-238, Pu-239, Po-210, etc. are used in neutron sources. The most commonly used isotopes are americium and plutonium. The strength of such sources is defined by the activity (Ci) of alpha emitter. 1 Ci of Am-Be source can emit around $2. \times 10^6$ n/s. The average energy of the source is around 4.2 MeV and the half-life around 432 years. The Pu-239-based source has an average energy around 5 MeV and can produce 1.5×10^6 n/s per Ci. Such sources are constructed by mixing the oxide of alpha emitters with beryllium metal and compressing in a cylindrical-shaped capsule.

The alpha-based sources can also be constructed using other elements like boron, lithium, or fluorine instead of beryllium.

The gamma-based source can be built through the following reactions:

$$Be^9 + \gamma \rightarrow Be^8 + Neutron$$

$$H^2 + \gamma \rightarrow H^1 + Neutron$$

The gamma source can produce monoenergetic neutrons but due to very less probability of interaction, most of gamma rays leak without interaction and cause high radiation exposure. A source made of Sb-124 and beryllium can produce around 2×10^5 n/s per Ci and half-life around 60 days.

Apart from the above-mentioned sources, neutrons are being produced through accelerator. The charged particles are accelerated using voltage difference and bombarded on a target to produce neutrons. The accelerator-based neutron sources are generally called a generator and is a controlled device unlike Am-Be or spontaneous fission-based sources. The source of 14 MeV neutron can be made by accelerating deuterium ion beam and hitting on the tritium target. It is the most common neutron generator. The yield of the generator depends on the beam energy.

$$D + T \rightarrow n + He^4$$

The neutrons can be also produced through other reactions like *D–T* as follows:

$$Be^9 + D \rightarrow B^{10} + neutron$$

$$Li^7 + p \rightarrow Be^7 + neutron$$

Neutron generators are also built for various applications of science. Accelerator-based neutron sources are quite useful for laboratory scale shielding-related experiments and material testing applications.

The shielding materials being developed for specific purposes cannot be tested using any kind of neutron source. As per the requirement of the materials, the neutron source should be selected for the shield capability testing.

11.4 Diagnostics for shielding efficiency measurement

The measurement of neutrons not only assures the conduction of the shielding experiments but also assures the shielding efficiency of the particular material. Various detectors are available to measure different energy ranges of neutrons. They are based on neutron interaction probability of the materials [12, 59, 60].

The low-energy neutrons especially having energy below 0.5 eV can be detected using high cross-section reactions such as ^{10}B(n, α), ^{6}Li(n, α), and ^{3}He(n, p). The cross sections of these reactions are 3830, 937, and 5330 barns, respectively. The boron-based neutron detector is BF_3 proportional counter which is enriched with ^{10}B. It is used for slow neutron detections. There is a scintillator counter based on lithium reaction. It has LiI crystal as a scintillation material. ^{3}He-based proportional counter is widely used for slow neutron detection.

^{235}U fission ionization chamber is also used as a slow neutron detector due to the property of the large fission at slow neutrons.

Fast neutrons can also be detected by thermal neutron detectors using moderator. Such detectors are made by covering a BF_3 or ^{3}He counter by dense hydrogenous material which converts the fast neutrons into a thermal neutron via elastic collisions. Examples of such detectors are ^{3}He spherical dosimeters, BF_3-based long counters, and many more.

The fast neutrons can be detected through its direct elastic scattering with nuclei. The recoil nuclei particle can be detected for the information of neutron. The recoils can be produced in a detector material or separate radiator. For energy <1 MeV, solid-state radiators cannot be used due to high-energy losses of recoil protons. To detect such neutrons, a gas-based proportional counter can be chosen which are filled with methane/hydrogen and propane. For high energy, the target-based organic scintillators are used. The target could be liquid or solid. Stilbene and anthracene are used for solid scintillator target and fluros-dissolved aromatic solvent is used for liquid.

Apart from the direct measurement of the neutrons, there is an indirect measurement process which is based on neutron activation; it is also called neutron dosimetry. In this process, various material foils are used and irradiated through neuron source. The foils get activated and emit the secondary radiation through its decay process. Secondary radiations can be measured to get information about neutron fluence and energy. The foil activation measurement is a kind of tedious and time-consuming procedure. The information on the fluence and energy can be obtained only after the experiment. Also, the foils need to be irradiated for a certain minimum duration to obtain their saturation activity.

As per the demand of the experiment, selection of diagnostics has to be made. In order to get complete and assure information, it is always recommended to use multiple detectors in the experiment.

11.5 Conclusion

The characterization of shielding ability is an essential and important aspect of the nuclear facility and shielding material development. The shield behavior directly depends on the affinity of the interaction of the neutron. Various elements such as boron, cadmium, iron, water, and many hydrogenous materials have a great affinity for the neutron interaction and some of them have the quality to absorb or eliminate neutrons. As described in the chapter neutrons interact with material through elastic scattering or inelastic scattering. Both processes contribute to the shielding feature of the materials. Few elements or materials attenuate the energy of the neutron through the number of successive elastic collisions whereas some eliminate the primary neutrons through capture or absorption reaction. The ideal shield requires both attenuation and absorption features inherently. Any material for the shielding application should be made of elements, or molecules which have qualities such as moderation and absorption.

The microscopic cross section represents the affinity of particular material or element interaction with neutrons in quantitatively. Boron isotope (^{10}B) has large cross section for thermal neutrons. The same feature of boron is also utilized in the shielding as well as detection of neutrons. Cadmium also has huge cross section for neutron capture, up to 0.5 eV neutrons. The quality of boron and cadmium is quite useful for controlling a chain fission reaction in a fission reactor. The cross section of hydrogen is quite high for elastic collision which makes it an efficient moderator. The profile of neutron cross section of intermediate-atomic weight elements like Cr, Ni, Fe, and Zn are quite similar. These elements make their presence in most of the structural materials which bare the loads. Such elements with sufficient affinity of the neutron positively contribute to the shielding.

The shield materials are developed keeping in mind their specific utilization. Few materials are developed for nuclear reactor shielding application whereas few are developed for space radiation protection. Some of them are made for flexible shielding but cannot work at higher temperature whereas ceramic-based materials can sustain a high temperature but do not have flexibility. Few of them can be utilized also as structural material but few cannot bear even the small load. As per their utilization and properties, the shielding characterization can be made. Moreover, a hand-based simple assessment can be done using the exponential expression of neutron attenuation which gives the feel of the uncollided fluence attenuation.

The collective feature of neutron attenuation can also be understood by macroscopic cross section or mean free path phenomena which present the realistic picture of the shielding. For example, the macroscopic cross section of hydrogen is quite high but hydrogen gas cannot make any significant contribution to shielding and, on the other side, water which has two hydrogen atoms is used as a moderator in fission reactor and many facilities. Such representation could only be understood by macroscopic cross section which actually provides the effective probability of interaction in a material. It depends on the density of the material. Although the cross section of iron is also not as high as cadmium for low energy, its density and abundance makes it a good attenuator.

The realistic testing of the materials can be done using the neutron source but the selection of the source should be made as per the quality of the materials. Various neutron sources are available worldwide. Some of them are based on nuclear fission whereas some of them are made of spontaneous fission processes such as Cf-252. There are sources that can be built using alpha emitter and beryllium whereas few of them are built using ion accelerator. The alpha emitter and beryllium-based sources are very commonly used for small-scale experiments and practical teaching applications. The ion accelerator is used in various applications like nuclear material detection, oil well logging, medical therapy, materials testing, and small-scale shield experiments.

The detectors play an equally important role as a neutron source in the characterization of shielding capability. The detectors have their working energy range. Like ^{3}He and BF_3 proportional counters are used only for slow neutron detection whereas recoil scintillators are used for fast neutron detection. The selection of the detectors should be made as per the requirement of the experiment.

The material's shielding capability characterization is essential and important for the design and development of innovative shielding materials. It is an inherent part of the development process and should be evaluated during and after the development of any kind of shield material.

References

[1] S. Glasstone, Nuclear Reactor Engineering, Delhi Cbs, 1986.
[2] A.R. Foster, Basic Nuclear Engineering, Boston Allynard Bacon, 1977.
[3] A.B. Chilton, J.K. Shultis, R.E. Faw, Principles of Radiation Shielding, Prentice Hall, Englewood Cliffs, 1984.
[4] S.J. Kenneth, R. Faw, Radiation Shielding, American Nuclear Society, Illinois, 2000.
[5] R.G. Jaeger, Engineering Compendium on Radiation Shielding, Vol-I: Shielding and Methods, Springer, 1968.
[6] R.G. Jaeger, Engineering Compendium on Radiation Shielding, Vol-II: Shielding Materials, Springer, 1975.
[7] H. Shulman, W.S. Ginell, Nuclear and Space Radiation Effects on Materials-Space Vehicle Design Criteria, 1970.
[8] C.L. Hanks, D.J. Hamman, Effect of Radiation on Electrical Insulating Materials, 1969.
[9] S.C. Ko, C.S. Pugh, et al., Boron containing polyimides for aerospace radiation shielding, MRS Online Proc. Libr. 551 (2011) 275.
[10] C. Jumpee, D. Wongsawaeng, Innovative neutron shielding materials composed of natural rubber-styrene butadiene rubber blends, boron oxide and iron(III) oxide, J. Phys. Conf. Ser. 611 (2015) 012019.
[11] K. Almenas, R. Lee, Nuclear Interaction With Matter, Nuclear Engineering, Springer, Berlin, Heidelberg, 1992.
[12] G. Knoll, Radiation Detection and Measurement, John Wiley & Sons, Toronto, 1979.
[13] D.A. Brown, et al., ENDF-VIII.0: the 8th Major release of the nuclear reaction data library with CIELO- project cross section, new standards and thermal scattering data, Nucl. Data Sheets 148 (2018) 1–148.
[14] M.B. Chadwick, et al., ENDF/BVII.1 Nuclear data from science and technology: cross sections, covariance, fission product yields and decay data, Nucl. Data Sheets 112 (12) (2011) 2887–2996.
[15] M.C. Han, et al., First assessment of ENDF/B-VIII and EPICS atomic data libraries, IEEE Trans. Nucl. Sci. 65 (8) (August 2018).

[16] C.L. Dunford, Evaluated nuclear data file, ENDF/B-VI, in: S.M. Qaim (Ed.), Nuclear Data for Science and Technology, Research Reports in Physics, Springer, Berlin, Heidelberg, 1992.

[17] Online Nuclear data Services of IAEA, Website link, www.nds.iaea.orgwww.nds.iaea.org/exfor/endf.htm.

[18] K. Shibata, O. Iwamoto, T. Nakagawa, et al., JENDL-4.0: A new library for nuclear science and engineering, J. Nucl. Sci. Technol. 48 (2011) 1–30.

[19] S. Kunieda, et al., JENDL/ImPACT-2018: a new nuclear data library for innovative studies on transmutation of long-lived fission products, J. Nucl. Sci. Technol. (2019), https://doi.org/10.1080/00223131.2019.1647889.

[20] A.R. Raffray, et al., Breeding blanket concepts for fusion and materials requirements, J. Nucl. Mater. 307–311 (Part 1) (2002) 21–30.

[21] M.A. Abdou, Tritium breeding in fusion reactors. in: K.H. Böckhoff (Ed.), Nuclear Data for Science and Technology, Springer, Dordrecht, 1983. https://doi.org/10.1007/978-94-009-7099-1_63.

[22] H.L. Swami, et al., Neutronic performance of Indian LLCB TBM set conceptual design in ITER, Fusion Eng. Des. 113 (December) (2016) 71–81.

[23] J.W. Shin, J.W. Lee, S. Yu, B.K. Baek, J.P. Hong, Y. Seo, W.N. Kim, S.M. Hong, C.M. Koo, Polyethylene/boron-containing composites for radiation shielding, Thermochim. Acta 585 (2014) 5–9.

[24] D. Sariyer, et al., Neutron shielding properties of concretes containing boron carbide and ferro – Boron, Procedia Soc. Behav. Sci. 195 (2015) 1752–1756.

[25] D. Sunil Kumar, et al., A feasibility study of ferro-boron as in-core shield material in fast breeder reactors, Nucl. Eng. Des. 240 (2010) 2972–2980.

[26] H.L. Swami, et al., Neutronic design optimization of ITER TBM port#2 bio-shield plug, Fusion Eng. Des. 137 (2018) 49–55.

[27] P.R. Knowlers, Design of Structural Steelwork, second ed., Taylor & Francis, 1987.

[28] R.B. Gunia, G.R. Woodrow, Nitrogen improves engineering properties of chromium-nickel stainless steels, J. Mater. 5 (1970) 413–430.

[29] A.J. Cooper, et al., Effect of oxygen content upon the microstructural and mechanical properties of type 316L austenitic stainless steel manufactured by hot isostatic pressing, Metall. Mater. Trans. A 47A (2016) 4467.

[30] W.J. Henderson, P.R. Tunnicliffe, The production of N16 and N17 in the cooling water of the NRX reactor, Nucl. Sci. Eng. 3 (2) (1958) 145–150.

[31] M. Celli, F. Grazzia, M. Zoppia, A new ceramic material for shielding pulsed neutron scattering instruments, Nucl. Instrum. Methods A 565 (2006) 861–863.

[32] A. Labouriau, et al., Boron filled siloxane polymers for radiation shielding, Radiat. Phys. Chem. 144 (2018) 288–294.

[33] R.L. Klueh, Reduced-activation bainitic and martensitic steels for nuclear fusion applications, Curr. Opinion Solid State Mater. Sci. 8 (3–4) (2004) 239–250.

[34] R.L. Klueh, Ferritic/martensitic steels for advanced nuclear reactors, Trans. Indian Inst. Metals 62 (2009) 81.

[35] H.L. Swami, et al., Activation characteristics of candidate structural materials for a near-term Indian fusion reactor and the impact of their impurities on design considerations, Plasma Sci. Technol. 20 (2018) 065602.

[36] G.T. Chapman, C.L. Storrs, Effective Neutron Removal Cross Sections for Shielding, 1955.

[37] T. Rockwell (Ed.), Reactor Shielding Design Manual, 1956. Usaec Report Tid-7004.

[38] J. Wood, Computational Methods in Reactor Shielding, Pergamon Press, 1982.

[39] Schaeffer, N. M. (Ed.), n.d. Reactor Shielding for Nuclear Engineers, Usaec Report Tid-25951, 1973, https://www.nrc.gov/docs/ML1000/ML100070680.pdf.

[40] Hydrogen details, https://en.wikipedia.org/wiki/Hydrogen.

[41] G. Hübschen et al., (Ed.), Materials Characterization Using Nondestructive Evaluation (NDE) Methods, Woodhead Publishing, 2016.

[42] C.J. Werner (Ed.), MCNP Users Manual-Code Version 6.2″, 2017. LA-UR-17-29981.

[43] J.M. McGhee, T.A. Wareing, D.A. Barnett, ATTILA Version 5: User Manual, Transpire Inc, Gig Harbour, WA, 2006.

[44] J. Allison, et al., Recent developments in GEANT4, Nucl. Inst. Methods Phys. Res. A 835 (2016) 186–225.

[45] G. Battistoni, et al., Overview of FLUKA, Ann. Nucl. Energy 82 (2015) 10–18.

[46] T. Piotrowski, et al., Experiments on neutron transport through concrete member and the potential for the use in material investigation, Acta Phys. Pol. A 128 (2015).

[47] H.R. Vega-Carrillo, et al., Neutron shielding for a 252Cf source, Memorias CIC Acapulco 2006 en CDROM, in: Proceedings IJM Acapulco 2006 on CDROM, 2006.

[48] S. Domański, et al., Experimental investigation on radiation shielding of high performance concrete for nuclear and radiotherapy facilities, Pol. J. Med. Phys. Eng. 22 (2) (2016) 41–47.

[49] R. Adeli, S.P. Shirmardi, S.J. Ahmadi, Neutron irradiation tests on B4C/epoxy composite for neutron shielding application and the parameters assay, Radiat. Phys. Chem. 127 (2016) 140–146.

[50] A. Seyhun Kipcak, et al., Characterization of boron carbide particles and its shielding behavior against neutron radiation, Energy Convers. Manag. 72 (2013) 39–44.

[51] R.J. McConn Jr., C.J. Gesh, R.T. Pagh, R.A. Rucker, R.G. Wlliams III, Radiation Portal Monitor Project: Compendium of Material Composition Data for Radiation Transport Modeling, Pacific Northwest National Laboratory, Washington, 2011.

[52] V.P. Singh, N.M. Badiger, Investigation of gamma and neutron shielding parameters for borate glass containing NiO and PbO, Phys. Res. Int. 2012 (2012) 954958.

[53] P. Gong, et al., Preparation and characteristics of a flexible neutron and g-ray shielding and radiation-resistant material reinforced by benzophenone, Nucl. Eng. Technol. 50 (2018) 470–477.

[54] M. Dong, et al., Preparation, shielding properties and mechanism of a novel neutron shielding material made from natural Szaibelyite resource, Prog. Nucl. Energy 106 (2018) 140–145.

[55] L. Seenappa, et al., Gamma, X-ray and neutron shielding properties of polymer concretes, Indian J. Pure Appl. Phys. 56 (2018) 383–391.

[56] H.L. Swami, et al., A neutronic experiment to support the design of an Indian TBM shield module for ITER, Plasma Sci. Technol. 21 (2019) 065601.

[57] Obodovskiy, Neutron Sources, Radiation, 2019.

[58] https://doi.org/10.1016/B978-0-444-63979-0.00019-7.

[59] Neutron detectors. In: Radioisotopes and Radiation Methodology, Med Phys 4RA3, 4RB3/6R03, n.d., https://www.science.mcmaster.ca/radgrad/images/6R06CourseResources/4RA34RB3_Lecture_Note_9_Neutron_Detectors.pdf.

[60] A.E. Profio, Radiation Shielding and Dosimetry, John Wiley & Sons, New York, 1979.

CHAPTER 12

Advanced multilayer composite structures for fast neutron detection and shielding protection applications

S.V. Naydenov[a], V.D. Ryzhikov[b], G.M. Onyshchenko[b], C.F. Smith[c]
[a]Institute for Single Crystals of the NAS of Ukraine, Kharkov, Ukraine
[b]Institute for Scintillation Materials of the NAS of Ukraine, Kharkov, Ukraine
[c]Naval Postgraduate School, Monterey, CA, United States

12.1 The challenge of developing new modern fast neutron detectors

One of the main challenges in nuclear security is the creation of detection systems for fast neutrons and mixed neutron/gamma radiation that would be highly efficient, compact, inexpensive, easy to use, rugged and robust with respect to unfavorable conditions, and reliable in operation. Reliable recognition of special nuclear materials (i.e., enriched uranium and plutonium), and other neutron-emitting materials require the creation of detectors with high detection efficiency for fast neutrons (not less than 50%–60%). At the same time, practically all of the state-of-the-art detectors proposed for the replacement of ^{3}He counters can efficiently detect only slow and/or thermal neutrons, relying on the radiative capture reactions of nuclei such as ^{6}Li or ^{10}B with very high thermal absorption cross sections, but relatively insensitive to fast neutrons. The probability of direct detection of fast neutrons with these systems without using moderators such as plastics or other hydrogenous materials is orders of magnitude lower, and the efficiency of direct detection therefore does not exceed a few percent. Even with massive and voluminous moderators to thermalize the fast neutrons, the fast neutron detection efficiency of such systems is not higher than 10%–20%, and for ^{3}He detectors about 10%.

At the same time, theoretical considerations, actual experiments, and numerical simulation of the interaction processes of fast neutrons passing through materials with heavy nuclei indicate that, alongside radiative capture (n, γ), which is not sufficiently efficient in the fast energy range, another

Micro and Nanostructured Composite Materials for Neutron Shielding Applications
https://doi.org/10.1016/B978-0-12-819459-1.00012-X
© 2020 Elsevier Ltd.
All rights reserved.

interaction mechanism can be used for efficient fast neutron detection—the reaction of inelastic scattering $(n, n'\gamma)$ of fast neutrons ([1–6]; and references therein). It has been found ([5–11], and others) that promising materials for such detectors are heavy-oxide scintillators with relatively large cross sections for inelastic scattering of fast neutrons on the heavy nuclei of their constituent atoms (i.e., ^{113}Cd, ^{155}Gd, ^{157}Gd, ^{184}W, ^{209}Bi, etc.). Such scintillators, $CdWO_4$ (CWO), $ZnWO_4$ (ZWO), $PbWO_4$ (PWO), $Bi_4Ge_3O_{12}$ (BGO), $Gd_2SiO_5(Ce)$ (GSO(Ce)), etc., have been used to create novel single-crystal detectors of fast neutrons and mixed gamma-neutron fields [8–12]. In these scintillators, the energy of fast neutrons is directly converted into the energy of gamma-quanta and conversion electrons, without the stage of preliminary moderation of the neutrons. In this case, the single-crystal scintillator plays a double role as an efficient converter of neutrons into secondary gamma-quanta of intermediate energies, and as a scintillator that detects these internal gamma-quanta in either a counting or spectrometric mode. These detectors show high detection efficiency of fast neutrons (in the range of 50%–70%) and high sensitivity [up to 49 cps/ (neutron/s·cm^2)] with compact scintillation assemblies using single crystals of dimensions ø40 × 80 mm coupled to 2″-photomultipliers. This allows the use of such neutron detectors in compact stationary systems and portal monitors for the detection of radioactive and fissionable nuclear materials [13, 14].

Recent studies [8–10, 13–15] have also shown the possibility to create fast neutron detectors of comparable efficiency on the basis of a novel multilayer composite scintillation structure that relies similarly on direct detection of fast neutrons through their interaction with materials of high effective atomic number. These studies describe an original heterogeneous scintillation structure (named ZEBRA), which comprises a series of alternating plates of two types—plates consisting of small particles of heavy crystalline scintillator material [i.e., CWO, ZWO, PWO, BGO, GSO(Ce), etc.] embedded in an organic matrix (silicon rubber), and plates of a clear plastic material (PMMA, polystyrene, or others), which simultaneously serve as a moderating material and light guides for the output of scintillation photons. In detecting fast neutrons, such a detector medium utilizes, to the maximum extent, not just one, but several channels of neutron interaction with heavy nuclei—inelastic scattering of fast neutrons scattered at different angles into the moderator, as well as resonance scattering and radiative capture of neutrons moderated inside the detector by elastic scattering in hydrogen-containing plastic. The detection of fast neutrons simultaneously over several channels of their interaction substantially increases the total detection efficiency. It should also be noted that such an approach, with a transition from homogeneous (single-layer) to heterogeneous (multilayer) detectors has been also considered in several other works [16–21] searching for new, more efficient types of composite neutron detectors.

12.2 Main nuclear mechanisms of fast neutron detection

There are several principal interaction phenomena related to detecting an incident flux of fast neutrons by materials comprising multilayer hybrid scintillator described here. In this chapter, we consider only those possible neutron reactions which are most important with respect to fast neutron detection by the ZEBRA detectors. Note that there are many other neutron reactions (including reactions such as $(n, 2n)$, (n, p) and other nonelastic processes apart from inelastic scattering) that are not the principal mechanisms for the ZEBRA detection system. To provide additional discussion about such reactions would only add unnecessary detail, and could introduce misunderstanding as to the processes that are important.

Several types of reactions of direct importance should be singled out: (i) inelastic scattering $(n, n'\gamma)$ of fast neutrons on heavy nuclei in the composite scintillator layers; (ii) elastic scattering (n, n) and deceleration (moderation) of neutrons of intermediate energies in the plastic layers of the detector; (iii) elastic $(n, n)_{res}$ and (iv) nonelastic resonance interactions, including resonant capture $(n, \gamma)_{res}$ of neutrons of resonance energies (from several eV to tens of keV) in the scintillator layers after their moderation in plastic layers; and (v) radiative capture (n, γ) of neutrons reaching the range of thermal energies, which would be especially efficient for scintillators with odd neutron-capturing nuclei, such as ^{113}Cd, ^{155}Gd, ^{157}Gd, etc.

Neutron inelastic scattering $(n, n'\gamma)$ in the range of energies E_n up to ~50 MeV occurs mainly through the formation of a compound nucleus. At fast neutron energies, about 5–6 MeV and higher, the excitation energy falls into a quasi-continuous spectrum of the compound nucleus levels, which allows the use of the statistical model of the nucleus [22, 23]. Within this model, the excitation energy (i.e., the incident neutron energy minus the nucleus recoil energy) is distributed onto the statistical fraction of the level spectrum, which determines the so-called nucleus temperature, T. The nucleus temperature is evaluated from the excitation energy U_{ex} as $T \approx \sqrt{U_{ex}/a}$, where the level density parameter $a \approx 10$. The excitation energy $U_{ex} = U^* + \varepsilon_n$ is the sum of the kinetic energy U^* brought by the incident neutron to the nucleus, and the binding energy ε_n of the captured particle (neutron), which then is followed by an the emission of the n' neutron from the compound nucleus. For a nucleus with mass number $A \approx 150$ and excitation energy $U_{ex} \approx 5 - 6$ MeV, the nucleus temperature is $T \approx 0.75$ MeV (see, e.g., [22]). The incident neutron energy $E_n \approx 4.5$ MeV is then of the order of the average energy of fast neutrons for a ^{239}Pu-Be source. In the statistical model of nucleus, the average nucleon energy in the nucleus is $\varepsilon_n = 2T$. Therefore, the average kinetic energy $E_{n'}$ of neutron emitted from the compound nucleus is, in this case, approximately equal to $E_{n'} \approx \varepsilon_n = 2T = 1.5$ MeV. In the residual nucleus, the remaining energy is ~3.5 MeV. This is sufficient for the excitation of several lower levels of the residual nucleus. This excitation is removed, as a rule, by the emission of accompanying gamma-quanta and/or conversion electrons (the probabilities of these transitions are nearly equal). For heavy nuclei, the energies of secondary gamma-quanta are in the range from tens of keV to several MeV. The conversion electron energies correspond to energies of the inner atomic shells, i.e., they are in the range of soft X-rays, typically tens of keV.

A peculiar feature of fast neutron inelastic scattering on heavy nuclei for neutrons in the 2–14 MeV energy range is rather significant (up to 80%) energy loss as a result of this reaction. Thus, the inelastically scattered neutron has much lower energy than the incident neutron. Because of this, fast neutrons of energies up to 10 MeV can be subject to inelastic scattering only once (or at most a few times), after which their energy becomes lower than the threshold required for inelastic scattering. The inelastic scattering channel is therefore closed, and such neutrons are not registered by a detector based on further inelastic scattering within the heavy-oxide scintillator. Therefore, when the scintillator thickness is increased, the recorded signal from inelastic scattering becomes saturated when such neutrons are detected. As a result, the detection efficiency becomes nearly constant after the thickness reaches 40–60 mm [8–10]. However, if the energy of these inelastically scattered neutrons could be lowered even more (to resonance energies of 1–10 keV or to thermal energies below the cadmium threshold of 0.5 eV), an additional detection channel of resonance scattering and radiative capture would be opened. In this channel, alongside elastic scattering, the reactions of resonance scattering and radiative capture and/or thermal radiative capture are also possible. Note that certain nuclei have large cross sections for such interactions (see Table 12.1). Resonance and thermal captures are accompanied by the emission of gamma-quanta in a broad energy

Table 12.1 Cross sections of neutron interactions with nuclei (mixtures of natural isotopes) present in heavy oxide scintillators.

Nuclei	$\sigma_{capture}$	$\sigma_{resonant}$	$\sigma_{inelestic}$
$_{30}$Zn	1.063	2.539	0.619
$_{32}$Ge	2.218	5.997	0.566
$_{48}$Cd	3.294×10^3	6.659×10^1	0.416
$_{64}$Gd	4.119×10^4	4.011×10^2	0.652
$_{74}$W	1.819×10^1	3.551×10^2	0.428
$_{82}$Pb	0.154	0.142	0.324
$_{83}$Bi	0.342	0.172	0.361

Cross-section values are given in barns (1 barn is equal to 10^{-24} cm^2).
Based on data from JENDL (Japanese Evaluated Nuclear Data Library), 2014. Japan Atomic Energy Agency, Nuclear Data Center, Japan. http://wwwndc.jaea.go.jp/jendl/j40/j40.html.

range, the recording of which can substantially increase the fast neutron detection efficiency.

Figs. 12.1 and 12.2 show the main interaction mechanisms between neutrons and the heavy nuclei (A, Z) of the scintillators used in this study. In Fig. 12.1, a scheme of inelastic neutron scattering is presented, with possible generation of the following interaction products:

(i) prompt gamma-quanta $(n, n'\gamma_1)$ from de-excitation of the compound nucleus $(A + 1, Z)^*$;
(ii) delayed (in the 0–30 μs range) gamma-quanta $(n, n'\gamma_2)$ from the de-excitation of the excited states $(A, Z)^*$ of the excited nucleus;
(iii) conversion electrons (e_1) in the transfer of the excess excitation $(A, Z)^*$ to the atomic orbitals of the final nucleus (A, Z);
(iv) inelastically scattered neutrons (n').

Fig. 12.2 illustrates the interaction channels of neutrons with resonance energies that appear as a result of deceleration of the initial fast neutrons in the plastic layers of the multilayer detector. This opens new channels for energy transformation in the composite heavy-oxide scintillators. As a result, in addition to the processes shown in Fig. 12.1, the following products can be generated:

(i) prompt gamma-quanta from resonance nonelastic reactions, including resonant capture $(n, \gamma_3)_{res}$;
(ii) prompt gamma-quanta from radiative capture $(n, \gamma_4)_{capt}$ in the thermal neutron range;
(iii) electrons from beta-decay of the excited parent compound nucleus $(A +1, Z)^*$ into the ground state $(A + 1, Z + 1)_{gs}$ or an excited state $(A + 1, Z + 1)^*$ of the daughter nucleus $(A + 1, Z + 1)$;

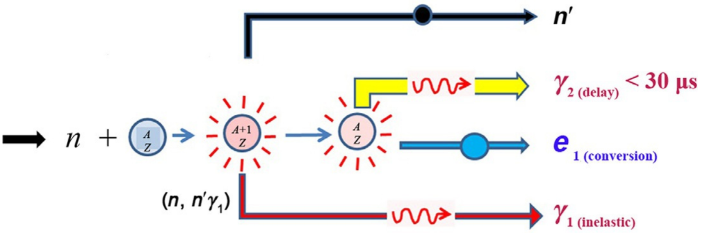

Fig. 12.1 Interaction products from inelastic scattering of fast neutrons with the heavy nuclei in the composite heavy-oxide scintillator.

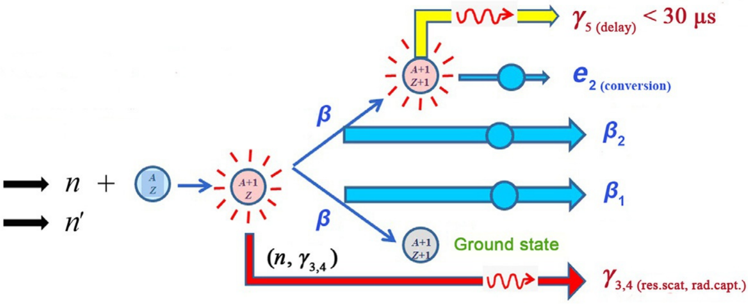

Fig. 12.2 Products resulting from the interaction of neutrons at resonance and/or thermal energies with the constituent nuclei of composite heavy-oxide scintillator. The index *n* denotes the neutrons moderated to resonance energies by elastic scattering in plastic layers and *n*′ the secondary neutrons with resonant energies emitted after inelastic scattering in inorganic scintillator, correspondently.

(iv) delayed (up to 30 μs) gamma-quanta γ_5 and conversion electrons e_2, which can be emitted in de-excitation of the daughter nucleus $(A+1, Z+1)^*$.

In the heavy-oxide scintillator layers of the composite structure, there is practically no deceleration of fast neutrons from elastic scattering reactions $(n, n)_{el}$ because energy transfer from neutrons to heavy and middle mass nuclei (as well as to oxygen nuclei) of the scintillator material is inversely proportional to atomic number, $\Delta E_{el} = 2EA/(A+1)^2 \approx E/A$ for $A >> 1$, and on average it does not exceed several percent of the neutron energy. If the detector includes (as in ZEBRA) periodically alternating plastic layers, which contain large amounts of hydrogen nuclei ($A = 1$), the picture is substantially changed. Theoretical estimates show that 35–40 mm of the total thickness of the plastic layers is sufficient to moderate the neutron energy of 1–2 MeV to 1 keV. The multilayered design of the ZEBRA detector is better than a double-layered design (i.e., one layer of scintillator plus one layer of moderator) or a three-layered design (i.e., a scintillator layer between two moderator layers), because the thicker scintillation layers record more completely the total flux of resonance neutrons—coming from deceleration of both the initial incident neutrons and the intermediary neutrons formed by inelastic scattering in the outer scintillation layers.

The resonance neutron cross sections (mostly due to radiative capture) for many heavy and middle mass nuclei are not generally less than the characteristic cross sections for inelastic scattering of neutrons (and sometimes they are even larger). Comparative values of microscopic radiative capture cross sections, based on an IAEA nuclear database [24], are presented in Table 12.1. They include cross-section data for radiative capture $\sigma_{capture}$ (in the energy range from 0.0253 to 0.5 eV), resonance scattering $\sigma_{resonant}$ with gamma-quanta escape (the resonance integral covers the energy range from 0.5 eV to 10 MeV), and inelastic scattering $\sigma_{inelastic}$ (for a fixed fast neutron energy 14 MeV) on nuclei that enter the composition of our heavy-oxide scintillators comprising ZWO, CWO, GSO(Ce), or BGO.

The resonance integral for resonance scattering (capture) cross section of such nuclei as ^{184}W or ^{157}Gd can reach hundreds of barns. Therefore, for recording the of resonance neutrons, a sufficient thickness of composite scintillators like ZWO or GSO(Ce) should not exceed 1 mm. Thus, with additional registration of resonance neutrons, the detection efficiency is increased, even though the total thickness of the active layers of heavy-oxide composite scintillators in our heterogeneous detectors is much smaller than the thickness of a single-crystal scintillator made of the same material (used in a conventional neutron detector with comparable efficiency).

12.3 Multilayer composite heavy-oxide fast neutron detectors (ZEBRA)

In studies by Ryzhikov et al. [8–10, 15], a new design (Fig. 12.3) of the multilayer composite scintillation ZEBRA-detector, which could detect mixed neutron and gamma radiation, was proposed and tested. The ZEBRA detector (Fig. 12.4) consists of alternating and optically connected (i.e., glued) planar parallel layers of two types: (1) 5–6 plates (films) of the scintillator material dispersed in a transparent organic matrix (rubber glue), with a thickness of ~1–2 mm; (2) 7–8 plates of a transparent plastic, with a thickness of ~5–7 mm, which act both as a moderator for neutrons and as a light guide for all scintillation photons.

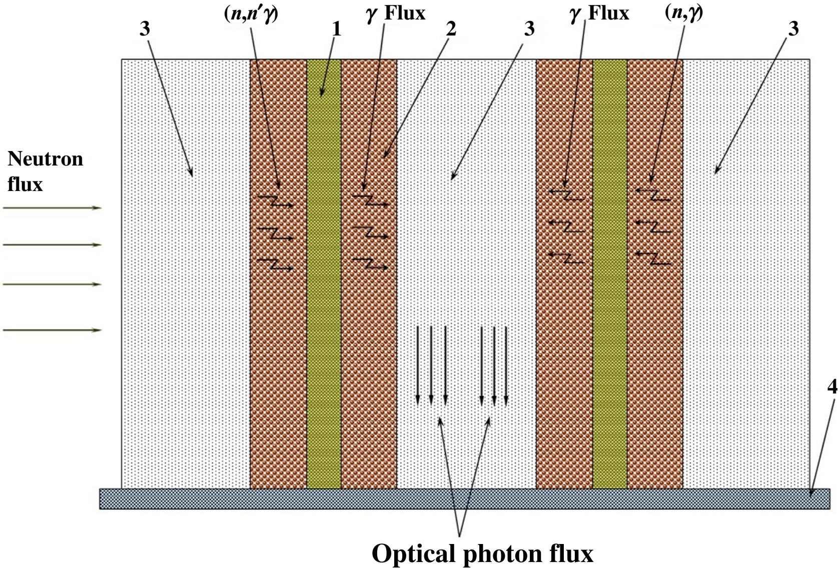
(n,n′γ)
γ Flux
γ Flux
(n,γ)
3
1
2
3
3
Neutron flux
4
Optical photon flux

Fig. 12.3 Design and functioning scheme of the multilayered composite detector (only few layers are shown): (1) internal reflector made of aluminized Mylar (it may be absent in many ZEBRA-detector variations); (2) active layer of composite scintillator material; (3) passive layer of light-conducting plastic; and (4) photoreceiver (PMT or Si-PM).

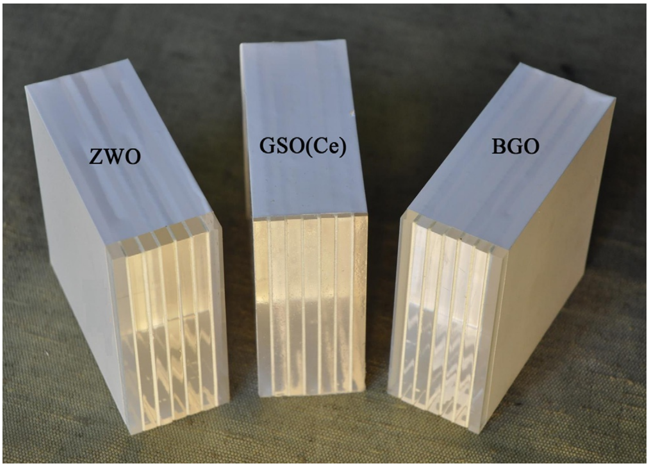
ZWO
GSO(Ce)
BGO

Fig. 12.4 Photos of ZEBRA detectors on the basis of the scintillators ZWO, GSO(Ce), BGO with dimensions 100 × 100 × 41 mm. The open end is to be connected to a photoreceiver.

The first layer type (i.e., the thin layers containing the dispersed heavy scintillator particles) required a transparent organic glue-like material with low-molecular weight and thermal shock resistance. For this layer type, the synthetic rubber SKTN-B, with a refractive index of $n_{glue} = 1.42$, was used. The average size of the heavy-oxide crystalline scintillator fragment in these composite scintillator layers was about 150–200 μm. The overall concentration of the small crystalline fragments (granules) was chosen such that the volume fraction of the active scintillator in the composite material was not less than 50%–60%.

For the second layer type (i.e., thicker light guides), transparent optical plastic polymethylmethacrylate (PMMA) with a refractive index of $n = 1.49$ (at light wavelength of 540 nm) and an absorption coefficient of $\alpha = 0.03\ \text{cm}^{-1}$ was used.

The outer surface of the detector is covered with a diffuse light-reflecting coating (except at the one face that is attached to the light-receiving device to provide optical contact and spectral matching). As an outer coating, a polytetrafluoroethylene (PTFE) membrane with a diffuse reflectivity coefficient of about 98% was used. The external reflector is very important for good light collection and high detection efficiency. An internal reflector as shown in Fig. 12.3 (i.e., an aluminized Mylar tape in the middle of the composite layers) was found not to be essential and is omitted in some of the detector variants tested. Although it provides a small increase in the scintillation output, it introduced production difficulties that did not justify the small improvement in performance. Nevertheless, detectors of both types were tested. The tested detectors without internal reflectors in the composite layers were found to have detection efficiencies approximately the same as those with reflectors.

It was experimentally found that a high detection efficiency of fast neutrons (up to 40%–50%) required that the full thickness of the detector be just 40 mm. This dimension is comparable to the diameter of the large single crystals generally used in homogeneous neutron detectors.

A set of ZEBRA detectors of large size ($100 \times 100 \times 41\ \text{mm}^3$) on the basis of different scintillators such as ZWO, BGO, GSO(Ce) were prepared and tested. Each detector had six composite layers of thickness 1 mm and seven layers of transparent plastic with thickness 5 mm (Fig. 12.4). The sensitive detector area under irradiation by neutron flux from the side (i.e., in the direction transverse to the plates) was $100\ \text{cm}^2$. In the general case, the multilayer detector comprises an arbitrary number of plates, without any limitations on their area.

For the transparent light-guide layers, use of a scintillating plastic transparent material was also considered. The neutron detection efficiency for the detectors incorporating scintillating plastic as the light guide material was determined to be much better, but the neutron-gamma rejection ratio was not as good. It is expected also that the production cost of this alternate configuration would be somewhat higher. Continued research and development of the ZEBRA detectors with scintillating plastics is anticipated to be a subject of future work.

The main difference between ZEBRA detectors and well-known conventional "capture gated detectors" [18, 19, 21] is that the latter are based on thermalization and the use of thermal neutron capture nuclei (such as ^{155}Gd, ^{157}Gd, ^{113}Cd) with very large thermal capture cross sections for the (n, γ) reaction for neutrons. In contrast, ZEBRA detectors include layers composed of composite heavy-oxide scintillators with heavy (Bi, W, Gd, Cd) and/or medium mass (Ge, Zn, Cd) nuclei with high probabilities of both fast neutron (above about $\sim$1 MeV) inelastic scattering and resonance neutron interactions (mainly, resonance capture with gamma-quanta and conversion electron emission) in an intermediate energy range from 10 s of eV to 10 s of keV. In addition to inelastic scattering, the resonance neutron interaction (capture) reaction is a key reaction for operation of ZEBRA detectors.

The ZEBRA detectors are designed for the direct detection of fast neutrons and for the discovery of small quantities of transuranic elements (by also detecting the accompanying gamma radiation). Detectors of this type are characterized by the following features:

(i) It is possible to prepare detectors of arbitrarily large working area of the detecting plates, which allows a substantial (by many times) increase in the sensitivity of such detectors in comparison with detectors based on inorganic single crystals.

(ii) The preparation of large-area layers of composite scintillators (on the basis of small-crystalline fractions of broken crystal fragments or microcrystalline powders obtained by solid-phase synthesis) is much simpler and less expensive than the growth of costly large-sized single crystals, the maximum size of which is essentially limited by the growth technology.

(iii) Within the framework of a multilayer design for such detectors, engineering combinations using different scintillation materials are possible, aiming at optimization of its productivity for different tasks.

The principle of operation of ZEBRA detectors is as follows. The incident neutrons interact with the layers of composite heavy-oxide scintillator and plastic. The composite scintillator layers contain heavy nuclei with high cross sections for both inelastic scattering and radiative capture in the region of resonant neutron scattering (the energy of epithermal and intermediate neutrons). The alternating transparent plastic layers serve as moderator of fast neutrons (from fast energies to epithermal/intermediate energies) and simultaneously as optical light guides through which the scintillation light can be transmitted. Fast neutrons interact directly with the layers of the composite scintillator through an inelastic scattering reaction if their energy is high enough for this [i.e., exceeding the energy threshold for inelastic neutron scattering (usually at least several hundred keV)]. Additionally, incident neutrons also interact with the heavy nuclei of composite scintillator material as a result of the resonance scattering reaction if their energy falls into the appropriate energy interval after moderation in the plastic layers. The moderation of the incident neutrons mainly occurs in the "thick" layers of hydrogen-containing plastic as a result of the elastic neutron scattering reaction. Elastic neutron scattering inside the "thin" layers of the composite can be neglected, since the volume fraction of the organic filler is small, and the energy loss due to scattering in the heavy-oxide scintillator granules is inversely proportional to the atomic mass of the heavy nuclei ($\Delta E_n \propto E_n/A \ll E_n$ if $A \gg 1$). Following elastic scattering in the transparent plastic layers, moderated neutrons may move in any direction, and most of them will reach the composite scintillator layers except the small fraction that are scattered out of the detector, primarily from the two outer plastic layers.

A feature of the ZEBRA detector is that the composite scintillator material consists of heavy nuclei with a large value of the resonance integral for the reaction $(n,\gamma)_{res}$ and/or concomitant resonance capture reactions with the emission of conversion electrons. If the value σ_{res} reaches several hundred barns (e.g., W, Gd, and Cd; see Table 12.1), then it can be shown that each neutron slowed down to the resonant energy region is highly likely to be absorbed and recorded as a secondary gamma quantum in a rather small volume of the scintillator of thickness of several hundred microns. Consequently, with high probability, fast neutrons moderated to resonance energies may be registered in each layer of the composite scintillator.

As a result of the reactions $(n,n'\gamma)_{fast}$ and $(n,\gamma)_{res}$ gamma-quanta of medium energies are produced which fall into the energy range of 20–300 keV, the energy range selected for signal registration in the

ZEBRA-detector system. In this case, gamma rays emitted in one active layer can be registered both in the same and in several adjacent layers of the heavy-oxide composite scintillator. Due to the small thickness of the transparent plastic layers, there is no significant attenuation of the secondary gamma radiation in them. The energy of gamma-quanta released by inelastic neutron scattering is more likely from 10 s of keV to 100 s of keV. The energies of gamma-quanta for resonant neutron capture (and/or energy of conversion electrons by accompanying reactions) are mainly about 10 s of keV, although they may reach 100 s of keV or even MeVs for some nuclei. The average energy of recoil protons released by fast neutrons (1–5 MeV) in the transparent plastic layers is about 100 s of keV, an energy range too small to produce many Compton electrons (much higher neutron energies would be required for this to be a significant factor). The most probable interaction of gamma-quanta with the heavy-oxide scintillator is via photoeffect because the energy of intrinsic gamma-quanta mainly lies in the range 20–300 keV as indicated by recent experiments.

The scintillation light obtained by the interaction of the secondary gamma-quanta (and/or conversion electrons) with the scintillator material, at first passes from the composite layer to the transparent plastic layer, and is transmitted to the photodetector (see Fig. 12.3). The geometry of the layers and the optical parameters of multilayer detectors (including optical and spectral correspondence of scintillators and light guides, interface to the PMT, characteristics related to total internal reflection and Fresnel losses, optical transparency of the composite scintillator and transparent plastic media, etc.) have been chosen specifically to optimize the light output.

Due to their design, ZEBRA detectors have gamma-ray sensitivity in addition to neutron sensitivity. But for fast neutron detection against background gamma radiation, the high-energy gamma rays are rejected by the choice of a special spectrometry range of 20–300 keV as previously proposed in methods for heavy-oxide scintillator fast neutron detection (see [5–11]). Lower energy gamma rays from background are also rejected by detector calibration (i.e., the use of initial and/or real-time special algorithms and software designed for neutron portal monitors based on our detectors), as well as the selected spectrometry range. Moreover, Compton gamma rays may be rejected by special separation methods including those developed previously and referred to as the "spectrometry windows" method [13, 14].

Unlike a homogeneous single-crystal detector in a heterogeneous detector, in the ZEBRA system, neutrons are detected by each active layer with a sensitive area equal to the cross-sectional area of the detector. Each active layer plays the role of an "internal" neutron mono-detector. In fact, neutrons are simultaneously recorded not by one but several such "internal" mono-detectors. The total area of all internal active layers will be higher than the sensitive area of the detector itself. Therefore, the sensitivity of the multilayer detector as a whole increases substantially, as evidenced in recent experiments. With a total thickness of active layers of 6–7 mm, the detection sensitivity of fast neutrons by a multilayer ZEBRA detector is comparable to the sensitivity of a single-crystal scintillation detector in which the scintillator layer is 10 times thicker in the direction of transmission (this is further discussed in Section 12.5).

12.4 Methods of fast neutron flux measurement and shield geometry

12.4.1 Problem of neutron radiative scattering in broad-beam geometry

Studies on detection efficiency and productivity of the prepared ZEBRA detectors under irradiation by ^{239}Pu-Be and ^{252}Cf fast neutron sources have been carried out. For these detectors, a large volume and a large sensitive area are characteristic features. This requires substantial changes in the procedures and geometry of measurements as compared with previous studies on neutron detection ([4–7]; and others) carried out for compact single crystals. In particular, the distance from the source to the detector was substantially increased (up to 100 cm) to preserve the geometry of a narrow (parallel) neutron beam falling on the detector, to avoid the effects of broad-beam geometry and the related edge effects, corrections, etc. Also, for detecting fast neutrons against the background of accompanying gamma radiation from one and the same source, it is necessary to use protection filters (as a rule, shields made of lead or iron with a thickness of up to 40–50 mm) for suppression of low- and medium-energy gamma-quanta. In the filter material, as well as in the objects surrounding the source and the detector (concrete walls, construction elements, parts of experimental installation, etc.), scattered radiation may appear due to the elastic and inelastic scattering of fast neutron flux. This stray emission can accumulate with time if long-lived nuclides are formed in interaction reactions with fast neutrons. This scattered radiation can distort the results of fast neutron detection by tens of percent or more.

The fast neutron measurement techniques described below were necessary to correctly determine fast neutron detection efficiency and to characterize the high fast neutron sensitivity of large-size/volume ZEBRA detectors.

In measurements using standard "broad-beam" geometry (Fig. 12.5), which is generally used for the measurement of the linear attenuation coefficient of particle beams, at specified distances between the source, detector, and filter (target), the number of neutrons coming to the detector is strongly dependent on the location and size of the filter, as well as on the detector size.

If, between the isotropic source and the detector (with small but finite dimensions), a protective disc-shaped screen is placed (Fig. 12.6), with radius R and a thickness h that is negligible as compared to its radius (i.e., $h \ll R$), it can be easily shown that losses in the full particle flux reaching the detector are determined only by the particles scattered by the screen at angles $0 \leq \theta \leq \theta_m$ (in analogy to the so-called Christi's theorem, see, for example, [25]), where θ is the angle between the direction of particles flowing through the screen and their direction after scattering.

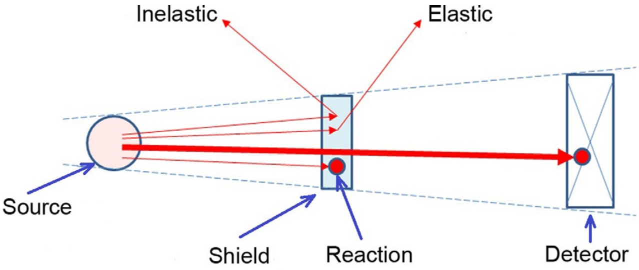

Fig. 12.5 Detection of fast neutrons in the "broad-beam" geometry (with a planar protective shield). Narrow neutron beams are subject to elastic and nonelastic reactions in the shield, distorting the neutron flux falling onto the detector.

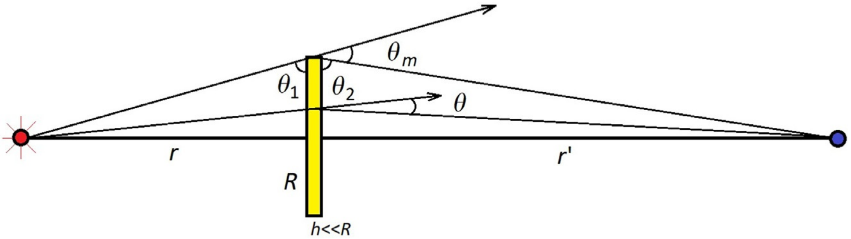

Fig. 12.6 Geometry of a planar shield between a source (on the left) and a detector (on the right) with a limiting scattering angle of θ_m.

Particles that are scattered at greater angles $\theta_m \le \theta \le \pi$ do not affect the total flux coming to the detector (as they would not reach the screen) and do not cause distortions.

The limiting scattering angle θ_m for particles falling onto the detector after scattering from the disc edge is calculated from the following relation (as shown in Fig. 12.6):

$$\theta_m + \theta_1 + \theta_2 = \pi; \quad \tan\theta_1 = \frac{r}{R}; \quad \tan\theta_2 = \frac{r'}{R}. \tag{12.1}$$

This limiting angle is equal to

$$\theta_m = \arctan\left[\frac{R(r+r')}{rr' - R^2}\right], \tag{12.2}$$

where r is the distance between the source and the screen and r' is the distance between the screen and the detector. The condition for minimum scattering-caused distortions is $\theta_m \ll 1$ (in this case any scattered neutrons do not affect the total flux arriving at the detector). For realistic cases, the condition for minimum scattering-caused distortions leads to the extremum condition for auxiliary "distortion" function $f(r; R, d)$:

$$f(r; R, d) = \min; \; f(r; R, d) \equiv |\tan\theta_m| = \frac{Rd}{|r(d-r) - R^2|}, \tag{12.3}$$

where $|\ldots|$ is the absolute value sign, and $d = r + r'$ is the distance between the source and the detector. Fixing the R and d values as parameters, the function $f(r; R, d)$ has a minimum at $r = r_* = d/2$. At this point $f_* = f(r_* = d/2) = (4R/d)/|1 - (2R/d)^2|$. From this it follows $f_* \approx 4R/d \ll 1$ if $d \gg 2R$, which yields the optimization condition

$$\text{planar shield}: \quad r = r' = \frac{d}{2}; \quad d \gg 2R \quad \Leftrightarrow \quad r \gg 4R. \tag{12.4}$$

The second condition in Eq. (12.4) is also necessary to avoid singularity of the function $f(r; R, d)$ in the special case that $r = d/2 = R$ which physically corresponds to strong scattering-caused distortions. To minimize distortions, the protection shield should be located exactly in the middle between the source and the detector, which should be sufficiently placed at a distance $r > 4R$ (i.e., the distance between the detector and the source should be much greater than the shield size). The distance between the source and the detector should also be large as compared to their linear dimensions, $R \gg l_s$, l_d, where l_s is the source dimension and l_d is the detector size.

Otherwise, the isotropic character of radiation would be violated with the appearance of edge effects. It should be noted that the relationship between the size of the screen, the detector, and the source could remain arbitrary. Also, condition (12.3) remains valid if the screen is not disc-like, but has the form of a rectangular plate with length and width much larger than thickness.

Scattering-caused distortions will be maximal under condition

$$f(r;R,d)=\max \quad \Rightarrow \quad rr'-R^2\approx 0. \tag{12.5}$$

Thus the closer the system is to condition (12.5), the worse the performance of neutron shield in providing radiation protection from shield scattering distortion. From Eq. (12.5) it follows:

$$r=r_\pm=\frac{d}{2}\left[1\pm\sqrt{1-4\left(\frac{R}{d}\right)^2}\right]\approx\frac{d}{2}\left[1\pm\left(1-2\left(\frac{R}{d}\right)^2\right)\right] \quad \text{if} \quad R\ll d. \tag{12.6}$$

There are two cases of strong shield distortion:

$$\begin{cases} 1) \quad r=r_+\approx d \quad \Rightarrow \quad r'\ll d \\ 2) \quad r=r_-\approx\dfrac{R^2}{d} \quad \Rightarrow \quad r\ll d \end{cases} \tag{12.7}$$

Therefore, neutron shielding will be worse if the planar shield is too close to either the source or the detector (the same is true for shields to protect other objects, personnel, and so on).

12.4.2 Spherical shield geometry

Condition (12.4) indicates only a way to minimize the effects of scattered radiation in the geometry of "broad beams." However, it does not allow us to exclude scattered radiation completely. A more efficient compensation of scattered radiation can be obtained if the measurements are carried out not in planar, but in spherical geometry (see, for example, [26]), using filters that fully surround the source and/or the detector (Fig. 12.7).

If the substance of which the protection is made (in the form of an ideal sphere of radius R) can only scatter neutrons, and practically does not absorb them (e.g., an iron or lead sphere), then the number of neutrons coming out of the sphere will not change along any direction from the source to the

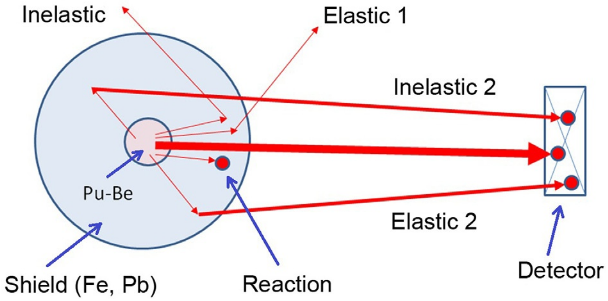

Fig. 12.7 Detection of fast neutrons from a spherically shielded source. Compensation is realized for narrow neutron beams scattered in different points of the sphere (beams 1 and 2), directed initially toward the detector (beam 1) and away from it (beam 2).

detector (due to spherical symmetry), so the neutron current will be unchanged in any point of the detector. The scattering of neutrons, i.e., their escape from the narrow beam directed to the detector, in certain points of the spherical layer is compensated by scattering of neutrons (with their "joining" the beam) in other points. The resulting neutron flux onto a finite-sized detector will be also unchanged. An important condition for this is the isotropic character of the radiation source. If this were not the case, after scattering, the angular distribution of the radiation will change, and, consequently, the beam falling onto the detector also changes (in the absence of protection). However, if the distance between the source and the detector is sufficiently large [estimates give the same condition (12.4) $r > 4R$ as in the case of planar geometry], the isotropic character of the radiation is preserved, and the inverse square law $I(r) \propto I_0/r^2$ for flux intensity at the distance r from the source is not violated. If we neglect also the dependence of detector efficiency on neutron energy, $\varepsilon(E) \approx \varepsilon = \text{const}$, the counting rate V of the detector, if spherical protection from gamma-quanta is used, can change only because of possible absorption of neutrons in the shielding material. The appropriate correction, which is the same for all measurements, is determined with an error of less than several percent. It is equal to

$$\text{spherical shield}: \quad V \rightarrow k_c V; \quad k_c = \frac{V^*}{V_0^*} = \exp\left(-n\sigma_a d_{sph}\right), \tag{12.8}$$

where k_c is the correction coefficient for the case when spherical protection is present, n is the concentration of heavy nuclei in the protection material, σ_a is the absorption cross section of fast neutrons, and d_{sph} is the thickness of spherical layer. Readings of calibration measurements with a test detector with and without protection are denoted as V^* and V_0^*, respectively.

Let us carry out calculations according to Eq. (12.8), e.g., for lead protection with a spherical layer of 40 mm thickness. The concentration of nuclei $n = N_A\rho/M$, where $N_A = 6.023 \times 10^{23}\,\text{mol}^{-1}$ is the Avogadro number, ρ is the density of the protection material, and M is the molar (atomic) mass. For lead, the molar mass is 208 $\text{g}\cdot\text{mol}^{-1}$, the density is 11.3 $\text{g}\cdot\text{cm}^{-3}$, the neutron absorption cross section averaged over the energy spectrum for ^{235}U fission is $\sigma_a = 0.0024$ barn, whence $k_c \approx 0.97$, i.e., the losses of the full neutron beam in the shield material are about 3%. For a spectrum of high-energy fast neutrons, these losses are even smaller. Thus, in lead the capture cross section of neutrons with 14 MeV energy is 0.00011 barn, which gives losses in protection from gamma-quanta not exceeding 0.14%.

The multiple elastic scattering of neutrons in the shield substantially distorts the simple expression (12.8), since multiple changes in the neutron movement direction violate the spherical symmetry of distribution of the scattered beams, and some of the advantages of the spherical shield are lost. However, elastic neutron scattering cross sections are not so large for heavy nuclei such as iron and lead as for light nuclei (in lead, the free path length reaches 15 cm at a neutron energy of 4 MeV). This make it possible to use spherical protection of large thickness, which will be sufficient for full absorption and discrimination of gamma-quanta emitted by the source up to energies of several MeV.

According to the method of fast neutron detection using heavy-oxide single crystals and multilayer composite scintillators, neutrons are detected mostly by gamma radiation that is emitted by scintillator nuclei from the reactions $(n, n'\gamma)$ and $(n, \gamma)_{res}$. To suppress the accompanying gamma radiation from the neutron source, experiments using a filter in the form of a lead sphere with an outer diameter of 100 mm, a spherical layer thickness of 40 mm, and an internal well to place the source in the center of the sphere were completed. To exclude the effects of external high-energy gamma-quanta on detector readings, the spectrometric range of gamma-quanta detection was chosen as 20–1000 keV. To quantitatively account for the effects of spherical protection on measurements, it is sufficient to measure the counting rate with and without a filter by a detector with a calibrated efficiency. In these experiments, a detector based on a ^{6}LiI (Eu) scintillator (96% enrichment with ^{6}Li) of dimensions ø15 × 10 mm was used. It was found that for ^{239}Pu-Be source inside the said lead sphere the neutron flux was weakened by not more than 3%–4%.

12.4.3 Fast-neutron energy transformation by spherical shield

The protection does also change the energy spectrum of neutrons coming from the source. The transformation is mainly felt in the low-energy range of the fast neutron spectrum, since energy losses due to elastic scattering on lead nuclei do not exceed 1%, while losses in the threshold reaction of inelastic scattering $(n, n'\gamma)$ at energies above 150 keV will be substantially higher. The results of model calculations (using the GEANT4 package) to determine the neutron spectrum after passing through spherical protection show that neutrons of 3–8 MeV energy participate very efficiently in the inelastic scattering reaction in lead. The energy range 1–3 MeV of the transformed spectrum gets an additional contribution from this reaction. The neutron flux in the 1–11 MeV range is only redistributed over energy values and remains essentially unchanged as compared with the neutron flux in the absence of lead protection. The number of neutrons escaping in the direction to detector remains nearly the same (i.e., changed by less than 0.5%) as in the absence of protection from gamma-quanta.

12.5 Fast neutron detection by heavy-oxide single-crystal and multilayer composite scintillator detectors

12.5.1 Typical experimental setup

Based on previous studies, an experimental scheme (Fig. 12.8) was developed and an experimental board was prepared for recording fast neutrons

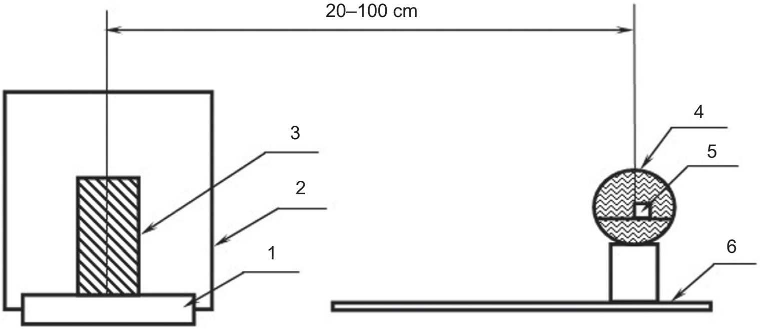

Fig. 12.8 Experimental setup for the measurement of fast neutron detection efficiency in direct spherical geometry of the source with protection from gamma-quanta: 1—photoreceiver (2″ or 3″ Hamamatsu R1307 PMT and 5″ ET Enterprises Limited 9390 KB PMT in correspondence with the different sizes of scintillation detectors from $10 \times 10 \times 10\ \mathrm{mm}^3$ up to $100 \times 100 \times 41\ \mathrm{mm}^3$ volume), 2—light protective housing, 3—detector under study (scintillation material), 4—lead sphere, 5—neutron source, and 6—supporting surface with source movement mechanism and scale bar.

by single-crystal detectors and multilayer ZEBRA detectors of different sizes. The neutron flux density at the detector location was determined according to the reference data of the source. Two different sources were used in these measurements:

- ^{239}Pu-Be isotropic source, with average neutron energy 4.5 MeV, output neutron flux 1.06×10^5 neutron/s, and flux density at $r = 100\,\text{cm}$ from the source 0.76 neutron/(см^2·s); the source dimensions were ø20 × 30 mm;
- ^{252}Cf source with average fast neutron energy 2.13 MeV, activity 20×10^6 Bq, output neutron flux 2.35×10^6 neutron/s, and flux density at $r = 100\,\text{cm}$ from the source 2.34 neutron/(см^2·s).

The lead shield ensured discrimination of the accompanying gamma radiation of the source. Additionally, the source could be coupled with a screen of gadolinium oxide to eliminate thermal neutrons. The neutron and gamma-radiation spectra of the sources are shown in Figs. 12.9 and 12.10.

The neutron spectra of ^{239}Pu-Be and ^{252}Cf sources are different (see, for example, [27]). In the first case, it is a characteristic spectrum of the nuclear reaction $^{9}Be(\alpha, n)^{12}C$ due to the capture of alpha particles formed as a result of ^{239}Pu decay. In the second case, it is a spectrum of spontaneous fission neutrons. However, after passing through the spherical lead protection, the transformed neutron spectrum from the ^{239}Pu-Be source also resembles that of the fission neutron spectrum. Therefore, the measurements of parameters of fast neutron detectors (detection efficiency and sensitivity) using both sources can be considered equivalent in the spherical geometry.

12.5.2 Fast neutron response for solid-state single-crystal and multilayer composite scintillator detectors

Within the framework of the measurement scheme in Fig. 12.8, a set of measurements was carried out for the detection of fast neutrons by heavy-oxide single-crystal and multilayer composite scintillators, including measurements of the spectrometric response of the detectors to the spectra of gamma-quanta emitted from fast neutron interactions with heavy scintillator nuclei, and measurements of neutron detection efficiency. This efficiency is defined as ratio of the number of registered neutrons N_{reg} to the total number of neutrons N entering the detector during a specified time interval:

$$\varepsilon(\%) = \frac{N_{reg}}{N}. \tag{12.9}$$

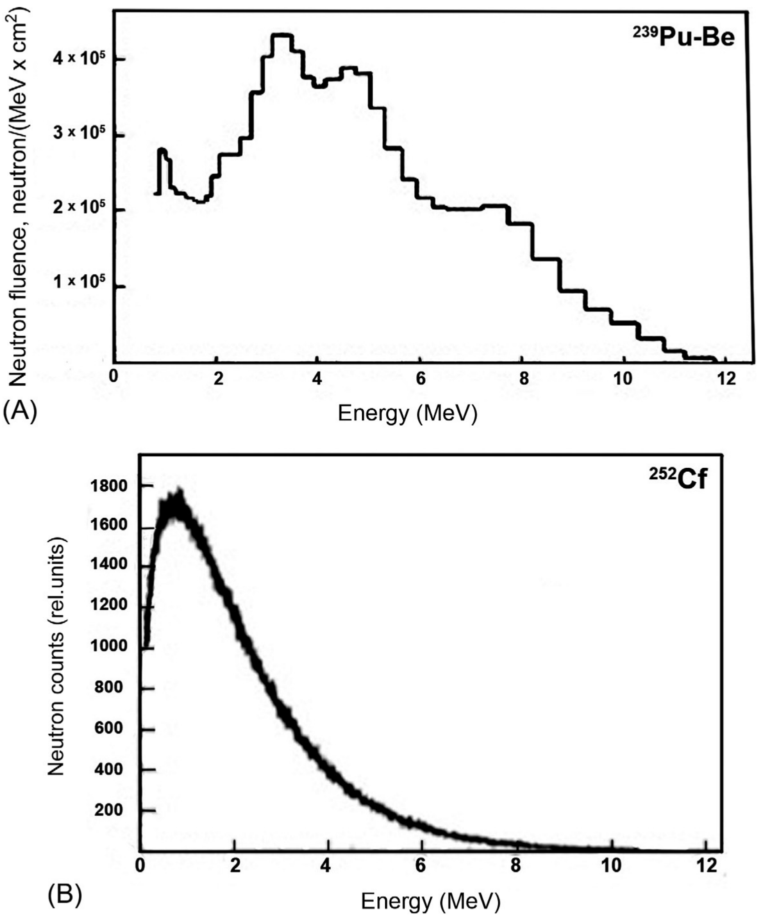

Fig. 12.9 Energy spectra of fast neutrons from ^{239}Pu-Be (A) and ^{252}Cf (B) radioactive sources.

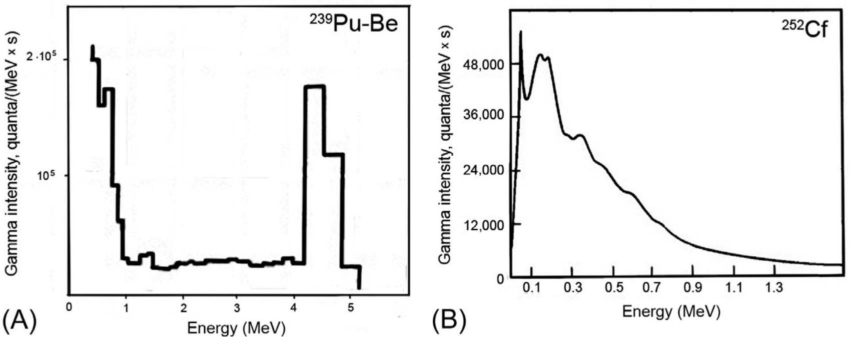

Fig. 12.10 Energy spectra of γ-radiation from ^{239}Pu-Be (A) and ^{252}Cf (B) radioactive sources.

For “heavy-oxide” single-crystal scintillators such as ZWO, CWO, GSO(Ce), BGO, and some others, it was found that the spectra of secondary gamma radiation recorded in the inelastic reactions $(n, n'\gamma)$ under irradiation by fast neutrons are qualitatively similar in the energy range $E_\gamma = 20\text{-}300\,\text{keV}$ (see Fig. 12.11) and even in a wider range $E_\gamma = 20\text{–}1000\,\text{keV}$. This supported the conclusion that the interaction mechanism of fast neutrons with the constituent material of the “heavy-oxide” scintillator (inelastic scattering) in the two energy ranges was also similar. The maximum sensitivity of the oxide scintillator response to fast neutrons was found in these ranges. Our estimates show that more than 90% of all the integral signal recorded by the pulse analyzer is in the spectrometric range of $E_\gamma = 20\text{–}300\,\text{keV}$. The measurements in the pulse analyzer channels below 20 keV are limited by internal noise of photomultiplier tube and other electronic components in the receiving-detecting circuit. Measurements above 1 MeV are characterized by small amplitude of the neutron response pulses, since gamma-quanta of such high energies are formed with low probability in inelastic scattering (with higher neutron energies and higher excitation energy of the compound nucleus, the more probable interactions are inelastic processes with the escape of particles, and not the emission of gamma-quanta [i.e., the processes of $(n, 2n)$, (n, α) and similar types]). Therefore, the 20–300 keV or 20–1000 keV ranges were chosen as working ranges for these measurements. With the selection of

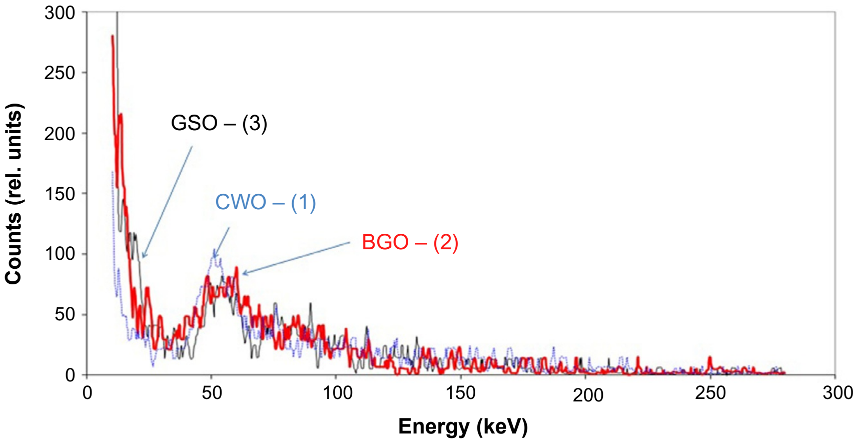

Fig. 12.11 Characteristic responses of fast neutron detectors based on heavy-oxide single crystals CWO, BGO, GSO(Ce) of the same size $10 \times 10 \times 10\,\text{mm}^3$ obtained from the ^{239}Pu-Be source with a 4 cm Pb-sphere gamma shield.

the wider window $E_\gamma = 20\text{–}1000\,\text{keV}$, the detector sensitivity is slightly increased, but the separation of the useful signal from the high-energy component of natural background becomes worse.

The scintillation response of multilayer ZEBRA detectors was also obtained from the same ^{239}Pu-Be source with Pb protection from the accompanying gamma radiation. The results are shown in Figs. 12.12–12.14. The neutron flux density was 0.46 neutron/s cm^{-2}. The value of pulse counts is given on a logarithmic scale. Channel number 200 corresponds to the detection of secondary gamma-quanta energy of about 5 keV, and channel number 2000 corresponds to gamma-equivalent energy of 50 keV. The main scintillation response of ZEBRA detectors to fast neutrons is limited by the low-energy spectrometric range below 60 keV for the detection of secondary gamma-quanta. This confirms that resonant neutron capture plays an important role in the response of ZEBRA detectors.

In the spectrometric mode, by cutting out the working energy range from the detector instrument spectrum and summing up the number of recorded pulses, the counting rate V for pulses of all recorded neutrons can be determined, as can the counting rate V_0 without the source. The counting rate can also be measured in the counting mode. As it can be seen from these measurements, the detection efficiency in the counting mode is about 30% higher than that in the spectrometric mode with the window $E_\gamma = 20\text{–}300\,\text{keV}$ (i.e., not all pulses from reactions of neutrons with

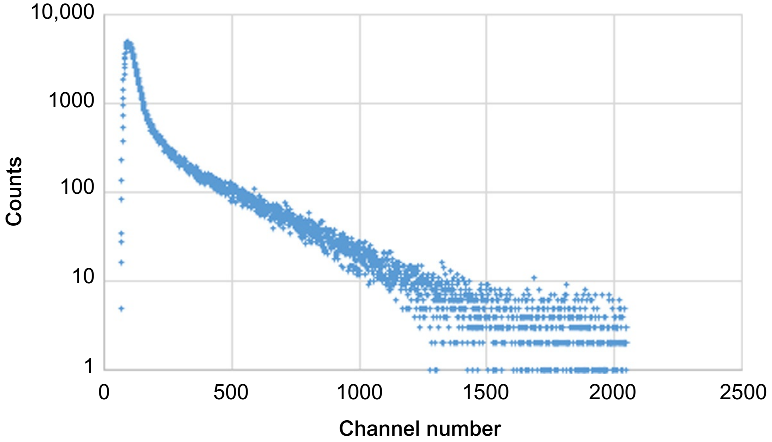

Fig. 12.12 Fast neutron scintillation response for a detector based on the multilayer composite scintillator ZEBRA-ZWO of size 100 mm × 100 mm × 41 mm.

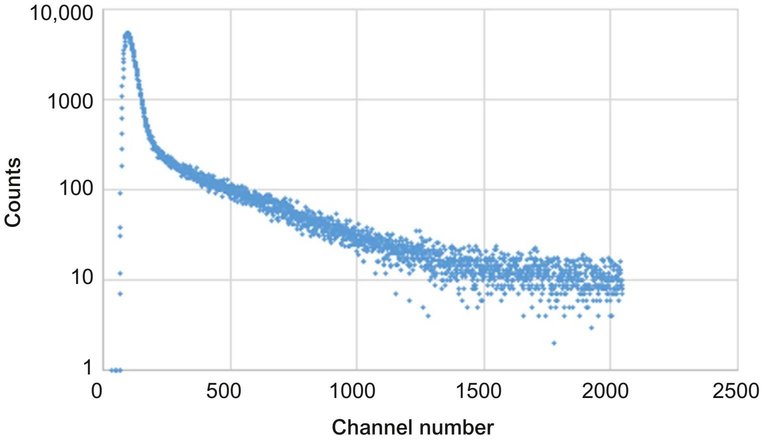

Fig. 12.13 Fast neutron scintillation response for a detector based on the multilayer composite scintillator ZEBRA-BGO of size 100 mm × 100 mm × 41 mm.

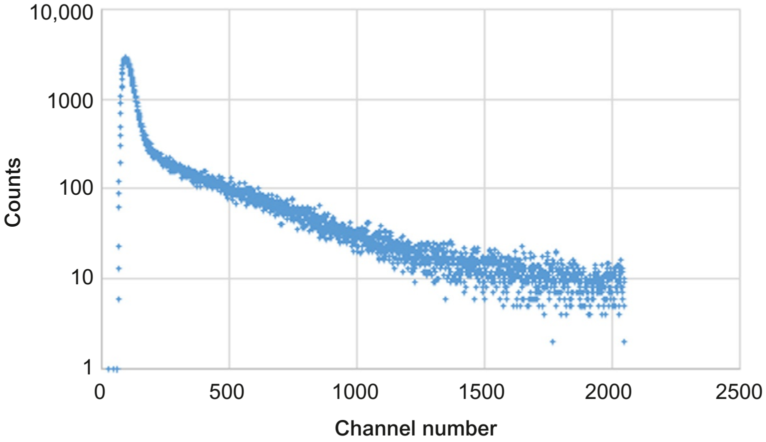

Fig. 12.14 Fast neutron scintillation response for a detector based on the multilayer composite scintillator ZEBRA-GSO(Ce) of size 100 mm × 100 mm × 41 mm.

scintillator material are recorded in the spectrometric mode). After calibration of the detecting system, we may obtain the detection efficiency as

$$\varepsilon = (kk_c)^{-1}\left(\frac{V - V_0}{F - F_0}\right), \tag{12.10}$$

where k is the calibration coefficient, which is equal to the average number of counting pulses per recorded neutron; k_c is the correction coefficient

(12.8) in the case when protection from gamma-quanta is present; F and F_0 are neutron fluxes from the source and in the absence of source (background), respectively, in the point of recording by the detector; the neutron background value $F_0 \ll F$ is usually neglected. The detection efficiency will be further given in percent, $[\varepsilon] = (counts \cdot s^{-1})/(neutrons \cdot s^{-1}) = [\%]$.

12.5.3 Neutron detection efficiency of heavy-oxide single-crystal scintillator detectors

In Table 12.2, we present the results of measurements of detection efficiency of fast neutrons, as well as neutrons moderated to resonance and slow (thermal) energies, in detectors with the heavy-oxide single-crystal scintillators ZWO, CWO, BGO, GSO(Ce), and some others in comparison with a ^{6}LiI(Eu) detector of thermal neutrons and a ^{3}He counter of fast neutrons.

To exclude contributions from slow neutrons (with energies below 0.5 eV) we used screens made of cadmium with thickness 0.5 mm or gadolinium oxide Gd_2O_3 with thickness up to 10 mm. The cadmium nuclei, when absorbing slow neutrons, can emit hard gamma-quanta with energies up to 7.5 MeV, which do not fall into the working spectrometric range of the detector (20–300 keV) and are thus cut out in the measurements. The gadolinium nuclei absorbing slow neutrons also practically do not emit gamma-quanta in the said energy range. For deceleration of fast neutrons

Table 12.2 The detection efficiency of fast neutron scattering by single-crystal scintillators of dimension 10 × 10 × 10 mm^3 in the absence of a moderator (ε_{fast}), with moderator (paraffin) of 1 cm thickness ($\varepsilon_{fast+res}$) and 6 cm thickness ($\varepsilon_{res+slow}$).

Scintillator	ε_{fast} (%)	$\varepsilon_{fast+res}$ (%)	$\varepsilon_{res+slow}$ (%)
ZWO	54	70	44
CWO	42	46	67
BGO	48	83	34
GSO(Ce)	46	90	65
LSO(Ce)	43	–	–
LuAG(Ce)	41	68	–
YSO(Ce)	17	–	–
^{6}LiI(Eu)	25	30	93[a]
^{3}He counter	5–8	–	95[b]

[a] Size ø12 × 10 mm. Response to reaction of radiative capture $^6Li(n,\alpha)^3H$ at $E_n = 0.0253$ eV.
[b] With massive 1000 × 200 × 50 mm plastic moderator of about 10 kg weight.
The neutron flux density at the recording point at the distance of 26 cm from the source ^{239}Pu-Be is 12.8 neutron/(s·cm^2).

in our measurements, the detector was surrounded from the outside by a layer of hydrogen-containing moderator (paraffin of 1 and 6 cm thicknesses, respectively).

For scintillators of small volume (1–10 cm^3) the differences in measured neutron detection efficiency for cases of planar or spherical protection from the source gamma-quanta are not significant. For detectors of larger size, better results are obtained with measurements in spherical geometry, when the scattered radiation in the protection is compensated better (see the previous section).

The results presented in Table 12.2 show that opening of additional channels of resonance scattering ($\varepsilon_{fast+res}$ column) in the detection of fast neutrons always increases the detection efficiency. At the same time, it can be seen ($\varepsilon_{res+slow}$ column) that, if the moderator thickness is excessive (i.e., above 40 mm), for most oxide scintillators not containing neutron-capturing nuclei of cadmium or gadolinium, the detection efficiency has strongly decreased. This is caused by the following: (i) after moderation the number of fast neutrons in the incident beam has decreased, and (ii) their energy becomes lower than the inelastic scattering threshold. This strongly reduces the contribution of this reaction to the signal recorded by the detector. Both these facts suggest physical reasons that make the multilayer design (with several alternating moderator layers of small thickness between layers of heavy-oxide scintillator) appears to be highly efficient for detection of fast neutrons.

12.5.4 Neutron detection sensitivity of heavy-oxide single-crystal scintillator detectors

Similar measurements of fast neutron detection efficiency with heavy-oxide scintillators of large volume (dimensions ø40 × 80 mm) yield results that are comparable with those presented earlier. However, with larger scintillator dimensions the detector sensitivity increases. The sensitivity is defined as ratio of the counting rate of the useful signal to the flux density of the incident neutrons:

$$\eta = \frac{(V - V_0)}{(I - I_0)}. \tag{12.11}$$

The detector sensitivity is formally expressed in area units, $[\eta] = cps/(nps \cdot cm^{-2}) = [\mathrm{cm}^2]$. Within the framework of geometry of planar parallel “narrow beams,” the following relationship can be obtained:

$$\eta \approx \varepsilon S_{eff}, \tag{12.12}$$

where the effective area $S_{eff} = S_{det} <\cos\psi>$ of the total sensitive surface of the detector is introduced; S_{det} is the apparent area of the detector surface in the direction of irradiation; and $<\cos\psi>$ is the average value of the cosine of angle between the surface normal and irradiation direction. For scintillators of rectangular shape, S_{eff} coincides with the area of their side surface in the direction of irradiation (i.e., perpendicular to the surface). For scintillators of cylindrical shape $D \times H$, under irradiation onto the end face S_{eff} coincides with the area of cylinder cross section $S_{eff} = \pi D^2/4$, and under irradiation onto the side normal to the cylinder axis $S_{eff} = (2/\pi)DH \approx 0.64\,DH$. Thus, for single crystals of dimensions 10 × 10 × 10 mm^3 the detector sensitivity is $\eta = \varepsilon \times 10^{-2}\,\text{cm}^2$. For single crystals of dimensions 40 × 80 mm under side irradiation, $\eta \approx \varepsilon \times 20.37\,\text{cm}^2$. For multilayer ZEBRA materials of dimensions 100 × 100 × 41 mm under irradiation normally to the plates $\eta \approx \varepsilon \times 10^4\,\text{cm}^2$.

Table 12.3 presents, for comparison, the obtained data on sensitivity of single-crystal and multilayer fast neutron detectors on the basis of heavy-oxide scintillators ZWO, BGO, GSO(Ce).

It should be noted that the sensitivity to fast neutrons of the proposed multilayer ZEBRA detectors of dimensions 100 × 100 × 41 mm is 2 times higher than the sensitivity of detectors based on heavy-oxide scintillator single crystals and is comparable to the sensitivity of a typical ^{3}He counter with size and weight that is more than 10 times larger.

12.5.5 Neutron detection efficiency of multilayer heavy-oxide composite ZEBRA detectors

To conclude, Table 12.4 presents the collected data on fast neutron detection efficiency measurements carried out using multilayer detectors on the basis of composite scintillators ZWO, BGO, and GSO(Ce) with the same number and thickness of the layers (i.e., with the same total thickness of the detector), but with different sensitive areas. The measurements were carried out in conditions of broad-beam geometry and conditions of spherical geometry accounting for corrections for the natural background. However, the experimental installation was placed in a closed space, and near the detector and neutron source there were elements of metal construction, laboratory furniture, concrete walls, etc., so, there was high probability of accumulation of scattered radiation from reactions of fast neutrons $(n, n'\gamma)$ (iron) and (n, γ) (concrete, etc.), as well as from gamma-ray scattering emitted by

Table 12.3 Sensitivity of fast neutron detectors on the basis of single-crystal and multilayer scintillators of different sizes.

Scintillator	Sizes (mm)	Counts rate (counts $\cdot$ s^{-1})	Neutron flux (neutron $\cdot$ s^{-1} $\cdot$ cm^{-2})	Sensitivity (cm^2)
CWO	ø45 × 42	9.5	0.76	12.50
ZWO	ø45 × 73	12.6	0.76	16.58
CWO	ø63 × 100	20	0.76	26.32
BGO	ø40 × 80	8.73	1.14	23.28
GSO(Ce)-ZEBRA	100 × 100x41	60	1.08	55.56
^{3}He counter[a]	1000 × 160 × 50	21	N/A	48.00

[a] With massive 1000 × 200 × 50 mm plastic moderator of about 10 kg weight.

Data are given for the counting rate of useful signal and flux density of neutrons falling onto the detector.

Table 12.4 Sensitivity and efficiency [calculated from Eq. (12.12)] of fast neutron detection by multilayer ZEBRA-detectors on the basis of heavy-oxide composite scintillators.

Composite scintillator	Size (mm)	Neutron flux (nps·cm^{-2})	Sensitivity, η (cps/nps·cm^{-2})	Efficiency, ε (%)
BGO-ZEBRA	40 × 40 × 41	3.85	6.4	40
ZWO-ZEBRA	40 × 40 × 41	3.85	7.04	44
GSO(Ce)-ZEBRA	40 × 40 × 41	3.85	7.8	49
BGO-ZEBRA	100 × 40 × 41	1.70	16.0	40
ZWO-ZEBRA	100 × 40 × 41	1.70	11.4	45
GSO(Ce)-ZEBRA	100 × 40 × 41	1.70	19.6	50
BGO-ZEBRA	100 × 100 × 41	1.08	40.0	40
ZWO-ZEBRA	100 × 100 × 41	1.08	46.0	46
GSO(Ce)-ZEBRA	100 × 100 × 41	1.08	51.0	51

The measurements were carried out in the counting mode. Neutron sources ^{239}Pu-Be and ^{252}Cf were used. The measurement errors do not exceed several percent.

neutron source and scattered by external metal and concrete constructions. According to our estimates, the measured values were higher than the physical detection efficiency of fast neutrons that should be measured in ideal conditions. However, in real conditions where the detection of hidden nuclear materials would be carried out, the efficiency and sensitivity of detection systems would be expected to correspond to these measured results.

As can be seen from Table 12.4, within experimental error, the detection efficiency of fast neutrons does not vary significantly with size (area) of the ZEBRA detectors, but sensitivity increases directly with growth of both dimensions, i.e., dependent on the cross-sectional area of the plates in a broad spatial range. The detection efficiency reaches 40%–50%, which indicates very high ability of ZEBRA detectors to discover fissionable nuclear materials hidden in containers. The detection sensitivity for detectors of dimensions $100 \times 100 \times 41\ \mathrm{mm}^3$ reaches the values of 51 cps/(neutron$\cdot$s$^{-1}\cdot$cm^{-2}). If we assume that the activity of 1 ng of "fresh" nuclide ^{252}Cf per solid angle unit is 2.314×10^3 neutron$\cdot$s$^{-1}\cdot$ng^{-1} (see, for example, [28]), the flux of fast neutrons at the distance of 200 cm passing through a surface of area S, expressed in [cm^2] units, is equal to $0.058 \times S$ neutron$\cdot$s$^{-1}\cdot$ng^{-1}. Hence, we obtain a convenient relationship between detector sensitivity η and equivalent threshold $\eta(_{^{252}Cf})$ of the counting rate for reliable recording of the ^{252}Cf source at the distance 2 m from the detector:

$$\eta_{^{252}Cf} \approx 0.058\eta. \tag{12.13}$$

For ZEBRA detectors of dimensions not less than $100 \times 100 \times 41\ \mathrm{mm}^3$ with sensitivity η above 50 cps/(neutron$\cdot$s$^{-1}\cdot$cm^{-2}), the equivalent threshold for the detection of ^{252}Cf, calculated according to Eq. (12.13), is 2.9 cps/ng, which is superior to the generally accepted standard IEC 62244 (IAEA [29]) for portal monitors—sensitivity to fast neutrons should not be less than 2.5 cps/ng. Therefore, the ZEBRA detectors can be considered promising for the creation of a new generation of solid-state portal monitors as an alternative to stationary ^{3}He counters.

Comparative analysis of the results presented in Tables 12.2 and 12.3 and Table 12.4 leads to two important conclusions. First, the detection efficiency of fast neutrons obtained with multilayer detectors with thickness comparable to characteristic dimensions of large and expensive single-crystal heavy-oxide scintillators (dimensions from ø40 × 80 and higher) are practically not inferior to the latter, reaching 50%. Also, the sensitivity of these multilayered detectors is several times higher as compared with detectors using single crystals and can be increased even more by increasing the sensitive area of the detecting plates.

It should be noted that measurements of detection efficiency of ZEBRA detectors based on one and the same heavy-oxide scintillation material depend on: (i) choice of the direction of irradiation, which can fall onto the multilayer detector parallel or perpendicular to the layers; (ii) total thickness of the detector; (iii) number and thickness of layers in the composite scintillator; and (iv) height of the detector in direction from the output window (distance between the outer boundaries of the detector from the photoreceiver). Thus, optimal detector design allows optimization of parameters to minimize losses in the detection of incident neutrons. Studies of these aspects are the subject of continuing investigation.

12.6 Insight on the use of multilayer composite ZEBRA materials for fast neutron shielding

Theoretical calculations and real experiments indicate the high efficiency of multilayer composite ZEBRA detectors for the detection of fast neutrons. This is due to the fact that the multilayer structures of "low-Z" material (plastic) combined with "high-Z" material (heavy-oxide scintillator) have higher efficiency in detecting inelastic and resonance scattering reactions for the conversion of fast neutrons into secondary radiation (gamma radiation, conversion electrons and/or Auger electrons, and accompanying X-ray which are then more easily shielded), in comparison with the conversion efficiency of fast neutrons in the elastic scattering reaction with the release of recoil protons in traditional plastic moderators. By constructing a structure that has very high interaction efficiency with fast neutrons for the purpose of detection, the potential for application of this approach to the function of fast neutron shielding can be also considered.

A contributing factor in the high efficiency of detection of fast neutrons in ZEBRA structures is intermediate moderation and subsequent absorption (in the range of resonance energies) provided by the multilayer composite configuration. Thus, the efficiency of fast neutron detection can be much higher than that of traditional detector systems relying on homogeneous plastic materials with moderation of fast neutrons to thermal energies and their subsequent absorption in neutron-capture elements such as Li, B, Cd, and Gd. The same principles will also apply to shielding in the sense that neutron interactions that reduce the neutron energy (i.e., elastic and inelastic scattering) or remove the neutron all together are mechanisms of dose reduction.

It is possible to estimate the probability of a conversion (absorption) of fast neutrons in multilayer ZEBRA material (see Fig. 12.15) containing in series n layers of thickness d_1 from "low-Z" plastic moderator and n thinner layers of thickness d_2 from "high-Z" material which contains heavy nuclei with sufficiently high values of the resonance integral (tens or hundreds of barns) and the upper boundary of the range of resonant energies (tens or hundreds of keV). For example, these are nuclei of various isotopes of W or Gd. Unlike ZEBRA detectors, it is not necessary to use too expensive composites from scintillation materials for conversion layers of ZEBRA materials designed for fast neutron shielding. It is quite sufficient to use much cheaper "high-Z" materials containing the abovementioned "resonant capture" nuclei, for example, composites based on the crude tungsten oxides

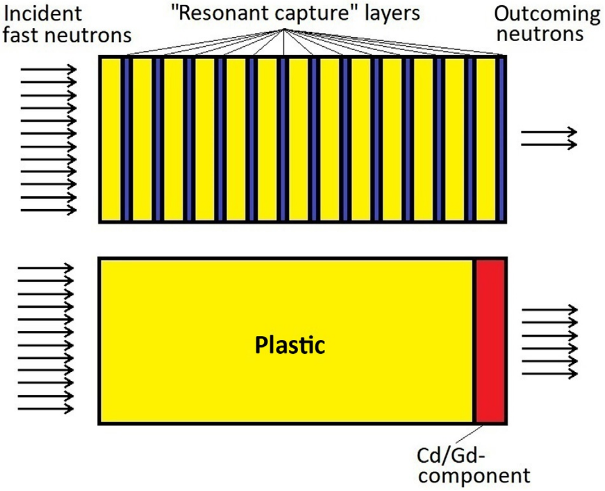

Fig. 12.15 Comparative design of multilayer composite ZEBRA shield (on the top) and ordinary homogeneous plastic shielding (on the bottom) from fast neutrons. Cd/Gd-component layer is intended for absorption of neutrons moderated by ordinary shielding up to thermal energy region. The efficiency of ZEBRA shield is 4–5 times better than the efficiency of ordinary shielding. The number of incident and outcoming neutrons are marked schematically.

WO_2 and/or gadolinium Gd_2O_3 powder. Typically, the values of the resonance scattering cross section for these materials are so large (see Table 12.1) that in each such layer of thickness of about ~1 mm there is radiation capture (absorption) of all neutrons moderated up to the region of resonance energies. The thickness of single moderator layer should be chosen to provide fast neutron moderation with probability close to 4%–5% from energy ~2 MeV to ~2 keV. For example, for PMMA plastic it is enough to take moderator layer with ~5 mm thickness. The total thickness of ZEBRA-shield is

$$d = n(d_1 + d_2) \approx nd_1; \quad d_1 \gg d_2. \tag{12.14}$$

It is supposed that after passing through each layer of moderator with d_1 thickness, a small part of the incident flux of fast neutrons reaches the region of resonant energies. We denote the probability for this "one-layer" moderation process by p_1. This probability is determined by the mean-squared slowdown length $L_s = L_s(E, E')$ needed for moderation of fast neutrons from energy E to energy E'

$$p_1 = 1 - \exp(-d_1/L_s). \tag{12.15}$$

Usually, $d_1 \ll L_s$. In such case we have

$$p_1 \approx \frac{d_1}{L_s}. \tag{12.16}$$

The probability of moderation of fast neutrons after passing through two consecutive moderation layers of total thickness $2d_1$ (divided by one thin conversion layer of thickness d_2) in the direction of propagation of the initial neutron flux is denoted y p_2 and so on. Under the assumption of weak moderation $p_k \ll 1$, it can be assumed that a set of these probabilities under condition $d_2 \ll d_1$ depends on the kth layer moderator as

$$p_k \approx kp_1 = \frac{kd_1}{L_s} \quad \text{if} \quad p_k \ll 1, \quad k = 1, 2, \ldots n. \tag{12.17}$$

Let us assume also that all resonant neutrons will be absorbed after passing through a conversion layer of small thickness $d_2 \ll d_1$. Then the total probability of attenuation of the initial fast neutron flux after passing through the entire ZEBRA-shield is

$$w_{zebra} \approx p_1 + (1-p_1)p_1 + (1-p_1)^2 p_1 + \ldots + (1-p_1)^{n-1} p_1 = 1 - (1-p_1)^n. \tag{12.18}$$

Under additional condition $p_1 \ll 1$ we may calculate the protection efficiency as [see also Eq. (12.17)]

$$w_{zebra} \approx \ np_1 + o(p_1). \tag{12.19}$$

From Eq. (12.19) some estimates follow. If one-layer moderation approaches $p_1 \sim 5\%$, then for the absorption of half of fast neutrons $w_{zebra} \sim 50\%$ a multilayer structure with about $n = 10$ moderator layers separated by the same quantity of thin conversion layers is needed. For weak one-layer moderation from Eq. (12.16) it follows

$$w_{zebra} \approx \frac{nd_1}{L_s^{res}}, \tag{12.20}$$

where $L_s^{res} = L_s(E, E_{res})$ is the neutron moderation length for moderation of fast neutrons from initial energy E to upper boundary E_{res} of the energies of resonant neutron scattering.

Let us now estimate the efficiency of shielding for homogeneous plastic moderator. For this, we consider the probability of moderation of fast neutrons up to the range of thermal energies. Slow or thermal neutrons can already be effectively absorbed in materials with neutron-capture elements.

Moderation of fast neutrons occurs due to the elastic scattering by light nuclei. The probability p of attenuation of incident fast neutron flux due to the moderation of neutrons from energy E to energy E' is determined as

$$p = 1 - \exp\left(-\frac{d}{L_s}\right), \tag{12.21}$$

where d is the thickness of a moderator. The mean-squared slowdown neutron length is determined by the relation (see, for example, [30]):

$$L_s = \sqrt{2q(E, E')\lambda_{tr}\lambda_{el}}; \quad \lambda_{tr} = \frac{\lambda_{el}}{1 - 2/(3A)}, \tag{12.22}$$

where $q(E, E')$ is the average number of collisions in elastic scattering, which is necessary to moderate the neutron from energy E to energy E'; λ_{tr} is the transport length of neutron scattering taking into account a scattering anisotropy; $\lambda_{el} = \Sigma_{el}^{-1}$ is the mean free path of neutron in elastic scattering; $\Sigma_{el} = n_A\sigma_{el}$ is the macroscopic cross section of neutron elastic scattering in material with concentration n_A of nuclei; σ_{el} is the microscopic cross section of neutron elastic scattering; and A is the atomic number of scattering nuclei.

The factor $q(E, E')$ depends on the parameter of moderation ξ:

$$q(E, E') = \xi^{-1} \ln\left(\frac{E}{E'}\right). \tag{12.23}$$

The parameter of moderation ξ is the logarithmic decrement of the average neutron energy loss per one collision. For complex compounds it is calculated from the expression (see, for example, [30]):

$$\xi = \frac{\sum_i k_i \xi_{A_i}}{\sum_i k_i}; \quad \xi_{A_i} = 1 - \frac{(A_i - 1)^2}{2A_i} \ln\frac{A_i + 1}{A_i - 1}, \tag{12.24}$$

where ξ_i is the partial decrement of deceleration on nuclei with atomic number A_i; k_i is the relative atomic concentration of simple elements in the molecule of a complex compound. For the PMMA (plexiglass) with the chemical formula $(C_4H_{12}O_2)_n$, a theoretical estimate with Eq. (12.24) gives a value $\xi \approx 0.628$.

In plastics, moderation mainly occurs on hydrogen nuclei with $A = 1$. Consequently, $\lambda_{tr} \approx 3\lambda_{el}$. A theoretical calculation by using cross-section data from the nuclear database [24] gives value $\lambda_{el} = 3.82\,\text{cm}$ for neutron scattering in PMMA plastic irradiated by ^{238}U source. For other fast neutron sources and/or for other plastic moderators, this value does not substantially change and remains about ~4 cm. From Eqs. (12.23) and (12.24) it follows that about $q_* \sim 29$ neutron collisions are required to moderate fast neutron from energy of 2 MeV to thermal energy of 0.025 eV. The estimate of corresponding moderation length by Eq. (12.22) gives value $L_s \sim 50$ cm. According to Eq. (12.21) the needed thickness of moderator for moderation of about 50% of initial fast neutron flux to thermal energies is about ~34 cm. Not considered here is neutron albedo-effect, i.e., backscattering of neutrons in thick moderator, which may decrease this value to half. Therefore, the corrected thickness of moderator should be about ~17 cm. For comparison, the moderation length experimentally obtained for reactor graphite for moderation of neutrons from 2 MeV to 0.025 eV is 17.7 cm.

The efficiency of ordinary shielding is determined by the probability of moderation of fast neutrons to thermal energies after multiple neutron collisions

$$w_{ordinary} \approx 1 - \exp\left(-\frac{d}{L_s^{th}}\right) \approx \frac{d}{L_s^{th}} \quad \text{if} \quad d \ll L_s^{th}, \tag{12.25}$$

where $L_s(E, E_{thermal})$ is the corresponding (thermal) moderation length for neutron flux.

The efficiencies of ZEBRA-type shield and ordinary shielding using the same plastic moderators in the case their equal total thicknesses $nd_1 \approx d$ are associated with the relation followed from Eq. (12.20) and Eq. (12.25):

$$\frac{w_{zebra}}{w_{ordinary}} \approx \frac{L_s^{th}}{L_s^{res}} = \sqrt{\frac{\ln(E/E_{thermal})}{\ln(E/E_{resonant})}}, \tag{12.26}$$

which is not dependent on the choice of material for a moderator.

Taking the initial neutron energy as $E \sim 10^6 eV$, energy thresholds as $E_{resonant} \sim 10^3 eV$ and $E_{thermal} \sim 10^{-2} eV$ we obtain from Eq. (12.26) theoretical estimate $w_{zebra}/w_{ordinary} \sim 3$. From this follows an important conclusion that the efficiency of the ZEBRA shield may be several times higher than the efficiency for ordinary detector structures for shielding from fast neutrons (Fig. 12.15).

12.7 Conclusion

Recent experiments have convincingly shown that the primary fast neutron interaction process enabling efficient fast neutron detection by heavy-oxide single crystals like ZWO, CWO, PWO, BGO, GSO(Ce), etc., is the reaction of inelastic scattering reaction. Experiments on detectors with external moderators, as well as theoretical estimates, show that it is possible to improve detection efficiency by capitalizing on the additional mechanisms of resonance scattering and radiative capture in cases when the scintillator material contains heavy nuclei with large cross sections for these reactions.

Optimum combination of inelastic and resonance scattering (in the presence of heavy nuclei such as W or Bi and medium nuclei such as Zn or Ge), as well as thermal neutron radiative capture (in the presence of nuclei such as Cd or Gd) are possible in the developed multilayer ZEBRA detectors based on heavy-oxide composite scintillators. Despite a much smaller amount of the active scintillating material (heavy-oxide composite) that detects neutrons in such detectors, the fast neutron detection efficiency in such detectors reaches 40%–50%, which is practically comparable with efficiency of detectors based on expensive and large-sized heavy-oxide single crystals. At the same time, the detection sensitivity and detection thresholds of fast neutrons from hidden special nuclear materials by ZEBRA detectors are several times higher than those of the single-crystal detectors. With a sensitivity to fast neutrons of 50 cps/(neutron $\cdot$ $s^{-1}\cdot cm^{-2}$) and better, these detectors are comparable or superior to ^{3}He counters, but are much smaller (by an order of magnitude or more) in size and weight.

An important distinction between this physical approach and most if not all alternative proposals to replace ^{3}He counters (e.g., by solid-state or gas discharge detectors) is that these methods propose to replace ^{3}He by other media that satisfactorily detect only thermal neutrons (^{6}Li and ^{10}B technologies), and require the use of massive plastic moderators to detect fast neutrons. Without these external moderators, this approach results in fast neutron detection efficiencies that do not exceed 10%. In the approaches described in this chapter, fast neutrons are detected directly by a heavy-oxide scintillator in the crystal itself or in a multilayer composite detector, and this enables much higher detection efficiency—up to 50%—with improved sensitivity of the detector to fast neutrons. As a consequence, the productivity (sensitivity per unit detector volume) of such detectors in detecting special nuclear materials, including those hidden in protective containers, will be substantially higher.

Finally, it should be noted that new multilayer composite ZEBRA materials can be used not only for advanced fast neutron detectors, but also as new materials for effective fast neutrons protection, and the effectiveness of this shielding can be in some cases several times higher than the effectiveness of traditional shielding.

References

[1] M. Anelli, G. Battistoni, S. Bertolucci, C. Bini, et al., Measurement and simulation of the neutron response and detection efficiency of a Pb-scintillating fiber calorimeter, Nucl. Instrum. Methods Phys. Res., Sect. A 580 (2007) 368–372.

[2] O. Hausser, M.A. Lone, T.K. Alexander, S.A. Kushneriuk, The prompt response of bismuth germanate and NaI(Tl) scintillation detectors to fast neutrons, Nucl. Instrum. Methods Phys. Res., Sect. A 213 (1983) 301–309.

[3] S. Kubota, T. Motobayashi, M. Ogiwara, H. Murakami, Y. Ando, J. Ruan(Gen), S. Shirato, Response of BaF_2, BaF_2-plastic, and BGO scintillators to neutrons with energies between 15 and 45 MeV, Nucl. Instrum. Methods Phys. Res., Sect. A 285 (1989) 436–440.

[4] V.D. Ryzhikov, B.V. Grinyov, G.M. Onyshchenko, L.A. Piven, O.K. Lysetska, L. L. Nagornaya, T. Pochet, The use of fast and thermal neutron detectors based on oxide scintillators in inspection systems for prevention of illegal transportation of radioactive substances, IEEE Trans. Nucl. Sci. 57 (5) (2010) 2747–2751.

[5] V.D. Ryzhikov, B.V. Grinyov, G.M. Onyshchenko, L.A. Piven, S. Naydenov, O. K. Lysetska, The highly efficient gamma-neutron detector for control of fissionable radioactive materials, Funct. Mater. 21 (3) (2014) 345–351.

[6] V.D. Ryzhikov, S.V. Naydenov, G.M. Onyshchenko, T. Pochet, C.F. Smith, High efficiency fast neutron detectors based on inorganic scintillators, in: Proceeding of the IEEE 2014 NSS-MIC Conference, Seattle, WA, 2014, 2014. https://doi.org/10.1109/NSSMIC.2014.7431165.

[7] V. Ryzhikov, B. Grinyov, G. Onyshchenko, L. Piven, O. Lysetska, L. Nagornaya, High efficiency method of fast neutron detection by oxide scintillators for detection systems of fissionable radioactive substances, in: Proceeding of the ANIMMA-2011 Conference, Ghent, Belgium, 2011, 2011. https://doi.org/10.1109/ANIMMA.2011.6172929.

[8] V.D. Ryzhikov, S.V. Naydenov, G.M. Onyshchenko, L.A. Piven, V.S. Zvereva, T. Pochet, C.F. Smith, A new multilayer scintillation detector for detection of neutron gamma radiation, in: Proceeding of the IEEE 2015 NSS-MIC Conference, San Diego, CA, 2015, 2015. https://doi.org/10.1109/NSSMIC.2015.7581996.

[9] V. Ryzhikov, C. Smith, B. Grinyov, L. Piven, G. Onyshchenko, S. Naydenov, T. Pochet, Detection of gamma-neutron radiation by novel solid-state scintillation detectors, in: Proceeding of the ANIMMA-2015 Conference, Lisbon, Portugal, 2015, 2015. https://doi.org/10.1109/ANIMMA.2015.7465541.

[10] V. Ryzhikov, V. Litichevskiy, L. Piven, G. Onyshchenko, et al., Combined detector of ionizing radiation, in particular for gamma-neutron radiation, 2015. Patent of Ukraine #UA109524 C2.

[11] V.D. Ryzhikov, B.V. Grinyov, S.V. Naydenov, G.M. Onyshchenko, L.A. Piven, Method of registration of fast neutrons and combined detector based thereon, 2018. Patent of Ukraine #UA117862 C2 (published 10.10.2018).

[12] B. Grynyov, V. Ryzhikov, L. Nagornaya, G. Onishcenko, L. Piven, Method of detection of fast neutrons, 2011. Patent US 8058624 B2.

[13] V.D. Ryzhikov, S.V. Naydenov, T. Pochet, G.M. Onyshchenko, L.A. Piven, C. F. Smith, Advanced multilayer composite heavy-oxide scintillator detectors for high efficiency fast neutron detection, in: Proceeding of the ANIMMA-2017 Conference, Liege, Belgium, 2017, 2017.

[14] V.D. Ryzhikov, S.V. Naydenov, L.A. Piven, G.M. Onyshchenko, C.F. Smith, T. Pochet, Fast neutron detectors and portal monitors based on solid-state heavy-oxide scintillators, Radiat. Meas. 105 (2017) 17–25, https://doi.org/10.1016/j.radmeas.2017.08.008.

[15] V.D. Ryzhikov, S.V. Naydenov, G.M. Onyshchenko, L.A. Piven, T. Pochet, C. F. Smith, Fast neutron detectors based on solid-state single crystalline and multilayer composite scintillators, in: Proceeding of the IEEE 2016 NSS-MIC Conference, Strasbourg, France, 2016, 2016.

[16] N.S. Bowden, P. Marleau, J.T. Steele, S. Mrowka, G. Aigeldinger, W. Mengesha, Improved fast neutron spectroscopy via detector segmentation, Nucl. Instrum. Methods Phys. Res., Sect. A 609 (2009) 32–37.

[17] Y.I. Chernukhin, A.A. Yudov, S.I. Streltsov, Fast-neutron heterogeneous scintillation detector with high discrimination of gamma background, Nucl. Energy Technol. 1 (2) (2015) 130–134.

[18] M. Flaska, S.D. Clarke, C.C. Lawrence, S.A. Pozzi, J.B. Czirr, L.B. Rees, Characterization of cadmium capture-gated detector for nuclear non-proliferation applications, in: Conference Records, 2010 IEEE Nuclear Science Symposium, Knoxville, TN, 2010, 2010, pp. 114–118.

[19] Y. Liu, Y.-G. Yang, Y. Tai, Z. Zhang, A capture-gated fast neutron detection method, Chin. Phys. C 40 (7) (2016) 076201/1–076201/8.

[20] M. Mohsen, Monte Carlo simulation of a fast neutron counter for use in neutron radiography, Nucl. Instrum. Methods Phys. Res., Sect. A 788 (2015) 73–78.

[21] I.A. Paweczak, J. Toke, E. Henry, M. Quinlan, H. Singh, W.U. Schroder, NSTAR – a capture gated plastic neutron detector, Nucl. Inst. Methods Phys. Res. A 629 (2011) 230–238.

[22] A. Akhiezer, I. Pomeranchuk, Certain Problems of Nuclear Theory, second ed., Gostekhizdat, Moscow, Leningrad, 1950 (in Russian).

[23] J.M. Blatt, V.F. Weisskopf, Theoretical Nuclear Physics, Springer, New York, 1979.

[24] JENDL (Japanese Evaluated Nuclear Data Library), Japan Atomic Energy Agency, Nuclear Data Center, Japan, 2014.http://wwwndc.jaea.go.jp/jendl/j40/j40.html.

[25] H.H. Barschall, J.H. Manley, V.F. Weisskopf, Measurement of transport and inelastic scattering cross sections for fast neutrons. I, Methods Phys. Rev. 72 (1947) 875.

[26] A.I. Abramov, Y.A. Kazanski, E.S. Matusevich, Foundation of Experimental Methods in Nuclear Physics, second ed., Atomizdat, Moscow, 1977 (in Russian).

[27] S.D. Clarke, M.C. Hamel, A. Di Fulvio, S.A. Pozzi, Neutron and gamma-ray energy reconstruction for characterization of special nuclear material. Nucl. Eng. Technol. 2017 (2017). https://doi.org/10.1016/j.net.2017.06.005.

[28] R.T. Kouzes, J.R. Ely, A.T. Lintereur, D.L. Stephens, Neutron Detector Gamma Insensitivity Criteria, Technical Report PNNL-18903, Pacific Northwest National Laboratory, Richland, WA, 2009.

[29] IEC/FDIS 62244 (2006–06), Installed radiation monitors for the detection of radioactive and special nuclear materials at national borders, Available from:http://www.iec.ch, 2006.

[30] K.H. Beckurts, K. Wirtz, Neutron Physics, Springer, New York, 1964.

CHAPTER 13

Neutron spectroscopy techniques

Antony Joseph
University of Calicut, Kerala, India

13.1 Introduction

As it is electrically neutral, one may presume that neutron may not have a significant role in the day-to-day developments in science and technology and may be playing the role of a mere spectator in common interactions. But it is the lack of the electric charge that makes neutron distinct among the plethora of particles in the universe. Regardless of whether it is the strong force or the weak force, neutron occupies a key position in the family of elementary particles. It is such an important particle that one can easily find its applications either directly or indirectly, in almost all areas of science and technology. It plays unique roles in nuclear physics, astrophysics, condensed matter physics, medical physics, energy production, industry, etc. Here we are making an attempt to understand the theory and practice of neutron scattering as a technique to unravel the structure and dynamics of different forms of materials, encountered mainly in condensed matter physics.

Generally, the structure of any material is determined by analyzing the data obtained from the interaction of charged or uncharged radiations with it. Any radiation which is used to characterize the structure of an object is called a probe. Laser light, X-rays, electrons, neutrons, etc., are examples of such probes. X-ray is the most commonly used probe. However, within few years after the discovery of neutrons, they were identified to be very effective for this purpose. When probe particles like neutrons interact with a medium three things can happen:

1. Transmission, where the neutrons simply go through the sample without deviation.
2. Absorption, during which neutrons are captured by the sample.
3. Scattering, where the neutrons are deviated from the initial direction.

The scattering process can be either elastic, with no exchange of energy, or inelastic, with exchange of energy between the partners. The phenomenon of diffraction and the resulting crystallography are the result of elastic scattering and spectroscopy is the result of inelastic scattering. The inelastic scattering causes motion of atoms or molecules or it can be due to the motion of atoms.

Micro and Nanostructured Composite Materials for Neutron Shielding Applications
https://doi.org/10.1016/B978-0-12-819459-1.00013-1
© 2020 Elsevier Ltd.
All rights reserved.

Hence inelastic scattering can reveal the pattern of their motion. In this chapter, the stress is on the use of neutrons in structural studies and molecular dynamics, treating them as the two aspects of neutron spectroscopic techniques. The process of neutron interaction with matter is still not a fully understood area of research. Its application areas are also expanding with the developments taking place in science. For those who are novice in this field, there are several resources to get exposed to the basic concepts and to the latest developments taking place in this interesting area of scientific research [1–5].

13.2 The physics of crystallography and spectroscopy

As we are aware of, the scattering of particles by atoms, molecules, or nuclei is immensely important in the sense that our very idea of how atoms or nuclei look like is conceived from the scattering experiments, the classic example being the scattering of alpha particles by gold foil. Scattering in fact has many facets. It is a word having different meanings in different contexts. W.L. Bragg and W.H. Bragg studied the scattering of X-rays by crystals, which is called Bragg scattering [6], and that paved the way for the development of solid-state physics. Bragg scattering is also called Bragg diffraction or at times called Bragg reflection. We are also aware of Raman scattering, Brillouin scattering, etc. If the process of scattering is from a spatially periodic structure like a grating or in the microscopic context, from a crystalline solid, the scattered beam represents this periodic structure as a finger print and it is called diffraction. Or more precisely, when the waves (or equivalently particles, due to wave particle duality) get scattered from spatially periodic structures, it gives rise to diffraction and subsequently to crystallography. On the other hand, when waves get scattered from time periodic structures, scattering gives rise to spectrum, like rotational spectrum, vibrational spectrum, etc. Spatial periodicity affects momentum and leads to diffraction. Time periodicity affects energy and leads to spectrum, which in turn give us the information about the energy levels and the potentials involved. Energy and time have a fundamental relationship just like the fundamental relationship between momentum and space. The whole essence of spectroscopy and crystallography are pivoted to this basic concept in physics.

Neutron diffraction is a special case of scattering from space periodic systems. Neutron diffraction pattern is not related to any appreciable energy change, but since there is direction change due to scattering, it involves momentum change. The neutron diffraction pattern gives a mapping of the momenta, which is characteristic of crystallography. Thus crystallography maps momentum space whereas spectroscopy maps energy space. In the case of thermal neutrons, it so happened that its energy is comparable to the lattice vibrational energy of the crystalline materials. This feature enables the investigation of the elementary excitations called phonons. In other words, we are able to understand the dynamics of the phonons in condensed matter. For analyzing high-energy excitations of more than 100 meV, hot neutrons are used. Since neutrons can penetrate deep into the sample, analysis of bulk samples is possible. At the same time, the corresponding de Broglie wavelength of neutrons is comparable to the lattice spacing or lattice parameters of the crystalline materials. As a result, neutrons are ideal probe for spectroscopy as well as crystallography. On comparison we can see that X-ray wavelengths are comparable to lattice parameters whereas their energy is more than 10,000 times larger than the lattice vibrational energy. More exactly, if the X-ray energy is of the order of 20,000 eV, the lattice vibration energy in materials is of the order of fraction of an electronvolt, that is, around 0.025 eV. Hence lattice vibration is not sufficient to influence the energy of X-rays, whereas the wavelength of X-rays can be affected by the typical distance between spatial lattice planes. As a result, momentum transfer occurs very easily and that causes diffraction. Hence X-rays are suitable only for crystallography. Similarly, the energy of infrared radiations is comparable to the lattice vibrational energy of crystals but their wavelengths are more than 10,000 times the lattice parameters of the crystals. As a result, infrared radiations are suitable only for spectroscopy. In a crystalline material, the resolution of neutron diffraction pattern is higher than that due to X-rays because X-ray energy is of the order of kilo electronvolt whereas the lattice dynamical or thermal energy is 0.025 eV and the corresponding de Broglie wavelengths are slightly different. Because of the tremendous impact that neutron spectroscopy and crystallography had on physics, the Nobel Prize in Physics for 1994 was awarded to Bertram N. Brockhouse for the development of neutron spectroscopy and to Clifford Shell for the development of neutron diffraction techniques [7].

13.3 Classification and basic properties of neutrons

The precision and nature of the structural and dynamic information that can be extracted from the neutron diffraction pattern and spectra very much depend on the energy of the incident free neutrons. Therefore, an understanding of the classification of neutrons based on their energy is a prerequisite. The essential information related to neutrons is presented in

Table 13.1 Energy wise classification of neutrons [8, 9].

Neutrons	Energy range	Wave length (Å)	Velocity (m s^{-1})
Ultracold	≤300 neV	≥500	≤8
Very cold	300 neV–0.12 meV	52.2–26.1	7.5–152
Cold	0.12–12 meV	26.1–2.6	152–1515
Thermal	12–100 meV	2.6–0.9	1515–4374
Epithermal	100 meV–1 eV	0.9–0.28	4374–13.8 × 10^3
Intermediate	1 eV–0.8 MeV		
Fast	>0.8 MeV		

Table 13.1. The neutron is a spin $\frac{1}{2}$ subatomic particle with mass equivalent to 1839 electrons (1.674928 × 10^{-27} kg), and a magnetic moment of $-1.9130427\ \mu_n$ ($-$ 9.6491783 × 10^{-27} J T^{-1}). The quantum mechanical state of a free neutron is decided by the momentum $|p\rangle$ ($p^{\rightarrow} = \hbar k^{\rightarrow}$, $k = \frac{2\pi}{\lambda}$) and spin $|s\rangle$.

13.4 Theory of neutron scattering

Traditionally, X-ray scattering leading to the diffraction was the only accepted characterization technique in materials science, until the power of neutrons in this regard was established. The theory of neutron scattering was formulated and established by Van Hove [10] in 1954, 22 years after the discovery of neutrons by James Chadwick [11]. This technique is especially applicable in condensed matter physics, where we deal with materials belonging to different types like crystalline, amorphous, magnetic, polymeric, etc. Neutron being electrically neutral can penetrate into a considerable distance in matter, without being absorbed. Another important property is that it is especially sensitive to hydrogen atoms. Also it responds differently to the isotopes of the same element. Due to these unique properties, neutron scattering had become one of the sought-after techniques to study the structure and dynamics of materials. An added advantage of neutron scattering technique when compared to X-ray scattering is that it can explore the motion of atoms and molecules at nanometer length scale and nanosecond time scale. By applying this technique, atomic motion involving time scale 10^{-14} to 10^{-6} s can be explored. It is this same reason that makes neutron spectroscopy a widely used technique to study the structure and motion of proteins and nucleic acids in biological systems and in biopolymers [12]. A very useful source of information for the detailed formalism of neutron scattering and spectroscopy is Ref. [13].

By making use of the wave property of neutrons, it was established that neutrons can undergo diffraction in a manner very similar to that of X-rays. It obeys the Bragg equation

$$n\lambda = 2d\sin\theta \tag{13.1}$$

where λ is the de Broglie wavelength of neutrons, d is the distance between adjacent planes of scattering particles, θ is the angle between the incident neutron source and the plane of the scattering particles, and n is an integer called the order of the diffraction (see Fig. 13.1). In a scattering experiment, neutrons of a particular wavelength are selected by means of diffraction at some selected angles from a monochromating crystal, which can appropriately filter out unwanted diffraction orders. Such an incident wave is characterized by a momentum

$$p_i = \hbar k_i \tag{13.2}$$

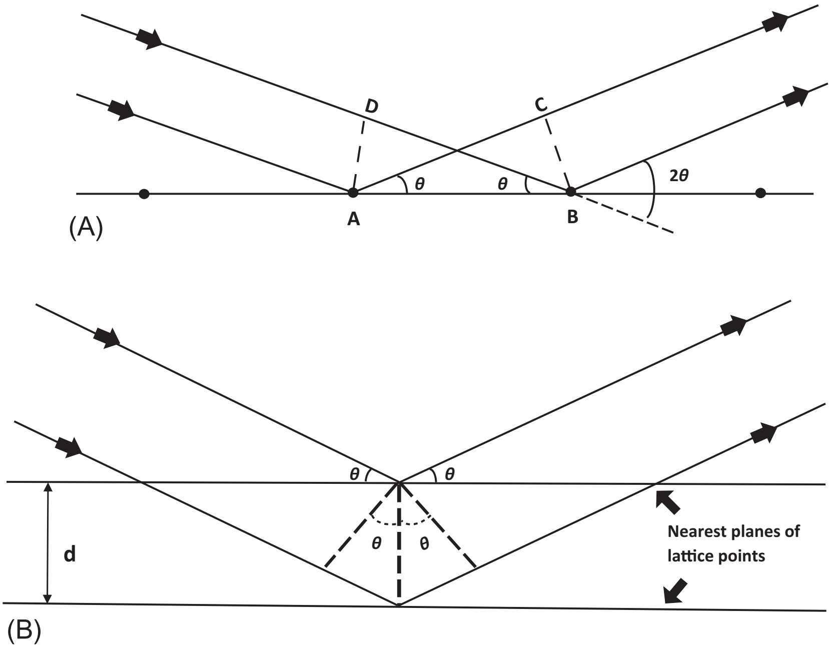

Fig. 13.1 (a) Scattering of neutrons from adjacent lattice points A and B. Scattered neutrons will be in phase if AC = DB. (b) Scattering of neutrons from adjacent planes, scattered neutrons will be in phase if the path difference 2*d*sin(θ) = $n\lambda$.

where $k_i = \frac{2\pi}{\lambda_i}$ is the associated wave vector, with λ_i being the wavelength of the initial/incident beam. Such a beam is directed to the sample either directly or after chopping into pulses. The sample scatters the beam in some specific manner depending on its structure, dynamics, isotopic, and magnetic properties. The wavelength of the final/scattered beam λ_f is also selected either by a monochromating crystal or by measuring the time of flight of the pulse traveling between the sample and the detector, which is placed at a known distance from the sample and at a known angle from the incident beam direction. The final state momentum is

$$p_f = \hbar k_f = \hbar \frac{2\pi}{\lambda_f} \tag{13.3}$$

From the law of conservation of momentum, the momentum transferred to the sample is

$$\hbar Q = \hbar(k_i - k_f) \tag{13.4}$$

Similarly, the energy transferred to the sample during scattering is

$$\Delta E = \hbar\omega = E_i - E_f = \frac{\hbar^2}{2m}\left(k_i^2 - k_f^2\right) \tag{13.5}$$

with m being the mass of the neutron. By measuring these two quantities one can understand a great deal about the structure and dynamics of the sample under investigation (see Fig. 13.2). Another quantity of interest is the spin state or spin orientation of the neutron, which is associated with its magnetic moment. The spin state of a polarized beam get changed on interacting with a magnetic material and the change can be measured with a spin-echo spectrometer. Thus, by selecting the initial and final wavelengths and spin states we can estimate the transfer of momentum, energy, and angular momentum from/or to the sample.

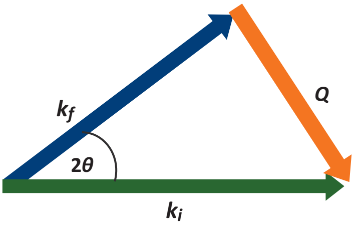

Fig. 13.2 Initial (k_i), final (k_f), and scattering (Q) wave vectors during the neutron scattering process. θ is the scattering angle.

In elastic scattering, $|k_i| = |k_f| = |k|$, say. Then,

$$|Q| = 2|k|\sin\theta = \frac{4\pi}{\lambda}\sin\theta \tag{13.6}$$

The Van Hove scattering function $S(Q, \omega)$, which is measurable in the scattering experiment, obtained from the double differential cross-section, contains all the physics of the system under study (in space and time) and depends only on the properties of the system. In fact, S is the Fourier transform of the space-time correlation function $G(r, t)$, which is used to extract the dynamics of the system.

As neutrons interact directly with the nuclei in a sample, this interaction is of short range. There is a characteristic quantity associated with this scattering, called scattering length (b). It is a measure of the strength of interaction between a neutron and a nucleus. It is a complex quantity and is different for different elements and also different for different isotopes of the same element. Again, its value varies with the spin of the atom. These are the unique properties which make neutron scattering different from scattering of matter with other probes such as laser light, electrons, X-rays, etc. The cross-section for scattering from a single stationary atom is expressed as $4\pi b^2$ [14].

When proposing a specimen for neutron spectroscopy, some of the factors to be considered are the size and the shape of single crystal and polycrystalline samples. The maximum size is fixed by the absorption cross-section and the minimum by the available neutron flux. More details on this can be obtained from Shmueli [15]. In biological sciences, an area of active research is related to the development of Protein Data Bank. It involves a large number of models developed based on data obtained from neutron diffraction alone or using data obtained from a hybrid procedure which combines X-ray and neutron diffraction. The specific advantage of neutron diffraction here is that with it the positions of all atoms can be determined, including hydrogen atoms, which is rarely obtained from X-ray diffraction [16, 17].

13.4.1 Coherent and incoherent scattering

In general, we consider two types of scattering. The first one is the scattering due to the average scattering length $\overline{b}$ and is called coherent scattering and the second one is due to the fluctuations from the average, $b - \overline{b}$, and is called incoherent scattering. In other words, when neutron waves interact with the whole sample as a unit, it leads to coherent scattering and consequent to this the scattered waves from different nuclei interfere with each other, showing interference effects leading to diffraction and the cross-section for this is proportional to $\overline{b}^2$. On the other hand, when the neutron waves interact independently with each nucleus, the resulting scattered waves do not show any interference effects and its cross-section is proportional to $(b-\overline{b})^2$ [18]. But if we observe diffraction patterns closely in terms of the fine structure, we can find a minute energy change and that is taken care of by the Debye-Waller factor. At this point, it is interesting to make a comparison of this with Lamb-Mossbauer factor. Even though Mossbauer effect is considered as recoilless gamma ray spectroscopy, in actual situation, if the source is embedded in a crystalline material, the otherwise negligible recoil momentum exists. Because of this reason, Mossbauer effect is widely applied in solid-state physics.

13.5 Neutron sources

It is known that free neutrons have a half-life of around 15 min [19, 20]. This time is sufficient to conduct neutron scattering experiments, without getting affected by their natural decays. Neutrons are strongly bound to atomic nuclei and so it is difficult to produce free neutrons. However, there are different techniques to produce free neutrons. The easiest provider of neutrons is an appropriate radioactive source. Except for the simplest scattering experiments, such neutrons will not be sufficient. All large-scale neutron scattering facilities will have a reactor or a spallation source for this purpose. Generally, neutron sources provide neutrons of either continuous flux or pulsed flux. Fission reactors provide high-energy neutron flux, which is continuous in time. After moderation, thermal neutrons with energy around 0.025 eV, corresponding to the room temperature, are obtained. These neutrons have Maxwell-Boltzmann distribution of speeds. This necessitates the incorporation of an appropriate energy selection method in the experimental setup. In a neutron scattering experiment, if neutrons of higher energy are required, the usual option is a spallation source. Pulse-type neutron flux is provided by spallation sources. In most of the common spallation sources, high-energy protons having energy in the range 800 MeV to 1 GeV from an accelerator are allowed to fall on a suitable target like U, Bi, Pb, Ta, Hg, etc. With such targets, each proton produces up to around 30 neutrons and the typical energy of the emitted neutrons are around 1 MeV. Polyethylene slabs of sufficient thickness are used as moderators in these setups. The main advantage of a spallation neutron source is that it can produce short

(100 μs) pulses of neutrons with very high peak flux (10^{16} cm^{-2} s^{-1}), suitable for the time-of-flight experiments (which we will see in a forthcoming section). Operational safety and nonproliferation issues, compared to nuclear reactors, are the added advantages of spallation neutron sources. The only stringent requirement and challenge is the availability of a high power, around 10 MW or more, high-energy proton accelerator. A term commonly encountered in neutron spectroscopy, related to the energy of neutrons, is white neutrons or polychromatic neutrons. These terms stand for a beam of neutrons of multiple energies. A beam of neutrons is said to be monochromatic if it contains neutrons of single energy.

13.6 Neutron spectroscopic methods

Even in this era of hectic scientific research, characterization of the newly developed materials is a challenge. To tackle such a situation, different characterization methods are used in a complementary approach. This is very essential to decide the applicability of these materials in diverse scientific and technological fields. Neutron scattering and associated spectroscopy is one such option. The most common neutron spectroscopic techniques are [18, 21]

- triple-axis spectroscopy
- time-of-flight spectroscopy
- backscattering spectroscopy
- quasielastic neutron scattering spectroscopy
- neutron spin-echo spectroscopy
- magnetic neutron spectroscopy
- vibrational neutron spectroscopy

Other methods such as neutron radiography [22], tomography, and reflectometry give images, carrying information different from what is obtained via the above-mentioned methods. Elastic neutron scattering is made use of in reflectometry, which is a technique usually used to study thin films. Neutron activation analysis [23] is another method, which provides precise and excellent composition information of samples.

13.6.1 Neutron triple-axis spectroscopy (TAS)

The basic instrument with which triple-axis spectroscopic studies are carried out is the triple-axis spectrometer. It is used for both elastic and inelastic scattering studies of steady-state neutrons. It probes for almost any coordinate in momentum and energy space, giving information mainly on the elementary excitation, that is, phonon properties of materials. Independent control of momentum and energy are possible here. (In time-of-flight spectrometers, they are linked via instrumental configuration.) The changes in both energy and momentum of the neutrons produced upon interaction of the neutrons with these excitations are studied here. Typical energy resolution of the spectrum is in the range 0.01–1.0 meV. They are ideal for phonon dispersion curves in single crystals. The hydrogen nucleus has the largest cross-section for scattering interaction and is predominantly incoherent [24]. Because of this, hydrogen vibrations in samples containing total hydrogen of even 0.01 mole can be detected and the time averaged structure of the atomic and molecular constituents of the sample can be accessed. Also polarized neutrons allow more detailed measurements of the magnetic properties. In magnetic materials, the structural description of magnetic moments reveals static properties whereas the behavior of magnons unveil the dynamic properties. The energy range of excitations accessible to TAS is much larger than that accessible with spin-echo and backscatter spectrometers. A prototype of this was developed by Brockhouse in early 1950s [25], and later modified it [7]. Many improvements have been incorporated in the latest models including robotic control systems. Generally, these types of spectrometers are installed near nuclear reactors. The major components of this spectrometers are monochromator and analyzer crystals, energy filters, collimators, and appropriate neutron detectors. The monochromator fixes both the direction and the magnitude of the momentum of the incident neutron beam. The analyzer analyzes the magnitude and the direction of the momentum of the scattered beam. Here there are three vertical axes about which the parts of the machine can rotate. The three axes correspond to the axis of rotation of the monochromator, that of the sample, and that of the analyzer. Each axis and crystal can be individually moved with a computer control mechanism. The monochromator, by its rotation about the first axis, selects a narrow band of neutron wavelengths centered around the intended wavelength λ from a white or wide spectrum supplied by the neutron source, satisfying the condition

$$n\lambda = 2d\sin\theta \tag{13.7}$$

where d is the lattice spacing of the monochromator crystal, 2θ is the angle through which the neutrons are scattered, and n is a possible integer. The collimator placed on either side of the monochromator decides this angle. The neutrons coming out of the second collimator falls on the sample. The second axis of rotation passes through the sample and allows to

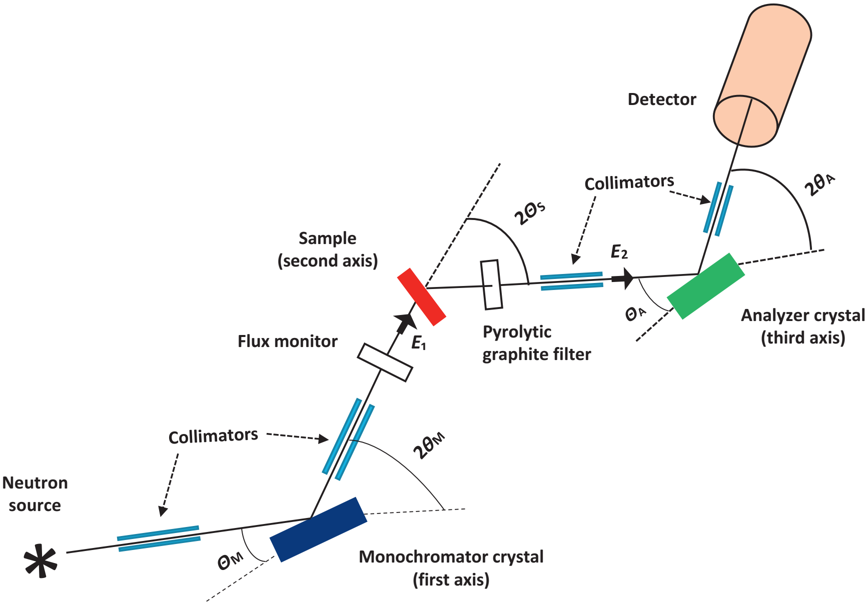
Detector
Collimators
2θA
E2
2θS
Sample
(second axis)
Pyrolytic
graphite filter
θA
Analyzer crystal
(third axis)
Flux monitor
E1
Collimators
2θM
Neutron
source
θM
Monochromator crystal
(first axis)

Fig. 13.3 Schematic diagram of a triple-axis spectrometer. E_1 and E_2 are the neutron energies before and after the scattering at the sample.

investigate the neutron scattering properties of the sample as a function of the scattering angle ϑ. The third axis passing through the analyzer crystal determines the center and the width of the neutron wavelengths to which the detector will respond. The final band width will be decided by the angular divergence of the last two collimators and the properties of the analyzer. Provision for extensive shielding will also be there. The schematic diagram of a triple-axis spectrometer is shown in Fig. 13.3.

Two types of scans are possible to collect data. The first one called constant energy scans (constant E scan) are performed by keeping the energy transfer $\Delta E = \hbar\omega = E_f - E_i$ fixed, while varying the momentum transfer $\vec{Q}$. The second one called constant momentum scans (constant $\vec{Q}$) are performed by holding the momentum transfer fixed, while varying the energy transfer ΔE. In inelastic scattering, the neutrons may lose or gain energy. Those neutrons which are scattered under a scattering angle θ and having a specified final energy are detected by the detector which is placed behind the analyzer. Bragg reflection at the analyzer selects the desired energy, which may be varied by rotating the analyzer crystal and the detector around the third axis of the spectrometer. This type of spectrometer is the most universal one. Variation in incident energy, final energy, scattering angle, and sample orientation provides scattered intensity at arbitrary points in the four-dimensional space, which is characteristic of the momentum and energy transfer. The measured quantity is the scattering function $S(Q^{\rightarrow}, \omega).G(\vec{r}, t)$. The experimental spectra yield information of the microscopic dynamics of the sample under investigation, which can only be obtained by neutron scattering because with this instrument particle motions are resolved simultaneously in space as well as in time.

The scattering vector $\vec{Q}$ and the energy transfer $\hbar\omega$ are determined by the angles $2\theta_s$ and $2\theta_A$ and are exactly in accordance with Eqs. (13.4), (13.5). The sign of energy transfer tells whether the neutron has gained energy ($k_i < k_f$, $\Delta E < 0$) or lost energy ($k_i > k_f$, $\Delta E > 0$) at the scattering. With a magnetic sample, this spectrometer is appropriate for measuring the dispersion of both phonons and magnons [26].

13.6.2 Neutron time-of-flight spectroscopy

The time-of-flight method is a very common procedure to determine the energy of particles if its mass is known or its mass if its energy is known [27]. Here we use this method to determine the energy of neutrons. By this method, we can measure the energy of neutrons with extreme accuracy. Since the mass of the neutron is known to be within less than 3 keV, energy resolution as good as 0.1% can be easily achieved. In a time-of-flight measurement, we determine the speed of the neutron v. The velocity of a neutron of wavelength 2 Å is around 2000 ms^{-1}. A velocity of this order can be determined by measuring the time the neutron takes for traveling over a distance of few meters, say L. The kinetic energy of the neutron of mass M, assuming the relativistic condition, is given by

$$E_R = Mc^2\left(\frac{1}{\sqrt{1-\beta^2}} - 1\right) = Mc^2\left(\frac{1}{\sqrt{1-\frac{L^2}{c^2t^2}}} - 1\right) \tag{13.8}$$

with $\frac{L}{t}$ being the velocity of the neutron and $Mc^2 = 939.552$ MeV, its rest mass. Under nonrelativistic condition,

$$E_{NR} = \frac{1}{2}Mv^2 = \frac{1}{2}M\frac{L^2}{t^2} \tag{13.9}$$

The choice of the equation depends on the range of energy measured and the resolution of the energy required. The energy resolution, respectively, under relativistic and nonrelativistic cases are

$$\frac{\Delta E}{E}=\frac{E+Mc^2}{E}\frac{\beta^2}{1-\beta^2}\sqrt{\left(\frac{\Delta L}{L}\right)^2+\left(\frac{\Delta t}{t}\right)^2} \tag{13.10}$$

and

$$\frac{\Delta E}{E}=2\sqrt{\left(\frac{\Delta L}{L}\right)^2+\left(\frac{\Delta t}{t}\right)^2} \tag{13.11}$$

The time-of-flight method is especially suited for pulsed neutrons. The time of starting of the flight is known if the neutrons are introduced into the spectrometer as pulses. The time at which the flight ends can be determined by noting the time of arrival at the detector. Neutrons of different energy within each pulse reach the detector at different times and this enable the energy discrimination in experiments involving pulsed neutron beam. The count rate at the detector is measured as a function of time of arrival. The schematic of a simple time-of-flight spectrometer for neutron diffraction study is shown further. The time of flight of elastically scattered neutrons of fixed wavelength λ and momentum $p = Mv$ can be used to determine the interplanar distances in crystalline materials. The time of fight

$$t=\frac{L}{v}=\frac{ML}{p}=\frac{hML}{hp}=\frac{\lambda ML}{h} \tag{13.12}$$

where L is the total length of the neutron path, from the source to the detector via the sample. According to Bragg's law the condition for diffraction is

$$n\lambda=2d\sin\theta \tag{13.13}$$

For a fixed detector position, angle θ is decided by the geometry of the experimental setup. Combining the last two equations,

$$t=\frac{\lambda ML}{h}=\frac{ML}{h}\frac{2d\sin\theta}{n} \tag{13.14}$$

Peaks appear in neutron count rate at times satisfying the above equation. There are two conditions which are to be satisfied for the above procedure to work.

1. The crystal planes must be oriented at the correct angle to the incident beam.

2. The beam must have neutrons of wavelength required to satisfy Bragg's law. This condition is ensured by using pulse of incident neutrons having a distribution of energies.

13.6.3 Neutron backscattering spectroscopy (BSS)

In science, especially in physics, backscattering is the reflection of waves, particles, or signals back to the incoming direction. To explain the theory behind the neutron backscattering spectroscopy, let us consider Bragg's law,

$$\lambda = 2d\sin\theta \tag{13.15}$$

By differentiating this we obtain

$$\frac{\Delta\lambda}{\lambda} = \frac{\Delta d}{d} + \frac{\Delta\theta}{\tan\theta} \tag{13.16}$$

As $\theta \rightarrow 90$ degrees, the angular term vanishes. In other words, the wavelength spread $\Delta\lambda$ of a Bragg diffracted neutron beam decreases as the scattering angle 2θ approaches 180 degrees. Hence it gives rise to a minimum value for $\frac{\Delta\lambda}{\lambda}$. The energy resolution depends on the spread Δd and d, which is the average value of the lattice spacing between the Bragg planes of the crystal. In the kinematical limit, this minimum is zero. Thus neutron backscattering has paved the way to a new branch of spectroscopy, that is, the μeV spectroscopy, in inelastic neutron scattering with diverse applications, ranging from hyperfine interactions to rotational tunneling. Here the energy and time scale accessible are 0.7–30 μeV and 20 ps to 1 ns, respectively [28].

13.6.4 Neutron spin-echo spectroscopy (NSE)

Neutron spin-echo spectroscopy is another form of spectroscopy that relies on the precession of a spinning neutron (spin quantum number $= \frac{1}{2}$), even though ultimately it is a time-of-flight measurement. It is different from other conventional neutron inelastic spectroscopies. Conventional inelastic neutron spectrocopies involves two steps. Step 1: Preparation of the incoming monochromatic beam. Step 2: Analysis of the scattered beam. Values of energy and momentum transfer are estimated by taking the differences between incoming and outgoing parameters measured in the above two steps into account. To overcome the fundamental intensity barrier to energy resolution, a radically new approach is used here—the decoupling of energy resolution from monochromatization, that is, wavelength spread of neutrons. The basic idea is that, instead of monochromatizing the beam falling on the target or sample, we make each neutron remember its initial velocity.

For this we use the natural individual clock in each neutron, which is nothing but its spin. The Larmor spin-spin precession frequency ω_L in an external magnetic field H conveniently offers itself to its use as a time base

$$\omega_L = \gamma_L H \tag{13.17}$$

where $\gamma_L = 2.916$ kHz Oe^{-1}.[a] In NSE velocities of both the incoming and outgoing neutrons are measured by making use of the Larmor precession of the neutron's spin. The energy transfer of the neutron is encoded in their polarization and not in the change of wavelength of the scattered neutrons.

Here a polarized beam of cold, polychromatic neutrons are allowed to propagate through a magnetic field. The number of Larmor precessions of the neutrons are set depending on the length and strength of the magnetic field. Subsequently, the beam scatters off the given sample and the resulting precessions after scattering are determined using a second magnetic field. The difference in the number of precessions is an indication of the change in velocity and hence the change in the energy of the neutrons. However, here the measurement is not a direct measure of the energy change. It is a time-dependent measurement and so has to be treated by a Fourier transform to convert it to the energy domain, that is, the corresponding spectrum. Neutron spin-echo measurements have energy resolutions of the order of nanoelectron volts (neV) [29, 30]. There are three variants of the spin-echo spectrometers: (1) neutron spin-echo, (2) neutron resonance spin-echo, and (3) MIEZE (Modulation of IntEnsity with Zero Effort) technique in a transverse geometry.

At this point, it is worth mentioning some details of the neutron resonance spin-echo spectrometer. It is a variant of the conventional neutron spin-echo technique. This is quite appropriate for exploring nondispersive processes such as diffusion, crystallization, tunneling processes, crystal electric field excitations, spin fluctuations, and other slow dynamic processes [31]. It can also be operated in the MIEZE configuration to carry out studies related to dynamics of flux lines in superconductors, magnetic fluctuations in ferromagnetic materials, and samples containing hydrogen.

Because of the versatility of the neutron spin-echo spectroscopy, it finds plenty of applications in diverse fields. These are widely used in biological sciences. For example, Heidare [32] used this technique in the analysis of malignant cancer cells and tissues before and after delivering synchrotron radiation. Several of similar studies also made use of this technique [33].

---

[a] For further reading refer to the books cited in bibliography as Refs. [46, 47].

Spin-echo small-angle neutron scattering is another efficient procedure based on spin-echo scattering, used to measure the structure of materials in real space. By this method structure can be estimated over the length scale from 20 nm to 20 μm. The accessible energy and time ranges are 0.7 neV to 0.7 meV and picosecond to microsecond, respectively. These are generated from the data obtained in terms of polarization as a function of spin-echo length. This is one order of magnitude larger in length scale than that is obtained from the usual small-angle neutron scattering (SANS). In conventional scattering methods, the data is available in reciprocal space, whereas in spin-echo SANS the data is obtained in real space and hence the interpretation is easier [34, 35].

13.6.5 Quasielastic neutron spectroscopy (QENS)

Quasielastic scattering is a limiting case of inelastic neutron scattering. In this case, Doppler type of broadening of the elastic line takes place due to small energy transfer between neutrons and the atoms of the sample. Quasielastic scattering is widely used for understanding the slow processes such as translational diffusion, molecular reorientation, relaxation processes, etc. These are more regularly applied in the case of specific materials like fuel cells, batteries, hydrogen storage devices, etc. This technique is also extensively used to analyze the properties of materials belonging to the soft matter category such as polymers, nanocomposites and blends, organic photovoltaics, polymer electrolytes, etc. [36, 37]. It is extensively used in other branches of science also. For example, in biology it is used to understand the dynamics of proteins, hydration water, etc. In chemistry it finds applications in studying the interactions at water-matter interfaces, ionic liquids and surface interactions, etc. Thus it is proved to be very efficient for understanding molecular dynamics and in verifying the results of molecular dynamics simulations. QENS spectrometers are generally categorized into two categories: (1) back scattering spectrometers and (2) time-of-flight spectrometers. The first category spectrometers possess higher energy resolution, but it cannot be changed as it is fixed by the neutron energy. It gives information on lower dynamics at nanosecond to picosecond time scale. It has limited dynamic range. The second category of spectrometers have lower resolution, but it can be varied by changing the energy of the incoming neutrons. In contrast to the first category spectrometers, they can give information on faster dynamics occurring at picosecond time scale. Also the dynamic range accessible is larger.

The scattering function is generally expressed as

$$S(Q,\omega) = p_0\delta(\omega) + \sum_{i=1}^{n} p_i \frac{1}{\pi}\frac{\Delta_i(Q)}{\omega^2 + \Delta_i^2} + B \tag{13.18}$$

From the dynamic scattering function, detailed information on the sample dynamic states can be understood.

A typical QENS spectrum is given further.

13.6.6 Magnetic neutron spectroscopy

We know that X-rays are scattered by extranuclear electrons, the electrons surrounding the nucleus of the atom, while neutrons are scattered by the nuclei themselves. In addition, in magnetic materials, there is another interaction for neutrons. Even though neutrons are electrically neutral, they possess a nonzero magnetic dipole moment, which is of the order of Bohr magneton and is very efficient in interacting with the unpaired electrons in magnetic materials belonging to ferromagnetic, ferrimagnetic, and antiferromagnetic types and gives valuable information about the magnetic structure and spin dynamics. The specific inherent properties of neutrons that enable it to act as a preferred probe for magnetic materials are that (1) it possess a spin and (2) neutron beams can be polarized and analyzed. Just 3 years after the discovery of neutrons, Bloch [38] developed the idea of magnetic scattering and recognized the potential of neutrons as a tool in undermining the properties of magnetic materials. The de Broglie wavelength associated with the neutron is comparable with the lattice parameters available in a spin lattice. In magnetic materials, the spin systems which are coupled by exchange interactions have wave-like low-lying energy states. The energy of these waves, called spin waves, are quantized and are designated as magnons. These magnons inelastically scatter the neutrons. In other words, when neutrons are incident on magnetic materials, spin waves are also concurrently excited at any finite temperature [39]. The energy of the spin waves in magnetic solids are in the meV range, which are comparable with the energy of the thermal neutrons. It is worthy to note that in magnetic materials the spin lattice parameter is about twice the spatial lattice parameter, related to the interaction of neutrons with the nucleus. Since the nearest atom spins are antiparallel, only spins of second nearest atoms are identical. Thus the lattice parameters become double when we consider magnetic scattering with the spin lattice. Hence, in the relation $2d\sin\theta = n\lambda$, d gets doubled, $\sin\theta$ becomes half so that λ remains constant. Hence corresponding to small angles, we get an extra Bragg scattering, that is, an extra peak. Neutron sources in general provide unpolarized neutrons. But it was later understood that more detailed and unambiguous structure and dynamics of magnetic materials can be obtained from scattering data provided by polarized neutrons. It is interesting to see that many materials which are playing crucial role in the present day science and technology had been developed based on the results from such studies. Accordingly neutron scattering is the method generally adopted for investigating the magnetic structure as well as spin waves and other excitations in magnetic materials. If the energy of the spin waves is around 0.1 meV, then cold neutron scattering is appropriate. It is known that in transition metal ferromagnets made up of Fe, Ni, Co, etc., the spin wave energies lie in the range 0–200 meV and scattering by hot neutrons are made use of. Spin waves are observed in all types of ordered spin systems. The energy of any scattered neutron will be equal to the energy of the incident neutron plus/minus the energy of the magnon.

Shull and Smart first experimentally confirmed neutron magnetic scattering in MnO [40]. From the experimentally observed dispersion relations, we extract the sign and magnitude of the exchange interactions. Magnetic structure study is crystallography whereas magnon spectra is the manifestation of the spectroscopy. Both are managed with neutrons. These processes are collectively called magnetic scattering. After the success of the first experiment, this area of research flourished over decades and still continues to be like that. These are evident from the number of books released and the papers published on the applications of this novel technique [41–45]. One can have a quick look at many of these things, including the basic theory, in the book edited by Tapan Chatterji [46] and that written by Randy et al. [47]. The experimental arrangement used in this type of spin wave dispersion studies is the triple-axis spectrometer [48].

The symmetry analysis of neutron diffraction data, based on the principles of group theory, provides valuable information on the structure of magnetic materials. A wealth of information in this regard is available from the investigations of Izyumov et al. [49–53].

13.6.7 Vibrational spectroscopy with neutrons

In neutron vibrational spectroscopy, inelastic neutron scattering is performed with a specific aim to obtain vibrational spectroscopic and bonding information in a wide range of materials. Here more interest is on inelastic neutron scattering from hydrogenous molecules, solids, and surfaces. The major benefits of using neutrons for vibrational spectroscopy are strong scattering by hydrogen and high penetration. Neutron scattering spectrum is a rich source of information on forces acting internally between atoms within molecules and externally between atoms and molecules in extended lattice sites. When neutrons exchange energy in scattering it is inelastic and gives spectroscopic information. It was early understood that vibrations of hydrogenations in compounds are easily amenable to neutron scattering techniques (for more details refer to Ref. [1], vol. 3). Neutron vibrational spectroscopy is such an active area of research that one particular session in the International Conference on Advanced Vibrational Spectroscopy is entirely dedicated to vibrational neutron spectroscopy. Also the importance of this can be seen in the recent reviews [54, 55].

Another spectroscopic technique, very close in principle to those discussed earlier is the time-resolved neutron spectroscopy. This spectroscopy is used to study the dynamic processes in materials or chemical compounds such as relaxation processes. Generally, the dynamic processes are studied after the illumination of the sample with the probe radiation. It can be applied to any process that leads to a change in the properties of the material. Pulsed neutron sources are used in these investigations. These are generally called in situ or time-resolved spectroscopy [56, 57].

13.7 Neutron amorphography

Amorphous materials like glass are playing very important role in the modern materials science. For explaining their properties several models have been suggested and are being used, especially based on random network theory. These are developed based on experimental observations. Just as in the case of crystalline materials, X-ray and neutron diffraction are the major probes for identifying the structure and dynamics of amorphous solids. Generally, the amorphous materials have no spatial periodicity and so symmetry principles cannot be applied. Ideal crystalline substances provide diffraction pattern characterized by well-defined sharp Bragg peaks. Crystalline materials are characterized by a long-range order which is absent in the case of amorphous materials. Hence diffraction pattern from amorphous materials do not exhibit sharp Bragg peaks. However, real amorphous substances are not collection of atoms with complete random distributions. On close observation of the diffraction pattern of X-rays or neutrons from an amorphous material, one can see the variation in intensity with scattering angle and hence very broad peaks. From the resulting inverse Fourier transform of this intensity distribution, we can infer the pair distribution function in the real space and it gives distances between atoms. These near-neighbor distances are, in most of the cases, very similar to that obtained from the crystalline analog of these materials. These procedures for identifying the structure of amorphous materials is called amorphography [58–60]. In a study carried out by Sabu et al. [61], the effectiveness of neutron scattering for understanding the morphology and structure of fillers in rubber matrix (which is an amorphous material) was firmly established.

13.8 Sources of additional information

In recent years, major neutron and X-ray facilities around the world had generated enormous amount of data and the users felt the necessity of having a common data format and it resulted in the NeXus data format. NeXus is built on top of the scientific data format HDF5. It is a binary file format available in public domain and is well supported by both commercial and free software tools. It is efficient and platform independent [62].

The capability of X-rays and neutrons as material characterization tools had been identified immediately after their discoveries. The data accumulated over the years was used to generate databases and was released under the name Joint Committee on Powder Diffraction Standards (JCPDS) reference databases (Powder Diffraction Files—PDF) and later became International Centre for Diffraction Data (ICDD) [63]. The latest version to be released in 2020, under the name PDF-4+ 2020, is announced to have 426,000+ entries. Though not free, institutional license can be had, and users can remain updated with these files.

There are open-access databases also, freely available to the users. One among them is Crystallography Open Database, containing more than 45 lakhs of entries of crystal structures of organic, inorganic, and metal-organic compounds, and minerals, excluding biopolymers [64].

It is worth noting that we have, in the discussions presented earlier, concentrated only on interactions of neutrons as a tool to understand the structure and dynamics of condensed matter. Apart from that there is a broad area in science where thermal and fast neutron interactions are used with a motivation to understand nuclear reactions and nuclear structure, with applications in neutron activation analysis, reactor physics, medical physics, etc. [65, 66], modulation spectrometry with neutrons, with diffractometry applications. Thus, neutron scattering technique, resulting in spectroscopy and crystallography, is a very versatile tool for investigating the structure and dynamics of crystalline materials, amorphous materials, polymers, nanomaterials, composite, and ceramic materials. It is also immensely used in engineering diagnostics, molecular biology, pharmacology, geophysics, earth science, etc.

In spite of all the above-mentioned advantages for neutron scattering technique, when compared to X-ray scattering, it suffers from few inherent limitations. (1) The instrumentation for neutron scattering require dedicated facilities. Developing, operating, and maintaining neutron sources are expensive, whereas the instrumentation for X-ray scattering are relatively of low cost and can be installed in an ordinary research lab. (2) Generally, intensity of neutron flux is lower than that of X-rays and as a result neutron irradiation needs more exposure time and often requires large amount of sample (which is a problem in the case of biological samples). (3) Since incoherent scattering cross-section with ^1H is relatively high, it acts as an unwanted background in many spectra or pattern.

Acknowledgments

The author (Antony Joseph) wishes to express sincere gratitude to Dr. T.N. Vasudevan for the fruitful discussions and to Dr. K. Muraleedhara Varier for patiently going through the manuscript and offering relevant suggestions.

References

[1] J.L. Finney, D.L. Worcestor(Eds.), Series of Neutron Techniques With Applications—vol. 1: Modulation Spectrometry of Neutrons With Diffractometry Applications, vol. 2: Single Crystal Neutron Diffraction From Molecular Materials, vol. 3: Vibrational Spectroscopy With Neutrons With Applications in Chemistry, Biology, Material Science, and Catalysis, World Scientific, Singapore, 2005.
[2] http://www.spectroscopyonline.com/neutron-spectroscopy.
[3] https://www.tandfonline.com/loi/gnnw20.
[4] http://nssi.org.in/.
[5] https://www.hindawi.com/journals/jspec/about/.
[6] A.M. Glazer, A Journey Into Reciprocal Space—A Crystallographer's Perspective, Morgan and Claypool Publishers, San Rafael, CA, 2017.
[7] B.N. Brockhouse, Slow neutron spectroscopy and the grand atlas of the physical world, Rev. Modern Phys. 67 (4) (1995) 735–751.
[8] https://psi.ch/en/niag/neutron-physics.
[9] L. Heilbrown, Neutron properties and definitions supplement, https://three.jsc.nasa.gov/articles/Heilbrown_Neutron_Supplement.pdf.
[10] L. Van Hove, Correlations in space and time and Born approximation scattering in systems of interacting particles, Phys. Rev. 95 (1954) 249.
[11] J. Chadwick, Possible existence of a neutron, Nature 129 (1932) 312.
[12] G.K. Dhindsa, Dynamics of Biopolymers on Nanomaterials Studied by Quasielastic Neutron Scattering and MD Simulations (Ph.D. thesis), Wayne State University, 2015.

[13] https://www.nist.gov/nist-research-library/journal-research-volume-98.

[14] G.L. Squires, Introduction to the Theory of Thermal Neutron Scattering, Dover publications Inc., New York, NY, 1996.

[15] U. Shmueli, International Tables for Crystallography, vol. B: Reciprocal Space, third ed, Wiley, New Jersey, 2008.

[16] L. Koester, A. Steyerl, Neutron Physics, Springer Tracts in Modern Physics Book Series, vol. 80, STMP, Switzerland, 1977.

[17] L. Dorothee, Evaluation of models determined by neutron diffraction and proposed improvements to their validation and deposition, Acta Crystallogr. D Struct. Biol. 74 (pt. 8) (2018) 800–813.

[18] R. Pynn, International Neutron Scattering Instrumentation School (INSIS), Neutron News. 24 (1) (2013) 7.

[19] W. Mampe, P. Ageron, C. Bates, J.M. Pendlebury, A. Steyer, Neutron lifetime measured with stored ultracold neutrons, Phys. Rev. Lett. 63 (1989) 593.

[20] A. Serebrov, A. Fomin, New analysis of neutron life-time experiments, Crystallogr. Rep. 56 (7) (2011) 1248–1252.

[21] D. Allan Bromley, Neutrons in science and technology, Nucl. Instrum. Methods Phys. Res. 225 (1984) 240–279.

[22] I.S. Anderson, R. McGreevy, H.Z. Bilheux, Neutron Imaging and Applications: A Reference for the Imaging Community (Neutron Scattering Applications and Techniques), Springer, US, 2010.

[23] K. Muraleedhara Varier, J. Antony, P.P. Pradyumnan, Advanced Experimental Techniques in Modern Physics, Pragati Prakashan, Meerut, 2006.

[24] S.F. Trevino, The triple axis and spins spectrometers, J. Res. Natl. Inst. Stan. Technol. 98 (1) (1993) 59–69.

[25] B.N. Brockhouse, A.T. Stewart, Scattering of neutrons by phonons in an aluminium single crystal, Phys. Rev. 100 (1955) 756.

[26] T. Dove, B.M. Powell, G.S. Pawley, S.L. Chaplot, A. Mierzejewski, Inelastic neutron scattering determination of phonon dispersion curves in the molecular crystal sym $C_6F_3Cl_3$, J. Chem. Phys. 90 (1989) 1918.

[27] N. Tsooulfanidis, Measurement and Detection of Radiation, Taylor & Francis, Washington, DC, 1995.

[28] M. Monkenbusch, D. Richten, High resolution neutron spectroscopy—a tool for the investigation of dynamics of polymers and soft matter, C.R. Physique 8 (2007) 845–864.

[29] F. Mezei, Neutron Spin Echo, in: Proceedings of a Laue-Langevin Institute Workshop, Grenoble, October 15–16, 1979.

[30] F. Mezei, Neutron spin-echo spectroscopy, Europhys. News 16 (4) (1985) 1–4.

[31] R. Georgii, J. Kendervater, C. Pfleiderer, P. Boni, RESPECT: neutron resonance spin-echo spectrometer for extreme studies, Nucl. Instrum. Methods Phys. Res. A 837 (2016) 123–135.

[32] A. Heidare, Neutron spin echo spectroscopy and spin noise spectroscopy—comparative study on malignant and benign cancer cells and tissues with a passage of time under synchrotron radiation, Int. J. Biopharm. Sci. 1 (1) (2018) 1–5.

[33] G. Krijger et al., Spin-echo small angle neutron scattering analysis of liposomes and bacteria, J. Phys. Conf. Ser. 247 (2010) 01206.

[34] E.L. Hahn, Spin echoes, Phys. Rev. 80 (4) (1950) 580.

[35] M.J. Hollamby, Practical applications of small angle neutron scattering, Phys. Chem. Chem. Phys. 15 (2013) 10566–10579.

[36] V.G. Sakai, C. Alba-Simionesco, Dynamics of Soft Matter—Neutron Applications, Neutron Scattering Applications and Techniques Series, Springer, US, 2012.

[37] J.P. Embs, F. Juranyi, R. Hempelmann, Introduction to quasielastic neutron scattering, Z. Phys. Chem. 224 (2010) 5–32.

[38] F. Bloch, On the magnetic scattering of neutrons, Phys. Rev. 50 (1936) 259.

[39] J.R. Hook, H.E. Hall, Solid State Physics, second ed., John Wiley & Sons, 2010.

[40] C.G. Shull, J.S. Smart, Detection of antiferromagnetism by neutron diffraction, Phys. Rev. 76 (1949) 1256.

[41] W. Marshell, S.W. Lovesey, Theory of Thermal Neutron Scattering, Oxford University Press, New York, NY, 1971.

[42] E. Balcar, S.W. Lovesey, Theory of Magnetic Neutron and Photon Scattering, Clarendon Press, Oxford, 1989.

[43] G.E. Bacon, Neutron Diffraction, Clarendon, Oxford, 1975.

[44] S. Lovesey, Theory of Neutron Scattering From Condensed Matter, vol. 1, Clarendon Press, Oxford, 1987.

[45] H.S. Nair, J.M. Brown, E. Coldren, G. Hester, M.P. Gelfand, A. Podlesnyak, Q. Huang, K.A. Ross, Short range order in the quantum XXZ honeycomb lattice material $BaCo_2(PO_4)_2$, Phys. Rev. B 97 (2018) 134409.

[46] T. Chatterji, Neutron Scattering From Magnetic Materials, Elsevier, 2006.

[47] R.S. Fishman, J.A. Fernandez-Baca, T. Room, Spin-Wave Theory and Its Applications to Neutron Scattering and THz Spectroscopy, IOP Publishers, San Rafael, CA, 2018.

[48] G. Shirane, S.M. Shapiro, J.M. Tranquada, Neutron Scattering With a Triple-Axis Spectrometer - Basic Techniques, Cambridge University Press, Cambridge, UK, 2002.

[49] Y.A. Izyumov, V.E. Naish, Symmetry analysis in neutron diffraction studies of magnetic structures—1. A phase transition concept to describe magnetic structures in crystals, J. Magn. Magn. Mater. 12 (1979) 239–248.

[50] Y.A. Izyumov, V.E. Naish, V.N. Syromiatnikov, Symmetry analysis in neutron diffraction studies of magnetic structures—2. Changes in periodicity at magnetic phase transitions, J. Magn. Magn. Mater. 12 (1979) 249–261.

[51] Y.A. Izymov, V. Naish, S. Petrov, Symmetry analysis in neutron diffraction studies of magnetic structures—3. An example: the magnetic structure of spinels, J. Magn. Magn. Mater. 13 (1979) 267–274.

[52] Y.A. Izymov, V.E. Naish, S.B. Petrov, Symmetry analysis in neutron diffraction studies of magnetic structures—4. Theoretical group analysis of exchange Hamiltonian, J. Magn. Magn. Mater. 13 (1979) 275–282.

[53] Y.A. Izymov, Symmetry analysis in neutron diffraction studies of magnetic structures—5. Polarization effects in the scattering of neutrons by magnetic structures, J. Magn. Magn. Mater. 21 (1980) 33–42.

[54] S.F. Parker, A.J. Remirez-Cuesta, L. Daemen, Vibrational spectroscopy with neutrons: recent developments, Spectrochim. Acta A Mol. Biomol. Spectrosc. 190 (2018) 518–523.

[55] F. Stewert Parker, D. Lennon, P.W. Albers, Vibrational spectroscopy with neutrons: a review of new directions, Appl. Spectrosc. 65 (12) (2011) 1325–1341.

[56] G. Eckold, Time-resolved triple-axis spectroscopy—a new method for real time neutron scattering, Nucl. Instrum. Methods Phys. Res. A289 (1990) 221–230.

[57] O. Isnard, A review of in situ and/or time resolved neutron scattering, C. R. Physique 8 (2007) 789–805.

[58] A.C. Wright et al., Neutron amorphography, J. Non Cryst. Solids 49 (1982) 63–102.

[59] A.C. Wright, Neutron and X-ray amorphography, J. Non Cryst. Solids 106 (1988) 1–16.

[60] S. Neov, V. Kozhukharov, Neutron diffraction in amorphous structure, in: J.M. Rincon, M. Romero (Eds.), Characterisation Techniques of Glasses and Ceramics, Springer-Verlag, Berlin, Heidelberg, 1999 (Chapter 12).

[61] J. Varghese, C.J. Chirayil, L. Somasekharan, S. Thomas, X-ray, light and neutron scattering studies on natural rubber composites and nanocomposites, in: H.J. Maria, J. Joy, C.H. Chan, L.A. Pothen, S. Thomas (Eds.), Natural Rubber Materials—vol. 2: Composites and Nanocomposites, RSC Publishing, Cambridge, UK, 2013 (Chapter 22).

[62] M. Konnecke, F.A. Akeroyd, H.J. Bernstein, A.S. Brewster, S.I. Campbell, B. Clausen, S. Cottrell, J.U. Hoffmann, P.R. Jemian, D. Mannicke, R. Osborn, P.F. Peterson, T. Richter, J. Suzuki, B. Watts, E. Wintersberger, J. Wuttke, The NeXus data format, J. Appl. Crystallogr. 48 (2015) 301–305.
[63] https://www.icdd.com/.
[64] http://www.crystallography.net/cod/index.php.
[65] G. Ericsson, Advanced neutron spectroscopy in fusion research, J. Fusion energy 38 (2019) 330–355.
[66] www.nds.iaea.org.

CHAPTER 14

Advancements in computational methods for neutron shielding

C. Danani, H.L. Swami
Institute for Plasma Research, Gandhinagar, India

14.1 Introduction

Neutron shielding evaluation is a key phenomenon to the design and development of nuclear facilities, i.e., nuclear power plants, test reactors, neutron generators, radioactive waste management, etc. [1–4]. It will assure the safety of humans working in such facilities and also the components. There are regulatory bodies that ensure the safety associated with nuclear facilities by evaluating the shielding design. Thus, the shielding design and evaluation becomes vital for the safe and smooth operation of any kind of nuclear facilities. There are many computational techniques to assess shielding capabilities. Computational modeling also helps to optimize the shielding for a particular machine as per the requirements. The evaluation and optimization of the shielding through computational methods are cost-effective and time-saving method. Thus, shielding evaluation through experiments is very costly and time consuming and also not safe in the case of big nuclear facilities like nuclear plants and accelerators. However, computational techniques opted to perform the shielding evaluation has to be validated through some laboratory-scale experiments to get assurance on predicted results [5–7].

Characteristics of the neutron source drive the shielding design in terms of shield material, thickness, etc. For the neutron shield design, the understanding of the neutron interaction with the matter is required. Neutron is a chargeless particle and due to the neutral charge it is unaffected by atomic orbital electrons and the electromagnetic force of the nucleus. The interaction of neutron is based on short-range nuclear forces. The basic interaction of the neutrons with material happens in three ways: elastic scattering, inelastic scattering, and transmutation. The neutron changes its energy and direction through elastic collision with nucleus. It transfers part of the energy to the nucleus which is also displaced from its lattice location. Inelastic scattering process happens in two parts: the neutron is captured by the nucleus followed

Micro and Nanostructured Composite Materials for Neutron Shielding Applications
https://doi.org/10.1016/B978-0-12-819459-1.00014-3
© 2020 Elsevier Ltd.
All rights reserved.

by the emission of the neutron from the nucleus which will leave the nucleus in the excited state. The excited nucleus returns to its ground state by emitting gamma rays. The transmutation also happens through neutron capture process but after that nucleus emits some other particles such as alpha particles, protons, neutrons, and the nucleus is converted to the nucleus of another element.

Shielding design requires the attenuation of energy and flux of neutron. The process of neutron attenuation happens through the above-explained interaction processes in the material. The neutron interaction process also depends on the constituents of the material. The interaction process depends on the energy of the incident neutron and elemental composition of the material. The steps involved in attenuation process in shielding material are as follows [8–10]:

Step 1: The high-energy neutrons, having energy above 1 MeV, can penetrate materials for a few cm thickness without interaction due to high velocity (high mean free path) and fewer collisions. The component which remains uncollided is identified as the uncollided neutrons in neutron transport theory.

Step 2: Neutrons slow down through elastic collisions which is a major part of the interaction. It converts most of the uncollided neutrons to secondary neutrons. The energy of secondary neutrons lies between 1 MeV and thermal energy. Inelastic scattering also plays a part in slowing down neutrons through the capture process.

Step 3: The neutrons are finally absorbed through the transmutation process, which is a vital part of shielding. It makes absolute removal of neutrons. The absorption mainly happens for thermal neutrons. The elastic and inelastic collisions reduce the energy of neutrons which makes them suitable for the absorption process.

The probability of a particular type of interaction (elastic, inelastic, absorption, etc.) is defined as microscopic cross section. It has the unit of area and depends on incident neutron energy, type of interaction, and target element. The total cross sections of some nuclides, i.e., hydrogen, boron, cadmium, iron, and tungsten are shown in Fig. 14.1. It has been taken from the nuclear data service through the interactive plot of ENDF [11–15]. As shown in Fig. 14.1, cross sections of cadmium and boron are very high for thermal neutrons. There is a resonance region in the cross-section profile between the energy of 100 eV and 1 MeV.

The cross sections of elastic scattering for some nuclides are plotted Fig. 14.2. It is clear from the cross-section curves in Figs. 14.1 and 14.2 that

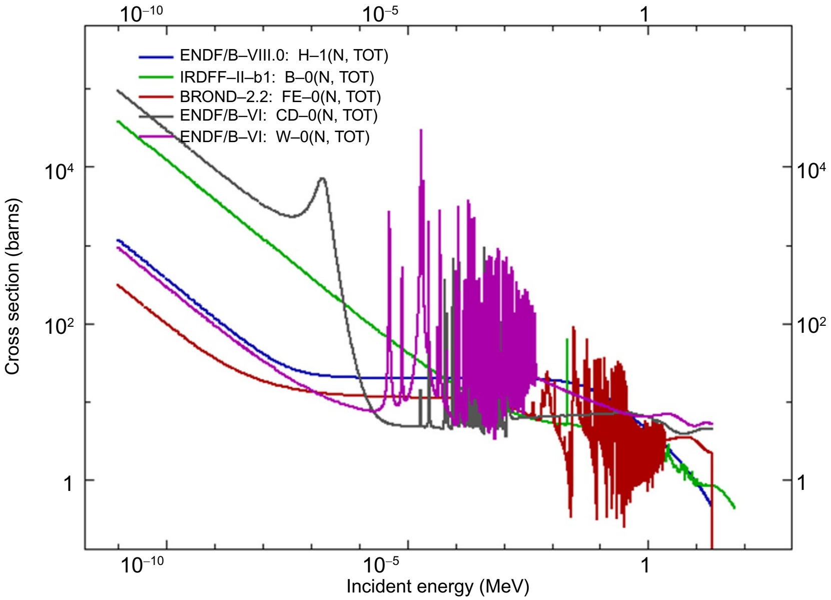

Fig. 14.1 Total neutron interaction cross section.

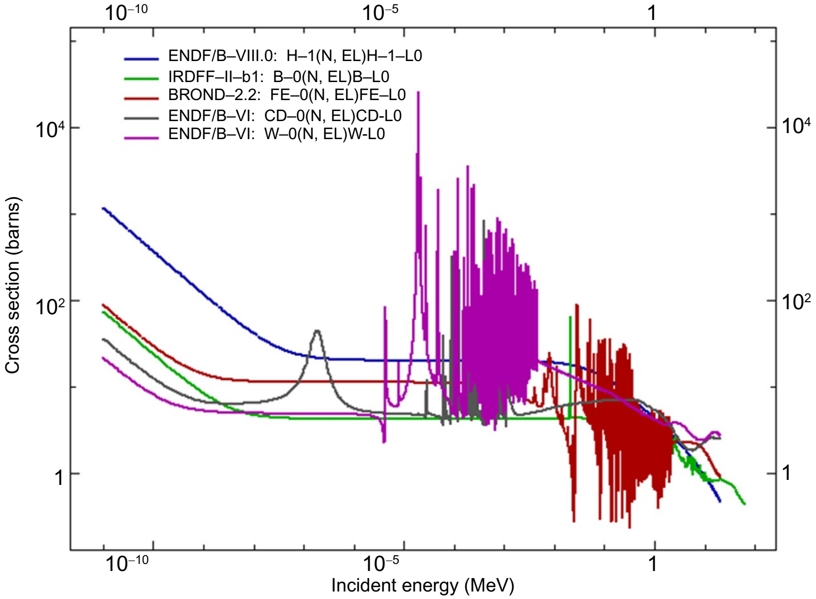

Fig. 14.2 Elastic scattering cross section.

the elastic scattering cross section is lower than total interaction cross section. Hydrogen has higher cross section for elastic scattering in low-energy region in comparison to other elements as shown in Fig. 14.2. The elastic scattering cross section decreases with an increase in atomic number.

The concept of cross section is very important, since it is a key term used in empirical and semiempirical formulas or advanced computational codes for shielding design.

In the early days of design and development of nuclear facilities, the exponential method of radiation attenuation was used to evaluate the required material thickness for shielding. The classical methods for the shielding assessment are described in Section 14.2.

As computational physics and nuclear physics progressed, various computational codes have also been developed for radiation transport in the one-dimensional to three-dimensional geometries. Most of the developed modeling codes are based on either the Monte Carlo method for particle sampling or deterministic method based on the Boltzmann transport equation. A brief introduction of these transport methods is given in Section 14.3.

The advancement in the neutron transport modeling tools such as MCNP, ATTILA, SUPER-MC, etc. have made it possible to use realistic system geometries through 3D CAD models for the shielding assessments. The advancement also provides more accurate and improved nuclear reaction cross-section data which help in reducing the uncertainty in design. The recent radiation transport codes have the ability to perform virtual experiments that will predict the reactor performance and safety with minimum uncertainty. The details of well-established codes are given in Section 14.4.

14.2 Numerical estimation of neutron shielding

In the early days of nuclear reactor designs and development, neutron shielding assessment was performed manually using empirical or semi-empirical formulas. The initial method was fast removal theory which was developed by Albert-Welton for systemizing the bulk shield data. The removal-diffusion theory was also employed as alternative and advancement of removal theory. Various theories were also based entirely on empirical formulations to solve the shielding problems. A glimpse of removal and diffusion theories is given in the following sections [5–10].

14.2.1 Albert-Welton kernel method

In 1950 Albert-Welton had established a semiempirical formula for neutron attenuation estimation in materials. The main objective of the method was to develop a theory for fission reactor neutron attenuation using a hydrogenous shield. The method considers that the removal of neutrons is dominated by hydrogen whereas other heavier elements play a partial role only. The effective removal cross section is the sum of the total cross section of hydrogen and partial cross section of other elements. The total removal flux is expressed as

$$\varnothing(R)=\frac{k}{4\pi R^2}\int_0^\infty f(E)e^{-\sum^{H}(E)R}\,dEe^{-\sum_i\left(g_i\sum_R^{(i)}\right)R} \tag{14.1}$$

where

$\varnothing(R)$: total removal flux density at distance R from source

$\sum_R(i)$: macroscopic effective removal cross section of the ith – elements other than hydrogen

g_i : volume fraction of the ith nonhydrogenous element

$f(E)dE$: fraction of fission neutrons with energy E in the interval $- dE$ for a total source of 1 fission per sec

$\sum^H(E)$: total macroscopic cross section of hydrogen

k : suitable constant of proability

The removal cross-section method is only applicable to minimum thickness of around 60 cm of hydrogenous material which should be followed by heavy material slab. This method was very useful during the early years of fission reactor shield design (during the 1950s).

14.2.2 Spinney kernel method

A method for shielding design was proposed by Spinney in 1957 which was based on the removal and diffusion concept. In the Spinney method, removal theory estimates the fast neutron penetration through the material and diffusion theory covers the thermalization and absorption process. The formulation of the method is given as.

$$\varnothing(R)=\frac{1}{4\pi R^2}\int_0^\infty f(E)e^{-\sum_R(E)R}dE \tag{14.2}$$

$\varnothing(R)$: total removal flux density at distance R from source

$\sum_R(E)$: macroscopic energy – depedent removal cross section

$f(E)dE$: fraction of fission neutrons with energy E in the interval dE for a total source of 1 fission per sec

Spinney method is also applicable for hydrogenous materials similar to Albert-Welton method.

14.2.3 Empirical neutron point kernel method

The shielding design expression and the attenuation function were derived from the experimentally obtained data during the operation of the fission reactors. These data had been fitted as Eq. (14.3) to get the shielding estimation and detector response for the reactor operation.

$$K(R) = \frac{1}{4\pi R^2} \sum_i A_i e^{-\alpha_i R} \tag{14.3}$$

where $K(R)$ is the response of the detector at a distance R from a unit source in an infinite medium of the moderator. Data obtained from experimental measurements for various kinds of shield materials such as H_2O, D_2O, or heavy materials and function as shown in Eq. (14.3) was derived. The parameters A_i, α_i are coefficients which fits experimental data with Eq. (14.3). Eq. (14.3) has been improvised to use mixture of moderator and heavier materials. The effective removal cross section has been added in the equation. Thus, $K(R)$ is expressed as.

$$K(R) = \frac{1}{4\pi R^2} \sum_i A_i exp\left[-g\alpha_i R - \sum_k g_k \sum\nolimits_R^{(k)} R\right] \tag{14.4}$$

where g and g_k are the volume fraction of the moderator and heavier element k in the region of interest respectively, $\sum_R$ is the effective removal cross section of the element k, and R is the thickness of the shield region along with the radiation path between the source and the point detector.

14.2.4 Simplified neutron point kernel method:

In order to get the general concept for shielding design which is applicable for all shielding materials, a simplified neutron point kernel method was developed. The equation used in this method is.

$$\varnothing(R) = \frac{1}{4\pi R^2} \int_0^\infty f(E) \exp\left[-\sum_k g_k \sum\nolimits_R^{(K)} (E) R\right] dE \tag{14.5}$$

where $\Phi(R)$ is the removal flux density at distance R, $f(E)dE$ represents the fission neutrons of energy E for a total source of 1 fission per second, and g_k is the volume fraction of kth elements. The formulation of a simplified neutron point kernel is also applicable for multilayer shielding.

14.3 Computational techniques for neutron shielding efficiency

The neutron transport in the material is better explained by the Boltzmann equation. It is the particle balance equation. The rate of particle change can be estimated by subtracting the loss terms from source terms. The Boltzmann equation for neutron transport is [8–10].

$$\frac{1}{v}\frac{d\varnothing}{dt} = -\boldsymbol{\Omega}.\nabla\varnothing - \sum\varnothing + \iint \sum{}' f'\varnothing' d\Omega dE' + S \tag{14.6}$$

where $\boldsymbol{\Phi}$ is the angular neutron flux, $\sum$ is the total macroscopic cross section, $\boldsymbol{\Omega}$ is the unit vector in the direction of motion in terms of solid angle, ν is the neutron velocity, f is the probability of interaction, and $S$is the neutron flux from external sources.

The LHS of Eq. (14.6) is the rate of change in neutron flux with time because interactions happen inside a certain volume of the materials.

In Eq. (14.6), terms on the right-hand side have two parts: one is for loss and the other for gain of the neutrons. The first and second terms on the right-hand side are loss terms. The first loss term is a neutron leakage rate from the volume. The second term indicates the rate of loss through all types of the nuclear interaction. The third and fourth terms are for gain of neutrons. The third term represents the gain of neutron through nuclear interaction including fission. The fourth term signifies the external sources of neutrons. For a steady-state situation, the rate of the change in neutron flux concerning time becomes zero.

The neutron transport equation is solved using two main numerical approaches as follows:

- deterministic method [16–18]
- Monte Carlo method [19–21]

These approaches are different from each other. The deterministic method solves the Boltzmann equation by simplifying the parameters. It opts for the discretization of the energy, space, and direction whereas the Monte Carlo method does not solve the transport equation. It tracks the particles from its origin to elimination. It simulates the physics associated with nuclear interaction by adopting random sampling techniques. Both methods are described in the following sections.

14.3.1 Deterministic method

The deterministic approach is used to solve the Boltzmann equation. The method plays a vital role in the shielding design of the reactor, especially for deep shield designs. It is also important for the modeling of the reactor core and other experimental facilities. Various popular neutron transport codes based on the deterministic method are ATTILA, THREEDANT, SNAM, ANISN, DORT, and TORT [22–25]. The deterministic method is based on discretizing various parameters of the Boltzmann transport equation to linearize it for the desired output. The following methodologies and approximations are opted by deterministic methods:

- energy discretization
- space discretization
- angle discretization
- spherical harmonics

Energy discretization is a multigroup energy approximation. The problem is considered a neutron energy-dependent problem. The neutron interaction cross-section data is divided into multigroups. The average energy of the group is considered interaction energy. The decision on the number of energy groups depends on the problem. For some problems such as fission reactor fuel design modeling, the resonance in cross-section data needs to be incorporated into model realistic conditions. It depends on the interaction with environment. Some elements do not show the resonance in cross sections whereas some have significant. In particular, for neutron shielding estimation, it does not make substantial difference. However, such cross-section approximation over a certain energy range becomes the source of uncertainty in reactor core design calculations.

Space discretization breaks the geometries in the finite small parts, i.e., mesh. The neutron transport is simulated using finite difference or finite element method at each point. To reduce the uncertainty in the space discretization, the boundary of specific material zones needs to be precisely considered. Fine meshes are also required where the drastic difference in the energy spectrum is expected. However, the uncertainty reduction in outcome through fine meshing of geometry leads to high computational power.

The direction of the particles can also be discretized through two processes. First is the P_N method, also known as spherical harmonics polynomial, and the other is the S_N method or discrete ordinate method.

In P_N approximation, the directional integral is represented by the summation of spherical harmonics. It includes scattering kernel, angular flux, and direction of the source particle. It can be solved by approximation of the truncation of infinite series. For the case of symmetrical geometry, Legendre polynomials can be used instead of spherical harmonicas. Thus, the transport equation becomes the set of N coupled differential equations.

S_N method is defined as segments in N number of directions. The continuous direction variable is replaced by several discrete directions which represent the discrete ordinates method. The angular flux is considered in a limited number of directions. It is linear between two points. The number of directions should be high enough to deal with anisotropy of angular flux. The enhancement in discretization can provide a good estimation of neutron flux distribution but consumes a lot of computational power.

14.3.2 Monte Carlo method

Unlike the deterministic method, the Monte Carlo method does not solve the neutron transport equation [19–21]. It simulates each particle trajectory in the area of interest from birth to death. It processes the microscopic physics associated with neutron in terms of energy, collision, and direction. It is a computer-based neutron transport experiment. It simulates the actual physical process as it happens in real. It creates a sequence of life histories of source neutrons using random sampling process and uses the probability of neutron interaction with specific elements. It predicts real-life neutron behavior in the medium. The history of the neutron is tracked until the neutron absorbed or escapes from the medium. It includes all scattering and absorption processes of neutrons. The neutrons tracked in the zones of interests are divided by the total number of histories to get the mean value of flux.

Monte Carlo technique is based on the random number generator and event sampling process as per physical phenomena.

The random numbers are an inherent part of the particle sampling process because each event in neutron transport is associated with a random number. It is generated through a computer-based algorithm thus it is not random, but pseudorandom. The algorithm can produce a series of random numbers from a certain uniform distribution between 0 and 1.

There are many algorithms that can generate a series of random numbers such as the middle square method, Mersenne Twister, Weyl sequence, CryptGenRandom, etc. [26–30]. The physics associated with neutron transport in the Monte Carlo method is represented by the probability distribution function. It is expressed as the probability of the event occurrence. Thus, the probability of the occurrence of an event between x and x +dx is given by

$$dP = f(x)dx \tag{14.7}$$

If it is seen in the interval $[x_0, x_1]$ then

$$P(\mathrm{x}_0 \leq \mathrm{x} \leq \mathrm{x}_1) = \int_{x_0}^{x_1} dP = \int_{x_0}^{x_1} f(x)dx \tag{14.8}$$

The probability of the occurrence of an event before a certain value is given by cumulative distribution function

$$F(x) = P(x' \leq x) = \int_{-\infty}^{x} f(x')dx' \tag{14.9}$$

The probability distribution integration must be equal to 1.

$$\lim_{x \to \infty} F(x) = 1 \tag{14.10}$$

The sampling of the various event outcomes like distance to collision site, type of interaction during collision, direction, and energy of scattered neutrons is done using the probability distributions. The inversion method is the simplest method for the sampling of a random value from distribution $f(x)$. It is derived through cumulative distribution function $F^{-1}(x)$ and uniformly distributed random variables ξ on unit interval. The value of the variable x is obtained from the inverse of the cumulative distribution function

$$x = F^{-1}(\xi) \tag{14.11}$$

It is not used if F or F^{-1} are two different distributions. In such case, the rejection sampling technique works. It uses two distribution functions, the original distribution $f(x)$ and majorant function $g(x)$ where

$$g(x) \geq f(x) \tag{14.12}$$

First x variable is sampled using $g(x)$ distribution via inversion method and through rejection sampling accept the sample with probability

$$P(x) = \frac{f(x)}{g(x)} \tag{14.13}$$

For a better understanding of the rejection method, an example of sampling points for a certain area (circle) inside the square envelope can be considered. Points fall inside the circle are accepted and outside the circle are rejected. These are the ways of sampling the variables in the Monte Carlo Method [31, 32].

Monte Carlo method is a statistical concept and the result of each event does not match. It lies in some range or distribution. The error associated with the result is a statistical approximation error. To unify the magnitude of the peak and reduce the bandwidth of outcome distribution, the number of particle histories should be large. High computational resources are required to run a large number of particle histories. For deep shielding problems, the number of particle histories should be maximized to get a good score at interesting zones that need a large number of random numbers. In such cases, non-analog technique is used to enhance the score of the particles in interesting zones. It is done using particle sampling biasing techniques. The particle biasing is applied in such a way that particle scores at the interesting zones should rise in a significant manner. It is done by generating pseudoparticles in the sampling process and adjusting the particles' statistical weight. It does not hinder the mean value and enhance the score in an interesting zone. It leads to a reduction in the statistical error [33–37]. Overall, the Monte Carlo method can solve any kind of neutron transport problem whether it is complex or simple. It directly applies neutron physics without major approximations. It needs large computing time and resources which makes it computationally expensive.

14.4 Advance simulation software for the simulation of realistic neutron shielding experiments

This section describes the popular codes in the current scenario for radiation transport phenomena and radiation shielding. These codes have advanced simulation capability in terms of geometry, physical process, and computational efficiency. The codes included here are MCNP, ATTILA, SuperMC, TRIPOLI, TORT, FLUKA, and GEANT. These codes are either based on Monte Carlo method or deterministic method of particle transport.

14.4.1 MCNP [38–41]

Monte Carlo N Particle (MCNP) code is developed by Los Alamos National Laboratory. It is the most popular code for radiation transport physics simulation. It can transport neutron, photon, electron, or coupled neutron/photon/electron. It solves an entire range of neutron transport physics problems such as fission and fusion reactor design, deep penetration problems, neutron source modeling, experiments design, detector design, nuclear oil logging, accelerator target design, nuclear critical safety, radiation shielding, radiography, decontamination, and decommissioning. The advanced capabilities of the MCNP code are handling complex 3D geometry, ease of general source inclusion, criticality source, and surface sources. It can plot geometry as well as nuclear responses. It has a broad range of non-analog techniques for statistical error reduction for the simulation of deep shielding and huge complex geometries. It also has the flexibility of modeling the desired outputs. It can simulate responses like surface current, flux volume flux or track length, radiation heating, detectors, detector pulse height for energy and charge deposition, radiography responses, and mesh-based responses. It has a wide collection of nuclear cross-section data. It uses the point-wise cross-section data.

Evaluated Nuclear Data Files (ENDF) for neutron transport is opted by MCNP. It has the flexibility to use other evaluated cross-section data files. Apart from the cross section, it has many inbuilt physics models to tackle the free gas treatments, $S(\alpha, \beta)$, etc.

MCNP takes the input as a text file format that has three basic cards, i.e., cell card, surface card, and data card. The cell card has details of specific volume geometry. Volume cells are formed through an algebraic combination of defined surfaces. The surface card has details of surfaces with plane definition. The data card has other remaining details of the problem except for geometry. It consists of various cards such as source, tally, particle transport information, etc. The source card has the details of the source. The source can be selected from predefined source distribution in the code such as Maxwell fission spectrum, Watt fission spectrum, Gaussian fusion spectrum, evaporation spectrum, Muir velocity Gaussian fusion spectrum, etc. It can be a user-defined source. A user can define the source in the form of energy and emission probability. MCNP can simulate multiple source problems in a single run. The tally card has information about the desired responses such as neutron flux distribution, reaction rates, dose rates, and nuclear heat deposition. The information related to the number of particle history, particle transport specifications such as neutron, photon, coupled neutron-photon transport has to be included in the data card. MCNP execution occurs as per defined inputs and generates output file. The output file has the desired information along with the statistical data. Overall, MCNP is the most relevant and worldwide accepted code for nuclear radiation transport simulation. It has an excellent quality to solve deep shielding problems.

14.4.2 ATTILA [42–45]

ATTILA is three-dimensional radiation transport simulation software. It is created to solve the Boltzmann transport equation using the deterministic numerical method. It was initially developed by Los Alamos National Laboratory (LANL). The advanced version of ATTILA was developed by the University of California (UCLA). It uses the SN method to solve linearized transport equations. It can solve multiparticle transport problems such as neutron-photon, electron-photon. ATTILA employs algorithm which has a set of individual discretization techniques. The discretization techniques are assembled in a way to provide solution for a wide variety of applications. The discretizations followed by ATTILA are as follows:

- energy discretization
- spatial discretization using unstructured tetrahedral finite element mesh
- discrete ordinates (S_N) differencing in angle
- spherical harmonics expansion of scattering source

The discretization produces a large, sparse linear system of equations in six-dimensional phase space. S_N, multigroup, discontinues fine element method with arbitrary order anisotropy scatter is a convergent method which is opted by ATTILA.

ATTILA code directly imports computer-aided drafting (CAD) model of problem geometry which reduces the error of geometry modeling. It brings the easiness and advancement of the critical nuclear calculations of complex nuclear facilities and reactors with minimum geometrical approximations.

Various source distributions are inbuilt with code and users can opt any source for their problem. However, ATTILA is capable enough to define user-specific sources and multisource in a single run like MCNP. The boundary conditions like refractive, vacuum, and source boundary can be easily included.

Various kinds of materials can be included by users as per the particular problem requirements. It needs group cross-section data to solve the problem which has a specific format. It can also solve deep penetration problems and streaming problems with a biased quadrature set.

The beauty of ATTILA is that it produces particle distribution in the entire geometry of the problem, unlike MCNP. Such a feature reduces multiple run time. The desired output can be generated through particle distribution. It has post-processing feature which can generate various kinds of nuclear responses as custom reports. It can provide reaction rates, dose rates, energy spectrum, heating, and many more responses through processing of particle flux distribution. ATTILA has the option of the visualization of the results which gives the users a clear picture of the nuclear field and response in the geometry. ATTILA has the capability of parallel processing which makes it viable for commercial utilization in nuclear analyses like MCNP. Overall, ATTILA is a well-developed, general-purpose radiation transport code that is capable of solving a wide variety of scientific and engineering problems.

14.4.3 TRIPOLI [46–49]

TRIPOLI is a radiation transport code based on Monte Carlo computational technique. It is useful for the design of the nuclear shielding, nuclear reactor fuel, and other radiation facilities. It was developed by the Atomic Energy Centre of France also known as CEA. The latest TRIPOLI version has the capability to simulate neutral particle transport. It can simulate neutrons from the 20 MeV to 10^{-5} eV and photons in the range from 20 MeV to 1 keV. Apart from neutral particles, it has capability of electron and positron transport up to 1 keV. The charge particle transport function is especially for radiation detection and instrumentation modeling. It also has coupled particle transport capabilities. The advanced feature of the code is that it gives the user options to simulate both kinds of source problem whether it is a fixed source or criticality. For the simulation of the radiation shielding and radiation protection-related problem, the fixed source option has to be considered. For fission reactor fuel design, the criticality mode has to be chosen. The criticality mode will track both initial neutrons and secondary neutrons which are generated through fission process.

Like MCNP and ATTILA, it also has inbuilt particle distribution sources which can be directly called for the problem. Additionally, it has the flexibility for the user to define its specific source as per the problem in terms of spatial, angular, energy, and time details. The nuclear cross-section data used by TRIPOLI for continuous energy radiation transport is point-wise along with secondary energy-angle distribution. It accepts the data format of the ENDF library.

TRIPOLI code has an inbuilt geometry tool. Geometry can be defined using a combination of surfaces. It also accepts the geometry represented in predefined shape combinations as well as Boolean operator-based surface combinations like MCNP. The TRIPOLI uses variance reduction techniques such as particle splitting, implicit capture, and Russian roulette to solve general particle transport and deep penetration problems. The code is operated in non-analog mode whereas MCNP has both analog and non-analog modes of transport. It has a variety of response estimators like MCNP. It can estimate surface flux, averaged flux, and reaction rates over the volume. It can also estimate point flux, pulse height for gamma-ray spectroscopy, dosimetry responses using IRDEF libraries, KERMA factors, and many more. It has also the capability to estimate material irradiation which is a recent advancement in the Monte Carlo radiation transport tools. The code has the capability to visualize estimated nuclear response through an interactive tool of displays. The code can be operated in parallel running mode which can reduce the simulation time.

The TRIPOLI code has the great capability of nuclear radiation transport simulation which made the code quite popular in nuclear community. It is widely used in European Countries for the design and development of nuclear facilities.

14.4.4 SuperMC [50–52]

SuperMC is Super Monte Carlo radiation transport simulation software with its inbuilt CAD conversion capability. It is designed to solve reactor physics, radiation physics, nuclear detection, radiation health physics, and radiation shielding problems. It can perform various kinds of particle transport calculations, depletion, material activation, burn-up calculations, and shutdown dose rate calculations. It has the capability to solve the multi-physics problem such as thermo-hydraulic, structural mechanics, and fuel performance. The advancement of the code is to solve multi-physics problem which reduces the error associated with data migration and geometrical modeling. It also makes the optimization of reactor parameters quite easy with small approximation errors. The transport calculations of SuperMC are based on the hybrid model as it uses both Monte Carlo and deterministic method to transport various particles like neutron, photon, electron, and proton with continuous energy cross-section data libraries. It has the ability to model fixed source problems and criticality problems. It has a module through which the radioactive nuclide inventories can be estimated after certain time of irradiation with details of pathways.

The SuperMC opts hybrid method of transport for the complex geometry-based deep shielding problems. It divides the CAD model into three regions: complex, regular, and common. In the complex region, it applies the Monte Carlo approach and for the regular deep penetrations, it uses the S_N method using geometrical mesh. It uses both the methods for common regions. It also has variance reduction techniques to solve the deep penetration problem. It is important for the sampling of particles along with particle weight adjustment in the variance reduction method. It uses the SN method to obtain target weight and biased source for dose rate estimation using the Monte Carlo approach. It has many methods to accelerate the calculation of deep shielding problems.

One of the attractive features of SuperMC is geometrical modeling. It can directly import CAD models which enhance the capability of simulating the complex fission and fusion reactors. It drastically reduces the error caused due to manual text modeling of geometry. Apart from importing CAD model, it has the capability to generate the geometrical model using a graphical user interface.

The SuperMC has nuclear data libraries for nuclear analyses. The libraries contain coarse group, fine group energy data, and point-wise cross-section data for transport, activation, burn-up, material damage, and material data, etc. The evaluated cross-section data are selected from the available nuclear data sources like ENDF, JENDL, and JEFF. The resonance cross-section, self-shielding, thermal neutron scattering, and Doppler effect on temperature are included as a physical effect correction. The architect of SuperMC allows the user to assess nuclear radiation transport calculations, after irradiation calculations and thermo-hydraulic calculations in sequence using the same geometrical model. Overall, SuperMC is an emerging tool for the nuclear community to simulate advanced complex nuclear systems.

14.4.5 TORT [53, 54]

TORT is a three-dimensional discrete ordinate radiation transport code. It is made to solve 2D and 3D neutron and photon transport with deep penetration problems. It was developed by the Oak Ridge National Laboratory (ORNL). The directional variable of the Boltzmann equation is handled by a discrete ordinate method whereas the spatial variables are treated through weight difference and nodal method. Multigroup formulation of energy has been opted to solve the Boltzmann equation. The code does not allow time evolution of the parameters.

TORT has the capability to calculate flux in the entire three-dimensional geometrical model. It includes the impact of incident particles on the system that is generated through external source or within the material through interaction in the material. The main application of the TORT is to solve the deep shielding problems for neutrons and photons. It can also solve reactor eigenvalue problems. The TORT code was quite popular for the reactor shielding problem in the late 1990s.

14.4.6 FLUKA [55–57]

The FLUKA code was developed for the high-energy particle interaction-related research by CERN and its associates. Now, it has become a general-purpose simulation tool based on the Monte Carlo computational method for the assessment of particle transport and interaction with matter. It covers proton and electron shielding, target design, calorimetry, dosimetry, activation, detector design, cosmic rays, radiotherapy, neutrino physics, accelerator-driven systems, etc. FLUKA can simulate transport of about 60 different particles. It has the capability to transport electrons and photons from ~1 keV to ~1000 TeV energy and the range of hadron is up to 20 TeV. It can also simulate neutrinos and muons of any energy. It can also transport neutrons down to thermal energy. FLUKA can handle very complex geometrical models using Combinational Geometry (CG) package. The FLUKA CG has been developed to track charged particles in the presence of magnetic and electric fields correctly. It also can perform time evolution and tracking of emitted radiation from unstable residual nuclei online. The FLUKA also has an advanced feature of using the biased mode and fully analog mode for the transport calculations. It also has facility for parallel computing. Moreover, FULKA is a kind code for a current generation that can solve a wide range of problems related to nuclear systems as well as accelerator systems.

14.4.7 GEANT [58–61]

The GEANT is software to simulate particle transport in matter. It is based on the Monte Carlo method and initially developed for detector designs. It is an open-source code and developed by CERN Laboratory and associates. Now, it is widely used in various scientific applications such as high-energy physics, nuclear physics, medical physics, space science, astrophysics, and radiation protection. GEANT tool kit has the capability to transport most of the particles like FLUKA. The GEANT has a various set of physics models for the interactions of particles with materials across a wide range of energy. Since the software is open-source, users can add their models of physics to simulate their area of interest which makes it unique and advance concerning other available codes. It has capability of multithread parallel computing which enhances the code applicability for complex and large geometrical problems. GEANT code latest version has improved capabilities for advanced simulation of high-energy physics detector design, radiation health protection. It has an improved biasing technique for particle scoring and improvisation in statistics of the results.

The GEANT is a comprehensive utility for the simulation of particle transport specifically for space and accelerator as an open source.

14.5 Concluding remarks

The particle transport phenomena govern multiple areas of science and cover various applications related to nuclear reactors, radiation physics, particle detections, health physics, high-energy physics, material science, and many more. The recent advancement of particle transport simulations has a huge contribution in medical science and space science. The simulation of radiation therapy for cancer treatment made a revolutionary contribution to medical science. The space radiation and particle transport physics simulation provides a tremendous support in the design of spacecraft and satellite. It helps in the development of instruments and control devices.

In the early days of nuclear reactors development, radiation transport simulation was done using certain empirical and numerical models through manual estimations. The Monte Carlo method is a kind of computational experiment of simulating realistic particle transport. Various numerical methods are available to solve the Boltzmann radiation transport equation for radiation transport simulation. Deterministic and Monte Carlo approaches have their pros and cons. A recent development suggests that hybrid methods, which utilize both approaches to get a good agreement with experimental observations, are the advanced approach for particle transport simulation. The enhancement in adopting the realistic CAD model makes the coupling of radiation transport calculations with engineering calculations more feasible. It also reduces the error in data migration and optimization time of the system. The availability of nuclear cross-section data in a wide and comprehensive range of energy makes the simulation more precise and viable.

As nuclear shielding materials development is concerned, the simulation can assess the shielding capability and neutron irradiation effects at the development stage. It can support the elemental composition optimization process of innovative material development for the various application of neutron shielding. Applicability of developed materials for various applications such as nuclear reactor shielding, medical sources shielding, spacecraft shielding, etc., can be assessed utilizing the advanced capabilities of simulation software. Based on the conducted review of advanced computational codes, it can be concluded that various computational transport codes are capable of simulating complex systems as well as deep shielding problems.

Shielding solutions for various dedicated and sophisticated systems like radiation therapy, spacecraft, etc., are also possible with great precision and reliability. Particle transport simulation software is also an asset for material developers in the present scenario.

References

[1] A.B. Chilton, et al., Principle of Radiation Shielding, Prentice-Hall, New Jersey, 1984.
[2] S.J. Kenneth, Radiation Shielding, American Nuclear Society, 2000.
[3] R.G. Jaeger, Engineering Compendium on Radiation Shielding, Vol-I: Shielding and Methods, Springer, 1968.
[4] R.G. Jaeger, Engineering Compendium on Radiation Shielding, Vol-Ii: Shielding Materials, Springer, 1975.
[5] T. Rockwell (Ed.), Reactor Shielding Design Manual, Usaec Report Tid-7004, 1956.
[6] J. Wood, Computational Methods in Reactor Shielding, Pergamon Press, 1982.
[7] N.M. Schaeffer (Ed.), 1973. Reactor Shielding for Nuclear Engineers. Usaec Report Tid-25951.
[8] S. Glasstone, Nuclear Reactor Engineering, Delhi Cbs, 1986.
[9] A.R. Foster, Basic Nuclear Engineering, Boston Allynard Bacon, 1977.
[10] K. Almenas, R. Lee, Nuclear Interaction With Matter, Nuclear Engineering, Springer, Berlin, Heidelberg, 1992.
[11] D.A. Brown, et al., ENDF-VIII.0: the 8th Major release of the nuclear reaction data library with CIELO - project cross section, new standards and thermal scattering data, Nucl. Data Sheets 148 (2018) 1–148.
[12] M.B. Chadwick, et al., ENDF/BVII.1 Nuclear data from science and technology: cross sections, covariance, fission product yields and decay data, Nucl. Data Sheets 112 (12) (2011) 2887–2996.
[13] M.C. Han, et al., First assessment of ENDF/B-VIII and EPICS atomic data libraries, IEEE Trans. Nucl. Sci. 65 (8) (2018).
[14] C.L. Dunford, Evaluated nuclear data file, ENDF/B-VI, in: S.M. Qaim (Ed.), Nuclear Data for Science and Technology, Research Reports in Physics, Springer, Berlin, Heidelberg, 1992.
[15] Online Nuclear data Services of IAEA, n.d. Website link: www.nds.iaea.org, www.nds.iaea.org/exfor/endf.htm.
[16] T. Nishimura, et al., Development of discrete ordinates SN code in three-dimensional (X, Y, Z) geometry for shielding design, J. Nucl. Sci. Technol. 17 (1980) 539–558.
[17] P.N. Stevens, Use of the discrete ordinates Sn method in radiation shielding calculations, Nucl. Eng. Des. 13 (3) (1970) 395–408.
[18] C.E. Lee, The Discrete Sn Approximation Theory, Los Alamos Scientific Laboratory Report LA-2595, March 1962.
[19] A. Haghighat, Monte Carlo Methods for Particle Transport, CRC Press, Taylor & Francis Group, 6000 Broken Sound Parkway, NW, Suite 300, Boca Raton, FL, 2014.
[20] E.D. Cashwell, C.J. Everett, A Practical Manual on the Monte Carlo Method for Random Walk Problems, Pergamon Press, Inc, New York, 1959.
[21] J. Spanier, E.M. Gelbard, Monte Carlo Principles and Neutron Transport Problems, Dover, Mineola, NY, 2008.
[22] W.W. Engle Jr., A Users Manual for ANISN, a One Dimensional Discrete Ordinates Transport Code with Anisotropic Scattering, K-25 Report K-1693, Union Carbide Corp., Nuclear Division, March 1967.

[23] W.A. Rhoades, D.B. Simpson, The TORT Three Dimensional Discrete Ordinates Neutron/Photon Transport Code (TORT Version 3), Oak Ridge National Laboratory, ORNL/TM-13221, 1997.

[24] H. Hu, et al., Benchmarking of SNAM with ITER 3D model, Fusion Eng. Des. 82 (2007) 2867–2871.

[25] W. A. Rhoades, R. L. Childs, DOORS-3.2a, One, Two-and Three-Dimensional Discrete Ordinates Neutron/Photon Transport Code System, RSICC Computer Code Collection CCC-650, OAK Ridge National Laboratory, Oak Ridge, TN.

[26] N.A. Frigerio, N.A. Clark, Random number set for Monte Carlo computations, Trans. Am. Nucl. Soc. 22 (1975) 283–284.

[27] J.E. Gentle, Random Number Generation and Monte Carlo Methods, second ed., Springer, New York, 2003.

[28] J. Von Neumann, Various techniques used in connection with random digits. National Bureau of Standards (U.S.), Appl. Math. Ser. 12 (1951) 36–38.

[29] M. Matsumoto, T. Nishimura, Mersenne twister: a 623-dimensionally equidistributed uniform pseudorandom number generator, ACM Trans. Model. Comput. Simul. 8 (1) (1998) 3–30.

[30] J. Kelsey, B. Schneier, N. Ferguson, Yarrow-160: notes on the design and analysis of the yarrow cryptographic pseudorandom number generator, in: Selected Areas in Cryptography, volume 1758 of LNCS, Springer, 1999, pp. 13–33.

[31] G.E.P. Box, M.E. Muller, A note on the generation of random normal deviates, Ann. Math. Stat. 29 (1958) 610–611.

[32] E.D. Cashwell, C.J. Everett, G.D. Turner, A Method of Sampling Certain Probability Densities Without Inversion of Their Distribution Functions, Report LA-5407+4S, Los Alamos Scientific Laboratory, Los Alamos, NM, 1973.

[33] T.E. Booth, Automatic importance estimation in forward Monte Carlo calculations, Trans. Am. Nucl. Soc. 41 (1982) 308–309.

[34] T.E. Booth, A weight window/importance generator for Monte Carlo streaming problems, in: Paper Presented at the Proceedings of the Sixth International Conference on Radiation Shielding, May 16–20, Tokyo, Japan, 1983.

[35] T.E. Booth, A Sample Problem in Variance Reduction in MCNP, Los Alamos National Laboratory, Los Alamos, NM, LA-10363-MS, 1985.

[36] T.E. Booth, Monte Carlo variance comparison for expected-value versus sampled splitting, Nucl. Sci. Eng. 89 (1985) 305.

[37] T.E. Booth, A caution on reliability using "optimal" variance reduction parameters, Trans. Am. Nucl. Soc. 66 (1992) 278.

[38] X-5 Monte Carlo Team, MCNP-A General N Particle Transport Code, Version 5, LA-UR-03-1987, April 2003.

[39] C.J. Werner (Ed.), MCNP Users Manual-Code Version 6.2, LA-UR-17-29981, 2017.

[40] D.A. Torres, et al., Comparison of MCNP5 and experimental results on neutron shielding effects for materials, in: 2004 Annual Meeting of the American Nuclear Society, Pittsburgh, PA, LA-UR-04-0122, 2004.

[41] T. Goorley, Using MCNP for medical physics applications, in: Computational Medical Physics Working Group Workshop II, Gainesville FL, October 1–3, 2007, LA-UR-07-6618, 2007.

[42] J.M. McGhee, T.A. Wareing, D.A. Barnett, ATTILA Version 5: User Manual, Transpire Inc, Gig Harbour, WA, 2006.

[43] R. Pampin, M.J. Loughlin, Evaluation of a three-dimensional discrete ordinates radiation transport tool for the support of ITER design, Fusion Eng. Des. 82 (2007) 2008–2014.

[44] W. Arter, M.J. Loughlin, Radiation transport analyses for IFMIF design by the ATTILA software using Monte-Carlo source model, Fusion Eng. Des. 84 (2009) 89–96.

[45] M.Z. Youssef, et al., Benchmarking the three-dimensional CAD-based discrete ordinates code "ATTILA" using integral dose-rate experiments and comparison to MCNP results, Fusion Sci. Technol. 56 (2) (2009) 718–725.

[46] E. Brun, F. Damian, et al., TRIPOLI-4, CEA, EDF and AREVA reference Monte Carlo code, Ann. Nucl. Energy 82 (2015) 151–160.

[47] J.P. Both, J.C. Nimal, T. Vergnaud, Automated importance generation and biasing techniques for Monte Carlo shielding techniques by the TRIPOLI-3 code, Prog. Nucl. Energy 24 (1990) 273–281.

[48] J.P. Both, Y. Pénéliau, Parallelization of the Monte Carlo code TRIPOLI-4, in: Proceedings of the M&C99 Conference, Madrid, Spain, 1999.

[49] S. Bourganel, O. Petit, C.M. Diop, Three-dimensional particle transport using Green's functions in TRIPOLI-4 Monte Carlo code: application to PWR neutron fluence and ex-core response studies, Nucl. Technol. 184 (2013) 29–41.

[50] Y. Wu, et al., CAD-based Monte Carlo program for integrated simulation of nuclear system SuperMC, Ann. Nucl. Energy 82 (2015) 161–168.

[51] J. Song, et al., Benchmarking of CAD-based SuperMC with ITER benchmark model, Fusion Eng. Des. 89 (2014) 2499–2503.

[52] C. Chen, et al., Validation of shielding analysis capability of SuperMC with SINBAD, EPJ Web Conf. 153 (2017) 02009.

[53] Y.Y. Azmy, The three-dimensional, discrete ordinates neutral particle transport code TORT: an overview, in: Presented at the OECD/NEA Meeting on 3D Deterministic Radiation Transport Computer Programs, Feature, Applications and Perspectives, Paris, France, December 2–3, 1996.

[54] W.A. Rhoades, Y.Y. Azmy, Three-dimensional SN calculations with the Oak Ridge TORT Code, in: Proc. Int. Conf. on Mathematics and Computations, Reactor Physics, and Environmental Analyses, Portland, Oregon, April 30–May 4, 1995, Vol. 1, American Nuclear Society, LaGrange Park, IL, 1995, p. 480.

[55] G. Battistoni, et al., Overview of FLUKA, Ann. Nucl. Energy 82 (2015) 10–18.

[56] G. Battistoni, S. Muraro, P. Sala, F. Cerutti, A. Ferrari, S. Roesler, A. Fassò, J. Ranft, The fluka code: description and benchmarking, in: M. Albrow, R. Raja (Eds.), Hadronic Shower Simulation Workshop 2006. Vol. 896 of AIP Conference Proceedings, Fermilab, 2006, , pp. 31–49.

[57] V. Andersen, et al., The FLUKA code for space applications: recent developments, Adv. Space Res. 34 (2004) 1302.

[58] J. Allison, et al., GEANT4 developments and applications, IEEE Trans. Nucl. Sci. 53 (2006) 270–278.

[59] J. Allison, et al., Recent developments in GEANT4, Nucl. Inst. Methods Phys. Res. A 835 (2016) 186–225.

[60] X. Dong, G. Cooperman, J. Apostolakis, Multithreaded Geant4: semi-automatic transformation in to scalable thread-parallel software, in: Euro-Par 2010 – Parallel Processing, Lect. Notes Comput. Sci 6272 (2010) 287–303.

[61] Geant4Collaboration, n.d. Toolkit Developers Guide, Available online at http://cern.ch/geant4 (Chapter 2).

CHAPTER 15

Effect of spent nuclear fuel neutron aging on dry cask shielding material

Yuan Gao, Andreas Enqvist, James Baciak
University of Florida, Nuclear Engineering Program, Gainesville, FL, United States

15.1 Introduction

Nuclear power uses the energy released by splitting the atoms of certain elements. It was developed in 1940s initially for nuclear weapons, and then turned to the peaceful use of nuclear energy. Around 11% of the world's electricity is generated by about 450 commercial nuclear power plants. Around 60 nuclear reactors are under construction. Spent nuclear fuel is a serious issue for nuclear industry, despite other nuclear energy advantages. The concentration of plutonium in the fuel increases with reactor fuel burnup to the point that it no longer can be used as a nuclear fuel. So, the nuclear fuel has to be removed from the reactor after 18–36 months depending on the reactor design. There are two alternatives for spent nuclear fuel: reprocessing to recycle, and long-term storage and final disposal. No reliable reprocessing method has been finalized in the past decades in the United States. Either long-term storage or semi-long-term storage becomes a practical solution for spent nuclear fuel. There are several safe long-term storage methods worldwide, such as reactor pool storage, off-site consolidated pool storage, and dry cask storage. All the long-term storage methods demonstrate the safety of spent fuel storage for long periods of time, according to the operating history of nuclear reactors worldwide. Pool storage provides important thermal, shielding, containment, and critically control of the spent fuel when it is thermally hot and highly radioactive. However, the defined capacity when the pool was built makes the pool storage limited [1]. Dry storage meets similar safety functions as pool storage and tend to have lower capital cost than pool expansion. This chapter describes the effect of spent nuclear fuel neutron source aging on dry cask shielding material.

Micro and Nanostructured Composite Materials for Neutron Shielding Applications
https://doi.org/10.1016/B978-0-12-819459-1.00015-5
© 2020 Elsevier Ltd.
All rights reserved.

15.2 Spent nuclear fuel

The production of electricity from nuclear power plant has created radioactive residues which have to be carefully stored and managed since the material is hazardous to human health [2]. The radioactive residues include solid and liquid nuclear waste from nuclear power production. The spent nuclear fuel (SNF) is declared a nuclear waste and is currently being stored in pool storage and dry storage, pending disposal in deep underground facilities, or being reprocessed into usable fuel. Fig. 15.1 demonstrates the general fuel production flow chart for light water reactors (LWR), while Fig. 15.2 shows the calculation results of material balance for the annual production of 1 GWe. Radioactive waste can be created during the entire nuclear fuel cycle, including mining and milling of uranium, as well as the nuclear power generation process. The nuclear power generation process causes the production of several kinds of radioactive wastes, including spent nuclear fuel (SNF), which contain the largest activity of the radioactive substances generated by the nuclear energy industry. According to theoretical calculation, from 1 year of operation of 1 GWe LWR, spent nuclear fuel assemblies

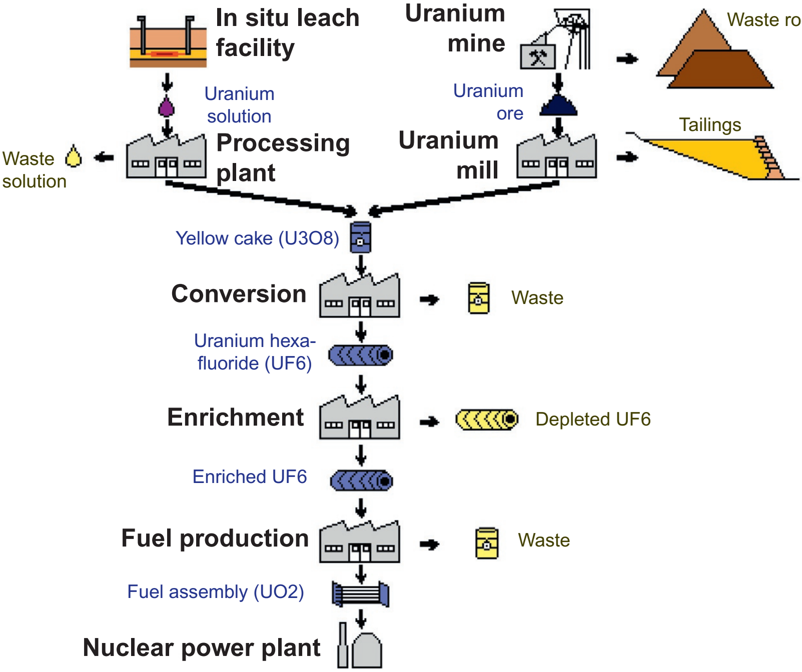
In situ leach facility
Uranium mine
Waste rock
Uranium solution
Uranium ore
Tailings
Waste solution
Processing plant
Uranium mill
Yellow cake (U3O8)
Conversion
Waste
Uranium hexa-fluoride (UF6)
Enrichment
Depleted UF6
Enriched UF6
Fuel production
Waste
Fuel assembly (UO2)
Nuclear power plant

Fig. 15.1 Nuclear fuel production chain for light water reactors [3].

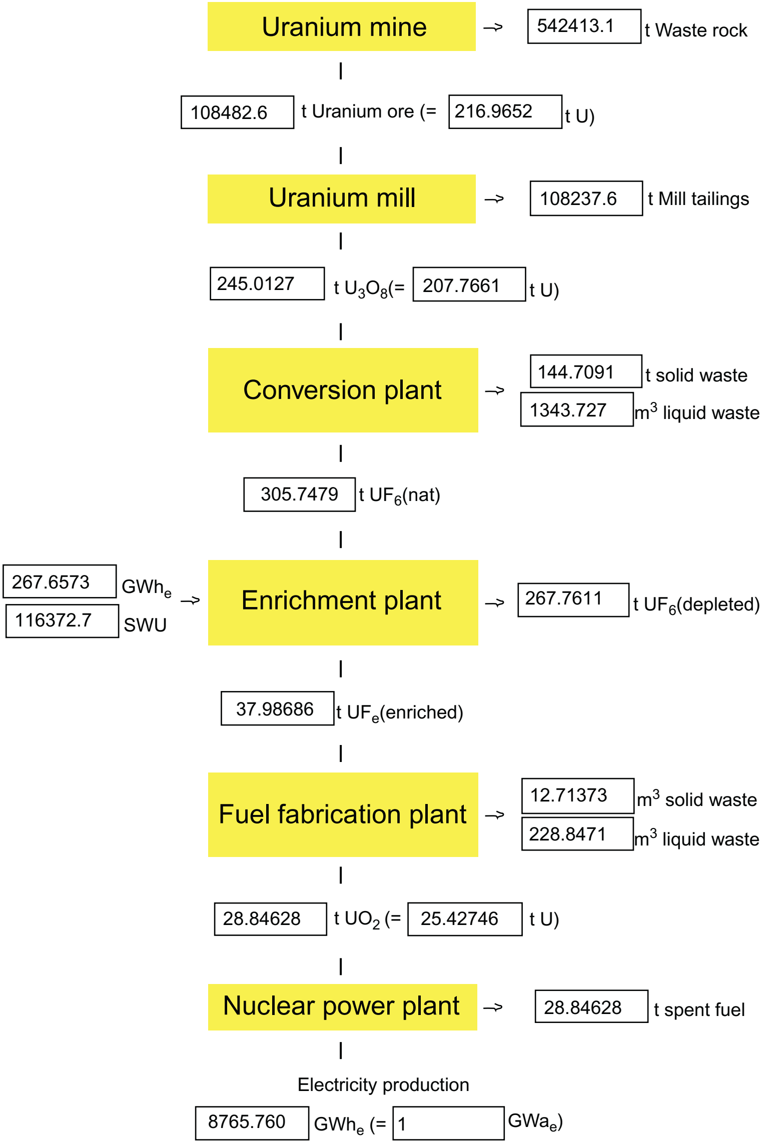
Uranium mine
542413.1 t Waste rock
108482.6 t Uranium ore (= 216.9652 t U)
Uranium mill
108237.6 t Mill tailings
245.0127 t U_3O_8(= 207.7661 t U)
Conversion plant
144.7091 t solid waste
1343.727 m^3 liquid waste
305.7479 t UF_6(nat)
267.6573 GWh_e
116372.7 SWU
Enrichment plant
267.7611 t UF_6(depleted)
37.98686 t UF_e(enriched)
Fuel fabrication plant
12.71373 m^3 solid waste
228.8471 m^3 liquid waste
28.84628 t UO_2 (= 25.42746 t U)
Nuclear power plant
28.84628 t spent fuel
Electricity production
8765.760 GWh_e (= 1 GWa_e)

Fig. 15.2 Nuclear fuel chain material balance for electricity production of 1 GWa(e) [3].

containing around 30–50 metrics tons of heavy metal (MTHM) are generated, while the initial activity is around 5.0–8.3 E6 TBq [2]. According to the SNF data collected from the National Reports submitted to the Second Review meeting of the Joint Convention on the safety of Spent Fuel

Management and on the Safety of Radioactive Waste Management [3], the total amount of SNF was approximately 180,000 MTHM by 2005. By 2014, the worldwide total amount of SNF increased to 371,000 MTHM [4]. And this amount grows by over 12,000 MTHM per year [5]. According to the IAEA report, until 2003 only 0.7% of SNF in volume capacity had been reprocessed [6]. The majority of SNF has been put into long-term storage pending disposal deep underground.

15.3 Dry storage

Long-term storage of SNF can be classified as pool storage or dry storage. As mentioned in the introduction, there are several limitations of pool storage compared with dry storage. The dry storage can now be expected to store more SNF until a permanent solution is finalized. Dry storage includes dry storage vaults and dry storage casks. In dry storage vaults, spent fuel is placed in thin-walled stainless steel canisters, which are dried and filled with helium gas, and then welded shut [1]. Then these canisters are inserted into a vault that was cooled passively by air or other gases. Dry storage casks for spent nuclear fuels were first employed at the Surry Nuclear Plant as a temporary solution for high level nuclear waste storage until a permanent solution is finalized [7]. By 2013, approximately 2300 dry casks were loaded in the United States, the United States continues to operate nearly 100 nuclear reactors. As a result, more spent nuclear fuel will be produced, and it is estimated that 4500 dry casks will be loaded by 2025 [8]. Research concerning the use of deep geological repositories started several decades ago, but to date, there is no operational deep geological repository for spent nuclear fuel worldwide. Considering the difficulty of such a project in many aspects, there is a possibility that a deep geological repository for spent nuclear fuel can be neither constructed nor operated within the next few decades. Thus, prolonged services lives of dry storage casks have become a realistic option for spent nuclear fuel. Thus, research on the impacts of aging neutron source on dry storage cask turns to be meaningful and necessary.

The TN-32 cask is a typical metal non-canistered dry storage cask, which was developed by Transnuclear. The TN-32 cask was designed to accommodate 32 intact pressurized water reactor assemblies, with or without burnable poison rod assemblies and thimble plug assemblies (as shown in Fig. 15.6). The overall length of the cask is 513.75 cm including its protective cover. And it has an outside diameter of 248.3 cm, the fully loaded weight is around 115.5 tons. The top part of the cask is a protective cover.

Below the protective cover are 10.2 cm of polypropylene encased in a 0.64-cm thick steel shell, and 26.7-cm thick steel in the lid, which compromises the top neutron and photon shielding materials. The diameter and length of the main containment vessel are 174.6 and 414.7 cm, respectively. Radial gamma-ray shielding is provided by 3.8-cm-thick inner steel shell, 20.3-cm-thick steel body wall, and 1.3-cm-thick outer steel shell. The neutron shielding material is what we discuss in this chapter. The neutron shielding is provided by an 11.4-cm-borated polyester resin compound. The bottom part is a 22.5-cm-thick steel bottom plate to shield gamma ray. There is no neutron shielding material on the bottom part, since the dry cask was designed to be placed vertically on the ground. The radiation shielding safety of TN-32 dry cask was checked with numerical simulation method. The maximum total dose rate over the cask surfaces is <10 mrem/h (9.258 ± 0.212 mrem/h) after 40 years, and this outcome fulfills all dose rate requirements from 10 CFR 71.47(b). After 300 years of storage, the average total dose rates on the side surface and top surface would be 0.150 ± 0.007 mrem/h and 0.057 ± 0.003 mrem/h, respectively, while the maxima would be 0.601 ± 0.014 mrem/h and 0.112 ± 0.006 mrem/h, respectively [9] (Figs. 15.3–15.8).

15.4 Spent nuclear fuel neutron

Spent nuclear fuel (SNF) is characterized by a very high neutron and gamma-ray emission due to spontaneous fission, and radioactive decay of fission products and actinides. There are two major neutron sources in SNF: neutrons generated from spontaneous and subcritical fission, and neutrons emitted from the (α, n) reaction of fissile material [7]. In nuclear

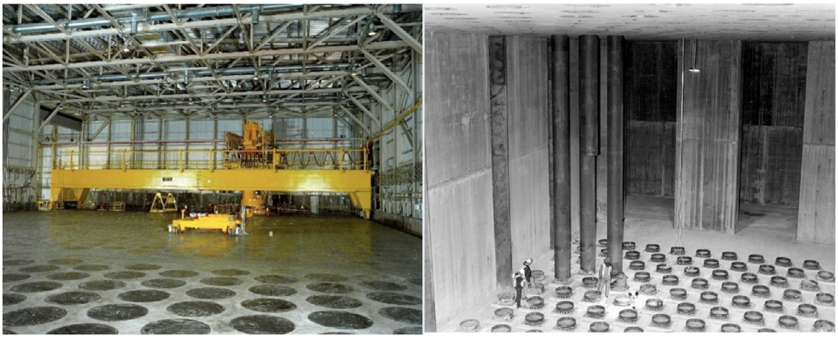

Fig. 15.3 Canister vault storage construction at Washington State Hanford Site.

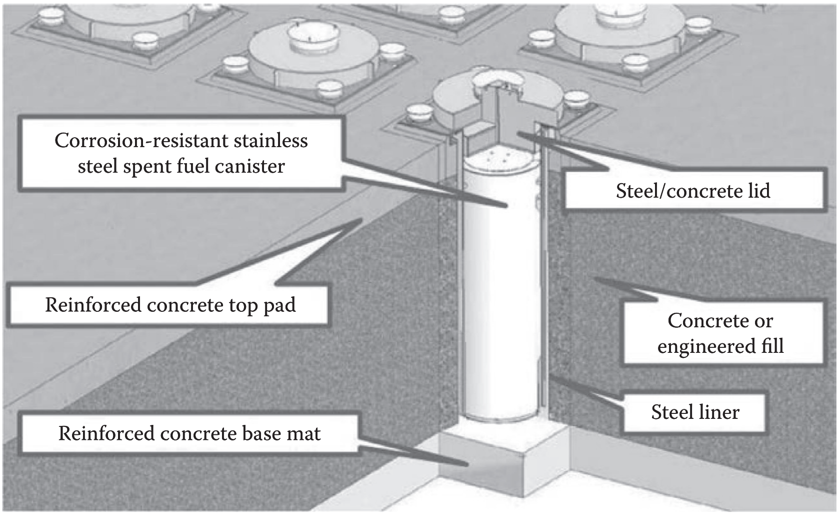
Corrosion-resistant stainless steel spent fuel canister
Steel/concrete lid
Reinforced concrete top pad
Concrete or engineered fill
Steel liner
Reinforced concrete base mat

Fig. 15.4 Schematic of vault storage construction [10].

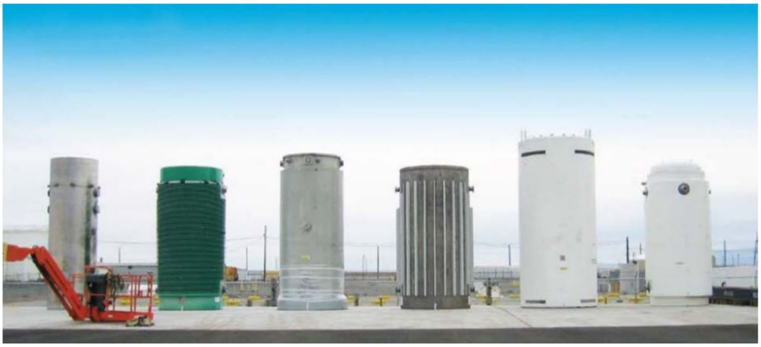

Fig. 15.5 NAC-128, CASTOR V/21, REA 2023, MC-10, VSC-17, and TN-24P dry storage casks.

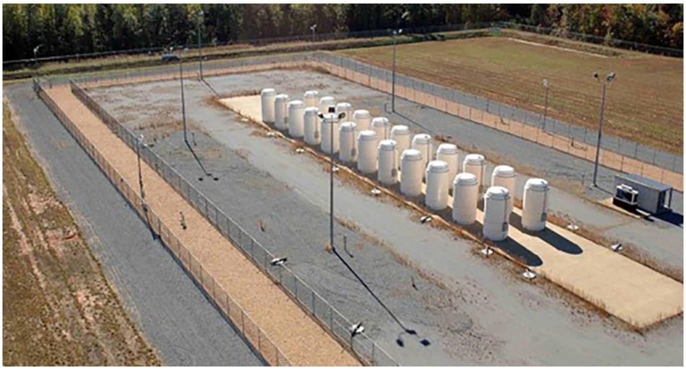

Fig. 15.6 Birdview of transnuclear TN-32 dry storage cask.

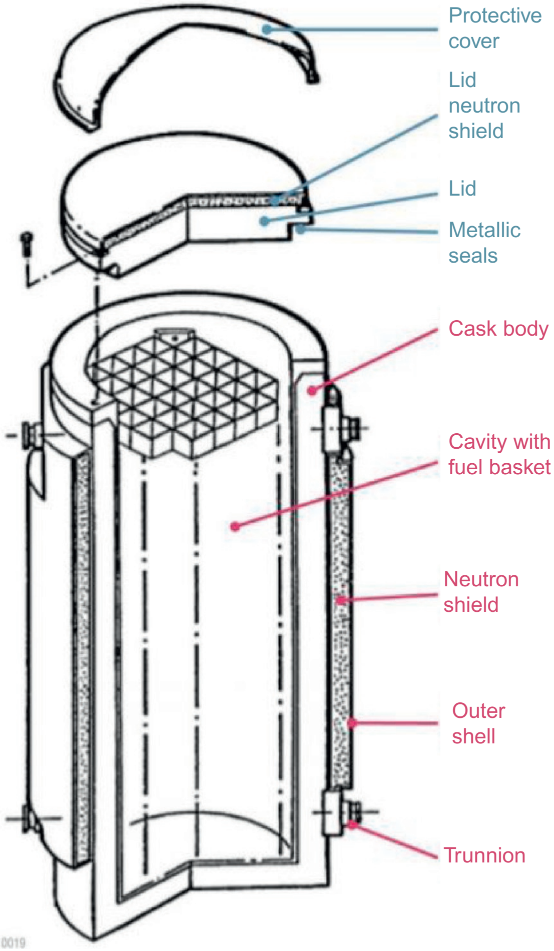
Protective cover
Lid neutron shield
Lid
Metallic seals
Cask body
Cavity with fuel basket
Neutron shield
Outer shell
Trunnion
0019

Fig. 15.7 Exploded/cutaway diagram of a TN-32 cask [2].

physics, nuclear fission is the process in which a heavy atomic nucleus (e.g., uranium, plutonium) breaks into two lighter nuclei, accompanied by the release of a large amount of energy. Spontaneous fission is a form of radioactive decay process and is only found in heavy nuclei. Spontaneous fission is feasible only for mass numbers greater than 232 (^{232}Th). In SNF, about 1% mass material are heavy transuranic elements (e.g., plutonium, californium), which are mainly generated from neutron capture in uranium ore with subsequent beta decays (e.g., $^{238}\mathrm{U} + \mathrm{n} \rightarrow {}^{239}\mathrm{U} \rightarrow {}^{239}\mathrm{Np} \rightarrow {}^{239}\mathrm{Pu}$). For transuranic elements, the spontaneous fission transition rate increases with the

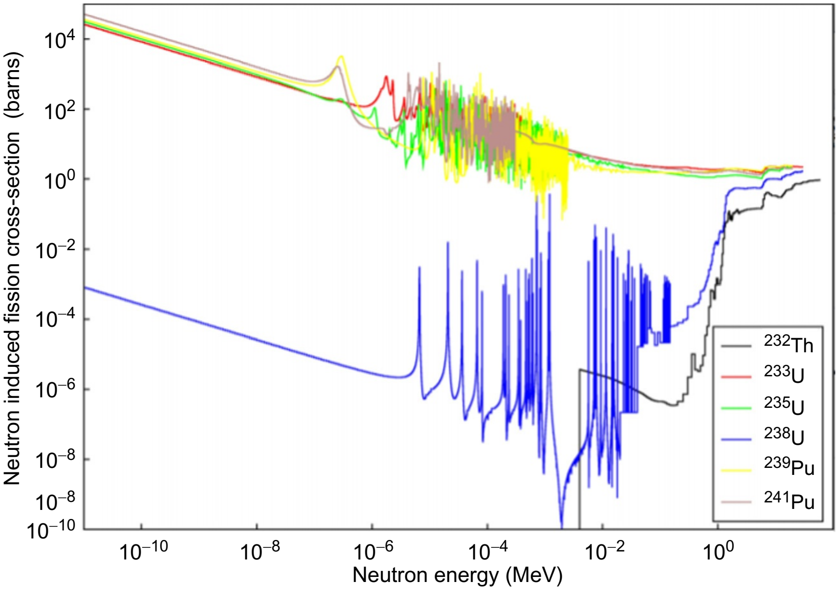

Fig. 15.8 Neutron induced fission cross section for major actinides [11].

mass number and may become the dominant decay mode when mass number is greater than 260. The (α , n) reaction occurs when an α particle is emitted by an actinide isotope, and then captured by the nucleus of a light element (e.g., $^{4}_{2}\alpha + ^{9}_{4}\mathrm{Be} \rightarrow ^{12}_{6}\mathrm{C} + ^{1}_{0}\mathrm{n}$). The main neutron emitters in SNF are ^{242}Cm, ^{244}Cm, ^{246}Cm, ^{248}Cm, ^{235}U, ^{238}U, ^{238}Pu, ^{239}Pu, ^{240}Pu, ^{241}Pu, ^{242}Pu, and ^{241}Am. Among all these neutron emitters, ^{242}Cm and ^{244}Cm with half-life of 162.8 days and 18.10 years, respectively, contribute a significant portion of the spontaneous fission neutrons [12]. Subcritical fission means the induced fission happens in SNF under subcritical condition. ^{238}U is the primary actinide present in the fuel at >95% by mass with an extremely low neutron-induced fission cross section for thermal and epithermal neutron. However, ^{238}U has a significant fission cross section for fast neutrons (above 1 MeV). The spontaneous fission and (α , n) neutrons can induce ^{238}U and other actinide fission. The neutron emission rate and energy spectra in SNF depend on the fuel initial enrichment (IE), burnup (BU), and cooling time (CT). In nuclear industry, the SNF neutron emission and energy spectra are calculated with computation code ORIGEN-ARP [13], which is a part of the SCALE package [14] and is developed by Oak Ridge National Laboratory, and discussed in detail in the following section.

15.5 ORIGEN-ARP

ORIGEN (Oak Ridge Isotope Generation code) calculates time-dependent concentrations, activities, and radiation source terms for many isotopes simultaneously generated or depleted by neutron transmission, fission, and radioactive decay. The main methodologies of ORIGEN used in calculation are as follows [14]:

- generation of problem-dependent transition matrices
- solution of the system of depletion equation
- conversion from power to flux
- calculation of emission spectra
- interpolation of progenerated sets of transition matrices

ORIGEN-ARP is one of the computation modules of ORIGEN, ARP is short for automated rapid processing, which uses interpolation of existing ORIGEN reactor libraries. ORIGEN-ARP employs a graphical user interface (GUI) to select several characteristics of the SNF, which is more user friendly than ORIGEN. As we have mentioned earlier, the most important characteristics of SNF are fuel initial enrichment (IE), burnup (BU), and cooling time (CT). The sensitivity test of various IE and BU on a standard 17 × 17 PWR (pressurized water reactor) spent fuel assembly are shown in Figs. 15.9 and 15.10. The variation in CT is the major discussion of this chapter, and the results are provided in following sections.

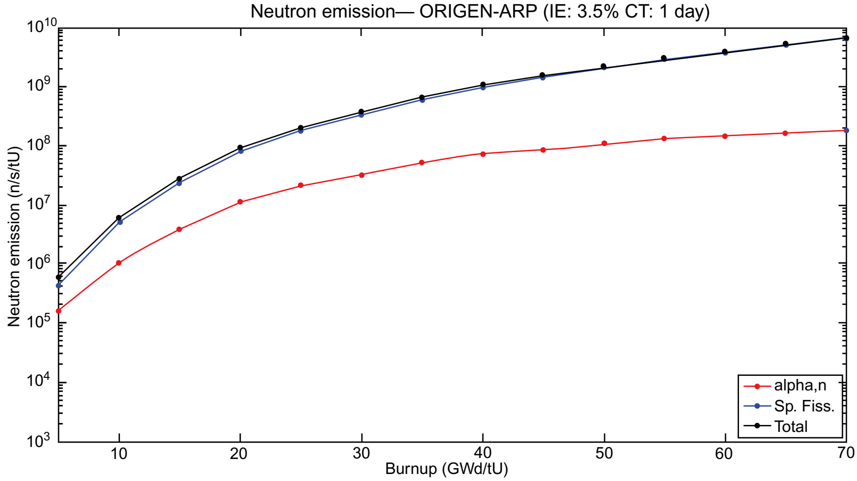

Fig. 15.9 Neutron emission as a function of the burnup for a 17 × 17 PWR spent fuel assembly with initial enrichment of 3.5% and cooling time of 1 day. The contribution due to (α , n) and spontaneous fission reactions as well as the total neutron emission are also shown [15].

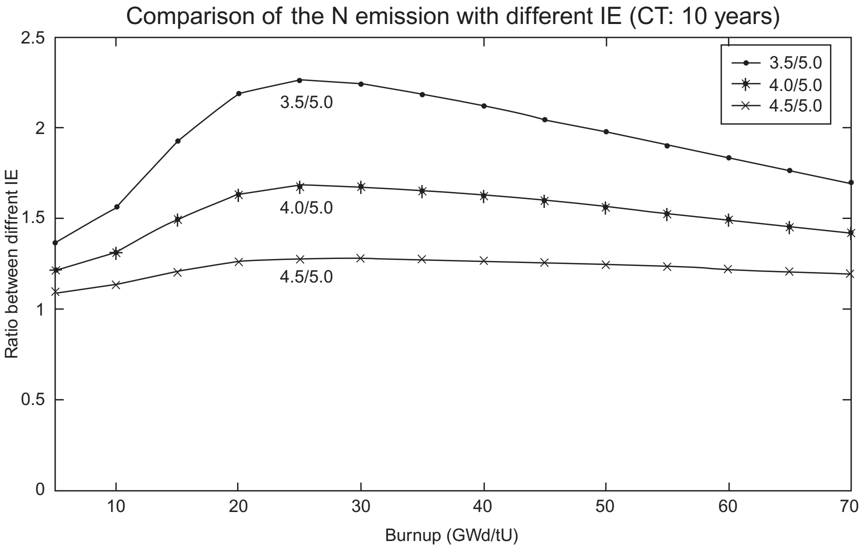

Fig. 15.10 Ratio of total neutron emission for different enrichments as a function of the burnup for a 17 × 17 PWR spent fuel assembly with cooling time of 10 years. The IE (initial enrichment) used for the ratio are indicated close to the corresponding curve [15].

15.6 Spent nuclear fuel neutron aging

This section discusses the SNF neutron aging during long-term storage. Fig. 15.11 shows the variation in neutron energy spectra at selected storage time, and Fig. 15.12 shows the variation in SNF neutron intensity per fuel assembly. The results were calculated with ORIGEN-ARP, as discussed in the previous section. In this analysis, 47 neutron energy groups were utilized. The SNF has an initial enrichment of 3.6% and the fuel operating history is normally three cycle, which is the most common fuel cycle in nuclear power plant, with a total burnup of 35,040 MWd/MTU. The boron concentration change and structure change are not considered in this simulation. The decay time after three fuel cycles was set from 10 to 300 years with 10-year steps. As shown in Figs. 15.11 and 15.12, the fast decrease time is 100 years. After 100 years, the decrease in the neutron is insignificant. Overall, the neutron emission from SNF decreases approximately two orders of magnitude after 300 years' storage time.

Nuclide masses from individual rods within spent fuel assemblies of varying initial enrichments, cooling times, and burnups were obtained from The Next-Generation Safeguards Initiative (NGSI) Spent Fuel Library. Weldon

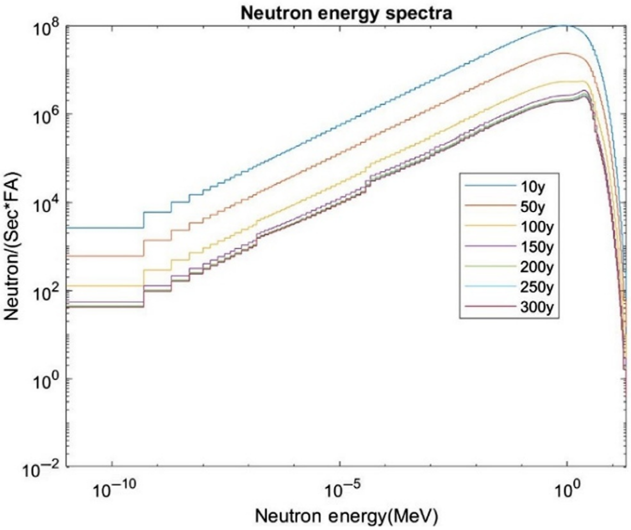

Fig. 15.11 Neutron energy spectra variation at selected storage time.

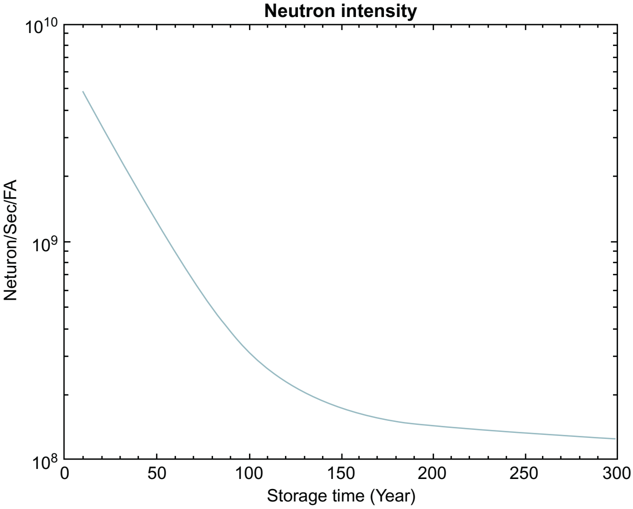

Fig. 15.12 Variation in the SNF neutron intensity per fuel assembly versus storage time.

Jr. et al. presented details of both a methodology for generating spatially dependent gross neutron emission (GNE) and a characterization of GNE for a particular NGSI spent fuel library [16]. Fig. 15.13 shows the SNF neutron source term fractions separated into spontaneous fission neutron flux and (α , n) reaction neutrons. All kinds of neutron flux decrease as storage

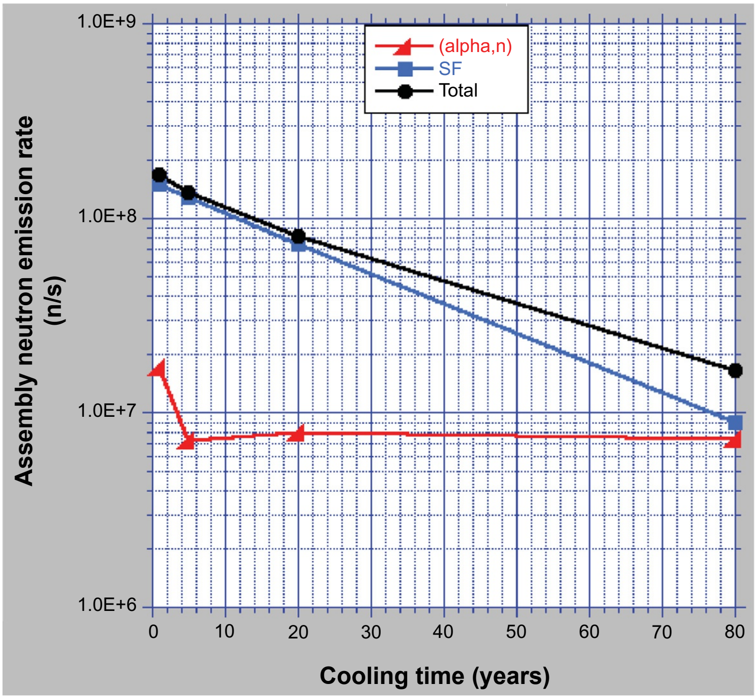

Fig. 15.13 Change in neutron source strength as a function of cooling time [17].

time increases, while the (α , n) reaction decreases much slower than total and spontaneous neutron flux. The spontaneous fission and (α , n) neutron emission isotopic component analysis are shown in Figs. 15.14 and 15.15. The analysis shows that the spontaneous fission emission is mostly dominated by ^{244}Cm and ^{242}Cm at early storage time. Then at later storage times, ^{242}Cm decays away due to its short half-life (163 days), and ^{240}Pu and ^{244}Cm makeup a large percentage of emission. Finally, at 80 years cooling time, most of the ^{244}Cm would decay and ^{240}Pu would be the dominant. The (α , n) reaction neutron emission contribution was considerably more diverse than the spontaneous fission emission contribution. The major contributors were ^{242}Cm, ^{244}Cm, ^{238}Pu, ^{240}Pu, ^{239}Pu, and ^{241}Am. The general trend is that at earlier storage times, the neutron emission was dominated by ^{242}Cm, ^{244}Cm, and ^{238}Pu; however, as storage time increases, the importance of ^{241}Am dramatically increases [16]. The ORIGEN-ARP can separate spontaneous fission neutrons from (α , n) reaction neutrons. Based on the characteristics of their spectra, the fission neutrons and (α , n) reaction neutrons can be estimated from a total neutron spectrum. The spontaneous fission neutrons peak between 0.8 and 1 MeV and have a long tail extending

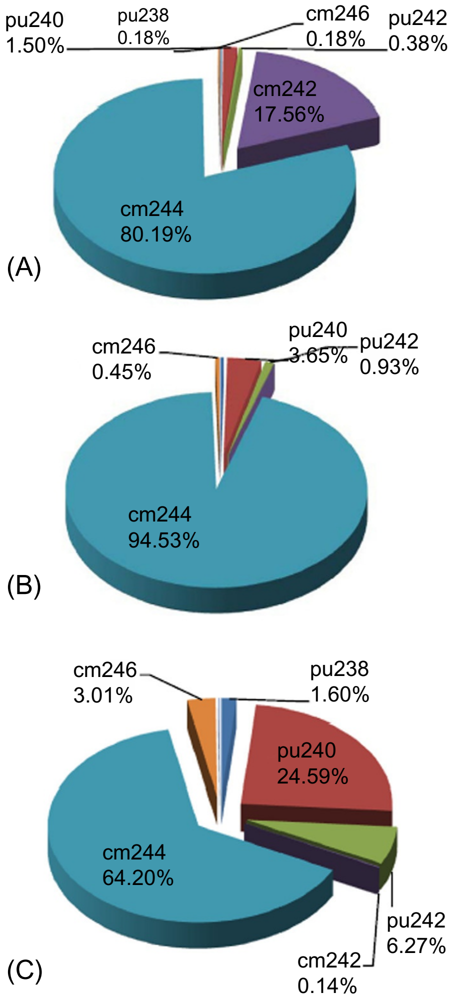

Fig. 15.14 Spontaneous fission neutron emission isotopic component percentage at 30,000 MWd/MTU: (A) 1 year, (B) 20 years, and (C) 80 years [16].

to 12–15 MeV. The spectrum for (α , n) reaction neutrons has a softer curve with a maximum between 2.5 and 3.0 MeV, and spectra tails ends at approximately 5 MeV [18]. Fig. 15.15 shows the characteristic ranges on a graph of the total neutron spectrum for a spent fuel rod with 4% initial enrichment, 15,000 Mwd/MTU burnup, and a 40-year cooling time [18]. As shown in Fig. 15.13, the spontaneous fission neutron emission decays much faster than (α , n) reaction, which means that low-energy neutrons (below 1 MeV) decays faster than high-energy neutrons (Fig. 15.16).

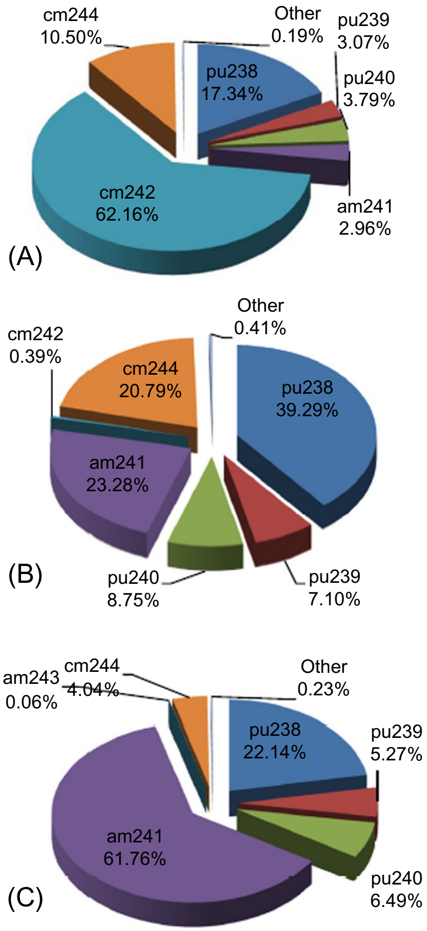

Fig. 15.15 Isotopic component percentage of the (α, n) neutron emission signal at 30,000 Mwd/MTU and (a) 1 year, (b) 5 years, (c) 40 years cooling.

15.7 Neutron interactions with shielding material in dry cask

Like gamma radiation, neutrons undergo scattering and absorption interactions with matter. These interactions are the fundamental to shield neutron radiation. However, unlike gamma radiation, which interacts primarily with the electrons in matter, neutrons interact primarily with the nucleus. The shielding materials for neutrons are quite different; high atomic number absorbers are more effective in gamma-ray radiation shielding. In general,

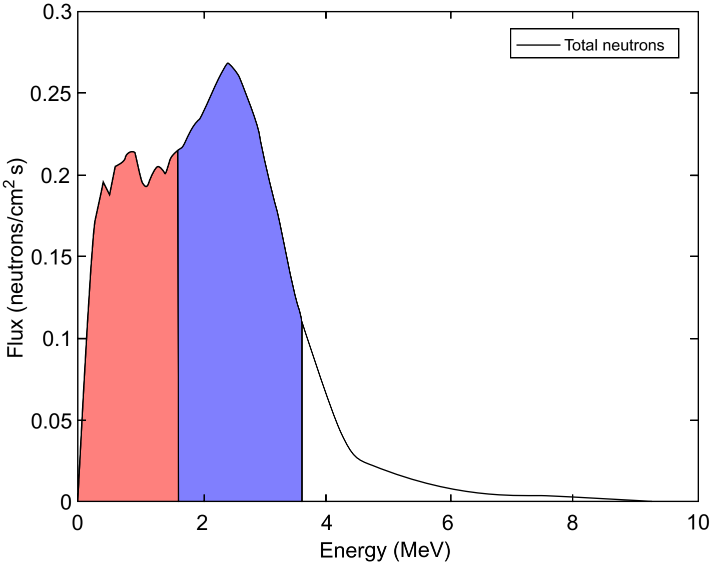

Fig. 15.16 Characteristic energy ranges for spontaneous fission and (α , n) neutrons. The range on the left from 0 to 1.6 MeV is for spontaneous fission neutrons and the range on the right from 1.6 to 3.6 MeV is for (α , n) neutrons [18].

for high-energy neutrons, scattering interactions are more likely than capture interactions. As the neutron energy is reduced through scattering interactions (neutron down scatter/moderation), the probability of both interactions increases and make the neutron capture interactions more significant. Neutron scattering interactions can be categorized into elastic and inelastic scattering. In elastic scattering means kinetic energy of neutron and scatter target system is conserved; in inelastic scattering the kinetic energy of neutron and scatter target system is lowered through excitation of the scatter target nucleus and gamma-ray emission. This gamma-ray radiation is also referred to as secondary gamma rays, which is a major radiation source for SNF in dry cask especially in long-term storage. A detailed discussion about neutron cross sections, mean free path, stopping power, and other neutron shielding knowledge is skipped, since these are included in other chapters.

Neutron shielding materials are typically constructed from low atomic number elements (hydrogen, carbon, and boron) with high scattering cross sections that can effectively moderate thermal neutron (low energy). Borated polyethylene, aluminum, boron-aluminum alloys, and boric acid

Table 15.1 TN-32 cask shield materials [19].

Component	Material	Density (g/cm^3)	Thickness (cm)
Cask body wall	Carbon steel	7.82	24.13
Lid	Carbon steel	7.82	26.67
Bottom	Carbon steel	7.82	26.04
Resin	Polyester resin styrene aluminum hydrate zinc borate	1.58	10.82
Aluminum box	Aluminum	2.7	0.31
Outer shell	Carbon steel	7.82	1.27
Basket	Stainless steel	7.92	0.53
	Aluminum	2.7	1.27
	Borated aluminum	2.65	0.1
Protective cover	Carbon steel	7.82	0.97
Polypropylene drum	Polypropylene	0.9	10.16
Polypropylene drum shell	Carbon steel	7.82	0.64

in water are examples of materials incorporating boron. As presented in Table 15.1, polyester resin is the neutron shielding material in TN-32 dry cask. Neutron shielding may also incorporate high atomic weight elements to shield secondary gamma-ray radiation. Lead, bismuth, and tungsten are often used as secondary gamma-ray shielding material due to their high density, and good gamma-ray attenuation characteristics [20]. For dry cask storage, concrete is always used as a gamma-ray shielding material. TN-32 cask is a metal sealed, non-canistered dry cask in which thick carbon steel layer is designed as gamma-ray shielding material. A TN-32 dry cask model is reproduced in MCNP to study neutron transmission [21], as shown in Figs. 15.17 and 15.18. An initial flux estimation using a superimposed mesh tally (fmesh) was used to examine how well neutrons transmitted through the cask. The source term was modeled as a monoenergetic 14.1 MeV neutron, corresponding to a deuterium and tritium reaction, conical source placed at the axial mid-plane of the cask. With no energy threshold the average event scatters 122 ± 80, but with a threshold of 11 MeV the average event scatters 8 ± 4 times. These result shows that most high-energy neutrons were slowed down and reduced to thermal neutron region, also proving the TN-32 neutron shielding design (Fig. 15.19).

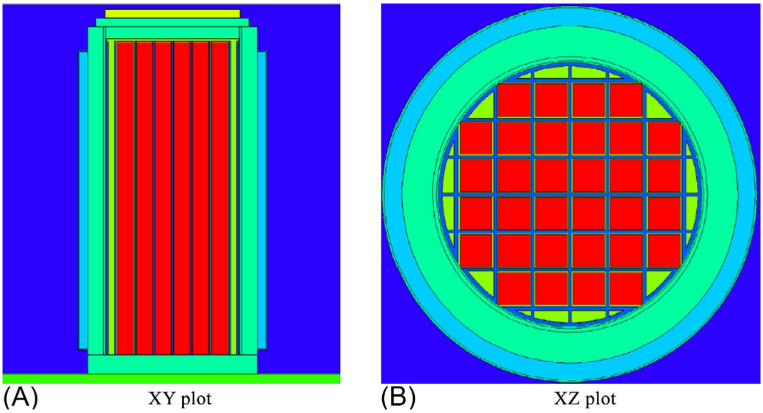

Fig. 15.17 The visualization of a TN-32 cask MCNP model using VISED with assemblies homogenized for ease of viewing [21].

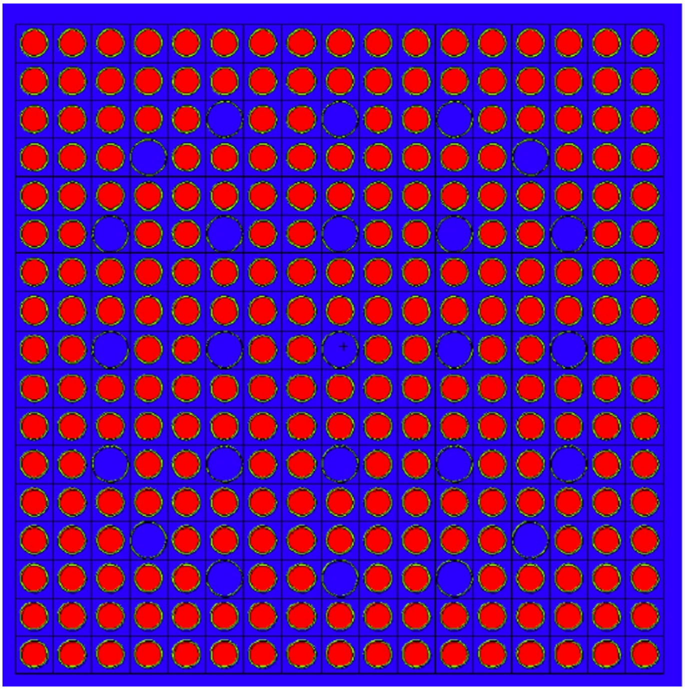

Fig. 15.18 A cross-sectional view of the modeled 17 × 17 Westinghouse PWR fuel assembly. Note that what may appear to be 15 empty spaces are instrumentation and guide tubes with very thin cladding [21].

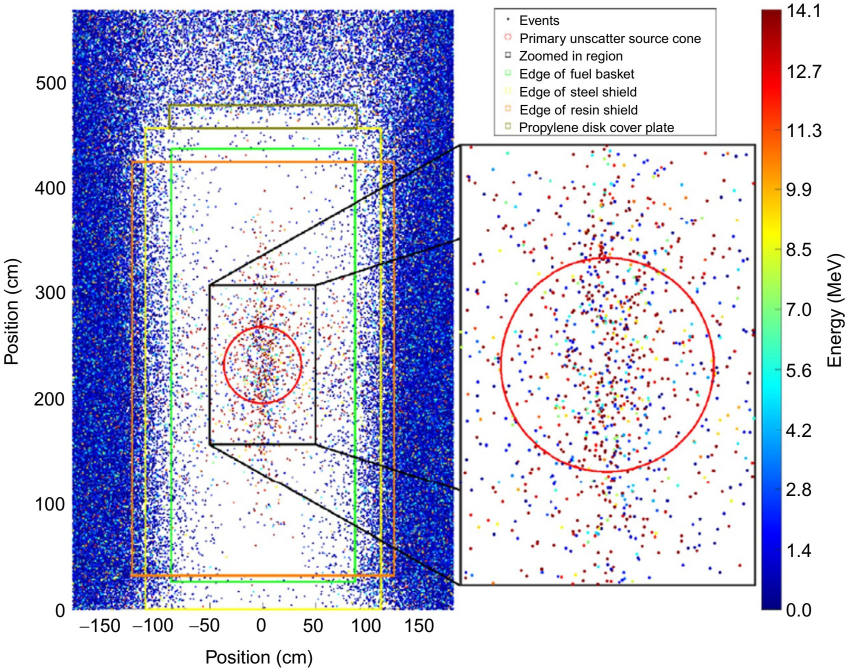

Fig. 15.19 The plotted events with fewer than 10 scatters colored by energy [21].

15.8 Discussion

This chapter provides general information about SNF neutron source, neutron source aging, and neutron shielding material in dry cask. The influence of neutron aging on dry cask shielding material is not discussed into detail, because not much research has been done on this topic. The dry cask storage has been employed for around 40 years; the oldest loaded dry casks are still in good condition. The dry cask storage has turned into a semipermanent solution, and the service life is much longer than several decades, thus further studies are needed to comprehend the effect of neutron-induced aging on neutron shielding material. According to the research results, we have now, if we do not consider any structural or material failure, dry casks which could fulfill the neutron shielding requirement. But the neutron in SNF could interact with the shielding over the course of half a century or a century, so none can conclude that the dry cask is safe without further research.

References

[1] K.B. Sorenson, Long-term storage of spent nuclear fuel and high-level radioactive waste: strategies and implications for package design, in: K.B. Sorenson (Ed.), Safe and Secure

Transport and Storage of Radioactive Materials, Woodhead Publishing, Sandia National Laboratories, Albuquerque, NM, ISBN: 9781782423096, 2015, pp. 311–324.

[2] International Atomic Energy Agency, Estimation of Global Inventories of Radioactive Waste and Other Radioactive Materials, IAEA-TECDOC-1591, IAEA, Vienna, 2010.

[3] International Atomic Energy Agency, Joint Convention on the Safety of Spent Fuel Management and on the Safety of Radioactive Waste Management, International Law Series No. 1, IAEA, Vienna, 2006.

[4] IAEA, Spent Fuel Performance Assessment and Research, IAEA-TECDOC-1771, IAEA, Vienna, 2015.http://www-pub.iaea.org/MTCD/Publications/PDF/TE-1771_web.pdf.

[5] Radioactive Waste Management, World Nuclear Association, http://www.world-nuclear.org/information-library/nuclear-fuel-cycle/nuclear-wastes/radioactive-waste-management.aspx. (updated October 2016).

[6] G.W. Csullog, I. Pozdniakov, The IAEA net enabled waste management database—development and implementation of version II, in: DISTEC 2004, an International Conference on Radioactive Waste Disposal, April 26–28, 2004, Berlin, Germany, 2004.

[7] Y. Gao, C.R. Hughes, C.R. Greulich, J.E. Tulenko, A. Enqvist, J.E. Baciak, Radiation dose rate distributions of spent fuel dry casks estimated with MAVRIC based on detailed geometry and continuous-energy models, Ann. Nucl. Energy 117 (2018) (2018) 84–97. ISSN 0306-4549, https://doi.org/10.1016/j.anucene.2018.03.015.

[8] U.S. Department of Energy, Fuel Cycle Research & Development, Nuclear Fuels Storage & Transportation (FCRD-NFST), Commercial Spent Nuclear Fuel and High-Level Radioactive Waste Inventory Report, 2013. FCRD-NFST-2013-263, Rev. 4.

[9] Transnuclear Inc., TN-32 Dry Storage Cask. Safety Analysis Report Final Safety Analysis Report, Rev.2, Table 5.2–11, p633, Transnuclear Inc., 2002.

[10] D.K. Kok, Nuclear Engineering Handbook, CRC Press, Boca Raton, FL, 2009, 378 pp.

[11] J.E. Fast, J.W. Chenault, B.D. Glasgow, D.C. Rodriguez, B.A. Van Devender, L.S. Wood, Spent Nuclear Fuel Measurements, PNNL-23561, 2014.

[12] O.W. Hermann, C.W. Alexander, A Review of Spent-Fuel Photon and Neutron Source Spectra, 1986.

[13] I. Gauld, S. Bowman, J. Horwedel, Origen-ARP: automatic rapid processing for spent fuel depletion, decay, and source term analysis, ORNL/TM-2005/39, January 2009.

[14] Oak Ridge National Laboratory (ORNL), SCALE: A Modular Code System for Performing Standardized Computer Analyses for Licensing Evaluation, ORNL/TM-2005/39, January 2009.

[15] R. Rossa, et al., Development of a reference spent fuel library of 17x17 PWR fuel assemblies, ESARDA Bull. 50 (2013) 48–60.

[16] M.L. Fensin, M.R. James, Biasing secondary particle interaction physics and production in MCNP6, Prog. Nucl. Energy 94 (2016) 618–625.

[17] J.G. Richard, M.L. Fensin, S.J. Tobin, M.T. Swinhoe, J. Baciak, H.O. Menlove, Characterization of the neutron source term and multiplicity of a spent fuel assembly in support of NDA safeguards of spent nuclear fuel, in: INMM 51st Annual Meeting, 2010.

[18] I. Harkness, T. Zhu, Y. Liang, E. Rauch, A. Enqvist, K.A. Jordan, Development of neutron energy spectral signatures for passive monitoring of spent nuclear fuels in dry cask storage, EPJ Web Conf. 170 (2017) 4–7.

[19] Y. Gao, et al., Dry cask radiation shielding validation and estimation of cask surface dose rate with MAVRIC during long-term storage, Ann. Nucl. Energy 140 (2020) 107145. ISSN 0306-4549.

[20] D.R. McAlister, Neutron Shielding Materials, PG Research Foundation, Inc., Lisle, IL, 2016. https://www.eichrom.com/wp-content/uploads/2018/02/neutron-attenuation-white-paper-by-d-m-rev-2-1.pdf

[21] C. Greulich, C. Hughes, Y. Gao, A. Enqvist, J. Baciak, High energy neutron transmission analysis of dry cask storage, Nucl. Instrum. Methods Phys. Res., Sect. A 874 (2017) 5–11.

Index

Note: Page numbers followed by *f* indicate figures and *t* indicate tables.

A

Absorption, 355
Active neutron interrogation techniques, 3
Additives of interest, 58–61
  boron carbide, 59–60
  boron nitride, 58–59
  boron nitride nanotubes, 60–61
  carbon fiber, 61
Advance simulation software, for realistic neutron shielding, 389–396
  ATTILA, 391–392
  FLUKA, 395
  GEANT, 395–396
  Monte Carlo N Particle, 389–390
  SuperMC, 393–394
  TORT, 394
  TRIPOLI, 392–393
Air humidity, 241–242
Albert-Welton kernel method, 383
Alloys, 144–145, 147
Alpha emitters, 309
Alternating transparent plastic layers, 327
Aluminum, 54, 55*t*, 264–265
  alloys, 147
  composites, 11–12, 147
Amorphous boron powder, 271
Amorphous materials, 373–374
Antirads, 130
Artificial intelligence (AI), 159–162
Atom, 139
Atomic composition
  of cement, 184–185
  of concrete, 184–185
Atomic force microscopy (AFM), 70–71
Attenuation coefficient, 131
Attenuation of neutrons through water, 304–305, 306*f*

B

Back scattering spectrometers, 370
Beer-Lambert law, 181
Benzophenone, 134
Beryllium, neutron cross section of, 293, 293*f*
Bio-based materials, 133
Bismuth oxide, 132
Blended cements, 199
Boltzmann equation, for neutron transport, 385, 396
Boral, 11–12
Borated concrete, 7–8, 251
Borated polyethylene, 147
Borated polymer composites, 6
Borated steel, 6
Borax, 85
Borax filled concrete, 8–9
Boric acid, 35, 128, 131, 268–269, 271
Boric oxide, 36
Borohydrides, 212
Boron, 151–153, 303–304
Boron atomic density (BAD), 11–12
Boron-based fillers, 27–37
  boron carbide, 28–31
  hexagonal boron nitride, 31–35
Boron carbide, 28–31, 59–60, 92*f*, 130–131, 134
Boron compounds, 8–9, 35–37, 200–212, 268–269
Boron-containing iron ore concentrate (BCIOC), 97
Boron-filled PUR composites, 272–279
Boron fillers, 8–9, 270–272
Boron-infused basalt fiber-reinforced concrete, 10
Boron isotopes, 293–294, 294*f*
Boron mud (BM), 97
Boron neutron capture therapy, 2
Boron nitride (BN), 13–14, 58–59, 85–86, 268–269
Boron nitride nanotubes (BNNTs), 33, 60–61, 69–70
Boron oxide, 36–37, 128
Boron-rich slag (BRS), 97
Boron trioxide (B_2O_3), 17

Borosilicate glass, 10
Bragg equation, 359–360
Bragg scattering, 356
"Broad-beam" geometry, 330
  detection of fast neutrons, 330*f*

C

Cadmium, 151–153, 300, 301*f*, 312
Canister-based systems, 243–245
Canister vault storage construction, 405*f*
Capture gated detectors, 326
Carbon fiber (CF), 12, 58, 61
Carbon fiber-reinforced polyimide (CFRP), 103
Carbon nanotubes, 230–231
Carbon, neutron cross section, 294, 295*f*
Carbon steel, 245
Cask-based systems, 243–244
CASTOR casks, 243–244
Cement
  atomic composition, 184–185
  paste, 10
  type on neutron attenuation and absorption, 199–200
Ceramic matrix composites, 147
Ceramics, 247
Chain scission, 66–67
Chemical vapor deposition (CVD), 31–32
Chloride (Cl), 178–181
Chloride ion, 240–241
Chloroprene, 130
Chromium, neutron cross section of, 297, 298*f*
Coherent and incoherent scattering, 361–362
Colemanite, 9, 188
Composite alloy neutron shielding material n-order gram evaluations, 154–158, 155–157*t*
Composites
  and alloys in the material classification, 144–148, 145*f*
  for neutron absorption, 251
  scintillator layers, 327
Compression tests of HDPE/BN composite, 72
Computational methods for neutron shielding, 385–389
  advance simulation software, 389–396
  deterministic method, 386–387
  Monte Carlo method, 387–389
  numerical estimation of neutron shielding (*see* Numerical estimation of neutron shielding)
Computational modeling, 379
Computer codes, 224
Computer simulation methods, 185
Concentration effects, thermoplastic micro- and nanocomposites, 63
Concrete, 1–2, 229, 247–249, 254, 415–416
  applications in neutron-generating, 87–88
  atomic composition, 184–185
  behavior, 248–249
  castings, 6
  characterization, 254
  in civil structures, 177
  degradation, 116
  density, 233
  mixtures, 10
  molecular weight, 248
  neutron radiation shielding, 251
  neutron shielding, 228–231
  scattering cross section, 251
  uses, 177, 229–230
Concrete-based neutron-shielding materials, 7–10, 87–88
Copper, 246
Corrosion, 241–242
Corrosion-resistant materials, 241–242
Cosmic radiation, 264–265
Cosmic rays, 264–265
Coupling agents, 130
Cross sections of neutron interactions with nuclei, 320–321, 321*t*
Crystalline materials, 373–374
Crystallography, 356–357
Cyclotrons, 220–222

D

Deep space missions, 264
  composites for radiation shielding, 268–269
  radiation dose to astronauts, 267–268
  spallation nuclear reactions, 266–267

De-excitation, 266
Degradation in neutron-shielding material, 116
Deterministic method, 386–387
Deuterium-tritium (D-T), 220
Diagnostics for shielding efficiency measurement, 310–311
Differential scanning calorimetry (DSC), 73–75
Discrete ordinate method, 387
Document classification, 153–154
Dry cask storage, 240–241, 401, 404–405, 418
  neutron interactions with shielding material, 414–417
  uses, 258
Dry storage containers (casks), 243
Dual-purpose systems, 243

E
Earth's magnetic field, 263–264
EDPM, 250
Elastic modulus, 126–127
Elastic neutron scattering, 25, 26*f*, 289–290, 327, 334, 361, 363, 380–382, 381*f*, 414–415
Elastomer composites, 15–16
Elastomeric micro- and nanocomposites, 128–135, 129*t*
Elastomeric neutron-shielding composites, 15–18, 126, 128
Elastomers, 126–127, 135
  glass transition temperature, 126–127
  types used in neutron shielding, 127
  typical stress-strain diagram, 126–127, 127*f*
Electrical charge in neutrons, 229
Elemental composition of materials, 291–302
Embedding steel in cement, 231
Empirical neutron point kernel method, 384
Energetic radiation particles, 83
Energy discretization, 386
Energy solutions systems, 244–245
Energy spectra
  of fast neutrons, 336, 337*f*
  of g-radiation, 337*f*
Engineering and gamma-ray shielding properties of heavy concrete samples, 231–232, 232*t*
Engineering materials, 145–146
EPDM rubber composites, 17
Epoxy-based thermoset neutron-shielding composites, 15
Epoxy-/boric-acid-based lightweight material, 15
Epoxy composites, 90–100
  fast neutron and gamma integral fluxes, 93*f*
  injecting mortar for cracks, 94
  macroscopic absorption cross section of, 93*t*
  mechanical properties, 94
  shielding parameters of, 92–93
  thermal neutron flux attenuation properties, 95–96, 95*f*
Epoxy-ferrochromium slag composites, 116
Epoxy/lithium borate composites, 15
Epoxy resins, 90, 250–251
Epoxy thermoset, 90
Ethylene-propylene diene rubber, 131
Evaluated Nuclear Data Files (ENDF), 390
Excitation energy, 319–320

F
Fast neutron attenuation, 188
Fast neutron detection
  heavy-oxide single-crystal and multilayer composite scintillators, 335–346
  by multilayer composite scintillator detectors, 335–346
  nuclear mechanisms, 319–323
Fast neutron detectors, challenge of developing, 317–319
Fast neutron flux measurement and shield geometry
  fast-neutron energy transformation by spherical shield, 335
  neutron radiative scattering in broad-beam geometry, 329–332
  spherical shield geometry, 332–334

Fast neutrons, 83, 178, 310–311
  energy transformation by spherical shield, 335
  mass removal cross section, 182–183
  measured fluxes, 92–93
  scintillation response, 339, 339*f*
Fast neutron shielding, multilayer composite ZEBRA materials, 347–351
Fe-based amorphous ribbons, 12–13
Ferrochromium (FeCr) slag, 116
Fillers, 25
  for neutron shielding, 25
Fission reactors, 307–308, 362–363
Flexible elastomeric neutron-shielding materials, 15–16
Flexible shield materials, 287
Flexural testing, 73
FLUKA, 395
  Combinational Geometry (CG), 394
  simulations, 67–69
Free neutron, 141

G

Gadolinium, 38–41, 134, 212, 268–269
  particles, 99
Galactic cosmic radiation (GCR), 264, 267, 279–280
Galactic cosmic rays, 2–3
Gamma radiation, 15
Gamma ray, 327–328
  radiation, 414–415
  shielding, 222
Gamma source neutrons, 309
GEANT, 395–396
Geomagnetic storms, 159–162
Graphene platelets, 134
Graphite, 268–269

H

Hadronic cascades, 222, 223*t*
Half-value layer (HVL), 184, 225
Half-value thickness values, 225, 225*t*
H_3BO_3 fillers, 17
Heavy concrete, 7–8
  shielding for photon and neutron shielding, 231–233
Heavy-oxide scintillator layers, 322–323
Heavy-oxide single-crystal scintillator detectors
  neutron detection efficiency, 341–342, 341*t*
  neutron detection sensitivity, 342–343, 344*t*
Heavyweight aggregate, 188, 212–213
Heterogeneous mixtures, 144
Hexagonal boron nitride (hBN), 31–35, 128, 132, 270–271
High-density concrete, 233
  materials, 230
High-density polyethylene (HDPE), 127, 249
  comparative properties, 57*t*
  composites, 13–14
  thermal properties, 57*t*
  use, 31
High-energy neutrons, 1–2, 53–54, 380
High-energy radiation in deep space, 263–265
High-level waste (HLW), 239–240
High secondary radiation, 2–3
High-temperature concrete, 7–8
HI-STAR cask, 244–245
HI-STORM overpacks, 244–245
Homogeneous mixtures, 144
Hot pressing sintering, 28–29
H-rich compounds, 242–243
Hydration heat, 200
Hydrogen, 55, 87–88
  in concrete, 18
  gas, 303–304
  of limonite and serpentine, 9
  neutron cross section, 291, 292*f*
Hydrogenous epoxy resin, 116
Hydrogenous materials, 6
Hydrogen-rich elastomeric materials, 135
Hydrogen-rich materials, 125–126
Hydrogen-rich polymer matrix, 269–270, 280
HZE particles, 264–265, 279–280
HZETRN simulations, 69–70

I

Incident neutrons, 327
Inelastic neutron scattering, 320–321, 322*f*, 372–373

Inelastic scattering, 26*f*, 221, 298, 355–356, 379–380
  kinetic energy of neutron and scatter target, 414–415
Inner concrete shielding, 252–253
In situ or time-resolved spectroscopy, 373
Intermediate-level waste (ILW), 239–240
International Centre for Diffraction Data (ICDD), 374
International Space Station (ISS), 263–264
Iron (Fe), 178–181
  neutron cross section, 298, 299*f*
Iron-based aggregates, 188
Isophthalic-bismuth polymer composites, 114–115
Isotopes, 289–290

J

Joint Committee on Powder Diffraction Standards (JCPDS), 374

K

Kapton, 57

L

Lattice vibration, 356–357
Lead, 302
  based aggregates, 188
  neutron cross section, 302, 302*f*
Legendre polynomials, 387
Light nanocomposites, 230–231
Light water reactors (LWR), 402–404, 402*f*
Lightweight polymer filler compounds, 25–26
Linear accelerators, 220
Lithium
  based compounds, 27
  neutron cross section, 291–293, 292*f*
Lithium bis(oxalate) borate (LiBOB), 271
Long-term storage methods, 401
Low atomic weight materials, 125–126
Low-density polyethylene (LDPE), 31, 55–56, 127
  comparative properties, 57*t*
  thermal properties, 57*t*
Low-energy neutrons, 53–54, 310
Low-field nuclear magnetic resonance (LF-NMR) technique, 115
Low-level waste (LLW), 239–240
Low-viscosity epoxy resin, 91

M

Macroscopic cross section, 302–303, 312
  mean free path of neutrons, 303, 304*t*
  uncollided flux estimation, 303, 303*f*
Macroscopic effective cross section of fast neutrons, 183–184
Magnesium oxide (MgO), 199
Magnetic neutron spectroscopy, 371–372
Magnetic scattering, 372
Mass absorption, 78
Material balance for electricity production, 402–404, 403*f*
Material degradation, thermoplastic micro- and nanocomposites, 66–67
Mechanical testing, thermoplastic micro- and nanocomposites, 67–69
  atomic force microscopy, 70–71
  compression testing, 72
  flexural testing, 73
Medical facilities utilizing neutron radiation, 220–221
Metal alloys, 239–240, 242–243
  for spent fuel containers
    carbon steel, 245
    ceramics, 247
    concrete, 247–249
    copper, 246
    nickel alloys, 247
    stainless steels, 245–246
    titanium alloys, 246
Metal neutron-shielding composites, 10–13, 18
Metals, 144, 242–243
Methyl vinyl silicon rubber, 16–17
Mixtures, 144
Modified boron nitride (mBN) fillers, 76
Monomers, 13
Monte Carlo (MC) method, 185, 387–389, 396
Monte Carlo N Particle (MCNP), 389–390
Monte Carlo simulation methods, 87
Morphological test, 115

Multilayer composites
  heavyoxide fast neutron detectors, 323–329, 324*f*
  thermoplastic micro- and nanocomposites, 64–66
  ZEBRA materials for fast neutron shielding, 347–351
Multilayer concrete, 253–254
Multilayer heavy-oxide composite ZEBRA detectors
  neutron detection efficiency, 343–346, 345*t*
Multiple elastic scattering of neutrons, 334
Multipurpose systems, 243
Multiwalled carbon nanotubes (MWCNTs), 101

N

Nano-boron carbide, 85–86
Natural elemental boron, 269
Natural rubber (NR) blend, 130–131, 135
Nature ludwigite green ore (NLGO), 97
Neutron, 140, 177, 219, 233, 289–290
  absorbers, 15–16
  absorption test, 91–92
  in atomic view, 141*f*
  backscattering spectroscopy, 368
  classification and basic properties, 357–358
  diffraction, 356–357
  diffusion, 290–291
  distribution, 221
  elastic collisions, 380
  emission, 83, 405–408, 409–410*f*
  emitted in reactors, 1–2
  energy, 221
  energy spectra variation, 410, 411*f*
  energy wise classification, 358*t*
  exchange energy, 372–373
  flux density, 339
  generators, 310
  high radiation weighting factors, 125
  induced fission cross section, 408*f*
  inelastic scattering, 319–321
  interaction, 287, 379–380, 381*f*
  interactions with shielding material in dry cask, 414–417
  particles, 125
  permeability, 76–78
  physics, 221–222
  production, 220
  radiation, 3–4, 15, 53, 83, 139, 220–221
  radiative scattering in broad-beam geometry, 329–332
  radiography, 3
  scattering, 159, 297, 371–373, 375, 414–415
  sources, 125, 362–363, 371–372
  therapy centers, 220*t*
  transmutation process, 380
  transmission factor, 109–112
  transport codes, 386
  transport equation, 385, 387
  vibrational spectroscopy, 372–373
Neutron-absorbing fillers, 25–27, 44–46
  boron-based fillers, 27–37
    boron carbide, 28–31
    boron compounds, 35–37
    hexagonal boron nitride, 31–35
  characteristics, 45*t*
  feature comparison chart, 44
  rare earths, 38–44
    gadolinium, 38–41
    samarium, 42–44
Neutron activation analysis (NAA) technique, 3
Neutron amorphography, 373–375
  sources of additional information, 374–375
Neutron attenuation and absorption, 78, 84, 99, 100*f*
  composites, 251
  by concrete with different aggregates, 188–198, 189–198*t*
  efficiency by special components of concrete, 200–212, 201–210*t*
  influence of cement type, 199–200
  quantities for description, 181–184
Neutron cross section, 287
  beryllium, 293, 293*f*
  boron isotopes, 293–294, 294*f*
  cadmium, 300, 301*f*
  carbon, 294, 295*f*
  chromium, 297, 298*f*

  - hydrogen, 291, 292*f*, 312
  - iron, 298, 299*f*
  - lead, 302, 302*f*
  - lithium, 291–293, 292*f*
  - nickel, 298, 299*f*
  - nitrogen, 294–295, 296*f*
  - oxygen, 295–297, 296*f*
  - sulfur, 297, 297*f*
  - tungsten, 300–302, 301*f*
  - zinc, 300, 300*f*
- Neutron detection efficiency, 326
  - of heavy-oxide single-crystal scintillator detectors, 341–342, 341*t*
  - of multilayer heavy-oxide composite ZEBRA detectors, 343–346, 345*t*
- Neutron detection sensitivity
  - of heavy-oxide single-crystal scintillator detectors, 342–343, 344*t*
- Neutron-gamma rejection ratio, 326
- Neutron-generating devices, 219
- Neutron radiation shielding, 280
  - boron-filled PUR composites, 272–280
  - other types of thermosetting composites, 115
  - of polyimide composite, 107–108
  - polymer composites, 84–88
  - thermosetting micro- and nanocomposites (*see* Thermosetting micro- and nanocomposites for neutron radiation shielding)
- Neutron resonance spin-echo spectrometer, 369
- Neutron shielding, 53–54, 222, 233, 415–416
  - characterization, 288–307, 289*f*
    - diagnostics for shielding efficiency measurement, 288, 310–311
    - importance of elemental composition of materials, 291–302
    - neutron source for shielding efficiency measurement, 288, 307–310
    - numerical estimation of macroscopic cross section, 302–305
    - shielding efficiency of materials, 302–305
    - small-scale shielding experiments, 306–307
  - concrete, 228–231
  - design, 379–380
  - effectiveness by individual atoms, 199–200
  - with elastomeric micro- and nanocomposites developed, 128–135, 129*t*
  - of EPDM rubber, 131
  - evaluation, 184–187, 379
  - including micro- and nanomaterial structures, 222–228
  - mechanism, 4
  - neutrons and, 140–144
  - numerical estimation of (*see* Numerical estimation of neutron shielding)
  - by particular atoms of concrete, 178–181, 179–180*t*
- Neutron shielding aerogel materials, 109, 110*f*, 111*t*
- Neutron-shielding composite (NSC), 103
- Neutron-shielding efficiency, 109
- Neutron-shielding fiber metal laminates (NSFMLs), 12, 103, 104*f*
- Neutron shielding materials, 4–18, 415–416
  - application in various sectors, 2*t*
  - classification, 6, 7*f*
  - concrete neutron-shielding materials, 7–10
  - metal neutron-shielding composites, 10–13
  - polymer neutron-shielding composites, 13–18
- Neutron source
  - characteristics, 379–380
  - shielding efficiency measurement, 307–310
- Neutron spectroscopy techniques
  - magnetic neutron spectroscopy, 371–372
  - neutron backscattering spectroscopy, 368
  - neutron spin-echo spectroscopy, 368–370
  - neutron time-of-flight spectroscopy, 366–368
  - neutron triple-axis spectroscopy, 363–366
  - quasielastic neutron spectroscopy, 370–371
  - vibrational spectroscopy with neutrons, 372–373

Neutron spectrum optimizer, 307
Neutron spin-echo measurements, 369
Neutron spin-echo spectroscopy, 368–370
Neutron time-of-flight spectroscopy, 366–368
Neutron triple-axis spectroscopy, 363–366
Next-Generation Safeguards Initiative (NGSI) spent fuel library, 410–413
Next-generation shielding systems, 139
Nickel
  alloys, 247
  neutron cross section, 298, 299*f*
Nitrogen, 294–295
  neutron cross section of, 294–295, 296*f*
Nonisocyanate polyurethane-filled concrete, 9
Novel polyester, 112–113
Nuclear fission, 405–408
Nuclear mechanisms of fast neutron detection, 319–323
  neutron inelastic scattering, 319–320
Nuclear power, 401
  generation, 402–404
  plants, 1–2
Nuclear reaction, 141
Nuclear security, 317
Nuclear waste, 239–240
Nucleus temperature, 319–320
Nuclide cross section, 287
Nuclide masses, 410–413
Numerical estimation of neutron shielding, 382–385
  Albert-Welton kernel method, 383
  empirical neutron point kernel method, 384
  simplified neutron point kernel method, 384–385
  Spinney kernel method, 383–384

O

Off-site consolidated pool storage, 401
ORIGEN, 409
ORIGEN-automated rapid processing, 409
Oxygen, 295–297
  neutron cross section, 295–297, 296*f*

P

Particles size, thermoplastic micro-and nanocomposites, 61–63
Particle transport physics simulation, 396
Phonons, 356–357
Photoneutrons, 2, 230
Photons, 224, 233
Plutonium, 401
Polyamide, 251
Poly(methyl methacrylate) composites, 101–102
Polyester
  composites, 112–115
  resin, 415–416
Polyether-polyurethane (PUR) composites, 272, 280
  linear and mass attenuation coefficient, 275–276, 277*t*
Polyethylene (PE), 31, 55–56, 165, 224, 268
Polyimides (PI), 56–57
  chemical structure, 57*f*
  composites, 102–108
  mechanical properties, 58*t*
  resins, 55
  thermal properties, 58*t*
Polymer, 9, 30–31, 34, 66, 239–240
Polymer-cement concrete, 211
Polymer composites, 6
  for neutron attenuation, 249–251
    epoxy compounds, 250–251
    high-density polyethylene, 249
    polyamide, 251
    rubbers, 250
    ultrahigh-molecular-weight polyethylene, 249–250
  for neutron radiation shielding, 84–87
Polymeric compounds, 242–243
Polymer neutron-shielding composites, 13–18
  elastomeric neutron-shielding composites, 15–18
  thermoplastic neutron-shielding composites, 13–15
  thermoset neutron-shielding composites, 15
Polymethylmethacrylate (PMMA), 165, 268, 325
Polypropylene fibers, 9

Polytetrafluoroethylene (PTFE), 325
Polyurethane (PUR), 108–112, 133, 269–270
Portland cement, 184–185, 200
  classification, 199–200
  clinker, 199
Pressureless sintering, 28–29
Prioritization criteria evaluation, 148–150
Prompt gamma NAA technique, 3
Protons, 139, 141, 222
Pulse-type neutron flux, 362–363
Pure substances, 144

Q

Quasielastic neutron spectroscopy (QENS), 370–371
Quasielastic scattering, 370

R

Radiation, 140
  attenuation, 229
  dose to astronauts in deep space missions, 267–268
  exposure, 55
  protection, 228
Radiation shielding, 53–54, 263
  boric acid, 35
  composites in deep space missions, 268–269
  historical approaches, 53–54
  models, 67–70
    FLUKA simulations, 67–69
    HZETRN simulations, 69–70
  necessary and desired applications, 55
  neutron shielding, 53–54
  prevalence of aluminum, 54, 55*t*
  property, 140
  size of filler particles, 26–27
  thermoplastics of interest, 55–57
  transport simulation, 396
  use of fillers, 26–27
Radiation testing, thermoplastic micro-and nanocomposites
  neutron absorption results, 78
  neutron permeability results, 76–78
Radiative capture, 25, 26*f*
Radioactive residues, 402–404
Radioactive waste, 402–404
Radiobiological effectiveness of by-product neutron, 2
Rare earth-doped high-density rubber, 130
Rare earths, 38–44
  gadolinium, 38–41
  samarium, 42–44
Reactor-generated neutrons, 221
Reactor pool storage, 401
Reinforced epoxy composites, 103
Relative attenuation factor (RAF), 86–87
Resins, 87–88
  matrix, 89
Resonance neutron cross sections, 323
Rubbers, 250

S

Samarium, 42–44
Samarium oxide, 134
Scattering, 355–356
Scintillating plastic transparent material, 326
Scintillation light, 328
Search engines, 153–154, 158
Secondary gamma radiation, 8–9
Semi-long-term storage, 401
Shield effectiveness, 78
Shielding capability of material, 306
Shielding efficiency
  evaluation, 306, 307*f*
  measurement
    diagnostics for, 310–311
    neutron source for, 307–310
Shielding high-energy neutrons, 229
Shielding materials, 142, 287
Silicone rubber, 132, 250–251
  composites, 16–17
Simplified neutron point kernel method, 384–385
Simulation
  model of shielding experiment, 307, 308*f*
  of radiation therapy, 396
  process, 288
Single-crystal scintillator, 317–318
Single-purpose systems, 243
Single-walled carbon nanotubes (SWCNTs), 101
Small-angle neutron scattering (SANS), 370

Small-scale shielding experiments, 306–307
Solar energetic particles, 2–3
Solar particle events (SPEs), 264
Spacecraft, 53
Space discretization, 386
Space exploration, 263–264
Space radiation, 53–54, 396
Spallation neutron source, 362–363
Spallation nuclear reactions, in deep space missions, 266–267
Spatial periodicity, 356
Spectroscopy, 356–357
Spent fuel containers, 239–240
  canister-based systems, 243–245
  cask-based systems, 243–244
  dry and wet storage systems, 243
  dry cask storage, 240–241
  dual-purpose systems, 243
  elements, 239–240
  factors that influence material choice, 240–243
  multilayer strategies, 252–254, 253*f*
  multipurpose systems, 243
  numerical simulations, 254–257
  single-purpose systems, 243
  types, 243–245
Spent nuclear fuel (SNF), 401–408
  neutron aging, 410–413
  variation in neutron intensity per fuel assembly, 410, 411*f*
Spherical harmonics polynomial, 387
Spherical shield geometry, 332–334
Spin-echo small-angle neutron scattering, 370
Spin-echo spectrometers, 369
Spinney kernel method, 383–384
Spontaneous fission, 405–408
  neutron emission isotopic component, 410–413, 413–414*f*
Stainless steels, 245–246
Stress corrosion cracking (SCC), 241–242
Styrene butadiene rubber (SBR), 135
Sulfur, neutron cross section of, 297, 297*f*
SuperMC, 393–394
Synthetic rubber SKTN-B, 325
Synthetic thermoset-based mortar, 87–88

T
Tenth value layer (TVL), 184
Thaumasite, 240–241
Theory of neutron scattering, 358–362
  coherent and incoherent scattering, 361–362
Thermal behavior, thermoplastic micro-and nanocomposites
  differential scanning calorimetry, 73–75
  thermogravimetric analysis, 75
Thermal neutrons, 8–9, 108–109, 186–187
  absorption, 27–28, 34, 91, 227
  attenuation, 131
  epoxy/ilmenite composites, 94
  radiation shielding, 108
Thermal neutron-shielding, 4, 5*f*
Thermogravimetric analysis (TGA), 75
Thermoplastic micro-and nanocomposites for neutron shielding
  additives of interest, 58–61
    boron carbide, 59–60
    boron nitride, 58–59
    boron nitride nanotubes, 60–61
    carbon fiber, 61
    concentration effects, 63
    material degradation, 66–67
    particle size of, 61–63
    thickness effects, 63–64
  concentration effects, 63
  current research approaches, 67–78
    mechanical testing, 67–69
    radiation shielding models, 67–70
    radiation testing of composites, 76–78
    thermal behavior, 73–75
  material degradation, 66–67
  multilayer composites, 64–66
  particles size effects, 61–63
  radiation shielding, 53–54
    historical approaches, 53–54
    models, 67–70
    necessary and desired applications, 55
    neutron shielding, 53–54
    prevalence of aluminum, 54, 55*t*
    thermoplastics of interest, 55–57
  thickness effects, 63–64
Thermoplastics, 55–57
  neutron-shielding composites, 13–15
  polyethylene, 55–56

  polyimides, 56–57
Thermoset neutron-shielding composites, 15
Thermosetting matrices, 88–89
Thermosetting micro-and nanocomposites for neutron radiation shielding, 89–115
  application of, 115–118
  epoxy composites, 90–100
  linear attenuation coefficients, 96, 96*t*
  other types, 115
  poly(methyl methacrylate) composites, 101–102
  polyester composites, 112–115
  polyimide composites, 102–108
  polyurethane composites, 108–112
Thermosetting polyimides, 102
Thermosetting polymers, 87–88
Thermosetting resins, 88–89
Thickness effects, thermoplastic micro- and nanocomposites, 63–64
Threshold energy, 178
Ti composites, 147
Time-of-flight method, 366–368
Time-of-flight spectrometers, 370
Time periodicity, 356
Time-resolved neutron spectroscopy, 373
Titanium alloys, 246
TN-32 dry storage cask, 404–405, 406–407*f*, 415–416, 417*f*
TORT, 394
Traditional spacecraft building material, 264–265
Transmission, 355
Transparent light-guide layers, 326
Transport codes, 227
TRIPOLI, 392–393
Tungsten, 130
  neutron cross section, 300–302, 301*f*

U

Ultrahigh-molecular-weight polyethylene (UHMWPE), 249–250

V

Van Hove scattering function, 361
Vibrational spectroscopy with neutrons, 372–373

W

Water, 224

X

X-ray scattering, 358–359

Z

ZEBRA-detector, 323, 324*f*, 326–327
  dimensions, 346
  efficiency and productivity, 329
  feature, 327
  gamma-ray sensitivity, 328
  layers of thickness, 325
  principle of operation, 327
  scintillation response, 339
Zinc borate, 128, 130
Zinc, neutron cross section, 300, 300*f*

WOODHEAD PUBLISHING SERIES IN COMPOSITES SCIENCE AND ENGINEERING

Recent advancements in the field of nuclear science and technology have increased the demand for new innovative advanced materials for radiation shielding applications. For example, exposure to neutron radiation can cause severe damage to human beings. **Micro and Nanostructured Composite Materials for Neutron Shielding Applications** focuses on recent developments and future possibilities for neutron-shielding materials. Emphasis is placed on the correlation between morphology, shielding mechanisms, and other desired properties such as the mechanical and thermal properties of materials. The effect of neutron absorbing fillers, including their size on the final properties, is also examined in detail. Recent advancements in the preparation, characterization, and simulation techniques are also covered. Written by specialists in their respective fields, the book will help professionals and students to understand the fundamentals of neutron shielding, as well as the properties of micro and nanopolymer-based composites, concrete materials, alloy materials, and metal-ceramic composites.

Key features

- Provides an up-to-date understanding of the fundamentals of shielding mechanisms, morphology, and material property correlations.
- Covers a broad range of micro and nanocomposite materials for neutron shielding.
- Discusses the recent advancements in neutron-shielding characterizations, neutron detectors, and computational methods.

About the Editors

Sajith Thottathil Abdulrahman is a senior researcher at the Universiti Teknologi Mara, Shah Alam, Malaysia. He holds an MTech in Nanotechnology and a BTech in Mechanical engineering. His areas of research include nanotechnology, mechanical engineering, materials engineering, and polymer composites.

Prof. Sabu Thomas is currently vice-chancellor of Mahatma Gandhi University, Kottayam, India. Prof. Thomas is an outstanding leader with sustained international acclaim for his work in nanoscience, polymer science and engineering, polymer nanocomposites, elastomers, polymer blends, interpenetrating polymer networks, polymer membranes, green composites and nanocomposites, nanomedicine, and green nanotechnology. He has received many national and international awards and has published more than 1000 peer-reviewed research papers. He has co-edited 135 books and has 15 patents to his credit.

Zakiah Ahmad is a full professor and the dean of Faculty of Civil Engineering, Universiti Teknologi Mara, Malaysia. Prof. Zakiah has specialized in timber-engineered composite and nano-polymer composites. She has published more than 300 papers in journals/proceedings and eight books. Prof. Zakiah is also the recipient of Malaysia's Top Research Scientist award.

Technology and Engineering/
Material Science

ISBN 978-0-12-819459-1

9 780128 194591

ELSEVIER

WP
WOODHEAD
PUBLISHING
An imprint of Elsevier
elsevier.com/books-and-journals